Complexity, Dynamics, Control, and Applications of Nonlinear Systems with Multistability 2021

Lead Guest Editor: Viet-Thanh Pham
Guest Editors: Sundarapandian Vaidyanathan, Jesus Manuel Muñoz-Pacheco, and Ahmad Taher Azar

Complexity, Dynamics, Control, and Applications of Nonlinear Systems with Multistability 2021

Complexity, Dynamics, Control, and Applications of Nonlinear Systems with Multistability 2021

Lead Guest Editor: Viet-Thanh Pham
Guest Editors: Sundarapandian Vaidyanathan, Jesus Manuel Muñoz-Pacheco, and Ahmad Taher Azar

Contents

Research Article

Synchronization of a New Chaotic System Using Adaptive Control: Design and Experimental Implementation

Alfredo Roldán-Caballero [ID],[1] J. Humberto Pérez-Cruz [ID],[2]
Eduardo Hernández-Márquez [ID],[3] José Rafael García-Sánchez [ID],[4] Mario Ponce-Silva [ID],[5]
Jose de Jesus Rubio [ID],[2] Miguel Gabriel Villarreal-Cervantes [ID],[6]
Jesús Martínez-Martínez [ID],[4] Enrique García-Trinidad [ID],[4]
and Alejandro Mendoza-Chegue [ID][2]

[1]*Unidad Profesional Interdisciplinaria de Ingeniería Campus Tlaxcala, Instituto Politécnico Nacional, Tlaxcala 90000, Mexico*
[2]*Sección de Estudios de Posgrado e Investigación, Escuela Superior de Ingeniería Mecánica y Eléctrica Unidad Azcapotzalco, Instituto Politécnico Nacional, Ciudad de México 02250, Mexico*
[3]*Departamento de Ingeniería Mecatrónica, Instituto Tecnológico Superior de Poza Rica, Tecnológico Nacional de México, Veracruz 93230, Mexico*
[4]*División de Ingeniería Mecatrónica, Tecnológico de Estudios Superiores de Huixquilucan, Tecnológico Nacional de México, La Magdalena Chichicaspa, Estado de México 52773, Mexico*
[5]*Departamento de Ingeniería Electrónica, Tecnológico Nacional de México-CENIDET, Cuernavaca 62490, Morelos, Mexico*
[6]*Centro de Innovación y Desarrollo Tecnológico en Cómputo, Instituto Politécnico Nacional, Ciudad de México 07700, Mexico*

Correspondence should be addressed to J. Humberto Pérez-Cruz; jhperez@ipn.mx

This paper presents the design of an adaptive controller that solves the synchronization control problem of two identical Nwachioma chaotic systems in a master-slave configuration. The closed-loop stability is guaranteed by means of a Lyapunov-like analysis. With the aim of verifying the feasibility and performance of the proposed approach, a comparison with an active control algorithm is developed at the numerical simulation level. Based on such results, the master-slave Nwachioma chaotic system in closed-loop with adaptive control is now being experimentally tested by using two personal computers and two low-cost Arduino UNO boards. The experimental results not only show the good performance of the adaptive control but also that Arduino UNO boards are an excellent option for the experimental setup.

1. Introduction

It is well known that complex chaotic systems are nonlinear dynamic systems characterized by being nonperiodic oscillators with high sensitivity to initial conditions and whose solution can be hardly predictable in the long term [1, 2]. Despite the latter, these kind of systems are deterministic, meaning that suitable control algorithms can be designed for them [3, 4]. In this regard, the first chaotic system was presented by Lorenz in [5]. From that moment on, several applications associated with chaotic systems have emerged. Some of those are in the areas of neurosystems [6, 7], chemical reactions [8, 9], secure communications [10–18], turbines [19, 20], robotics [21–24], cryptosystems [25–29], medicine [30–33], lasers [25, 34], among others.

When control strategies for complex chaotic systems are designed, the tasks to be solved can be divided into the following: (1) chaos suppression and (2) synchronization. The

present paper is focused on the second control task. Hence, the following state-of-the-art review describes some relevant contributions related to the synchronization of chaotic systems.

1.1. Related Works.

The purpose of synchronization in chaotic systems is to achieve that one or more systems, with similar or different dynamics, converge to the same pre-scribed trajectory. Such a synchronization is generally carried out by means of a master-slave configuration. In this di-rection, the pioneer paper of Pecora and Carroll [35] de-scribed, for the first time, the synchronization of the Lorenz and the Rossler chaotic systems. Based on Pecora and Car-roll's contribution, the research related to the design of controllers for synchronization of chaotic systems has been intensively studied during the last four decades [36–89]. The proposed control strategies reported in those works can be classified as active control [36–42], nonlinear control [43–57], linear feedback control [58–65], sliding modes [66–72], and adaptive control [73–89]. Such a literature is described below.

1.1.1. Active Control.

Based on the literature, the active control approach was one of the first control methods for solving the synchronization problem. In this sense, Bai and Lonngren in [36, 37] demonstrated that coupled Lorenz sys-tems can be synchronized by active control theory. The syn-chronization was verified at the simulation level. Meanwhile, Tang et al. [38] introduced a control strength matrix in the active control. With this extended method, the authors showed that the chaos complete synchronization can be achieved more easily. Numerical simulations on Rossler, Liu's four-scroll, and Chen systems confirmed the latter. Also, Yassen [39] presented simulation results of synchronizations between two different chaotic systems: the Lorenz and Lü systems, the Chen and Lü systems, and the Lorenz and Chen systems. On the other hand, Pérez-Cruz et al. [40] investigated the synchronization of a new three-dimensional chaotic system and, by means of Lyapunov analysis, a nonlinear controller was designed in such a way that the exponential convergence of the synchronization error was guaranteed and the results of the numeric simulation verified the good performance of this controller. In [41] Varan and Akful synchronized a hyperchaotic system and by using a Lyapunov function, achieved global asymptotic stability; numerical analysis was used to check the effectiveness of the proposed active control design. Lastly, Zhu and Du in [42] solved the antisynchronization of systems by using the active control, and the feasibility of control was verified via numerical simulations.

1.1.2. Nonlinear Control.

Related to the design of nonlinear controllers for solving the synchronization problem, Suna et al. [43] proposed a nonlinear control strategy for synchronizing five chaotic systems, where the performance of the proposed approach was verified by numerical simulations. Zheng designed a nonlinear control in [44] to study multi-switching combination synchronization of three different chaotic sys-tems, i.e., two drive chaotic systems and a controlled response chaotic system; simulation results depicted good performance

of the system in closed-loop. Likewise, Hettiarachchi et al. presented a nonlinear control algorithm for solving the syn-chronization problem over two time-delay coupled Hind-marsh–Rose neurons [45], whose effectiveness of the proposed approach was investigated through numerical simulations. Additionally, Yadav et al. [46] developed a nonlinear control method for combination-combination phase synchronization in fractional-order nonidentical complex chaotic systems. Simulation results were obtained, by using the Adams–Bashforth–Moulton method, with the aim of showing the performance of the system in closed-loop. Also, Yadav et al. [47] analyzed a nonlinear control for the triple compound synchronization among eight chaotic systems with external disturbances, and the feasibility of the proposed control was depicted through numerical simulations by using the Run-ge–Kutta method. Ouannas et al. [48] used a nonlinear control algorithm for the synchronization of a fractional hyperchaotic Rabinovich master-slave pair and numerical simulations demonstrated the validity and convergence of the proposed synchronization scheme. Whereas, Abdurahman and Jiang [49] introduced a nonlinear control strategy to investigate the general decay projective synchronization (GDPS) problem of a type of delayed memristor-based BAM neural networks; numerical results were obtained and the effectiveness of the proposed control was verified. On the other hand, Al-Hayali and Al-Azzawi [50] addressed the problem of synchronizing 4D identical Rabinovich hyperchaotic systems by using two strategies: active and nonlinear control; the good performance of the hyperchaotic systems in closed-loop was verified via simulation results. Another research was conducted by Al-Obeidi and Al-Azzawi [51], where they reported a nonlinear control strategy for chaos synchronization by using a 6D hyperchaotic system and numerical simulations were carried out to validate the effectiveness of the proposed control technique. Subsequently, Al-Azzawi and Al-Obeidi [52] pro-vided a nonlinear control for a new 6D hyperchaotic system with real variables and a self-excited attractor. The proposed control allowed finding the stability of error dynamics and its performance was tested through numerical simulations. Also, Trikha et al. [53] introduced a novel 3D fractional chaotic system with two quadratic terms and designed a nonlinear control strategy for solving the synchronization problem; the simulations results demonstrated the effectiveness of the proposed strategy. Lin et al. [54] addressed the issue of global exponential synchronization for delayed impulsive and time-varying delayed inertial memristor-based quaternion-valued neural networks and the closed-loop system was verified via numerical simulations. Additionally, Jahanzaib et al. [55] elaborated a nonlinear control scheme for a novel fractional-order chaotic model with the aim of achieving the synchro-nization of the system; simulations were obtained and the good performance of the closed-loop system was demonstrated. Another work was developed by Ouannas et al. [48], where linear and nonlinear feedback controls were investigated and both force the slave system to follow the trajectory set by the master given different initial states; numerical simulations validated the synchronization schemes. Also, Ouannas et al. [56] developed two nonlinear control schemes to achieve as-ymptotic convergence with the aim of solving the

synchronization problem; experimental and simulation results supported the proposed theory. Later, Mesdoui et al. [57] designed nonlinear controls for solving the synchronization problem in a nonlinear bacterial cultures reaction-diffusion model and the effectiveness of the proposed control was verified via simulation results.

1.1.3. Linear Feedback Control. Regarding this kind of control, Wu [58] investigated the synchronization of the general master-slave identical generalized Lorenz systems, and the developed theory was validated via numerical simulations. Also, Yan and Yun [59] studied the synchronization of an LC chaotic system via three types of state feedback controls: (i) linear feedback control; (ii) adaptive feedback control; and (iii) a combination of linear feedback and adaptive feedback controls, where numerical simulations demonstrated the obtained theoretical results. Whereas, Rafikov and Balthazar in [60] formulated linear feedback controllers for the control and synchronization of chaos through an application of optimal control and Lyapunov stability theories to guarantee the global stability of the nonlinear error system; numerical simulations were provided in order to demonstrate the effectiveness of this control approach by achieving the synchronization of the hyper-chaotic Rössler system. Later, Chen et al. [61] proposed the global synchronization criteria for a class of third-order nonautonomous chaotic systems consisting of cubic and (or) intersecting nonlinearity terms under the master-slave linear state error feedback control, whose effectiveness was verified through a numerical example. Likewise, Mobayen and Tchier [62] studied the chaos synchronization problem for a class of uncertain chaotic systems with Lipschitz non-linearity conditions using an LMI-based state feedback stabilization control method and simulation results were given to show the efficiency of the control scheme. On the other hand, Zhao et al. addresses H_∞ synchronization for uncertain chaotic systems with one-sided Lipschitz nonlinearity under the output and intrinsic state delays [63], where numerical simulations proved the effectiveness of the proposed methodology by achieving the synchronization of Chua's circuit chaotic systems. Moreover, Mahmoud et al. [64] designed a single-state feedback track synchronization control algorithm and the effectiveness of the proposed algorithm is well illustrated via an exhaustive numerical simulation. Lastly, Azar et al. [65] explored the stabilization and synchronization of a chaotic system by means of a state feedback control that moves the eigenvalues of the linearized chaotic system to a point where the state variables reach equilibrium; numerical experiments and simulation results were reported with the aim of showing the effectiveness of the proposed approach.

1.1.4. Sliding Mode Control. Another control technique used for synchronization of chaotic systems is the sliding mode. For example, Siddique and Rehman [66] presented an adaptive integral sliding mode control design method for parameter identification and hybrid synchronization of chaotic systems connected in ring topology, where the effectiveness of the proposed technique was validated through

numerical examples. Also, Mufti et al. [67] developed the control design method for the transmission projective synchronization of multiple nonidentical coupled chaotic systems, whose performance in closed-loop was checked via numerical simulations. Another work was realized by Mufti et al. [68], where the synchronization and antisynchronization between the Chua and modified Chua oscillators were obtained and the effectiveness of the control strategies was validated via numerical simulations. Based on the Lyapunov stability theory and fractional-order integral sliding surface, a novel active sliding mode controller to synchronize fractional-order complex chaotic systems was proposed by Nian et al. [69] and was verified through numerical simulations. Another work was developed by Song et al. [70], where they focused on the robust synchronization issue for drive-response fractional-order chaotic systems applying the sliding mode control scheme; practical examples to illustrate the feasibility of the theoretical results are developed. In [71], Wan et al. proposed a discrete sliding mode controller to ensure the synchronization of chaotic systems and experimental results were given to demonstrate the performance of the proposed cryptosystems. The synchronization problem of chaotic systems using the integral-type sliding mode control for hyper-chaotic systems is considered in [72], where simulation results confirm the success of the designed control.

1.1.5. Adaptive Control. This approach is used when the parameters of the chaotic system are unknown. For example, Wu et al. [73] showed how adaptive controllers can be used to adjust the parameters of two Chua's oscillators to synchronize them via simulations. Whereas, based on the Lyapunov stability theory, Liao developed an adaptive control law [74] for synchronizing two Lorenz systems; the simulation results validated the proposed approach. In [75], Behinfaraz et al. developed a new fractional-order chaotic system where the parameter's adaption laws were obtained to design adaptive controllers using the Lyapunov stability theory and numerical examples were carried out to verify the performance of the controllers. By means of the Lyapunov theory, Wang et al. [76] proposed a nonlinear adaptive system to ensure the synchronization of two Hindmarsh–Rose neuron models and its simulation results verified the feasibility and effectiveness of the designed controller. Also, Pérez-Cruz [77] added a robustifying term to the adaptive control law for the stabilization and synchronization of an uncertain Zhang system; the performance of this robust approach was verified through numerical simulations. In [78], Khennaoui et al. proposed a one-dimensional adaptive control strategy that forces the states of discrete-time chaotic systems to tend asymptotically to zero; numerical results were presented to confirm the success of these synchronization schemes. Later, Luo et al. [79] proposed an adaptive synchronization scheme, which combines the best of the Chebyshev neural network, extended state tracking differentiator, and adaptive backstepping for the fractional-order chaotic arch microelectro-mechanical system; the effectiveness of the proposed adaptive synchronization scheme was demonstrated through simulation results. On the other hand, Xu et al. in [80] investigated an adaptive event-triggered

transmission strategy for the exponential synchronization of chaotic Lur'e systems; the designed control scheme was verified through numerical examples. Based on the complex-variable inequality and stability theory for the fractional-order complex-valued system, Zhang et al. presented [81] a new scheme for adaptive synchronization of fractional-order complex-variable chaotic systems with unknown complex parameters, where simulation results proved the effectiveness of the synchronization scheme. Liu et al. [82] developed the fractional Mittag–Leffler stability theory, that is, an adaptive, large-scale, and asymptotic synchronization control method for the synchronization of two different fractional-order chaotic systems under the conditions of determined parameters and uncertain parameters; the simulation results proved the good reliability of the controller. Another work was reported by Singh and Roy in [83] developed three different well-known control techniques: nonlinear active control, sliding mode control, and adaptive control, which are used for synchronization between various pairs of chaotic systems; simulation results are presented, which reflect the successful achievement of the objectives. In [84], Gao et al. proposed the cluster synchronization of a class of nonlinearly coupled Lur'e networks through a novel adaptive pinning control strategy, whose performance was depicted through numerical simulations. Another work was reported by Azar and Serrano in [85], where the design of an adaptive terminal sliding mode control for the stabilization of chaotic systems was proposed and experimental results were introduced for validating the control scheme. Javan et al. [86] showed a synchronization scheme using a robust-adaptive control procedure with the help of the Lyapunov stability theorem and the experimental results revealed the capability and flexibility of this method in synchronization of chaotic systems. Later, Javan et al. [87] developed an adaptive control method, and the definition of appropriate Lyapunov function was used for synchronization for chaotic systems; the results showed the effectiveness of the proposed synchronization technique in the medical images encryption for telemedicine application. One more piece of research was introduced by Wang and Rongwei [88], where they applied the adaptive control method to investigate the design of a universal controller to achieve the hybrid synchronization of a class of chaotic systems; numerical examples verify and validate the effectiveness of the proposed theoretical results. In addition, Khennaoui et al. [89] proposed adaptive control laws for solving the synchronization problem in three different types of chaotic systems, the Stefanski, Rossler, and Wang systems where the performance of the systems in closed-loop was verified by simulation results.

1.2. Discussion of Related Work, Motivation, and Contribution. The literature shows that several types of complex chaotic systems have been proposed with the aim of solving the synchronization control problem. The control strategies, usually developed, are active control [36–42], nonlinear control [43–57], linear feedback control [58–65], sliding modes [66–72], and adaptive control [73–89]. Also, on the one hand, it was observed that experimental results about synchronization of chaotic systems are

very scarce [90–97]. On the other hand, recently a new 3D chaotic system with four nonlinearities was proposed in [98]. Surprisingly, a control algorithm for solving the synchronization control problem for this system has not been yet proposed.

Motivated by the aforementioned and by the fact that complex chaotic systems can be applied in a wide range of fields, the contribution of this paper is to solve the synchronization for the chaotic system [98] by means of proposing an adaptive control. Moreover, with the purpose of enhancing this contribution, a comparison between an active control scheme and the adaptive control algorithm developed in this research is presented. Later, the experimental implementation of the adaptive control on the Nwachioma chaotic system is carried out through a novel experimental realization. For this latter, a low-cost testbed composed of two personal computers and two Arduino UNO boards along with MATLAB-Simulink are used.

The rest of the paper is structured as follows: in Section 2, the mathematical model of the new Nwachioma chaotic system in the master-slave configuration is presented and the adaptive control for solving the synchronization control problem is developed. The comparison between an active control and the adaptive control proposed here along with its experimental implementation is presented in Section 3. Finally, conclusions related to this research and future work are described in Section 4.

2. Materials and Methods

This section presents the generalities of the Nwachioma chaotic system and the master-slave configuration to be used throughout this paper. Also, the design of the adaptive control that achieves the synchronization of the master-slave configuration is introduced.

2.1. Nwachioma Chaotic System and Master-Slave Configuration. The Nwachioma chaotic system was proposed in [98]. The mathematical model describing its behavior is given by the following equations:

$$
\begin{aligned}
\dot{x}_1 &= a_1 x_1 + a_2 x_1 x_3 + a_3 x_2 x_3, \\
\dot{x}_2 &= a_4 x_2 + a_5 x_1 x_3 + a_6, \\
\dot{x}_3 &= a_7 x_3 + a_8 x_1^2 x_2 + a_9,
\end{aligned}
\tag{1}
$$

where a_i (for $i = 1, 2, \ldots, 9$) are constants and $a_8 x_1^2 x_2$ assures the boundedness of the system [98]. As can be observed in the previous equations, the Nwachioma system is autonomous, i.e., the system does not have inputs that modify its dynamics. On the other hand, the behavior of such a system is purely chaotic when the following constant values are considered in (1):

$$
\begin{aligned}
&a_1 = -0.1, a_2 = 0.15, a_3 = 0.18, a_4 = 3.9, \\
&a_5 = -1.5, a_6 = -4, a_7 = -4.9, a_8 = 2.5, a_9 = 0,
\end{aligned}
\tag{2}
$$

and also when the initial conditions are set to $x_1(0) = 1$, $x_2(0) = 3$, and $x_3(0) = 8$ (see Figure 1).
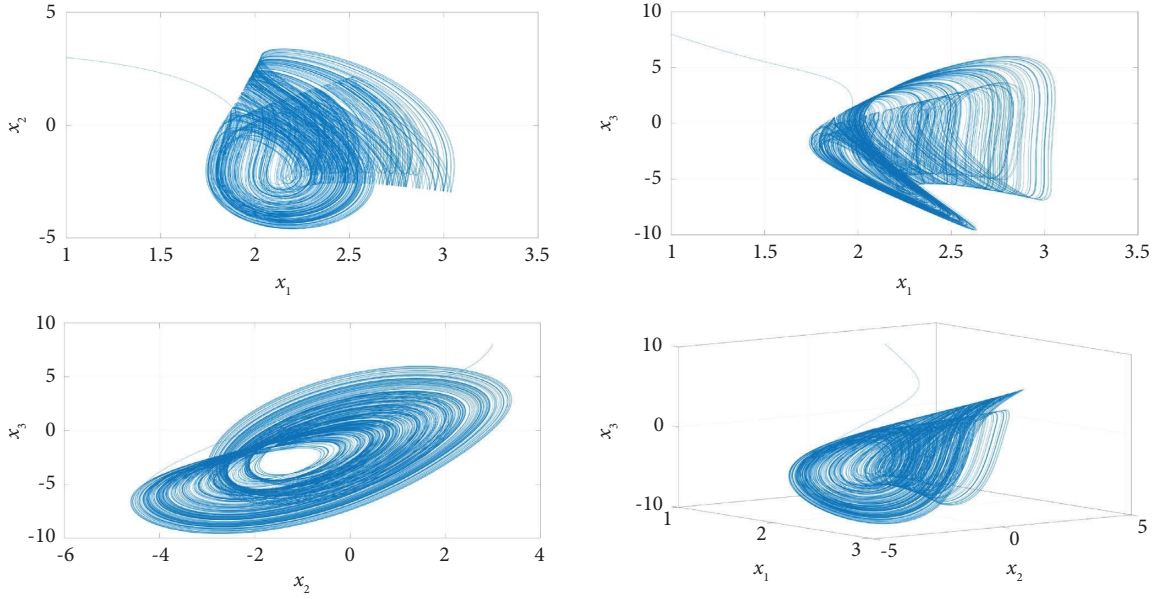
FIGURE 1: Planes and phase portraits of the Nwachioma chaotic system, where the self-attractor of the system can be observed. The initial conditions considered for the plane and the phase portrait are $x_1(0) = 1$, $x_2(0) = 3$, and $x_3(0) = 8$.

As can be observed in Figure 1, the planes and phase portraits of system (1) show the self-excited attractor, meaning that the states of the system are bounded over a specific region. It is worth mentioning that the system is very sensitive to initial conditions due to the chaoticity of its dynamics. This can be confirmed through the simulation results depicted in Figure 2. Such results show the behavior of the Nwachioma system when two sets of initial conditions are used. The first set of initial conditions were reported in [98] and were defined as $x_1(0) = 1$, $x_2(0) = 3$, and $x_3(0) = 8$, whereas the second set are those proposed in this paper and are prescribed to be $x_{1b}(0) = 1$, $x_{2b}(0) = 3.002$, and $x_{3b}(0) = 8$.

The master-slave Nwachioma chaotic system is composed of two subsystems: a master Nwachioma system and a slave Nwachioma-alike system. The first one is defined by the following autonomous dynamics:

$$\dot{x}_{1m} = a_1 x_{1m} + a_2 x_{1m} x_{3m} + a_3 x_{2m} x_{3m},$$
$$\dot{x}_{2m} = a_4 x_{2m} + a_5 x_{1m} x_{3m} + a_6, \qquad (3)$$
$$\dot{x}_{3m} = a_7 x_{3m} + a_8 x_{1m}^2 x_{2m} + a_9,$$

and it is identified through the subscript m. On the other hand, the slave system is denoted with the subscript s and, compared with the master, it is not an autonomous system, since it is commanded through inputs u_1, u_2, and u_3. The dynamics of the slave is defined as follows:

$$\dot{x}_{1s} = a_1 x_{1s} + a_2 x_{1s} x_{3s} + a_3 x_{2s} x_{3s} + u_1,$$
$$\dot{x}_{2s} = a_4 x_{2s} + a_5 x_{1s} x_{3s} + a_6 + u_2, \qquad (4)$$
$$\dot{x}_{3s} = a_7 x_{3s} + a_8 x_{1s}^2 x_{2s} + a_9 + u_3,$$

where constants a_i are equal in both systems. However, when the adaptive control is designed such constants are considered to be unknown.

2.2. Adaptive Synchronization.
The objective of the adaptive synchronization control proposed in this section is to achieve that $(x_{1s}, x_{2s}, x_{3s}) \longrightarrow (x_{1m}, x_{2m}, x_{3m})$. For such an aim, the following synchronization errors are defined:

$$e_1 = x_{s1} - x_{m1},$$
$$e_2 = x_{s2} - x_{m2}, \qquad (5)$$
$$e_3 = x_{s3} - x_{m3}.$$

Thus, from (5), the error dynamics is given by

$$\dot{e}_1 = \dot{x}_{s1} - \dot{x}_{m1},$$
$$\dot{e}_2 = \dot{x}_{s2} - \dot{x}_{m2}, \qquad (6)$$
$$\dot{e}_3 = \dot{x}_{s3} - \dot{x}_{m3}.$$

After replacing the dynamics (3) and (4) in (6), the following error dynamics in open-loop is obtained:

$$\dot{e}_1 = a_1 x_{s1} + a_2 x_{s1} x_{s3} + a_3 x_{s2} x_{s3} + u_1 - \left(a_1 x_{m1} + a_2 x_{m1} x_{m3} + a_3 x_{m2} x_{m3} \right),$$
$$\dot{e}_2 = a_4 x_{m2} + a_5 x_{s1} x_{s3} + a_6 + u_2 - \left(a_4 x_{m2} + a_5 x_{m1} x_{m3} + a_6 \right), \qquad (7)$$
$$\dot{e}_3 = a_7 x_{s3} + a_8 x_{s1}^2 x_{s2} + a_9 + u_3 - \left(a_7 x_{m3} + a_8 x_{m1}^2 x_{m2} + a_9 \right).$$
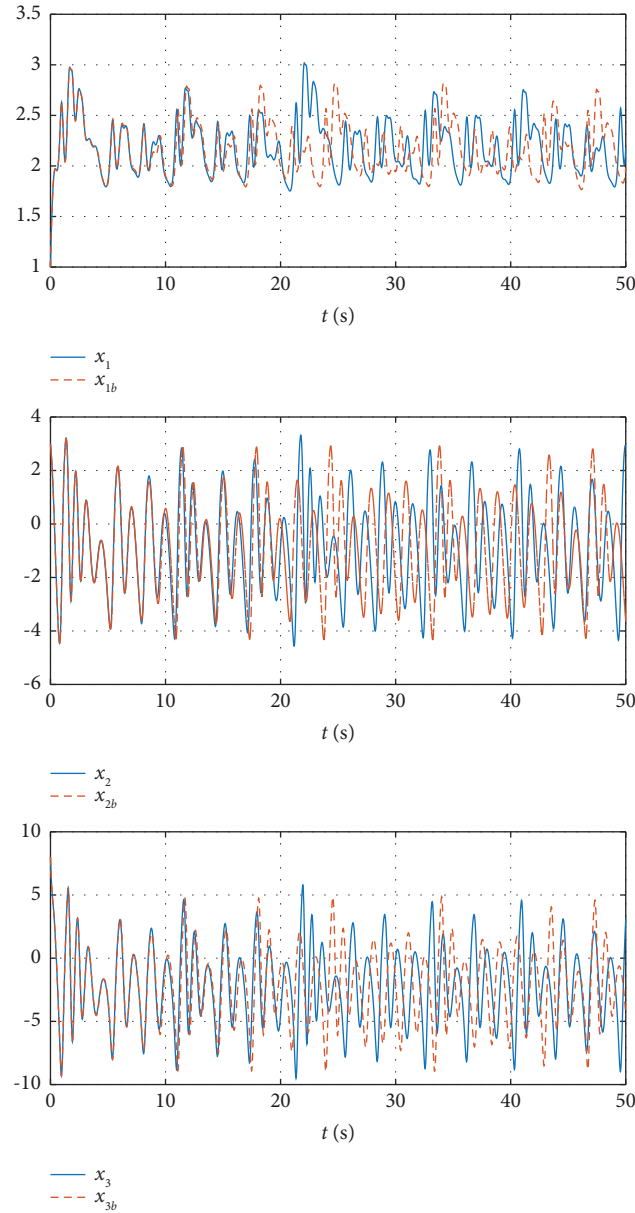
FIGURE 2: Simulation results showing the sensitivity of the Nwachioma chaotic system when small variations are considered in the initial conditions. The initial conditions considered in this simulation are $x_1(0) = 1$, $x_2(0) = 3$, $x_3(0) = 8$, $x_{1b}(0) = 1$, $x_{2b}(0) = 3.002$, and $x_{3b}(0) = 8$.

Lastly, by considering (5) into (7), the error dynamics in open-loop can be expressed in terms of the master dynamics and the synchronization errors as follows:

$$\dot{e}_1 = a_1 e_1 + a_2 \left(e_1 e_3 + x_{m3} e_1 + x_{m1} e_3\right) + a_3 \left(e_2 e_3 + x_{m2} e_3 + x_{m3} e_2\right) + u_1,$$
$$\dot{e}_2 = a_4 e_2 + a_5 \left(e_1 e_3 + x_{m1} e_3 + x_{m3} e_1\right) + u_2,$$
$$\dot{e}_3 = a_7 e_3 + a_8 \left(e_1^2 e_2 + 2 x_{m1} e_1 + x_{m1}^2 e_2 + x_{m2} e_1^2 + 2 x_{m1} x_{m2} e_1\right) + u_3.$$

$$(8)$$

2.2.1. Adaptive Control Design. With the intention of achieving that the slave subsystem tracks the master subsystem, i.e., $(x_{1s}, x_{2s}, x_{3s}) \longrightarrow (x_{1m}, x_{2m}, x_{3m})$, the following adaptive inputs u_1, u_2, and u_3 are designed:

$$
\begin{aligned}
u_1 &= -\hat{a}_1 e_1 - \hat{a}_2 \left(e_1 e_3 + x_{m3} e_1 + x_{m1} e_3\right) - \hat{a}_3 \left(e_2 e_3 + x_{m2} e_3 + x_{m3} e_2\right) - k_1 e_1, \\
u_2 &= -\hat{a}_4 e_2 - \hat{a}_5 \left(e_1 e_3 + x_{m1} e_3 + x_{m3} e_1\right) - k_2 e_2, \\
u_3 &= -\hat{a}_7 e_3 - \hat{a}_8 \left(e_1^2 e_2 + 2 x_{m1} e_1 + x_{m1}^2 e_2 + x_{m2} e_1^2 + 2 x_{m1} x_{m2} e_1\right) - k_3 e_3.
\end{aligned}
\tag{9}
$$

where $\hat{a}_i$ (for $i = 1, 2, 3, 4, 5, 7, 8$) are the estimated parameters and gains k_i (for $i = 1, 2, 3$) are greater than zero. When replacing (9) in (8), and after defining the error in the unknown parameters as $\tilde{a}_i = \hat{a}_i - a_i$ (for $i = 1, 2, 3, 4, 5, 7, 8$), then the following error dynamics in closed-loop is obtained:

$$
\begin{aligned}
\dot{e}_1 &= -\tilde{a}_1 e_1 - \tilde{a}_2 \left(e_1 e_3 + x_{m3} e_1 + x_{m1} e_3\right) - \tilde{a}_3 \left(e_2 e_3 + x_{m2} e_3 + x_{m3} e_2\right) - k_1 e_1, \\
\dot{e}_2 &= -\tilde{a}_4 e_2 - \tilde{a}_5 \left(e_1 e_3 + x_{m1} e_3 + x_{m3} e_1\right) - k_2 e_2, \\
\dot{e}_3 &= -\tilde{a}_7 e_3 - \tilde{a}_8 \left(e_1^2 e_2 + 2 x_{m1} e_1 + x_{m1}^2 e_2 + x_{m2} e_1^2 + 2 x_{m1} x_{m2} e_1\right) - k_3 e_3.
\end{aligned}
\tag{10}
$$

2.2.2. Stability Proof and Learning law. For demonstrating the stability of the closed-loop system (10) by means of the Lyapunov theory, the first step is to propose and analyze an energy candidate function defined in terms of states e_i (for $i = 1, 2, 3$) and parameters $\tilde{a}_i$. Thus, the following function is proposed:

$$
V(t) = \frac{1}{2} \left(\sum_{i=1}^{3} e_i^2 + \sum_{i=1}^{5} \tilde{a}_i^2 + \sum_{i=7}^{8} \tilde{a}_i^2 \right).
\tag{11}
$$

With the aim of verifying the stability of the closed-loop system (10), the time-derivative of (11) along with (10) must be analyzed [99]; that is,

$$
\begin{aligned}
\dot{V}(t) = {} & \tilde{a}_1 \left[\dot{\hat{a}}_1 - e_1^2\right] + \tilde{a}_2 \left[\dot{\hat{a}}_2 - \left(e_1^2 e_3 + x_{m3} e_1^2 + x_{m1} e_1 e_3\right)\right] \\
& + \tilde{a}_3 \left[\dot{\hat{a}}_3 - \left(e_1 e_2 e_3 + x_{m2} e_1 e_3 + x_{m3} e_1 e_2\right)\right] - k_1 e_1^2 + \tilde{a}_4 \left[\dot{\hat{a}}_4 - e_2^2\right] \\
& + \tilde{a}_5 \left[\dot{\hat{a}}_5 - \left(e_1 e_2 e_3 + x_{m1} e_2 e_3 + x_{m3} e_1 e_2\right)\right] - k_2 e_2^2 + \tilde{a}_7 \left[\dot{\hat{a}}_7 - e_3^2\right] \\
& + \tilde{a}_8 \left[\dot{\hat{a}}_8 - \left(e_1^2 e_2 e_3 + 2 x_{m1} e_1 e_3 + x_{m1}^2 e_2 e_3 + x_{m2} e_1^2 e_3 + 2 x_{m1} x_{m2} e_1 e_3\right)\right] - k_3 e_3^2.
\end{aligned}
\tag{12}
$$

Now, it is easily observed that a suitable learning law for parameter estimation is the following:

$$
\begin{aligned}
\dot{\hat{a}}_1 &= e_1^2, \\
\dot{\hat{a}}_2 &= e_1^2 e_3 + x_{m3} e_1^2 + x_{m1} e_1 e_3, \\
\dot{\hat{a}}_3 &= e_1 e_2 e_3 + x_{m2} e_1 e_3 + x_{m3} e_1 e_2, \\
\dot{\hat{a}}_4 &= e_2^2, \\
\dot{\hat{a}}_5 &= e_1 e_2 e_3 + x_{m1} e_2 e_3 + x_{m3} e_1 e_2, \\
\dot{\hat{a}}_7 &= e_3^2, \\
\dot{\hat{a}}_8 &= e_1^2 e_2 e_3 + 2 x_{m1} e_1 e_3 + x_{m1}^2 e_2 e_3 + x_{m2} e_1^2 e_3 + 2 x_{m1} x_{m2} e_1 e_3.
\end{aligned}
\tag{13}
$$

After replacing (13) in (12), the following is obtained:

$$
\dot{V}(t) = -k_1 e_1^2 - k_2 e_2^2 - k_3 e_3^2.
\tag{14}
$$

Notice that (14) is negative semidefinite, i.e., $\dot{V}(t) \leq 0$. Hence, system (10) is stable in the sense of Lyapunov [99].

However, with the aim of demonstrating the asymptotic stability of (10) the Barbalat's lemma needs to be invoked [100].

Lemma 1 (Barbalat's Lemma). *If* $e(t)\colon \mathbb{R}^+ \longrightarrow \mathbb{R}^+$ *is uniformly continuous for* $t \geq 0$ *and if*

$$
\lim_{t \to \infty} \int_0^t \|e(\tau)\| d\tau \leq \epsilon,
\tag{15}
$$

for $\epsilon \in \mathbb{R}^+$, *then*

$$
\lim_{t \to \infty} e(t) = 0.
\tag{16}
$$

Corollary 1. *If* $e(t) \in L_2 \cap L_\infty$ *and* $\dot{e}(t) \in L_\infty$, *then*

$$
\lim_{t \to \infty} e(t) = 0.
\tag{17}
$$

From Corollary 1 and when replacing $k = \min\{k_1, k_2, k_3\}$ in (14), the following is obtained:

$$\dot{V} \le -k\left(e_1^2 + e_2^2 + e_3^2\right). \tag{18}$$

Now, after integrating from 0 to t both sides of (18),

$$\int_0^t \left(e_1^2 + e_2^2 + e_3^2\right) d\tau \le \frac{V(0) - V(t)}{k}, \tag{19}$$

and since $V(t) > 0$, it means that $V(0) - V(t) < V(0)$. Hence,

$$\frac{V(0) - V(t)}{k} < \frac{V(0)}{k}. \tag{20}$$

When replacing the latter expression in (19) and after finding lim when $t \longrightarrow \infty$, then

$$\lim_{t \longrightarrow \infty} \int_0^t \left(e_1^2 + e_2^2 + e_3^2\right) d\tau \le \frac{V(0)}{k}. \tag{21}$$

Thus, it is concluded that

$$e_i \in L_2. \tag{22}$$

In the following, the rest of conditions related to Corollary 1 are verified. By considering that $\dot{V}(t) \le 0$ and after integrating such an expression from 0 to t, it is found that $V(t) \le V(0)$. Also, it is observed that $V(t)$ is bounded since $V(t) > 0$. Thus, from (11) e_i and $\tilde{a}_i$ are also bounded and, consequently,

$$e_i \in L_\infty. \tag{23}$$

On the other hand, since e_i, $\tilde{a}_i$, and the master system (3) are bounded (it is worth remembering that the vector state of a chaotic system is bounded), then $\dot{e}_i$ in (10) is also bounded. Thus,

$$\dot{e}_i \in L_\infty. \tag{24}$$

Lastly, after considering (22), (23), and (24), it is easily observed that Lemma 1 guarantees that

$$\lim_{t \longrightarrow \infty} e_i(t) = 0. \tag{25}$$

Remark 1. Note that the estimation errors $\tilde{a}_i$ are bounded but not tend to zero; however, the errors e_i does tend to zero when the time is large enough, as will be shown in the next section.

Remark 2. It is important to mention that according to the previous proof, from a strictly theoretical point of view, the synchronization can be achieved for any value of the system

constant parameters a_i whenever the control gains are $k_1 > 0$, $k_2 > 0$, and $k_3 > 0$.

3. Results

In order to enhance the contribution of this paper, in this section, a comparison between an active control scheme and the adaptive control algorithm previously developed in Section 2 is presented. Such a comparison is executed via simulation results with the aim of verifying the performance in closed-loop of the Nwachioma chaotic system, in master-slave configuration, with both controls. Later, the experimental implementation of the adaptive control on the Nwachioma chaotic system is carried out through a novel experimental realization.

3.1. Comparison with respect to Active Control. Although active control was one of the first methods proposed for solving the synchronization problem, currently, is still frequently used [101–105]. This method can be considered a kind of feedback linearization one. Active control comprises two stages: one for compensation of nonlinearities and another one for decoupling. In this regard, and with the purpose of executing the comparison with the adaptive control developed in this paper; in the following, an active control is designed for solving the synchronization problem associated with the Nwachioma chaotic system.

3.1.1. Design of the Active Control. With the intention of avoiding any kind of confusion regarding both control algorithms, i.e. the adaptive control and the active control, new variables are defined for the design of the active control. Now the slave system, where the active control is applied, has the following dynamics:

$$\begin{aligned}
\dot{x}_{a1s} &= a_1 x_{a1s} + a_2 x_{a1s} x_{a3s} + a_3 x_{a2s} x_{a3s} + u_{a1}, \\
\dot{x}_{a2s} &= a_4 x_{a2s} + a_5 x_{a1s} x_{a3s} + a_6 + u_{a2}, \\
\dot{x}_{a3s} &= a_7 x_{a3s} + a_8 x_{a1s}^2 x_{a2s} + a_9 + u_{a3},
\end{aligned} \tag{26}$$

whereas the tracking error is given by

$$\begin{aligned}
e_{a1} &= x_{a1s} - x_{m1}, \\
e_{a2} &= x_{a2s} - x_{m2.}, \\
e_{a3} &= x_{a3s} - x_{m3}.
\end{aligned} \tag{27}$$

By considering (26) and (27), the following error dynamics in open-loop is obtained:

$$\begin{aligned}
\dot{e}_{a1} &= a_1 e_{a1} + a_2 \left(e_{a1} e_{a3} + x_{m3} e_{a1} + x_{m1} e_{a3}\right) + a_3 \left(e_{a2} e_{a3} + x_{m2} e_{a3} + x_{m3} e_{a2}\right) + u_{a1}, \\
\dot{e}_{a2} &= a_4 e_2 + a_5 \left(e_{a1} e_{a3} + x_{m1} e_{a3} + x_{m3} e_{a1}\right) + u_{a2}, \\
\dot{e}_{a3} &= a_7 e_{a3} + a_8 \left(e_{a1}^2 e_{a2} + 2 x_{m1} e_{a1} + x_{m1}^2 e_{a2} + x_{m2} e_{a1}^2 + 2 x_{m1} x_{m2} e_{a1}\right) + u_{a3}.
\end{aligned} \tag{28}$$

In (28), note the nonlinearities and the coupling of the variables. Hence, the following active control is proposed:

$$u_{a1} = -a_1 e_{a1} - a_2 \left(e_{a1} e_{a3} + x_{m3} e_{a1} + x_{m1} e_{a3} \right) - a_3 \left(e_{a2} e_{a3} + x_{m2} e_3 + x_{m3} e_{a2} \right) - k_1 e_{a1},$$
$$u_{a2} = -a_4 e_{a2} - a_5 \left(e_{a1} e_{a3} + x_{m1} e_{a3} + x_{m3} e_{a1} \right) - k_2 e_{a2}, \tag{29}$$
$$u_{a3} = -a_7 e_{a3} - a_8 \left(e_{a1}^2 e_{a2} + 2 x_{m1} e_{a1} + x_{m1}^2 e_{a2} + x_{m2} e_{a1}^2 + 2 x_{m1} x_{m2} e_{a1} \right) - k_3 e_{a3}.$$

After replacing the proposed control (29) in the error dynamics (28), the following error dynamics in closed-loop is obtained:

$$\dot{e}_{a1} = -k_1 e_{a1},$$
$$\dot{e}_{a2} = -k_2 e_{a2}, \tag{30}$$
$$\dot{e}_{a3} = -k_3 e_{a3}.$$

It is easily observed that the dynamics (30) is linear and the time-varying error variables are decoupled. Additionally, if $k_1 > 0$, $k_2 > 0$, and $k_3 > 0$, then $(e_{a1}, e_{a2}, e_{a3}) \longrightarrow (0,0,0)$.

3.1.2. Simulation Results. On the one hand, the efficiency of both controls, the adaptive one and the active one, is validated by using the criterion of the quadratic error integral as an index performance. For the adaptive control, the index performance is defined as

$$\phi(t) = \int_0^t \left(e_1^2 + e_2^2 + e_3^2 \right) d\xi, \tag{31}$$

whereas the index performance for the active control is defined as

$$\phi_a(t) = \int_0^t \left(e_{a1}^2 + e_{a2}^2 + e_{a3}^2 \right) d\xi. \tag{32}$$

By using these indexes it is possible to obtain a measure, for comparative purposes, between both controls. Such a measure allows to observe graphically the sum of both errors, the transient one and the stable one (if exists). On the other hand, with the intention of comparing the performance of the adaptive control and the active control, four simulations are carried out when the parameters a_i defined in (2) of the master-slave Nwachioma chaotic system are changed according to the values specified in Table 1.

The rest of parameters for the active control (29) were defined previously in (2) and were given as

$$a_1 = -0.1, a_2 = 0.15, a_3 = 0.18, a_4 = 3.9,$$
$$a_5 = -1.5, a_6 = -4, a_7 = -4.9, a_8 = 2.5, a_9 = 0. \tag{33}$$

The gains of both controls were chosen as $(k_1, k_2, k_3) = (1, 1, 1)$, while the initial conditions for the master system were defined as $(x_{1m}(0), x_{2m}(0), x_{3m}(0)) = (1, 3, 8)$, the initial conditions for the slave system when using the adaptive control were selected as $(x_{1s}(0), x_{2s}(0), x_{3s}(0)) = (0, 0, 0)$, and those for the same slave system when using the active control were selected as $(x_{1as}(0), x_{2as}(0), x_{3as}(0)) = (0, 0, 0)$. All simulations were executed in MATLAB-Simulink with the variable-step solver ode23s.

(a) Numerical simulation 1: The results presented in Figure 3 show that both control algorithms solved the synchronization control task. This is accomplished because the parameters of the Nwachiona chaotic system, in the master-salve configuration, and those of the active control were the same.

(b) Numerical simulation 2: Figure 4 depicts the performance of the Nwachioma chaotic system in closed-loop with both controls, the adaptive one and the active one. Although the synchronization control task is achieved, the transient response of the slave system due to the active control is greater than the one obtained in the previous simulation.

(c) Numerical simulation 3: As can be observed in Figure 5, the synchronization control task is solved for the master-slave Nwachioma chaotic system in closed-loop with the adaptive control. However, such a task is not solved for the active control.

(d) Numerical simulation 4: Similar to the previous simulation results, those presented in Figure 6 show that the chaotic system in closed-loop with the adaptive control solved the synchronization control problem. But when using the active control the synchronization is not achieved. It is worth mentioning that this numerical simulation was executed only for 4 s, since $x_{a2s} \longrightarrow \infty$ and $\phi_a(t) \longrightarrow \infty$ when $t \longrightarrow \infty$, as can be observed in Figure 6.

3.1.3. Comments on the Numerical Simulations. As can be noted in Figures 3–6, the adaptive control exhibits a better performance compared with the performance achieved by the active control. Such a superior behavior on the closed-loop Nwachioma system, in the master-slave configuration, with the adaptive control is observed through the performance indexes of the quadratic error integral calculated for both controls. The results associated with the indexes $\phi(t)$ and $\phi_a(t)$, for each numerical simulation, are shown in Table 2.

3.2. Experimental Implementation. With the aim of highlighting the effectiveness of the adaptive control (9) developed in this paper, a novel and easy to understand implementation in closed-loop of the proposed approach with the Nwachioma chaotic system, in the master-slave configuration, is presented in this section. The experimental realization of the adaptive control is carried out by using MATLAB-Simulink and two computers, one for the master system and a second one for the slave system. The testbed is depicted in Figure 7, where the connections diagram between the master computer and the slave computer along with their corresponding Arduino UNO boards are shown.

TABLE 1: Changes in parameters a_i for comparison purposes between the adaptive control and the active control via numerical simulations.

	a_1	a_2	a_3	a_4	a_5	a_6	a_7	a_8	a_9
Numerical simulation 1	−0.10	0.15	0.180	3.90	−1.5	−4	−4.90	2.5	0
Numerical simulation 2	−0.14	0.21	0.252	5.46	−2.1	−5.6	−6.86	3.5	0
Numerical simulation 3	−0.18	0.27	0.324	7.02	−2.7	−7.2	−8.82	4.5	0
Numerical simulation 4	−0.22	0.33	0.396	8.58	3.3	−8.8	−10.78	5.5	0
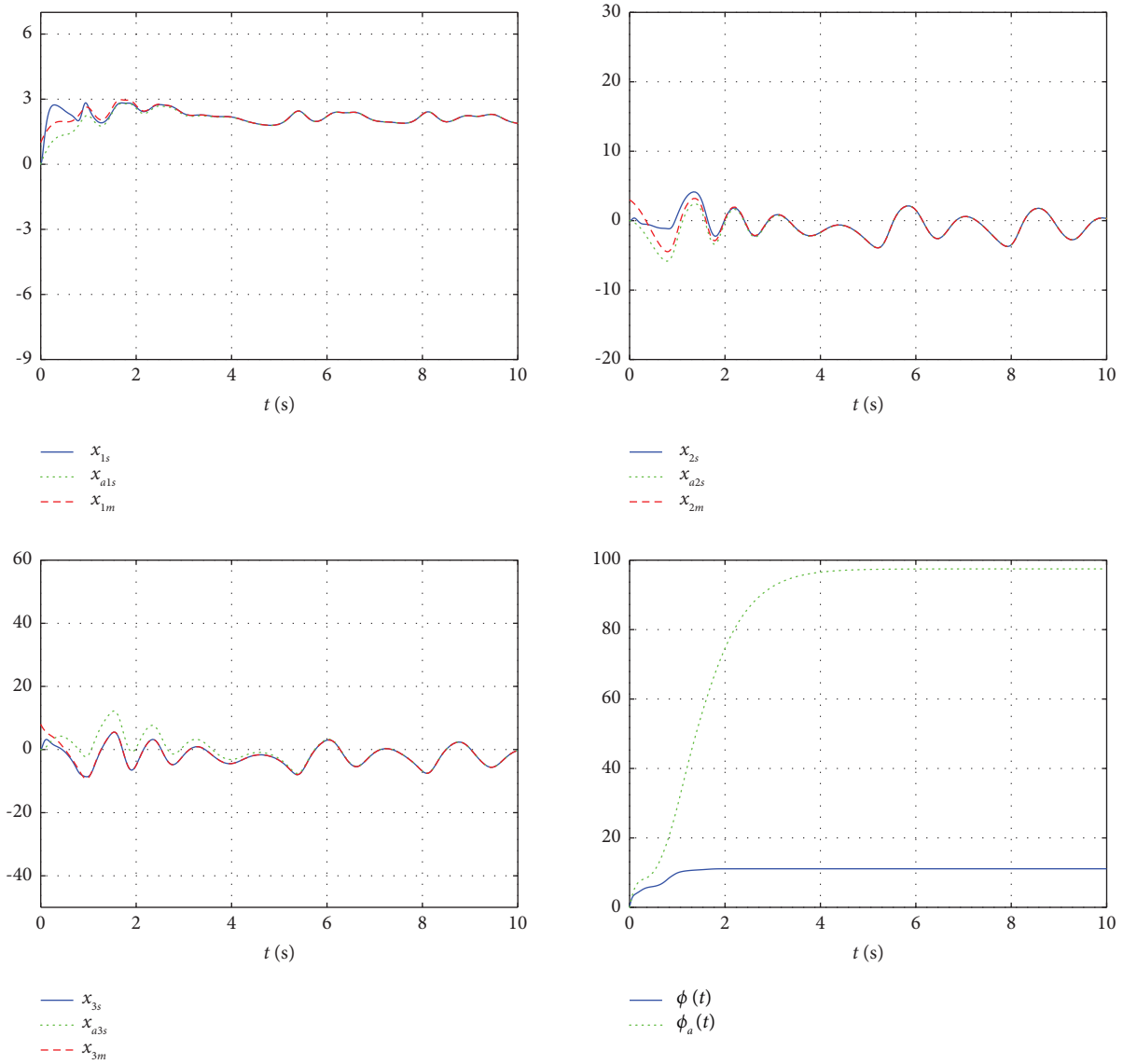
FIGURE 3: Numerical simulation 1. Comparison between the adaptive control and the active control in closed-loop with the Nwachioma chaotic system. The used parameters are in accordance with those specified on the first line in Table 1. The indexes obtained for this simulation are $\phi(10\,\text{s}) = 11.11$ and $\phi_a(10\,\text{s}) = 97.48$.

The master system and the slave system are implemented by programming their mathematical models (3) and (4), respectively, in MATLAB-Simulink by using the numeric method ode4 with sampling step of 1 ms. Both the computers are interconnected via the serial communication protocol RS-232 along with two Arduino UNO development boards [106]. It is worth mentioning that using MATLAB-Simulink along with the RS-232 serial protocol and the

Arduino UNO board is, indeed, a low-cost implementation of the approach presented in this paper. In fact, the synchronization problem in chaotic systems is tremendously affordable when using these kind of computational tools.

3.2.1. Synchronization of the Master-Slave Nwachioma Chaotic System. The synchronization of the master-slave Nwachioma chaotic system is realized through the
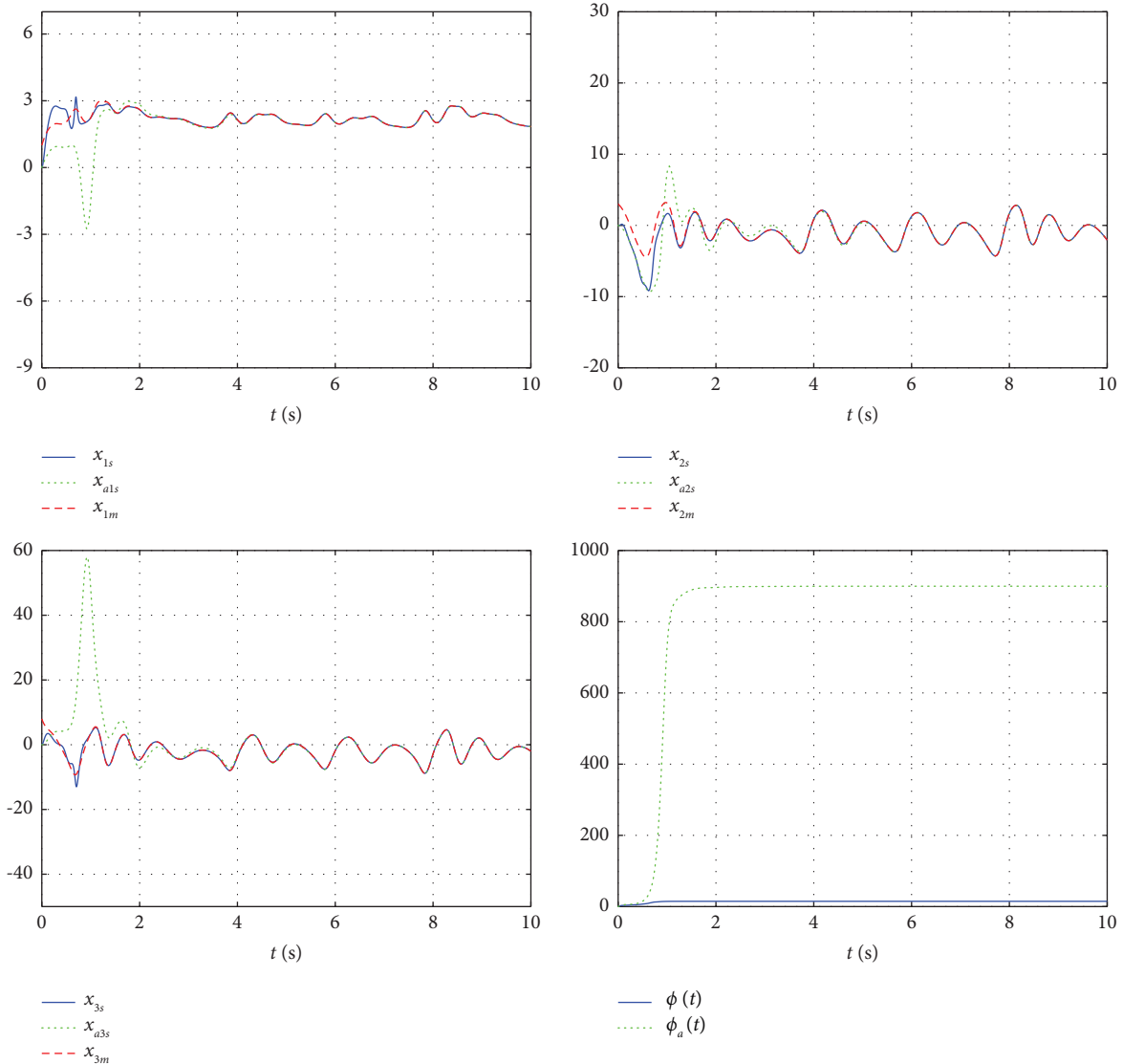
FIGURE 4: Numerical simulation 2. Results of the adaptive control and the active control in closed-loop with the Nwachioma chaotic system. The used parameters are in accordance with those specified on the second line in Table 1. The indexes obtained for this simulation are $\phi(10\,\mathrm{s}) = 14.76$ and $\phi_a(10\,\mathrm{s}) = 899.7$.

connections shown in Figure 7, whereas the flowchart shown in Figure 8 depicts the process to be followed for achieving the communication between the master system and the slave system.

It is worth noticing that for achieving the synchronization of the chaotic system, the Arduino UNO boards and the computers must be configured. In this regard, the Arduino UNO boards are interconnected to each other by using a virtual serial port. The code shown in the Listing 1 commands both Arduino UNO boards and establishes the flow of information, i.e., master computer-board-board-slave computer. The virtual port directs the communication between both Arduino boards. The data are received from the virtual (or the physical) serial port and are saved and sent via the variable *InData* to the remaining serial port, respectively.

On the one hand, Computer 1 is interconnected to the Arduino UNO 1 board via a USB cable, where the Arduino driver is used so that the connection is viewed as a serial port. On the other hand, both Arduino UNO boards are interconnected through pins RX and TX, as can be observed in the code presented in the Listing 1. This is the RX pin of the first board, which is connected to the TX pin and vice versa. Lastly, the Arduino UNO 2 board is connected to Computer 2 in the same way as computer 1 is connected to its corresponding Arduino board.

Once the connections have been made, the next step is the implementation of dynamics associated with the master system (3) and the slave system (4) in computer 1 and computer 2, respectively. Figure 9 depicts the block diagram programmed in MATLAB-Simulink with the intention of acquiring the response of master system (3) and send it to
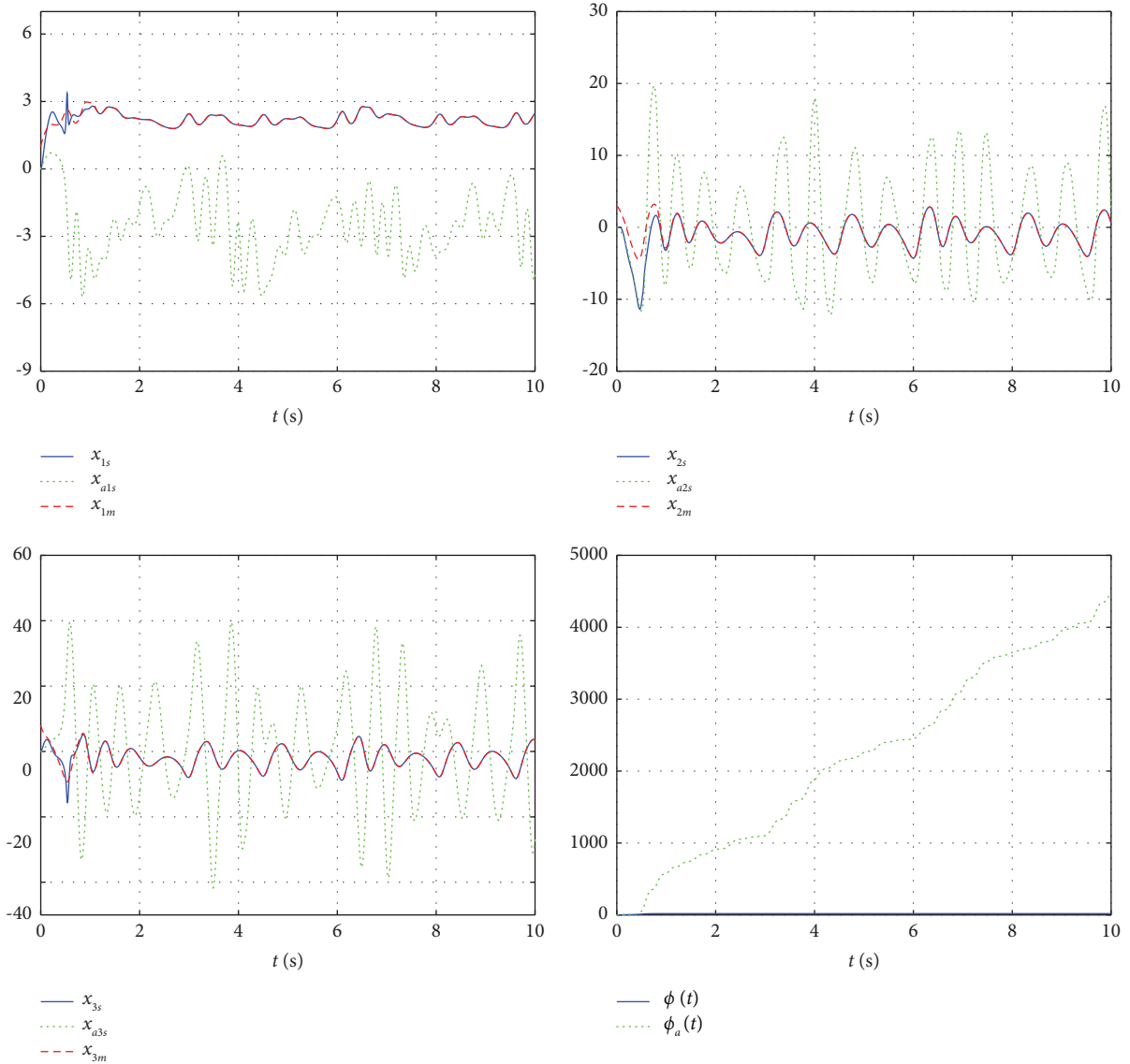
FIGURE 5: Numerical simulation 3. Comparison between the adaptive control and the active control in closed-loop with the Nwachioma chaotic system. The used parameters are in accordance with those specified on the third line in Table 1. The indexes obtained for this simulation are $\phi (10 \text{ s}) = 18.57$ and $\phi_a (10 \text{ s}) = 4490$.

computer 2. Since the two Nwachioma systems of the master-slave configuration are equal, the parameters (2) are programmed in both systems for implementation purposes. However, such parameters are considered to be unknown and, consequently, are not used by the adaptive control (9).

In the following, the block diagram of Figure 9 is described.

(i) Nwachioma master system: This block is composed of the blocks a_i, *Master*, and *Integrator*. The block a_i contains this constant parameters of the system (3), considered to be unknown. However, for implementation purposes, the parameters a_i given by (2) are programmed instead. The equations (3) are programmed in *Master* block, whose output is the time-derivative of the vector state. Lastly, block *Integrator* generates the vector state, i.e., the vector

whose elements are x_{1m}, x_{2m}, x_{3m} along with its corresponding initial conditions.

(ii) Sampling and scaling: With the aim of sending the vector state of the master system, a *Zero-Order Hold* is required for sampling the response of the system. Additionally, since the data are sent in 1 byte packages, a scaling factor is implemented through the *Scale* block so that the elements of the vector state are mapped into the interval [0, 255].

(iii) Data sending: All parameters for establishing the serial communication, such as velocity transmission, COM port, etc., are specified in the *Serial Configuration* block, whereas the *Conversion* block transforms double type data into uint8 type (equivalent to 1 byte). Lastly, data are sent through the COM port specified in the *Serial Send* block.
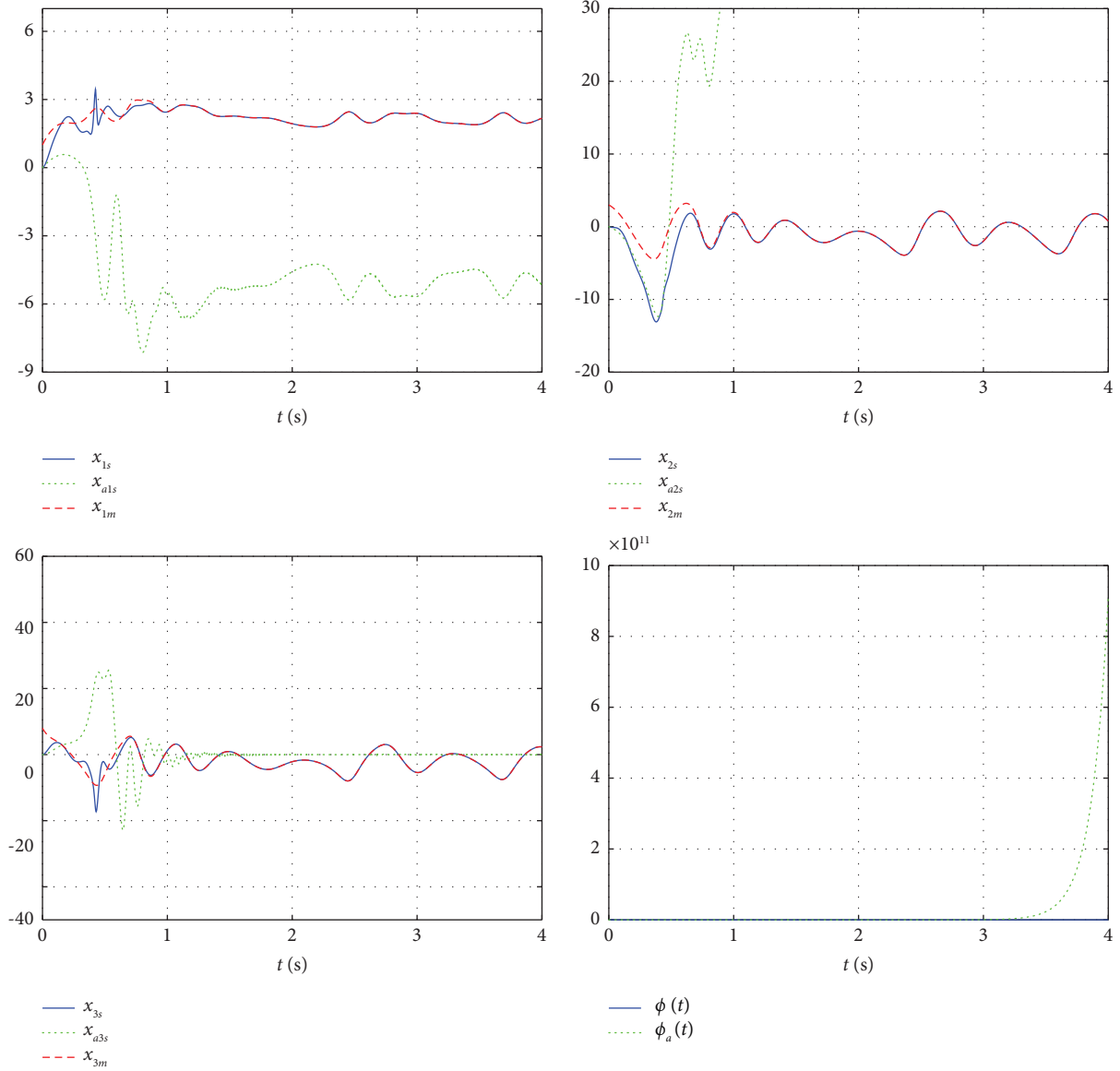
FIGURE 6: Numerical simulation 4. Results of the adaptive control and the active control in closed-loop with the Nwachioma chaotic system. The used parameters are in accordance with those specified on the fourth line in Table 1. The indexes obtained for this simulation are $\phi (10 \text{ s}) = 21.86$ and $\phi_a (10 \text{ s}) = 9.3 \times 10^{11}$.

TABLE 2: Performance indexes of the quadratic error integral for the numerical simulations.

	$\phi(t)$	$\phi_a(t)$	t (s)
Numerical simulation 1	11.11	97.48	10
Numerical simulation 2	14.76	899.70	10
Numerical simulation 3	18.57	4490	10
Numerical simulation 4	21.86	9.3×10^{11}	4

The index $\phi(t)$ represents the performance of the adaptive control, whereas the index $\phi_a(t)$ shows the performance of the active control.

On the other hand, the block diagram programmed in MATLAB-Simulink for implementing the slave system is presented in Figure 10 and is divided into the following parts:

(i) Data receiving: In this block, the *Serial Configuration* is used again with the purpose of selecting the communication parameters. The *Serial Receive* acquires the uint8 data of the slave system, which are
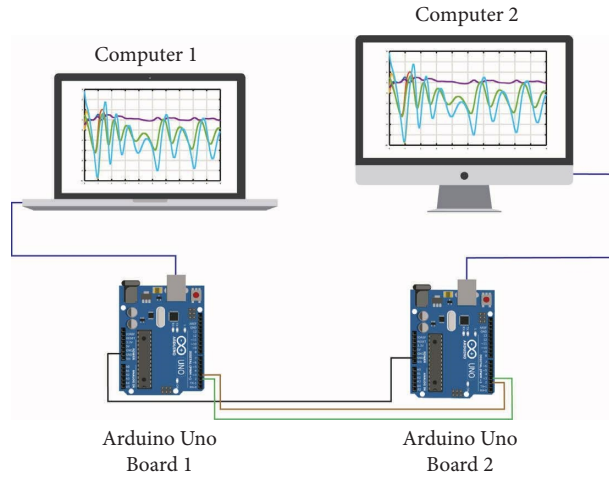
FIGURE 7: Experimental implementation of the Nwachioma chaotic system in the master-slave configuration. The master system and the slave system are implemented independently in two computers. The communication between both systems is realized through the protocol RS-232 via two Arduino UNO boards.
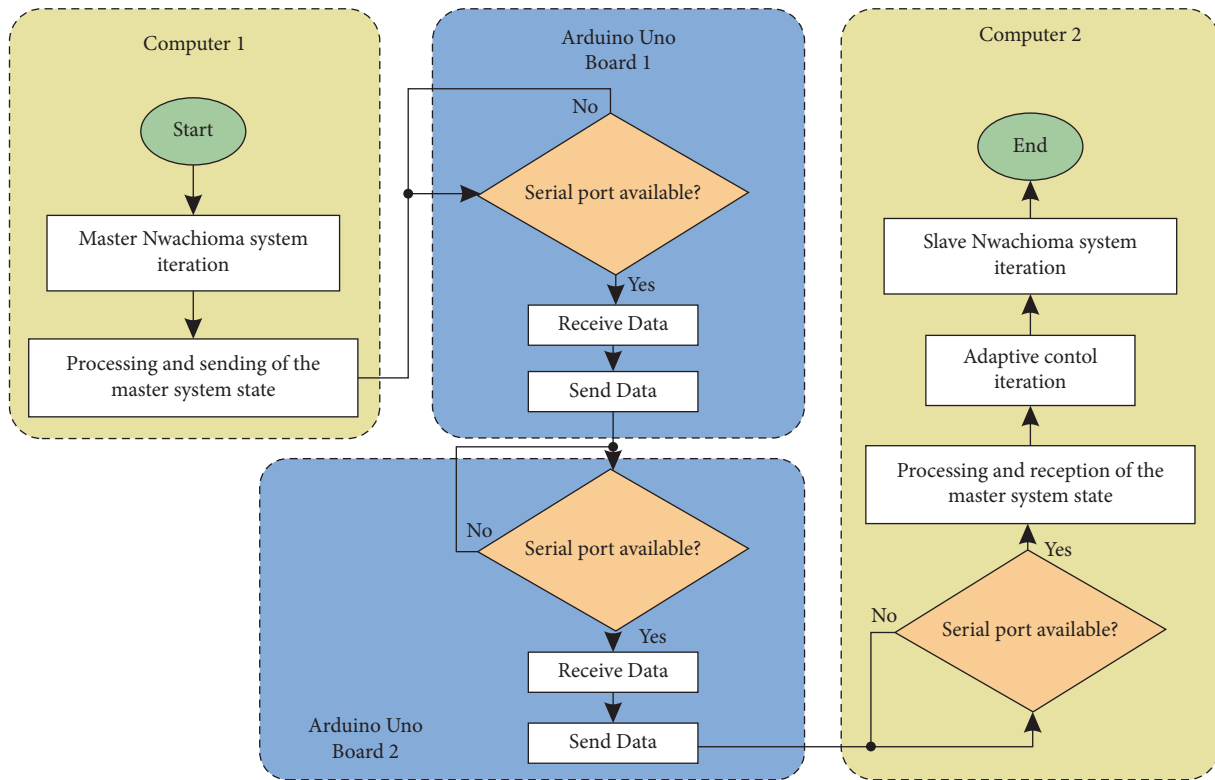
FIGURE 8: Flowchart for implementing the adaptive control on the Nwachioma chaotic system, in the master-slave configuration, through two computers and two Arduino UNO boards.

mapped in the scale [0, 255], and by using the *Conversion* block the data are converted into type double. Later, the block *Scale* recovers the original scaling factor of the state vector.

(ii) Nwachioma slave system: It comprises the block of parameters a_i, where constants (2) are programmed again for implementation purposes. The block *Slave*

is where the equations (4) are programmed with the aim of obtaining the time-derivatives $\dot{x}_{1s}$, $\dot{x}_{2s}$, and $\dot{x}_{3s}$. The states x_{1s}, x_{2s}, and x_{3s} are obtained by considering the initial conditions of the slave system through the block *Integrator2*.

(iii) Learning law: Equations (13) are programmed into the block *Update law* with the intention of obtaining

```
# include <SoftwareSerial.h>
# define rxPin 2
# define txPin 3
SoftwareSerial VirtualSerial = SoftwareSerial(rxPin, txPin);
void setup()
{
    Serial.begin(9600);
    VirtualSerial.begin(9600);
}
void loop()
{
    byte InData;
    if (Serial.available())
    {
      InData = Serial.read();
      VirtualSerial.write(InData);
    }
    if(VirtualSerial.available())
    {
      InData = VirtualSerial.read();
      Serial.write(InData);
    }
}
```

LISTING 1: Arduino code programming language for implementing the RS-232 serial communication.
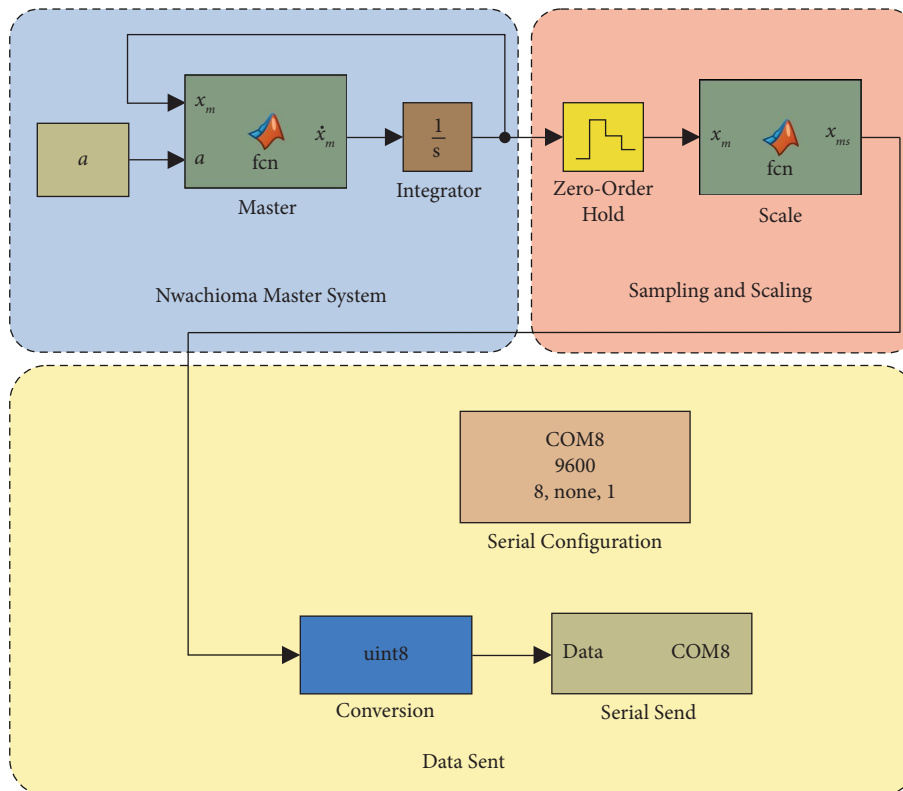
FIGURE 9: Block diagram programmed in MATLAB-Simulink for computer 1. With this program, the master system is implemented and the corresponding data associated with the states are sent via the communication protocol RS-232 to the slave system.
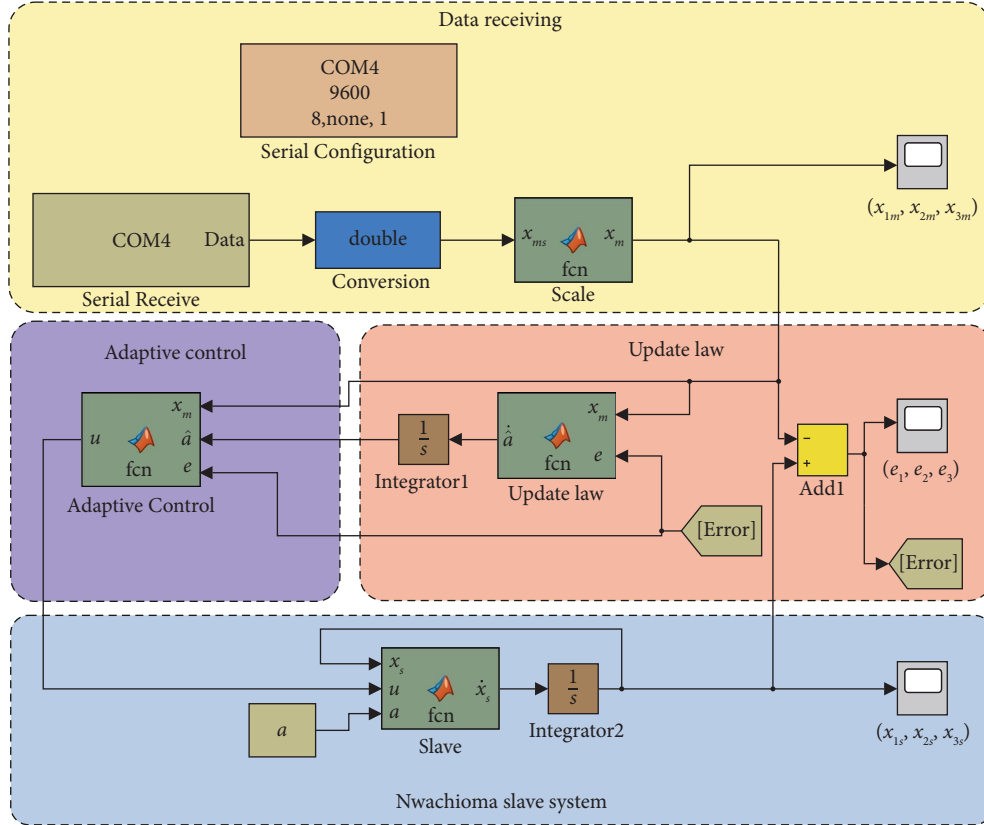
FIGURE 10: Block diagram programmed in MATLAB-Simulink for computer 2. With this program, the slave system is implemented, the data associated with the master system are acquired via the communication protocol RS-232, and the adaptive control is executed.

$\dot{\widehat{a}}_i$. It is easily observed that after using the block *Integrator1*, over the time-derivatives previously mentioned, the corresponding signals $\widehat{a}_i$ are obtained (after considering initial conditions equal to zero) and now can be used into the proposed adaptive control.

(iv) Adaptive control: This block generates the corresponding inputs u_1, u_2, and u_3 through (9) and by taking into account, as parameters, the signals e_1, e_2, e_3, the estimated ones $\widehat{a}_i$, and the states x_{1m}, x_{2m}, and x_{3m}.

3.2.2. Experimental Results. The master system (3) is experimentally implemented in computer 1, where the parameters given in (2) and the initial conditions ($x_{1m}(0) = 1$, $x_{2m}(0) = 3$, and $x_{3m}(0) = 8$ retaken from [98]) for the Nwachioma system, are specified. On the other hand, the slave system (4) is implemented in computer 2 and the parameters given in (2) are used again. The initial conditions for the slave system are considered to be $x_{1s}(0) = 0$,

$x_{2s}(0) = 0$, and $x_{3s}(0) = 0$, whereas for the learning law, and the initial condition of the time-derivative of the estimated values, $\dot{\widehat{a}}_i = 0$. The gains of the proposed adaptive control are chosen to be $k_1 = 5$, $k_2 = 7$, and $k_3 = 5$. With all these values, the system in closed-loop achieves the synchronization objective, i.e., $(x_{1s}, x_{2s}, x_{3s}) \longrightarrow (x_{1m}, x_{2m}, x_{3m})$, as can be observed in Figure 11.

Figure 12(a) shows that $(e_1, e_2, e_3) \longrightarrow (0, 0, 0)$ even when the initial conditions of both systems are not equal, whereas Figure 12(b) depicts the control inputs of the slave system, whose behavior not only allows that $(e_1, e_2, e_3) \longrightarrow (0, 0, 0)$ but also that $(u_1, u_2, u_3) \longrightarrow (0, 0, 0)$.

3.2.3. Comments on the Experimental Results. As was previously mentioned, chaotic systems are very sensitive to initial conditions (this phenomenon can be observed in Figure 2). Notice that, in Figures 11 and 12, although such initial conditions are different in both, the master and the slave systems, the synchronization problem is solved. Also, despite the master-slave communication is low-cost and
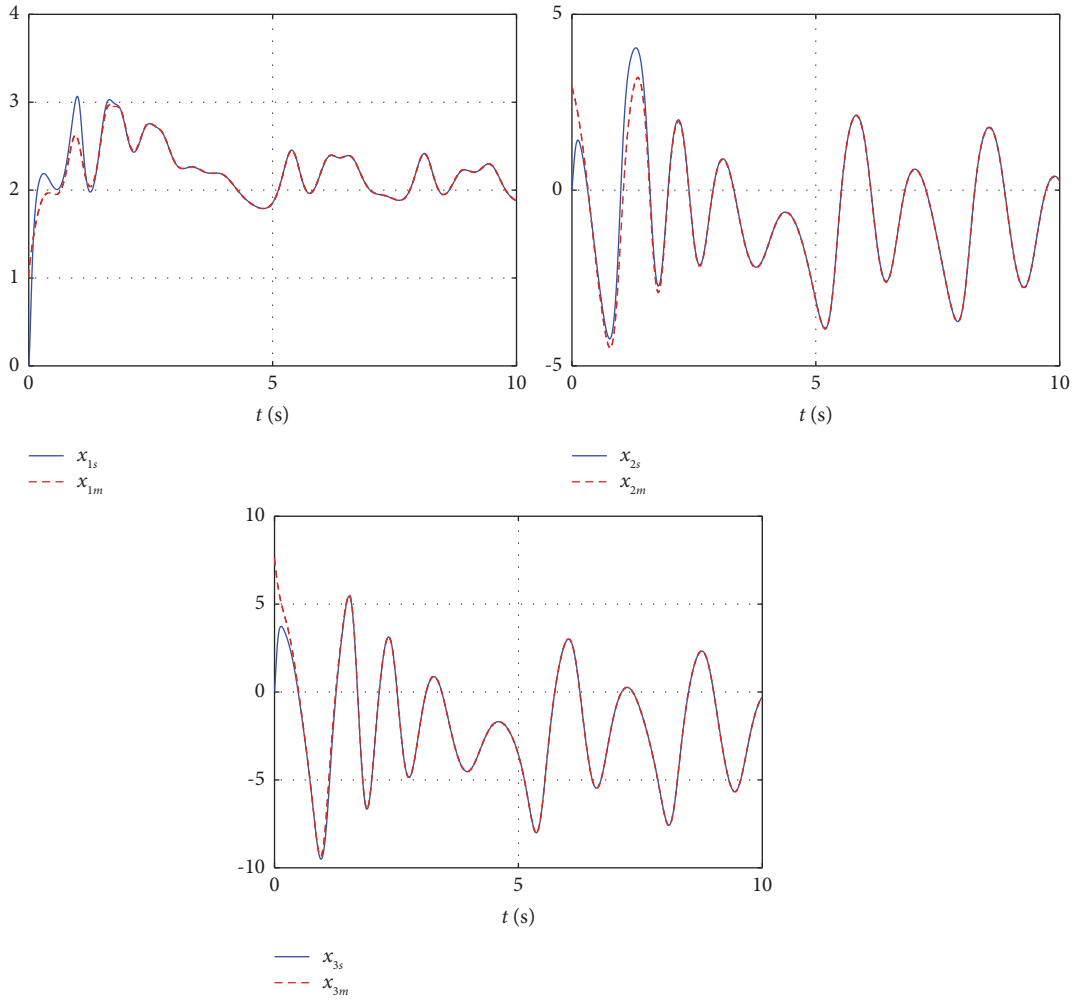
FIGURE 11: Experimental comparison between the states of the master system versus the corresponding states of the slave system. The initial conditions of the master system are $x_{1m}(0) = 1$, $x_{2m}(0) = 3$, and $x_{3m}(0) = 8$, whereas those of the slave system are $x_{1s}(0) = 0$, $x_{2s}(0) = 0$, and $x_{3s}(0) = 0$.
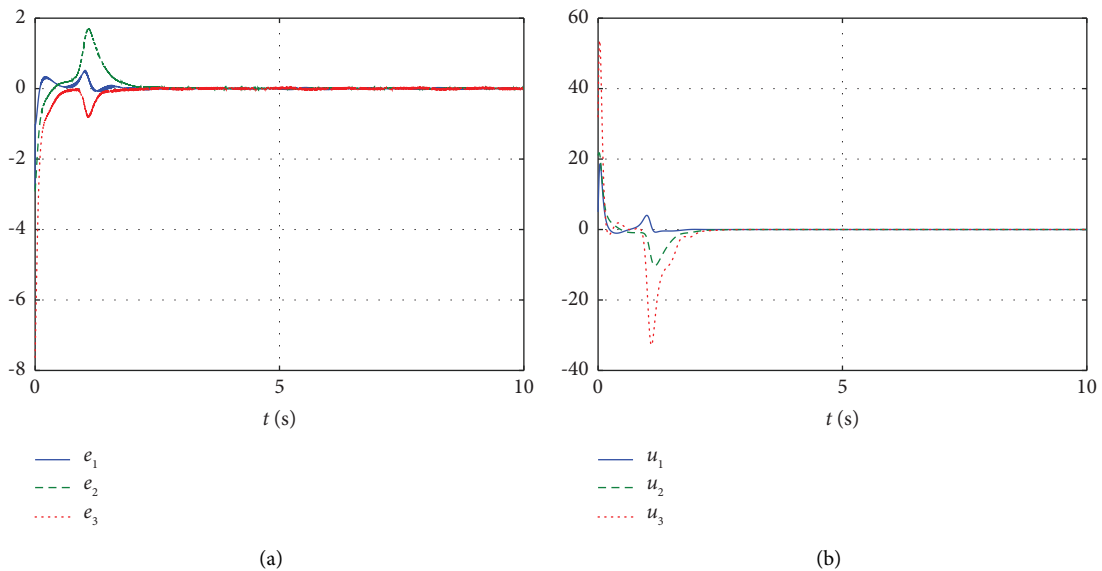
FIGURE 12: Experimental results indicators. (a) Synchronization errors of the Nwachioma master-slave system, described by (5). (b) Inputs of the slave system allowing that $(x_{1s}, x_{2s}, x_{3s}) \longrightarrow (x_{1m}, x_{2m}, x_{3m})$ are achieved.
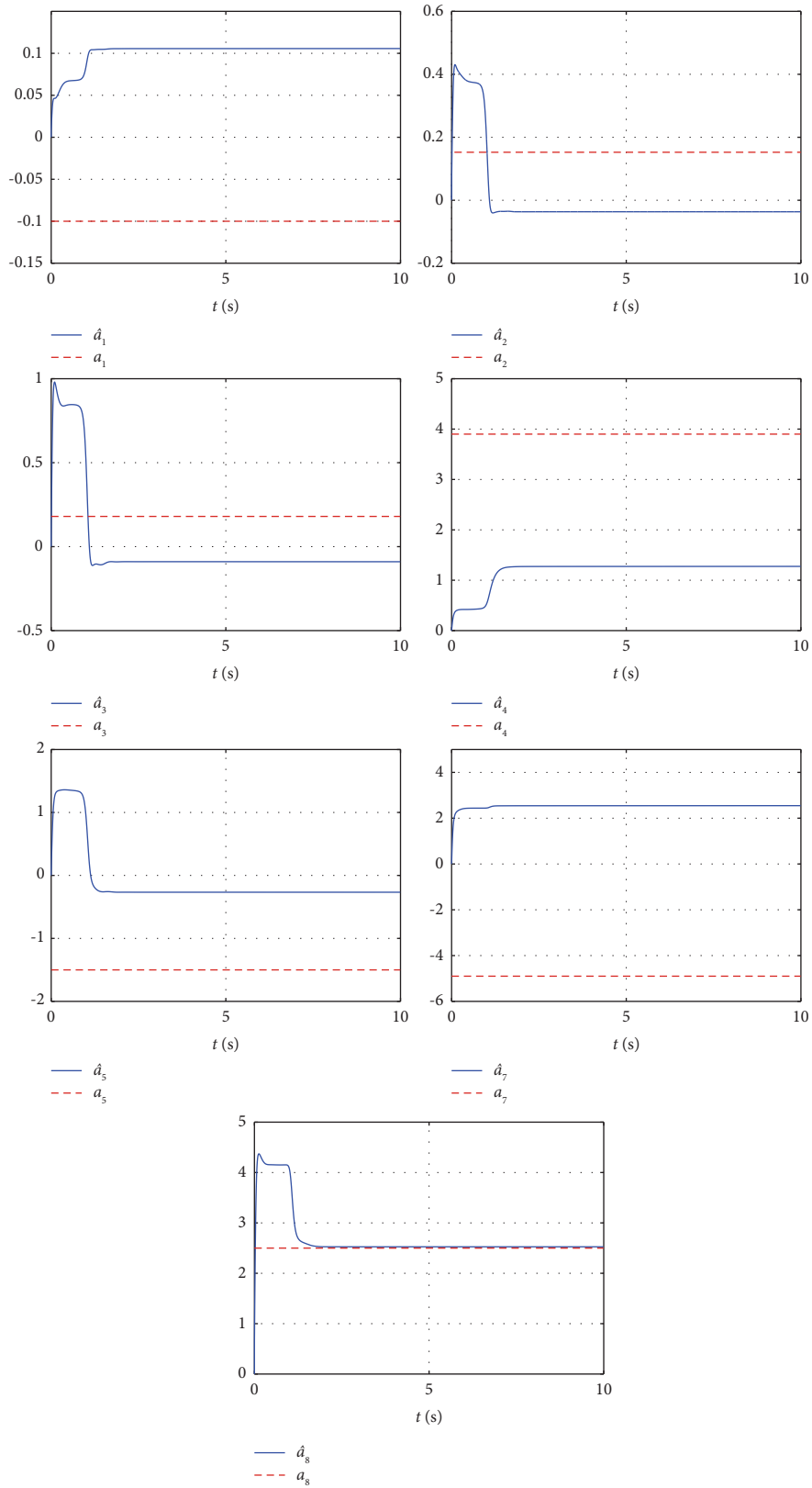
FIGURE 13: Comparison between the adaptive parameters $\hat{a}_i$ of the proposed adaptive control and the constants a_i of the Nwachioma system.

with communication delays, the synchronization is achieved in a short period of time. As depicted in Figure 13, although $\hat{a}_i \longrightarrow a_i$ is not true, the errors $\tilde{a}_i = \hat{a}_i - a_i$ are bounded.

4. Conclusions and Future Work

For the first time in literature, an adaptive control algorithm for solving the synchronization task on the Nwachioma master-slave chaotic system was presented in this paper. The feasibility and performance of the closed-loop system were demonstrated in two senses. The first one was by comparing via numerical simulations the adaptive control with an active control by implementing them in closed-loop on the master-slave Nwachioma chaotic system via MATLAB-Simulink. The simulation results showed that the performance of the adaptive control is superior to the one obtained with the active control, i.e., $(x_{1s}, x_{2s}, x_{3s}) \longrightarrow (x_{1m}, x_{2m}, x_{3m})$, and was verified through the performance indexes of the quadratic error integral associated with both controls in closed-loop. In all simulations, the parameters a_i of the master system and those of the slave system were different for both control algorithms. The second one was by executing the experimental implementation of the adaptive control on a testbed of the master-slave Nwachioma chaotic system. The experimental implementation of the master system was carried out on a computer via MATLAB-Simulink. This computer sent the states x_{1m}, x_{2m}, and x_{3m} through the Arduino UNO board and the RS-232 serial protocol. Then, the computer associated with the slave system received such states and executed the corresponding learning law and the adaptive control, also via MATLAB-Simulink, with the aim of solving the synchronization task. The experimental results showed that the proposed adaptive control achieves in finite time that $(x_{1s}, x_{2s}, x_{3s}) \longrightarrow (x_{1m}, x_{2m}, x_{3m})$.

As a future work, the current results will be generalized to several slave systems synchronized only to one master system [107]. Also, a potential extension of the results presented in this paper could include external disturbances [108] on the Nwachioma chaotic system in the master-slave configuration.

Data Availability

The data used to support the findings of this study are available from the corresponding author upon request.

Conflicts of Interest

The authors declare that they have no conflicts of interest.

Acknowledgments

References

[1] H. Tirandaz and S. Saeidiaminabadi, "Identical and non-identical synchronization of three scroll unified chaotic system (TSUCS) with unknown parameter using a modified function projective control method," *Iranian Journal of Science and Technology - Transactions of Electrical Engineering*, vol. 41, pp. 319–334, 2017.

[2] C. Nwachiona and J. H. Pérez-Cruz, "Realization and implementation of polynomial chaotic Sun system," *Physical Science International Journal*, vol. 16, pp. 1–7, 2018.

[3] G. Chen, "On some controllability conditions for chaotic dynamics control," *Chaos, Solitons & Fractals*, vol. 8, no. 9, pp. 1461–1470, 1997.

[4] L. M. Pecora and T. L. Carroll, "Synchronization of chaotic systems," *Chaos: An Interdisciplinary Journal of Nonlinear Science*, vol. 25, no. 9, pp. 097611-097612, 2015.

[5] E. N. Lorenz, "Deterministic nonperiodic flow," *Journal of the Atmospheric Sciences*, vol. 20, no. 2, pp. 130–141, 1963.

[6] A. A. Ewees, M. A. Elaziz, Z. Alameer, H. Ye, and Z. Jianhua, "Improving multilayer perceptron neural network using chaotic grasshopper optimization algorithm to forecast iron ore price volatility," *Resources Policy*, vol. 65, pp. 101555–101612, 2020.

[7] S. K. Palit and S. Mukherjee, "A study on dynamics and multiscale complexity of a neuro system," *Chaos, Solitons & Fractals*, vol. 145, pp. 110737–110810, 2021.

[8] J. Gao, C. Gu, and H. Yang, "Spiral waves with interfacial oscillatory chemical reactions emerge in a model of reaction-diffusion systems," *Chemical Physics*, vol. 528, pp. 110507–110516, 2020.

[9] K. M. Owolabi and B. Karaagac, "Chaotic and spatiotemporal oscillations in fractional reaction-diffusion system," *Chaos, Solitons & Fractals*, vol. 141, pp. 110302–110315, 2020.

[10] J. Luo, S. Qu, Z. Xiong, E. Appiagyei, and L. Zhao, "Observer-based finite-time modified projective synchronization of multiple uncertain chaotic systems and applications to secure communication using DNA encoding," *IEEE Access*, vol. 7, pp. 65527–65543, 2019.

[11] T. Karimov, D. Butusov, V. Andreev, A. Karimov, and A. Tutueva, "Accurate synchronization of digital and analog chaotic systems by parameters re-identification," *Electronics*, vol. 7, pp. 123–210, 2018.

[12] R. Babajans, D. Cirjulina, J. Grizans et al., "Impact of the chaotic synchronization's stability on the performance of QCPSK communication system," *Electronics*, vol. 10, no. 6, pp. 640–714, 2021.

[13] L. Moysis, C. Volos, I. Stouboulos et al., "A novel chaotic system with a line equilibrium: analysis and its applications to secure communication and random bit generation," *Tele.com*, vol. 1, no. 3, pp. 283–296, 2020.

[14] A. S. Muhammad and F. S. I. E. A. Ózkaynak, "SIEA: secure image encryption algorithm based on chaotic systems optimization algorithms and PUFs," *Symmetry*, vol. 13, no. 5, pp. 824–921, 2021.

[15] C. Wang, Y. Di, J. Tang, J. Shuai, Y. Zhang, and Q. Lu, "The dynamic analysis of a novel reconfigurable cubic chaotic map and its application in finite field," *Symmetry*, vol. 13, no. 8, pp. 1420–1424, 2021.

[16] O. Mofid, M. Momeni, S. Mobayen, and A. Fekih, "A disturbance-observer-based sliding mode control for the robust synchronization of uncertain delayed chaotic systems: application to data security," *IEEE Access*, vol. 9, pp. 16546–16555, 2021.

[17] B. Vaseghi, S. S. Hashemi, S. Mobayen, and A. Fekih, "Finite time chaos synchronization in time-delay channel and its application to satellite image encryption in OFDM communication systems," *IEEE Access*, vol. 9, pp. 21332–21344, 2021.

[18] S. Hashemi, M. A. Pourmina, S. Mobayen, and M. R. Alagheband, "Multiuser wireless speech encryption using synchronized chaotic systems," *International Journal of Speech Technology*, vol. 24, no. 3, pp. 651–663, 2021.

[19] K. Rajagopal, H. Jahanshahi, S. Jafari, R. Weldegiorgis, A. Karthikeyan, and P. Duraisamy, "Coexisting attractors in a fractional order hydro turbine governing system and fuzzy PID based chaos control," *Asian Journal of Control*, vol. 23, no. 2, pp. 894–907, 2020.

[20] X. Xu and W. Guo, "Chaotic behavior of turbine regulating system for hydropower station under effect of nonlinear turbine characteristics," *Sustainable Energy Technologies and Assessments*, vol. 44, p. 101088, 2021.

[21] L. Moysis, E. Petavratzis, M. Marwan, C. Volos, H. Nistazakis, and S. Ahmad, "Analysis, synchronization, and robotic application of a modified hyperjerk chaotic system," *Complexity*, vol. 2020, Article ID 2826850, pp. 1–15, 2020.

[22] C. Nwachioma and J. H. Pérez Cruz, "Analysis of a new chaotic system, electronic realization and use in navigation of differential drive mobile robot," *Chaos, Solitons & Fractals*, vol. 144, pp. 1–12, 2021.

[23] E. K. Petavratzis, C. K. Volos, L. Moysis et al., "An inverse pheromone approach in a chaotic mobile robot's path planning based on a modified logistic map," *Technologies*, vol. 7, no. 4, pp. 84–16, 2019.

[24] E. Petavratzis, L. Moysis, C. Volos, I. Stouboulos, H. Nistazakis, and K. Valavanis, "A chaotic path planning generator enhanced by a memory technique," *Robotics and Autonomous Systems*, vol. 143, pp. 103826–1039, 2021.

[25] S. Takougang Kingni, C. Alnamon, V. Kamdoum Tamba, and J. B. Chabi Orou, "Directly modulated semiconductor ring lasers: chaos synchronization and applications to cryptography communications," *Chaos Theory and Applications*, vol. 2, pp. 31–39, 2020.

[26] R. Montero Canela, E. Zambrano Serrano, E. I. Tamariz Flores, J. M. Muñoz Pacheco, and R. Torrealba Meléndez, "Fractional chaos based-cryptosystem for generating encryption keys in Ad Hoc networks," *Ad Hoc Networks*, vol. 97, pp. 1–21, 2020.

[27] J. Machicao, O. M. Bruno, and M. S. Baptista, "Zooming into chaos as a pathway for the creation of a fast, light and reliable cryptosystem," *Nonlinear Dynamics*, vol. 104, pp. 753–764, 2021.

[28] S. Mobayen, C. Volos, and U. Cavusoglu, "A simple chaotic flow with hyperbolic sinusoidal function and its application to voice encryption," *Symmetry*, vol. 12, pp. 2047–2118, 2020.

[29] B. Vaseghi, S. Mobayen, S. S. Hashemi, and A. Fekih, "Fast reaching finite time synchronization approach for chaotic systems with application in medical image encryption," *IEEE Access*, vol. 9, pp. 25911–25925, 2021.

[30] J. Guo, Z. Zhao, F. Shi, R. Wang, and S. Li, "Observer-based synchronization control for coronary artery time-delay chaotic system," *IEEE Access*, vol. 7, pp. 51222–51235, 2019.

[31] C. J. Ye, Z. Sharpe, and H. H. Heng, "Origins and consequences of chromosomal instability: from cellular adaptation to genome chaos-mediated system survival," *Genes*, vol. 11, no. 10, pp. 1162–1213, 2020.

[32] J. M. Muñoz-Pacheco, C. Posadas-Castillo, and E. Zambrano-Serrano, "The effect of a non-local fractional operator in an asymmetrical glucose-insulin regulatory system: analysis, synchronization and electronic implementation," *Symmetry*, vol. 12, no. 9, pp. 1395–1422, 2020.

[33] H. Jahanshahi, J. M. Muñoz-Pacheco, S. Bekiros, and N. D. Alotaibi, "A fractional-order SIRD model with time-dependent memory indexes for encompassing the multi-fractional characteristics of the COVID-19," *Chaos, Solitons & Fractals*, vol. 143, pp. 110632–110711, 2021.

[34] S. Liu, N. Jiang, A. Zhao, Y. Zhang, and K. Qiu, "Secure optical communication based on cluster chaos synchronization in semiconductor lasers network," *IEEE Access*, vol. 8, pp. 11872–11879, 2020.

[35] L. M. Pecora and T. L. Carroll, "Synchronization in chaotic systems," *Physical Review Letters*, vol. 64, no. 8, pp. 821–824, 1990.

[36] E. W. Bai and K. E. Lonngren, "Synchronization of two Lorenz systems using active control," *Chaos, Solitons & Fractals*, vol. 8, no. 1, pp. 51–58, 1997.

[37] E. W. Bai and K. E. Lonngren, "Sequential synchronization of two Lorenz systems using active control," *Chaos, Solitons & Fractals*, vol. 11, no. 7, pp. 1041–1044, 2000.

[38] R. A. Tang, Y. L. Liu, and J. K. Xue, "An extended active control for chaos synchronization," *Physics Letters A*, vol. 373, no. 16, pp. 1449–1454, 2009.

[39] M. T. Yassen, "Chaos synchronization between two different chaotic systems using active control," *Chaos, Solitons & Fractals*, vol. 23, no. 1, pp. 131–140, 2005.

[40] J. H. Pérez-Cruz, E. A. Portilla-Flores, P. A. Niño-Suárez, and R. Rivera-Blas, "Design of a nonlinear controller and its intelligent optimization for exponential synchronization of a new chaotic system," *Optik*, vol. 130, pp. 201–212, 2017.

[41] M. Varan and A. Akgul, "Control and synchronisation of a novel seven-dimensional hyperchaotic system with active control," *Pramana*, vol. 90, no. 4, pp. 54–58, 2018.

[42] X. Zhu and W. S. Du, "New chaotic systems with two closed curve equilibrium passing the same point: chaotic behavior, bifurcations, and synchronization," *Symmetry*, vol. 11, no. 8, pp. 951–1010, 2019.

[43] J. Sun, Y. Wang, Y. Wang, G. Cui, and Y. Shen, "Compound-combination synchronization of five chaotic systems via nonlinear control," *Optik*, vol. 127, no. 8, pp. 4136–4143, 2016.

[44] S. Zheng, "Multi-switching combination synchronization of three different chaotic systems via nonlinear control," *Optik*, vol. 127, no. 21, pp. 10247–10258, 2016.

[45] I. T. Hettiarachchi, S. Lakshmanan, A. Bhatti et al., "Chaotic synchronization of time-delay coupled Hindmarsh–Rose neurons via nonlinear control," *Nonlinear Dynamics*, vol. 86, no. 2, pp. 1249–1262, 2016.

[46] V. K. Yadav, G. Prasad, M. Srivastava, and S. Das, "Combination–combination phase synchronization among non-identical fractional order complex chaotic systems via nonlinear control," *International Journal of Dynamics and Control*, vol. 7, no. 1, pp. 330–340, 2019.

[47] V. K. Yadav, G. Prasad, M. Srivastava, and S. Das, "Triple compound synchronization among eight chaotic systems with external disturbances via nonlinear approach," *Differential Equations and Dynamical Systems*, vol. 30, no. 3, pp. 549–572, 2019.

[48] A. Ouannas, S. Bendoukha, C. Volos, N. Boumaza, and A. Karouma, "Synchronization of fractional hyperchaotic Rabinovich systems via linear and nonlinear control with an application to secure communications," *International Journal of Control, Automation and Systems*, vol. 17, no. 9, pp. 2211–2219, 2019.

[49] A. Abdurahman and H. Jiang, "Nonlinear control scheme for general decay projective synchronization of delayed

memristor-based BAM neural networks," *Neurocomputing*, vol. 357, pp. 282–291, 2019.

[50] S. Y. Al-Hayali and S. F. Al-Azzawi, "An optimal control for complete synchronization of 4D Rabinovich hyperchaotic systems," *Telkomnika*, vol. 18, no. 2, pp. 994–1000, 2020.

[51] A. S. Al-Obeidi and S. F. Al-Azzawi, "Chaos synchronization in a 6-D hyperchaotic system with self-excited attractor," *Telkomnika*, vol. 18, no. 3, pp. 1483–1490, 2020.

[52] S. F. Al-Azzawi and A. S. Al-Obeidi, "Chaos synchronization in a new 6D hyperchaotic system with self-excited attractors and seventeen terms," *Asian-European Journal of Mathematics*, vol. 14, no. 05, Article ID 2150085, 2021.

[53] P. Trikha, L. S. Jahanzaib, Nasreen, and D. Baleanu, "Dynamical analysis and triple compound combination antisynchronization of novel fractional chaotic system," *Journal of Vibration and Control*, vol. 28, no. 9-10, pp. 1057–1073, 2021.

[54] D. Lin, X. Chen, G. Yu, Z. Li, and Y. Xia, "Global exponential synchronization via nonlinear feedback control for delayed inertial memristor-based quaternion-valued neural networks with impulses," *Applied Mathematics and Computation*, vol. 2021, Article ID 126093, 401 pages, 2021.

[55] L. S. Jahanzaib, P. Trikha, and D. Baleanu, "Analysis and application using quad compound combination antisynchronization on novel fractional-order chaotic system," *Arabian Journal for Science and Engineering*, vol. 46, no. 2, pp. 1729–1742, 2021.

[56] A. Ouannas, A. A. Khennaoui, Z. Odibat, V. T. Pham, and G. Grassi, "On the dynamics, control and synchronization of fractional-order Ikeda map," *Chaos, Solitons & Fractals*, vol. 123, pp. 108–115, 2019.

[57] F. Mesdoui, A. Ouannas, N. Shawagfeh, G. Grassi, and V. T. Pham, "Synchronization methods for the Degn-Harrison reaction-diffusion systems," *IEEE Access*, vol. 8, pp. 91829–91836, 2020.

[58] X. Wu, G. Chen, and J. Cai, "Chaos synchronization of the master-slave generalized Lorenz systems via linear state error feedback control," *Physica D: Nonlinear Phenomena*, vol. 229, no. 1, pp. 52–80, 2007.

[59] Z. Yan and P. Yu, "Linear feedback control, adaptive feedback control and their combination for chaos (lag) synchronization of LC chaotic systems," *Chaos, Solitons & Fractals*, vol. 33, no. 2, pp. 419–435, 2007.

[60] M. Rafikov and J. M. Balthazar, "On control and synchronization in chaotic and hyperchaotic systems via linear feedback control," *Communications in Nonlinear Science and Numerical Simulation*, vol. 13, no. 7, pp. 1246–1255, 2008.

[61] Y. Chen, X. Wu, and Z. Gui, "Global synchronization criteria for a class of third-order non-autonomous chaotic systems via linear state error feedback control," *Applied Mathematical Modelling*, vol. 34, no. 12, pp. 4161–4170, 2010.

[62] S. Mobayen and F. Tchier, "Synchronization of a class of uncertain chaotic systems with lipschitz nonlinearities using state-feedback control design: a matrix inequality approach," *Asian Journal of Control*, vol. 20, no. 1, pp. 71–85, 2018.

[63] Z. Zhao, F. Lv, J. Zhang, and Y. Du, "H∞ Synchronization for Uncertain Time-Delay Chaotic Systems with One-Sided Lipschitz Nonlinearity," *IEEE Access*, vol. 6, pp. 19798–19806, 2018.

[64] E. E. Mahmoud, M. Higazy, and O. A. Althagafi, "A novel strategy for complete and phase robust synchronizations of chaotic nonlinear systems," *Symmetry*, vol. 12, no. 11, pp. 1765–1818, 2020.

[65] A. T. Azar, F. E. Serrano, Q. Zhu et al., "Robust stabilization and synchronization of a novel chaotic system with Input saturation constraints," *Entropy*, vol. 23, no. 9, pp. 1110–1127, 2021.

[66] N. Siddique and F.-U. Rehman, "Parameter identification and hybrid synchronization in an array of coupled chaotic systems with ring connection: an adaptive integral sliding mode approach," *Mathematical Problems in Engineering*, vol. 2018, Article ID 6581493, 15 pages, 2018.

[67] M. R. Mufti, H. Afzal, F. Ur-Rehman, W. Aslam, and M. I. Qureshi, "Transmission projective synchronization of multiple non-identical coupled chaotic systems using sliding mode control," *IEEE Access*, vol. 7, pp. 17847–17861, 2019.

[68] M. R. Mufti, H. Afzal, F.-U. Rehman, Q. R. Butt, and M. I. Qureshi, "Synchronization and antisynchronization between two non-identical chua oscillators via sliding mode control," *IEEE Access*, vol. 6, pp. 45270–45280, 2018.

[69] F. Nian, X. Liu, and Y. Zhang, "Sliding mode synchronization of fractional-order complex chaotic system with parametric and external disturbances," *Chaos, Solitons & Fractals*, vol. 116, pp. 22–28, 2018.

[70] C. Song, S. Fei, J. Cao, and C. Huang, "Robust synchronization of fractional-order uncertain chaotic systems based on output feedback sliding mode control," *Mathematics*, vol. 7, pp. 599–610, 2019.

[71] P. Y. Wan, T. L. Liao, J. J. Yan, and H. H. Tsai, "Discrete sliding mode control for chaos synchronization and its application to an improved El-Gamal cryptosystem," *Symmetry*, vol. 11, no. 7, pp. 843–913, 2019.

[72] K. A. Alattas, J. Mostafaee, A. Sambas et al., "Nonsingular integral-type dynamic finite-time synchronization for hyperchaotic systems," *Mathematics*, vol. 10, pp. 115–122, 2021.

[73] C. W. Wu, T. Yang, and L. O. Chua, "On adaptive synchronization and control of nonlinear dynamical systems," *International Journal of Bifurcation and Chaos*, vol. 06, no. 03, pp. 455–471, 1996.

[74] T. L. Liao, "Adaptive synchronization of two Lorenz Systemsfn1fn1Communicated by prof. Y. H. Ichikawa," *Chaos, Solitons & Fractals*, vol. 9, pp. 1555–1561, 1998.

[75] R. Behinfaraz, S. Ghaemi, and S. Khanmohammadi, "Adaptive synchronization of new fractional-order chaotic systems with fractional adaption laws based on risk analysis," *Mathematical Methods in the Applied Sciences*, vol. 42, no. 6, pp. 1772–1785, 2019.

[76] T. Wang, D. Wang, and K. Wu, "Chaotic adaptive synchronization control and application in chaotic secure communication for industrial internet of things," *IEEE Access*, vol. 6, pp. 8584–8590, 2018.

[77] J. H. Pérez-Cruz, "Stabilization and synchronization of uncertain zhang system by means of robust adaptive control," *Complexity*, vol. 2018, Article ID 4989520, 19 pages, 2018.

[78] A.-A. Khennaoui, A. Ouannas, S. Bendoukha, X. Wang, and V.-T. Pham, "On chaos in the fractional-order discrete-time unified system and its control synchronization," *Entropy*, vol. 20, no. 7, pp. 530–615, 2018.

[79] S. Luo, S. Li, F. Tajaddodianfar, and J. Hu, "Adaptive synchronization of the fractional-order chaotic arch micro-electro-mechanical system via Chebyshev neural network," *IEEE Sensors Journal*, vol. 18, no. 9, pp. 3524–3532, 2018.

[80] L. Xu, H. Ma, and S. Xiao, "Exponential synchronization of chaotic lur´e systems using an adaptive event-triggered mechanism," *IEEE Access*, vol. 6, pp. 61295–61304, 2018.

[81] R. Zhang, Y. Liu, and S. Yang, "Adaptive synchronization of fractional-order complex chaotic system with unknown complex parameters," *Entropy*, vol. 21, no. 2, pp. 207–212, 2019.

[82] L. Liu, C. Du, X. Zhang, J. Li, and S. Shi, "Adaptive synchronization strategy between two autonomous dissipative chaotic systems using fractional-order mittag–leffler stability," *Entropy*, vol. 21, no. 4, pp. 383–419, 2019.

[83] P. P. Singh and B. K. Roy, "Comparative performances of synchronisation between different classes of chaotic systems using three control techniques," *Annual Reviews in Control*, vol. 45, pp. 152–165, 2018.

[84] Y. Gao, D. Ding, and Z. Tang, "Adaptive cluster synchronization of complex networks with identical and non-identical Lur'e systems," *Electronics*, vol. 9, no. 5, pp. 706–716, 2020.

[85] A. T. Azar and F. E. Serrano, "Stabilization of port Hamiltonian chaotic systems with hidden attractors by adaptive terminal sliding mode control," *Entropy*, vol. 22, pp. 122–215, 2020.

[86] A. A. K. Javan, A. Shoeibi, A. Zare et al., "Design of adaptive-robust controller for multi-state synchronization of chaotic systems with unknown and time-varying delays and its application in secure communication," *Electronics*, vol. 21, pp. 1–21, 2021.

[87] A. A. K. Javan, M. Jafari, A. Shoeibi et al., "Medical images encryption based on adaptive-robust multi-mode synchronization of Chen hyper-chaotic systems," *Sensors*, vol. 21, no. 11, pp. 3925–3934, 2021.

[88] Z. Wang and G. Rongwei, "Hybrid synchronization problem of a class of chaotic systems by an universal control method," *Symmetry*, vol. 10, pp. 1–18, 2018.

[89] A. A. Khennaoui, A. Ouannas, S. Bendoukha et al., "Chaos, control, and synchronization in some fractional-order difference equations," *Advances in Difference Equations*, vol. 2019, p. 423, 2019.

[90] Z.-A. S. A. Rahman, B. H. Jasim, Y. I. A. Al-Yasir, R. A. Abd-Alhameed, and B. N. Alhasnawi, "A new No equilibrium fractional order chaotic system, dynamical investigation, synchronization, and its digital implementation," *Inventions*, vol. 6, no. 3, p. 49, 2021.

[91] Y.-M. Chu, S. Bekiros, E. Zambrano-Serrano et al., "Artificial macro-economics: a chaotic discrete-time fractional-order laboratory model," *Chaos, Solitons and Fractals*, vol. 145, Article ID 110776, 2021.

[92] H. Takhi, K. Kemih, L. Moysis, and C. Volos, "Passivity based sliding mode control and synchronization of a perturbed uncertain unified chaotic system," *Mathematics and Computers in Simulation*, vol. 181, pp. 150–169, 2021.

[93] A. Ouannas, A. A. Khennaoui, T. E. Oussaeif, V. T. Pham, G. Grassi, and Z. Dibi, "Hyperchaotic fractional Grassi-Miller map and its hardware implementation," *Integration*, vol. 80, pp. 13–19, 2021.

[94] H. Hamiche, H. Takhi, M. Messadi, K. Kemih, O. Megherbi, and M. Bettayeb, "New synchronization results for a class of nonlinear discrete-time chaotic systems based on synergetic observer and their implementation," *Mathematics and Computers in Simulation*, vol. 185, pp. 194–217, 2021.

[95] T. Bonny, "Chaotic or hyper-chaotic oscillator? Numerical solution, circuit design, MATLAB HDL-coder implementation, VHDL code, security analysis, and FPGA realization," *Circuits, Systems, and Signal Processing*, vol. 40, no. 3, pp. 1061–1088, 2021.

[96] J. Wang, L. Xiao, K. Rajagopal, A. Akgul, S. Cicek, and B. Aricioglu, "Fractional-order analysis of modified Chua's circuit system with the smooth degree of 3 and its microcontroller-based implementation with analog circuit design," *Symmetry*, vol. 13, no. 2, pp. 340–413, 2021.

[97] V. A. Adeyemi, J. C. Nuñez-Pérez, Y. Sandoval-Ibarra, F. J. Pérez-Pinal, and E. Tlelo-Cuautle, "FPGA realization of the parameter-switching method in the Chen oscillator and application in image transmission," *Symmetry*, vol. 13, no. 6, pp. 923–1021, 2021.

[98] C. Nwachioma, J. Humberto Perez-Cruz, A. Jimenez, M. Ezuma, and R. Rivera-Blas, "A new chaotic oscillator—properties, analog implementation, and secure communication application," *IEEE Access*, vol. 7, pp. 7510–7521, 2019.

[99] D. R. Merkin, *Introduction to the theory of stability*, Springer Science and Business Media, Berlin, Germany, 2012.

[100] A. S. Pozniak, E. N. Sanchez, and W. Yu, *Differential Neural Networks for Robust Nonlinear Control: Identification, State Estimation and Trajectory Tracking*, World Scientific, Singapore, 2001.

[101] A. S. Al-Obeidi, S. Fawzi Al-Azzawi, A. Abdullah Hamad et al., "A novel of new 7D hyperchaotic system with self-excited attractors and its hybrid synchronization," *Computational Intelligence and Neuroscience*, vol. 2021, Article ID 3081345, 11 pages, 2021.

[102] A. S. lshomrani, M. Z. Ullah, and D. Baleanu, "A new approach on the modelling, chaos control and synchronization of a fractional biological oscillator," *Advances in Difference Equations*, vol. 2021, pp. 1–20, 2021.

[103] A. A. Velamore, A. Hegde, A. A. Khan, and S. Deb, "Dual cascaded fractional-order chaotic synchronization for secure communication with analog circuit realisation," in *Proceedings of the 2021 IEEE Second International Conference on Control, Measurement and Instrumentation (CMI)*, pp. 30–35, Kolkata, India, January 2021.

[104] L. Yan, J. Liu, F. Xu, K. L. Teo, and M. Lai, "Control and synchronization of hyperchaos in digital manufacturing supply chain," *Applied Mathematics and Computation*, vol. 391, p. 391, Article ID 125646, 2021.

[105] F. Aydogmus and E. Tosyali, "Master–slave synchronization in a 4D dissipative nonlinear fermionic system," *International Journal of Control*, vol. 95, no. 3, pp. 620–625, 2022.

[106] C. Arduino, "Arduino reference," 2019, https://www.arduino.cc/reference/en/language/functions/communication/serial/.

[107] S. Mobayen, A. Fekih, S. Vaidyanathan, and A. A. Sambas, "Chameleon chaotic systems with quadratic nonlinearities: an adaptive finite-time sliding mode control approach and circuit simulation," *IEEE Access*, vol. 9, pp. 64558–64573, 2021.

[108] H. Karami, S. Mobayen, M. Lashkari, F. Bayat, and A. Chang, "LMI-observer-based stabilizer for chaotic systems in the existence of a nonlinear function and perturbation," *Mathematics*, vol. 9, no. 10, pp. 1128–1215, 2021.

WILEY | Hindawi

Research Article

Analytical Solution for the Cubic-Quintic Duffing Oscillator Equation with Physics Applications

Alvaro H. Salas [ID],[1] Lorenzo J. Martínez H,[1,2] and David L. Ocampo R [ID][1,2]

[1]*Department of Mathematics and Statistics, Universidad Nacional de Colombia-Sede Manizales, Manizales, Caldas, Colombia*
[2]*Universidad de Caldas, Departamento de Matemáticas y Estadística, Manizales, Colombia*

Correspondence should be addressed to Alvaro H. Salas; ahsalass@unal.edu.co

The nonlinear differential equation governing the periodic motion of the one-dimensional, undamped, and unforced cubic-quintic Duffing oscillator is solved exactly by obtaining the period and the solution. The period is given in terms of the complete elliptic integral of the first kind and the solution involves Jacobian elliptic functions. We solve the cubic-quintic Duffing equation under arbitrary initial conditions. Physical applications are provided. The solution to the mixed parity Duffing oscillator is also formally derived. We illustrate the obtained results with concrete examples. We give high accurate trigonometric approximations to the Jacobian function cn.

1. Introduction

It is well known that many engineering problems are not linear and their analytical solutions are not easy to obtain. Disturbance methods are among the known methods for solving nonlinear problems, which are based on the existence of small/large parameters, the so-called disturbance parameters. Our approach is different from known solutions to this problem [1–5]. On the contrary, here, we express the solutions without imaginary quantities: both frequency and modulus are real numbers. The quintic term appearing in the cubic-quintic Duffing equation makes this nonlinear oscillator not only more complex but also more interesting to study.

2. The Analytical Solution to the Cubic-Quintic Duffing Equation

Let p, q, r, y_0, and $\dot{y}_0$ be arbitrary real numbers. We will solve the initial value problem:

$$y''(t) + p y(t) + q y(t)^3 + r y(t)^5 = 0 \text{ given that } y(0)$$
$$= y_0 \text{ and } y'(0) \qquad (1)$$
$$= \dot{y}_0.$$

We will assume that $y_0^2 + \dot{y}_0^2 > 0$. Multiplying (1) by $y'(t)$ and integrating it with respect to t gives

$$\frac{1}{2}y'(t)^2 + \frac{p}{2}y(t)^2 + \frac{q}{4}y(t)^4 + \frac{r}{6}y(t)^6 = \frac{1}{2}\dot{y}_0^2 + \frac{p}{2}y_0^2 + \frac{q}{4}y_0^4 + \frac{r}{6}y_0^6. \qquad (2)$$

Let

$$y(t) = \frac{c_0 \operatorname{cn}\left(\sqrt{\omega}\, t + c_1 | m\right)}{\sqrt{1 + \lambda \cdot \operatorname{cn}\left(\sqrt{\omega}\, t + c_1 | m\right)^2 + \mu \cdot \operatorname{cn}\left(\sqrt{\omega}\, t + c_1 | m\right)^4}}, \qquad (3)$$

where the parameter values c_0, c_1, m, ω, λ, and μ are to be determined. If the solution in (3) is periodic, it will have the same period as the function $\operatorname{cn}\left(\sqrt{\omega}\, t + c_1 | m\right)$ and this period may be evaluated by means of the formula

$$T = \frac{4}{\sqrt{\omega}} K(m). \qquad (4)$$

In the case, when $-1 \le m \le 1/2$, we may approximate the value of $K(m)$ using the formula

$$K(m) \approx \frac{\pi(m(409m - 3984) + 4864)}{50m(41m - 208) + 9728}. \qquad (5)$$

The error for this approximation is given by

$$\text{Error} = \max_{-1 \leq m \leq 1/2} |K(m) - K(m)| < 0.000314. \quad (6)$$

On the contrary, we may obtain approximate trigonometric solution making use of the following approximation formula:

$$\begin{aligned} \text{cn}(t,m) &\approx \cos{}_m(t) \\ &= \frac{\sqrt{1+\kappa}\cos\left(\sqrt{1+\kappa}\,t\right)}{\sqrt{1+\kappa}\cos^2\left(\sqrt{1+\kappa}\,t\right)}, \text{ where } \kappa \\ &= \frac{1}{14}\left(\sqrt{m^2 - 144m + 144} - (m+12)\right). \end{aligned} \quad (7)$$

See Table 1, for the error $= \max_{-2K(m) \leq t \leq 2K(m)} |\cos{}_m(t) - \text{cn}(t,m)|$.

A more accurate trigonometric approximation may be obtained using the formula

$$\text{cn}(t,m) \approx \cos_m(t) := \frac{\sqrt{1+\rho+\kappa}\cos\left(\sqrt{w}\,t\right)}{\sqrt{1 + \rho\cos^2\left(\sqrt{w}\,t\right) + \kappa\cos^4\left(\sqrt{w}\,t\right)}}, \quad (8)$$

being

$$w = \frac{(\kappa - 1)(m - 2)}{\kappa + 2}, \rho = \frac{(\kappa - 7)\kappa - (\kappa - 1)^2 m}{\kappa + 2}, \quad (9)$$

and

$$\kappa = \frac{8m^2\left(2409m^4 - 29600m^3 + 111520m^2 - 163840m + 81920\right)}{35767m^6 - 831840m^5 + 6197600m^4 - 21217280m^3 + 36823040m^2 - 31457280m + 10485760}.$$

See Table 2, for the error $= \max_{-2K(m) \leq t \leq 2K(m)} |\cos_m(t) - \text{cn}(t,m)|$.

Let

$$\begin{aligned} R(t) &= \frac{1}{2}y'(t)^2 + \frac{p}{2}y(t)^2 + \frac{q}{4}y(t)^4 + \frac{r}{6}y(t)^6 \\ &\quad - \left(\frac{1}{2}\dot{y}_0^2 + \frac{p}{2}y_0^2 + \frac{q}{4}y_0^4 + \frac{r}{6}y_0^6\right): \text{Residual.} \end{aligned} \quad (10)$$

Introduce the notation:

$$\text{cn} = \text{cn}\left(\sqrt{\omega}\,t|m\right) \text{ and cn} = \sqrt{\zeta}. \quad (11)$$

Definition 1. The discriminant to the i.v.p. (1) is defined as

$$\begin{aligned} \Delta &= \left(p + qy_0^2 + ry_0^4\right)^2\left(3q^2 - 16pr - 4qry_0^2 - 4r^2y_0^4\right) \\ &\quad + \left(6\left(q + 2ry_0^2\right)\left(q^2 - 6pr - 2qry_0^2 - 2r^2y_0^4\right)\right)\dot{y}_0^2 - 36r^2\dot{y}_0^4. \end{aligned} \quad (12)$$

2.1. First Case: $\Delta > 0$. We define $\mu = 0$. Inserting the ansatz (3) into (10), we obtain

$$R(t) = \frac{1}{12(1+\lambda\zeta)^3}\begin{bmatrix} \left(-6c_0^2 m\omega + 6c_0^2\omega - 6py_0^2 - 3qy_0^4 - 2ry_0 - 6\dot{y}_0{}^2\right)+ \\ \\ 3\left(4c_0^2 m\omega + 2c_0^2 p - 2c_0^2\omega - 6\lambda py_0^2 - 3\lambda qy_0^4 - 2\lambda ry_0^6 - 6\lambda\dot{y}_0{}^2\right)\zeta, \\ \\ 3\left(-2c_0^2 m\omega + 4c_0^2\lambda p + c_0^4 q - 6\lambda^2 py_0 - 3\lambda^2 qy_0 - 2\lambda^2 ry_0^6 - 6\lambda^2\dot{y}_0^2\right)\zeta^2 \\ \\ \left(6c_0^2\lambda^2 p + 3c_0^4\lambda q + 2c_0^6 r - 6\lambda^3 py_0^2 - 3\lambda^3 qy_0^2 - 2\lambda^3 ry_0^2 - 6\lambda^3\dot{y}_0{}^2\right)\zeta^3 \end{bmatrix}. \quad (13)$$

Equating to zero the coefficients of ζ^j ($j = 0, 1, 2, 3$) in the numerator of the last expression gives an algebraic system. Solving it, we obtain

TABLE 1: Error of approximating the Jacobian cn function by means of the cosine function (7) with $T = 4K(m)$.

m	Error	m	Error
−1	0.0068	0	0
−0.95	0.00624	0.05	0.0000332
−0.9	0.005742	0.1	0.00014
−0.85	0.0053	0.15	0.00033
−0.8	0.0045	0.2	0.00061
−0.75	0.0043	0.25	0.0010
−0.7	0.0039	0.3	0.00153
−0.65	0.00344	0.35	0.00212
−0.6	0.00301	0.4	0.003
−0.55	0.00261	0.45	0.0041
−0.5	0.00222	0.5	0.0054
−0.45	0.00186	0.55	0.007
−0.4	0.001517	0.6	0.009
−0.35	0.0012	0.65	0.0116
−0.3	0.0009	0.7	0.0145
−0.25	0.00066	0.75	0.0188
−0.2	0.00044	0.8	0.0241
−0.15	0.00025	0.85	0.0314
−0.1	0.00012	0.9	0.042
−0.05	0.000031	0.95	0.059

TABLE 2: Error of approximating the Jacobian cn function by means of the cosine function (8) with $T = 4K(m)$.

m	Error	m	Error
−1	0.000074	0	0
−0.95	0.000063	0.05	$2.002e-9$
−0.9	0.000054	0.1	$3.52e-8$
−0.85	0.0000452	0.15	$1.98e-7$
−0.8	0.0000378	0.2	$6.93e-7$
−0.75	0.00003	0.25	$1.89e-6$
−0.7	0.000025	0.3	$4.40e-6$
−0.65	0.000012	0.35	$9.22e-6$
−0.6	0.000015	0.4	0.000018
−0.55	0.000011	0.45	0.000033
−0.5	$8.37e-6$	0.5	0.00006
−0.45	$5.88e-6$	0.55	0.0000991
−0.4	$3.94e-6$	0.6	0.00017
−0.35	$2.48e-6$	0.65	0.00023
−0.3	$1.44e-6$	0.7	0.00045
−0.25	$7.5e-7$	0.75	0.00074
−0.2	$3.322e-7$	0.8	0.0012
−0.15	$1.145e-7$	0.85	0.0021
−0.1	$2.44e-8$	0.9	0.0036
−0.05	$1.67e-9$	0.95	0.015

$$m = \frac{3\lambda\omega - p + \omega}{(3\lambda + 2)\omega}.\omega$$

$$= \frac{(3\lambda + 2)\left(6py_0^2 + 3qy_0^4 + 2ry_0^6 + 6\dot{y}_0^2\right)}{6c_0^2} - p. \tag{14}$$

For these choices, we obtain the following system:

$$\left(-18py_0^2 - 9qy_0^4 - 6ry_0^6 - 18\dot{y}_0^2\right)\lambda^2$$
$$+ \left(12c_0^2 p - 18py_0^2 - 9qy_0^4 - 6ry_0^6 - 18\dot{y}_0^2\right)\lambda$$
$$+ \left(6c_0^2 p + 3c_0^4 q - 6py_0^2 - 3qy_0^4 - 2ry_0^6 - 6\dot{y}_0^2\right) = 0. \tag{15}$$
$$\left(-6py_0^2 - 3qy_0^4 - 2ry_0^6 - 6\dot{y}_0^2\right)\lambda^3$$
$$+ 6c_0^2 p\lambda^2 + 3c_0^4 q\lambda + 2c_0^6 r = 0.$$

Eliminating c_0 from system (15) gives the sextic

$$d_0 + d_1\lambda + d_2\lambda^2 + d_3\lambda^3 + d_4\lambda^4 + d_5\lambda^5 + d_6\lambda^6 = 0, \qquad (16)$$

where

$$d_0 = 4r^2\left(6py_0^2 + 3qy_0^4 + 2ry_0^6 + 6\dot{y}_0^2\right)^2,$$

$$d_1 = 36r\left(6py_0^2 + 3qy_0^4 + 2ry_0^6 + 6\dot{y}_0^2\right)\left(pq + 6pry_0^2 + 3qry_0^4 + 2r^2y_0^6 + 6r\dot{y}_0^2\right),$$

$$d_2 = 9\begin{pmatrix} 48p^3r + 240p^2qry_0^2 + 576p^2r^2y_0^4 - 18pq^3y_0^2 + 120pq^2ry_0^4 + 656pqr^2y_0^6 + \\ 240pqr\dot{y}_0^2 + 384pr^3y_0^8 + 1152pr^2\dot{y}_0^2y_0^2 - 9q^4y_0^4 - 6q^3ry_0^6 - 18q^3\dot{y}_0^2 + \\ 144q^2r^2y_0^8 + 192qr^3y_0^{10} + 576qr^2\dot{y}_0^2y_0^4 + 64r^4y_0^{12} + 384r^3\dot{y}_0^2y_0^6 + 576r^2\dot{y}_0^4 \end{pmatrix},$$

$$d_3 = 162\begin{pmatrix} 16p^3r - 2p^2q^2 + 48p^2qry_0^2 + 72p^2r^2y_0^4 - 6pq^3y_0^2 + 24pq^2ry_0^4 + 88pqr^2y_0^6 + \\ 48pqr\dot{y}_0^2 + 48pr^3y_0^8 + 144pr^2\dot{y}_0^2y_0^2 - 3q^4y_0^4 - 2q^3ry_0^6 - 6q^3\dot{y}_0^2 + \\ 18q^2r^2y_0^8 + 24qr^3y_0^{10} + 72qr^2\dot{y}_0^2y_0^4 + 8r^4y_0^{12} + 48r^3\dot{y}_0^2y_0^6 + 72r^2\dot{y}_0^4 \end{pmatrix},$$

$$d_4 = 27\begin{pmatrix} 208p^3r - 36p^2q^2 + 504p^2qry_0^2 + 576p^2r^2y_0^4 - 78pq^3y_0^2 + 252pq^2ry_0^4 + 744pqr^2y_0^6 + \\ 504pqr\dot{y}_0^2 + 384pr^3y_0^8 + 1152pr^2\dot{y}_0^2y_0^2 - 39q^4y_0^4 - 26q^3ry_0^6 - 78q^3\dot{y}_0^2 + \\ 144q^2r^2y_0^8 + 192qr^3y_0^{10} + 576qr^2\dot{y}_0^2y_0^4 + 64r^4y_0^{12} + 384r^3\dot{y}_0^2y_0^6 + 576r^2\dot{y}_0^4 \end{pmatrix},$$

$$d_5 = 324\begin{pmatrix} 16p^3r - 3p^2q^2 + 36p^2qry_0^2 + 36p^2r^2y_0^4 - 6pq^3y_0^2 + \\ 18pq^2ry_0^4 + 48pqr^2y_0^6 + 36pqr\dot{y}_0^2 + 24pr^3y_0^8 + 72pr^2\dot{y}_0^2y_0^2 - 3q^4y_0^4 - \\ 2q^3ry_0^6 - 6q^3\dot{y}_0^2 + 9q^2r^2y_0^8 + 12qr^3y_0^{10} + 36qr^2\dot{y}_0^2y_0^4 + 4r^4y_0^{12} + 24r^3\dot{y}_0^2y_0^6 + 36r^2\dot{y}_0^4 \end{pmatrix},$$

$$d_6 = 108\begin{pmatrix} 16p^3r - 3p^2q^2 + 36p^2qry_0^2 + 36p^2r^2y_0^4 - 6pq^3y_0^2 + 18pq^2ry_0^4 + 48pqr^2y_0^6 + \\ 36pqr\dot{y}_0^2 + 24pr^3y_0^8 + 72pr^2\dot{y}_0^2y_0^2 - 3q^4y_0^4 - 2q^3ry_0^6 - 6q^3\dot{y}_0^2 + \\ 9q^2r^2y_0^8 + 12qr^3y_0^{10} + 36qr^2\dot{y}_0^2y_0^4 + 4r^4y_0^{12} + 24r^3\dot{y}_0^2y_0^6 + 36r^2\dot{y}_0^4 \end{pmatrix}.$$

$$(17)$$

Sextic (16) is solvable by radicals. Indeed, let

$$\lambda = \sqrt{z} - \frac{1}{2}. \qquad (18)$$

Then,

$$s_0 + s_1z + s_2z^2 + s_3z^3 = 0, \qquad (19)$$

where

$$s_0 = \left(9pq + 6pry_0^2 + 3qry_0^4 + 2r^2y_0^6 + 6r\dot{y}_0^2\right)^2,$$

$$s_1 = 9\begin{pmatrix} 48p^3r - 27p^2q^2 - 12p^2qry_0^2 + 36p^2r^2y_0^4 - \\ 18pq^3y_0^2 - 6pq^2ry_0^4 + 32pqr^2y_0^6 - 12pqr\dot{y}_0^2 + \\ 24pr^3y_0^8 + 72pr^2\dot{y}_0^2y_0^2 - 9q^4y_0^4 - 6q^3ry_0^6 - \\ 18q^3\dot{y}_0^2 + 9q^2r^2y_0^8 + 12qr^3y_0^{10} + 36qr^2\dot{y}_0^2y_0^4 + \\ 4r^4y_0^{12} + 24r^3\dot{y}_0^2y_0^6 + 36r^2\dot{y}_0^4 \end{pmatrix},$$

$$s_2 = -27\begin{pmatrix} 32p^3r - 9p^2q^2 + 36p^2qry_0^2 - 36p^2r^2y_0^4 - \\ 12pq^3y_0^2 + 18pq^2ry_0^4 - 24pqr^2y_0^6 + 36pqr\dot{y}_0^2 - 24pr^3y_0^8 - \\ 72pr^2\dot{y}_0^2y_0^2 - 6q^4y_0^4 - 4q^3ry_0^6 - 12q^3\dot{y}_0^2 - 9q^2r^2y_0^8 - 12qr^3y_0^{10} - \\ 36qr^2\dot{y}_0^2y_0^4 - 4r^4y_0^{12} - 24r^3\dot{y}_0^2y_0^6 - 36r^2\dot{y}_0^4 \end{pmatrix},$$

$$s_3 = 27\begin{pmatrix} 16p^3r - 3p^2q^2 + 36p^2qry_0^2 + 36p^2r^2y_0^4 - 6pq^3y_0^2 + 18pq^2ry_0^4 + 48pqr^2y_0^6 + \\ 36pqr\dot{y}_0^2 + 24pr^3y_0^8 + 72pr^2\dot{y}_0^2y_0^2 - 3q^4y_0^4 - 2q^3ry_0^6 - 6q^3\dot{y}_0^2 + \\ 9q^2r^2y_0^8 + 12qr^3y_0^{10} + 36qr^2\dot{y}_0^2y_0^4 + 4r^4y_0^{12} + 24r^3\dot{y}_0^2y_0^6 + 36r^2\dot{y}_0^4 \end{pmatrix}.$$

$$(20)$$

The discriminant to cubic (19) is

$$\delta_{\text{cubic}} = 20639121408 r^2 \left(6 p y_0^2 + 3 q y_0^4 + 2 r y_0^6 + 6 \dot{y}_0^2\right)^2$$
$$\left(16 p^3 r + 6 p q^3 y_0^2 + 3 q^4 y_0^4 + 2 q^3 r y_0^6 + 6 q^3 \dot{y}_0^2\right)^2 \Delta > 0. \tag{21}$$

Cubic (19) has three real roots and at least one of them must be *positive*. Indeed, let z_1, z_2, and z_3 be the roots to this cubic. Then,

$$z_1 z_2 z_3 = -\frac{s_0}{s_3}$$

$$= \frac{\left(9 p q + 6 p r y_0^2 + 3 q r y_0^4 + 2 r^2 y_0^6 + 6 r \dot{y}_0^2\right)^2}{1728\Delta} > 0. \tag{22}$$

Since $z_1 z_2 z_3 > 0$, at least one of the numbers z_1, z_2, and z_3 must be positive. We choose the closest to $1/4$ positive root to cubic (19) so that, in view of (17), the number λ will be the closest to zero real root to the sextic in (15). Observe also that the condition $\Delta > 0$ implies that $q^2 - 4pr > 0$. Thus, if $q^2 - 4pr \leq 0$, then $\Delta \leq 0$. Moreover, the discriminant to the cubic (17) and Δ have the same sign.

The numbers c_0 and c_1 are determined from the initial conditions:

$$c_1 = \text{cn}^{-1}\left(\pm \frac{y_0}{\sqrt{c_0^2 - \lambda y_0^2}} | m\right). \tag{23}$$

The number c_0 is a solution to the sextic:

$$\lambda(\lambda + 1)(2\lambda + 1) y_0^2 \left(6 p y_0^2 + 3 q y_0^4 + 2 r y_0^6 + 6 \dot{y}_0^2\right)$$

$$+ \left(\begin{array}{c} -24\lambda^2 p y_0^2 - 24\lambda p y_0^2 - 6 p y_0^2 - 9\lambda^2 q y_0^4 - 9\lambda q y_0^4 - \\ 3 q y_0^4 - 6\lambda^2 r y_0^6 - 6\lambda r y_0^6 - 2 r y_0^6 - 18\lambda^2 \dot{y}_0^2 - 18\lambda \dot{y}_0^2 - 6 \dot{y}_0^2 \end{array}\right) c_0^2$$

$$+ 6(2\lambda + 1) p c_0^4 + \left(3q + 2 r y_0^2\right) c_0^6 = 0. \tag{24}$$

Example 1. Let

$$p = 1,$$
$$q = 5,$$
$$r = 1, \tag{25}$$
$$y_0 = 1 \text{ and}$$
$$\dot{y}_0 = 1.$$

Sextic (15) reads

$$213084\lambda^6 + 639252\lambda^5 + 598887\lambda^4 + 132354\lambda^3$$
$$- 75861\lambda^2 - 35496\lambda - 3364 = 0. \tag{26}$$

The roots to this sextic are
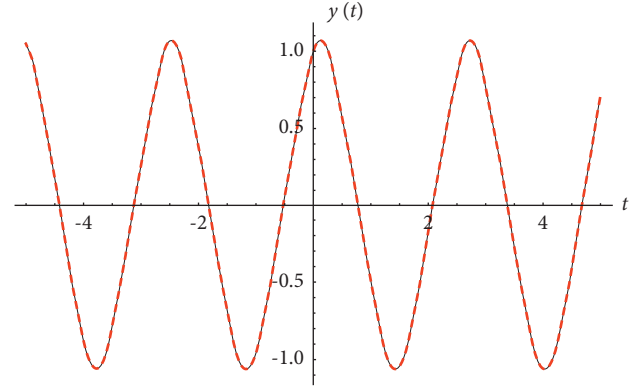
FIGURE 1: Comparison between the exact and the approximate numerical solution.

$$\lambda_1 = -1.39266,$$
$$\lambda_2 = -0.855911,$$
$$\lambda_3 = -0.626144.$$
$$\lambda_4 = -0.373856, \tag{27}$$
$$\lambda_5 = -0.144089,$$
$$\lambda_6 = 0.392663.$$

We choose the value $\lambda = \lambda_5 = -0.144089$. The values of c_0 and c_1 are determined from the initial conditions. They read

$$c_0 = 0.985102 \text{ and}$$
$$c_1 = -0.327845. \tag{28}$$

The exact solution to the i.v.p.,

$$y''(t) + y(t) + 5 y(t)^3 + y(t)^5 = 0 \text{ given that } y(0)$$
$$= 1 \text{ and } y'(0) \tag{29}$$
$$= 1,$$

reads

$$y(t) = \frac{0.985102 \text{cn}(2.60927 t - 0.327845, 0.268447)}{\sqrt{1 - 0.144089 \text{cn}(2.60927 t - 0.327845, 0.268447)^2}}. \tag{30}$$

The solution is periodic with period $T = 4K(m)/\sqrt{\omega} = 2.5997790766024407$. The approximate trigonometric solution is given by

$$y_{\text{trigo}}(t) = \frac{3.41275 \cos(2.41528(t - 0.125818))}{\sqrt{14 - 3.72995 \cos^2(2.41528(t - 0.125818))}}. \tag{31}$$

The error of this trigonometric approximant compared with the exact solution on $0 \leq t \leq T$ equals 0.00352816, see Figure 1.

2.2. Second Case: $\Delta < 0$. Let $\mu \neq 0$. Inserting the ansatz (3) into (10), we obtain

$$\left(12\zeta^6\mu^3 + 36\zeta^5\lambda\mu^2 + 12\zeta^4\left(3\lambda^2\mu + 3\mu^2\right) + 12\zeta^3\left(\lambda^3 + 6\lambda\mu\right) + 12\zeta^2\left(3\lambda^2 + 3\mu\right) + 36\zeta\lambda + 12\right)R(t) =$$

$$- 6c_0^2 m\omega + 6c_0^2\omega - 6py_0^2 - 3qy_0^4 - 2ry_0^6 - 6\dot{y}_0^2$$

$$+ 3\begin{pmatrix} 4c_0^2\mu\omega - 4c_0^2\mu m\omega + 2c_0^2 m\omega - 4c_0^2\lambda p - c_0^4 q+ \\ 6\lambda^2 py_0^2 + 6\mu py_0^2 + 3\lambda^2 qy_0^4 + 3\mu qy_0^4+ \\ 2\lambda^2 ry_0^6 + 2\mu ry_0^6 + 6\lambda^2\dot{y}_0^2 + 6\mu\dot{y}_0^2 \end{pmatrix}\zeta^2$$

$$+ 3\zeta\left(4c_0^2 m\omega + 2c_0^2 p - 2c_0^2\omega - 6\lambda py_0^2 - 3\lambda qy_0^4 - 2\lambda ry_0^6 - 6\lambda\dot{y}_0^2\right)$$

$$- \begin{pmatrix} 12c_0^2\mu\omega - 24c_0^2\mu m\omega + 6c_0^2\lambda^2 p + 12c_0^2\mu p + 3c_0^4\lambda q+ \\ 2c_0^6 r - 6\lambda^3 py_0^2 - 36\lambda\mu py_0^2 - 3\lambda^3 qy_0^4 - 18\lambda\mu qy_0^4- \\ 2\lambda^3 ry_0^6 - 12\lambda\mu ry_0^6 - 6\lambda^3\dot{y}_0^2 - 36\lambda\mu\dot{y}_0^2 \end{pmatrix}\zeta^3 \tag{32}$$

$$- 3\mu\begin{pmatrix} -2c_0^2\mu\omega + 2c_0^2\mu m\omega - 4c_0^2 m\omega - 4c_0^2\lambda p- \\ c_0^4 q + 6\lambda^2 py_0^2 + 6\mu py_0^2 + 3\lambda^2 qy_0^4 + 3\mu qy_0^4+ \\ 2\lambda^2 ry_0^6 + 2\mu ry_0^6 + 6\lambda^2\dot{y}_0^2 + 6\mu\dot{y}_0^2 \end{pmatrix}\zeta^4$$

$$+ 3\mu^2\left(4c_0^2 m\omega + 2c_0^2 p - 2c_0^2\omega - 6\lambda py_0^2 - 3\lambda qy_0^4 - 2\lambda ry_0^6 - 6\lambda\dot{y}_0^2\right)\zeta^5$$

$$- \mu^2\left(6c_0^2 m\omega + 6\mu py_0^2 + 3\mu qy_0^4 + 2\mu ry_0^6 + 6\mu\dot{y}_0^2\right)\zeta^6.$$

Equating to zero the coefficients of ζ^j ($j = 0, 1, 2, 3, 4, 5, 6$) gives an algebraic system. Solving it gives

$$\omega = \frac{(3\lambda + 2)\left(6py_0^2 + 3qy_0^4 + 2ry_0^6 + 6\dot{y}_0^2\right)}{6c_0^2} - p,$$

$$m = \frac{\mu}{\mu - 1}, \tag{33}$$

$$\mu = \frac{6c_0^2 p}{6py_0^2 + 3qy_0^4 + 2ry_0^6 + 6\dot{y}_0^2} - 3\lambda - 1.$$

The system reduces to

$$\left(-24pc_0^2 + 3qc_0^4 + 24py_0^2 + 12qy_0^4 + 8ry_0^6 + 24\dot{y}_0^2\right)$$
$$+ 12\lambda\left(pc_0^2 + 6py_0^2 + 3qy_0^4 + 2ry_0^6 + 6\dot{y}_0^2\right) - 3\lambda^2\left(6py_0^2 + 3qy_0^4 + 2ry_0^6 + 6\dot{y}_0^2\right) = 0,$$

$$2c_0^2\begin{pmatrix} 72p^2c_0^2 - 72p^2y_0^2 + 6prc_0^4y_0^2 - 36pqy_0^4 + 3qrc_0^4y_0^4 - 24pry_0^6+ \\ 2r^2c_0^4y_0^6 - 72p\dot{y}_0^2 + 6rc_0^4\dot{y}_0^2 \end{pmatrix} \tag{34}$$
$$- 3\left(48pc_0^2 - qc_0^4 - 24py_0^2 - 12qy_0^4 - 8ry_0^6 - 24\dot{y}_0^2\right)\left(6py_0^2 + 3qy_0^4 + 2ry_0^6 + 6\dot{y}_0^2\right)\lambda$$
$$+ 6\left(6py_0^2 + 3qy_0^4 + 2ry_0^6 + 6\dot{y}_0^2\right)\left(pc_0^2 + 36py_0^2 + 18qy_0^4 + 12ry_0^6 + 36\dot{y}_0^2\right)\lambda^2$$
$$- \left(6py_0^2 + 3qy_0^4 + 2ry_0^6 + 6\dot{y}_0^2\right)^2\lambda^3 = 0.$$

Eliminating c_0 from this system gives the sextic

$$D_0 + D_1\lambda + D_2\lambda^2 + D_3\lambda^3 + D_4\lambda^4 + D_5\lambda^5 + D_6\lambda^6 = 0, \tag{35}$$

where

$$D_0 = 64\left(2ry_0^6 + 3qy_0^4 + 6py_0^2 + 6\dot{y}_0^2\right)\left(2r^2y_0^6 + 3qry_0^4 + 6pry_0^2 + 6r\dot{y}_0^2 + 9pq\right)^2,$$

$$D_1 = 576\left(2r^2y_0^6 + 3qry_0^4 + 6pry_0^2 + 6r\dot{y}_0^2 + 9pq\right)$$

$$quad\begin{pmatrix} 4r^3y_0^{12} + 12qr^2y_0^{10} + 24pr^2y_0^8 + 9q^2ry_0^8 + 24r^2\dot{y}_0^2y_0^6 + \\ 50pqry_0^6 + 21pq^2y_0^4 + 36qr\dot{y}_0^2y_0^4 + 36p^2ry_0^4 + 72pr\dot{y}_0^2y_0^2 + 42p^2qy_0^2 + \\ 36r\dot{y}_0^4 + 24p^3 + 42pq\dot{y}_0^2 \end{pmatrix},$$

$$D_2 = 144\begin{pmatrix} 88r^5y_0^{18} + 396qr^4y_0^{16} + 792pr^4y_0^{14} + 594q^2r^3y_0^{14} + \\ 3056pqr^3y_0^{12} + 309q^3r^2y_0^{12} + 792r^4\dot{y}_0^2y_0^{12} + 2376p^2r^3y_0^{10} + \\ 3822pq^2r^2y_0^{10} + 2376qr^3\dot{y}_0^2y_0^{10} + 36q^4ry_0^{10} + 27q^5y_0^8 + \\ 7644p^2qr^2y_0^8 + 4752pr^3\dot{y}_0^2y_0^8 + 1782q^2r^2\dot{y}_0^2y_0^8 + 1602pq^3ry_0^8 + \\ 108pq^4y_0^6 + 2376r^3\dot{y}_0^4y_0^6 + 2664p^3r^2y_0^6 + 11208pqr^2\dot{y}_0^2y_0^6 + \\ 72q^3r\dot{y}_0^2y_0^6 + 7254p^2q^2ry_0^6 + 3564qr^2\dot{y}_0^4y_0^4 + 1809p^2q^3y_0^4 + \\ 108q^4\dot{y}_0^2y_0^4 + 7128p^2r^2\dot{y}_0^2y_0^4 + 6120pq^2r\dot{y}_0^2y_0^4 + \\ 6552p^3qry_0^4 + 7128pr^2\dot{y}_0^4y_0^2 + 3402p^3q^2y_0^2 + \\ 216pq^3\dot{y}_0^2y_0^2 + 12240p^2qr\dot{y}_0^2y_0^2 + 864p^4ry_0^2 + 2376r^2\dot{y}_0^6 + \\ 108q^3\dot{y}_0^4 + 6120pqr\dot{y}_0^4 + 3402p^2q^2\dot{y}_0^2 + 864p^3r\dot{y}_0^2 + 1728p^4q \end{pmatrix},$$

$$D_3 = 864\begin{pmatrix} 8r^5y_0^{18} + 36qr^4y_0^{16} + 72pr^4y_0^{14} + 54q^2r^3y_0^{14} + 312pqr^3y_0^{12} + 39q^3r^2y_0^{12} + 72r^4\dot{y}_0^2y_0^{12} + \\ 216p^2r^3y_0^{10} + 450pq^2r^2y_0^{10} + 216qr^3\dot{y}_0^2y_0^{10} + 36q^4ry_0^{10} + 27q^5y_0^8 + 900p^2qr^2y_0^8 + 432pr^3\dot{y}_0^2y_0^8 + \\ 162q^2r^2\dot{y}_0^2y_0^8 + 288pq^3ry_0^8 + 108pq^4y_0^6 + 216r^3\dot{y}_0^4y_0^6 + 232p^3r^2y_0^6 + 1224pqr^2\dot{y}_0^2y_0^6 + \\ 72q^3r\dot{y}_0^2y_0^6 + 1038p^2q^2ry_0^6 + 324qr^2\dot{y}_0^4y_0^4 + 369p^2q^3y_0^4 + 108q^4\dot{y}_0^2y_0^4 + 648p^2r^2\dot{y}_0^2y_0^4 + \\ 864pq^2r\dot{y}_0^2y_0^4 + 888p^3qry_0^4 + 648pr^2\dot{y}_0^4y_0^2 + 522p^3q^2y_0^2 + 216pq^3\dot{y}_0^2y_0^2 + 1728p^2qr\dot{y}_0^2y_0^2 + \\ 48p^4ry_0^2 + 216r^2\dot{y}_0^6 + 108q^3\dot{y}_0^4 + 864pqr\dot{y}_0^4 + 522p^2q^2\dot{y}_0^2 + 48p^3r\dot{y}_0^2 + 216p^4q \end{pmatrix},$$

$$D_4 = 108\begin{pmatrix} -88r^5y_0^{18} - 396qr^4y_0^{16} - 792pr^4y_0^{14} - 594q^2r^3y_0^{14} - 2496pqr^3y_0^{12} - 145q^3r^2y_0^{12} - 792r^4\dot{y}_0^2y_0^{12} - \\ 2376p^2r^3y_0^{10} - 2142pq^2r^2y_0^{10} - 2376qr^3\dot{y}_0^2y_0^{10} + 456q^4ry_0^{10} + 342q^5y_0^8 - 4284p^2qr^2y_0^8 - \\ 4752pr^3\dot{y}_0^2y_0^8 - 1782q^2r^2\dot{y}_0^2y_0^8 + 642pq^3ry_0^8 + 1368pq^4y_0^6 - 2376r^3\dot{y}_0^4y_0^6 - 2440p^3r^2y_0^6 - \\ 7848pqr^2\dot{y}_0^2y_0^6 + 912q^3r\dot{y}_0^2y_0^6 - 510p^2q^2ry_0^6 - 3564qr^2\dot{y}_0^4y_0^4 + \\ 2223p^2q^3y_0^4 + 1368q^4\dot{y}_0^2y_0^4 - 7128p^2r^2\dot{y}_0^2y_0^4 - 1080pq^2r\dot{y}_0^2y_0^4 - \\ 1176p^3qry_0^4 - 7128pr^2\dot{y}_0^4y_0^2 + 1710p^3q^2y_0^2 + 2736pq^3\dot{y}_0^2y_0^2 - 2160p^2qr\dot{y}_0^2y_0^2 - \\ 192p^4ry_0^2 - 2376r^2\dot{y}_0^6 + 1368q^3\dot{y}_0^4 - 1080pqr\dot{y}_0^4 + 1710p^2q^2\dot{y}_0^2 - 192p^3r\dot{y}_0^2 + 576p^4q \end{pmatrix},$$

$$D_5 = 324\begin{pmatrix} 8r^5y_0^{18} + 36qr^4y_0^{16} + 72pr^4y_0^{14} + 54q^2r^3y_0^{14} + 216pqr^3y_0^{12} + 35q^3r^2y_0^{12} + 72r^4\dot{y}_0^2y_0^{12} + 216p^2r^3y_0^{10} + 162pq^2r^2y_0^{10} + \\ 216qr^3\dot{y}_0^2y_0^{10} + 24q^4ry_0^{10} + 18q^5y_0^8 + 324p^2qr^2y_0^8 + 432pr^3\dot{y}_0^2y_0^8 + \\ 162q^2r^2\dot{y}_0^2y_0^8 + 48pq^3ry_0^8 + 72pq^4y_0^6 + 216r^3\dot{y}_0^4y_0^6 + 200p^3r^2y_0^6 + 648pqr^2\dot{y}_0^2y_0^6 + \\ 48q^3r\dot{y}_0^2y_0^6 + 30p^2q^2ry_0^6 + 324qr^2\dot{y}_0^4y_0^4 + 117p^2q^3y_0^4 + 72q^4\dot{y}_0^2y_0^4 + 648p^2r^2\dot{y}_0^2y_0^4 - 24p^3qry_0^4 + \\ 648pr^2\dot{y}_0^4y_0^2 + 90p^3q^2y_0^2 + 144pq^3\dot{y}_0^2y_0^2 - 48p^4ry_0^2 + 216r^2\dot{y}_0^6 + 72q^3\dot{y}_0^4 + 90p^2q^2\dot{y}_0^2 - 48p^3r\dot{y}_0^2 + 24p^4q \end{pmatrix},$$

$$D_6 = -27\left(2ry_0^6 + 3qy_0^4 + 6py_0^2 + 6\dot{y}_0^2\right)\begin{pmatrix} 4r^4y_0^{12} + 12qr^3y_0^{10} + 24pr^3y_0^8 + 9q^2r^2y_0^8 + \\ 48pqr^2y_0^6 + 24r^3\dot{y}_0^2y_0^6 - 2q^3ry_0^6 - 3q^4y_0^4 + 36p^2r^2y_0^4 + 36qr^2\dot{y}_0^2y_0^4 + \end{pmatrix},$$

$$D_6 = -27\left(2ry_0^6 + 3qy_0^4 + 6py_0^2 + 6\dot{y}_0^2\right).$$

(36)

Sextic (34) has at least one real root. Indeed, let z_j ($j = 1, 2, 3, 4, 5, 6$) be its roots. Then,

$$z_1 z_2 z_3 z_4 z_5 z_6 = \frac{D_0}{D_6}$$

$$= \frac{64\left(9pq + 6pr y_0^2 + 3qr y_0^4 + 2r^2 y_0^6 + 6r \dot{y}_0^2\right)^2}{27\Delta} < 0.$$

$$(37)$$

We will choose the closest to zero real root to sextic (34). The values for c_0 and c_1 are determined from the initial conditions:

$$c_1 = \mathrm{cn}^{-1}\left(\sqrt{\frac{c_0^2 - \lambda y_0^2 \pm \sqrt{\left(c_0^2 - \lambda y_0^2\right)^2 - 4\mu y_0^4}}{2\mu y_0^2}} \,\middle|\, m \right). \quad (38)$$

The number c_0 is found from the algebraic equation:

$$\left(6\lambda y_0^6 - 15\lambda y_0^4 + 15\lambda y_0^2 + 3\lambda \dot{y}_0^2 + 2y_0^6 - 5y_0^4 + 5y_0^2 + \dot{y}_0^2 - 5c_0^2\right)$$

$$\left(\left(2y_0^6 - 5y_0^4 + \dot{y}_0^2\right)c_0^2 + 4\lambda y_0^8 - 10\lambda y_0^6 + 10\lambda y_0^4 + 2\lambda \dot{y}_0^2 y_0^2\right)$$

$$\begin{pmatrix} \left(2y_0^6 - 5y_0^4 + 5y_0^2 + \dot{y}_0^2\right)c_0^4 + \\ \left(-4\lambda y_0^8 + 10\lambda y_0^6 - 10\lambda y_0^4 - 2\lambda \dot{y}_0^2 y_0^2 - 20y_0^4\right)c_0^2 + \\ 2\lambda^2 y_0^{10} - 5\lambda^2 y_0^8 + 5\lambda^2 y_0^6 + \lambda^2 \dot{y}_0^2 y_0^4 + 24\lambda y_0^{10} - 60\lambda y_0^8 + \\ 60\lambda y_0^6 + 12\lambda \dot{y}_0^2 y_0^4 + 8y_0^{10} - 20y_0^8 + 20y_0^6 + 4\dot{y}_0^2 y_0^4 \end{pmatrix} = 0.$$

$$(39)$$

Example 2. Let $p = q = r = y_0 = \dot{y}_0 = 1$. The i.v.p. problem to be solved is

$$y''\prime(t) + y(t) + y(t)^3 + y(t)^5 = 0 \text{ given that } y(0)$$

$$= 1 \text{ and } y'(0) \quad (40)$$

$$= 1.$$
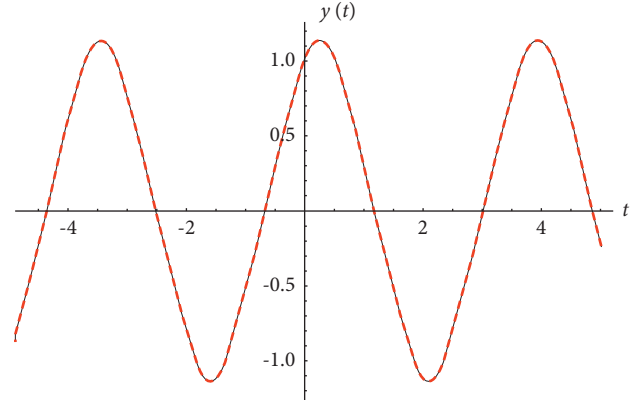
FIGURE 2: Comparison between the numerical and the exact solution for the i.v.p. (40).

This problem has a negative discriminant $\Delta = -387$. Sextic (35) reads

$$177633\lambda^6 - 1825416\lambda^5 + 5060232\lambda^4 - 12568608\lambda^3$$

$$- 16971120\lambda^2 - 6469632\lambda - 735488 = 0. \quad (41)$$

The roots are

$$\lambda_1 = -0.404933 - 0.145779i,$$

$$\lambda_2 = -0.404933 + 0.145779i,$$

$$\lambda_3 = -0.208601,$$

$$\lambda_4 = 1.63821 - 3.26816i, \quad (42)$$

$$\lambda_5 = 1.63821 + 3.26816i,$$

$$\lambda_6 = 8.01838.$$

We choose $\lambda = \lambda_3 = -0.208601$. The values for c_0 and c_1 are

$$c_0 - 0.993235, c_1 = 2.72596. \quad (43)$$

The exact solution is given by

$$y(t) = -\frac{0.993235\,\mathrm{cn}\,(1.71662t + 2.72596|0.0253557)}{\sqrt{-0.0260153\,\mathrm{cn}\,(1.71662t + 2.72596|0.0253557)^4 - 0.208601\,\mathrm{cn}\,(1.71662t + 2.72596|0.0253557)^2 + 1}}. \quad (44)$$

See Figure 2, for a comparison with the numerical solution.

2.3. Third Case: $\Delta = 0$. In this case, we have two roots to the cubic:

$$z_1 = \frac{1}{9}\left(\frac{8p^2}{4p^2 + q\left(6py_0^2 + 3qy_0^4 + 2ry_0^6 + 6\dot{y}_0^2\right)} + \frac{4pr + q^2}{q^2 - 4pr}\right),$$

and $\quad (45)$

$$z_2 = \frac{1}{9}\left(\frac{8p^2}{4p^2 + q\left(6py_0^2 + 3qy_0^4 + 2ry_0^6 + 6\dot{y}_0^2\right)} + \frac{4pr + q^2}{q^2 - 4pr}\right).$$

At least one of these two numbers must be positive. So, we proceed the same way as we did for a positive discriminant.

2.4. Two Particular Cases

2.4.1. First Particular Case: $\dot{y}_0 = 0$. Let

$$y''(t) + py(t) + qy(t)^3 + ry(t)^5 = 0 \text{ given that } y(0)$$
$$= y_0 \text{ and } y'(0) \quad (46)$$
$$= 0.$$

The discriminant to the i.v.p. (46) equals

$$\Delta_1 = \left(p + qy_0^2 + ry_0^4\right)^2 \left(3q^2 - 4qry_0^2 - 4r^2y_0^4 - 16pr\right). \quad (47)$$

If $\Delta_1 > 0$, then the exact solution is given by

$$y(t) = \frac{\sqrt{\lambda + 1}y_0 \operatorname{cn}(t\sqrt{\omega}\,|m)}{\sqrt{1 + \lambda \operatorname{cn}(t\sqrt{\omega}\,|m)^2}}, \quad (48)$$

where

$$m = \frac{2\lambda(3\lambda + 2)p + (\lambda + 1)(3\lambda + 1)qy_0}{(\lambda + 1)((6\lambda + 2)p + (3\lambda + 2)qy_0)},$$

$$\omega = \frac{(\lambda + 1)((6\lambda + 2)p + (3\lambda + 2)qy_0)}{6\lambda(\lambda + 1) + 2},$$

$$\lambda = -\frac{y_0\left(3q + 6ry_0 \pm \sqrt{3}\sqrt{3q^2 - 16pr - 4qry_0 - 4r^2y_0}\right)}{12(p + qy_0 + ry_0)}. \quad (49)$$

Assume now a negative discriminant. The exact solution reads

$$\omega = \frac{2p(\lambda(3\lambda + 4) - 5\mu + 1) + (3\lambda + 2)qy_0^2(\lambda + \mu + 1)}{6\lambda(\lambda + 1) + 10\mu + 2},$$

$$m = \frac{2p(\lambda(3\lambda + 2) - 5\mu) + (3\lambda + 1)qy_0^2(\lambda + \mu + 1)}{2p(\lambda(3\lambda + 4) - 5\mu + 1) + (3\lambda + 2)qy_0^2(\lambda + \mu + 1)},$$

$$\lambda = \frac{2\left(3q + 2ry_0^2\right)\left(-2\sqrt{6}\,\Delta_2 + 12p + 9qy_0^2 + 6ry_0^4\right)}{3y_0^2\left(16pr - 3q^2 + 4ry_0^2\left(q + ry_0^2\right)\right)}, \quad (50)$$

$$\mu = \frac{-96p^2 + 16p\left(\sqrt{6}\,\Delta_2 - 9qy_0^2 - 7ry_0^4\right) + y_0^2\left(3q + 2ry_0^2\right)\left(4\sqrt{6}\,\Delta_2 - 17qy_0^2 - 14ry_0^4\right)}{y_0^4\left(16pr - 3q^2 + 4ry_0^2\left(q + ry_0^2\right)\right)},$$

where

$$\Delta_2 = \sqrt{\left(p + qy_0^2 + ry_0^4\right)\left(6p + 3qy_0^2 + 2ry_0^4\right)}.$$

We claim that $\Delta_2 > 0$. Indeed, let

$$\delta = 3q^2 - 4qry_0^2 - 4r^2y_0^4 - 16pr. \quad (51)$$

Then, $\delta < 0$. However,

$$\Delta_2 = \frac{\left(3\left(q + 2ry_0^2\right)^2 - \delta\right)\left(\left(3q + 2ry_0^2\right)^2 - 3\delta\right)}{128r^2}. \quad (52)$$

From the last identity, it is clear that $\Delta_2 > 0$.

Assume now that $\Delta_1 = 0$. In this case, we have the following solutions:

$$y(t) = \frac{y_0\sqrt{3q + 2ry_0^2}\cos\left(1/4\sqrt{(q + 2ry_0^2)(3q + 2ry_0^2)/r}\,t\right)}{\sqrt{3q + 4ry_0^2 - 2ry_0^2\cos\left(1/4\sqrt{(q + 2ry_0^2)(3q + 2ry_0^2)/r}\,t\right)}} \text{ for } \frac{(q + 2ry_0^2)(3q + 2ry_0^2)}{r} > 0,$$

(53)

$$y(t) = \frac{y_0\sqrt{3q + 2ry_0^2}\cosh\left(1/4\sqrt{-(q + 2ry_0^2)(3q + 2ry_0^2)/r}\,t\right)}{\sqrt{3q + 4ry_0^2 - 2ry_0^2\cosh\left(1/4\sqrt{-(q + 2ry_0^2)(3q + 2ry_0^2)/r}\,t\right)}} \text{ for } \frac{(q + 2ry_0^2)(3q + 2ry_0^2)}{r} < 0.$$

Solutions (53) are called solitons. They arise in soliton theory.

2.4.2. Second Particular Case: $y_0 = 0$. Let

$$y''(t) + py(t) + qy(t)^3 + ry(t)^5 = 0 \text{ given that } y(0) = 0 \text{ and } y'(0) = \dot{v}_0.$$

(54)

The solution has the form

$$y(t) = \frac{\dot{v}_0\sqrt{\lambda + \mu + 1}\cdot \text{sn}\left(x\sqrt{-p(\lambda + \mu + 1)/2\lambda + 4\mu - 1}\,|\mu/\lambda + \mu + 1\right)}{\sqrt{-p(\lambda + \mu + 1)/2\lambda + 4\mu - 1}\sqrt{1 + \mu\cdot \text{cn}\left(x\sqrt{-p(\lambda + \mu + 1)/2\lambda + 4\mu - 1}\,|\mu/\lambda + \mu + 1\right)^4 + \lambda\cdot \text{cn}\left(x\sqrt{-p(\lambda + \mu + 1)/2\lambda + 4\mu - 1}\,|\mu/\lambda + \mu + 1\right)^2}}.$$

(55)

The values of λ and μ are obtained by solving the two sextics:

$$P(\lambda) = 0 \text{ and } Q(\mu) = 0,$$

(56)

where

$$\begin{aligned}
P(\lambda) = {}& \dot{v}_0^2\left(9q^3 - 48pqr - 64r^2\dot{v}_0^2\right) + 12\left(-3p^2q^2 + 16p^3r - 3q^3\dot{v}_0^2 + 20pqr\dot{v}_0^2 + 16r^2\dot{v}_0^4\right)\lambda \\
& + 6\left(-3p^2q^2 + 16p^3r + 3q^3\dot{v}_0^2 - 12pqr\dot{v}_0^2 - 16r^2\dot{v}_0^4\right)\lambda^2 + 4\dot{v}_0^2\left(9q^3 - 48pqr - 32r^2\dot{v}_0^2\right)\lambda^3 \\
& + 3\dot{v}_0^2\left(3q^3 - 16pqr + 16r^2\dot{v}_0^2\right)\lambda^4 + 48r^2\dot{v}_0^4\lambda^5 + 8r^2\dot{v}_0^4\lambda^6,
\end{aligned}$$

(57)

and

$$\begin{aligned}
Q(\mu) = {}& 3\dot{v}_0^4\left(3p^2q^2 - 16p^3r + 6q^3\dot{v}_0^2 - 36pqr\dot{v}_0^2 - 36r^2\dot{v}_0^4\right) \\
& - 144\left(4p^6 + 17p^4q\dot{v}_0^2 + 21p^2q^2\dot{v}_0^4 + 14p^3r\dot{v}_0^4 + 6q^3\dot{v}_0^6 + 27pqr\dot{v}_0^6 + 18r^2\dot{v}_0^8\right)\mu \\
& + 96\left(6p^6 + 48p^4q\dot{v}_0^2 + 129p^2q^2\dot{v}_0^4 - 124p^3r\dot{v}_0^4 + 114q^3\dot{v}_0^6 - 252pqr\dot{v}_0^6 - 198r^2\dot{v}_0^8\right)\mu^2 \\
& - 768\dot{v}_0^2\left(3p^4q + 15p^2q^2\dot{v}_0^2 - 10p^3r\dot{v}_0^2 + 18q^3\dot{v}_0^4 - 18pqr\dot{v}_0^4 + 36r^2\dot{v}_0^6\right)\mu^3 \\
& + 768\dot{v}_0^4\left(3p^2q^2 + 8p^3r + 6q^3\dot{v}_0^2 + 28pqr\dot{v}_0^2 + 132r^2\dot{v}_0^4\right)\mu^4 - 12288r\dot{v}_0^6\left(pq + 6r\dot{v}_0^2\right)\mu^5 + 16384r^2\dot{v}_0^8\mu^6.
\end{aligned}$$

(58)

3. Applications

The cubic-quintic Duffing oscillator has many interesting applications in soliton theory, optics, nonlinear circuits, plasma physics, and other areas of science and engineering.

3.1. Nonlinear Odd Parity Oscillators.

3.1. Nonlinear Odd Parity Oscillators. Let us consider the nonlinear oscillator:

$$u\prime\prime(t) + f(u(t)) = 0 \text{ subjected to } u(0)$$
$$= u_0 \text{ and } u\prime(0) \quad (59)$$
$$= 0,$$

where $f(x)$ is and odd function:

$$f(-x) = -f(x). \quad (60)$$

We may approximate the function $f = f(x)$ by means of a Chebyshev polynomial on some interval $[-A, A]$ $(A > 0)$ as follows:

$$f(x) \approx px + qx^3 + rx^5, \quad (61)$$

where

$$\begin{cases} p = \dfrac{f(-A\sqrt{2}/2) - f(A\sqrt{2}/2) - (5+3\sqrt{3})f(-1/2\sqrt{2-\sqrt{3}}\,A) + (5+3\sqrt{3})f(1/2\sqrt{2-\sqrt{3}}\,A) + (5-3\sqrt{3})(f(-1/2\sqrt{2+\sqrt{3}}\,A) - f(1/2\sqrt{2+\sqrt{3}}\,A))}{3\sqrt{2}\,A}, \\[3mm] q = \dfrac{\sqrt{2}\,(-8f(-A\sqrt{2}/2) + 8f(A\sqrt{2}/2) + (7+5\sqrt{3})f(-1/2\sqrt{2-\sqrt{3}}\,A) - (7+5\sqrt{3})f(1/2\sqrt{2-\sqrt{3}}\,A) + (5\sqrt{3}-7)(f(-1/2\sqrt{2+\sqrt{3}}\,A) - f(1/2\sqrt{2+\sqrt{3}}\,A)))}{3A^3}, \\[3mm] r = \dfrac{4\sqrt{2}\,(1+\sqrt{3})((\sqrt{3}-1)f(-A\sqrt{2}/2) - (\sqrt{3}-1)f(A\sqrt{2}/2) - f(-1/2\sqrt{2-\sqrt{3}}\,A) + f(1/2\sqrt{2-\sqrt{3}}\,A) + (\sqrt{3}-2)(f(-1/2\sqrt{2+\sqrt{3}}\,A) - f(1/2\sqrt{2+\sqrt{3}}\,A)))}{3A^5}. \end{cases} \quad (62)$$

Then, we may obtain an approximated analytic solution to oscillator (59) by solving the cubic-quintic Duffing oscillator:

$$y\prime\prime(t) + py(t) + qy(t)^3 + ry(t)^5 = 0 \text{ subjected to } y(0)$$
$$= u_0 \text{ and } y'(0) \quad (63)$$
$$= 0.$$

Example 3. Let us obtain an approximate analytical solution to the pendulum equation:

$$\theta\prime\prime(t) + k^2 \sin(\theta(t)) = 0 \text{ subjected to } \theta(0)$$
$$= \theta_0 \text{ and } \theta\prime(0) \quad (64)$$
$$= 0,$$

having the analytical solution [9]

$$\theta(t) = 2\tan^{-1}\left(\tan\left(\frac{\theta_0}{2}\right)\text{cn}\left(k\cdot t \mid \sin^2\left(\frac{\theta_0}{2}\right)\right)\right). \quad (65)$$

The Chebyshev approximant $P(x)$ of $f(x) = \sin x$ on $[-\pi/2, \pi/2]$ reads

$$P(x) = 16\sqrt{2}\left(\sin\left(\frac{\pi}{\sqrt{2}}\right) - \sqrt{3}\,\sin\left(\frac{1}{2}\sqrt{\frac{3}{2}}\pi\right)\cos\left(\frac{\pi}{2\sqrt{2}}\right) + \sin\left(\frac{\pi}{2\sqrt{2}}\right)\cos\left(\frac{1}{2}\sqrt{\frac{3}{2}}\pi\right)\right) - 3\pi^5 x^5$$

$$+ 4\sqrt{2}\left(4\sin\left(\frac{\pi}{\sqrt{2}}\right) - 5\sqrt{3}\,\sin\left(\frac{1}{2}\sqrt{\frac{3}{2}}\pi\right)\cos\left(\frac{\pi}{2\sqrt{2}}\right) + 7\sin\left(\frac{\pi}{2\sqrt{2}}\right)\cos\left(\frac{1}{2}\sqrt{\frac{3}{2}}\pi\right)\right)3\pi^3 x^3 \quad (66)$$

$$- \sqrt{2}x\left(\sin\left(\frac{\pi}{\sqrt{2}}\right) - 6\sqrt{3}\,\sin\left(\frac{1}{2}\sqrt{\frac{3}{2}}\pi\right)\cos\left(\frac{\pi}{2\sqrt{2}}\right) + 10\sin\left(\frac{\pi}{2\sqrt{2}}\right)\cos\left(\frac{1}{2}\sqrt{\frac{3}{2}}\pi\right)\right)3\pi.$$

We may rationalize this expression up to 10^{-7} to obtain

$$P(x) = \frac{17x^5}{2926} - \frac{2461x^3}{15601} + \frac{1641x}{1649}. \quad (67)$$

The square mean error is

$$\sqrt{\int_{-\pi}^{\pi} (\sin x - P(x))^2} = 0.0141773. \qquad (68)$$

Thus, our aim is to solve the cubic-quintic Duffing oscillator:

$$y\prime\prime(t) + \frac{1641k^2}{1649} y(t) - \frac{2461k^2}{15601} y^3(t) + \frac{17k^2}{2926} y^5(t) = 0 \text{ subjected to } y(0)$$

$$= \theta_0 \text{ and } y'(0)$$

$$= 0. \qquad (69)$$

Let $k = 1$ and $\theta_0 = 5\pi/6$. For these data, we have a positive discriminant and the solution to the initial value problem,

$$y\prime\prime(t) + \frac{1641}{1649} y(t) - \frac{2461}{15601} y^3(t) + \frac{17}{2926} y^5(t) = 0 \text{ subjected to } y(0)$$

$$= \frac{5\pi}{6} \text{ and } y'(0)$$

$$= 0, \qquad (70)$$

may be obtained making use of formula (48).

3.2. The Duffing–Helmholtz Oscillator.

Let us consider the i.v.p.:

$$x\prime\prime(t) + \alpha x(t) + \beta x^2(t) + \gamma x^3(t) = 0 \text{ given that } x(0)$$

$$= x_0 \text{ and } x\prime(0) \qquad (71)$$

$$= \dot{x}_0.$$

Suppose that the function $y = y(t)$ is the solution to the cubic-quintic Duffing equation:

$$y\prime\prime(t) + \frac{1}{4}\left(\alpha + 2A\beta + 3A^2\gamma\right)y(t)$$

$$-\frac{1}{3}(A - x_0)(\beta + 3A\gamma)y(t)^3 + \frac{3}{8}(A - x_0)^2\gamma y(t)^5$$

given that

$$y(0)$$

$$= 1 \text{ and } y'(0)$$

$$= \frac{\dot{x}_0}{2(x_0 - A)}. \qquad (72)$$

Then, the function,

$$x(t) = A + (x_0 - A)y^2(t), \qquad (73)$$

is the solution to the i.v.p. (71) provided that A is a solution to the quartic:

$$3\gamma A^4 + 4\beta A^3 + 6\alpha A^2 - 6\alpha x_0^2 - 4\beta x_0^3 - 3\gamma x_0^4 - 6\dot{x}_0^2 = 0. \qquad (74)$$

3.3. Nonlinear Conservative Oscillators.

Suppose we are given to sole the i.v.p.:

$$u\prime\prime(t) + g(u(t)) = 0 \text{ subjected to } u(0)$$

$$= u_0 \text{ and } u\prime(0) \qquad (75)$$

$$= \dot{u}_0.$$

Assume that $|u| \le A$. We approximate the function $g = g(u)$ by means of a cubic polynomial on $-A \le u \le A$ using Chebyshev approach so that

$$g(u) \approx a_0 + a_1 u + a_2 u^2 + a_3 u^3, -A \le u \le A, \qquad (76)$$

where

$$a_0 = \frac{\cos^2(\pi/8)(g(-A\sin(\pi/8)) + g(A\sin(\pi/8))) - \sin^2(\pi/8)(g(-A\cos(\pi/8)) + g(A\cos(\pi/8)))}{\sqrt{2}},$$

$$a_1 = \frac{(\sqrt{2} - 1)\left(8\sec(\pi/8)(g(-A\cos(\pi/8)) - g(A\cos(\pi/8))) + \csc^5(\pi/8)(g(A\sin(\pi/8)) - g(-A\sin(\pi/8)))\right)}{32A},$$

$$a_2 = \frac{-g(-A\sin(\pi/8)) - g(A\sin(\pi/8)) + g(-A\cos(\pi/8)) + g(A\cos(\pi/8))}{\sqrt{2}A^2},$$

$$a_3 = \frac{(\sqrt{2} - 1)\csc^2(\pi/8)\sec(\pi/8)(-g(-A\cos(\pi/8)) + g(A\cos(\pi/8)) + \cot(\pi/8)(g(-A\sin(\pi/8)) - g(A\sin(\pi/8))))}{4A^3}.$$

$$(77)$$

We now replace the i.v.p. (75) with the i.v.p.:

$$u\prime\prime(t) + a_0 + a_1 u(t) + a_2 u^2(t) + a_3 u^3(t) = 0 \text{ subjected to } u(0)$$
$$= u_0 \text{ and } u\prime(0)$$
$$= \dot{u}_0. \tag{78}$$

Let

$$u(t) = \rho + x(t), \text{ where } a_0 + a_1\rho + a_2\rho^2 + a\rho^3. \tag{79}$$

The problem reduces to the i.v.p.:

$$x\prime\prime(t) + \left(a_1 + 2\rho a_2 + 3\rho^2 a_3\right)x(t)$$
$$+ \left(a_2 + 3\rho a_3\right)x^2(t) + a_3 x^3(t) = 0 \text{ given that } x(0)$$
$$= u_0 - \rho \text{ and } x\prime(0) \tag{80}$$
$$= \dot{u}_0.$$

This is a Duffing–Helmholtz oscillator (71) with

$$\alpha = a_1 + 2\rho a_2 + 3\rho^2 a_3, \beta$$
$$= a_2 + 3\rho a_3 \text{ and } \gamma \tag{81}$$
$$= a_3.$$

4. Analysis and Discussion

We have solved the cubic-quintic Duffing oscillator equation for any given arbitrary initial conditions. In [1], authors considered the particular case:

$$\frac{d^2 x}{dt^2} + a_1 x + a_3 x^3 + a_5 x^5 = 0 \text{ given that } x(0)$$
$$= A > 0 \text{ and } \frac{dx}{dt}(0) \tag{82}$$
$$= 0,$$

under the restrictions,

$$a_1 \geq 0, a_3 \geq 0 \text{ and } a_5 \geq 0. \tag{83}$$

These conditions, however, are too restrictive. In [6], author considered the ansatz:

$$y^2(t) = \frac{1}{a + b\text{cn}^2\left(\omega t + \phi, k^2\right)}. \tag{84}$$

This approach does not allow to determine the sign of $y(t)$. On the contrary, this ansatz sometimes gives complex values for ω or k, which makes it difficult to interpret the obtained solution physically. Our approach avoids obtaining such complex values.

Other authors solved this equation using perturbative methods [2, 4, 7–9]. In [5], author studied the stability analysis to a cubic-quintic Duffing equation. There are other numerical and analytical methods that allow to solve this oscillator equation.

The cubic-quintic Duffing oscillator may also be solved making use of perturbative methods. One of them is the famous Krylov–Bogoliubov–Mitropolsky method (KBM). For example, let us consider the following oscillator:

$$y''(t) + \omega_0^2 y(t) + \alpha y(t)^3 + \beta y(t)^5 = 0 \text{ given that } y(0)$$
$$= y_0 \text{ and } y'(0) \tag{85}$$
$$= \dot{y}_0.$$

Using the Krylov–Bogoliubov–Mitropolsky method gives the following approximate analytical solution:

$$y(t) = A\cos(\omega) - \frac{123\alpha A^4\beta + 63\alpha^2 A^2 - 96\alpha\omega_0^2 + 55A^6\beta^2 - 120A^2\beta\omega_0^2}{3072\omega_0^4}A^3\cos(3\omega)$$
$$+ \frac{9\alpha^2 + 5A^4\beta^2 + 9\alpha A^2\beta + 24\beta\omega_0^2}{9216\omega_0^4}A^5\cos(5\omega) + \frac{\beta\left(72\alpha + 95A^2\beta\right)}{294912\omega_0^4}A^7\cos(7\omega) + \frac{\beta^2}{98304\omega_0^4}A^9\cos(9\omega), \tag{86}$$

where

$$\omega = \omega(t)$$

$$= \left[\omega_0 + \frac{3\alpha}{8\omega_0}A^2 - \frac{5\left(3\alpha^2 - 16\beta\omega_0^2\right)}{256\omega_0^3}A^4 - \frac{5\alpha\beta}{64\omega_0^3}A^6 - \frac{55\beta^2}{3072\omega_0^3}A^8\right]t + B. \tag{87}$$

For the damped oscillator,

$$y'\prime(t) + 2\varepsilon y'(t) + \omega_0^2 y(t) + qy(t)^3 + ry(t)^5 = 0 \text{ given that } y(0)$$
$$= y_0 \text{ and } y'(0)$$
$$= \dot{y}_0. \tag{88}$$

The KBM gives

$$y(t) = a(t)\cos(\psi(t)) + \frac{4q + 5ra(t)^2}{128\omega_0^2} a(t)^3 \cos(3\psi(t))$$

$$+ \frac{r}{384\omega_0^2} a(t)^5 \cos(5\psi(t)),$$

$$(89)$$

where

$$a(t) = A \exp(-\varepsilon t) \text{ and } \psi(t)$$

$$= \omega_0 t + B + \frac{3\left(1 - e^{-2t\varepsilon}\right)}{16\varepsilon\omega_0} qA^2 + \frac{5\left(1 - e^{-4t\varepsilon}\right)}{64\varepsilon\omega_0} rA^4.$$

$$(90)$$

The constants A and B are determined from the initial conditions. These results are also valid for the cubic Duffing oscillator $(r = 0)$:

$$y''(t) + 2\varepsilon y'(t) + \omega_0^2 y(t) + qy(t)^3 = 0 \text{ given that } y(0)$$

$$= y_0 \text{ and } y'(0) \qquad (91)$$

$$= \dot{y}_0.$$

5. Conclusions

The cubic-quintic Duffing oscillator has been solved exactly for arbitrary initial conditions. The obtained results may be applied to solve strongly nonlinear conservative oscillators like the pendulum oscillator equation. We may go further by considering a damped oscillator of the form $\ddot{x} + 2\varepsilon\dot{x} + F(x) = 0$. In the case when $F(-x) = -F(x)$, we may approximate the function $F(x)$ by means of some cubic-quintic polynomial using Chebyshev approximation formulas. The solution is then assumed in the form $x(t) = \exp(-\rho t)y(t)$, where ρ is some parameter having a value near $\rho = \varepsilon$ and $y = y(t)$ is the exact solution to some cubic-quintic Duffing oscillator equation.

Data Availability

No data were used to support this study.

Conflicts of Interest

The authors declare that they have no conflicts of interest.

References

[1] A. Beléndez, T. Beléndez, F. J. Martínez, C. Pascual, M. L. Alvarez, and E. Arribas, "Exact solution for the unforced Duffing oscillator with cubic and quintic nonlinearities," *Nonlinear Dynamics*, vol. 86, no. 3, pp. 1687–1700, 2016.

[2] D. D. Ganji, M. Gorji, S. Soleimani, and M. Esmaeilpour, "Solution of nonlinear cubic-quintic Duffing oscillators using He's Energy Balance Method," *Journal of Zhejiang University - Science*, vol. 10, no. 9, pp. 1263–1268, 2009.

[3] A. I. Maïmistov, "Propagation of an ultimately short electromagnetic pulse in a nonlinear medium described by the fifth-order Duffing model," *Optics and Spectroscopy*, vol. 94, no. 2, pp. 251–257, 2003.

[4] A. H. Salas and S. C. Trujillo, "A new approach for solving the complex cubic-quintic duffing oscillator equation for given arbitrary initial conditions," *Mathematical Problems in Engineering*, vol. 2020, Article ID 3985975, 8 pages, 2020.

[5] M. O. Oyesanya and J. I. Nwamba, "Stability analysis of damped cubic-quintic duffing oscillator," *World Journal of Mechanics*, vol. 03, no. 01, pp. 43–57, 2013.

[6] A. Elías-Zúñiga, "Exact solution of the cubic-quintic Duffing oscillator," *Applied Mathematical Modelling*, vol. 37, no. 4, pp. 2574–2579, 2013.

[7] M. A. Hammad, A. H. Salas, and S. A. El-Tantawy, "New method for solving strong conservative odd parity nonlinear oscillators: applications to plasma physics and rigid rotator," *AIP Advances*, vol. 10, no. 8, Article ID 085001, 2020.

[8] A. V. Tsiganov, "On exact discretization of cubic-quintic Duffing oscillator," *Journal of Mathematical Physics*, vol. 59, no. 7, 2018.

WILEY | Hindawi

Research Article

Identities on Changhee Polynomials Arising from λ-Sheffer Sequences

Byung Moon Kim,[1] **Taekyun Kim** [iD],[2] **Jin-Woo Park** [iD],[3] **and Taha Ali Radwan**[4,5]

[1]*Department of Mechanical System Engineering, Dongguk University, 123 Dongdae-ro, Gyungju-si,
Gyeongsangbuk-do 38066, Republic of Korea*
[2]*Department of Mathematics, Kwangwoon University, Seoul 139-401, Republic of Korea*
[3]*Department of Mathematics Education, Daegu University, Gyungju-si 38453, Republic of Korea*
[4]*Department of Mathematics, College of Science and Arts, Qassim University, Ar Rass, Saudi Arabia*
[5]*Department of Mathematics and Statistics, Faculty of Management Technology and Information Systems, Port Said University,
Port Said, Egypt*

Correspondence should be addressed to Taekyun Kim; tkkim@kw.ac.kr and Jin-Woo Park; a0417001@daegu.ac.kr

In this paper, authors found a new and interesting identity between Changhee polynomials and some degenerate polynomials
such as degenerate Bernoulli polynomials of the first and second kind, degenerate Euler polynomials, degenerate Daehee
polynomials, degenerate Bell polynomials, degenerate Lah–Bell polynomials, and degenerate Frobenius–Euler polynomials and
Mittag–Leffer polynomials by using λ-Sheffer sequences and λ-differential operators to find the coefficient polynomial when
expressing the n-th Changhee polynomials as a linear combination of those degenerate polynomials. In addition, authors derive
the inversion formulas of these identities.

1. Introduction

Umbral calculus from 1850 to 1970 consisted primarily of symbolic techniques for sequence manipulation, and its mathematical rigor left little room for demands. In the 1970s, Gian-Carlo Rota began building a completely rigid foundation for theories based on relatively modern ideas of linear functions, linear operators, and adjacency functions (see [1–4]). Umbral calculus contributed to the generalization of Lagrange inversion formula and has been applied in many fields such as combinatorial counting with linear recurrences and lattice path counting, graph theory using chromatic polynomials, probability theory, link invariant theory, statistics, topology, and physics (see [3]). It is being actively applied in various fields by researchers (see [1–16]).

In the past few years, many distinct umbral calculus types have begun to be studied (see [2, 4, 6, 10]). In particular, Kim–Kim defined the degenerate Sheffer sequences,

λ-Sheffer sequence, a family of λ-linear functionals, and λ-differential operators as follows (see [2]).

Let $\mathbb{C}$ be the field of complex numbers:

$$\mathcal{F} = \left\{ f(t) = \sum_{n=0}^{\infty} a_k \frac{t^n}{n!} \middle| a_k \in \mathbb{C} \right\}, \tag{1}$$

and let

$$\mathbb{P} = \mathbb{C}[x] = \left\{ \sum_{k=0}^{\infty} a_l x^k \middle| a_k \in \mathbb{C} \text{ with } a_k \right.$$

$$\left. = 0 \text{ for all but finite number of } k \right\}. \tag{2}$$

Let $\mathbb{P}^*$ be the vector space of all linear functionals on $\mathbb{P}$.

Then, each real number λ gives rise to the linear functional $\left\langle f(t) \middle| \cdot \right\rangle_\lambda$ on $\mathbb{P}$, called λ-linear functional given by $f(t)$, which is defined by (see [2])

$$\left\langle f(t)|(x)_{n,\lambda}\right\rangle_{\lambda} = a_n, \quad (n \geq 0), \qquad (3)$$

and by linear extension where $(x)_{0,\lambda} = 1$, $(x)_{n,\lambda} = x(x - \lambda)$ $\cdots (x - (n-1)\lambda)$, $(n \geq 1)$. From (3), we have

$$\left\langle t^k|(x)_{n,\lambda}\right\rangle_{\lambda} = n!\delta_{n,k}, \quad (n, k \geq 0), \qquad (4)$$

where $\delta_{n,k}$ is Kronecker's symbol (see [2]).

For each real number λ and each positive integer k, Kim and Kim defined the differential operator on $\mathbb{P}$ in [2] as follows:

$$\left(t^k\right)_\lambda (x)_{n,\lambda} = \begin{cases} (n)_k (x)_{n-k,\lambda}, & \text{if } k \leq n, \\ 0, & \text{if } k > n, \end{cases} \qquad (5)$$

and for any $f(t) = \sum_{k=0}^\infty a_k (t^k/k!) \in \mathscr{F}$,

$$\left(f(t)\right)_\lambda (x)_{n,\lambda} = \sum_{k=0}^n \binom{n}{k} a_k (x)_{n-k,\lambda}. \qquad (6)$$

In addition, they showed that for $f(t), g(t) \in \mathscr{F}$ and $p(x) \in \mathbb{P}$,

$$\begin{aligned} \left\langle f(t)g(t)|p(x)\right\rangle_\lambda &= \left\langle g(t)|(f(t))_\lambda p(x)\right\rangle_\lambda \\ &= \left\langle f(t)|(g(t))_\lambda p(x)\right\rangle_\lambda. \end{aligned} \qquad (7)$$

The order $o(f(t))$ of $f(t) \in \mathscr{F} - \{0\}$ is the smallest integer k for which the coefficient of t^k does not vanish. If $o(f(t)) = 0$, then $f(t)$ is called invertible and such series has a multiplicative inverse $1/f(t)$ of $f(t)$. If $o(f(t)) = 1$, then $f(t)$ is called delta series and it has a compositional inverse $\overline{f}(t)$ of $f(t)$ with $\overline{f}(f(t)) = f(\overline{f}(t)) = t$ (see [1, 2, 12, 16]).

Let $f(t)$ be a delta series and let $g(t)$ be an invertible series. Then, there exists a unique sequence $S_{n,\lambda}(x)$ $(\deg S_{n,\lambda}(x) = n)$ of polynomials satisfying the orthogonality conditions (see [2])

$$\left\langle g(t)(f(t))^k|S_{n,\lambda}(x)\right\rangle_\lambda = n!\delta_{n,k}, \quad (n, k \geq 0). \qquad (8)$$

Here, $S_{n,\lambda}(x)$ is called the λ-Sheffer sequence for $(g(t), f(t))$, which is denoted by $S_{n,\lambda}(x) \sim (g(t), f(t))_\lambda$. The sequence $S_{n,\lambda}(x)$ is the λ-Sheffer sequence for $(g(t), f(t))$ if and only if

$$\frac{1}{g(\overline{f}(t))} e_\lambda^y(\overline{f}(t)) = \sum_{n=0}^\infty S_{n,\lambda}(y) \frac{t^n}{n!}, \qquad (9)$$

for all $y \in \mathbb{C}$, where $\overline{f}(t)$ is the compositional inverse of $f(t)$ such that $f(\overline{f}(t)) = \overline{f}(f(t)) = t$ (see [1, 2, 12, 16]).

Let $S_{n,\lambda}(x) \sim (g(t), f(t))_\lambda$ and let $h(x) = \sum_{l=0}^n a_l S_{l,\lambda}(x) \in \mathbb{P}$. Then, by (8), we have

$$\begin{aligned} \left\langle g(t)(f(t))^k|h(x)\right\rangle_\lambda &= \sum_{l=0}^n a_l \left\langle g(t)(f(t))^k|S_{l,\lambda}(x)\right\rangle_\lambda \\ &= k!a_k, \end{aligned} \qquad (10)$$

and thus we know that

$$a_k = \frac{1}{k!} \left\langle g(t)(f(t))^k \middle| h(x) \right\rangle_\lambda. \qquad (11)$$

The following theorem is proved by Kim and Kim [2] and is a very useful tool for researching degenerate versions of special polynomials and numbers.

Theorem 1. *Let* $s_{n,\lambda} \sim (g(t), f(t))_\lambda$, $r_{n,\lambda} = (h(t), l(t))_\lambda$. *Then, we have*

$$s_{n,\lambda} = \sum_{k=0}^n c_{n,k} r_{k,\lambda}, \qquad (12)$$

where

$$c_{n,k} = \frac{1}{k!} \left\langle \frac{h(\overline{f}(t))}{g(\overline{f}(t))} (l(\overline{f}(t)))^k \middle| (x)_{n,\lambda} \right\rangle_\lambda. \qquad (13)$$

For $n \geq 0$, the Stirling numbers of the first kind $\begin{bmatrix} n \\ k \end{bmatrix}$ and Stirling numbers of the second kind $\begin{Bmatrix} n \\ k \end{Bmatrix}$, respectively, are given by the following (see [11, 12, 17–20]):

$$(x)_n = \sum_{k=0}^n \begin{bmatrix} n \\ k \end{bmatrix} x^k \text{ and } x^n = \sum_{k=0}^n \begin{Bmatrix} n \\ k \end{Bmatrix} (x)_k. \qquad (14)$$

For each positive integer k, it is well known that (see [11, 12, 17–20])

$$\frac{1}{k!} (\log(1+t))^k = \sum_{n=k}^\infty \begin{bmatrix} n \\ k \end{bmatrix} \frac{t^n}{n!}, \frac{1}{k!} (e^t - 1)^k = \sum_{n=k}^\infty \begin{Bmatrix} n \\ k \end{Bmatrix} \frac{t^n}{n!}. \qquad (15)$$

For any nonzero real number λ, the degenerate exponential function is defined by (see [1, 21–27])

$$e_\lambda^x(t) = (1 + \lambda t)^{x/\lambda}, \quad e_\lambda(t) = (1 + \lambda t)^{1/\lambda}, \qquad (16)$$

Note that

$$\frac{e_\lambda(t) + 1}{2} = 1 + \frac{1}{2} \sum_{n=1}^\infty (1)_{n,\lambda} \frac{t^n}{n!}. \qquad (17)$$

A study of degenerate versions of some special numbers and polynomials was initiated by Carlitz who found interesting relationships connected with important numbers in combinatorics, Bernoulli polynomials, and Eulerian polynomials (see [28]). In the past decades, the study of degenerate versions of various special polynomials or numbers has been studied by many researchers (see [1, 2, 21–27, 29–32]).

By using (16), the higher-order degenerate Bernoulli polynomials are defined as follows (see [1, 10, 12, 30, 33, 34]):

$$\sum_{n=0}^\infty B_{n,\lambda}^{(r)}(x) \frac{t^n}{n!} = \left(\frac{t}{e_\lambda(t) - 1}\right)^r e_\lambda^x(t). \qquad (18)$$

When $x = 0$, $B_{n,\lambda}^{(r)}(0) = B_{n,\lambda}^{(r)}$ are called the higher-order degenerate Bernoulli numbers. In addition, when $r = 1$, we denote $B_{n,\lambda}^{(1)}(x) = B_{n,\lambda}(x)$.

On the other hand, Kim and Kim defined $\log_\lambda(t)$ called the degenerate logarithm function as the compositional inverse function of $e_\lambda(t)$ satisfying $\log_\lambda(e_\lambda(t)) = t$. Then, we have (see [1, 10, 22, 24, 32])

$$\log_\lambda (1 + t) = \sum_{n=1}^{\infty} \lambda^{n-1} (1)_{n,1/\lambda} \frac{t^n}{n!}. \qquad (19)$$

By using (19), the degenerate Bernoulli polynomials of the second kind are defined by the generating function to be (see [16])

$$\sum_{n=0}^{\infty} \beta_{n,\lambda} (x) \frac{t^n}{n!} = \frac{t}{\log_\lambda (1 + t)} e_\lambda^x (\log_\lambda (1 + t)). \qquad (20)$$

In the special case $x = 0$, $\beta_{n,\lambda} = \beta_{n,\lambda} (0)$ are called the Bernoulli numbers of the second kind.

As degenerate version of the Stirling numbers of the first and second kind in (14), the degenerate Stirling numbers of the first kind $\begin{bmatrix} n \\ k \end{bmatrix}_\lambda$ and the degenerate Stirling numbers of the second kind $\begin{Bmatrix} n \\ k \end{Bmatrix}_\lambda$ are, respectively, introduced by Kim–Kim (see [1, 2, 21, 22, 24, 26–30, 35, 36]) as follows:

$$\frac{1}{k!} (\log_\lambda (1 + t))^k = \sum_{n=k}^{\infty} \begin{bmatrix} n \\ k \end{bmatrix}_\lambda \frac{t^n}{n!} \text{ and } \frac{1}{k!} (e_\lambda (t) - 1)^k$$

$$= \sum_{n=k}^{\infty} \begin{Bmatrix} n \\ k \end{Bmatrix}_\lambda \frac{t^n}{n!}. \qquad (21)$$

Let $(x)_n = \sum_{k=0}^{n} c_{n,k} (x)_{k,\lambda}$. Since

$$(x)_{k,\lambda n} \sim (1, e_\lambda (t) - 1)_\lambda,$$
$$(x)_{n,\lambda} \sim (1, t)_\lambda, \qquad (22)$$

by Theorem 1, we obtain

$$c_{n,k} = \frac{1}{k!} \left\langle (\log_\lambda (1 + t))^k \middle| (x)_{n,\lambda} \right\rangle_\lambda$$

$$= \sum_{l=k}^{\infty} S_{1,\lambda} (l, k) \frac{1}{l!} \left\langle t^l \middle| (x)_{n,\lambda} \right\rangle_\lambda \qquad (23)$$

$$= \begin{bmatrix} n \\ k \end{bmatrix}_\lambda,$$

and thus, we know that

$$(x)_n = \sum_{k=0}^{n} \begin{bmatrix} n \\ k \end{bmatrix}_\lambda (x)_{k,\lambda}, \qquad (24)$$

where $(x)_0 = 1$, $(x)_n = x(x-1)\dots(x-n+1)$, $(n \geq 1)$ is the falling factorial sequences. In the similar way, we also know that

$$(x)_{n,\lambda} = \sum_{k=0}^{n} \begin{Bmatrix} n \\ k \end{Bmatrix}_\lambda (x)_k. \qquad (25)$$

The aim of this paper is to find some new and interesting identities related to the Changhee polynomials and some

special polynomials by using λ-Sheffer sequences and λ-differential operators. In more detail, we find the coefficients which are also polynomials or numbers when the n-th Changhee polynomial is expressed as a linear combination of some degenerate special polynomials by using the λ-Sheffer sequences and λ-differential operators (see Theorems 2–10), and by using the λ-Sheffer sequences and the linear combinations of those polynomials (see Theorems 5–8 and 10), and derive the inversion formulas of these identities.

2. Changhee Polynomials Arising from λ-Sheffer Sequences

In this section, we find some relationships between the Changhee polynomials and some special polynomials arising from λ-Sheffer sequences.

The Changhee polynomials are given by

$$\sum_{n=0}^{\infty} Ch_n (x) \frac{t^n}{n!} = \frac{2}{2 + t} (1 + t)^x. \qquad (26)$$

By (24) and (26), we obtain

$$\sum_{n=0}^{\infty} Ch_n (x) \frac{t^n}{n!} = \left(\sum_{n=0}^{\infty} Ch_n \frac{t^n}{n!} \right) \left(\sum_{n=0}^{\infty} (x)_n \frac{t^n}{n!} \right)$$

$$= \sum_{n=0}^{\infty} \left(\sum_{m=0}^{n} \binom{n}{m} Ch_{n-m} (x)_m \right) \frac{t^n}{n!}$$

$$= \sum_{n=0}^{\infty} \left(\sum_{m=0}^{n} \sum_{k=0}^{m} \binom{n}{m} \begin{bmatrix} m \\ k \end{bmatrix}_\lambda Ch_{n-m} (x)_{k,\lambda} \right) \frac{t^n}{n!}, \qquad (27)$$

and, by (27), we have

$$Ch_n (x) = \sum_{m=0}^{n} \sum_{k=0}^{m} \binom{n}{m} \begin{bmatrix} m \\ k \end{bmatrix}_\lambda Ch_{n-m} (x)_{k,\lambda}, \quad (n \geq 0). \qquad (28)$$

By (28), we compute the first few Changhee polynomials as follows:

$$Ch_0 (x) = 1,$$

$$Ch_1 (x) = x - \frac{1}{2},$$

$$Ch_2 (x) = x^2 - 2x + \frac{1}{2},$$

$$Ch_3 (x) = -x^3 + \frac{9}{2} x^2 - 5x + \frac{3}{4}, \qquad (29)$$

$$Ch_4 (x) = x^4 - 8x^3 + 20x^2 - 16x + \frac{3}{2},$$

$$Ch_5 (x) = -x^5 + \frac{25}{2} x^4 - 55x^3 + 100x^2 - 64x + \frac{15}{4}.$$

In addition, graphs for some Changhee polynomials are shown in Figure 1.
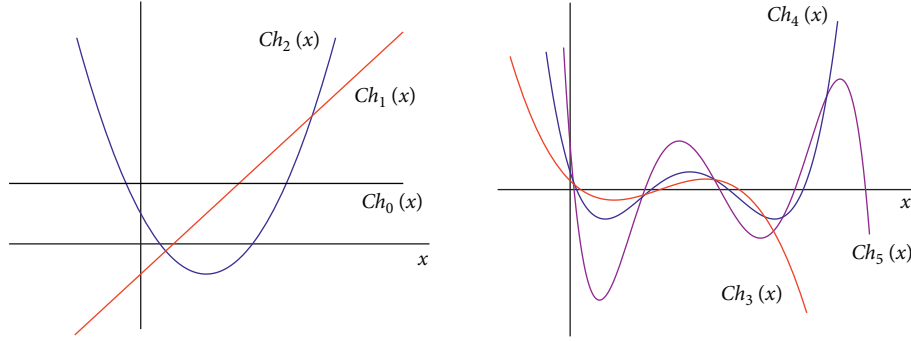
FIGURE 1: The shapes of Changhee polynomials $Ch_n(x)$.

Note that

$$\frac{1}{(t+2)^k} = (t+2)^{-k} = \sum_{l=0}^{\infty} \binom{-k}{l} t^l 2^{-k-l}$$

$$= \sum_{l=0}^{\infty} \frac{\langle k \rangle_l (-1)^l}{2^{l+k}} \frac{t^l}{l!}, \tag{30}$$

where $\langle x \rangle_0 = 1$, $\langle x \rangle_n = x(x+1)(x+2)\ldots(x+(n-1))$, $(n \geq 1)$.

Theorem 2. *For each nonnegative integer n, we have*

$$Ch_n(x) = \sum_{k=0}^{n} \left(\sum_{l=k}^{n} \binom{n}{l} \left[\begin{matrix} l \\ k \end{matrix} \right]_\lambda Ch_{n-l} \right) (x)_{k,\lambda}. \tag{31}$$

As the inversion formula of (31), we have

$$(x)_{n,\lambda} = \sum_{k=0}^{n} \left(\left\{ \begin{matrix} n \\ k \end{matrix} \right\}_\lambda + \frac{1}{2} \sum_{m=1}^{n-k} (1)_{m,\lambda} \binom{n}{m} \left\{ \begin{matrix} n-m \\ k \end{matrix} \right\}_\lambda \right) Ch_k(x). \tag{32}$$

Proof. Let $Ch_n(x) = \sum_{k=0}^{n} c_{n,k}(x)_{k,\lambda}$. Since

$$Ch_n(x) \sim \left(\frac{e_\lambda(t)+1}{2}, e_\lambda(t) - 1 \right)_\lambda, \tag{33}$$

$$(x)_{n,\lambda} \sim (1,t)_\lambda,$$

by Theorem 1 and (30), we have

$$c_{n,k} = \frac{1}{k!} \left\langle \frac{1}{((t+2)/2)} (\log_\lambda(1+t))^k \Big| (x)_{n,\lambda} \right\rangle_\lambda$$

$$= \left\langle \frac{2}{t+2} \Big| \left(\frac{1}{k!} (\log_\lambda(1+t))^k \right)_\lambda (x)_{n,\lambda} \right\rangle_\lambda$$

$$= \sum_{l=k}^{n} \binom{n}{l} \left[\begin{matrix} l \\ k \end{matrix} \right]_\lambda \left\langle \frac{2}{t+2} \Big| (x)_{n-l,\lambda} \right\rangle_\lambda \tag{34}$$

$$= \sum_{l=k}^{n} \binom{n}{l} \left[\begin{matrix} l \\ k \end{matrix} \right]_\lambda Ch_{n-l}.$$

Conversely, we assume that $(x)_{n,\lambda} = \sum_{k=0}^{n} d_{n,k} Ch_k(x)$. By (6) and (17), we obtain

$$d_{n,k} = \frac{1}{k!} \left\langle \frac{e_\lambda(t)+1}{2} (e_\lambda(t) - 1)^k \Big| (x)_{n,\lambda} \right\rangle_\lambda$$

$$= \left\langle \frac{1}{k!} (e_\lambda(t) - 1)^k \Big| \left(\frac{e_\lambda(t)+1}{2} \right)_\lambda (x)_{n,\lambda} \right\rangle_\lambda$$

$$= \left\langle \frac{1}{k!} (e_\lambda(t) - 1)^k \Big| \left(1 + \frac{1}{2} \sum_{m=1}^{\infty} (1)_{m,\lambda} \frac{t^m}{m!} \right)_\lambda (x)_{n,\lambda} \right\rangle_\lambda$$

$$= \left\langle \sum_{l=k}^{\infty} \left\{ \begin{matrix} l \\ k \end{matrix} \right\}_\lambda \frac{t^l}{l!} \Big| (x)_{n,\lambda} \right\rangle_\lambda$$

$$+ \frac{1}{2} \sum_{m=1}^{n} \binom{n}{m} (1)_{m,\lambda} \left\langle \sum_{l=k}^{\infty} \left\{ \begin{matrix} l \\ k \end{matrix} \right\}_\lambda \frac{t^l}{l!} \Big| (x)_{n-m,\lambda} \right\rangle_\lambda$$

$$= \left\{ \begin{matrix} n \\ k \end{matrix} \right\}_\lambda + \frac{1}{2} \sum_{m=1}^{n-k} \binom{n}{m} (1)_{m,\lambda} \left\{ \begin{matrix} n-m \\ k \end{matrix} \right\}_\lambda. \tag{35}$$

□

Since

$$\sum_{n=0}^{\infty} B_{n,\lambda}^{(r)}(x) \frac{t^n}{n!} = \left(\frac{t}{e_\lambda(t) - 1} \right)^r e_\lambda^x(t)$$

$$= \left(\sum_{n=0}^{\infty} B_{n,\lambda}^{(r)} \frac{t^n}{n!} \right) \left(\sum_{n=0}^{\infty} (x)_{n,\lambda} \frac{t^n}{n!} \right) \tag{36}$$

$$= \sum_{n=0}^{\infty} \left(\sum_{m=0}^{n} \binom{n}{m} B_{n-m,\lambda}^{(r)}(x)_{m,\lambda} \right) \frac{t^n}{n!},$$

and thus we know that

$$B_{n,\lambda}^{(r)}(x) = \sum_{m=0}^{n} \binom{n}{m} B_{n-m,\lambda}^{(r)}(x)_{m,\lambda}. \tag{37}$$

Theorem 3. *For each $n \geq 0$, we have*

$$Ch_n(x) = \sum_{k=0}^{n}\left(\sum_{l=k}^{n}\sum_{m=0}^{n-l}\binom{n}{l}\binom{n-l}{m}\begin{bmatrix}l\\k\end{bmatrix}_\lambda B_{m,\lambda}Ch_{n-l-m}\right)$$
$$\cdot B_{k,\lambda}(x).$$

(38)

As the inversion formula of (38), we have

$$B_{n,\lambda}(x) = \sum_{k=0}^{n}\left(\sum_{m=0}^{n}\binom{n}{m}B_{n-m,\lambda}\left(\begin{Bmatrix}m\\k\end{Bmatrix}_\lambda\right.\right.$$
$$\left.\left.+\frac{1}{2}\sum_{l=1}^{m}\binom{m}{l}\begin{Bmatrix}m-l\\k\end{Bmatrix}_\lambda(1)_{l,\lambda}\right)\right)Ch_k(x)$$

$$= \sum_{k=0}^{n}\left(\sum_{m=k}^{n}\binom{n}{m}\begin{Bmatrix}m\\k\end{Bmatrix}_\lambda B_{n-m,\lambda}\right.$$
$$\left.+\frac{1}{2}\sum_{l=1}^{n}\sum_{m=l}^{n-l}\binom{n}{l}\binom{n-l}{m}(1)_{l,\lambda}\begin{Bmatrix}m\\k\end{Bmatrix}_\lambda B_{n-l-m,\lambda}\right)Ch_k(x).$$

(39)

Proof. Let $Ch_n(x) = \sum_{k=0}^{n}c_{n,k}B_{k,\lambda}(x)$. Since

$$Ch_n(x) \sim \left(\frac{e_\lambda(t)+1}{2},e_\lambda(t)-1\right)_\lambda,$$
$$B_{n,\lambda}(x) \sim \left(\frac{e_\lambda(t)-1}{t},t\right)_\lambda,$$

(40)

by Theorem 1, we obtain

$$c_{n,k} = \frac{1}{k!}\left\langle\frac{t/\log_\lambda(1+t)}{t+2/2}(\log_\lambda(1+t))^k\middle|(x)_{n,\lambda}\right\rangle_\lambda$$

$$= \left\langle\frac{2}{t+2}\frac{t}{\log_\lambda(1+t)}\middle|\left(\frac{1}{k!}(\log_\lambda(1+t))^k\right)_\lambda(x)_{n,\lambda}\right\rangle_\lambda$$

$$= \sum_{l=k}^{n}\binom{n}{l}\begin{bmatrix}l\\k\end{bmatrix}_\lambda\left\langle\frac{2}{t+2}\middle|\left(\frac{t}{\log_\lambda(1+t)}\right)_\lambda(x)_{n-l,\lambda}\right\rangle_\lambda$$

$$= \sum_{l=k}^{n}\sum_{m=0}^{n-l}\binom{n}{l}\binom{n-l}{m}\begin{bmatrix}l\\k\end{bmatrix}_\lambda\beta_{m,\lambda}\left\langle\frac{2}{t+2}\middle|(x)_{n-l-m,\lambda}\right\rangle_\lambda$$

$$= \sum_{l=k}^{n}\sum_{m=0}^{n-l}\binom{n}{l}\binom{n-l}{m}\begin{bmatrix}l\\k\end{bmatrix}_\lambda\beta_{m,\lambda}Ch_{n-l-m}.$$

(41)

Conversely, let $B_{n,\lambda}(x) = \sum_{k=0}^{n}d_{n,k}Ch_k(x)$. By (8), (12), (15) and (37), we obtain

$$d_{n,k} = \frac{1}{k!}\left\langle\frac{e_\lambda(t)+1}{2}(e_\lambda(t)-1)^k\middle|B_{n,\lambda}(x)\right\rangle_\lambda$$

$$= \sum_{m=0}^{n}\binom{n}{m}B_{n-m,\lambda}\frac{1}{k!}\left\langle\frac{e_\lambda(t)+1}{2}(e_\lambda(t)-1)^k\middle|(x)_{m,\lambda}\right\rangle_\lambda$$

$$= \sum_{m=0}^{n}\binom{n}{m}B_{n-m,\lambda}\frac{1}{k!}\left\langle(e_\lambda(t)-1)^k\middle|\left(\frac{e_\lambda(t)+1}{2}\right)_\lambda(x)_{m,\lambda}\right\rangle_\lambda$$

$$= \sum_{m=0}^{n}\binom{n}{m}B_{n-m,\lambda}\frac{1}{k!}\left\langle(e_\lambda(t)-1)^k\middle|\left(1+\frac{1}{2}\sum_{l=1}^{\infty}(1)_{l,\lambda}\frac{t^l}{l!}\right)_\lambda(x)_{m,\lambda}\right\rangle_\lambda$$

$$= \sum_{m=0}^{n}\binom{n}{m}B_{n-m,\lambda}\left\langle\frac{1}{k!}(e_\lambda(t)-1)^k\middle|(x)_{m,\lambda}+\frac{1}{2}\sum_{l=1}^{m}\binom{m}{l}(1)_{l,\lambda}(x)_{m-l,\lambda}\right\rangle_\lambda$$

$$= \sum_{m=0}^{n}\binom{n}{m}B_{n-m,\lambda}\begin{Bmatrix}m\\k\end{Bmatrix}_\lambda$$
$$+\frac{1}{2}\sum_{m=0}^{n}\sum_{l=1}^{m}\binom{n}{m}\binom{m}{l}B_{n-m,\lambda}\begin{Bmatrix}m-l\\k\end{Bmatrix}_\lambda(1)_{l,\lambda}.$$

(42)

On the other hand, by Theorem 1, we have

$$d_{n,k} = \frac{1}{k!}\left\langle\frac{e_\lambda(t)+1/2}{e_\lambda(t)-1/t}(e_\lambda(t)-1)^k\middle|(x)_{n,\lambda}\right\rangle_\lambda$$

$$= \frac{1}{k!}\left\langle\frac{t}{e_\lambda(t)-1}(e_\lambda(t)-1)^k\middle|\left(\frac{e_\lambda(t)+1}{2}\right)_\lambda(x)_{n,\lambda}\right\rangle_\lambda$$

$$= \frac{1}{k!}\left\langle\frac{t}{e_\lambda(t)-1}(e_\lambda(t)-1)^k\middle|(x)_{n,\lambda}\right\rangle$$
$$+\frac{1}{2}\sum_{l=1}^{n}\binom{n}{l}(1)_{l,\lambda}\frac{1}{k!}\left\langle\frac{t}{e_\lambda^t-1}(e_\lambda^t-1)^k\middle|(x)_{n-l,\lambda}\right\rangle_\lambda$$

$$= \left\langle\frac{t}{e_\lambda(t)-1}\middle|\left(\frac{1}{k!}(e_\lambda(t)-1)^k\right)_\lambda(x)_{n,\lambda}\right\rangle_\lambda$$
$$+\frac{1}{2}\sum_{l=1}^{n}\binom{n}{l}(1)_{l,\lambda}\left\langle\frac{t}{e_\lambda(t)-1}\middle|\left(\frac{1}{k!}(e_\lambda(t)-1)^k\right)_\lambda(x)_{n-l,\lambda}\right\rangle_\lambda$$

$$= \sum_{m=k}^{n}\binom{n}{m}\begin{Bmatrix}m\\k\end{Bmatrix}_\lambda\left\langle\frac{t}{e_\lambda(t)-1}\middle|(x)_{n-m,\lambda}\right\rangle_\lambda$$
$$+\frac{1}{2}\sum_{l=1}^{n}\sum_{m=k}^{n-l}\binom{n}{l}\binom{n-l}{m}(1)_{l,\lambda}\begin{Bmatrix}m\\k\end{Bmatrix}_\lambda\left\langle\frac{t}{e_\lambda(t)-1}\middle|(x)_{n-l-m}\right\rangle_\lambda$$

$$= \sum_{m=k}^{n}\binom{n}{m}\begin{Bmatrix}m\\k\end{Bmatrix}_\lambda B_{n-m,\lambda}$$
$$+\frac{1}{2}\sum_{l=1}^{n}\sum_{m=k}^{n-l}\binom{n}{l}\binom{n-l}{m}(1)_{l,\lambda}\begin{Bmatrix}m\\k\end{Bmatrix}_\lambda B_{n-l-m,\lambda},$$

(43)

and hence our proofs are completed.

The degenerate Euler polynomials are defined by the generating function to be (see [28])

$$\frac{2}{e_\lambda(t)+1}e_\lambda^x(t) = \sum_{n=0}^{\infty} \mathscr{E}_{n,\lambda}(x)\frac{t^n}{n!}. \tag{44}$$

When $x = 0$, $\mathscr{E}_{n,\lambda} = \mathscr{E}_{n,\lambda}(0)$ are called the degenerate Euler numbers.

By (44), we know that

$$\sum_{n=0}^{\infty} \mathscr{E}_{n,\lambda}(x)\frac{t^n}{n!} = \frac{2}{e_\lambda(t)+1}e_\lambda^x(t)$$

$$= \left(\sum_{n=0}^{\infty} \mathscr{E}_{n,\lambda}\frac{t^n}{n!}\right)\left(\sum_{n=0}^{\infty} (x)_{n,\lambda}\frac{t^n}{n!}\right) \tag{45}$$

$$= \sum_{n=0}^{\infty}\left(\sum_{m=0}^{n}\binom{n}{m}\mathscr{E}_{n-m,\lambda}(x)_{m,\lambda}\right)\frac{t^n}{n!},$$

and so

$$\mathscr{E}_{n,\lambda}(x) = \sum_{m=0}^{n}\binom{n}{m}\mathscr{E}_{n-m,\lambda}(x)_{m,\lambda}. \tag{46}$$

$\square$

Theorem 4. *For each $n \geq 0$, we have*

$$Ch_n(x) = \sum_{k=0}^{n}\begin{bmatrix} n \\ k \end{bmatrix}_\lambda \mathscr{E}_{k,\lambda}(x). \tag{47}$$

As the inversion formula of (47), we have

$$\mathscr{E}_{n,\lambda}(x) = \sum_{k=0}^{n}\left\{\begin{matrix} n \\ k \end{matrix}\right\}_\lambda Ch_k(x)$$

$$= \sum_{k=0}^{n}\left(\sum_{m=k}^{n}\binom{n}{m}\left\{\begin{matrix} m \\ k \end{matrix}\right\}_\lambda \mathscr{E}_{n-m,\lambda}\right.$$

$$\left. +\frac{1}{2}\sum_{m=k+1}^{n}\sum_{l=k}^{m-1}\binom{n}{m}\binom{m}{l}\left\{\begin{matrix} l \\ k \end{matrix}\right\}_\lambda \mathscr{E}_{n-m,\lambda}(1)_{m-l,\lambda}\right)Ch_k(x). \tag{48}$$

Proof. Let $Ch_n(x) = \sum_{k=0}^{n} c_{n,k}\mathscr{E}_{k,\lambda}(x)$. Since

$$Ch_n(x) \sim \left(\frac{e_\lambda(t)+1}{2}, e_\lambda(t)-1\right)_\lambda,$$
$$\tag{49}$$
$$\mathscr{E}_{n,\lambda}(x) \sim \left(\frac{e_\lambda(t)+1}{2}, t\right)_\lambda,$$

by Theorem 1, we obtain

$$c_{n,k} = \frac{1}{k!}\left\langle \frac{t+2/2}{t+2/2}(\log_\lambda(1+t))^k \bigg| (x)_{n,\lambda}\right\rangle_\lambda$$

$$= \left\langle \frac{1}{k!}(\log_\lambda(1+t))^k\bigg|(x)_{n,\lambda}\right\rangle_\lambda = \left\langle \sum_{l=k}^{\infty}\begin{bmatrix} l \\ k \end{bmatrix}_\lambda\frac{t^l}{l!}\bigg|(x)_{n,\lambda}\right\rangle_\lambda$$

$$= \begin{bmatrix} n \\ k \end{bmatrix}_\lambda. \tag{50}$$

Conversely, we assume that $\mathscr{E}_{n,\lambda}(x) = \sum_{k=0}^{n} d_{n,k}Ch_k(x)$. Then,

$$d_{n,k} = \frac{1}{k!}\left\langle \frac{e_\lambda(t)+1/2}{e_\lambda(t)+1/2}(e_\lambda(t)-1^k\bigg|(x)_{n,\lambda}\right\rangle_\lambda$$

$$= \left\langle \frac{1}{k!}(e_\lambda(t)-1)^k\bigg|(x)_{n,\lambda}\right\rangle_\lambda = \left\langle \sum_{l=k}^{\infty}\left\{\begin{matrix} l \\ k \end{matrix}\right\}_\lambda\frac{t^l}{l!}\bigg|(x)_{n,\lambda}\right\rangle_\lambda$$

$$= \left\{\begin{matrix} n \\ k \end{matrix}\right\}_\lambda. \tag{51}$$

On the other hand, by (11) and (46), we obtain

$$d_{n,k} = \frac{1}{k!}\left\langle \frac{e_\lambda(t)+1}{2}(e_\lambda(t)-1)^k\bigg|\mathscr{E}_{n,\lambda}(x)\right\rangle_\lambda$$

$$= \sum_{m=0}^{n}\binom{n}{m}\mathscr{E}_{n-m,\lambda}\left\langle \frac{e_\lambda(t)+1}{2}\bigg|\left(\frac{1}{k!}(e_\lambda(t)-1)^k\right)_\lambda(x)_{m,\lambda}\right\rangle_\lambda$$

$$= \sum_{m=0}^{n}\sum_{l=k}^{m}\binom{n}{m}\binom{m}{l}\left\{\begin{matrix} l \\ k \end{matrix}\right\}_\lambda \mathscr{E}_{n-m,\lambda}\left\langle \frac{e_\lambda(t)+1}{2}\bigg|(x)_{m-l,\lambda}\right\rangle_\lambda$$

$$= \sum_{m=0}^{n}\sum_{l=k}^{m}\binom{n}{m}\binom{m}{l}\left\{\begin{matrix} l \\ k \end{matrix}\right\}_\lambda \mathscr{E}_{n-m,\lambda}\left\langle 1+\frac{1}{2}\sum_{a=1}^{\infty}(1)_{a,\lambda}\frac{t^a}{a!}\bigg|(x)_{m-l,\lambda}\right\rangle_\lambda$$

$$= \sum_{m=0}^{n}\sum_{l=k}^{m}\binom{n}{m}\binom{m}{l}\left\{\begin{matrix} l \\ k \end{matrix}\right\}_\lambda \mathscr{E}_{n-m,\lambda}$$

$$\times\left(\left\langle 1\bigg|(x)_{m-l,\lambda}\right\rangle_\lambda + \frac{1}{2}\sum_{a=1}^{\infty}\frac{(1)_{a,\lambda}}{a!}\left\langle t^a\bigg|(x)_{m-l,\lambda}\right\rangle_\lambda\right)$$

$$= \sum_{m=k}^{n}\binom{n}{m}\left\{\begin{matrix} m \\ k \end{matrix}\right\}_\lambda \mathscr{E}_{n-m,\lambda}$$

$$+\frac{1}{2}\sum_{m=k+1}^{n}\sum_{l=k}^{m-1}\binom{n}{m}\binom{m}{l}\left\{\begin{matrix} l \\ k \end{matrix}\right\}_\lambda \mathscr{E}_{n-m,\lambda}(1)_{m-l,\lambda}, \tag{52}$$

and so our proofs are completed.

By (46), we compute the first few degenerate Euler polynomials as follows:

$$\mathscr{E}_{0,\lambda}(x) = 1,$$

$$\mathscr{E}_{1,\lambda}(x) = x - \frac{1}{2},$$

$$\mathscr{E}_{2,\lambda}(x) = x^2 - (\lambda+1)x + \frac{1}{2}\lambda,$$

$$\mathscr{E}_{3,\lambda}(x) = -x^3 + \left(3\lambda + \frac{3}{2}\right)x^2 - \left(2\lambda^2 + 3\lambda\right)x + \lambda^2 - \frac{1}{4},$$

$$\mathscr{E}_{4,\lambda}(x) = -x^4 + (2+6\lambda)x^3 - \left(11\lambda^2 + 9\lambda\right)x^2$$

$$+ \left(6\lambda^3 + 11\lambda^2 - 1\right)x - 3\lambda^2 + \frac{3}{2}\lambda. \tag{53}$$
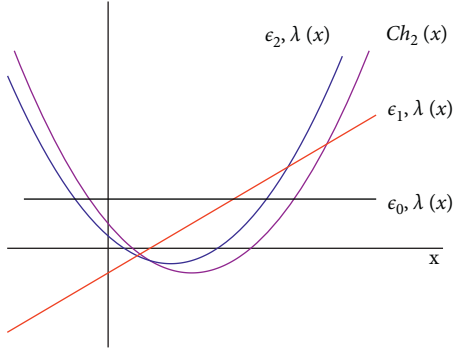
FIGURE 2: The shapes of $Ch_2(x)$, $\mathscr{E}_{0,\lambda}(x)$, $\mathscr{E}_{1,\lambda}(x)$, and $\mathscr{E}_{2,\lambda}(x)$ when $\lambda = 0.5$.

Although $Ch_2(x) = \sum_{l=0}^{2} a_l(x)\mathscr{E}_{l,\lambda}(x)$, it is difficult to find $a_i(x)$, $i = 0, 1, 2$ through Figure 2. But by Theorem 4, we see that $a_i(x) = \begin{bmatrix} 2 \\ i \end{bmatrix}_{0.5}$, $i = 0, 1, 2$.

The degenerate Daehee polynomials are defined by the generating function to be

$$\frac{\log_\lambda(1+t)}{t}e_\lambda^x(\log_\lambda(1+t)) = \sum_{n=0}^{\infty} D_{n,\lambda}(x)\frac{t^n}{n!}. \tag{54}$$

In the special case of $x = 0$, $D_{n,\lambda} = D_{n,\lambda}(0)$ are called the degenerate Daehee numbers (see [32, 37]).

Note that

$$\sum_{n=0}^{\infty} D_{n,\lambda}(x)\frac{t^n}{n!} = \frac{\log_\lambda(1+t)}{t}(1+t)^x$$

$$= \left(\sum_{n=0}^{\infty} D_{n,\lambda}\frac{t^n}{n!}\right)\left(\sum_{n=0}^{\infty}(x)_n\frac{t^n}{n!}\right) \tag{55}$$

$$= \sum_{n=0}^{\infty}\left(\sum_{l=0}^{n}\binom{n}{l}D_{n-l,\lambda}(x)_l\right)\frac{t^n}{n!},$$

and by (24), we have

$$D_{n,\lambda}(x) = \sum_{l=0}^{n}\sum_{k=0}^{l}\binom{n}{l}\begin{bmatrix} l \\ k \end{bmatrix}_\lambda D_{n-l,\lambda}(x)_{k,\lambda}. \tag{56}$$

$\square$

Theorem 5. *For each nonnegative integer n, we have*

$$Ch_n(x) = \sum_{k=0}^{n}\left(\binom{n}{k}\sum_{m=0}^{n-k}\binom{n-k}{m}Ch_m\beta_{n-k-m,\lambda}\right)D_{k,\lambda}(x)$$

$$= \sum_{k=0}^{n}\left(\sum_{l=0}^{n}\sum_{m=0}^{l}\sum_{a=k}^{m}\binom{n}{l}\binom{m}{a}\right.$$

$$\left.\times\frac{(1)_{m-a+1,\lambda}Ch_{n-l}}{m-a+1}\begin{bmatrix} l \\ m \end{bmatrix}_\lambda\begin{Bmatrix} a \\ k \end{Bmatrix}_\lambda\right)D_{k,\lambda}(x). \tag{57}$$

As the inversion formula of (57), we have

$$D_{n,\lambda}(x) = \sum_{k=0}^{n}\left(\binom{n}{k}\left(D_{n-k,\lambda} + \frac{n-k}{2}D_{n-k-1,\lambda}\right)\right)Ch_k(x)$$

$$= \sum_{k=0}^{n}\left\{\sum_{l=0}^{n}\sum_{r=0}^{l}\binom{n}{l}\begin{bmatrix} l \\ r \end{bmatrix}_\lambda D_{n-l,\lambda}\left(\begin{Bmatrix} r \\ k \end{Bmatrix}_\lambda\right.\right.$$

$$\left.\left.+\frac{1}{2}\sum_{a=1}^{r}\binom{r}{a}(1)_{a,\lambda}\begin{Bmatrix} r-a \\ k \end{Bmatrix}_\lambda\right)\right\}Ch_k(x). \tag{58}$$

Proof. Let $Ch_n(x) = \sum_{k=0}^{n} c_{n,k}D_{k,\lambda}(x)$. Since

$$Ch_n(x) \sim \left(\frac{e_\lambda(t)+1}{2}, e_\lambda(t)-1\right)_\lambda,$$

$$D_{n,\lambda}(x) \sim \left(\frac{e_\lambda(t)-1}{t}, e_\lambda(t)-1\right)_\lambda, \tag{59}$$

by Theorem 1, we have

$$c_{n,k} = \frac{1}{k!}\left\langle \frac{t/\log_\lambda(1+t)}{t+2/2}t^k \middle| (x)_{n,\lambda}\right\rangle_\lambda$$

$$= \frac{1}{k!}\left\langle \frac{t}{\log_\lambda(1+t)}\frac{2}{t+2}\middle|(t^k)_\lambda(x)_{n,\lambda}\right\rangle_\lambda$$

$$= \binom{n}{k}\left\langle \frac{t}{\log_\lambda(1+t)}\frac{2}{t+2}\middle|(x)_{n-k,\lambda}\right\rangle_\lambda$$

$$= \binom{n}{k}\left\langle \frac{t}{\log_\lambda(1+t)}\middle|\left(\frac{2}{t+2}\right)_\lambda(x)_{n-k,\lambda}\right\rangle_\lambda$$

$$= \binom{n}{k}\sum_{m=0}^{n-k}\binom{n-k}{m}Ch_m\left\langle\frac{t}{\log_\lambda(1+t)}\middle|(x)_{n-k-m,\lambda}\right\rangle_\lambda$$

$$= \binom{n}{k}\sum_{m=0}^{n-k}\binom{n-k}{m}Ch_m\beta_{n-k-m,\lambda}. \tag{60}$$

On the other hand, by (11) and (28), we obtain

$$c_{n,k} = \frac{1}{k!}\left\langle \frac{e_\lambda(t)-1}{t}(e_\lambda(t)-1)^k \middle| Ch_n(x) \right\rangle$$

$$= \sum_{l=0}^{n}\sum_{m=0}^{l}\binom{n}{l}[lm]_\lambda Ch_{n-l}\left\langle \frac{e_\lambda(t)-1}{t}\middle|\left(\frac{1}{k!}(e_\lambda(t)-1)^k\right)_\lambda(x)_{m,\lambda}\right\rangle_\lambda$$

$$= \sum_{l=0}^{n}\sum_{m=0}^{l}\sum_{a=k}^{m}\binom{n}{l}\binom{m}{a}\begin{bmatrix}l\\m\end{bmatrix}_\lambda\begin{Bmatrix}a\\k\end{Bmatrix}_\lambda Ch_{n-l}\left\langle \frac{e_\lambda(t)-1}{t}\middle|(x)_{m-a,\lambda}\right\rangle_\lambda$$

$$= \sum_{l=0}^{n}\sum_{m=0}^{l}\sum_{a=k}^{m}\binom{n}{l}\binom{m}{a}\begin{bmatrix}l\\m\end{bmatrix}_\lambda\begin{Bmatrix}a\\k\end{Bmatrix}_\lambda Ch_{n-l}$$

$$\times \left\langle \sum_{b=0}^{\infty}\frac{(1)_{b+1,\lambda}}{b+1}\frac{t^b}{b!}\middle|(x)_{m-a,\lambda}\right\rangle_\lambda$$

$$= \sum_{l=0}^{n}\sum_{m=0}^{l}\sum_{a=k}^{m}\binom{n}{l}\binom{m}{a}\frac{(1)_{m-a+1,\lambda}Ch_{n-l}}{m-a+1}\begin{bmatrix}l\\m\end{bmatrix}_\lambda\begin{bmatrix}a\\k\end{bmatrix}_\lambda. \tag{61}$$

Conversely, we assume that $D_{n,\lambda}(x)=\sum_{k=0}^{n}d_{n,k}Ch_k(x)$. Then, by Theorem 1 and (6), we obtain

$$d_{n,k} = \frac{1}{k!}\left\langle \frac{t+2/2}{(t/\log_\lambda(1+t))}t^k \middle| (x)_{n,\lambda}\right\rangle_\lambda$$

$$= \frac{1}{k!}\left\langle \frac{t+2}{2}\frac{\log_\lambda(1+t)}{t}\middle|(t^k)_\lambda(x)_{n,\lambda}\right\rangle_\lambda$$

$$= \binom{n}{k}\left\langle \frac{\log_\lambda(1+t)}{t}\middle|\left(\frac{t+2}{2}\right)_\lambda(x)_{n-k,\lambda}\right\rangle_\lambda$$

$$= \binom{n}{k}\left\langle \frac{\log_\lambda(1+t)}{t}\middle|(x)_{n-k,\lambda}+\frac{n-k}{2}(x)_{n-k-1,\lambda}\right\rangle_\lambda$$

$$= \binom{n}{k}\left(\left\langle \frac{\log_\lambda(1+t)}{t}\middle|(x)_{n-k,\lambda}\right\rangle_\lambda+\frac{n-k}{2}\left\langle \frac{\log_\lambda(1+t)}{t}\middle|(x)_{n-k-1,\lambda}\right\rangle_\lambda\right)$$

$$= \binom{n}{k}\left(D_{n-k,\lambda}+\frac{n-k}{2}D_{n-k-1,\lambda}\right). \tag{62}$$

On the other hand, by (11) and (56), we obtain

$$d_{n,k} = \frac{1}{k!}\left\langle \frac{e_\lambda(t)+1}{2}(e_\lambda(t)-1)^k \middle| D_{n,\lambda}(x) \right\rangle_\lambda$$

$$= \frac{1}{k!}\sum_{l=0}^{n}\sum_{r=0}^{l}\binom{n}{l}\begin{bmatrix}l\\r\end{bmatrix}_\lambda D_{n-l,\lambda}\left\langle \frac{e_\lambda(t)+1}{2}(e_\lambda(t)-1)^k\middle|(x)_{r,\lambda}\right\rangle_\lambda$$

$$= \sum_{l=0}^{n}\sum_{r=0}^{l}\binom{n}{l}\begin{bmatrix}l\\r\end{bmatrix}_\lambda D_{n-l,\lambda}\left\langle \frac{1}{k!}(e_\lambda(t)-1)^k\middle|\left(\frac{e_\lambda(t)+1}{2}\right)_\lambda(x)_{r,\lambda}\right\rangle_\lambda$$

$$= \sum_{l=0}^{n}\sum_{r=0}^{l}\binom{n}{l}\begin{bmatrix}l\\r\end{bmatrix}_\lambda D_{n-l,\lambda}$$

$$\times \left\langle \frac{1}{k!}(e_\lambda(t)-1)^k\middle|\left(1+\sum_{a=1}^{\infty}\frac{(1)_{a,\lambda}}{2}\frac{t^a}{a!}\right)_\lambda(x)_{r,\lambda}\right\rangle_\lambda$$

$$= \sum_{l=0}^{n}\sum_{r=0}^{l}\binom{n}{l}\begin{bmatrix}l\\r\end{bmatrix}_\lambda D_{n-l,\lambda}$$

$$\times \left\langle \sum_{b=k}^{\infty}\begin{Bmatrix}b\\k\end{Bmatrix}_\lambda\frac{t^b}{b!}\middle|(x)_{r,\lambda}+\frac{1}{2}\sum_{a=1}^{r}\binom{r}{a}(1)_{a,\lambda}(x)_{r-a,\lambda}\right\rangle_\lambda$$

$$= \sum_{l=0}^{n}\sum_{r=0}^{l}\binom{n}{l}\begin{bmatrix}l\\r\end{bmatrix}_\lambda D_{n-l,\lambda}\left(\begin{Bmatrix}r\\k\end{Bmatrix}_\lambda+\frac{1}{2}\sum_{a=1}^{r}\binom{r}{a}(1)_{a,\lambda}\begin{Bmatrix}r-a\\k\end{Bmatrix}_\lambda\right). \tag{63}$$

The degenerate Bell polynomials are defined by the generating function to be (see [1, 23])

$$e_\lambda^x((e_\lambda(t)-1)) = \sum_{n=0}^{\infty}Bel_{n,\lambda}(x)\frac{t^n}{n!}. \tag{64}$$

Note that

$$\sum_{n=0}^{\infty}Bel_{n,\lambda}(x)\frac{t^n}{n!} = e_\lambda^x((e_\lambda(t)-1)) = \sum_{m=0}^{\infty}(x)_{m,\lambda}\frac{1}{m!}(e_\lambda(t)-1)^m$$

$$= \sum_{m=0}^{\infty}(x)_{m,\lambda}\sum_{l=m}^{\infty}\begin{Bmatrix}l\\m\end{Bmatrix}_\lambda\frac{t^l}{l!}$$

$$= \sum_{n=0}^{\infty}\left(\sum_{m=0}^{n}\begin{Bmatrix}n\\m\end{Bmatrix}_\lambda(x)_{m,\lambda}\right)\frac{t^n}{n!}, \tag{65}$$

and thus

$$Bel_{n,\lambda}(x) = \sum_{m=0}^{n}n\backslash brace m_\lambda(x)_{m,\lambda}. \tag{66}$$

In addition, we know that

$$\frac{1}{k!}(\log_\lambda(1+\log_\lambda(1+t)))^k = \sum_{l=k}^\infty \begin{bmatrix} l \\ k \end{bmatrix}_\lambda \frac{1}{l!}(\log_\lambda(1+t))^l$$

$$= \sum_{l=k}^\infty \sum_{m=l}^\infty \begin{bmatrix} l \\ k \end{bmatrix}_\lambda \begin{bmatrix} m \\ l \end{bmatrix}_\lambda \frac{t^m}{m!} \qquad (67)$$

$$= \sum_{l=k}^\infty \sum_{m=k}^l \begin{bmatrix} m \\ k \end{bmatrix}_\lambda \begin{bmatrix} l \\ m \end{bmatrix}_\lambda \frac{t^l}{l!}.$$

$$\frac{e_\lambda(e_\lambda(t)-1)+1}{2} = \frac{1}{2}\left(1+\sum_{a=0}^\infty (1)_{a,\lambda}\frac{1}{a!}(e_\lambda(t)-1^a\right)$$

$$= 1+\frac{1}{2}\sum_{a=1}^\infty \sum_{b=a}^\infty (1)_{a,\lambda}\begin{Bmatrix} b \\ a \end{Bmatrix}_\lambda \frac{t^b}{b!}$$

$$= 1+\frac{1}{2}\sum_{a=1}^\infty \sum_{b=1}^a (1)_{b,\lambda}\begin{Bmatrix} a \\ b \end{Bmatrix}_\lambda \frac{t^a}{a!}.$$

$$(68) \quad \square$$

Theorem 6. *For each nonnegative integer n, we have*

$$Ch_n(x) = \sum_{k=0}^n \left(\sum_{l=k}^n \sum_{m=k}^l \binom{n}{l}\begin{bmatrix} l \\ k \end{bmatrix}_\lambda \begin{bmatrix} l \\ m \end{bmatrix}_\lambda Ch_{n-l} \right) Bel_{k,\lambda}(x).$$

$$(69)$$

As the inversion formula of (69), we have

$$Bel_{n,\lambda}(x)$$

$$= \sum_{k=0}^n \left(\sum_{m=0}^{n-k} \begin{Bmatrix} m+k \\ k \end{Bmatrix}_\lambda \begin{Bmatrix} n \\ m+k \end{Bmatrix}_\lambda \right.$$

$$\left. +\frac{1}{2}\sum_{l=k}^{n-1}\sum_{m=0}^{l-k}\sum_{b=1}^{n-l} (1)_{b,\lambda}\binom{n}{l}\begin{Bmatrix} m+k \\ k \end{Bmatrix}_\lambda \begin{Bmatrix} l \\ m+k \end{Bmatrix}_\lambda \begin{Bmatrix} n-l \\ b \end{Bmatrix}_\lambda \right) Ch_k(x)$$

$$= \sum_{k=0}^n \left(\sum_{m=k}^n \begin{Bmatrix} n \\ m \end{Bmatrix}_\lambda \begin{Bmatrix} m \\ k \end{Bmatrix}_\lambda \right.$$

$$\left. +\frac{1}{2}\sum_{m=k+1}^n \sum_{l=k}^{m-1} \binom{m}{l}\begin{Bmatrix} n \\ m \end{Bmatrix}_\lambda \begin{Bmatrix} l \\ k \end{Bmatrix}_\lambda (1)_{m-l,\lambda} \right) Ch_k(x).$$

$$(70)$$

Proof. Let $Ch_n(x) = \sum_{k=0}^n c_{n,k} Bel_{k,\lambda}(x)$. Since

$$Ch_n(x) \sim \left(\frac{e_\lambda(t)+1}{2}, e_\lambda(t)-1 \right)_\lambda,$$

$$(71)$$

$$Bel_{n,\lambda}(x) \sim (1, \log_\lambda(1+t))_\lambda,$$

by Theorem 1and (67), we obtain

$$c_{n,k} = \frac{1}{k!}\left\langle \frac{1}{((t+2)/2)}(\log_\lambda(1+\log_\lambda(1+t)))^k \middle| (x)_{n,\lambda} \right\rangle_\lambda$$

$$= \left\langle \frac{2}{t+2} \middle| \left(\frac{1}{k!}(\log_\lambda(1+\log_\lambda(1+t)))^k \right)_\lambda (x)_{n,\lambda} \right\rangle_\lambda$$

$$= \left\langle \frac{2}{t+2} \middle| \left(\sum_{l=k}^\infty \sum_{m=k}^l \begin{bmatrix} m \\ k \end{bmatrix}_\lambda \begin{bmatrix} l \\ m \end{bmatrix}_\lambda \frac{t^l}{l!} \right)_\lambda (x)_{n,\lambda} \right\rangle_\lambda$$

$$= \sum_{l=k}^n \sum_{m=k}^l \binom{n}{l}\begin{bmatrix} m \\ k \end{bmatrix}_\lambda \begin{bmatrix} l \\ m \end{bmatrix}_\lambda \left\langle \frac{2}{t+2} \middle| (x)_{n-l,\lambda} \right\rangle_\lambda$$

$$= \sum_{l=k}^n \sum_{m=k}^l \binom{n}{l}\begin{bmatrix} m \\ k \end{bmatrix}_\lambda \begin{bmatrix} l \\ m \end{bmatrix}_\lambda Ch_{n-l}.$$

$$(72)$$

Conversely, we assume that $Bel_{n,\lambda}(x) = \sum_{k=0}^n d_{n,k} Ch_k(x)$. By (68), we obtain

$$d_{n,k} = \frac{1}{k!}\left\langle \frac{e_\lambda(e_\lambda(t)-1)+1}{2}(e_\lambda(e_\lambda(t)-1)-1)^k \middle| (x)_{n,\lambda} \right\rangle_\lambda$$

$$= \left\langle \frac{e_\lambda(e_\lambda(t)-1)+1}{2} \middle| \left(\frac{1}{k!}(e_\lambda(e_\lambda(t)-1)-1)^k \right)_\lambda (x)_{n,\lambda} \right\rangle_\lambda$$

$$= \left\langle \frac{e_\lambda(e_\lambda(t)-1)+1}{2} \middle| \left(\sum_{l=k}^\infty \begin{Bmatrix} l \\ k \end{Bmatrix}_\lambda \frac{1}{l!}(e_\lambda(t)-1)^l \right)_\lambda (x)_{n,\lambda} \right\rangle_\lambda$$

$$= \left\langle \frac{e_\lambda(e_\lambda(t)-1)+1}{2} \middle| \left(\sum_{l=k}^\infty \sum_{m=l}^\infty \begin{Bmatrix} l \\ k \end{Bmatrix}_\lambda \begin{Bmatrix} m \\ l \end{Bmatrix}_\lambda \frac{t^m}{m!} \right)_\lambda (x)_{n,\lambda} \right\rangle_\lambda$$

$$= \sum_{l=k}^n \sum_{m=0}^{l-k} \binom{n}{l}\begin{Bmatrix} m+k \\ k \end{Bmatrix}_\lambda \begin{Bmatrix} l \\ m+k \end{Bmatrix}_\lambda \left\langle \frac{e_\lambda(e_\lambda(t)-1)+1}{2} \middle| (x)_{n-l,\lambda} \right\rangle_\lambda$$

$$= \sum_{l=k}^n \sum_{m=0}^{l-k} \binom{n}{l}\begin{Bmatrix} m+k \\ k \end{Bmatrix}_\lambda \begin{Bmatrix} l \\ m+k \end{Bmatrix}_\lambda$$

$$\times \left(\left\langle 1 \middle| (x)_{n-l,\lambda} \right\rangle +\frac{1}{2}\left\langle \sum_{a=1}^\infty \sum_{b=1}^a (1)_{b,\lambda}\begin{Bmatrix} a \\ b \end{Bmatrix}_\lambda \frac{t^a}{a!} \middle| (x)_{n-l,\lambda} \right\rangle \right)$$

$$= \sum_{m=0}^{n-k} \begin{Bmatrix} m+k \\ k \end{Bmatrix}_\lambda \begin{Bmatrix} n \\ m+k \end{Bmatrix}_\lambda$$

$$+\frac{1}{2}\sum_{l=k}^{n-1}\sum_{m=0}^{l-k}\sum_{b=1}^{n-l} (1)_{b,\lambda}\binom{n}{l}\begin{Bmatrix} m+k \\ k \end{Bmatrix}_\lambda \begin{Bmatrix} l \\ m+k \end{Bmatrix}_\lambda \begin{Bmatrix} n-l \\ b \end{Bmatrix}_\lambda.$$

$$(73)$$

On the other hand, by (11) and (66), we have

$$d_{n,k} = \frac{1}{k!}\left\langle \frac{e_\lambda(t)+1}{2}(e_\lambda(t)-1)^k \middle| Bel_{n,\lambda}(x)\right\rangle_\lambda$$

$$= \frac{1}{k!}\sum_{m=0}^{n}\begin{Bmatrix} n \\ m \end{Bmatrix}_\lambda \left\langle \frac{e_\lambda(t)+1}{2}(e_\lambda(t)-1)^k \middle| (x)_{m,\lambda}\right\rangle_\lambda$$

$$= \sum_{m=0}^{n}\begin{Bmatrix} n \\ m \end{Bmatrix}_\lambda \left\langle \frac{e_\lambda(t)+1}{2}\middle| \left(\frac{1}{k!}(e_\lambda(t)-1)^k\right)_\lambda (x)_{m,\lambda}\right\rangle_\lambda$$

$$= \sum_{m=0}^{n}\sum_{l=k}^{m}\binom{m}{l}\begin{Bmatrix} n \\ m \end{Bmatrix}_\lambda \begin{Bmatrix} l \\ k \end{Bmatrix}_\lambda \left\langle \frac{e_\lambda(t)+1}{2}\middle|(x)_{m-l,\lambda}\right\rangle_\lambda$$

$$= \sum_{m=0}^{n}\sum_{l=k}^{m}\binom{m}{l}\begin{Bmatrix} n \\ m \end{Bmatrix}_\lambda \begin{Bmatrix} l \\ k \end{Bmatrix}_\lambda \left\langle 1+\frac{1}{2}\sum_{a=1}^{\infty}(1)_{a,\lambda}\frac{t^a}{a!}\middle|(x)_{m-l,\lambda}\right\rangle_\lambda$$

$$= \sum_{m=0}^{n}\sum_{l=k}^{m}\binom{m}{l}\begin{Bmatrix} n \\ m \end{Bmatrix}_\lambda \begin{Bmatrix} l \\ k \end{Bmatrix}_\lambda$$

$$\cdot\left(\left\langle 1\middle|(x)_{m-l,\lambda}\right\rangle_\lambda + \frac{1}{2}\sum_{a=1}^{\infty}\frac{(1)_{a,\lambda}}{a!}\left\langle t^a\middle|(x)_{m-l,\lambda}\right\rangle_\lambda\right)$$

$$= \sum_{m=k}^{n}\begin{Bmatrix} n \\ m \end{Bmatrix}_\lambda \begin{Bmatrix} m \\ k \end{Bmatrix}_\lambda + \frac{1}{2}\sum_{m=k+1}^{n}\sum_{l=k}^{m-1}\binom{m}{l}\begin{Bmatrix} n \\ m \end{Bmatrix}_\lambda \begin{Bmatrix} l \\ k \end{Bmatrix}_\lambda (1)_{m-l,\lambda},$$

$$(74)$$

and thus our proofs are completed.

The unsigned Lah number $L(n,k)$ counts the number of ways a set of n elements can be partitioned into k nonempty linearly ordered subsets and has the explicit formula (see [1, 20, 23, 38, 39])

$$L(n,k) = \binom{n-1}{k-1}\frac{n!}{k!}. \qquad (75)$$

By (75), we can derive the generating function of $L(n,k)$ to be (see [1, 20, 23, 38, 39])

$$\frac{1}{k!}\left(\frac{t}{1-t}\right)^k = \sum_{n=k}^{\infty} L(n,k)\frac{t^n}{n!}, \ (k\geq 0). \qquad (76)$$

Recently, Kim–Kim introduced the degenerate Lah–Bell polynomials as follows (see [1, 20]):

$$e_\lambda^x\left(\frac{1}{1-t}-1\right) = \sum_{n=0}^{\infty} B_{n,\lambda}^L(x)\frac{t^n}{n!}. \qquad (77)$$

In the special case of $x = 1$, $B_n^L = B_n^L(1)$ are called Lah–Bell numbers. Note that n-th Lah–Bell number B_n^L $(n\geq 0)$ is the number of ways a set of n elements can be partitioned into nonempty linearly ordered subsets. By (77), we can derive the following:

$$\sum_{n=0}^{\infty} B_{n,\lambda}^L(x)\frac{t^n}{n!} = e_\lambda^x\left(\frac{t}{1-t}\right)$$

$$= \sum_{n=0}^{\infty}(x)_{n,\lambda}\frac{1}{n!}\left(\frac{t}{1-t}\right)^n$$

$$= \sum_{n=0}^{\infty}(x)_{n,\lambda}\sum_{m=n}^{\infty} L(m,n)\frac{t^m}{m!}$$

$$= \sum_{n=0}^{\infty}\left(\sum_{m=0}^{n} L(n,m)(x)_{m,\lambda}\right)\frac{t^n}{n!},$$

$$(78)$$

and thus, we obtain

$$B_{n,\lambda}^L(x) = \sum_{m=0}^{n} L(n,m)(x)_{m,\lambda}. \qquad (79)$$

$$\square$$

Theorem 7. *For each nonnegative integer n, we have*

$$Ch_n(x) = \sum_{k=0}^{n}\left(\sum_{l=0}^{n}\sum_{m=0}^{l}(-1)^{m-k}\binom{n}{l}\binom{m}{k}\langle k\rangle_{m-k}\begin{bmatrix} l \\ m \end{bmatrix}_\lambda Ch_{n-l}\right)B_k^L(x). \qquad (80)$$

As the inversion formula of (80), we have

$$B_n^L(x) = \sum_{k=0}^{n}\left(\sum_{l=k}^{n}\begin{Bmatrix} l \\ k \end{Bmatrix}_\lambda L(n,l)\right.$$

$$\left.+\frac{1}{2}\sum_{m=k}^{n-1}\sum_{l=k}^{m}\sum_{b=1}^{n-m}\binom{n}{m}(1)_{b,\lambda}\begin{Bmatrix} l \\ k \end{Bmatrix}_\lambda (m,l)L(n-m,b)\right)Ch_k(x)$$

$$= \sum_{k=0}^{n}\left(\sum_{m=k}^{n}\begin{Bmatrix} m \\ k \end{Bmatrix}_\lambda L(n,m)\right.$$

$$\left.+\frac{1}{2}\sum_{m=0}^{n}\sum_{l=k}^{m-1}\binom{m}{l}(1)_{m-l,\lambda}\begin{Bmatrix} l \\ k \end{Bmatrix}_\lambda L(n,m)\right)Ch_k(x). \qquad (81)$$

Proof. Let $Ch_n(x) = \sum_{k=0}^{n} c_{n,k}B_k^L(x)$. Since

$$Ch_n(x) \sim \left(\frac{e_\lambda(t)+1}{2}, e_\lambda(t)-1\right)_\lambda,$$

$$B_n^L(x) \sim \left(1, \frac{t}{1+t}\right)_\lambda, \qquad (82)$$

by (11) and (28), we obtain

$$c_{n,k} = \frac{1}{k!}\left\langle \left(\frac{t}{1+t}\right)^k \middle| Ch_n(x)\right\rangle_\lambda$$

$$= \frac{1}{k!}\sum_{l=0}^{n}\sum_{m=0}^{l}\binom{n}{l}\begin{bmatrix} l \\ m \end{bmatrix}_\lambda Ch_{n-l}\left\langle \left(\frac{t}{1+t}\right)^k \middle| (x)_{m,\lambda}\right\rangle_\lambda$$

$$= \frac{1}{k!}\sum_{l=0}^{n}\sum_{m=0}^{l}\binom{n}{l}\begin{bmatrix} l \\ m \end{bmatrix}_\lambda Ch_{n-l}\left\langle (1+t)^{-k}\middle| (t^k)_\lambda (x)_{m,\lambda}\right\rangle_\lambda$$

$$= \sum_{l=0}^{n}\sum_{m=0}^{l}\binom{n}{l}\binom{m}{k}\begin{bmatrix} l \\ m \end{bmatrix}_\lambda Ch_{n-l}\left\langle \sum_{a=0}^{\infty}\frac{(-1)^a\langle k\rangle_a}{a!}t^a\middle| (x)_{m-k,\lambda}\right\rangle_\lambda$$

$$= \sum_{l=0}^{n}\sum_{m=0}^{l}\binom{n}{l}\binom{m}{k}(-1)^{m-k}\langle k\rangle_{m-k}\begin{bmatrix} l \\ m \end{bmatrix}_\lambda Ch_{n-l}. \tag{83}$$

Conversely, we assume that $B_{n,\lambda}^L(x) = \sum_{k=0}^{n} d_{n,k}Ch_k(x)$. Then,

$$d_{n,k} = \frac{1}{k!}\left\langle \frac{e_\lambda(t/1-t)+1}{2}(e_\lambda(t/1-t)-1)^k \middle| (x)_{n,\lambda}\right\rangle_\lambda$$

$$= \left\langle \frac{e_\lambda(t/1-t)+1}{2}\middle| \left(\frac{1}{k!}(e_\lambda((t/1-t))-1)^k\right)_\lambda (x)_{n,\lambda}\right\rangle_\lambda$$

$$= \left\langle \frac{e_\lambda((t/1-t))+1}{2}\middle| \left(\sum_{l=k}^{\infty}\begin{Bmatrix} l \\ k \end{Bmatrix}_\lambda \frac{1}{l!}((t/1-t))^l\right)_\lambda (x)_{n,\lambda}\right\rangle_\lambda$$

$$= \left\langle \frac{e_\lambda((t/1-t))+1}{2}\middle| \left(\sum_{l=k}^{\infty}\sum_{m=l}^{\infty}\begin{Bmatrix} l \\ k \end{Bmatrix}_\lambda L(m,l)\frac{t^m}{m!}\right)_\lambda (x)_{n,\lambda}\right\rangle_\lambda$$

$$= \sum_{m=k}^{n}\sum_{l=k}^{m}\binom{n}{m}\begin{Bmatrix} l \\ k \end{Bmatrix}_\lambda L(m,l)\left\langle \frac{e_\lambda((t/1-t))+1}{2}\middle| (x)_{n-m,\lambda}\right\rangle_\lambda$$

$$= \sum_{m=k}^{n}\sum_{l=k}^{m}\binom{n}{m}\begin{Bmatrix} l \\ k \end{Bmatrix}_\lambda L(m,l)$$

$$\left\langle 1+\frac{1}{2}\sum_{a=1}^{\infty}\sum_{b=a}^{\infty}(1)_{a,\lambda}L(b,a)\frac{t^b}{b!}\middle| (x)_{n-m,\lambda}\right\rangle_\lambda$$

$$= \sum_{m=k}^{n}\sum_{l=k}^{m}\binom{n}{m}\begin{Bmatrix} l \\ k \end{Bmatrix}_\lambda L(m,l)$$

$$\times \left(\left\langle 1\middle| (x)_{n-m,\lambda}\right\rangle_\lambda + \frac{1}{2}\left\langle \sum_{a=1}^{\infty}\sum_{b=1}^{a}(1)_{b,\lambda}L(a,b)\frac{t^a}{a!}\middle| (x)_{n-m,\lambda}\right\rangle_\lambda\right)$$

$$= \sum_{l=k}^{n}\begin{Bmatrix} l \\ k \end{Bmatrix}_\lambda L(n,l)$$

$$+ \frac{1}{2}\sum_{m=k}^{n-1}\sum_{l=k}^{m}\sum_{b=1}^{n-m}\binom{n}{m}(1)_{b,\lambda}\begin{Bmatrix} l \\ k \end{Bmatrix}_\lambda L(m,l)L(n-m,b). \tag{84}$$

On the other hand, by (11) and (79), we obtain

$$d_{n,k} = \frac{1}{k!}\left\langle \frac{e_\lambda(t)+1}{2}(e_\lambda(t)-1)^k \middle| B_{n,\lambda}^L(x)\right\rangle$$

$$= \frac{1}{k!}\sum_{m=0}^{n}L(n,m)\left\langle \frac{e_\lambda(t)+1}{2}(e_\lambda(t)-1)^k \middle| (x)_{m,\lambda}\right\rangle_\lambda$$

$$= \sum_{m=0}^{n}L(n,m)\left\langle \frac{e_\lambda(t)+1}{2}\middle| \left(\frac{1}{k!}(e_\lambda(t)-1)^k\right)_\lambda (x)_{m,\lambda}\right\rangle_\lambda$$

$$= \sum_{m=0}^{n}\sum_{l=k}^{m}\binom{m}{l}L(n,m)\begin{Bmatrix} l \\ k \end{Bmatrix}_\lambda \left\langle \frac{e_\lambda(t)+1}{2}\middle| (x)_{m-l,\lambda}\right\rangle_\lambda$$

$$= \sum_{m=0}^{n}\sum_{l=k}^{m}\binom{m}{l}L(n,m)\begin{Bmatrix} l \\ k \end{Bmatrix}_\lambda \left\langle 1+\frac{1}{2}\sum_{a=1}^{\infty}(1)_{a,\lambda}\frac{t^a}{a!}\middle| (x)_{m-l,\lambda}\right\rangle_\lambda$$

$$= \sum_{m=0}^{n}\sum_{l=k}^{m}\binom{m}{l}L(n,m)\begin{Bmatrix} l \\ k \end{Bmatrix}_\lambda$$

$$\times \left(\left\langle 1\middle| (x)_{m-l,\lambda}\right\rangle_\lambda + \frac{1}{2}\left\langle \sum_{a=1}^{\infty}\frac{(1)_{a,\lambda}}{a!}t^a\middle| (x)_{m-l,\lambda}\right\rangle_\lambda\right)$$

$$= \sum_{m=k}^{n}\begin{Bmatrix} m \\ k \end{Bmatrix}_\lambda L(n,m)$$

$$+ \frac{1}{2}\sum_{m=0}^{n}\sum_{l=k}^{m-1}\binom{m}{l}(1)_{m-l,\lambda}\begin{Bmatrix} l \\ k \end{Bmatrix}_\lambda L(n,m), \tag{85}$$

and so our proofs are completed.

By the definition of the degenerate Bernoulli polynomials of the second kind, we note that

$$\sum_{n=0}^{\infty}\beta_{n,\lambda}(x)\frac{t^n}{n!} = \frac{t}{\log_\lambda(1+t)}e_\lambda^x(\log_\lambda(1+t))$$

$$= \sum_{n=0}^{\infty}\left(\sum_{m=0}^{n}\sum_{l=0}^{m}\binom{n}{m}\begin{bmatrix} m \\ l \end{bmatrix}_\lambda \beta_{n-m,\lambda}(x)_{l,\lambda}\right)\frac{t^n}{n!}, \tag{86}$$

and thus, we obtain

$$\beta_{n,\lambda}(x) = \sum_{m=0}^{n}\sum_{l=0}^{m}\binom{n}{m}\begin{bmatrix} m \\ l \end{bmatrix}_\lambda \beta_{n-m,\lambda}(x)_{l,\lambda}. \tag{87}$$

□

Theorem 8. *For each $n \geq 0$, we have*

$$Ch_n(x) = \left(\sum_{l=0}^{n-k}\binom{n}{k}\binom{n-k}{l}Ch_l D_{n-k-l,\lambda}\right)\beta_{k,\lambda}(x). \tag{88}$$

As the inversion formula of (88), we have

$$\beta_{n,\lambda}(x) = \sum_{k=0}^{n} \left(\binom{n}{k} \beta_{n-k,\lambda} + \binom{n}{k} \frac{n-k}{2} \beta_{n-k-1,\lambda} \right) Ch_k(x)$$

$$= \sum_{k=0}^{n} \left(\sum_{m=0}^{n} \sum_{l=0}^{m} \binom{n}{m} \beta_{n-m,\lambda} \left\{ \begin{matrix} m \\ l \end{matrix} \right\}_{\lambda} \left\{ \begin{matrix} l \\ k \end{matrix} \right\}_{\lambda} \right.$$

$$\left. + \frac{1}{2} \sum_{m=0}^{n} \sum_{l=k+1}^{m} \sum_{a=k}^{l-1} \binom{n}{m} \binom{l}{a} \beta_{n-m,\lambda} \left[\begin{matrix} m \\ l \end{matrix} \right]_{\lambda} \left\{ \begin{matrix} a \\ k \end{matrix} \right\}_{\lambda} (1)_{l-a,\lambda} \right) Ch_k(x).$$

$$(89)$$

Proof. Let $Ch_n(x) = \sum_{k=0}^{n} c_{n,k} \beta_{k,\lambda}(x)$. Since

$$Ch_n(x) \sim \left(\frac{e_\lambda(t) + 1}{2}, e_\lambda(t) - 1 \right)_\lambda,$$

$$\beta_{n,\lambda}(x) \sim \left(\frac{t}{e_\lambda(t) - 1}, e_\lambda(t) - 1 \right)_\lambda,$$

$$(90)$$

by Theorem 1, we obtain

$$c_{n,k} = \frac{1}{k!} \left\langle \frac{\log_\lambda (1+t)/t}{t+2/2} t^k \middle| (x)_{n,\lambda} \right\rangle_\lambda$$

$$= \frac{1}{k!} \left\langle \frac{2}{t+2} \frac{\log_\lambda (1+t)}{t} \middle| (t^k)_\lambda (x)_{n,\lambda} \right\rangle_\lambda$$

$$= \binom{n}{k} \left\langle \frac{2}{t+2} \frac{\log_\lambda (1+t)}{t} \middle| (x)_{n-k,\lambda} \right\rangle_\lambda$$

$$= \binom{n}{k} \left\langle \frac{\log_\lambda (1+t)}{t} \middle| \left(\frac{2}{t+2} \right)_\lambda (x)_{n-k,\lambda} \right\rangle_\lambda$$

$$(91)$$

$$= \sum_{l=0}^{n-k} \binom{n}{k} \binom{n-k}{l} Ch_l \left\langle \frac{\log_\lambda (1+t)}{t} \middle| (x)_{n-k-l,\lambda} \right\rangle_\lambda$$

$$= \sum_{l=0}^{n-k} \binom{n}{k} \binom{n-k}{l} Ch_l D_{n-k-l,\lambda}.$$

Conversely, we assume that $\beta_{n,\lambda}(x) = \sum_{k=0}^{n} d_{n,k} Ch_k(x)$. Then,

$$d_{n,k} = \frac{1}{k!} \left\langle \frac{t+2/2}{\log_\lambda (1+t)/t} t^k \middle| (x)_{n,\lambda} \right\rangle_\lambda$$

$$= \frac{1}{k!} \left\langle \frac{t}{\log_\lambda (1+t)} \frac{t+2}{2} \middle| (t^k)_\lambda (x)_{n,\lambda} \right\rangle_\lambda$$

$$= \binom{n}{k} \left\langle \frac{t}{\log_\lambda (1+t)} \middle| \left(1 + \frac{1}{2} t \right) (x)_{n-k,\lambda} \right\rangle_\lambda$$

$$(92)$$

$$= \binom{n}{k} \left\langle \sum_{m=0}^{\infty} \beta_{m,\lambda} \frac{t^m}{m!} \middle| (x)_{n-k,\lambda} + \frac{n-k}{2} (x)_{n-k-1,\lambda} \right\rangle_\lambda$$

$$= \binom{n}{k} \beta_{n-k,\lambda} + \binom{n}{k} \frac{n-k}{2} \beta_{n-k-1,\lambda}.$$

On the other hand, by (11) and (87), we obtain

$$d_{n,k} = \frac{1}{k!} \left\langle \frac{e_\lambda(t) + 1}{2} (e_\lambda(t) - 1)^k \middle| \beta_{n,\lambda}(x) \right\rangle_\lambda$$

$$= \frac{1}{k!} \sum_{m=0}^{n} \sum_{l=0}^{m} \binom{n}{m} \beta_{n-m,\lambda} \left\{ \begin{matrix} m \\ l \end{matrix} \right\}_{\lambda} \left\langle \frac{e_\lambda(t) + 1}{2} (e_\lambda(t) - 1)^k \middle| (x)_{l,\lambda} \right\rangle_\lambda$$

$$= \sum_{m=0}^{n} \sum_{l=0}^{m} \binom{n}{m} \beta_{n-m,\lambda} \left\{ \begin{matrix} m \\ l \end{matrix} \right\}_{\lambda} \left\langle \frac{e_\lambda(t) + 1}{2} \middle| \left(\frac{1}{k!} (e_\lambda(t) - 1)^k \right)_\lambda (x)_{l,\lambda} \right\rangle_\lambda$$

$$= \sum_{m=0}^{n} \sum_{l=0}^{m} \sum_{a=k}^{l} \binom{n}{m} \binom{l}{a} \beta_{n-m,\lambda} \left\{ \begin{matrix} m \\ l \end{matrix} \right\}_{\lambda} \left\{ \begin{matrix} a \\ k \end{matrix} \right\}_{\lambda} \left\langle \frac{e_\lambda(t) + 1}{2} \middle| (x)_{l-a,\lambda} \right\rangle_\lambda$$

$$= \sum_{m=0}^{n} \sum_{l=0}^{m} \sum_{a=k}^{l} \binom{n}{m} \binom{l}{a} \beta_{n-m,\lambda} \left\{ \begin{matrix} m \\ l \end{matrix} \right\}_{\lambda} \left\{ \begin{matrix} a \\ k \end{matrix} \right\}_{\lambda}$$

$$\left\langle 1 + \frac{1}{2} \sum_{b=1}^{\infty} (1)_{b,\lambda} \frac{t^b}{b!} \middle| (x)_{l-a,\lambda} \right\rangle_\lambda$$

$$= \sum_{m=0}^{n} \sum_{l=0}^{m} \binom{n}{m} \beta_{n-m,\lambda} \left\{ \begin{matrix} m \\ l \end{matrix} \right\}_{\lambda} \left\{ \begin{matrix} l \\ k \end{matrix} \right\}_{\lambda}$$

$$+ \frac{1}{2} \sum_{m=0}^{n} \sum_{l=k+1}^{m} \sum_{a=k}^{l-1} \binom{n}{m} \binom{l}{a} \beta_{n-m,\lambda} \left\{ \begin{matrix} m \\ l \end{matrix} \right\}_{\lambda} \left\{ \begin{matrix} a \\ k \end{matrix} \right\}_{\lambda} (1)_{l-a,\lambda},$$

$$(93)$$

and thus our proofs are completed.

The Mittag–Leffler polynomials are defined by the generating function to be see ([14, 34, 36])

$$\left(\frac{1+t}{1-t} \right)^x = \sum_{n=0}^{\infty} M_n(x) \frac{t^n}{n!}.$$

$$(94)$$

□

Theorem 9. *For each nonnegative integer n, we have*

$$Ch_n(x) = \sum_{k=0}^{n} \left(\binom{n}{k} \frac{(-1)^{n-k} \langle k+1 \rangle_{n-k}}{2^n} \right) M_k(x).$$

$$(95)$$

As the inversion formula of (95), we have

$$M_n(x) = \sum_{k=0}^{n} \left(2^k \sum_{l=k}^{n} \binom{n}{l} L(l,k)(n-l)! \right) Ch_k(x).$$

$$(96)$$

Proof. Let $Ch_n(x) = \sum_{k=0}^{n} c_{n,k} M_k(x)$. Since

$$Ch_n(x) \sim \left(\frac{e_\lambda(t) + 1}{2}, e_\lambda(t) - 1 \right)_\lambda,$$

$$M_n(x) \sim \left(1, \frac{e_\lambda(t) - 1}{e_\lambda(t) + 1} \right)_\lambda,$$

$$(97)$$

by Theorem 1 and (30), we obtain

$$c_{n,k} = \frac{1}{k!}\left\langle \frac{1}{t+2/2}\left(\frac{t}{t+2}\right)^k \middle| (x)_{n,\lambda}\right\rangle_\lambda = \frac{1}{k!}\left\langle \frac{2t^k}{(t+2)^{k+1}} \middle| (x)_{n,\lambda}\right\rangle_\lambda$$

$$= \frac{1}{k!}\left\langle \sum_{m=0}^\infty \frac{(-1)^m \langle k+1\rangle_m}{2^{k+m}}\frac{t^m}{m!}\middle| \left(t^k\right)_\lambda (x)_{n,\lambda}\right\rangle_\lambda$$

$$= \binom{n}{k}\left\langle \sum_{m=0}^\infty \frac{(-1)^m \langle k+1\rangle_m}{2^{k+m}}\frac{t^m}{m!}\middle| (x)_{n-k,\lambda}\right\rangle_\lambda$$

$$= \binom{n}{k}\frac{(-1)^{n-k}\langle k+1\rangle_{n-k}}{2^n}.$$

$$(98)$$

Conversely, we assume that $M_n(x) = \sum_{k=0}^n d_{n,k} Ch_k(x)$. Then, by (76), we obtain

$$d_{n,k} = \frac{1}{k!}\left\langle \frac{e_\lambda\left(\log_\lambda 1 + t/1 - t\right) + 1}{2}\left(e_\lambda\left(\log_\lambda \frac{1+t}{1-t}\right) - 1\right)^k \middle| (x)_{n,\lambda}\right\rangle_\lambda$$

$$= \frac{1}{2k!}\left\langle \frac{2}{1-t}\left(\frac{2t}{1-t}\right)^k \middle| (x)_{n,\lambda}\right\rangle_\lambda$$

$$= 2^k\left\langle \frac{1}{1-t}\middle| \left(\frac{1}{k!}\left(\frac{t}{1-t}\right)^k\right)_\lambda (x)_{n,\lambda}\right\rangle_\lambda$$

$$= 2^k \sum_{l=k}^n \binom{n}{l} L(l,k)\left\langle \frac{1}{1-t}\middle| (x)_{n-l,\lambda}\right\rangle_\lambda$$

$$= 2^k \sum_{l=k}^n \binom{n}{l} L(l,k)\left\langle \sum_{m=0}^\infty \langle 1\rangle_m \frac{t^m}{m!}\middle| (x)_{n-l,\lambda}\right\rangle_\lambda$$

$$= 2^k \sum_{l=k}^n \binom{n}{l} L(l,k)(n-l)!,$$

$$(99)$$

and so our proofs are completed.

The degenerate Frobenius–Euler polynomials of order α are defined by the generating function to be (see [1, 2, 31, 40])

$$\left(\frac{1-u}{e_\lambda(t)-u}\right)^\alpha e_\lambda^x(t) = \sum_{n=0}^\infty h_{n,\lambda}^{(\alpha)}(x|u)\frac{t^n}{n!}, \quad (u \neq 1, u \in \mathbb{C}), (r \geq 0).$$

$$(100)$$

In the special case $x = 0$, $h_{n,\lambda}^{(\alpha)}(u) = h_{n,\lambda}^{(\alpha)}(0|u)$ are called the degenerate Frobenius–Euler numbers of order α. By the definition of the Frobenius–Euler polynomials of order α, we note that

$$\sum_{n=0}^\infty h_{n,\lambda}^{(\alpha)}(x|u)\frac{t^n}{n!} = \left(\frac{1-u}{e_\lambda(t)-u}\right)^\alpha e_\lambda^x(t)$$

$$= \left(\sum_{n=0}^\infty h_{n,\lambda}^{(\alpha)}(u)\frac{t^n}{n!}\right)\left(\sum_{n=0}^\infty (x)_{n,\lambda}\frac{t^n}{n!}\right)$$

$$= \sum_{n=0}^\infty \left(\sum_{l=0}^n \binom{n}{l} h_{n-l,\lambda}^{(\alpha)}(u)(x)_{l,\lambda}\right)\frac{t^n}{n!},$$

$$(101)$$

and thus we have

$$h_{n,\lambda}^{(\alpha)}(x|u) = \sum_{l=0}^n \binom{n}{l} h_{n-l,\lambda}^{(\alpha)}(u)(x)_{l,\lambda}.$$

$$(102)$$

Furthermore, we see that

$$\left(e_\lambda(t)-u\right)^{-\alpha} = \left((e_\lambda(t)-1)+(1-u)\right)^{-\alpha}$$

$$= \sum_{a=0}^\infty \binom{-\alpha}{a}(1-u)^{-\alpha-a}\left(e_\lambda(t)-1\right)^a$$

$$= \sum_{a=0}^\infty (-1)^a \langle\alpha\rangle_a (1-u)^{-\alpha-a}\frac{1}{a!}\left(e_\lambda(t)-1\right)^a$$

$$= \sum_{m=0}^\infty \sum_{a=0}^m \frac{(-1)^a \langle\alpha\rangle_a}{(1-u)^{\alpha+a}}\left\{\begin{matrix} m \\ a \end{matrix}\right\}_\lambda \frac{t^m}{m!}.$$

$$(103)$$
□

Theorem 10. *For each nonnegative integer n, we have*

$$Ch_n(x) = \sum_{k=0}^n \left(\sum_{l=k}^n \sum_{m=0}^{n-l} \binom{n}{l}\binom{\alpha}{m}\frac{(n-l)_m}{(1-u)^m}\left\{\begin{matrix} l \\ k \end{matrix}\right\}_\lambda Ch_{n-l-m}\right)h_{k,\lambda}^{(\alpha)}(x|u).$$

$$(104)$$

As the inversion formula of (104), we have

$$h_{n,\lambda}^{(\alpha)}(x) = \sum_{k=0}^{n} \left(\sum_{m=k}^{n} \sum_{b=0}^{n-m} \binom{n}{m} \frac{(-1)^b \langle \alpha \rangle_b}{(1-u)^b} \begin{Bmatrix} m \\ k \end{Bmatrix}_\lambda \begin{Bmatrix} n-m \\ b \end{Bmatrix}_\lambda \right.$$

$$+ \frac{1}{2} \sum_{m=k}^{n-1} \sum_{a=0}^{n-m-1} \sum_{b=0}^{a} \binom{n}{m} \binom{n-m}{a}$$

$$\left. \times \frac{(-1)^b \langle \alpha \rangle_b}{(1-u)^b} \{mk\}_\lambda \begin{Bmatrix} a \\ b \end{Bmatrix}_\lambda (1)_{n-m-a,\lambda} \right) Ch_k(x)$$

$$= \sum_{k=0}^{n} \left(\sum_{l=0}^{n} \binom{n}{l} \begin{Bmatrix} l \\ k \end{Bmatrix}_\lambda h_{n-l,\lambda}^{(\alpha)}(u) \right.$$

$$\left. + \frac{1}{2} \sum_{l=k+1}^{n} \sum_{m=k}^{l-1} \binom{n}{l} \binom{l}{m} \begin{Bmatrix} m \\ k \end{Bmatrix}_\lambda h_{n-l,\lambda}^{(\alpha)}(u)(1)_{l-m,\lambda} \right) Ch_k(x).$$

$$(105)$$

Proof. Let $Ch_n(x) = \sum_{k=0}^{n} c_{n,k} h_{k,\lambda}^{(\alpha)}(x|u)$. Since

$$Ch_n(x) \sim \left(\frac{e_\lambda(t)+1}{2}, e_\lambda(t)-1 \right)_\lambda,$$

$$h_{n,\lambda}^{(\alpha)}(x|u) \sim \left(\left(\frac{e_\lambda(t)-u}{1-u} \right)^\alpha, t \right)_\lambda,$$

$$(106)$$

by Theorem 1, we obtain

$$c_{n,k} = \frac{1}{k!} \left\langle \frac{((1+t)-u/1-u)^\alpha}{t+2/2} (\log_\lambda(1+t))^k \middle| (x)_{n,\lambda} \right\rangle_\lambda$$

$$= \left\langle \frac{2}{t+2} \left(\frac{t+(1-u)}{1-u} \right)^\alpha \middle| \left(\frac{1}{k!} (\log_\lambda(1+t))^k \right)_\lambda (x)_{n,\lambda} \right\rangle_\lambda$$

$$= \frac{1}{(1-u)^\alpha} \sum_{l=k}^{n} \binom{n}{l} \begin{bmatrix} l \\ k \end{bmatrix}_\lambda \left\langle \frac{2}{t+2} (t+(1-u))^\alpha \middle| (x)_{n-l,\lambda} \right\rangle_\lambda$$

$$= \frac{1}{(1-u)^\alpha} \sum_{l=k}^{n} \binom{n}{l} \begin{bmatrix} l \\ k \end{bmatrix}_\lambda \left\langle \frac{2}{t+2} \middle| ((t+(1-u))^\alpha)_\lambda (x)_{n-l,\lambda} \right\rangle_\lambda$$

$$= \sum_{l=k}^{n} \sum_{m=0}^{n-l} \binom{n}{l} \binom{\alpha}{m} \frac{\begin{bmatrix} l \\ k \end{bmatrix}_\lambda (n-l)_m}{(1-u)^m} \left\langle \frac{2}{t+2} \middle| (x)_{n-l-m,\lambda} \right\rangle_\lambda$$

$$= \sum_{l=k}^{n} \sum_{m=0}^{n-l} \binom{n}{l} \binom{\alpha}{m} \frac{(n-l)_m}{(1-u)^m} \begin{bmatrix} l \\ k \end{bmatrix}_\lambda Ch_{n-l-m}.$$

$$(107)$$

Conversely, we assume that $h_{n,\lambda}^{(\alpha)}(x|u) = \sum_{k=0}^{n} d_{n,k} Ch_k(x)$. Then, by Theorem 1 and (103), we have

$$d_{n,k} = \frac{1}{k!} \left\langle \frac{e_\lambda(t)+1/2}{(e_\lambda(t)-u/1-u)^\alpha} (e_\lambda(t)-1)^k \middle| (x)_{n,\lambda} \right\rangle_\lambda$$

$$= \left\langle \left(\frac{1-u}{e_\lambda(t)-u} \right)^\alpha \frac{e_\lambda(t)+1}{2} \middle| \left(\frac{1}{k!} (e_\lambda(t)-1)^k \right)_\lambda (x)_{n,\lambda} \right\rangle_\lambda$$

$$= \sum_{m=k}^{n} \binom{n}{m} \begin{Bmatrix} m \\ k \end{Bmatrix}_\lambda \left\langle \left(\frac{1-u}{e_\lambda(t)-u} \right)^\alpha \frac{e_\lambda(t)+1}{2} \middle| (x)_{n-m,\lambda} \right\rangle_\lambda$$

$$= (1-u)^\alpha \sum_{m=k}^{n} \binom{n}{m} \begin{Bmatrix} m \\ k \end{Bmatrix}_\lambda$$

$$\left\langle \frac{e_\lambda(t)+1}{2} \middle| ((e_\lambda(t)-u)^{-\alpha})_\lambda (x)_{n-m,\lambda} \right\rangle_\lambda$$

$$= \sum_{m=k}^{n} \sum_{a=0}^{n-m} \sum_{b=0}^{a} \binom{n}{m} \binom{n-m}{a} \frac{(-1)^b \langle \alpha \rangle_b}{(1-u)^b} \begin{Bmatrix} m \\ k \end{Bmatrix}_\lambda$$

$$\{ab\}_\lambda \left\langle \frac{e_\lambda(t)+1}{2} \middle| (x)_{n-m-a,\lambda} \right\rangle_\lambda$$

$$= \sum_{m=k}^{n} \sum_{a=0}^{n-m} \sum_{b=0}^{a} \binom{n}{m} \binom{n-m}{a} \frac{(-1)^b \langle \alpha \rangle_b}{(1-u)^b} \begin{Bmatrix} m \\ k \end{Bmatrix}_\lambda \begin{Bmatrix} a \\ b \end{Bmatrix}_\lambda$$

$$\times \left\langle 1 + \frac{1}{2} \sum_{l=1}^{\infty} (1)_{l,\lambda} \frac{t^l}{l!} \middle| (x)_{n-m-a,\lambda} \right\rangle_\lambda$$

$$= \sum_{m=k}^{n} \sum_{b=0}^{n-m} \binom{n}{m} \frac{(-1)^b \langle \alpha \rangle_b}{(1-u)^b} \begin{Bmatrix} m \\ k \end{Bmatrix}_\lambda \begin{Bmatrix} n-m \\ b \end{Bmatrix}_\lambda$$

$$+ \frac{1}{2} \sum_{m=k}^{n-1} \sum_{a=0}^{n-m-1} \sum_{b=0}^{a} \binom{n}{m} \binom{n-m}{a} \frac{(-1)^b \langle \alpha \rangle_b}{(1-u)^b}$$

$$\begin{Bmatrix} m \\ k \end{Bmatrix}_\lambda \begin{Bmatrix} a \\ b \end{Bmatrix}_\lambda (1)_{n-m-a,\lambda}.$$

$$(108)$$

In addition, by (11) and (102), we obtain

$$
d_{n,k} = \frac{1}{k!} \left\langle \frac{e_\lambda(t)+1}{2} (e_\lambda(t)-1)^k \middle| h_{n,\lambda}^{(\alpha)}(x|u) \right\rangle_\lambda
$$

$$
= \frac{1}{k!} \sum_{l=0}^{n} \binom{n}{l} h_{n-l,\lambda}^{(\alpha)}(u) \left\langle \frac{e_\lambda(t)+1}{2} (e_\lambda(t)-1)^k \middle| (x)_{l,\lambda} \right\rangle_\lambda
$$

$$
= \sum_{l=0}^{n} \binom{n}{l} h_{n-l,\lambda}^{(\alpha)}(u) \left\langle \frac{e_\lambda(t)+1}{2} \middle| \left(\frac{1}{k!}(e_\lambda(t)-1)^k \right)_\lambda (x)_{l,\lambda} \right\rangle_\lambda
$$

$$
= \sum_{l=0}^{n} \sum_{m=k}^{l} \binom{n}{l} \binom{l}{m} \left\{ \begin{matrix} m \\ k \end{matrix} \right\}_\lambda h_{n-l,\lambda}^{(\alpha)}(u) \left\langle \frac{e_\lambda(t)+1}{2} \middle| (x)_{l-m,\lambda} \right\rangle_\lambda
$$

$$
= \sum_{l=0}^{n} \sum_{m=k}^{l} \binom{n}{l} \binom{l}{m} \left\{ \begin{matrix} m \\ k \end{matrix} \right\}_\lambda h_{n-l,\lambda}^{(\alpha)}(u)
$$

$$
\left\langle 1 + \frac{1}{2} \sum_{a=1}^{\infty} (1)_{a,\lambda} \frac{t^a}{a!} \middle| (x)_{l-m,\lambda} \right\rangle_\lambda
$$

$$
= \sum_{l=0}^{n} \binom{n}{l} \left\{ \begin{matrix} l \\ k \end{matrix} \right\}_\lambda h_{n-l,\lambda}^{(\alpha)}(u)
$$

$$
+ \frac{1}{2} \sum_{l=k+1}^{n} \sum_{m=k}^{l-1} \binom{n}{l} \binom{l}{m} \left\{ \begin{matrix} m \\ k \end{matrix} \right\}_\lambda h_{n-l,\lambda}^{(\alpha)}(u) (1)_{l-m,\lambda}.
$$

$$
\tag{109}
$$

$\square$

3. Conclusion

In this paper, we studied the Changhee polynomials related to the lambda falling factorial (Theorem 2), the degenerate Bernoulli polynomials (Theorem 3), the degenerate Euler polynomials (Theorem 4), the degenerate Daehee polynomials (Theorem 5), the degenerate Bell polynomials (Theorem 6), the degenerate Lah–Bell polynomials (Theorem 7), the degenerate Bernoulli polynomials of the second kind (Theorem 8), the Mittag–Leffler polynomials (Theorem 9), and the degenerate Frobenius–Euler polynomials (Theorem 10) by finding the coefficients which are also polynomials or numbers when the n-th Changhee polynomial is expressed as a linear combination of those degenerate special polynomials by using the λ-Sheffer sequences and λ-differential operators. In addition, we derive the inversion formulas of these identities.

Umbral calculus has been applied in many fields such as combinatorial counting with linear recurrences and lattice path counting, graph theory using chromatic polynomials, probability theory, link invariant theory, statistics, topology, and physics. It is being actively applied in various fields by researchers. As one of our future projects, we would like to continue to study degenerate versions of certain special polynomials and numbers by using λ-Umbral calculus. [41].

Data Availability

No data were used to support this study.

Conflicts of Interest

The authors declare that they have no conflicts of interest.

Authors' Contributions

TK and JWP conceived the framework and structured the whole manuscript. TK and JWP wrote the paper. BMK and TAR checked the results of the manuscript. All authors read and approved the final paper.

Acknowledgments

References

[1] H. K. Kim, "Degenerate lah-bell polynomials arising from degenerate sheffer sequences," *Adv. Difference Equ*, p. 16, 2020.

[2] D. S. Kim and T. Kim, "Degenerate Sheffer sequences and λ-Sheffer sequences," *Journal of Mathematical Analysis and Applications*, vol. 493, Article ID 124521, 2021.

[3] K. S. Nisar, *Umbral Calculus*, LAP LAMBERT Academic Publishing, Sunnyvale, 2012.

[4] S. Roman, *The Umbral Calculus*, Dover Publ. Inc, New York, NY, USA, 2005.

[5] S. Araci, "Novel identities involving Genocchi numbers and polynomials arising from applications of umbral calculus," *Applied Mathematics and Computation*, vol. 233, pp. 599–607, 2014.

[6] S. Araci, M. Acikgoz, T. Diagana, and H. M. Srivastavav, "A novel approach for obtaining new identities for the λ extension of q-Euler polynomials arising from the q-umbral calculus," *The Journal of Nonlinear Science and Applications*, vol. 10, no. 4, pp. 1316–1325, 2017.

[7] S. Araci, X. Kong, M. Acikgoz, and E. Sen, "A new approach to multivariate q-Euler polynomials using the umbral calculus," *Journal of Integer Sequences*, vol. 17, no. 1, p. 10, 2014.

[8] R. Dere and Y. Simsek, "Applications of umbral algebra to some special polynomials," *Adv. Stud. Contemp. Math. (Kyungshang)*, vol. 22, no. 3, pp. 433–438, 2012.

[9] R. Dere, Y. Simsek, and H. M. Srivastava, "A unified presentation of three families of generalized Apostol type polynomials based upon the theory of the umbral calculus and the umbral algebra," *Journal of Number Theory*, vol. 133, no. 10, pp. 3245–3263, 2013.

[10] L.-C. Jang, D. San Kim, H. Kim, T. Kim, and H. Lee, "Study of degenerate poly-Bernoulli polynomials by λ-umbral calculus," *Computer Modeling in Engineering and Sciences*, vol. 129, no. 1, pp. 393–408, 2021.

[11] H. K. Kim, D. V. Dolgy, and D. V. Dolgy, "Degenerate Catalan-Daehee numbers and polynomials of order $ r $ arising from degenerate umbral calculus," *AIMS Mathematics*, vol. 7, no. 3, pp. 3845–3865, 2022.

[12] T. Kim, D. S. Kim, D. V. Dolgy, and J.-W. Park, "On the type 2 poly-Bernoulli polynomials associated with umbral calculus," *Open Mathematics*, vol. 19, no. 1, pp. 878–887, 2021.

[13] T. Komatsu and Y. Simsek, "Identities related to the stirling numbers and modified apostol-type numbers on umbral

calculus," *Miskolc Mathematical Notes*, vol. 18, no. 2, pp. 905–916, 2017.

[14] G.-C. Rota and B. D. Taylor, "The classical umbral calculus," *SIAM Journal on Mathematical Analysis*, vol. 25, no. 2, pp. 694–711, 1994.

[15] Y. Simsek, "Special numbers and polynomials including their generating functions in Umbral analysis methods," *Axioms*, vol. 7, no. 2, p. 22, 2018.

[16] H. M. Srivastava, K. S. Nisar, and M. A. Khan, "Some umbral calculus presentations of the chan-chyan-srivastava polynomials and the erkuḷ-srivastava polynomials," *Proyecciones (Antofagasta)*, vol. 33, no. 1, pp. 77–90, 2014.

[17] L. Comtet, "Advanced combinatorics," *Dordrecht-Holland*, Springer, Netherlands, 1974.

[18] L.-C. Jang, C. S. Ryoo, J. J. Seo, and H. In Kwon, "Some properties of the twisted Changhee polynomials and their zeros," *Applied Mathematics and Computation*, vol. 274, pp. 169–177, 2016.

[19] T. Kim and D. S. Kim, "Degenerate zero-truncated Poisson random variables," *Russian Journal of Mathematical Physics*, vol. 28, no. 1, pp. 66–72, 2021.

[20] H. K. Kim and D. S. Lee, "Some identities of degenerate r-extended Lah-Bell polynomials," *Proceedings of the Jangjeon Mathematical Society*, vol. 24, no. 1, pp. 47–61, 2021.

[21] M. Acikgoz and U. Duran, "Unified degenerate central Bell polynomials," *Journal of Mathematical Analysis and Applications*, vol. 11, no. 2, pp. 18–33, 2020.

[22] J. Jeong and S.-H. Rim, "On finite times degenerate higher-order Cauchy numbers and polynomials," *Bulletin of the Korean Mathematical Society*, vol. 53, no. 5, pp. 1427–1437, 2016.

[23] T. Kim, D. V. Dolgy, D. S. Kim, H. K. Kim, and S. H. Park, "A note on degenerate generalized Laguerre polynomials and Lah numbers," *Advances in Difference Equations*, 2021.

[24] T. Kim and D. S. Kim, "Some identities on truncated polynomials associated with Degenerate Bell polynomials," *Russian Journal of Mathematical Physics*, vol. 28, no. 3, pp. 342–355, 2021.

[25] T. Kim and D. S. Kim, "Degenerate polyexponential functions and degenerate Bell polynomials," *Journal of Mathematical Analysis and Applications*, vol. 487, no. 2, p. 15, Article ID 124017, 2020.

[26] T. Kim, D. S. Kim, H. Lee, and J. W. Park, "A note on degenerate r-Stirling numbers," *Journal of Inequalities and Applications*, vol. 225, p. 12, 2020.

[27] T. Komastu and P. T. Young, "Convolutions of generalized Stirling numbers and degenerate Bernoulli polynomials," *Fibonacci Quarterly*, vol. 58, no. 4, pp. 361–366, 2020.

[28] L. Carlitz, "Degenerate stirling, bernoulli and eulerian numbers," *Util. Math*, vol. 15, pp. 51–88, 1979.

[29] B. M. Kim, L. C. Jang, W. Kim, and H. I. Kwon, "On Carlitz's type modified degenerate q-Changhee polynomials and numbers," *Discrete Dynamics in Nature and Society*, vol. 2018, Article ID 9520269, 5 pages, 2018.

[30] D. S. Kim and T. Kim, "A note on a new type of degenerate Bernoulli numbers," *Russian Journal of Mathematical Physics*, vol. 27, no. 2, pp. 227–235, 2020.

[31] G. Muhiuddin, W. A. Kahn, and D. Al-Kadi, "Construction on the degenerate poly-Frobenius-Euler polynomials of complex variable," *Journal of Function Spaces*, vol. 2021, Article ID 3115424, 9 pages, 2021.

[32] S. K. Sharma, W. A. Khan, S. Araci, and S. S. Ahmed, "New type of degenerate Daehee polynomials of the second kind," *Advances in Difference Equations*, vol. 428, p. 16, 2020.

[33] W. A. Khan, G. Muhiuddin, A. Muhyi, and D. Al-Kadi, "Analytical properties of type 2 degenerate poly-Bernoulli polynomials associated with their applications," *Advances in Difference Equations*, vol. 420, p. 18, 2021.

[34] T. Kim, L.-C. Jang, D. S. Kim, and H. Y. Kim, "Some identities on type 2 degenerate Bernoulli polynomials of the second kind," *Symmetry*, vol. 12, no. 4, p. 510, 2020.

[35] T. Kim and D. S. Kim, "Some relations of two type 2 polynomials and discrete harmonic numbers and polynomials," *Symmetry*, vol. 12, no. 6, 2020.

[36] T. Kim, D. S. Kim, L. C. Jang, and H. Leek, "Jindalrae and Gaenari numbers and polynomials in connection with Jindalrae? Stirling numbers," *Advances in Difference Equation*, vol. 2020, no. 245, 19 pages, 2020.

[37] D. Lim, "Degenerate, partially degenerate and totally degenerate Daehee numbers and polynomials," *Advances in Difference Equations*, vol. 2015, no. 1, p. 14, 2015.

[38] G. Nyul and G. Rácz, "The r-Lah numbers," *Discrete Mathematics*, vol. 338, no. 10, pp. 1660–1666, 2015.

[39] S. Tauber, "Lah numbers for fibonacci and lucas polynomials," *Fibonacci Quarterly*, vol. 6, no. 5, pp. 93–99, 1968.

[40] S. Araci and M. Acikgoz, "A note on the Frobenius-Euler numbers and polynomials associated with Bernstein polynomials," *Adv. Stud. Contemp. Math. (Kyungshang)*, vol. 22, no. 3, pp. 399–406, 2012.

[41] B.-M. Kim, J. Jeong, and S.-H. Rim, "Some explicit identities on Changhee-Genocchi polynomials and numbers," *Advances in Difference Equations*, vol. 2016, no. 1, p. 202, 2016.

WILEY | Hindawi

Research Article

New Periodic and Localized Traveling Wave Solutions to a Kawahara-Type Equation: Applications to Plasma Physics

Haifa A. Alyousef [iD],[1] **Alvaro H. Salas** [iD],[2] **M. R. Alharthi** [iD],[3] **and S. A. El-Tantawy** [iD][4,5]

[1]Department of Physics, College of Science, Princess Nourah bint Abdulrahman University, P.O. Box 84428, Riyadh 11671, Saudi Arabia
[2]Department of Mathematics and Statistics, Universidad Nacional de Colombia, FIZMAKO Research Group, Sede Manizales, Colombia
[3]Department of Mathematics and Statistics, College of Science, Taif University, P.O. Box 11099, Taif 21944, Saudi Arabia
[4]Department of Physics, Faculty of Science, Port Said University, Port Said 42521, Egypt
[5]Research Center for Physics (RCP), Department of Physics, Faculty of Science and Arts, Al-Makhwah, Al-Baha University, Al Bahah, Saudi Arabia

Correspondence should be addressed to S. A. El-Tantawy; tantawy@sci.psu.edu.eg

In this study, some new hypotheses and techniques are presented to obtain some new analytical solutions (localized and periodic solutions) to the generalized Kawahara equation (gKE). As a particular case, some traveling wave solutions to both Kawahara equation (KE) and modified Kawahara equation (mKE) are derived in detail. Periodic and soliton solutions to this family are obtained. The periodic solutions are expressed in terms of Weierstrass elliptic functions (WSEFs) and Jacobian elliptic functions (JEFs). For KE, some direct and indirect approaches are carried out to derive the periodic and localized solutions. For mKE, two different hypotheses in the form of WSEFs are used to derive the periodic and localized solutions. Also, the cnoidal wave solutions in the form of JEFs are obtained. As a realistic physical application, the solutions obtained can be dedicated to studying many nonlinear waves that propagate in plasma.

1. Introduction

Both ordinary and partial differential equations succeed in modelling and describing many complex nonlinear systems that are widely used in various fields of science such as optical fiber, fluid mechanics, nonlinear optics, biology, ecology, astronomy, oceans, economics, and plasma physics [1–10]. Due to the importance of these applications, the great success has achieved by differential equations in clarifying and interpreting the ambiguity of many complex systems, which prompted many authors to look for different analytical and numerical methods in solving such models [5–11]. In recent years, many new analytical and numerical methods have been discovered, and some improvements have been made to many of the existing methods in order to either obtain real solutions related to realistic problems or to obtain more accurate solutions to many integrable and nonintegrable differential equations [12–16]. In particular, there are a large number of partial differential equations (PDEs) that have been used for modelling a lot of nonlinear phenomena such as solitary waves, shock waves, cnoidal waves, peakons, and compactons that arise in different plasma models [5–11]. One of the most important of these equations and the most famous due to its great success not only in the field of fluid mechanics and plasma physics but also in various fields of science is Korteweg–de Vries (KdV) equation [5]:

$$\partial_t u(x,t) + \alpha_1 u(x,t)\partial_x u(x,t) + \beta\partial_x^3 u(x,t) = 0, \qquad (1)$$

where (α_1, β) are the real coefficients which are related to the physical model under study. This equation and its one-dimensional family including a modified KdV (mKdV) equation [5, 10], a Gardner equation, KdV–Burger's equation [5], damped KdV/mKdV equation [11], and so on have been widely used until this day in interpreting the mechanism and properties of many nonlinear phenomena that can propagate in plasma physics. This family is characterized by the third-order dispersion, but there is another family characterized by the fifth-order dispersion which is called the family of Kawahara equation (KE) [17].

$$R_{KE} \equiv \partial_t u(x,t) + \alpha_1 u(x,t)\partial_x u(x,t) \\ + \beta \partial_x^3 u(x,t) - \gamma \partial_x^5 u(x,t) = 0. \tag{2}$$

This is a nonlinear dispersive equation which generalizes the well-known KdV equation. Kawahara equation (2), sometimes referred to as the fifth-order KdV/or super KdV equation [18], is a model that describes solitary waves, cnoidal waves, and periodic waves propagating in nonlinear and high-dispersive media. This equation and many related equations with fifth-order dispersion have been extensively studied in literature [19]. It has important applications in the theory of magnetoacoustic waves in plasma and in the theory of shallow water waves with surface tension [17, 18, 20–30]. However, equation (2) fails to explain the nonlinear waves at some critical values of the plasma compositions due to the disappearance of the nonlinear term, i.e., $\alpha_1 = 0$. Accordingly, modified Kawahara equation (mKE) with higher-order nonlinearity was derived to describe some nonlinear phenomena at the critical plasma compositions:

$$R_{mKE} \equiv \partial_t u(x,t) + \alpha_2 u^2(x,t)\partial_x u(x,t) \\ + \beta \partial_x^3 u(x,t) - \gamma \partial_x^5 u(x,t) = 0. \tag{3}$$

Both KE equation (2) and mKE equation (3) are integrable Hamiltonian systems which are due to the many applications related to this family; many methodologies have been applied for analyzing it [17, 18, 20–24, 27–30]. There remain many secrets about the solutions of this family that appear and become clear day after day as a result of using new analytical and numerical methods for solving this family. This is one of our motives for obtaining a new generation of solutions to this family, which can contribute in understanding the mysterious of many phenomena in plasma physics and other fields related to this family. Thus, our aim is to provide new traveling wave (localized and periodic) solutions to the following generalized KE [29] using several new hypotheses and techniques:

$$\partial_t u(x,t) + \alpha_p u^P(x,t)\partial_x u(x,t) + \beta \partial_x^3 u(x,t) - \gamma \partial_x^5 u(x,t) = 0, \tag{4}$$

where p is a real number. Note that KE equation (2) can be obtained for $p = 1$, while for $p = 2$, mKE equation (3) is recovered.

2. General Analytical Solutions to the Generalized KE

To find a general analytic solution to the evolution equation (4), we suppose

$$\begin{cases} u = v^{(1/p)}, \\ v \equiv v(\xi) \qquad \xi = x + \lambda t, \end{cases} \tag{5}$$

where λ represents the frame velocity.

Inserting ansatz equations (5) into (4) gives the nonlinear ODE:

$$\alpha p^4 v^5 v' + p^4 v^4 \left(\beta v^{(3)} + \lambda v' - \gamma v^{(5)}\right) \\ + (p-1)p^3 v^3 \left(5\gamma v^{(4)} v' + 10\gamma v^{(3)} v'' - 3\beta v' v''\right) \\ + (p-1)p^2(2p-1)v^2 v'\left(-15\gamma(v'')^2\right. \\ \left. + \beta(v')^2 - 10\gamma v^{(3)} v'\right) \\ - \gamma(p-1)(2p-1)(3p-1)(4p-1)(v')^5 \\ + 10\gamma(p-1)p(2p-1)(3p-1)v(v')^3 v'' = 0, \tag{6}$$

where $v' \equiv \partial_\xi v$, $v'' \equiv \partial_\xi^2 v$, $v^{(3)} \equiv \partial_\xi^3 v$, $v^{(4)} \equiv \partial_\xi^4 v$, and $v^{(5)} \equiv \partial_\xi^5 v$.

In the following subsections, two important particular cases ($p = 1$ and $p = 2$), i.e., KE equation (2) and mKE equation (3)are analyzed.

2.1. Solutions of the Planar Kawahara Equation.
In the following sections, we try to find some new solutions including the periodic wave solutions, cnoidal wave solutions, and solitary wave solutions to the planar KE equation (2) ($p = 1$).

2.1.1. Periodic and Solitary Wave Solutions.
For planar KE equation (2), ODE equation (6) reduces to

$$-\gamma v^{(5)} + \beta v^{(3)} + \alpha v v' + \lambda v' = 0. \tag{7}$$

Integrating equation (7) once over ξ gives us

$$c_0 - \gamma v^{(4)} + \beta v'' + \frac{1}{2}\alpha v^2 + \lambda v = 0, \tag{8}$$

where c_0 is the integration constant.

Multiplying equation (8) by v' and then integrating it again, we get

$$c_0 v + c_1 + \frac{1}{2}\gamma(v'')^2 + \frac{1}{2}\beta(v')^2 - \gamma v^{(3)} v' + \frac{1}{6}\alpha v^3 + \frac{1}{2}\lambda v^2 = 0, \tag{9}$$

where c_1 the new constant of integration. The solution of equation (2) via several approaches is discussed as follows.

We seek a solution in the ansatz form:

$$v = \sum_{k=0}^{N} d_j \varphi^j, \tag{10}$$

where $\varphi \equiv \varphi(\xi)$ is a solution to the following Helmholtz equation [31].

$$\begin{cases} \varphi'' + A\varphi + B\varphi^2 = 0, \\ (\varphi')^2 = -A\varphi^2 - \dfrac{2}{3}B\varphi^3 + 2c_2. \end{cases} \tag{11}$$

Balancing the highest linear and nonlinear terms in equation (11) gives $N = 2$, so that

$$v = d_0 + d_1\varphi + d_2\varphi^2. \tag{12}$$

Inserting ansatz equation (12) into equation (9), we obtain

$$\sum_{j=0}^{6} F_j\varphi^j = 0, \tag{13}$$

where the values of $F_j (j = 0, 1, \cdots 6)$ are defined in Appendix A, and by solving the following system,

$$F_j = 0, \tag{14}$$

we get

$$c_0 = \frac{-1}{57122\alpha\gamma^2}\left(4598321A^4\gamma^4 - 54418A^2\beta^2\gamma^2 + 1457\beta^4 - 28561\gamma^2\lambda^2\right),$$

$$c_1 = \frac{-1}{28960854\alpha^2\gamma^3}\left(\begin{array}{c} 19394118562A^6\gamma^6 - 183532986A^4\beta^2\gamma^4 + 2331348747A^4\gamma^5\lambda \\ \\ +134862A^2\beta^4\gamma^2 - 27589926A^2\beta^2\gamma^3\lambda + 94922\beta^6 + 738699\beta^4\gamma\lambda - 4826809\gamma^3\lambda^3 \end{array}\right),$$

$$c_2 = \frac{(13A\gamma + \beta)}{263640B^2\gamma^3}\left(1690A^2\gamma^2 - 403A\beta\gamma + 31\beta^2\right),$$

$$d_0 = \frac{-1}{507\alpha\gamma}\left(1183A^2\gamma^2 - 910A\beta\gamma + 31\beta^2 + 507\gamma\lambda\right),$$

$$d_1 = \frac{140B(13A\gamma + \beta)}{39\alpha},$$

$$d_2 = \frac{140B^2\gamma}{3\alpha}. \tag{15}$$

Equation (11) has many formulas for its general solutions such as

$$\varphi = -\frac{A}{2B} - \frac{6}{B}\wp\left(\xi + e_0; A^2/12, g_3\right), \tag{16}$$

where $\wp \equiv \wp(\xi + e_0; A^2/12, g_3)$ indicates the Weierstrass elliptic function (WSEF) and the values of e_0 and g_3 are undetermined parameters which can be obtained from the initial conditions.

Also, the general solution to equation (11) can be expressed by

$$\varphi = e_1 - \frac{6e_1(A + Be_1)}{A + 2Be_1 + 12\wp\left(\xi + e_0; A^2/12, 1/216\left(A^3 - 6B^2e_1^2A - 4B^3e_1^3\right)\right)}, \tag{17}$$

where the values of e_0 and e_1 are determined from the initial conditions.

Thus, a periodic solution to KE equation (2) according to the values of parameters given in system equation (15) and the value of φ given in equation (16) is obtained as

$$u = \frac{910\beta A\gamma - 7098A^2\gamma^2 - 910A\beta\gamma - 31\beta^2 - 507\gamma\lambda}{507\alpha\gamma}$$

$$- \frac{280\beta}{13\alpha}\wp\left(x + \lambda t + \xi_0; A^2/12, g_3\right)$$

$$+ \frac{1680\gamma}{\alpha}\wp^2\left(x + \lambda t + \xi_0; A^2/12, g_3\right). \tag{18}$$

The constants A, B, λ, and ξ_0 are the arbitraries.

Using relation equation (9) with of the parameters given in system equation (15) and the value of φ given in equation (17), the solution to KE equation (2) can be expressed by

$$u = \frac{-31\beta^2 - 13\gamma\left(39\lambda - 70A\beta + 91A^2\gamma\right) + 1820B\gamma e_0\left(\beta + 13A\gamma + 13B\gamma e_0\right)}{507\alpha\gamma}$$

$$- \frac{280Be_0\left(A + Be_0\right)\left(\beta + 13A\gamma + 26B\gamma e_0\right)}{13\alpha\left[A + 2Be_0 + 12\wp\left(x + \lambda t + \xi_0; A^2/12, 1/216\left(A^3 - 2B^2 e_0^2\left(3A + 2Be_0\right)\right)\right)\right]}$$

$$+ \frac{1680B^2\gamma e_0^2\left(A + Be_0\right)^2}{\alpha\left[A + 2Be_0 + 12\wp^2\left(x + \lambda t + \xi_0; A^2/12, 1/216\left(A^3 - 2B^2 e_0^2\left(3A + 2Be_0\right)\right)\right)\right]},$$

(19)

where the constants A, B, λ, and e_0 are the arbitraries.

From the periodic solution equation (18), the soliton solutions can be obtained using the following hypotheses:

$$\begin{cases} cg_2 = A^2/12 = \dfrac{4}{3}, \\[2mm] g_3 = \dfrac{\beta\left(3549A^2\gamma^2 - 31\beta^2\right)}{4745520\gamma^3} = \dfrac{8}{27}, \end{cases}$$

(20)

which lead to $(A, \beta) = (4, 52\gamma)$, and by rearrange solution (18), the following soliton solution is obtained:

$$= -\frac{1168\gamma + 3\lambda}{3\alpha} - \frac{1120\gamma}{\alpha}\wp\left(x + \lambda t; \frac{4}{3}, -\frac{8}{27}\right),$$

$$+ \frac{1680\gamma}{\alpha}\wp\left(x + \lambda t; \frac{4}{3}, -\frac{8}{27}\right)^2.$$

(21)

Moreover, the solitary wave solution can be obtained by

$$\begin{cases} g_2 = A^2/12 = 1/12, \\[2mm] g_3 = \dfrac{\beta\left(3549A^2\gamma^2 - 31\beta^2\right)}{4745520\gamma^3} = -1/216, \end{cases}$$

(22)

which leads to $(A, \beta) = (1, 13\gamma)$; then, the periodic solution (18) reduces to the following soliton solution:

$$= -\frac{73\gamma + 3\lambda}{3\alpha} - \frac{280\gamma\wp\left(x + \lambda t + \xi_0; 1/12, -1/216\right)}{\alpha}$$

$$+ \frac{1680\gamma\wp\left(x + \lambda t + \xi_0; 1/12, -1/216\right)^2}{\alpha}.$$

(23)

Also, the periodic solution to KE (2) can be derived directly in terms of WSEF $\wp \equiv \wp\left(x + \lambda t + \xi_0; g_2, g_3\right)$ by inserting the following ansatz in (9).

$$u = a_0 + a_1\wp + a_2\wp^2,$$

(24)

which leads to

$$\sum_{j=0}^{6} S_j\varphi^j = 0,$$

(25)

where the values of $S_j\,(j = 0, 1, \cdots)$ are defined in Appendix B , and by solving the following system,

$$S_j = 0,$$

(26)

we have

$$a_1 = -\frac{280\beta k^2}{13\alpha},\ a_2 = \frac{1680\gamma k^4}{\alpha},$$

$$c_1 = -\frac{1}{14394744\alpha\gamma^2 k}\begin{bmatrix} 11661\alpha a_0\gamma k\left(507\alpha a_0\gamma k + 1014\gamma\lambda + 146\beta^2 k\right) \\ -1285245\gamma^2\lambda^2 + 449159\beta^4 k^2 + 1702506\beta^2\gamma k\lambda \end{bmatrix},$$

$$c_2 = \frac{1}{21894405624\alpha^2\gamma^3 k}\begin{bmatrix} 1521\alpha a_0\gamma\begin{pmatrix} 507\alpha a_0\gamma k\left(6929\alpha a_0\gamma k + 9126\gamma\lambda + 2189\beta^2 k\right) \\ +5\left(277\beta^2 k - 507\gamma\lambda\right)\left(507\gamma\lambda + 73\beta^2 k\right) \end{pmatrix} \\ -7\left(128781549\beta^2\gamma^2\lambda^2 + 9635389\beta^6 k^2 + 75627162\beta^4\gamma k\lambda\right) \end{bmatrix},$$

$$g_2 = -\frac{507\alpha a_0\gamma k + 507\gamma\lambda + 31\beta^2 k}{85176\gamma^2 k^5},$$

$$g_3 = -\frac{\beta\left(169\alpha a_0\gamma k + 169\gamma\lambda + 31\beta^2 k\right)}{3163680\gamma^3 k^7}.$$

(27)

Collecting both equations (24) and (27), we finally get

$$u = a_0 - \frac{280\beta k^2}{13\alpha} \wp\left(kx + t\lambda + \xi_0; -\frac{31k\beta^2 + 507\gamma\lambda + 507k\alpha\gamma a_0}{85176k^5\gamma^2}, -\frac{\beta(31k\beta^2 + 169\gamma\lambda + 169k\alpha\gamma a_0)}{3163680k^7\gamma^3}\right)$$

$$+ \frac{1680\gamma k^4}{\alpha} \wp\left(kx + t\lambda + \xi_0; -\frac{31k\beta^2 + 507\gamma\lambda + 507k\alpha\gamma a_0}{85176k^5\gamma^2}, -\frac{\beta(31k\beta^2 + 169\gamma\lambda + 169k\alpha\gamma a_0)}{3163680k^7\gamma^3}\right)^2. \tag{28}$$

Solution equation (28) satisfies KE equation (2).

2.1.2. Cnoidal and Solitary Wave Solutions.

We look for a solution to KE equation (2) in the ansatz form

$$u(x,t) = v(\xi) = \sum_{j=0}^{N} d_j cn^j(\xi), \tag{29}$$

where $\xi = \sqrt{\omega}(x + \lambda t)$ and N is an integer and positive number. From the balance between the highest-order linear $(N + 4)$ and nonlinear $(2N)$ terms of equation (8), we have $N = 4$. Substituting ansatz equation (29) into equation (6) gives a very complicated system. By solving this system using Mathematica package, we found that the coefficients of the odd power in ansatz equation (29) vanish. Thus, the solution of KE equation (2) could be written in the following ansatz:

$$u = A + Bcn^2(\xi,m) + Ccn^4(\xi,m). \tag{30}$$

Inserting ansatz equation (30) into KE equation (2), we get

$$R_{KE} = \sum_{j=0}^{3} W_j cn^{2j} = 0, \tag{31}$$

the values of $W_j (j = 0, 1, \cdots 3)$ are given in Appendix C, and by solving the system,

$$W_j = 0, \tag{32}$$

we have

$$A = \frac{1}{507\alpha\gamma}\left[\begin{array}{c} -31\beta^2 + 3640\beta\gamma(1 - 2m)\omega \\ +169\gamma(112\gamma(14(m-1)m-1)\omega^2 - 3\lambda) \end{array}\right],$$

$$B = \frac{-280m\omega}{13\alpha}(52\gamma(2m-1)\omega - \beta), \quad C = \frac{1680\gamma m^2\omega^2}{\alpha}, \tag{33}$$

where ω is a solution to the following cubic equation:

$$31\beta^3 - 56784\beta\gamma^2(m^2 - m + 1)\omega^2$$
$$+ 703040\gamma^3(m-2)(m+1)(2m-1)\omega^3 = 0. \tag{34}$$

Finally, the cnoidal wave solutions to KE equation (2) are obtained as

$$= \frac{-31\beta^2 + 3640\beta\gamma(1 - 2m)\omega + 169\gamma(112\gamma(14(m-1)m-1)\omega^2 - 3\lambda)}{507\alpha\gamma},$$

$$-\frac{280m\omega(52\gamma(2m-1)\omega - \beta)}{13\alpha}cn^2(\xi,m) + \frac{1680\gamma m^2\omega^2}{\alpha}cn^4(\xi,m), \tag{35}$$

where λ is the arbitrary constant, $\xi = \sqrt{\omega}(x + \lambda t)$, and ω is a root to equation (34).

The cnoidal wave solution equation (35) can be directly reduced to the soliton solution for $m \longrightarrow 1$ as

$$u = -\frac{36\beta^2 + 169\gamma\lambda}{169\alpha\gamma} + \frac{105\beta^2}{169\alpha\gamma}\sec h^4\left[\frac{1}{2}\sqrt{\frac{\beta}{13\gamma}}(x + \lambda t)\right]. \tag{36}$$

Moreover, solution equation (36) coincides with the obtained one by means of the tanh method:

$$u = \frac{105\beta^2}{169\alpha\gamma}\sec h^4\left[\frac{1}{2}\sqrt{\frac{\beta}{13\gamma}}\left(x - \frac{36\beta^2}{169\gamma}t\right)\right]. \tag{37}$$

The obtained solutions can be employed for investigating the propagation of nonlinear structures in different plasma models. For instance, we can apply these solutions to study cnoidal and solitary waves in the ultracold neutral plasma (UCNP) which is composed of strongly coupled positive ions and non-Maxwellian electron distributions [32–35]. Based on this model and for Maxwellian electrons, the values of the coefficients (α, β) are given by (to prevent stuffing and repetition, all the details can be found [32])

$$\alpha = \lambda_{ph} \text{ and } \beta = \frac{1}{2\lambda_{ph}}, \tag{38}$$

and the phase velocity λ_{ph} of the ion-acoustic waves (IAWs) reads

$$\lambda = \sqrt{1 + \sigma_*}, \tag{39a}$$

where $\sigma_* \equiv \sigma_*(T_e, T_i)$ represents the effective temperature ratio which is a function of electron and ion temperatures (T_e, T_i) [32–35]. For $(T_e, T_i) = (25K, 1K)$, we get $\sigma_* = 0.401169$, and for $(T_e, T_i) = (900K, 1K)$, we obtain $\sigma_* = 0.0120837$ [32–35]. With respect to the coefficient of the fifth-order dispersion γ, in general, it has a small value $0 < \gamma \ll 1$. The impact of effective temperature ratio σ^* on the profile of the cnoidal wave solution equation (35) and the solitary wave solution equation (36) for $(\gamma, \lambda) = (0.1, 0.1)$ is shown in Figures 1 and 2, respectively. It is observed that increasing the electron temperature, i.e., decreasing σ^*, leads

(a)

$\sigma^{*}=0.40117$
$\sigma^{*}=0.0.0121$

(b)
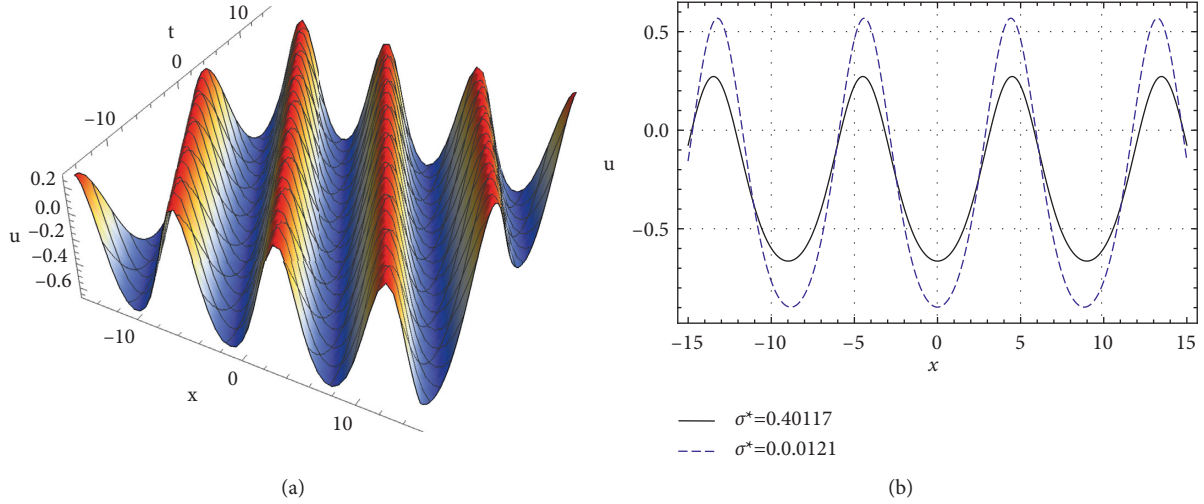
FIGURE 1: The profile of the periodic wave solution equation (35) to KE equation (2) plotted in (x, t) plane.

(a)

$\sigma^{*}=0.40117$
$\sigma^{*}=0.0.0121$

(b)

FIGURE 2: The profile of the solitary wave solution equation (36) to KE equation (2) is plotted in (x, t) plane.

to the enhancement (reduction) of the amplitude (width) of both localized and periodic waves.

2.2. Solutions of Planar Modified Kawahara Equation.
The generalized KE equation (4) can reduce the planar mKE equation (3) for $p = 2$. Making the traveling wave transformation $u = v(\xi)$, where $\xi = x + \lambda t + \xi_0$, we get

$$\lambda v' + \alpha v^2 v' + \beta v^{(3)} - \gamma v^{(5)} = 0, \qquad (40)$$

and integrating equation (40) twice over ξ, we obtain

$$\mathbb{R} \equiv c_0 v + c_1 - \gamma v^{(3)} v' + 1/12\alpha v^4 + \frac{1}{2}\lambda v^2$$
$$+ \frac{1}{2}\beta(v')^2 + \frac{1}{2}\gamma(v'')^2 = 0. \qquad (41)$$

Some new localized and periodic solutions to equation (41) are discussed using different approaches in the following sections.

2.2.1. First Ansatz in Terms of WSEFs.
The following ansatz is introduced to find a periodic wave solution to equation (41) in terms of WSEFs:

$$v = A + B\wp, \qquad (42)$$

where $\wp \equiv \wp(\xi + \xi_0; g_2, g_3)$, g_2 and g_3 denote the elliptic invariants, while the other parameters A, B, g_2, and g_3 are the constants and will be determined later.

Inserting the ansatz equations (42) into (40), we obtain

$$\left(A^2\alpha + 18\gamma g_2 + \lambda\right) + \left(2A\alpha B + 12\beta\right)\wp + \left(\alpha B^2 - 360\gamma\right)\wp^2 = 0. \qquad (43)$$

Equating the coefficients of $\wp^0$, $\wp$, and $\wp^2$ to zero and solving the obtained system, we have

$$A = \pm \frac{\beta}{\sqrt{10\alpha\gamma}}, B = \mp 6\sqrt{\frac{10\gamma}{\alpha}}, \text{and} g_2 = \frac{-\beta^2 - 10\gamma\lambda}{180\gamma^2}. \quad (44)$$

Note that g_3 is an arbitrary constant. Using the initial condition $v(0) = v_0$, we can get

$$A + B\wp(\xi_0; g_2, g_3) = v_0, \quad (45)$$

which leads to

$$\xi_0 = \wp^{-1}\left(\frac{v_0 - A}{B}; g_2, g_3\right). \quad (46)$$

By substituting the values of (A, B, g_2) given in equation (44) into the ansatz equation (42), we finally obtain the solutions of cnoidal wave as

$$u_{1,2}(x,t) = \pm \frac{\beta}{\sqrt{10\alpha\gamma}} \mp 6\sqrt{\frac{10\gamma}{\alpha}}\wp\left(x + \lambda t + \xi_0; \frac{-\beta^2 - 10\gamma\lambda}{180\gamma^2}, g_3\right), \quad (47)$$

and these solutions satisfy the evolution equation (3).

For the following choice,

$$g_2 = \frac{4}{3} \text{and} g_3 = -\frac{8}{27}, \quad (48)$$

the solitary wave solutions are recovered:

$$u_{1,2}(x,t) = \pm \frac{\beta}{\sqrt{10\alpha\gamma}} \mp 6\sqrt{\frac{10\gamma}{\alpha}}\wp\left(x + \lambda t + \xi_0; \frac{4}{3}, -\frac{8}{27}\right). \quad (49)$$

2.2.2. Second Ansatz in Terms of WSEFs.
The following rational hypothesis/ansatz is assumed to find some analytical solution to equation (41):

$$v(\xi) = A + \frac{B}{1 + C\wp}, \quad (50)$$

where A, B, and C are the undetermined constants and $\wp \equiv \wp(\xi + \xi_0; g_2, g_3)$.

Inserting the ansatz equations (50) into (41), we have

$$\sum_{j=0}^{6} Z_j \wp^j = 0, \quad (51)$$

where the coefficients Z_j $(j = 0, 1, \ldots, 6)$ are defined in Appendix D, and by solving the following system,

$$Z_0 = 0, Z_1 = 0, \ldots, Z_6 = 0, \quad (52)$$

we obtain the nontrivial solution:

$$A = \frac{60\gamma + \beta C}{\sqrt{10\alpha\gamma}C},$$

$$\lambda = -\frac{\beta^2}{10\gamma} - \frac{6}{5C^2}\left(\sqrt{10\alpha\gamma}\,BC + 180\gamma\right),$$

$$c_0 = \frac{\gamma^{-(3/2)}\sqrt{10/\alpha}\left(86400\gamma^3 + \beta^3 C^3 - 2160\beta\gamma^2 C\right) - 120BC(\beta C - 60\gamma)}{150C^3},$$

$$c_1 = \frac{1}{400\alpha\gamma^2 C^4}\left[-800\gamma^3\left(\alpha B^2 C^2 + 36\sqrt{10\alpha\gamma}\,BC + 3240\gamma\right)\right.$$

$$\left. + 56\beta^2\gamma^{3/2}C^2\left(\sqrt{10\alpha}\,BC + 180\sqrt{\gamma}\right) + 2880\beta\gamma^{5/2}C\left(\sqrt{10\alpha}\,BC + 120\sqrt{\gamma}\right) + \beta^4\left(-C^4\right)\right],$$

$$g_2 = \frac{\sqrt{(10\alpha/\gamma)}BC + 180}{15C^2},$$

$$g_3 = \frac{BC}{15C^3}\left(\sqrt{(10\alpha/\gamma)} + 120\right). \quad (53)$$

Thus, the traveling wave solutions to mKE equation (3) are expressed by

$$u = \frac{60\gamma + \beta C}{\sqrt{10\alpha\gamma}C} + \frac{B}{1 + C\wp\left(x - \left(\beta^2/10\gamma + 6(\sqrt{10\alpha\gamma}\,BC + 180\gamma)/5C^2\right)t + \xi_0; \left(\sqrt{10\alpha/\gamma}\,BC + 180/15C^2\right), \left(\sqrt{10\alpha/\gamma} + 120/15C^3\right)BC\right)}. \quad (54)$$

(a)

(b)

(c)

(d)
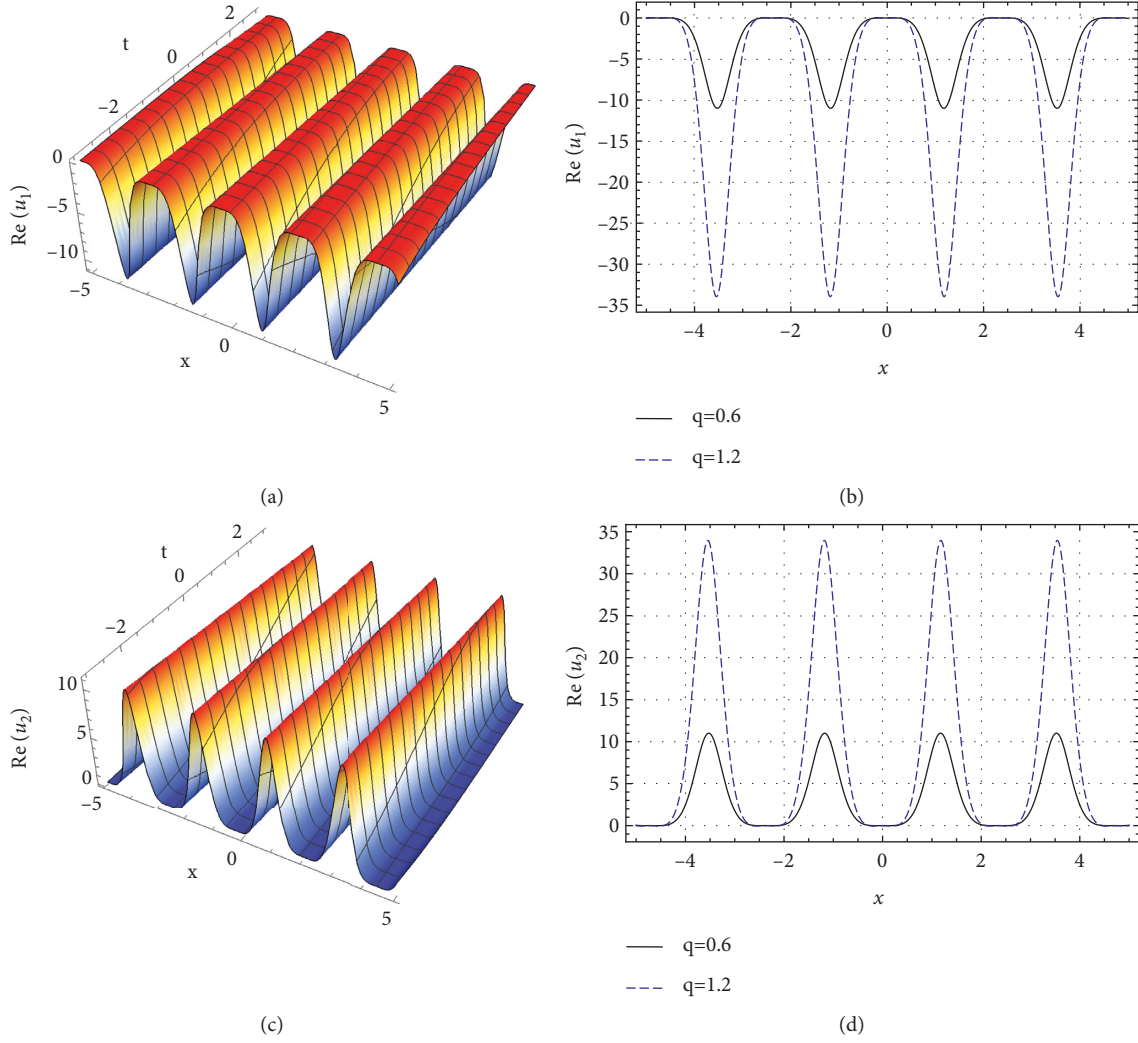
FIGURE 3: The profile of the cnoidal wave solution equation (47) to mKE equation (3) is plotted in (x, t) plane.

The values of the constants B and C are arbitrary.

The solitary wave solutions can be obtained from the periodic solution equation (54) according to the following choices:

$$\begin{cases} g_2 = 1/12, \quad g_3 = -1/216, \\ \\ g_2 = \dfrac{4}{3}, \qquad g_3 = -\dfrac{8}{27}. \end{cases} \tag{55}$$

For the choices equation (55), the soliton solutions are obtained:

$$u = \frac{\beta}{\sqrt{10\alpha\gamma}} + \frac{1}{2}\sqrt{\frac{5\gamma}{2\alpha}}\left[4 - \frac{9}{1 + 6\wp\left(x - \left(\beta^2 + 15\gamma^2/10\gamma\right)t + \xi_0; (1/12), -(1/216)\right)}\right], \tag{56}$$

$$u = \frac{\beta}{\sqrt{10\alpha\gamma}} + \sqrt{\frac{10\gamma}{\alpha}}\left(1 - \frac{18}{2 + 3\wp\left(x - \left(\beta^2 + 15\gamma^2/10\gamma\right)t + \xi_0; (4/3), -(8/27)\right)}\right). \tag{57}$$

2.2.3. Third Ansatz in Terms of JEFs. Using the following ansatz in equation (41),

we have

$$v(\xi) = A + B\,\mathrm{cn}^2, \tag{58}$$

$$\sum_{j=0}^{2n} Y_j cn^j = 0, \qquad (59)$$

where the coefficients Y_j ($j = 0, 2, 4, 6$) are defined in Appendix E, and by solving the following system,

$$A = \frac{-\beta - 20\gamma\omega + 40\gamma m\omega}{\sqrt{10}\sqrt{\alpha}\sqrt{\gamma}}, \quad B = \frac{6\sqrt{10}\sqrt{\gamma}m\omega}{\sqrt{\alpha}},$$

$$\lambda = -\frac{\beta^2 + 240\gamma^2\omega^2 + 240\gamma^2 m^2\omega^2 - 240\gamma^2 m\omega^2}{10\gamma},$$

$$c_0 = \frac{1}{15\sqrt{10}\sqrt{\alpha}\gamma^{3/2}} \begin{pmatrix} -240\beta\gamma^2\omega^2 + 3200\gamma^3\omega^3 \\ +3200\gamma^3 m^3\omega^3 - 240\beta\gamma^2 m^2\omega^2 \\ -4800\gamma^3 m^2\omega^3 + 240\beta\gamma^2 m\omega^2 \\ -4800\gamma^3 m\omega^3 + \beta^3 \end{pmatrix},$$

$$c_1 = -\frac{1}{400\alpha\gamma^2} \begin{pmatrix} \beta^4 - 1120\beta^2\gamma^2\omega^2 - 12800\beta\gamma^3\omega^3 \\ +32000\gamma^4\omega^4 + 32000\gamma^4 m^4\omega^4 \\ -12800\beta\gamma^3 m^3\omega^3 - 64000\gamma^4 m^3\omega^4 \\ -1120\beta^2\gamma^2 m^2\omega^2 + 19200\beta\gamma^3 m^2\omega^3 \\ +96000\gamma^4 m^2\omega^4 + 1120\beta^2\gamma^2 m\omega^2 \\ +19200\beta\gamma^3 m\omega^3 - 64000\gamma^4 m\omega^4 \end{pmatrix}.$$

$cn \equiv cn(\xi, m)$ and $\xi = x + \lambda t + \xi_0$.

$$Y_j = 0, \qquad (60)$$

we get

Using equation (61), the following cnoidal wave solution is obtained:

$$= \frac{\beta + 20\gamma\omega - 40\gamma m\omega}{\sqrt{10}\sqrt{\alpha}\sqrt{\gamma}}$$

$$+ \frac{6\sqrt{10}\sqrt{\gamma}m\omega}{\sqrt{\alpha}} cn^2 \left[\sqrt{\omega}\left(x - \frac{t(\beta^2 + 240m^2\gamma^2\omega^2 - 240m\gamma^2\omega^2 + 240\gamma^2\omega^2)}{10\gamma} \right) | m \right]. \qquad (62)$$

For letting $m \longrightarrow 1$, solution equation (62) can recover the soliton solution as

$$u = \frac{\beta - 20\gamma\omega}{\sqrt{10}\sqrt{\alpha}\sqrt{\gamma}} + \frac{6\sqrt{10}\sqrt{\gamma}\omega}{\sqrt{\alpha}}$$

$$\sec h^2 \left[\sqrt{\omega}\left(x - \frac{t(\beta^2 + 240\gamma^2\omega^2)}{10\gamma} \right) \right]. \qquad (63)$$

(a)

(b)

(c)

(d)
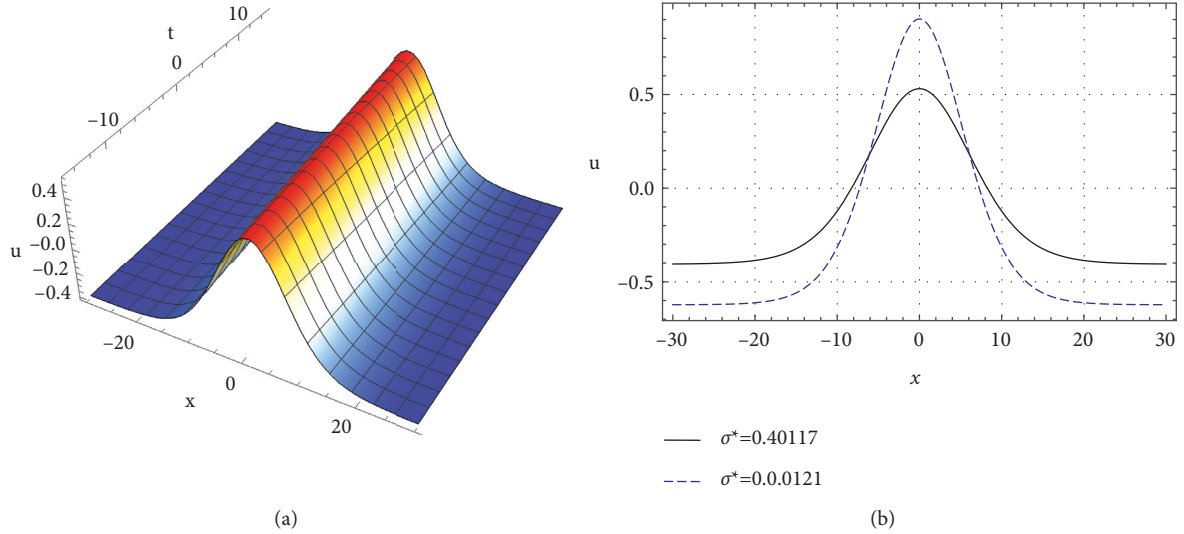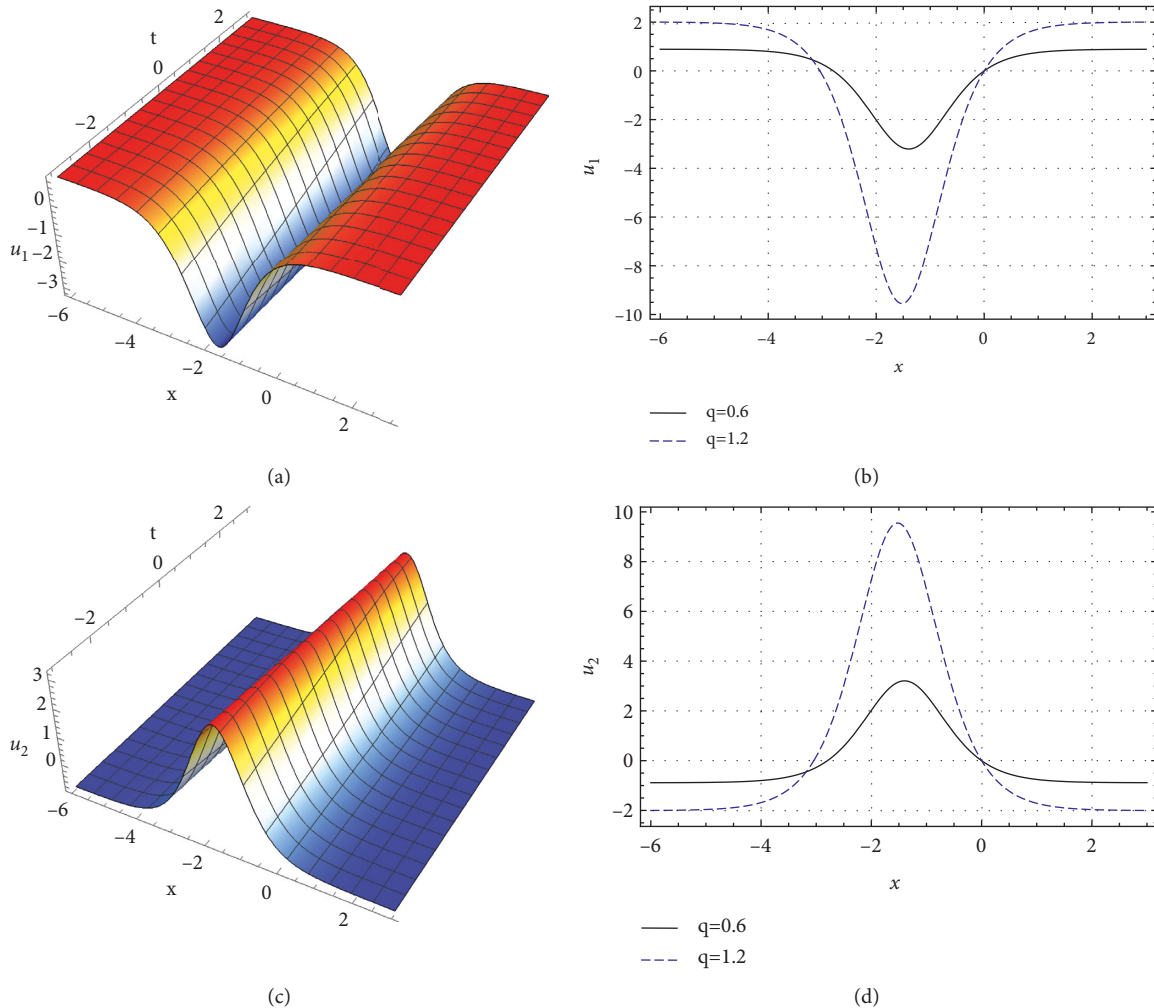
FIGURE 4: The profile of the solitary wave solution equation (49) to mKE equation (3) is plotted in (x, t) plane.

Furthermore, solution equation (54) can be reduced to the following cnoidal wave solution using the relation

$$
\begin{aligned}
= \frac{60\gamma + \beta C + \beta Cm - 120\gamma m}{\sqrt{10\alpha\gamma} C (m+1)} + \\
\frac{18\sqrt{10\gamma} m}{\sqrt{\alpha} C (m+1)} cn^2 \left(\sqrt{\frac{3}{C(m+1)}} \left(x - \left(\frac{\beta^2}{10\gamma} - \frac{216(m^2 - m + 1)\gamma}{C^2 (m+1)^2} \right) t \right) + \xi_0, m \right).
\end{aligned}
\tag{64}
$$

between WSEFs and JEFs [36] (more details are inserted in Appendix F):

Also, the soliton solution can be obtained from solution equation (64) for letting $m \longrightarrow 1$:

$$
u = \frac{2\beta C - 60\gamma}{2\sqrt{10\alpha\gamma C}} + \frac{9}{C}\sqrt{\frac{10\gamma}{\alpha}} \sec h^2 \left(\sqrt{\frac{3}{2C}} \left(x - \frac{\beta^2 C^2 - 540\gamma^2}{10\gamma C^2} t \right) + \xi_0 \right).
\tag{65}
$$

The propagation of higher-order ion-acoustic structures in a collisionless and unmagnetized plasma consisting of inertialess nonextensive electrons and positrons and inertial warm ions and nonextensive electrons as well as positrons [10] is investigated. El-Tantawy[10] derived both two-coupled KdV equations and two-coupled modified KdV (mKdV) equations for studying the KdV and mKdV solitons

collisions. For some external perturbation or at some certain conditions, the derivatives fifth-order should be taken into consideration which leads to both KE equation (2) and mKE (3). Now, to analyze the obtained solutions, we can use the same values of the coefficients of mKdV equation (26) in [10]. Based on this plasma model $(\alpha_2 = \alpha, \beta) =$ (2.14663, 0.698771) at $q = 0.6$ and $(\alpha_2 = \alpha, \beta) =$ (0.269511, 0.957799) at $q = 1.2$, where q indicates the nonextensive parameter, the profile of the periodic solution equation (47) is illustrated as shown in Figure 3 for the parameter values $(\gamma, \lambda, g_3, \xi_0, v_0) =$ (0.1, −0.1, 5, 0, 0). Moreover, the profiles of the solitary wave solutions equation (48) are shown in Figure 4 using the same parameters used in Figure 3 replacing $(g_2, g_3) = (4/3, -8/27)$. It is clear that the two solutions have opposite polarity, i.e., positive and negative potential. Furthermore, it is noticed that both amplitude and width increase with the increase of the nonextensive parameter q.

3. Conclusions

New localized and periodic traveling wave solutions to the generalized KE have been derived in detail using different new approaches and ansatz. As a particular case, several traveling wave solutions to both KE and mKE have been obtained using (in)direct methods. For the indirect method, KE has been solved with the help of Helmholtz equation. After that, we can use any solution to the Helmholtz equation in order to express the solution of the planar KE. We used two different formulas for WSEFs to get some periodic solutions to KE. In the direct method, a new ansatz in the terms of WSEFs has been introduced for getting a cnoidal solution to KE. In all cases and at certain conditions, the periodic solutions have been reduced to the localized solitary wave solutions. In the third (direct) method, the periodic and solitary wave solutions have been derived in the form of JEFs, and it was found that the obtained solutions coincide with that obtained by means of the tanh method. The obtained solutions have been used for interpreting several nonlinear structures that propagate in different plasma models. Furthermore, two new hypotheses in terms of WSEFs have been proposed to find some periodic solutions to mKE. Also, the conditions for reducing the periodic solutions of mKE to the localized solitary waves have been presented. The obtained solutions have been employed for investigating many nonlinear structures in different plasma models.

Appendix

A.

The values of the coefficients F_j ($j = 0, 1, \cdots 6$) are given by

$$F_0 = c_1 + c_0 d_0 + \frac{\lambda d_0^2}{2} + \frac{\alpha d_0^3}{6} + \beta c_2 d_1^2 + 2A\gamma c_2 d_1^2 + 8\gamma c_2^2 d_2^2,$$

$$F_1 = \frac{1}{2}d_1\left(2c_0 + 2\lambda d_0 + \alpha d_0^2 + 8B\gamma c_2 d_1 + 8\beta c_2 d_2 + 32A\gamma c_2 d_2\right),$$

$$F_2 = -\frac{1}{2}\left(\begin{array}{c} A\beta d_1^2 + A^2\gamma d_1^2 - \lambda d_1^2 - \alpha d_0 d_1^2 - 2c_0 d_2 - 2\lambda d_0 d_2 \\ -\alpha d_0^2 d_2 - 48B\gamma c_2 d_1 d_2 - 8\beta c_2 d_2^2 - 32A\gamma c_2 d_2^2 \end{array}\right),$$

$$F_3 = -\frac{1}{6}\left(\begin{array}{c} 2B\beta d_1^2 + 10AB\gamma d_1^2 - \alpha d_1^3 + 12A\beta d_1 d_2 + 36A^2\gamma d_1 d_2 \\ -6\lambda d_1 d_2 - 6\alpha d_0 d_1 d_2 - 160B\gamma c_2 d_2^2 \end{array}\right),$$

$$F_4 = -\frac{1}{6}\left(\begin{array}{c} 5B^2\gamma d_1^2 + 8B\beta d_1 d_2 + 80AB\gamma d_1 d_2 - 3\alpha d_1^2 d_2 \\ +12A\beta d_2^2 + 48A^2\gamma d_2^2 - 3\lambda d_2^2 - 3\alpha d_0 d_2^2 \end{array}\right),$$

$$F_5 = -\frac{1}{6}d_2\left(36B^2\gamma d_1 + 8B\beta d_2 + 104AB\gamma d_2 - 3\alpha d_1 d_2\right),$$

$$F_6 = -\frac{1}{18}d_2^2\left(140B^2\gamma - 3\alpha d_2\right).$$

(A.1)

B

The values of the coefficients S_j ($j = 0, 1, \cdots 6$) are given by

$$S_0 = \frac{1}{24}\left(\begin{array}{c} 24a_0 c_1 - 12a_1^2\beta g_3 k^3 + 3a_1^2\gamma g_2^2 k^5 + 48a_2^2\gamma g_3^2 k^5 \\ -48a_1 a_2\gamma g_2 g_3 k^5 + 4\alpha a_0^3 k + 12a_0^2\lambda + 24c_2 \end{array}\right),$$

$$S_1 = \frac{1}{2}a_1\left(\begin{array}{c} -a_1\beta g_2 k^3 - 4a_2\beta g_3 k^3 - 3a_2\gamma g_2^2 k^5 + 24a_1\gamma g_3 k^5 \\ +\alpha a_0^2 k + 2a_0\lambda + 2c_1 \end{array}\right),$$

$$S_2 = \frac{1}{2}\left(\begin{array}{c} 2a_2 c_1 - 4a_1 a_2\beta g_2 k^3 - 4a_2^2\beta g_3 k^3 - 3a_2^2\gamma g_2^2 k^5 + 18a_1^2\gamma g_2 k^5 \\ +144a_1 a_2\gamma g_3 k^5 + \alpha a_0 a_1^2 k + \alpha a_0^2 a_2 k + a_1^2\lambda + 2a_0 a_2\lambda \end{array}\right),$$

$$S_3 = \frac{1}{6}\left(\begin{array}{c} -12a_2^2\beta g_2 k^3 + 408a_1 a_2\gamma g_2 k^5 + 480a_2^2\gamma g_3 k^5 \\ +12a_1^2\beta k^3 + \alpha a_1^3 k + 6\alpha a_0 a_1 a_2 k + 6a_1 a_2\lambda \end{array}\right),$$

$$S_4 = \frac{1}{2}\left(168a_2^2\gamma g_2 k^5 + 16a_1 a_2\beta k^3 - 60a_1^2\gamma k^5 + \alpha a_0 a_2^2 k + \alpha a_1^2 a_2 k + a_2^2\lambda\right),$$

$$S_5 = -\frac{1}{2}a_2 k\left(-\alpha a_1 a_2 - 16a_2\beta k^2 + 432a_1\gamma k^4\right),$$

$$S_6 = -\frac{1}{6}a_2^2 k\left(1680\gamma k^4 - \alpha a_2\right).$$

(B.1)

C

The values of the coefficients W_j ($j = 0, 1, 2, 3$) are given by

$$W_3 = 2sn(\xi,m)cn(\xi,m)dn(\xi,m)\sqrt{\omega}\left(-2C\left(C\alpha - 1680m^2\gamma\omega^2\right)\right.$$

$$W_2 = -3\begin{pmatrix} BC\alpha - 20Cm\beta\omega - 1040Cm\gamma\omega^2 \\ \\ -120Bm^2\gamma\omega^2 + 2080Cm^2\gamma\omega^2 \end{pmatrix}$$

$$W_1 = \begin{pmatrix} -B^2\alpha - 2AC\alpha - 2C\lambda + 32C\beta\omega + 12Bm\beta\omega \\ \\ -64Cm\beta\omega + 512C\gamma\omega^2 + 240Bm\gamma\omega^2 - 3392Cm\gamma\omega^2 \\ \\ -480Bm^2\gamma\omega^2 + 3392Cm^2\gamma\omega^2 \end{pmatrix} \tag{C.1}$$

$$W_0 = \begin{pmatrix} -AB\alpha - B\lambda + 4B\beta\omega - 12C\beta\omega - 8Bm\beta\omega \\ \\ +12Cm\beta\omega + 16B\gamma\omega^2 - 240C\gamma\omega^2 - 136Bm\gamma\omega^2 \\ \\ +720Cm\gamma\omega^2 + 136Bm^2\gamma\omega^2 - 480Cm^2\gamma\omega^2 \end{pmatrix}.$$

D

The values of the coefficients Z_j $(j = 0, 1, 2 \cdots 6)$ are given by

$$Z_0 = 8\alpha AB^3 + 24AB\lambda + 24Ac_0 + 2\alpha B^4 - 96B^2\gamma C^4 g_3^2 + 48B^2\gamma C^3 g_2 g_3 - 12\beta B^2 C^2 g_3$$

$$+ 3B^2\gamma C^2 g_2^2 + 12B^2\lambda + 24Bc_0 + 24c_1 + 2\alpha A^4 + 8\alpha A^3 B + 12\alpha A^2 B^2 + 12A^2\lambda$$

$$Z_1 = 2C\begin{pmatrix} 6\alpha A^4 + 20\alpha A^3 B + 24\alpha A^2 B^2 + 36A^2\lambda + 12\alpha AB^3 + 60AB\lambda + \\ \\ 72Ac_0 + 2\alpha B^4 - 72B^2\gamma C^3 g_2 g_3 - 12\beta B^2 C^2 g_3 + 27B^2\gamma C^2 g_2^2 - \\ \\ 6\beta B^2 Cg_2 + 144B^2\gamma Cg_3 + 24B^2\lambda + 60Bc_0 + 72c_1 \end{pmatrix},$$

$$Z_2 = C^2\begin{pmatrix} 30\alpha A^4 + 80\alpha A^3 B + 72\alpha A^2 B^2 + 180A^2\lambda + 24\alpha AB^3 + 240AB\lambda + \\ \\ 360Ac_0 + 2\alpha B^4 - 12\beta B^2 C^2 g_3 - 45B^2\gamma C^2 g_2^2 - \\ \\ 24\beta B^2 Cg_2 + 216B^2\gamma g_2 + 72B^2\lambda + 240Bc_0 + 360c_1 \end{pmatrix},$$

$$Z_3 = 4C^2\begin{pmatrix} 10\alpha A^4 C + 20\alpha A^3 BC + 12\alpha A^2 B^2 C + 60A^2 C\lambda + 2\alpha AB^3 C + \\ \\ 60ABC\lambda + 120Ac_0 C + 12\beta B^2 - 3\beta B^2 C^2 g_2 + 120B^2\gamma C^2 g_3 - \\ \\ 84B^2\gamma Cg_2 + 12B^2 C\lambda + 60Bc_0 C + 120c_1 C \end{pmatrix}, \tag{D.1}$$

$$Z_4 = 2C^2\begin{pmatrix} 15\alpha A^4 C^2 + 20\alpha A^3 BC^2 + 6\alpha A^2 B^2 C^2 + 90A^2 C^2\lambda + \\ \\ 60ABC^2\lambda + 180Ac_0 C^2 - 360B^2\gamma + 108B^2\gamma C^2 g_2 + \\ \\ 6B^2 C^2\lambda + 48\beta B^2 C + 60Bc_0 C^2 + 180c_1 C^2 \end{pmatrix},$$

$$Z_5 = 4C^3\begin{pmatrix} 3\alpha A^4 C^2 + 2\alpha A^3 BC^2 + 18A^2 C^2\lambda + 6ABC^2\lambda + 36Ac_0 C^2 + \\ \\ 216B^2\gamma + 12\beta B^2 C + 6Bc_0 C^2 + 36c_1 C^2 \end{pmatrix},$$

$$Z_6 = 2C^4\left(\alpha A^4 C^2 + 6A^2 C^2\lambda + 12Ac_0 C^2 + 24B^2\gamma + 12c_1 C^2\right).$$

E

The values of the coefficients Y_j ($j = 0, 2, 4, 6, 8$) are given by

$$Y_0 = 1/12 \begin{pmatrix} \alpha A^4 + 6A^2\lambda + 12Ac_0 + 24B^2\gamma\omega^2 \\ +24B^2\gamma m^2\omega^2 - 48B^2\gamma m\omega^2 + 12c_1 \end{pmatrix},$$

$$Y_2 = 1/12 \begin{pmatrix} 4\alpha A^3 B + 12AB\lambda + 24\beta B^2\omega + 96B^2\gamma\omega^2 + \\ 192B^2\gamma m^2\omega^2 - 24\beta B^2 m\omega - 288B^2\gamma m\omega^2 + 12Bc_0 \end{pmatrix},$$

$$Y_4 = 1/12 \begin{pmatrix} 6\alpha A^2 B^2 - 24\beta B^2\omega - 96B^2\gamma\omega^2 + 6B^2\lambda - \\ 816B^2\gamma m^2\omega^2 + 48\beta B^2 m\omega + 816B^2\gamma m\omega^2 \end{pmatrix},$$

$$Y_6 = 1/12 \left(4\alpha AB^3 + 960B^2\gamma m^2\omega^2 - 24\beta B^2 m\omega - 480B^2\gamma m\omega^2 \right),$$

$$Y_8 = 1/12 \left(\alpha B^4 - 360B^2\gamma m^2\omega^2 \right).$$

$$(E.1)$$

F

Relation between the Jacobian cn elliptic function and the Weierstrass elliptic function.

It is known that

$$\left(\wp' \right)^2 = 4\wp^3 - g_2\wp - g_3, \quad \wp \equiv \wp(t; g_2, g_3). \tag{F.1}$$

On the other hand, if $v(t) = \text{cn}(\sqrt{\omega}\, t, m)$, we get

$$\frac{1}{2}\dot{v}^2 - (1 - m)\omega + (1 - 2m)\omega v^2(t) + m\omega v^4(t) = 0. \tag{F.2}$$

Define

$$w(t) = 1 + \frac{B}{1 + C\wp(t; g_2, g_3)}, \tag{F.3}$$

then,

$$\frac{1}{2}\dot{w}^2 - (1 - m)\omega + (1 - 2m)\omega w^2(t) + m\omega w^4(t)$$

$$= \frac{B}{(1 + C\wp)^4} \begin{bmatrix} B^3 m\omega + 4B^2 m\omega - BC^2 g_3 + 4Bm\omega + B\omega + 2\omega + \\ C\left(4B^2 m\omega - BCg_2 + 8Bm\omega + 2B\omega + 6\omega\right)\wp + \\ +C\omega\left(4Bm + B + 6\right)\wp^2 + 2C^2\left(2B + C\omega\right)\wp^3 \end{bmatrix}. \tag{F.4}$$

Equating to zero the coefficients of $\wp^j$ ($j = 0, 1, 2, 3$) gives an algebraic system, and by solving this system, we finally have

$$B = -\frac{6}{4m + 1},$$

$$C = \frac{12}{(4m + 1)\omega},$$

$$g_2 = 1/12 \left(16m^2 - 16m + 1 \right)\omega^2, \tag{F.5}$$

$$g_3 = 1/216 (2m - 1)\left(32m^2 - 32m - 1 \right)\omega^3.$$

Then,

$$\text{cn}(\sqrt{\omega}\, t, m)$$

$$= 1 - \frac{6}{(4m + 1)\left(1 + 12/(4m + 1)\omega\wp\left(t; (1/12)\left(16m^2 - 16m + 1\right)\omega^2, (1/216)(2m - 1)\left(32m^2 - 32m - 1\right)\omega^3\right)\right)}. \tag{F.6}$$

This identity shows that the function cn is expressible trough the function $\wp$. Now, if we know the function $\wp$, we want to write it in terms of cn. To this end, we must write ω and m in terms of g_2 and g_3. This is not too easy. Define

$$z = 16m^2 - 16m + 1. \tag{F.7}$$

Now, we eliminate ω and m from the system,

$$g_2 = 1/12 \left(16m^2 - 16m + 1 \right)\omega^2,$$

$$g_3 = 1/216 (2m - 1)\left(32m^2 - 32m - 1 \right)\omega^3, \tag{F.8}$$

$$z = 16m^2 - 16m + 1,$$

to obtain

$$27g_2^3 - 27g_2^3 z + 4\left(g_2^3 - 27g_3^2 \right)z^3 = 0. \tag{F.9}$$

This cubic is solvable by means of Tartaglia formula which leads to

$$m = \frac{1}{4}\left(2 \pm \sqrt{z + 3} \right), \omega = 2\sqrt{\frac{3g_2}{z}}. \tag{F.10}$$

Finally, we solve the following equation for $\wp(t; g_2, g_3)$:

$$1 + \frac{B}{1 + C\wp(t; g_2, g_3)} = \text{cn}(\sqrt{\omega}\, t, m). \tag{F.11}$$

The desired expression reads

$$\wp(t; g_2, g_3) = -\frac{\omega}{12}\left(1 + 4m - \frac{6}{1 - \text{cn}(\sqrt{\omega}\, t | m)} \right). \tag{F.12}$$

In conclusion, if some ODE or some PDE have a solution that is expressible in terms of the Jacobian cn function, then such solution may also be written in terms of the Weierstrass $\wp$ function and vice versa. So, cnoidal waves and $\wp$ solutions have the same meaning. Observe also that the last formula allows us to obtain the main period of the Weierstrass function in the form

$$T = \frac{4K(m)}{\sqrt{\omega}}. \qquad \text{(F.13)}$$

Data Availability

Conflicts of Interest

The authors declare that they have no conflicts of interest.

Authors' Contributions

All authors contributed equally and approved the final manuscript.

Acknowledgments

References

[1] Y.-Y. Fan, J. Manafian, Z. Syed Maqsood, Dinh Tran Ngoc Huy, and Le Trung-Hieu, "Analytical treatment of the generalized hirota-satsuma-ito equation Arising in shallow water wave," *Adv. Math. Phys.*vol. 2021, p. 1164838, 2021.

[2] J. Manafian, "Novel solitary wave solutions for the (3+1)-dimensional extended Jimbo-Miwa equations," *Computers & Mathematics with Applications*, vol. 76, no. 5, pp. 1246–1260, 2018.

[3] J. Manafian, ".An optimal Galerkin-homotopy asymptotic method applied to the nonlinear second-order BVPs," *Proceedings of the Institute of Mathematics and Mechanics, National Academy of Sciences of Azerbaijan*, vol. 47, p. 156, 2021.

[4] "An analytical analysis to solve the fractional differential equations," *Advanced Mathematical Models & Applications*, vol. 6, no. 2, p. 128, 2021.

[5] A.-M. Wazwaz, *Partial Differential Equations and Solitary Waves Theory*, Higher Education Press, Beijing, USA, 2009.

[6] A.-M. Wazwaz, *Partial Differential Equations : Methods and Applications*, Balkema, cop, Lisse, 2002.

[7] B. S. Kashkari, S. A. El-Tantawy, A. H. Salas, and L. S. El-Sherif, "Homotopy perturbation method for studying dissipative nonplanar solitons in an electronegative complex plasma," *Chaos, Solitons & Fractals*, vol. 130, Article ID 109457, 2020.

[8] J.-W. Xia, Yi-W. Zhao, and L. ü Xing, "Predictability, Fast calculation and simulation for the interaction solution to the cylindrical Kadomtsev-Petviashvili equation," *Commun. Nonlinear Sci. Numer. Simul.*vol. 90, Article ID 105260, 2020.

[9] S. Zhang and X. Zheng, "N-soliton solutions and nonlinear dynamics for two generalized Broer-Kaup systems," *Nonlinear Dynamics*, vol. 107, no. 1, pp. 1179–1193, 2022.

[10] S. A. El-Tantawy, "Nonlinear dynamics of soliton collisions in electronegative plasmas: The phase shifts of the planar KdV-and mkdV-soliton collisions," *Chaos, Solitons & Fractals*, vol. 93, pp. 162–168, 2016.

[11] B. S. Kashkari and S. A. El-Tantawy, "Homotopy perturbation method for modeling electrostatic structures in collisional plasmas," *The European Physical Journal Plus*, vol. 136, no. 1, p. 121, 2021.

[12] Yu-L. Ma, A.- M Wazwaz, and B.-Q. Li, "Novel bifurcation solitons for an extended Kadomtsev–Petviashvili equation in fluids," *Phys. Lett.*vol. 413, Article ID 127585, 2021.

[13] S. Malik, A. Hassan, S. Kumar, M. S. A-M Wazwaz, and A. Osman, "2+1)-dimensional Kadomtsev–Petviashvili equation with competing dispersion effect: painlevé analysis, dynamical behavior and invariant solutions," *Results Phys*, vol. 23, Article ID 104043, 2021.

[14] L. ü Xing and S.-J. Chen, "Interaction solutions to nonlinear partial differential equations via Hirota bilinear forms: one-lump-multi-stripe and one-lump-multi-soliton types," *Nonlinear Dyn*, vol. 103, p. 947, 2021.

[15] S.-J. Chen, W.-X. Ma, and L. U. Xing, "Bäcklund transformation, exact solutions and interaction behaviour of the (3 + 1)-dimensional Hirota-Satsuma-Ito-like equation," *Commun. Nonlinear Sci. Numer. Simul.*vol. 83, Article ID 105135, 2020.

[16] B. Ghanbari, "Employing Hirota's bilinear form to find novel lump waves solutions to an important nonlinear model in fluid mechanics," *Results Phys*, vol. 29, Article ID 104689, 2021.

[17] T. Kawahara, "Oscillatory solitary waves in dispersive media," *Journal of the Physical Society of Japan*, vol. 33, no. 1, pp. 260–264, 1972.

[18] S. E. Haupt and J. P. Boyd, "Modeling nonlinear resonance: A modification to the stokes' perturbation expansion," *Wave Motion*, vol. 10, no. 1, pp. 83–98, 1988.

[19] S. A. El-Tantawy, A. H. Salas, and M. R. Alharthi, "On the dissipative extended Kawahara solitons and cnoidal waves in a collisional plasma: novel analytical and numerical solutions," *Phys. Fluids*, vol. 33, Article ID 043106, 2021.

[20] T. Kakutani and H. Ono, "Weak non-linear hydromagnetic waves in a cold collision-free plasma," *Journal of the Physical Society of Japan*, vol. 26, no. 5, pp. 1305–1318, 1969.

[21] U. Sevil Çulha, A. Daşcıoğlu, and B. Dilek Varol, "New exact solutions of space and time fractional modified Kawahara equation," *Physica A*, vol. 551, Article ID 124550, 2020.

[22] Z. Pinar and T. Öziş, "The periodic solutions to Kawahara equation by means of the auxiliary equation with a sixth-degree nonlinear term," *Journal of Mathematics*, vol. 2013, Article ID 106349, 2013.

[23] A.-M. Wazwaz, "Compacton solutions of the Kawahara-type nonlinear dispersive equation," *Applied Mathematics and Computation*, vol. 145, no. 1, pp. 133–150, 2003.

[24] A.-M. Wazwaz, "New solitary wave solutions to the Kuramoto-Sivashinsky and the Kawahara equations," *Applied Mathematics and Computation*, vol. 182, no. 2, pp. 1642–1650, 2006.

[25] H. Noufe Aljahdaly and S. A. El-Tantawy, "Novel anlytical solution to the damped Kawahara equation and its application for modeling the dissipative nonlinear structures in a fluid medium," *J. Ocean Eng. Sci.*, 2021, https://doi.org/10.1016/j.joes.2021.10.001.

[26] S. A. El-Tantawy, A. H. Salas, and M. R. Alharthi, "Novel analytical cnoidal and solitary wave solutions of the Extended Kawahara equation," *Chaos, Solitons & Fractals*, vol. 147, p. 110965, 2021, In press.

[27] Sirendaoreji, "New exact travelling wave solutions for the Kawahara and modified Kawahara equations," *Chaos, Solitons & Fractals*, vol. 19, no. 1, pp. 147–150, 2004.

[28] Y. Khan, "A new necessary condition of soliton solutions for Kawahara equation arising in physics," *Optik*, vol. 155, pp. 273–275, 2018.

[29] A. Biswas, "Solitary wave solution for the generalized Kawahara equation," *Applied Mathematics Letters*, vol. 22, no. 2, pp. 208–210, 2009.

[30] E. Yusufoğlu, A. Bekir, and M. Alp, "Periodic and solitary wave solutions of Kawahara and modified Kawahara equations by using Sine–Cosine method," *Chaos, Solitons and Fractals*, vol. 37, p. 1193, 2008.

[31] S. A. El-Tantawy, A. H. Salas, and M. R. Alharthi, "A new approach for modelling the damped Helmholtz oscillator: applications to plasma physics and electronic circuits," *Communications in Theoretical Physics*, vol. 73, Article ID 035501, 2021.

[32] S. A. El-Tantawy, N. A. El-Bedwehy, and S. K. El-Labany, "Ion-acoustic super rogue waves in ultracold neutral plasmas with nonthermal electrons," *Phys. Plasmas*, vol. 20, Article ID 072102, 2013.

[33] S. A. El-Tantawy, W. M. Moslem, R. Sabry, S. K. El-Labany, M. El-Metwally, and R. Schlickeiser, "Nonplanar solitons collision in ultracold neutral plasmas," *Phys. Plasmas*, vol. 20, Article ID 092126, 2013.

[34] S. A. El-Tantawy, W. M. Moslem, R. Sabry, S. K. El-Labany, M. El-Metwally, and R. Schlickeiser, "Head-on collision of ion-acoustic solitons in an ultracold neutral plasma," *Astrophysics and Space Science*, vol. 350, no. 1, pp. 175–184, 2014.

[35] S. A. El-Tantawy, N. A. El-Bedwehy, and W. M. Moslem, "Super rogue waves in ultracold neutral nonextensive plasmas," *Journal of Plasma Physics*, vol. 79, no. 6, pp. 1049–1056, 2013.

[36] A. H. Salas, J. Lorenzo, H. Martinez, L. R. David, and R. Ocampo, "Approximation of elliptic functions by means of trigonometric functions with applications," *Math. Probl. Eng.*vol. 2021, Article ID 5546666, 16 pages, 2021.

WILEY | Hindawi

Research Article

Stability Analysis for Differential Equations of the General Conformable Type

Abdellatif Ben Makhlouf ,[1] **El-Sayed El-Hady** ,[1] **Salah Boulaaras** ,[2] **and Mohamed Ali Hammami** [3]

[1]*Department of Mathematics, College of Science, Jouf University, P.O. Box: 2014, Sakaka, Saudi Arabia*
[2]*Department of Mathematics, College of Sciences and Arts ArRas, Qassim University, Buraydah, Saudi Arabia*
[3]*University of Sfax, Faculty of Sciences of Sfax, Department of Mathematics, Route Soukra, BP 1171, 3000 Sfax, Tunisia*

Correspondence should be addressed to Abdellatif Ben Makhlouf; abmakhlouf@ju.edu.sa

Fractional calculus is nowadays an efficient tool in modelling many interesting nonlinear phenomena. This study investigates, in a novel way, the Ulam–Hyers (HU) and Ulam–Hyers–Rassias (HUR) stability of differential equations with general conformable derivative (GCD). In our analysis, we employ some version of Banach fixed-point theory (FPT). In this way, we generalize several earlier interesting results. Two examples are given at the end to illustrate our results.

1. Introduction

The stability issue gained a considerable attention in various research fields through applications. There are many kinds of stability, among them is the stability introduced by S. M. Ulam, in his famous talk at a conference held in Wisconsin University in 1940. Since then, it is known as HU stability or simply Ulam stability. Its applications for various types of differential equations have been investigated by many researchers. The readers can see the interesting results in 1–7, for more details. The stability problem of Ulam can be rewritten in the following form.

Consider a group G^* and a metric group (G^{**}, χ_1). Is it true that given $\varepsilon > 0$, there exist $\delta > 0$ such that if $\Lambda: G^* \longrightarrow G^{**}$ satisfies

$$\chi_1(\Lambda(x_1 x_2), \Lambda(x_1)\Lambda(x_2)) < \delta. \qquad (1)$$

For all $x_1, x_2 \in G^*$, then a homomorphism $\Xi: G^* \longrightarrow G^{**}$ exists such that

$$\chi_1(\Lambda(x_1), \Xi(x_1)) < \varepsilon, \qquad (2)$$

for every $x_1 \in G^*$?

The problem of Ulam has been extended in many directions for various interesting settings. In particular, Rassias (see [8]) generalized Ulam's result for Banach spaces.

Initial and boundary value problems with fractional-order derivatives are natural generalization of the classical initial and boundary value problems. It is much more complicated to investigate stability issues of fractional-order problems than their classical analogues; this is because of the singularity and nonlocality in the kernel of fractional differential operators. Fractional derivatives, in general, play negligible roles in a number of fields of science and engineering (see, e.g., [9–13] and the references there in).

In particular, during the last few decades, the area of fractional calculus has been investigated qualitatively by using different tools of functional analysis. These tools include but are not limited to *Gronwall Lemma*, see, e.g., [14], *Pachpatte's inequality*, see, e.g., [15], *Schaefer's FPT*, see, e.g., [16], *Schauder's FPT*, see, e.g., [17], *Banach FPT*, see, e.g., [18], and *Picard operator*, see, e.g., [15]. Various approaches have been used to define fractional derivatives (see, e.g., 19–28, for more details).

It should be remarked that generalized conformable derivative plays an essential role in many applications. For instance, the authors in [29] utilized it to examine some nonlinear evolution equations. Generalized conformable derivative also has been used in [30] to investigate some nonlinear evolution equations. A new generalized version of conformable derivative is given and in [31] with some applications in biological population. In the present study, we generalize several recent interesting works as follows. We use Theorem 2 to generalize the interesting results in [32, 33] by dropping some of the basic assumptions that have been used there. We also use Theorem 3 to generalize the work in [34].

The organization of the study is as follows. In Section 2, we present some preliminaries and some basic definitions. In Section 3, we introduce our stability results in the sense of HU and HUR. In Section 4, two examples are written to show the validity of our results, and in Section 5, we conclude our work.

2. Preliminaries

In this section, some definitions, lemmas, and theorems are given [35–39].

Definition 1. Let us consider a function ϕ defined on $[c, d]$; then, the GCD starting from the real c of a function ϕ is defined by

$$T_c^{v, \psi_c} \phi(z) = \lim_{\sigma \longrightarrow 0} \frac{\phi(z + \sigma \psi_c(z, v)) - \phi(z)}{\sigma}. \quad (3)$$

For all $z > c$, $v \in (0, 1)$ and $\psi_c(z, v)$ is a nonnegative continuous function that satisfies

$$\psi_c(z, 1) = 1,$$

$$\psi_c(., v_1) \neq \psi_c(., v_2), \text{where } v_1 \neq v_2 \text{ and } v_1, v_2 \in (0, 1]. \quad (4)$$

If $T_c^{v, \psi_c} \phi(z)$ exists, for every $z \in (c, a)$; for some $a > c$, $\lim_{t \longrightarrow c^+} T_c^{v, \psi_c} \phi(z)$ exists; then, by definition,

$$T_c^{v, \psi_c} \phi(c) = \lim_{t \longrightarrow c^+} T_c^{v, \psi_c} \phi(z). \quad (5)$$

Remark 1. To further study the properties of GCD, we suppose that $\psi_c(z, v) > 0$, for all $z > c$, and $1/\psi_c(., v)$ is locally integrable.

Definition 2. Let $0 < v < 1$. The conformable fractional integral starting from c of a function ϕ is defined by

$$I_c^{v, \psi_c} \phi(z) = \int_c^z \frac{\phi(x)}{\psi_c(x, v)} dx. \quad (6)$$

Lemma 1. *Suppose that $\phi \in C([c, d])$. Thus,*

$$T_c^{v, \psi} I_c^{v, \psi_c} \phi(z) = \phi(z), \quad \forall z \geq c. \quad (7)$$

Lemma 2. *Suppose that $\phi \in AC^1([c, d])$. Thus,*

$$I_c^{v, \psi_c} T_c^{v, \psi} \phi(z) = \phi(z) - \phi(c), \quad \forall z \geq c. \quad (8)$$

Remark 2. Assume that $\vartheta \in \mathbb{R}^*$. If $g(z) := \mathbb{E}_v^{\psi_c}(\vartheta, z, c) = e^{\vartheta \int_c^z 1/\psi_c(x, v) dx}$, then $T_c^{v, \psi_c} g(z) = \vartheta g(z)$ and $I_c^{v, \psi_c} g(z) = 1/\vartheta (g(z) - 1)$.

The following is the notion of a generalized metric on some set $\mathcal{S}_1$.

Definition 3 (see 40). Consider a mapping $\varrho: \mathcal{S}_1 \times \mathcal{S}_1 \longrightarrow [0, \infty]$. The mapping ϱ is called a generalized metric on set $\mathcal{S}_1$ iff ϱ satisfies:

M1 $\varrho(o_1, o_2) = 0$ if and only if $o_1 = o_2$

M2 $\varrho(o_1, o_2) = \varrho(o_2, o_1)$, for all $o_1, o_2 \in \mathcal{S}_1$

M3 $\quad \varrho(o_1, o_3) \leq \varrho(o_1, o_2) + \varrho(o_2, o_3)$, for all $o_i \in \mathcal{S}_1, i = 1, 2, 3$

The following theorem (see [40]) represents one of the interesting results of FPT. This theorem plays a fundamental role in our study.

Theorem 1. *Suppose that (Q, F) is a metric space that is generalized complete. Let $B: Q \longrightarrow Q$ be a strictly contractive operator. If there is an integer $t \geq 0$ with $F(\Gamma^{t+1}c, \Gamma^t c) < \infty$ for some $c \in Q$, thus*

(a) *$\lim_{s \longrightarrow +\infty} B^s c = c^*$, where c^* is the unique fixed point of Γ in Q^*: $= \{c_1 \in Q: F(B^t c, c_1) < \infty\}$*

(b) *If $c_1 \in Q^*$, then $F(c_1, c^*) \leq 1/1 - LF(Bc_1, c_1)$*

Define the space X as $X := C(I, \mathbb{R})$, with $I = [a, a + T]$ (a is some real number).

Lemma 3. *Define a metric $\eta: X \times X \longrightarrow [0, \infty]$ in such a way that*

$$\eta(\beta_1, \beta_2) = \inf \left\{ A \in [0, \infty]: \frac{|\beta_1(z) - \beta_2(z)|}{\mathbb{E}_\theta^{\psi_a}(\vartheta, z, a)} \leq A\lambda(z), z \in I \right\}, \quad (9)$$

where $\vartheta > 0$, $\theta \in (0, 1)$, and λ is positive and continuous. Thus, (X, η) is a generalized complete metric space.

The goal of this study is to investigate the stability of the following initial value problem:

$$T_a^{\theta, \psi_a} y(z) = \xi(z, y(z)), y(a) = y_a, \quad (10)$$

in the sense of HU and HUR. Notice that the solution of the initial value problem (10) is the solution of

$$y(z) = \int_a^z \frac{\xi(p, y(p))}{\psi_a(p, \theta)} dp + y_a, z \in I. \quad (11)$$

3. Ulam–Hyers–Rassias Stability Results

We use this section to present our main results. The theorem below represents the stability of (10) in the sense of HU.

Theorem 2. *Suppose ξ is continuous and satisfies*

$$|\xi(z, \gamma_1) - \xi(z, \gamma_2)| \le P|\gamma_1 - \gamma_2|, \quad \forall z \in I, \gamma_i \in \mathbb{R}, i = 1, 2.$$
(12)

If an absolutely continuous function $x: I \longrightarrow \mathbb{R}$ satisfies

$$|T_a^{\theta, \psi_a} x(z) - \xi(z, x(z))| \le \epsilon,$$
(13)

for some $\epsilon > 0$, therefore, there is a unique solution x^* of (10) with

$$|x(z) - x^*(z)| \le \epsilon \frac{P + \varrho}{\varrho} M \mathbb{E}_\theta^{\psi_a}((P + \varrho), a + T, a),$$
(14)

for every $z \in I$, where ϱ is any positive constant and $M = \sup_{s \in [a, a+T]} (I_a^{\theta, \psi_a}(1)(s)/\mathbb{E}_\theta^{\psi_a}((P + \varrho), s, a))$.

Proof. For any $B_1, B_2 \in X$, we define the metric d in this way:

$$d(B_1, B_2) = \inf \left\{ V \in [0, \infty] : \frac{|B_1(z) - B_2(z)|}{\mathbb{E}_\theta^{\psi_a}((P + \varrho), z, a)} \le V, z \in I \right\}.$$
(15)

Define the operator $\mathcal{G}: X \longrightarrow X$ such that

$$(\mathcal{G}y)(z) := x(a) + \int_a^z \frac{\xi(s, y(s))}{\psi_a(s, \theta)} ds, \quad \forall y \in X.$$
(16)

Since

$$\frac{|(\mathcal{G}y_0)(z) - y_0(z)|}{\mathbb{E}_\theta^{\psi_a}((P + \varrho), z, a)} < \infty, \quad \forall y_0 \in X, z \in I,$$
(17)

so that it is clear that $d(\mathcal{G}y_0, y_0) < \infty$, in addition, we get $\{y \in X : d(y_0, y) < \infty\} = X$.

Now, we prove that $\mathcal{G}$ is strictly contractive:

$$|(\mathcal{G}y_1)(z) - (\mathcal{G}y_2)(z)| \le \left| \int_a^z \frac{(\xi(s, y_1(s)) - \xi(s, y_2(s)))}{\psi_a(s, \theta)} ds \right|$$

$$\le \int_a^z \frac{|\xi(s, y_1(s)) - \xi(s, y_2(s))|}{\psi_a(s, \theta)} ds$$

$$\le P \int_a^z \frac{|y_1(s) - y_2(s)|}{\psi_a(s, \theta)} ds$$

$$\le P \int_a^z \frac{1}{\psi_a(s, \theta)} \frac{|y_1(s) - y_2(s)|}{\mathbb{E}_\theta^{\psi_a}((P + \varrho), s, a)} \mathbb{E}_\theta^{\psi_a}((P + \varrho), s, a) ds$$

$$\le \frac{P\, d(y_1, y_2)}{P + \varrho} \left(\mathbb{E}_\theta^{\psi_a}((P + \varrho), z, a) - 1 \right)$$

$$\le \frac{P\, d(y_1, y_2)}{P + \varrho} \mathbb{E}_\theta^{\psi_a}((P + \varrho), z, a) \text{for all } z \in I.$$
(18)

So, it is clear that

$$\frac{|(\mathcal{G}y_1)(z) - (\mathcal{G}y_2)(z)|}{\mathbb{E}_\theta^{\psi_a}((P + \varrho), z, a)} \le \frac{P}{P + \varrho} d(y_1, y_2),$$
(19)

which implies that

$$d(\mathcal{G}y_1, \mathcal{G}y_2) \le \frac{P}{P + \varrho} d(y_1, y_2),$$
(20)

which prove that the operator $\mathcal{G}$ is a strictly contractive one.

We get, from (27),

$$|x(z) - \mathcal{G}x(z)| \le \epsilon \int_a^t \frac{1}{\psi_a(s, \theta)} ds \le \epsilon I_a^{\theta, \psi_a}(1)(z).$$
(21)

Therefore,

$$d(x, \mathcal{G}x) \le \epsilon M.$$
(22)

Now, according to Theorem 1, there is some solution x^* of (10) satisfying

$$d(x, x^*) \le \epsilon \frac{P + \varrho}{\varrho} M,$$
(23)

so that

$$\frac{|x(z) - x^*(z)|}{\mathbb{E}_\theta^{\psi_a}((P + \varrho), z, a)} \le \epsilon \frac{P + \varrho}{\varrho} M,$$
(24)

which implies that

$$|x(z) - x^*(z)| \le \epsilon \frac{P + \varrho}{\varrho} M \mathbb{E}_\theta^{\psi_a}((P + \varrho), a + T, a).$$
(25)
□

Remark 3. It is clear that our findings in the sense of HU are some generalized version of the results obtained in [32, 33] as follows. In our analysis, we do not impose any constrains on P unlike equation 5 in Theorem 2 in [32]. In [33], the authors assumed conditions on the function φ which is not the case in our study.

The following theorem represents the stability of (10) in HUR sense.

Theorem 3. *Suppose ξ is continuous and satisfies*

$$|\xi(z, \gamma_1) - \xi(z, \gamma_2)| \le P|\gamma_1 - \gamma_2|, \quad \forall z \in I, \gamma_i \in \mathbb{R}, i = 1, 2.$$
(26)

If an absolutely continuous function $x: I \longrightarrow \mathbb{R}$ satisfies

$$|T_a^{\theta, \psi_a} x(z) - \xi(z, x(z))| \le \kappa(z),$$
(27)

where $\kappa(z)$ is a nondecreasing, continuous function, therefore, there is a unique solution x^* of (10) with

$$|x(z) - x^*(z)| \le \frac{P + \varrho}{\varrho} M \mathbb{E}_\theta^{\psi_a}((P + \varrho), a + T, a)\kappa(z),$$
(28)

for every $z \in I$, where ϱ is any positive constant and $M = \sup_{s \in [a, a+T]} (I_a^{\theta, \psi_a}(1)(s)/\mathbb{E}_\theta^{\psi_a}((P + \varrho), s, a))$.

Proof. For any $B_1, B_2 \in X$, we define the metric d as follows:

$$d(B_1, B_2) = \inf \left\{ V \in [0, \infty] : \frac{|B_1(z) - B_2(z)|}{\mathbb{E}_\theta^{\psi_a}((P + \varrho), z, a)} \le V\kappa(z), z \in I \right\}.$$
(29)

Define the operator $\mathscr{G}: X \longrightarrow X$ such that

$$(\mathscr{G}y)(z) := x(a) + \int_a^z \frac{\xi(s, y(s))}{\psi_a(s, \theta)} ds, \quad \forall y \in X. \tag{30}$$

We have $d(\mathscr{G}y_0, y_0) < \infty$, for all y_0. In addition, we get $\{y \in X: d(y_0, y) < \infty\} = X$.

Now, we prove that $\mathscr{G}$ is strictly contractive:

$$\left|(\mathscr{G}y_1)(z) - (\mathscr{G}y_2)(z)\right| \le \left|\int_a^z \frac{(\xi(s, y_1(s)) - \xi(s, y_2(s)))}{\psi_a(s, \theta)} ds\right|,$$

$$\le P \int_a^z \frac{|y_1(s) - y_2(s)|}{\psi_a(s, \theta)} ds$$

$$\le P\, d(y_1, y_2)\kappa(z) \int_a^z \frac{\mathbb{E}_\theta^{\psi_a}((P + \varrho), s, a)}{\psi_a(s, \theta)} ds$$

$$\le \frac{P\, d(y_1, y_2)}{P + \varrho} \mathbb{E}_\theta^{\psi_a}((P + \varrho), z, a)\kappa(z)\, \text{for all } z \in I.$$
$$\tag{31}$$

So,

$$d(\mathscr{G}y_1, \mathscr{G}y_2) \le \frac{P}{P + \varrho} d(y_1, y_2), \tag{32}$$

which prove that the operator $\mathscr{G}$ is a strictly contractive one.

We get, from (13),

$$|x(z) - \mathscr{G}x(z)| \le \int_a^t \frac{\kappa(s)}{\psi_a(s, \theta)} ds \le \kappa(z) I_a^{\theta, \psi_a}(1)(z). \tag{33}$$

Hence,

$$d(x, \mathscr{G}x) \le M. \tag{34}$$

Using Theorem 1, there is a solution x^* of (10) with

$$d(x, x^*) \le \frac{P + \varrho}{\varrho} M. \tag{35}$$

Thus,

$$|x(z) - x^*(z)| \le \frac{P + \varrho}{\varrho} M \mathbb{E}_\theta^{\psi_a}((P + \varrho), a + T, a)\kappa(z). \tag{36}$$
$$\square$$

Remark 4. Notice that the authors in [34] used conformable fractional Laplace transform to study the HUR stability of several kinds of differential equations. They had to assume some specific conditions, see, e.g., condition 12 in Theorem 3.6 is given in [34].

Remark 5. The authors in [41] obtained stability results for differential equations with integer-order derivatives $\psi_a = 1$, while in our study it is for GCD. In this sense, we introduce a generalized version of the interesting results [41].

4. Examples

This section uses two examples to show the validity of results.

Example 1. Consider equation (10) for $\psi_a(z, \theta) = (z - a)^{1-\theta}$, $a = 0$, $\theta = 0.6$, $T = 2$, and $\xi(z, \nu) = z^4 \sin(\nu)$.

We have

$$|z^4 \sin(\nu_1) - z^4 \sin(\nu_2)| \le 16|\nu_1 - \nu_2|, \quad \forall z \in [0, 9], \nu_1, \nu_2 \in \mathbb{R}. \tag{37}$$

Then, $L = 16$.

Suppose that ν satisfies

$$|T_0^{0.6, \psi_0} \nu(z) - \xi(z, \nu(z))| \le 0.01, \tag{38}$$

for all $z \in [0, 2]$.

Here, $\epsilon = 0.01$. Using Theorem 2, there is ν^* and $M > 0$ such that

$$|\nu(z) - \nu^*(z)| \le 0.01M, \quad \forall z \in [0, 2]. \tag{39}$$

Example 2. Consider equation (10) for $\psi_a(z, \theta) = (z - a)^{1-\theta}$, $a = 3$, $\theta = 0.3$, $T = 3$, and $\xi(z, \nu) = z \cos(\nu)$.

We have

$$|z \cos(\nu_1) - z \cos(\nu_2)| \le 6|\nu_1 - \nu_2|, \quad \forall z \in [3, 6], \nu_1, \nu_2 \in \mathbb{R}. \tag{40}$$

Then, $L = 6$.

Suppose that ν satisfies

$$|T_3^{0.3, \psi_3} \nu(z) - \xi(z, \nu(z))| \le (z + 2), \tag{41}$$

for all $z \in [3, 6]$.

Here, $\kappa(z) = z + 2$. Using Theorem 3, there is ν^* and $M > 0$ such that

$$|\nu(z) - \nu^*(z)| \le M(z + 2), \quad \forall z \in [0, 2]. \tag{42}$$

5. Conclusion

We managed to utilize a version of Banach FPT to present stability results in the sense of HU and HUR for some differential equations involving GCDs. In our analysis, we generalized some interesting results by dropping some of the basic assumptions that have been used in recent known investigations. We used two examples to show the validity of our main findings. We believe that the methodology used in this study can be further applied to many other fractional differential equations.

Data Availability

No data were used to support this study.

Conflicts of Interest

The authors declare that they have no conflicts of interest.

Acknowledgments

References

[1] R. P. Agarwal, O. Bazighifan, and M. A. Ragusa, "Nonlinear neutral delay differential equations of fourth-order: oscillation of solutions," *Entropy*, vol. 23, no. 2, 2021.

[2] R. P. Agarwal, S. Gala, and M. A. Ragusa, "A regularity criterion in weak spaces to Boussinesq equations," *Mathematics*, vol. 8, no. 6, p. 920, 2020.

[3] S. András and A. R. Mészáros, "Ulam-Hyers stability of dynamic equations on time scales via Picard operators," *Applied Mathematics and Computation*, vol. 219, no. 9, pp. 4853–4864, 2013.

[4] D. S. Cimpean and D. Popa, "Hyers-Ulam stability of Euler's equation," *Applied Mathematics Letters*, vol. 24, no. 9, pp. 1539–1543, 2011.

[5] B. Hegyi and S.-M. Jung, "On the stability of Laplace's equation," *Applied Mathematics Letters*, vol. 26, no. 5, pp. 549–552, 2013.

[6] S.-M. Jung, "Hyers-Ulam stability of linear differential equations of first order," *Applied Mathematics Letters*, vol. 17, no. 10, pp. 1135–1140, 2004.

[7] M. Inc, A. Yusuf, A. I. Aliyu, and D. Baleanu, "Soliton solutions and stability analysis for some conformable nonlinear partial differential equations in mathematical physics," *Optical and Quantum Electronics*, vol. 50, no. 4, p. 190, 2018.

[8] T. M. Rassias, "On the stability of the linear mapping in Banach spaces," *Proceedings of the American Mathematical Society*, vol. 72, no. 2, pp. 297–300, 1978.

[9] F. Liu and K. Burrage, "Novel techniques in parameter estimation for fractional dynamical models arising from biological systems," *Computers & Mathematics with Applications*, vol. 62, no. 3, pp. 822–833, 2011.

[10] K. B. Oldham, "Fractional differential equations in electrochemistry," *Advances in Engineering Software*, vol. 41, no. 1, pp. 9–12, 2010.

[11] I. Podlubny, *Fractional Differential Equations: An Introduction to Fractional Derivatives, Fractional Differential Equations, to Methods of Their Solution and Some of Their Applications*, Elsevier, Amsterdam, Netherland, 1999.

[12] R. Hilfer, *Applications of Fractional Calculus in Physics*, World Scientific, Singapore, 2000.

[13] A. A. Kilbas, H. M. Srivastava, and J. J. Trujillo, *Theory and Applications of Fractional Differential Equations*, Elsevier Science Limited, Elsevier, Amsterdam, Netherland, 2006.

[14] N. Lungu, S. A. Ciplea, and S. A. Ciplea, "Ulam-Hyers-Rassias stability of pseudoparabolic partial differential equations," *Carpathian Journal of Mathematics*, vol. 31, no. 2, pp. 233–240, 2015.

[15] P. U. Shikhare and K. D. Kucche, "Existence, uniqueness and Ulam stabilities for nonlinear hyperbolic partial integrodifferential equations," *International Journal of Algorithms, Computing and Mathematics*, vol. 5, no. 6, p. 156, 2019.

[16] H. Choi, Y. Sin, and K. Jong, "Existence results for nonlinear multiorder fractional differential equations with integral and antiperiodic boundary conditions," *Journal of Applied Mathematics*, vol. 2020, Article ID 1212040, 9 pages, 2020.

[17] R. I. Butt, T. Abdeljawad, and M. ur Rehman, "Stability analysis by fixed point theorems for a class of non-linear Caputo nabla fractional difference equation," *Advances in Difference Equations*, vol. 2020, no. 1, pp. 1–11, 2020.

[18] K. Liu, M. Fečkan, and J. Wang, "A fixed-point Approach to the hyers-ulam stability of caputo-fabrizio fractional differential equations," *Mathematics*, vol. 8, no. 4, p. 647, 2020.

[19] M. Caputo and M. Fabrizio, "A new definition of fractional derivative without singular kernel," *Progr. Fract. Differ. App.*vol. 1, no. 2, 2015.

[20] D. Baleanu, H. Mohammadi, and S. Rezapour, "Analysis of the model of HIV-1 infection of $C\,D4 + CD^4$ T-cell with a new approach of fractional derivative," *Advances in Difference Equations*, vol. 2020, no. 1, pp. 1–17, 2020.

[21] D. Baleanu, A. Jajarmi, H. Mohammadi, and S. Rezapour, "A new study on the mathematical modelling of human liver with Caputo-Fabrizio fractional derivative," *Chaos, Solitons & Fractals*, vol. 134, Article ID 109705, 2020.

[22] S. Alizadeh, D. Baleanu, and S. Rezapour, "Analyzing transient response of the parallel RCL circuit by using the Caputo-Fabrizio fractional derivative," *Advances in Difference Equations*, vol. 2020, no. 1, p. 55, 2020.

[23] A. Atangana and D. Baleanu, "New fractional derivatives with nonlocal and non-singular kernel: theory and application to heat transfer model," *Thermal Science*, vol. 20, no. 2, pp. 763–769, 2016.

[24] A. Atangana, "Non validity of index law in fractional calculus: a fractional differential operator with Markovian and non-Markovian properties," *Physica A: Statistical Mechanics and Its Applications*, vol. 505, pp. 688–706, 2018.

[25] A. Atangana and J. F. Gómez-Aguilar, "Fractional derivatives with no-index law property: application to chaos and statistics," *Chaos, Solitons & Fractals*, vol. 114, pp. 516–535, 2018.

[26] I. Koca, "Modelling the spread of Ebola virus with AtanganaBaleanu fractional operators," *The European Physical Journal Plus*, vol. 133, no. 3, pp. 1–11, 2018.

[27] V. F. Morales-Delgado, J. F. Gómez-Aguilar, M. A. TanecoHernández, R. F. Escobar-Jiménez, and V. H. Olivares-Peregrino, "Mathematical modeling of the smoking dynamics using fractional differential equations with local and nonlocal kernel," *The Journal of Nonlinear Science and Applications*, vol. 11, no. 8, pp. 1004–1014, 2018.

[28] K. Shah, T. Abdeljawad, I. Mahariq, and F. Jarad, "Qualitative analysis of a mathematical model in the time of COVID-19," *BioMed Research International*, vol. 2020, Article ID 5098598, 11 pages, 2020.

[29] A. A. Hyder and A. H. Soliman, "An extended Kudryashov technique for solving stochastic nonlinear models with generalized conformable derivatives," *Communications in Nonlinear Science and Numerical Simulation*, vol. 97, Article ID 105730, 2021.

[30] A. A. Hyder and A. H. Soliman, "Exact solutions of space-time local fractal nonlinear evolution equations: a generalized conformable derivative approach," *Results in Physics*, vol. 17, Article ID 103135, 2020.

[31] A. A. Hyder and A. H. Soliman, "A new generalized θ-conformable calculus and its applications in mathematical physics," *Physica Scripta*, vol. 96, no. 1, Article ID 015208, 2020.

[32] S. Öğrekçi, Y. Başci, and A. Misir, "Ulam type stability for conformable fractional differential equations," *Rendiconti del Circolo Matematico di Palermo Series*, vol. 2, pp. 1–11, 2020.

[33] M. Li, J. Wang, and D. O'Regan, "Existence and ulam's stability for conformable fractional differential equations with constant coefficients," *Bulletin of the Malaysian Mathematical Sciences Society*, vol. 42, no. 4, pp. 1791–1812, 2019.

[34] S. Wang, W. Jiang, J. Sheng, and R. Li, "Ulam's stability for some linear conformable fractional differential equations," *Advances in Difference Equations*, vol. 2020, no. 1, pp. 1–18, 2020.

[35] F. Azouz, D. Boucenna, A. Ben Makhlouf, L. Mchiri, and A. Benchaabane, "Controllability of differential systems with the general conformable derivative," *Complexity*, vol. 2021, Article ID 2817092, 11 pages, 2021.

[36] D. Zhao and M. Luo, "General conformable fractional derivative and its physical interpretation," *Calcolo*, vol. 54, pp. 903–917, 2015.

[37] S. Li, S. Zhang, and R. Liu, "The existence of solution of diffusion equation with the general conformable derivative," *Journal of Function Spaces*, vol. 2020, p. 10, Article ID 3965269, 2020.

[38] T. Abdeljawad, "On conformable fractional calculus," *Journal of Computational and Applied Mathematics*, vol. 279, pp. 57–66, 2015.

[39] R. Khalil, M. Al Horani, A. Yousef, and M. Sababheh, "A new definition of fractional derivative," *Journal of Computational and Applied Mathematics*, vol. 264, pp. 65–70, 2014.

[40] J. B. Diaz and B. Margolis, "A fixed point theorem of the alternative, for contractions on a generalized complete metric space," *Bulletin of the American Mathematical Society*, vol. 74, no. 2, pp. 305–309, 1968.

[41] Y. Başci, A. Misir, and S. Öğrekç i, "On the stability problem of differential equations in the sense of Ulam," *Results in Mathematics*, vol. 75, no. 1, p. 6, 2020.

WILEY | Hindawi

Research Article

Chaotic Behaviors and Coexisting Attractors in a New Nonlinear Dissipative Parametric Chemical Oscillator

Y. J. F. Kpomahou [ID],[1] **A. Adomou,**[2] **J. A. Adéchinan** [ID],[3] **A. E. Yamadjako** [ID],[4] **and I. V. Madogni**[4]

[1]*Department of Industrial and Technical Sciences, ENSET-Lokossa, UNSTIM-Abomey, Abomey, Benin*
[2]*National Higher Institute of Industrial Technology,*
 National University of Sciences, Technologies, Engineering and Mathematics (UNSTIM) of Abomey, Abomey, Benin
[3]*Department of Physics, FAST-Natitingou, UNSTIM-Abomey, Abomey, Benin*
[4]*Department of Physics, University of Abomey-Calavi, Abomey-Calavi, Benin*

Correspondence should be addressed to Y. J. F. Kpomahou; fkpomahou@gmail.com

In this study, complex dynamics of Briggs–Rauscher reaction system is investigated analytically and numerically. First, the Briggs–Rauscher reaction system is reduced into a new nonlinear parametric oscillator. The Melnikov method is used to derive the condition of the appearance of horseshoe chaos in the cases $\omega = \Omega$ and $\omega \neq \Omega$. The performed numerical simulations confirm the obtained analytical predictions. Second, the prediction of coexisting attractors is investigated by solving numerically the new nonlinear parametric ordinary differential equation via the fourth-order Runge–Kutta algorithm. As results, it is found that the new nonlinear chemical system displays various coexisting behaviors of symmetric and asymmetric attractors. In addition, the system presents a rich variety of bifurcations phenomena such as symmetry breaking, symmetry restoring, period doubling, reverse period doubling, period-m bubbles, reverse period-m bubbles, intermittency, and antimonotonicity. On the contrary, emerging chaotic band attractors and period-1, period-3, period-9, and period-m bubbles routes to chaos occur in this system.

1. Introduction

Nonlinear oscillations remain up to now an attractive topic of research due to their applications to physics, biology, chemistry, and engineering [1–4]. To that end, various analytical methods and numerical tools have been proposed and successfully used in study of nonlinear dynamics of oscillatory systems [4–10]. Recently, nonlinear chemical oscillations have received attention of many researchers from theoretical and experimental point of view [11–27]. This is due to dynamic complexities that can exhibit the new nonlinear chemical oscillators and their potential applications in engineering. For example, Cassani et al. [19] studied the nonlinear behavior of Belousov–Zhabotinsky-type reactions focusing on modeling under different operating conditions, from the simplest to the most widely applicable

models. The stability analysis of simplified models as a function of bifurcation parameter has been studied. Adéchinan et al. [20] studied the dynamics and active control of chemical oscillations governed by a forced generalized Rayleigh oscillator. The condition of the appearance of chaos has been derived using the Melnikov method. The control efficiency has been shown through the control gain parameter on the behavior of the system. Monwanou et al. [21] investigated the effect of an amplitude modulated excitation on the nonlinear dynamics of reactions between four molecules. The stability analysis of the autonomous system has been made in detail. The dynamics of the nonautonomous chemical system showed various routes to chaos. Olabodé et al. [22] used the Melnikov method and derived analytically the domains boundaries where horseshoe chaos appears in chemical oscillations. They afterward controlled

chaotic oscillations by subjecting the nonlinear chemical system to fluctuation hydrodynamic drag forces. On the contrary, the effects of passive hydrodynamics force on harmonic and chaotic oscillations in nonlinear chemical oscillations governed by a forced modified Van der pol–Duffing oscillator have been analyzed by Olabodé et al. [23]. Recently, Ghosh and Ray [24] showed that a class of arbitrary, autonomous kinetic equations in two variables, describing chemical and biochemical oscillations, can be reduced to the form of a Liénard oscillator. Binous and Bellagi [25] studied various important aspects of nonlinear dynamics such as limit cycles, quasi-periodic and chaotic behaviors, time series and phase portraits, power spectra, the time-delay reconstruction diagrams, Hopf bifurcation, bifurcation diagrams, steady-state multiplicity of four problems drawn from the chemical, and biochemical engineering field of study. Shabunin et al. [26] modeled chemical reactions by the forced limit-cycle oscillator and studied synchronization phenomena and transition to chaos.

The most theoretical studies on nonlinear dissipative chemical systems in general and on Briggs–Rauscher reaction system in particular have been performed with periodically external excitation [20, 22, 23, 27]. However, the aspects of nonlinear dynamics of Briggs–Rauscher reaction system under the influence of the parametric and two external periodic excitations have not been yet studied. Such a study will be important to perform since it is well known that the dynamics of a nonlinear system subjected to parametric and external excitations exhibits complex and rich dynamical behaviors [9, 28–30]. Thus, the problem of interest is to show that the Briggs–Rauscher reaction system can be modeled by the following new nonlinear parametric oscillator:

$$
\begin{aligned}
x + \mu\left(1 + x^2 + p\gamma\cos\omega t\right)\dot{x} \\
+ \left(1 + p\cos\omega t\right)\left(\alpha_1 x + \alpha_3 x^3\right) \\
= -\alpha_0\left(1 + p\cos\omega t\right) + f\cos\Omega t,
\end{aligned}
\tag{1}
$$

where the dots indicate differentiation with respect to time t and μ, p, α_i f, ω, and Ω are real system parameters.

The originality of this work is brought by the parameter p which controls the presence of the parametric and external excitations of frequency ω. It is important to point out that Si-yu and Jin-yan [29] considered a particular case of this strong nonlinear parametric equation in the study of the parameter stability and global bifurcations. It is now easy to see through this equation that when $p = 0$, the classical nonautonomous Van der Pol–Duffing oscillator is obtained. This classical driven oscillator has been widely studied in the context of various physical, chemical, and engineering problems. Some theoretical and numerical results for some particular cases of the strong nonlinear parametric system (1) have been found in the open literature. Therefore, the dynamics study of system (1) is of a crucial importance in nonlinear chemical oscillations for a better understanding of the dynamical behaviors of the system. In addition, the

investigation of nonlinear phenomena in dynamical system (1) is even significance in practical applications.

In order to predict the chaotic behavior in a driven nonlinear system, the Melnikov theory is often used [9, 27, 42]. From this theory, the condition for the existence of homoclinic bifurcation to occur in the case where the potential is an asymmetric or symmetric double well exists in the open literature for $p = 0$. However, for $p \neq 0$, the prediction of horseshoe chaos in a new nonlinear parametric system (1) under two periodic external excitations has not been investigated up to now. Thus, the presence of the parameter p would contribute to nonlinear dynamics of Briggs–Rauscher reaction system modeled by equation (1).

The coexisting attractors exist in many natural and artificial systems. This phenomenon has received the attention of many investigators in nonlinear dynamics fields [13, 20, 21, 31]. This is due to the fact that it provides multiple optional steady states for the system to respond to different needs. To that end, various studies on some driven nonlinear systems have shown the existence of multiple coexisting attractors [32–39]. In nonlinear chemical dynamics, the coexistence of two or more stable dynamical states (steady state, periodic oscillation, and chaos) of a system, under the same set of external constraints-input concentration of reactants, temperature, pressure, and so on, is one of the most interesting and significant phenomena. Although the coexistence of attractors offers important advantages to systems to respond to different solicitations, it also affects the performance of the system to some extent. For this reason, its prediction is become a necessity for the scientific community in recent years. Therefore, the study of coexisting of symmetric and asymmetric attractors in a new parametric chemical oscillator described by (1) is of fundamental and even practical interest. Furthermore, the prediction of coexisting attractors in a Briggs–Rauscher reaction system modeled by a strong nonlinear oscillator with damping and stiffness time-varying described by (1) has not yet been studied. So, the second problem that attracts our attention in this work is the prediction of chaos and coexisting attractors in a new nonlinear parametric chemical system governed by equation of motion (1).

In order to attain our objective, we firstly show that the Briggs–Rauscher kinetic equations can be reduced to a new nonlinear parametric oscillator given by equation (1), and we apply the Melnikov method for deriving the condition of the appearance of horseshoe chaos (Section 2). Second, we investigate the existence of coexisting of attractors by solving numerically the equation of motion (1) via the fourth-order Runge–Kutta algorithm (Section 3). Finally, we end with a conclusion (Section 4).

2. Mathematical Model and Melnikov Analysis

2.1. Mathematical Model. We consider in this work the Briggs–Rauscher reaction system [40] which represents a simple model for designing a chemical oscillator. Such a

reaction was proposed by Boissonade and de Kepper [41]. The governing equations are defined as follows:

$$\dot{u} = -u^3 + \mu_0 u - kv - \lambda,$$

$$\dot{v} = \frac{1}{s}(u - v),$$

(2)

where μ_0 and k are the positive parameters, s is the characteristic evolution time of the feedback $-kv$, and λ is here considered as constant negative feedback for the system. In theoretical studies performed up to now, system (2) has been transformed into a Liénard-type oscillator by considering s as a constant parameter [20, 22–24, 27]. The novelty of this work constitutes to express the characteristic evolution time s under the following form:

$$s^{-1} = s_0^{-1}(1 + p\cos\omega t).$$

(3)

By differencing the first equation of system (2) and taking into account its second equation and equation (3), we obtain after some mathematical manipulations the following equation:

$$x + \mu\left(1 + x^2 + p\gamma\cos\omega t\right)\dot{x}$$
$$+ (1 + p\cos\omega t)\left(\alpha_1 x + \alpha_3 x^3\right)$$
$$= -\alpha_0(1 + p\cos\omega t),$$

(4)

where $\mu = (1/s_0) - \mu_0$, $\alpha_0 = (\lambda/s_0)\sqrt{(3/\mu)}$, $\alpha_1 = (k - \mu_0)/s_0$, $\alpha_3 = (\mu/3s_0)$, $\gamma = 1/s_0\mu$, $A = \sqrt{3s_0/(\mu_0 s_0 - 1)}$, and $u = (1/A)x$.

Now, taking into account the influence of the external excitation of the form $g\cos\Omega t$, we finally obtain the desired equation of motion (1). It is easy to see that when $p = 0$, a similar equation (1) has been used to describe the nonlinear chemical oscillations of Briggs–Rauscher reaction system [22, 27]. After establishment of the equation of motion (1), we use in the next section the Melnikov method for deriving the condition of the appearance of horseshoe chaos in the cases, where $\omega = \Omega$ and $\omega \neq \Omega$.

2.2. Melnikov Analysis. The Melnikov method is a powerful analytical tool widely used to predict the existence of horseshoe chaos in a nonautonomous system [9, 27, 42]. In order to perform such a prediction, we rewrite (1) under the form of a first ordinary differential equation, that is,

$$\dot{x} = y,$$
$$\dot{y} = -\alpha_0 - \alpha_1 x - \alpha_3 x^3 - \varepsilon\mu\left(1 + x^2 + p\gamma\cos\omega t\right)y$$
$$- \varepsilon p\left(\alpha_0 + \alpha_1 x + \alpha_3 x^3\right)\cos\omega t + \varepsilon f\cos\Omega t,$$

(5)

where ε is a small perturbation quantity, that is, $0 < \varepsilon < 1$. From the system of (5), the unperturbed system obtained with $\varepsilon = 0$ becomes

$$\dot{x} = y,$$

$$\dot{y} = -\alpha_0 - \alpha_1 x - \alpha_3 x^3.$$

(6)

System (6) is Hamiltonian, and the potential function and associated Hamiltonian are

$$V(x) = \alpha_0 x + \frac{1}{2}\alpha_1 x^2 + \frac{1}{4}\alpha_3 x^4,$$

$$H(x, y) = \frac{1}{2}y^2 + V(x),$$

(7)

respectively. The homoclinic orbits corresponding to system (6) are given by the following expressions [27]:

$$x_h = x_0 + \frac{\sqrt{2}\sigma^2}{\alpha_3\left(x_0 \pm \delta\cosh\sigma\tau\right)},$$

$$y_h = \mp\frac{\sqrt{2}\delta\sigma^3\sinh(\sigma\tau)}{\alpha_3\left(x_0 \pm \delta\cosh(\sigma\tau)\right)^2},$$

(8)

where $x_0 = \alpha_0/2\alpha_1\sqrt{-3\alpha_3/\alpha_1}$, $\delta^2 = -\alpha_1/\alpha_3 - 1/2x_0^2$, $\sigma^2 = -\alpha_1 - 3/2\alpha_3 x_0^2$, $\tau = t - t_0$, and t_0 is the cross-section time of the Poincaré and can be considered as the initial time of the forcing time. When $\varepsilon \neq 0$, the Melnikov method can be applied. Thus, the Melnikov integral function is defined as follows:

$$M(t_0) = -\mu\left(\int_{-\infty}^{+\infty} y_h^2 d\tau + \int_{-\infty}^{+\infty} x_h^2 y_h^2 d\tau\right)$$
$$- \frac{p}{s_0}\int_{-\infty}^{+\infty} y_h^2\cos(\omega t)d\tau - p\alpha_1\int_{-\infty}^{+\infty} x_h y_h\cos(\omega t)d\tau$$
$$- p\alpha_3\int_{-\infty}^{+\infty} x_h^3 y_h\cos(\omega t)d\tau - p\alpha_0\int_{-\infty}^{+\infty} y_h\cos(\omega t)d\tau$$
$$+ f\int_{-\infty}^{+\infty} y_h\cos(\Omega t)d\tau.$$

(9)

Taking into consideration the expressions of the quantities x_h and y_h given by (8) and using the standard integral table [43], the Melnikov integral function (9) yields after some mathematical manipulations to the following equation:

$$M(t_0) = K_0 + pK_1\cos(\omega t_0) + pK_2\sin(\omega t_0) + fK_3\sin(\Omega t_0).$$

(10)

Assuming that $\Omega = \omega$, the Melnikov function (10) becomes

$$M(t_0) = K_0 + pK_1\cos(\omega t_0) + (pK_2 + fK_3)\sin(\omega t_0),$$

(11)

where the expression of K_i, $i = \overline{0, 3}$, are given in Appendix. It is easy to remark that (11) can be rewritten as follows:

$$M(t_0) = K_0 + \sqrt{K_1^2 p^2 + (K_2 p + K_3 f)^2}\cos(\omega t_0 - \phi),$$

(12)
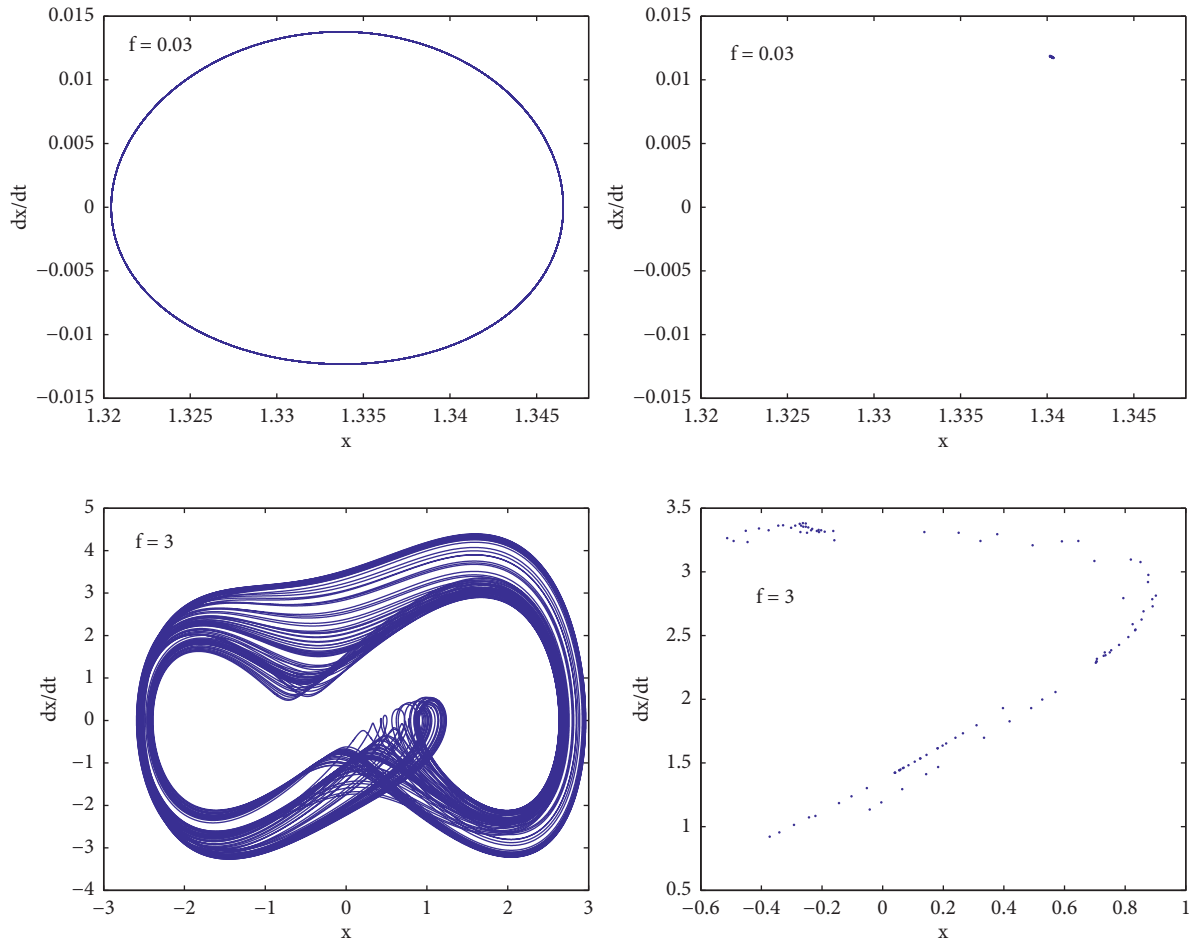
FIGURE 1: Phase portraits and its corresponding Poincaré maps showing the validation of the proposed analytical prediction of horseshoe chaos in the case $\omega = \Omega$.

(a)

(b)

(c)
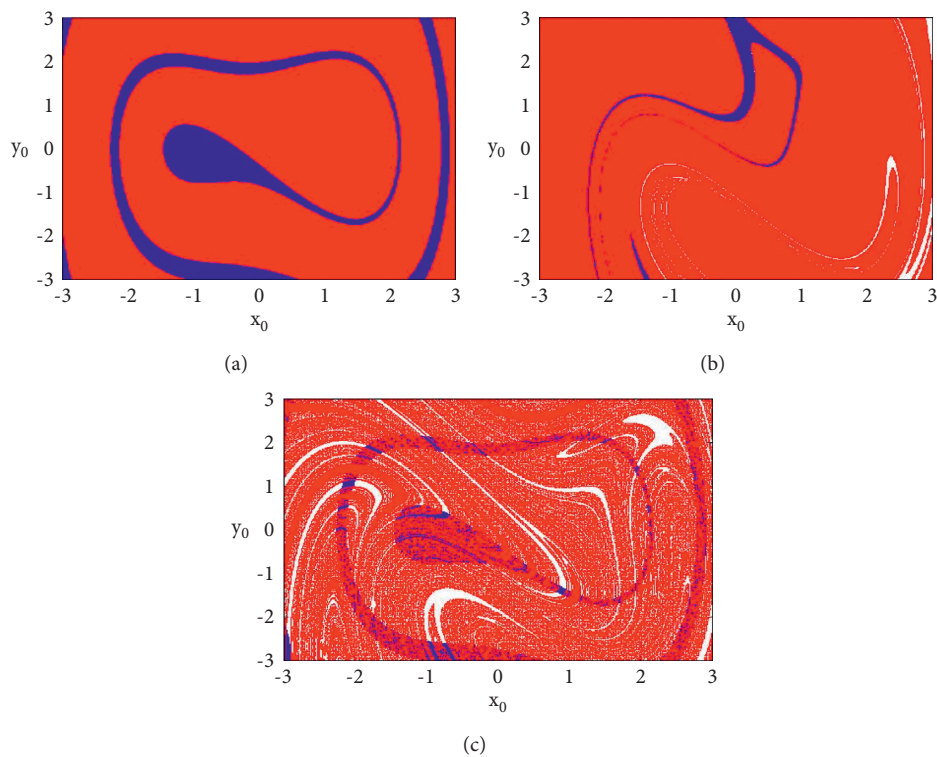
FIGURE 2: Basins of attraction of the new parametric chemical system (1) with the parameters of Figure 1 for three different values of f: (a) $f = 0.03$, (b) $f = 2$, and (c) $f = 3$.
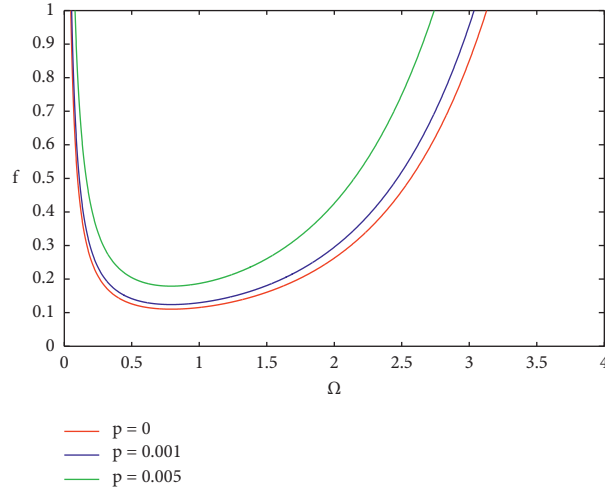
FIGURE 3: Melnikov threshold curves for homoclinic chaos in the (f, Ω) plane with $\omega = (\sqrt{5} - 1)/2$ and for three different values of p. The other parameters of Figure 1 are kept constant.

(a)

(b)

(c)
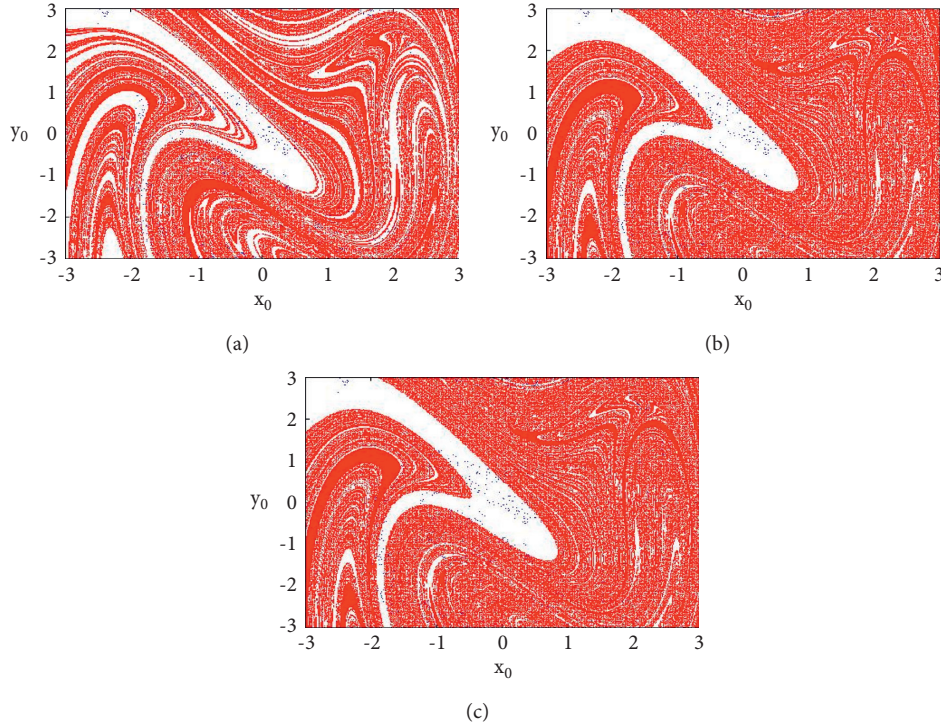
FIGURE 4: Basins of attraction of the new parametric chemical system (1) showing the effect of p with the parameters of Figure 3 for $\omega = (\sqrt{5} - 1)/2$ and $\Omega = 1$: (a) $p = 0$, (b) $p = 0.001$, and (c) $p = 0.05$.

with $\phi = \arctan(K_2 p + K_3 f / K_1 p)$.

To determine the Melnikov criterion for appearance of horseshoe chaos in our new nonlinear dissipative parametric oscillator, it is necessary to let $M(t_0) = 0$ with $M'(t_0) \neq 0$. Thus, $M(t_0) = 0$ leads to

$$\cos(\omega t_0 - \phi) = -\frac{K_0}{\sqrt{K_1^2 p^2 + (K_2 p + K_3 f)^2}}. \tag{13}$$

Since
$M'(t_0) = -\omega\sqrt{K_1^2 p^2 + (K_2 p + K_3 f)^2} \sin(\omega t_0 - \phi) \neq 0$ implies $\sin(\omega t_0 - \phi) \neq 0$, then $\cos(\omega t_0 - \phi) \neq 0$. Thus, $|\cos(\omega t_0 - \phi)| < 1$. Therefore, the condition for the existence of chaos is obtained if

$$M_1 = \left| \frac{K_0}{\sqrt{K_1^2 p^2 + (K_2 p + K_3 f)^2}} \right| < 1. \tag{14}$$
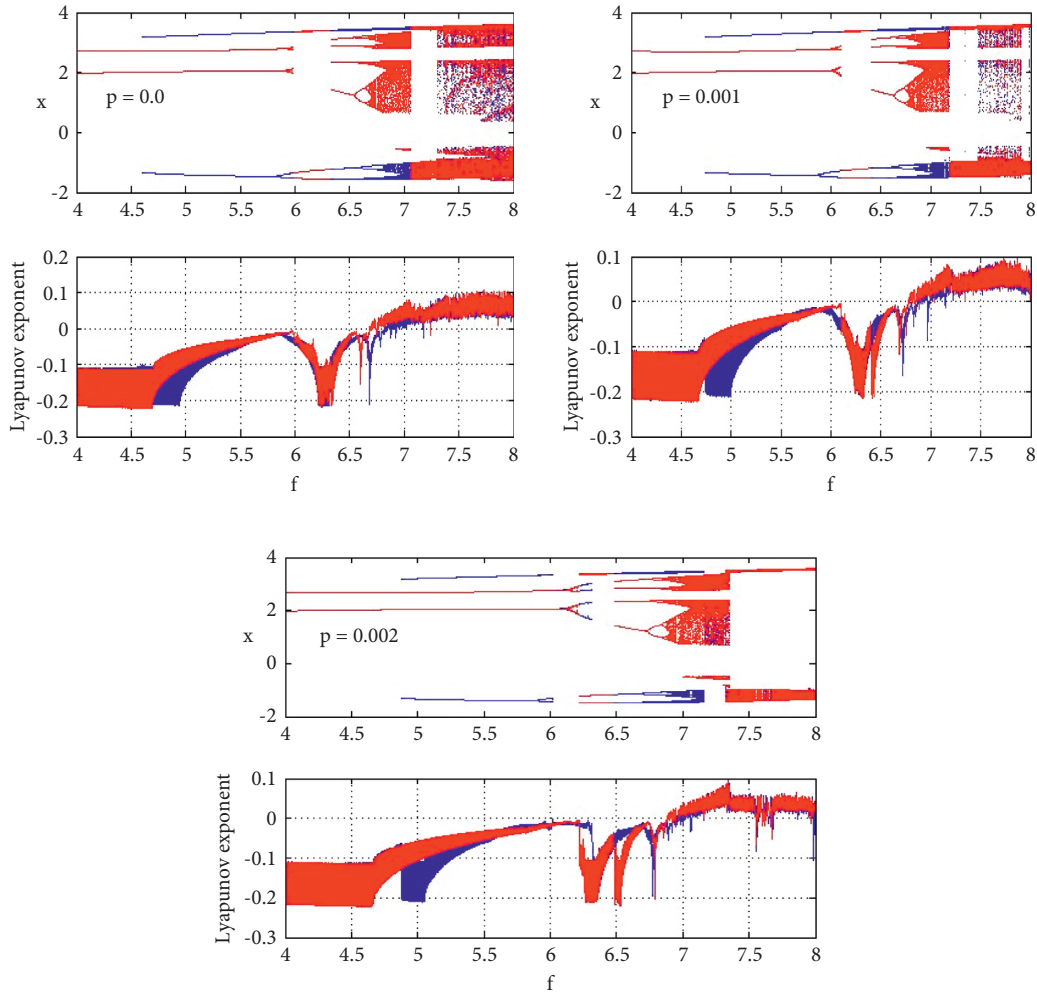
FIGURE 5: Bifurcation diagrams and its corresponding Lyapunov exponents vs. f exhibiting the effect of p with the parameters of Figure 1.

From this analytical result, the following theorem can be formulated.

Theorem 1. *If condition (14) is verified, then a homoclinic bifurcation occurs and the new parametric chemical system (1) may exhibit chaotic behavior.*

Using the following system parameters $k = 25.361$, $\mu_0 = 25.41$, $s_0 = 0.0392$, $\lambda = -0.0025$, $\omega = \Omega = 1.0$, and $p = 0.001$, we obtain $M_1 > 1$ for $f = 0.03$ and $M_1 < 1$ for $f = 3$. Therefore, the desired system given by (1) may display periodic motion for $f = 0.03$. However, when $f = 3$, the new chemical system (1) may exhibit chaotic behavior. The numerical simulations realized in Figure 1 under initial conditions $x(0) = 0.5$ and $\dot{x}(0) = 0.5$ confirm the analytical prediction. To test again the validity of the proposed analytical prediction, we have plotted in Figure 2, the basins of attraction of the new nonlinear chemical system (1) which represent a best tool to study numerically the regularity or

irregularity of the attractors. These basins of attraction are obtained by solving numerically the equation of motion (1) and collecting the initial conditions for which the dynamics of the new chemical system is sensitive. From Figure 2(a), we obtain that the new parametric chemical oscillator show a regular behavior when $f = 0.03$. However, the erosion of the basin of attraction appears and becomes more and more visible for $f = 2$ and $f = 3$. Thus, we can conclude that the analytical and numerical results are in good agreement.

Now, in the case where $\omega \neq \Omega$, the Melnikov function (10) becomes

$$M(t_0) = K_0 + p\sqrt{K_1^2 + K_2^2}\sin(\omega t_0 + \psi) + fK_3\sin\Omega t_0,$$

(15)

with $\tan\psi = K_1/K_2$. For $p \neq 0$ and $\omega \neq \Omega$, the condition of a zero of this Melnikov function is obtained from $|\sin(\omega t_0 + \psi)| < 1$ and $|\sin(\Omega t_0)| < 1$. Therefore, a sufficient condition for the onset of Melnikov chaos in our new chemical system (1) can be expressed from [44, 45] as follows:
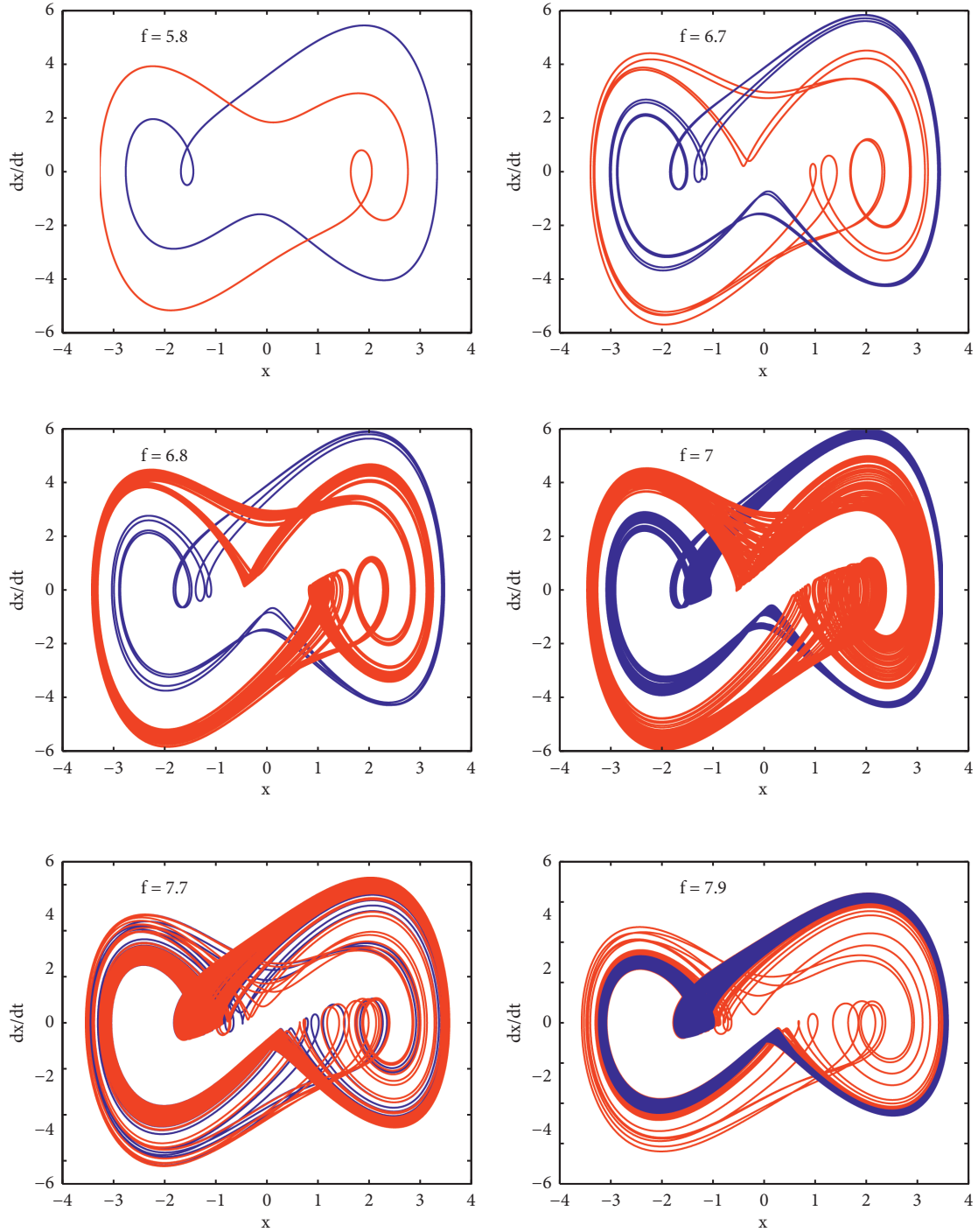
FIGURE 6: Various phase portraits illustrating the coexistence of two attractors for different values of f with the parameters of Figure 5.

$$f \geq \left| \frac{p\sqrt{K_1^2 + K_2^2} - K_0}{K_3} \right|. \qquad (16)$$

From (16), the following theorem can be formulated.

Theorem 2. *If condition (16) is satisfied, then a homoclinic bifurcation occurs and the new chemical system (1) may display chaotic motion.*

Figure 3 shows the dependence of the amplitude f of the periodic external excitation on the frequency Ω for three different

(a)   (b)   (c)
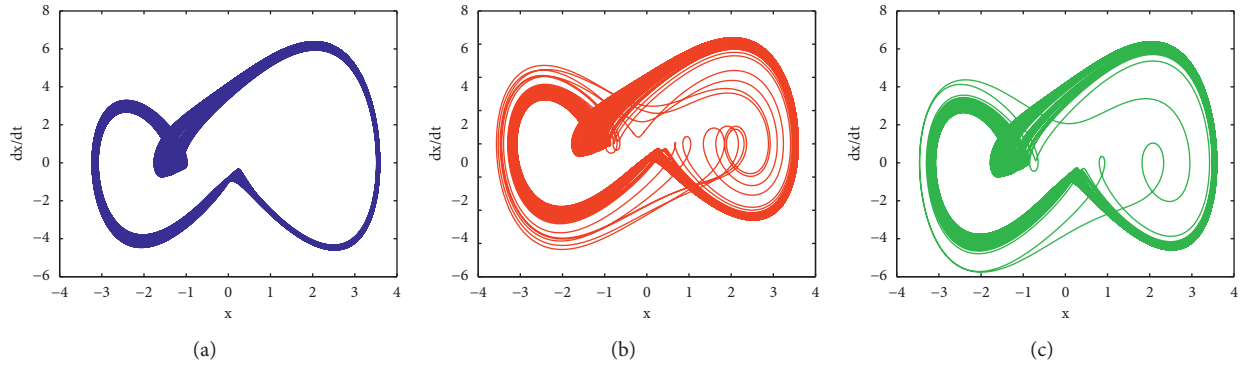
FIGURE 7: Phase portraits showing the coexistence of three different chaotic attractors for $f = 7.9$ under three initial conditions: (a) (0.5, 0.5), (b) (−0.5, − 0.5), and (c) (−0.8, 0).
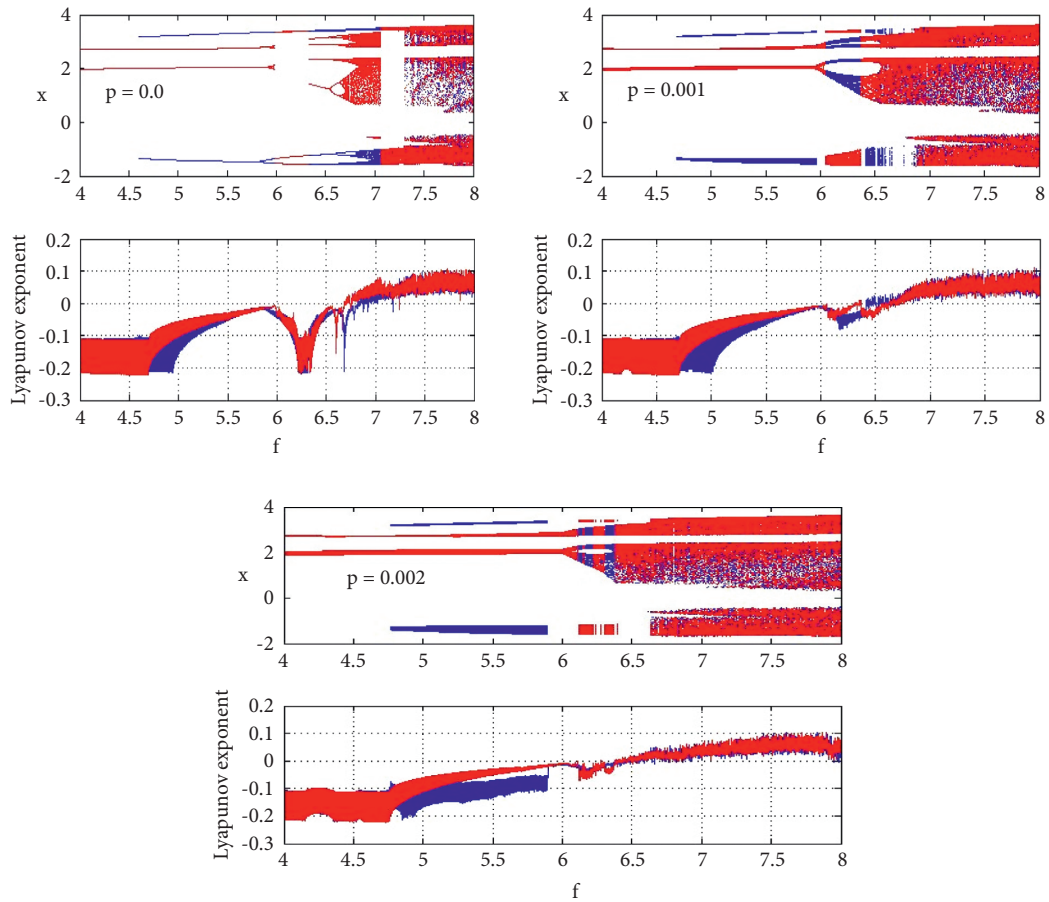
FIGURE 8: Bifurcation diagrams and its corresponding Lyapunov exponents versus f showing the effect of p when $\omega = (\sqrt{5} - 1)/2$ and $\Omega = 1$. The parameters of Figure 3 are kept constant.

values of p. Through this figure, we notice that the horseshoe chaos region decreases when p increases. This observation is confirmed by the basins of attraction shown in Figure 4.

3. Coexisting Attractors

The aim of this section is to investigate the coexisting behaviors of attractors and the eventual transitions to chaos that can arise in the Biggs–Rauscher (BR) reaction system

governed by equation of motion (1) when the parameter p varies. For this, we solve numerically the equation of motion (1) by using the fourth-order Runge–Kutta algorithm with the following system parameters: $k = 25.361$, $\mu_0 = 25.41$, $s_0 = 0.0392$, and $\lambda = -0.0025$. The initial conditions and the calculation step used to realize the numerical simulations are (0.5, 0.5) (blue color), (−0.5, −0.5) (red color), (−0.8, 0.0) (green color), (0.2, 0.2) (yellow color), and $h = 0.005$, respectively.
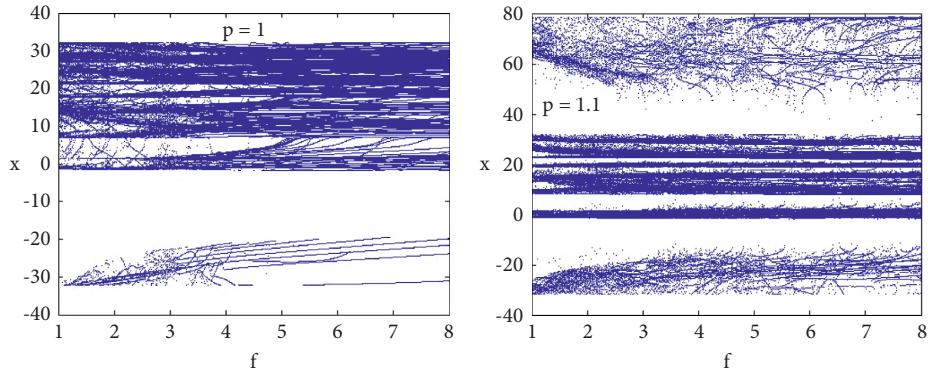
FIGURE 9: Effect of p on the bifurcation diagrams of the new nonlinear parametric chemical system (1) with the parameters of Figure 8.

(a)

(b)
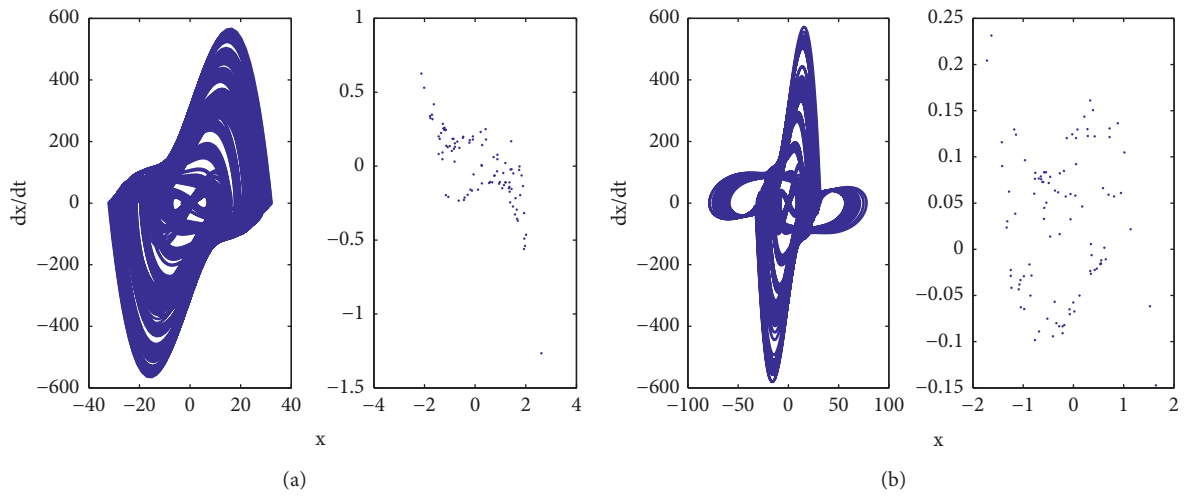
FIGURE 10: Phase portraits and its corresponding Poincaré maps illustrating the chaotic behavior of the new chemical system (1) with the parameters of Figure 9 for (a) $f = 3$, $p = 1.0$ and (b) $f = 1.8$, $p = 1.1$.
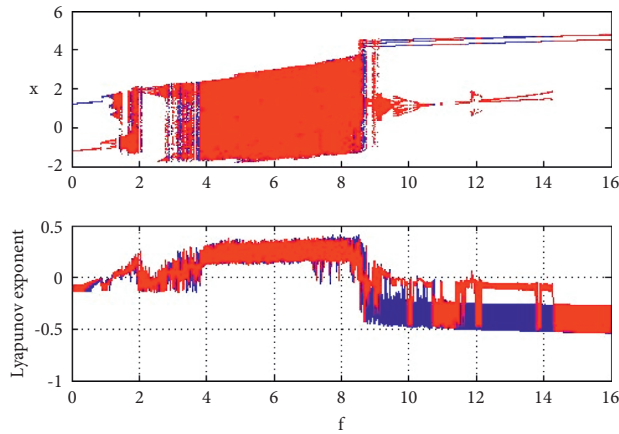
FIGURE 11: Bifurcation diagrams and its corresponding Lyapunov exponents with $\alpha_0 = -0.0193$, $p = 0.005$, $\omega = 1$, and $\Omega = 3$. The other system parameters are fixed.
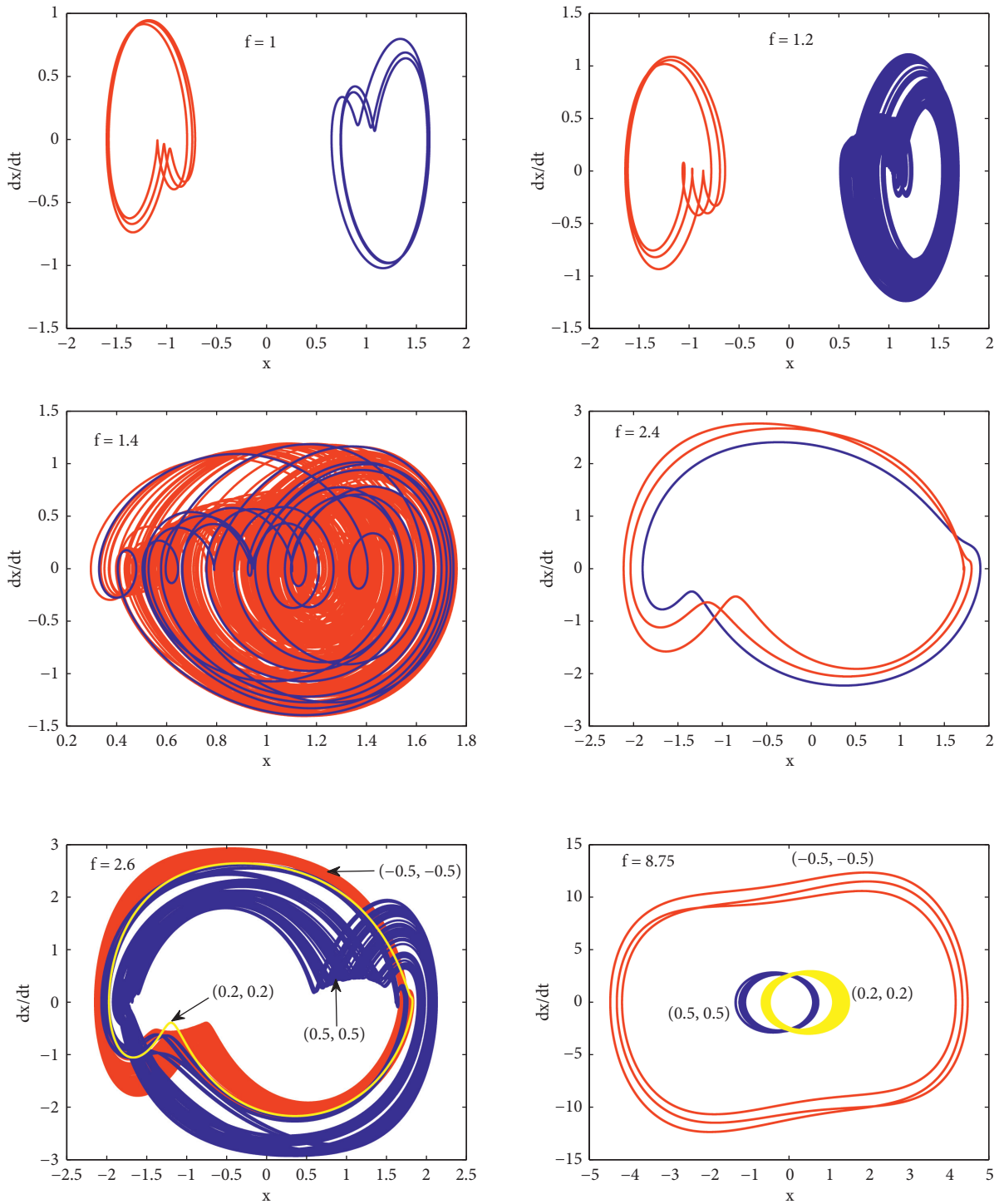
Figure 12: Coexisting behaviors of attractors in a new parametric chemical system (1) with $\Omega = 3$, $\omega = 1$, $p = 0.005$, and $\alpha_0 = -0.0193$. The other system parameters are kept constant.

Figure 5 shows the influence of p on the bifurcation diagrams of Biggs–Rauscher (BR) reaction system described by equation (1). Through this figure, we notice that this parameter accentuates the symmetry breaking phenomenon and removes the symmetry restoring phenomenon. Moreover, the coexistence of attractors
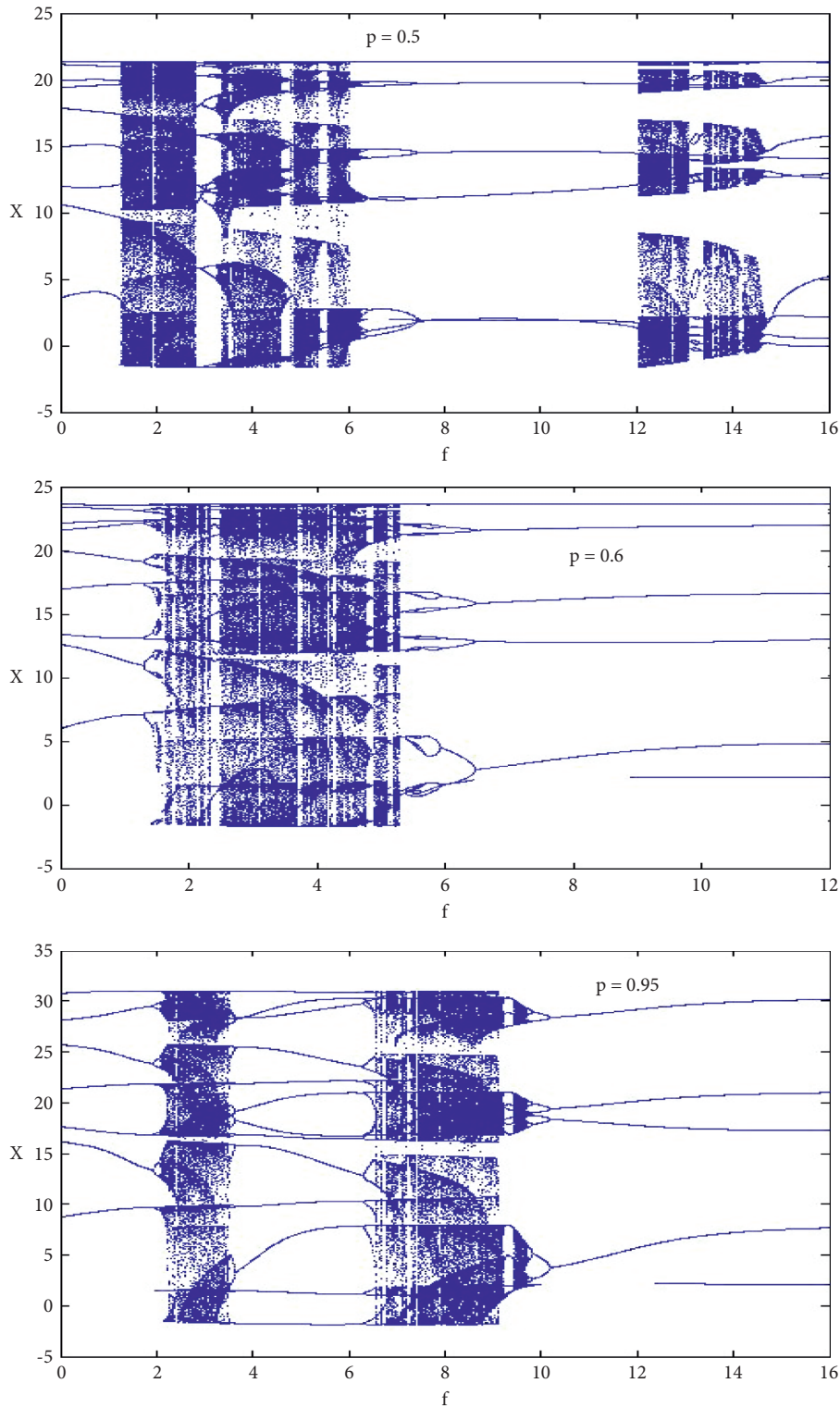
FIGURE 13: Effect of p on the bifurcation diagram of Figure 11 of the new chemical system obtained under initial conditions (0.5, 0.5).

remains in the system under the study when $p \neq 0$. Figure 6 illustrates the coexisting behaviors of attractors for several different values of f for $p = 0.001$. From this figure, we

clearly see that the new nonlinear dissipative parametric chemical system presents multiple coexisting attractors. For example, when $f = 5.8$, the left period-2 orbit coexists
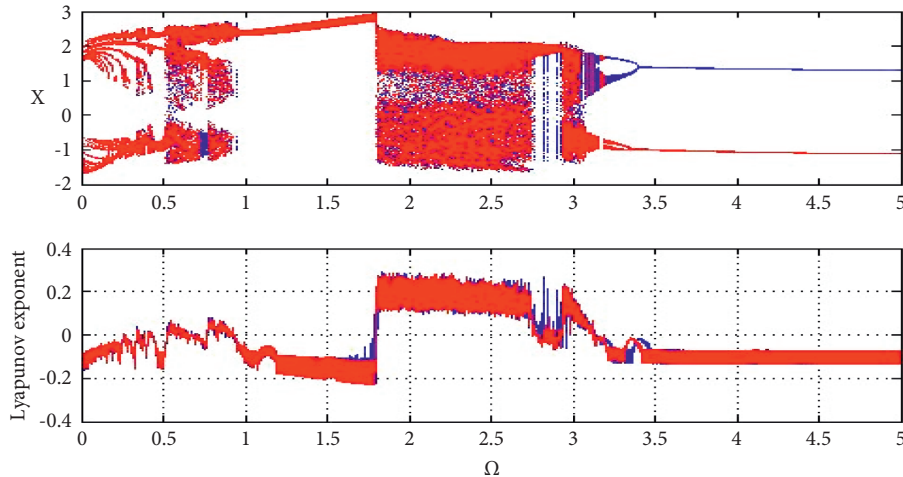
FIGURE 14: Bifurcation diagrams and its corresponding Lyapunov exponents vs. Ω with $f = 1.8$, $\alpha_0 = -0.0193$, and $p = 0.005$ The other parameters are kept constant.

with the right period-2 orbit. For $f = 6.7$, asymmetric period-6 and period-8 orbits coexist. As $f = 6.8$, the left period-6 orbit coexists with the right chaotic attractor. When $f = 7$, two chaotic asymmetric attractors of different topologies coexist. On the contrary, chaotic symmetric attractors of different complexities coexist when $f = 7.7$ and $f = 7.9$. In addition, we found that, for $f = 7.9$, the new parametric chemical system (1) displays with three different initial conditions and chaotic behaviors of different topologies (see Figure 7).

We have afterward analyzed the influence of the parameter p on the bifurcation diagrams of the chemical reaction system under consideration when $\omega \neq \Omega$. Thus, by keeping constant the other parameters and taking $\omega = (\sqrt{5} - 1)/2$ and $\Omega = 1$, the obtained results are shown in Figure 8. From this figure, we notice that the presence of the parameter p provokes always a symmetry breaking. In addition, the geometrical shape of attractors is modified, and we note the disappearance of the symmetry restoring crisis phenomenon. For $p = 1.0$ and $p = 1.1$, the bifurcation structures have completely changed, as shown in Figure 9. In addition, we clearly see through this figure that the amplitude of oscillations becomes important. In order to have an idea about the new chemical system behavior as predicted by these bifurcation diagrams, two phase portraits and its corresponding Poincaré maps are plotted in Figure 10 for two values of f. Through this figure, we notice that the new parametric chemical system (1) exhibits for these chosen system parameters and chaotic behaviors which are confirmed by the Poincaré maps. When ω/Ω is rational, that is, $\omega = 1$ and $\Omega = 3$, the new parametric chemical system (1) displays bistability phenomenon, symmetric coexisting attractors, and asymmetric coexisting attractors (see Figure 11). The coexisting behaviors of asymmetric attractors of

different topologies are illustrated in Figure 12. We also notice that, for $f = 2.6$, two chaotic symmetric attractors of different complexities coexist with a period-1 orbit. Moreover, when $f = 8.75$, two asymmetric quasi-periodic orbits coexist with a period-3 orbit of large oscillation amplitude. We have also investigated, in this case of oscillation, the effect of p on the bifurcation diagram of Figure 11 obtained with initial conditions (0.5, 0.5). The obtained numerical results are shown in Figure 13. From this figure, we observe that the new chemical system (1) exhibits various bifurcations such as period-doubling and reverse period-doubling bifurcations, period windows, period-m bubbles and reverse period-m bubbles, antimonotonicity, intermittency, symmetry breaking, and symmetry restoring. In addition, period-9 orbit route to chaos and period-m bubbles route to chaos occur in the system. On the contrary, we also observe merging of chaotic regions between the forward and reverse period-doubling sequences.

When we use the external excitation frequency, Ω, as the control parameter, with $f = 1.8$, $p = 0.005$, and $\alpha_0 = -0.0193$, the new nonlinear chemical oscillator under the study displays a period-3 route to chaos, period-1 route to chaos, periodic windows, reverse period doubling, symmetry breaking and symmetry restoring, bistable chaotic oscillations, and various coexisting behaviors of symmetric and asymmetric attractors (see Figure 14). Figure 15 illustrates the different attractors predicted by bifurcation diagrams of Figure 14 for several different values of Ω. Through this figure, we notice that our new chemical model presents several bistable symmetric and asymmetric attractors of different topologies and remarkable routes to chaos. We can conclude that the new nonlinear parametric oscillator under consideration displays a rich variety of dynamical behaviors with unusual transitions to chaos.
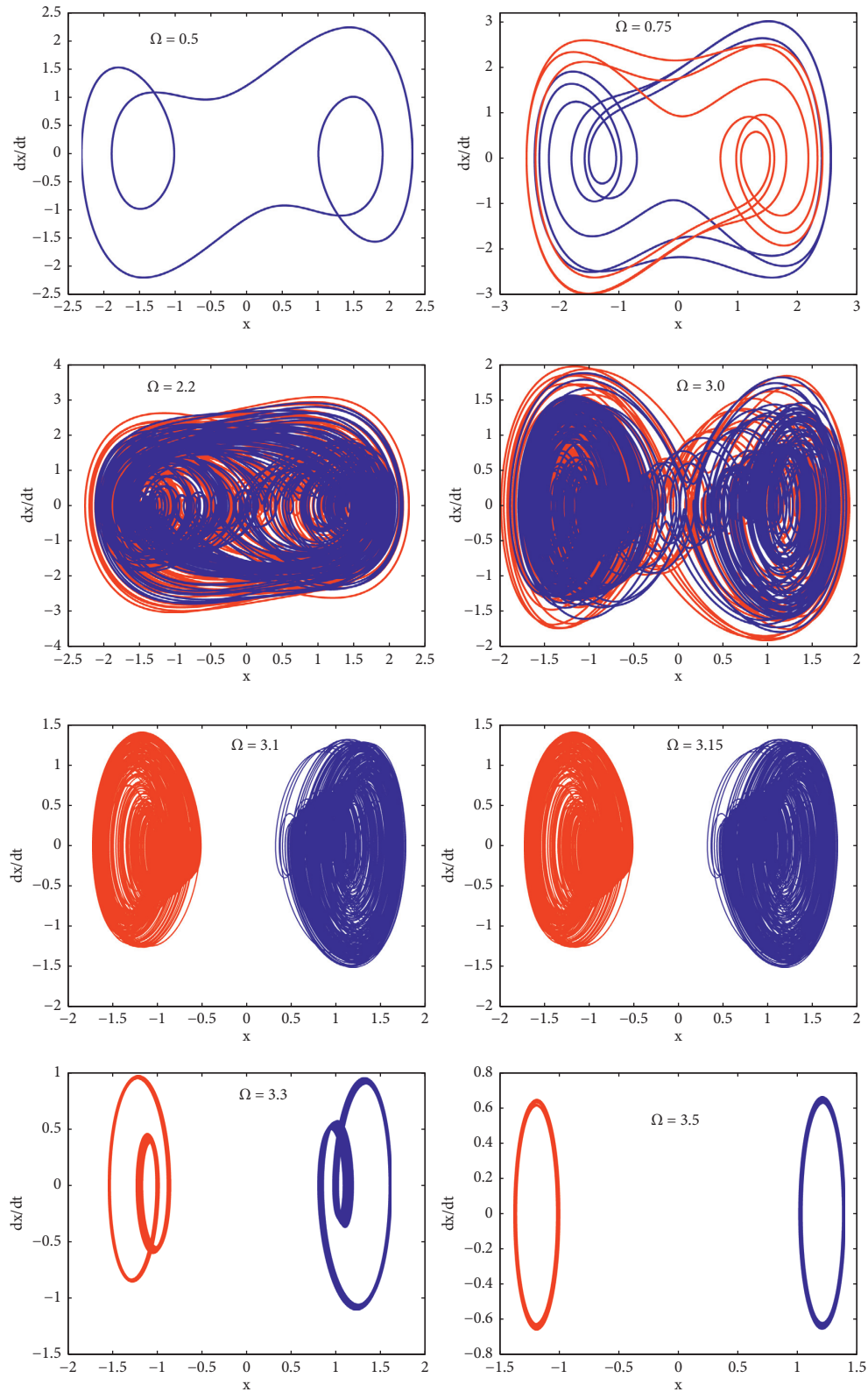
Figure 15: Various phase portraits illustrating monostability, bistability, and coexistence of attractors for different values of Ω with the parameters of Figure 13.

4. Conclusions

This study deals with nonlinear dynamics of Briggs–Rauscher reaction system modeled by a new non-linear parametric oscillator. The Melnikov method is used to derive the condition of the appearance of horseshoe chaos in a new nonlinear parametric chemical oscillator in the cases, where $\Omega = \omega$ and $\Omega \neq \omega$. The numerical simulations realized confirm the obtained analytical predictions. On the contrary, the complex dynamics of the new nonlinear parametric chemical oscillator (1) is investigated numerically by using the fourth-order Runge–Kutta algorithm. The obtained results show that the parametric parameter p also induces in the new chemical parametric system and the symmetry breaking phenomenon and removes the symmetry restoring crisis phenomenon when p increases. Note that the new nonlinear parametric chemical system presents bistability phenomenon and coexisting behaviors of asymmetric attractors in the case $\Omega = \omega$. Moreover, it is found that three chaotic attractors of different topologies coexist for $f = 7.9$. As ω/Ω is irrational, the geometrical shape of attractors has completely changed. In addition, the symmetry restoring crisis phenomenon disappears in the new chemical system under the study. The dynamical behavior of our new chemical system becomes rich when ω/Ω is rational. In this case, the coexisting behavior of symmetric and asymmetric attractor appears in the system as well as the bistability phenomenon. Furthermore, for $f = 2.6$ and $f = 8.75$, multiple coexisting attractors take place in the system. As p varies in this case of oscillation, the new chemical parametric system (1) exhibits various bifurcations such as symmetry breaking and symmetry restoring, period doubling and reverse period doubling, period windows, intermittency, period-m bubbles and reverse period-m bubbles, intermittency, and antimonotonicity. In addition, period-9 orbit route chaos and period-m bubbles transition to chaos occur in the system as well as remerging chaotic band attractors. When Ω is used as control parameter, the new nonlinear chemical oscillator displays also various symmetric and asymmetric bistable attractors. Moreover, symmetry breaking, symmetry restoring, reverse period doubling, period-3 orbit route to chaos, and period-1 motion leading to chaos are obtained.

Appendix

A. Expression of $K_{i \in \{0,1,2,3\}}$

$$K_0 = -\frac{4\mu\sigma^5}{15\alpha_3^2\delta^2}\left(1 + x_0^2\right)_2F_1\left(2, 1; \frac{7}{2}; \frac{1}{1 - \nu^2}\right) \mp \frac{16\mu\sqrt{2}\sigma^7 x_0}{105\alpha_3^3\delta^3}\,{}_2F_1\left(\frac{5}{2}, \frac{3}{2}; \frac{9}{2}; \frac{1}{1 - \nu^2}\right)$$

$$- \frac{16\mu\sigma^9}{315\alpha_3^4\delta^4}\,{}_2F_1\left(3, 2; \frac{11}{2}; \frac{1}{1 - \nu^2}\right),$$

$$K_2 = -\frac{2\sqrt{2}\sigma\omega\pi\alpha_0}{\alpha_3\sqrt{x_0^2 - \delta^2}}\frac{\sin\left((\omega/\sigma)\cosh^{-1}(x_0/\delta)\right)}{\sinh(\omega\pi/\sigma)} - \frac{2\sqrt{2}\omega\pi\alpha_1 x_0\,\sigma}{\alpha_3\sqrt{x_0^2 - \delta^2}}\frac{\sin\left((\omega/\sigma)\cosh^{-1}(x_0/\delta)\right)}{\sinh(\omega\pi/\sigma)}$$

$$- \frac{2\alpha_1\,\sigma\omega\left(\sigma^2 + \omega^2\right)\pi}{3\alpha_3^2\delta^2\sinh(\omega\pi/\sigma)}\,{}_2F_1\left(1 + i\frac{\omega}{2\sigma}, 1 - i\frac{\omega}{2\sigma}; \frac{5}{2}; \frac{1}{1 - \nu^2}\right) - \frac{2\sqrt{2}\omega\pi\sigma x_0^3}{\sqrt{x_0^2 - \delta^2}}\frac{\sin\left((\omega/\sigma)\cosh^{-1}(x_0/\delta)\right)}{\sinh(\omega\pi/\sigma)} \quad\text{(A.1)}$$

$$- \frac{2\sigma\omega x_0^2\left(\sigma^2 + \omega^2\right)\pi}{\alpha_3\delta^2\,\sinh(\omega\pi/\sigma)}\,{}_2F_1\left(1 + i\frac{\omega}{2\sigma}, 1 - i\frac{\omega}{2\sigma}; \frac{5}{2}; \frac{1}{1 - \nu^2}\right)$$

$$\mp \frac{2\sqrt{2}x_0\sigma\omega\left(4\sigma^2 + \omega^2\right)\left(\sigma^2 + \omega^2\right)\pi}{15\alpha_3^2\delta^3\sinh(\omega\pi/\sigma)}\,{}_2F_1\left(\frac{3}{2} + i\frac{\omega}{2\sigma}, \frac{3}{2} - i\frac{\omega}{2\sigma}; \frac{7}{2}; \frac{1}{1 - \nu^2}\right)$$

$$- \frac{\sigma\pi\omega\left(9\sigma^2 + \omega^2\right)\left(4\sigma^2 + \omega^2\right)\left(\sigma^2 + \omega^2\right)}{315\alpha_3^3\delta^4\sinh(\omega\pi/\sigma)}\,{}_2F_1\left(2 + i\frac{\omega}{2\sigma}, 2 - i\frac{\omega}{2\sigma}; \frac{9}{2}; \frac{1}{1 - \nu^2}\right),$$

with

$$\frac{1}{1-\nu^2} = 1 - \frac{x_0^2}{\delta^2},$$

$$K_3 = \frac{2\sqrt{2}\sigma\Omega\pi}{\alpha_3\sqrt{x_0^2-\delta^2}} \frac{\sin\left((\Omega/\sigma)\cosh^{-1}(x_0/\delta)\right)}{\sinh(\Omega\pi/\sigma)}. \tag{A.2}$$

Data Availability

All the data are included within the article.

Conflicts of Interest

The authors declare that there are no conflicts of interest regarding the publication of this paper.

References

[1] L. Cveticanin, *Strong Nonlinear Oscillators*, Springer, 2nd edition, 2018.

[2] S. Strogatz, *Nonlinear Dynamics and Chaos: With Applications to Physics, Biology, Chemistry, and Engineering*, Perseus Books, New York, NY, USA, 1994.

[3] A. H. Nayfeh and D. T. Mook, *Nonlinear Oscillations*, John Wiley & Sons, New York, NY, USA, 1995.

[4] M. Bayat, I. Pakar, and G. Domairry, "Recent developments of some asymptotic methods and their applications for nonlinear vibration equations in engineering problems: a review," *Latin American Journal of Solids and Structures*, vol. 9, no. 2, pp. 1–93, 2012.

[5] S. Fiori, "Nonlinear damped oscillators on Riemannian manifolds: numerical simulation," *Communications in Nonlinear Science and Numerical Simulation*, vol. 47, pp. 207–222, 2017.

[6] A. H. Nayfeh, *Perturbation Methods*, Wiley-VCH Verlag GmbH & Co.KGaA, 2004.

[7] M. Siewe Siewe, F. M. Moukam Kakmeni, C. Tchawoua, and P. Woafo, "Bifurcations and chaos in the triple-well φ^6 Van der Pol oscillator driven by external and parametric excitations," *Physica A: Statistical Mechanics and Its Applications*, vol. 357, no. 3-4, pp. 383–396, 2005.

[8] L. A. Hinvi, A. A. Koukpémèdji, V. A. Monwanou, C. H. Miwadinou, V. Kamdoum Tamba, and J. B. Chabi Orou, "Resonance, chaos and coexistence of attractors in a position dependent mass-driven Duffing-type oscillator," *Journal of the Korean Physical Society*, vol. 79, no. 8, pp. 755–771, 2021.

[9] Y. J. F. Kpomahou and J. A. Adéchinan, "Nonlinear dynamics and active control in a Liénard-type oscillator under parametric and external periodic excitations," *American Journal of Computational and Applied Mathematics*, vol. 10, no. 2, pp. 48–61, 2020.

[10] T. K. Dutta and P. K. Prajapati, "Some dynamical properties of the Duffing equation," *International Journal of Engineering Research & Technologies*, vol. 5, no. 12, pp. 500–503, 2016.

[11] I. R. Epstein and J. A. Pojman, *An Introduction to Nonlinear Chemical Dynamics*, Oxford University Press, Oxford, UK, 1998.

[12] A. B. Cambel, *An Introduction to Nonlinear Chemical Dynamics*, Academic Press, Cambridge, MA, USA, 1993.

[13] I. R. Epstein and K. Showalter, "Nonlinear chemical dynamics: oscillations, patterns, and chaos," *The Journal of Physical Chemistry*, vol. 100, no. 31, pp. 13132–13147, 1996.

[14] K. Showalter and I. R. Epstein, "From chemical systems to systems chemistry: patterns in space and time," *Chaos: An Interdisciplinary Journal of Nonlinear Science*, vol. 25, no. 9, pp. 97613–97621, 2015.

[15] M. A. Budroni, I. Calabrese, Y. Miele, M. Rustici, N. Marchettini, and F. Rossi, "Control of chemical chaos through medium viscosity in a batch ferroin-catalysed Belousov-Zhabotinsky reaction," *Physical Chemistry Chemical Physics*, vol. 19, no. 48, pp. 32235–32241, 2017.

[16] R. J. Field, "Chaos in the belousov-zhabotinsky reaction," *Modern Physics Letters B*, vol. 29, no. 34, pp. 1–39, 2015.

[17] V. Voorsluijs, I. G. Kevrekidis, and Y. De decker, "Nonlinear behavior and fluctuation-induced dynamics in the photosensitive Belousov-Zhabotinsky reaction," *Physical Chemistry Chemical Physics*, vol. 19, no. 33, pp. 22528–22537, 2017.

[18] Y.-N. Li, H. Song, Z.-S. Cai et al., "New chaotic behavior and its effective control in Belousov–Zhabotinsky reaction," *Canadian Journal of Chemistry*, vol. 79, no. 1, pp. 29–34, 2001.

[19] A. Cassani, A. Monteverde, and M. Piumetti, "Belousov-Zhabotinsky type reactions: the non-linear behavior of chemical systems," *Journal of Mathematical Chemistry*, vol. 59, no. 3, pp. 792–826, 2021.

[20] J. A. Adéchinan, Y. J. F. Kpomahou, C. H. Miwadinou, and L. A. Hinvi, "Dynamics and active control of chemical oscillations modeled as a forced generalized Rayleigh oscillator with asymmetric potential," *International Journal of Basic and Applied Sciences*, vol. 10, no. 2, pp. 20–31, 2021.

[21] A. V. Monwanou, A. A. Koukpémèdji, C. Aïnamon, P. R. Nwagoun Tuwa, C. H. Miwadinou, and J. B. Chabi Orou, "Nonlinear dynamics in a chemical reaction under an amplitude-modulated excitation: hysteresis, vibrational, resonance, multistability, and chaos," *Complexity*, vol. 2021, Article ID 8823458, 16 pages, 2021.

[22] D. L. Olabodé, C. H. Miwadinou, A. V. Monwanou, and J. B. Orou, "Horseshoes chaos and its passive control in nonlinear chemical dynamics," *Physica Scripta*, vol. 93, no. 8, pp. 1–19, 2018.

[23] D. L. Olabodé, C. H. Miwadinou, A. Monwanou, and J. B. C. Orou, "Effects of passive hydrodynamics force on harmonic and chaotic oscillations in dissipative nonlinear chemical dynamics," *Physica D*, vol. 386-387, pp. 49–59, 2019.

[24] S. Ghosh and D. S. Ray, "Liénard-type chemical oscillator," *The European Physical Journal B*, vol. 87, no. 65, pp. 1–7, 2014.

[25] H. Binous and A. Bellagi, "Introducing nonlinear dynamics to chemical and biochemical engineering graduate students using mathematica," *Computer Applications in Engineering Education*, vol. 27, no. 1, pp. 1–19, 2018.

[26] A. Shabunin, V. Astakhov, V. Demidov et al., "Modeling chemical reactions by forced limit-cycle oscillator: synchronization phenomena and transition to chaos," *Chaos, Solitons & Fractals*, vol. 15, no. 2, pp. 395–405, 2003.

[27] C. H. Miwadinou, A. V. Monwanou, J. Yovogan, L. A. Hinvi, P. R. Nwagoum Tuwa, and J. B. Chabi Orou, "Modeling nonlinear dissipative chemical dynamics by a forced modified Van der Pol-Duffing oscillator with asymmetric potential: chaotic behaviors predictions," *Chinese Journal of Physics*, vol. 56, no. 3, pp. 1089–1104, 2018.

[28] M. V. S. Meenakshi, S. Athisayanathan, V. Chinnathambi, and S. Rajasekar, "Homoclinic Bifurcation in a parametrically driven nonlinearly damped Duffing-vander Pol oscillator," *International Journal of Advances in Applied Mathematics and Mechanics*, vol. 6, no. 1, pp. 10–20, 2018.

[29] C. Si-yu and T. Jin-yuan, "Study on a new nonlinear parametric excitation equation: stability and bifurcation," *Journal of Sound and Vibration*, vol. 318, no. 4-5, pp. 1109–1118, 2008.

[30] J. Y. Tang, S. Y. Chen, and J. Zhong, "A improved nonlinear model of a spur gear pair system," *Engineering Mechanics*, vol. 1, no. 25, pp. 217–223, 2008.

[31] F. Sagués and I. R. Epstein, *Nonlinear dynamics," Dalton Transactions*, vol. 34, no. 7, pp. 1201–1217, 2003.

[32] Z. Wang, H. R. Abdolmohammadi, F. E. Alsaadi, T. Hayat, and V.-T. Pham, "A new oscillator with infinite coexisting asymmetric attractors," *Chaos, Solitons & Fractals*, vol. 110, no. C, pp. 252–258, 2018.

[33] K. Sun, A. D.-L. D. Li-kun, Y. Dong, H. Wang, and K. Zhong, "Multiple coexisting attractors and hysteresis in the generalized Ueda oscillator," *Mathematical Problems in Engineering*, vol. 2013, Article ID 256092, 7 pages, 2013.

[34] K. Zang, M. D. Vijayakumar, S. S. Jamal et al., "A novel megastable oscillator with a strange structure of coexisting attractors: design, analysis and FPGA implementation," *Complexity*, vol. 2021, Article ID 2594965, 11 pages, 2021.

[35] B. Deruni, A. S. Hacinliyan, E. Kandiran et al., "Coexisting attractors and bubbling route to chaos in modified coupled Duffing oscillators," *Australian Journal of Mathematical Analysis and Applications*, vol. 18, no. 1, pp. 1–13, 2021.

[36] M. Yan and H. Xu, "A chaotic system with a nonlinear term and multiple coexistence attractors," *The European Physical Journal Plus*, vol. 135, no. 6, pp. 1–9, 2020.

[37] N. Wang, G. Zhang, and H. Bao, "Bursting oscillations and coexisting attractors in a simple memristor-capacitor-based chaotic circuit," *Nonlinear Dynamics*, vol. 97, no. 4, pp. 1477–1494, 2019.

[38] N. Wang, G. Zhang, and N. V. K. H. Bao, "Hidden attractors and multistability in a modified Chua's circuit," *Communications in Nonlinear Science and Numerical Simulation*, vol. 92, Article ID 105494, 2021.

[39] B. Bao, T. Jiang, Q. Xu, M. Chen, H. Wu, and Y. Hu, "Coexisting infinitely many attractors in active band-pass filter-based memristive circuit," *Nonlinear Dynamics*, vol. 86, no. 3, pp. 1711–1723, 2016.

[40] T. S. Briggs and W. C. Rauscher, "An oscillating iodine clock," *Journal of Chemical Education*, vol. 50, no. 7, p. 496, 1973.

[41] J. Boissonade and P. De Kepper, "Transitions from bistability to limit cycle oscillations. Theoretical Analysis and experimental evidence in an open chemical system," *The Journal of Physical Chemistry*, vol. 84, no. 5, pp. 501–506, 1980.

[42] Y. J. F. Kpomahou, L. A. Hinvi, J. A. Adechinan, and C. H. Miwadinou, "Chaotic dynamic of a Mixed Rayleigh-Liénard oscillator driven by parametric damping and external excitations," *Complexity*, vol. 2021, Article ID 6631094, 18 pages, 2021.

[43] I. S. Gradshteyn and I. M. Ryzhik, *Table of Integrals, Series, and Products*, Academic Press, New York, NY, USA, 2007.

[44] X. Chen, X. Fu, X. Fu, and Z. Jing, "Chaos control in a special pendulum system for ultra-subharmonic resonance," *Discrete & Continuous Dynamical Systems-B*, vol. 26, no. 2, pp. 847–860, 2021.

[45] B. R. Chacon, "Melnikov method approach to control of homoclinic/heteroclinic chaos by weak harmonic excitations," *Philosophical Transactions of the Royal Society A*, vol. 364, pp. 2335–2351, 2012.

WILEY | Hindawi

Research Article

Synchronous Reluctance Motor: Dynamical Analysis, Chaos Suppression, and Electronic Implementation

Balamurali Ramakrishnan (ID),[1] **Andre Chéagé Chamgoué** (ID),[2] **Hayder Natiq** (ID),[3] **Jules Metsebo** (ID),[4] **and Alex Stephane Kemnang Tsafack** (ID)[5]

[1]*Center for Nonlinear Systems, Chennai Institute of Technology, Chennai-600069, Tamilnadu, India*
[2]*Department of Basic Sciences, School of Geology and Mining Engineering, University of Ngaoundere, P. O. BOX 115, Meiganga, Cameroon*
[3]*Information Technology College, Imam Ja'afar Al-Sadiq University, Baghdad 10001, Iraq*
[4]*Department of Hydraulics and Water Management, National Advanced School of Engineering, University of Maroua, P. O. Box 46, Maroua, Cameroon*
[5]*Research Unit of Condensed Matter of Electronics and Signal Processing Department of Physics, Faculty of Sciences, University of Dschang, P. O. Box 67, Dschang, Cameroon*

Correspondence should be addressed to Jules Metsebo; jmetsebo@gmail.com

Dynamical analysis, chaos suppression and electronic implementation of the synchronous reluctance motor (SynRM) without external inputs are investigated in this paper. The different dynamical behaviors (including monostable periodic behaviors, bistable periodic behaviors, monostable chaotic behaviors, and bistable chaotic behaviors) found in the SynRM without external inputs are illustrated in the two parameters largest Lyapunov exponent (LLE) diagrams, one parameter bifurcation diagram, and phase portraits. The three single controllers are designed to suppress the chaotic behaviors found in SynRM without external inputs. The three proposed single controllers are simple and easy to implement. Numerical simulation results show that the three proposed single controllers are effective. Finally, the dynamical behaviors found in the SynRM without external inputs and the physical feasibility of the three proposed single controllers are validated through circuit implementation on OrCAD-PSpice software.

1. Introduction

An electrical motor converts electrical energy into mechanical energy thank to the discovery by Michael Faraday in the 19th century. He stated that a current carrying coil within a magnetic field will experience a force. Electrical motors can be found in steel rolling mills, drilling machines, railway traction, industrial robots, and in most household items and office equipment [1–6]. Today, there are several variants of electric motors including the induction motor [7,8], permanent-magnet brushless motor [9–12], and variable-reluctance motor. The variable-reluctance motor class takes the advantages of a simple and rugged structure, good compatibility with the power converter, and high recyclability for the core and winding [13]. The variable-reluctance motor is divided into the switched reluctance motor [14,15] and synchronous reluctance motor (SynRM). The SynRM uses a distributed winding and sinusoidal wave which can essentially eliminate the torque pulsation and acoustic noise problems. It is broadly used in the field of transportation, industrial and agricultural production, commercial and household appliances, medical appliances and equipment, and so on [16–20]. Because of its advantage over other types of electrical motors in simple mechanical construction, there were no slip ring and no permanent magnet and over other

servomotors in high efficiency, high power density, and low manufacturing cost [21].

For industrial automation manufacturing, the secure and stable operation of the SynRM is an essential requirement because chaotic behaviors can extremely destabilize the SynRM and even cause the drive system to fail [20]. Hopf Bifurcation and chaos have been found in the SynRM [13]. In this paper, it is demonstrated that the SynRM can exhibit monostable periodic behaviors, bistable periodic behaviors, monostable chaotic behaviors, and bistable chaotic behaviors. The chaotic behaviors found in the SynRM induces instability in this motor and shortens its service time [9]. Thereafter, a variety of methods to control chaos have been used to suppress the chaotic behavior in SynRM. A passive adaptive controller [21], a nonlinear feedback controller [22], a controller based on tridiagonal structure matrix stability theory [23], a vector controller [24–26], a sliding mode controller [27], and an adaptive sliding mode controller [28] were used for the control of chaotic behavior in SynRM. Most of the existing techniques for the control of chaotic behavior in SynRM use a nonlinear and complicated controller.

To the best of authors' knowledge, no study on the chaos suppression in SynRM without external inputs has been carried out with the single state feedback controller. The single state feedback control method is simple, concise, and easy to implement. Therefore, the main contribution of this paper is to investigate the dynamical analysis of SynRM without external inputs and to design three single and simple controllers to suppress chaos in SynRM. The dynamical analysis and chaos suppression via a single controller of SynRM without external inputs are analytically, numerically, and electronically analysed in this paper. The dynamical analysis of SynRM without external inputs is investigated in Section 2. In Section 3, three proposed single controllers are employed to achieve the suppression of chaos in SynRM without external inputs. Section 4 presents the electronic implementation in order to check the existence of dynamical behaviors found in SynRM and the effectiveness of the three proposed single controllers. Finally, conclusions are given in Section 5.

2. Dynamical Analysis of SynRM without External Inputs

The SynRM can be described by the following rate equations [1, 2, 13]:

$$\frac{d\tilde{i}_d}{d\tilde{t}} = \frac{\left(\tilde{u}_d - R_s \tilde{i}_d + \omega_e L_q \tilde{i}_q\right)}{L_d}, \tag{1a}$$

$$\frac{d\tilde{i}_q}{d\tilde{t}} = \frac{\left[-R_s \tilde{i}_q - \omega_e L_d \tilde{i}_d + k_p \left(\tilde{\omega} - \omega_{ref}\right)\right]}{L_q}, \tag{1b}$$

$$\frac{d\tilde{\omega}}{d\tilde{t}} = \frac{\left[3P\left(L_d - L_q\right)\tilde{i}_d \tilde{i}_q/4 - B\tilde{\omega} + \tilde{T}_L\right]}{J}, \tag{1c}$$

where $\tilde{i}_d, \tilde{i}_q$ are the d (direct)- and q (quadrature)-axis stator currents, $\tilde{\omega}$ is the mechanical rotor speed, ω_e is the

electrical rotor speed, $\tilde{u}_d$ is the stator voltage on d axis, R_s is the stator resistance per phase, k_p is the feedback coefficient, and ω_{ref} is the reference rotor speed, L_d, L_q are the d- and q-axis stator inductors, P is the number of poles, $J, \tilde{T}_L$, and B are the inertia constant of the motor and load, load torque, and viscous friction coefficient, respectively. The normalization of equations (1a)–(1c) leads to the following dimensionless form of the mathematical model of SynRM:

$$\frac{dx}{dt} = u_d - bx + yz, \tag{2a}$$

$$\frac{dy}{dt} = -y - xz + c\left(z - z_{ref}\right), \tag{2b}$$

$$\frac{dz}{dt} = xy - az + T_L, \tag{2c}$$

with the following rescaling variables and parameters: $\tau = L_q/R_s, \tilde{t} = \tau t, a = BL_q/(JR_s)$, $b = L_q/L_d$, $k = \sqrt{8J/[3bP^2(L_d - L_q)(L_q/R_s)^2]}$, $\omega_{ref} = \tau z_{ref}$, $x = [1/(bk)]\tilde{i}_d, y = (1/k\tilde{i}_q), z = (L_q/R_s)\tilde{\omega}, c = 2k_d/(kPL_q), u_d = \tilde{u}_d/(kR_s), T_L = P\tau^2\tilde{T}_L/(2J)$. The external inputs are removed ($u_d = z_{ref} = T_L = 0$), and System (2a)–(2c) becomes

$$\frac{dx}{dt} = -bx + yz, \tag{3a}$$

$$\frac{dy}{dt} = -y - xz + cz, \tag{3b}$$

$$\frac{dz}{dt} = xy - az. \tag{3c}$$

System (3a)–(3c) is invariant under the transformation: $(x, y, z) \Leftrightarrow (x, -y, -z)$ and dissipative if $\nabla V = (\partial(dx/dt)/\partial x) + (\partial(dy/dt)/\partial y) + (\partial(dz/dt)/\partial z) = -(a + b + 1) < 0$. It has only one equilibrium point $O(0, 0, 0)$ if $\Delta = c^2 - 4a < 0$, three equilibrium points $O(0, 0, 0)$, $E_{1,2}(c/2, \pm\sqrt{ab}, \pm c\sqrt{b/a}/2)$ if $\Delta = 0$, and five equilibrium points $O(0, 0, 0)$, $E_{11,21}((c + \sqrt{\Delta})/2, \pm\sqrt{ab}, \pm(c + \sqrt{\Delta})\sqrt{b/a}/2)$, $E_{11,21}((c - \sqrt{\Delta})/2, \pm\sqrt{ab}, \pm(c - \sqrt{\Delta})\sqrt{b/a}/2)$ if $\Delta > 0$ [13]. The linear stability analysis of system (2) revealed that the equilibrium points displayed Hopf bifurcation [13]. When the parameters a, b, c are varied, SynRM without external inputs can be expected to exhibit steady state, periodic, and chaotic behaviors. In order to identify the dynamical behaviors of SynRM without external inputs, two parameters LLE diagrams are constructed in Figure 1.

From Figure 1, periodic or steady state regions are characterized as a combination of light blue-light blue-green colors, and chaotic regions are characterized by yellow and red colors. For $b = 0.2$ and $c = 22$, the bifurcation diagrams and LLE of SynRM without external inputs as a function of the parameter a are plotted in Figure 2.

Figure 2 shows that the SynRM without external inputs exhibits monostable period-3 oscillations, bistable period-3
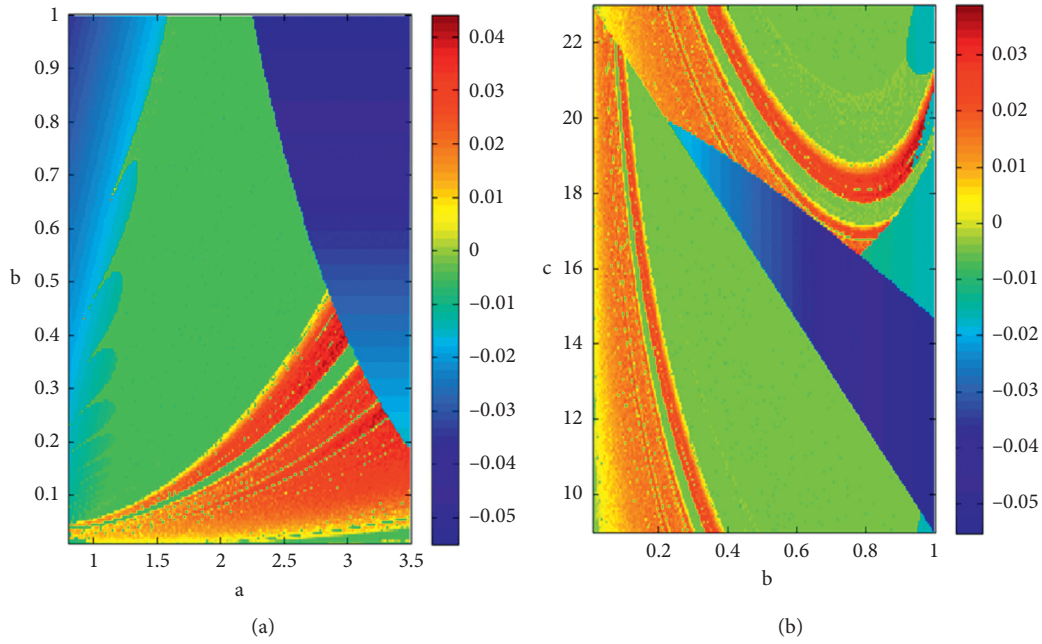
FIGURE 1: Two parameters LLE diagrams in (a) (a, b) space for $c = 22$ and (b) (b, c) space for $a = 1.53$.
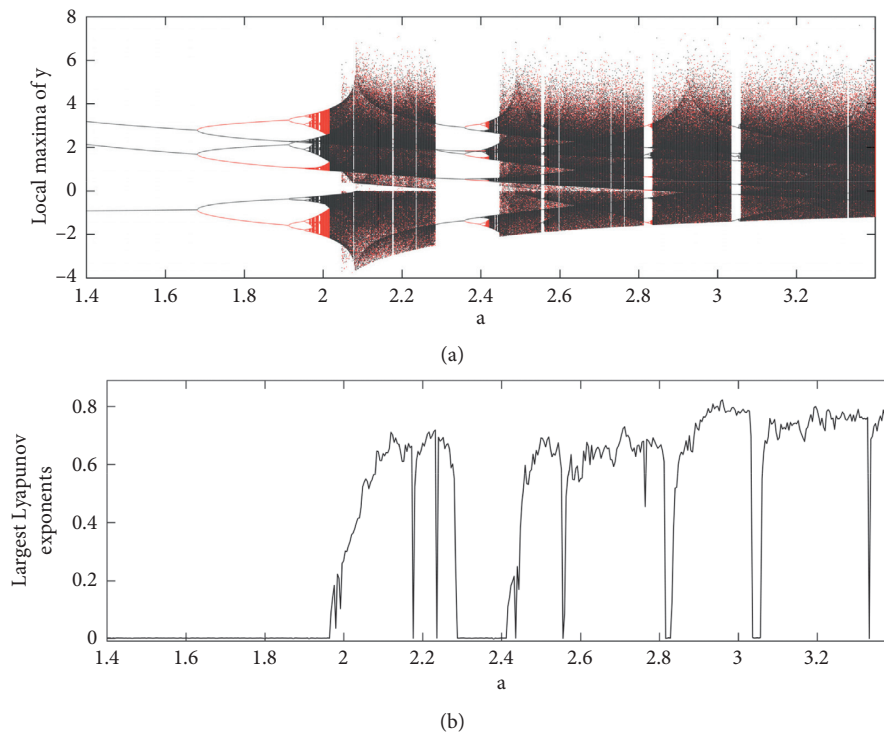
FIGURE 2: Bifurcation diagrams of $y(t)$ (a) and LLE (b) of SynRM versus the parameter a for $b = 0.2$ and $c = 22$. Bifurcation diagrams are obtained by scanning the parameter a upwards (black) and downwards (red). The initial conditions are $(x(0), y(0), z(0)) = (0.1, 0.2, 0.2)$.

oscillations followed to period tripling to bistable chaos and monostable chaos interspersed with bistable and monostable periodic regions. The dynamical behaviors shown in Figure 2 are illustrated in Figure 3 for a specific value of a.

The SynRM without external inputs exhibits monostable periodic attractors in Figure 3(a), bistable periodic attractors in Figure 3(b), bistable one-scroll chaotic attractors in Figure 3(c), and monostable double-scroll chaotic attractors in Figure 3(d). The bifurcation diagrams of SynRM without external inputs obtained numerically by the parameters b and c reveal monostable chaos and bistable chaos interspersed with monostable and bistable periodic regions
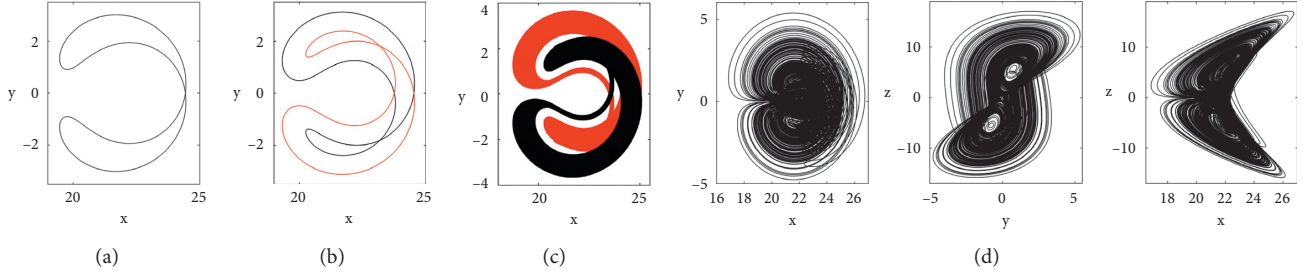
FIGURE 3: Phase planes of SynRM without external inputs for a specific value of parameter a: (a) $a = 1.5$, (b) $a = 1.8$, (c) $a = 2$, and (d) $a = 3$. The curves in black line are obtained by using the initial conditions $(x(0), y(0), z(0)) = (0.1, 0.2, 0.2)$, while the curves in red line are obtained by using the initial conditions $(x(0), y(0), z(0)) = (0.1, -0.2, -0.2)$. The remaining parameters are $b = 0.2$ and $c = 22$.

followed by monostable period-3-oscillations, but the results have not presented here for brevity.

3. Chaos Suppression in SynRM without External Inputs Using Single Controller

In this section, three single controllers are mathematically designed by using the principle of Lyapunov's method for asymptotic global stability to suppress the chaotic behavior found in SynRM without external inputs [29].

3.1. Proposed Controller 1.
System (3a)–(3c) with the first single controller $u_1 = -yz$ is described by

$$\frac{dx}{dt} = -bx + yz + u_1, \tag{4a}$$

$$\frac{dy}{dt} = -y - xz + cz, \tag{4b}$$

$$\frac{dz}{dt} = xy - az. \tag{4c}$$

The controlled system (4a)–(4c) can be rewritten as

$$\frac{dx}{dt} = -bx, \tag{5a}$$

$$\frac{dy}{dt} = -y - xz + cz, \tag{5b}$$

$$\frac{dz}{dt} = xy - az. \tag{5c}$$

The solution of equation (5a) is $x(t) = x(0)e^{-bt}$. That is, yield $\lim_{t \to \infty} x(t) = 0$. So, system (5a)–(5c) can be reduced as follows:

$$\frac{dy}{dt} = -y + cz, \tag{6a}$$

$$\frac{dz}{dt} = -az. \tag{6b}$$

The solution of equation (6b) is $z(t) = z(0)e^{-at}$. That is, yield $\lim_{t \to \infty} z(t) = 0$. So, system (6a) and (6b) can be rewritten as follows

$$\frac{dy}{dt} = -y. \tag{7}$$

The solution of equation (7) is $y(t) = y(0)e^{-t}$. That is, yield $\lim_{t \to \infty} y(t) = 0$. Therefore, the chaotic behavior found in the SynRM without external inputs can be controlled using the controller $u_1 = -yz$. The curves of the state responses and the output of the controller 1 are shown in Figure 4.

The results of Figure 4 show the efficiency of the controller u_1.

3.2. Proposed Controller 2.
System (3a)–(3c) with the second single controller $u_2 = z(x - c)$ is described by

$$\frac{dx}{dt} = -bx + yz, \tag{8a}$$

$$\frac{dy}{dt} = -y - xz + cz + u_2, \tag{8b}$$

$$\frac{dz}{dt} = xy - az. \tag{8c}$$

The controller u_2 into the controlled system (8a)–(8c) can be rewritten as

$$\frac{dx}{dt} = -bx + yz, \tag{9a}$$

$$\frac{dy}{dt} = -y, \tag{9b}$$

$$\frac{dz}{dt} = xy - az. \tag{9c}$$

The solution of equation (9b) is $y(t) = y(0)e^{-t}$. That is, yield $\lim_{t \to \infty} y(t) = 0$. Thus, the system (9a)–(9c) can be reduced as follows:

$$\frac{dx}{dt} = -bx, \tag{10a}$$

$$\frac{dz}{dt} = -az. \tag{10b}$$

The solution of system (10a) and (10b) is given by
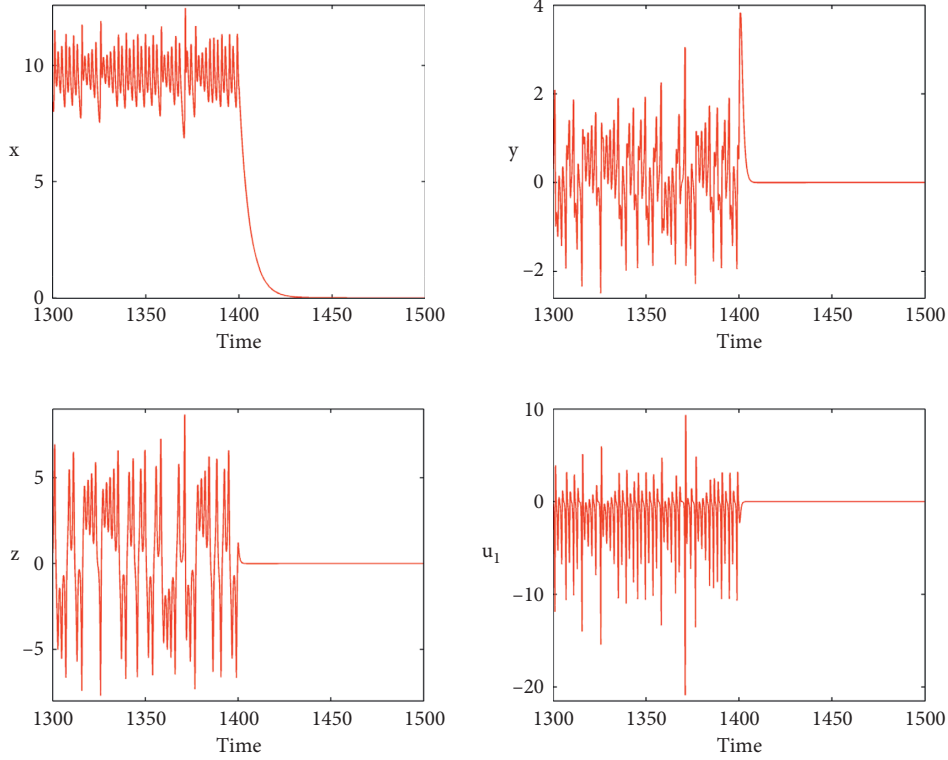
FIGURE 4: Time series of x, y, z, u_1 for $a = 3$, $b = 0.2$, and $c = 22$. The initial conditions are $(x(0), y(0), z(0)) = (0.1, 0.2, 0.2)$.

$$x(t) = x(0)e^{-bt}, \tag{11a}$$

$$z(t) = z(0)e^{-at}. \tag{11b}$$

That is, yield $\lim_{t \to \infty} y(t) = 0$ and $\lim_{t \to \infty} z(t) = 0$. Therefore, the chaotic behavior found in the SynRM without external inputs can be controlled using the controller $u_2 = z(x - c)$. The curves of the state responses and the output of the controller are shown in Figure 5.

The results of Figure 4 reveal the efficiency of the controller u_2.

3.3. Proposed Controller 3.
System (3a)–(3c) with the third single controller $u_3 = -xy$ is described by

$$\frac{dx}{dt} = -bx + yz, \tag{12a}$$

$$\frac{dy}{dt} = -y - xz + cz, \tag{12b}$$

$$\frac{dz}{dt} = xy - az + u_3. \tag{12c}$$

Substituting the expression of the controller u_3 into the controlled system (12a)–(12c) becomes

$$\frac{dx}{dt} = -bx + yz, \tag{13a}$$

$$\frac{dy}{dt} = -y - xz + cz, \tag{13b}$$

$$\frac{dz}{dt} = -az. \tag{13c}$$

The solution of equation (13c) is $z(t) = z(0)e^{-at}$. That, is yield $\lim_{t \to \infty} z(t) = 0$. Thus, system (13a)–(13c) can be reduced as follows:

$$\frac{dx}{dt} = -bx, \tag{14a}$$

$$\frac{dy}{dt} = -y. \tag{14b}$$

The solution of system (14a) and (14b) can be rewritten as follows:

$$x(t) = x(0)e^{-bt}, \tag{15a}$$

$$y(t) = y(0)e^{-t}. \tag{15b}$$

That is, yield $\lim_{t \to \infty} x(t) = 0$ and $\lim_{t \to \infty} y(t) = 0$. Therefore, the chaotic behavior found in SynRM without external inputs can be controlled using the controller $u_3 = -xy$. The curves of the state responses and the output of the single controller 3 are shown in Figure 6.
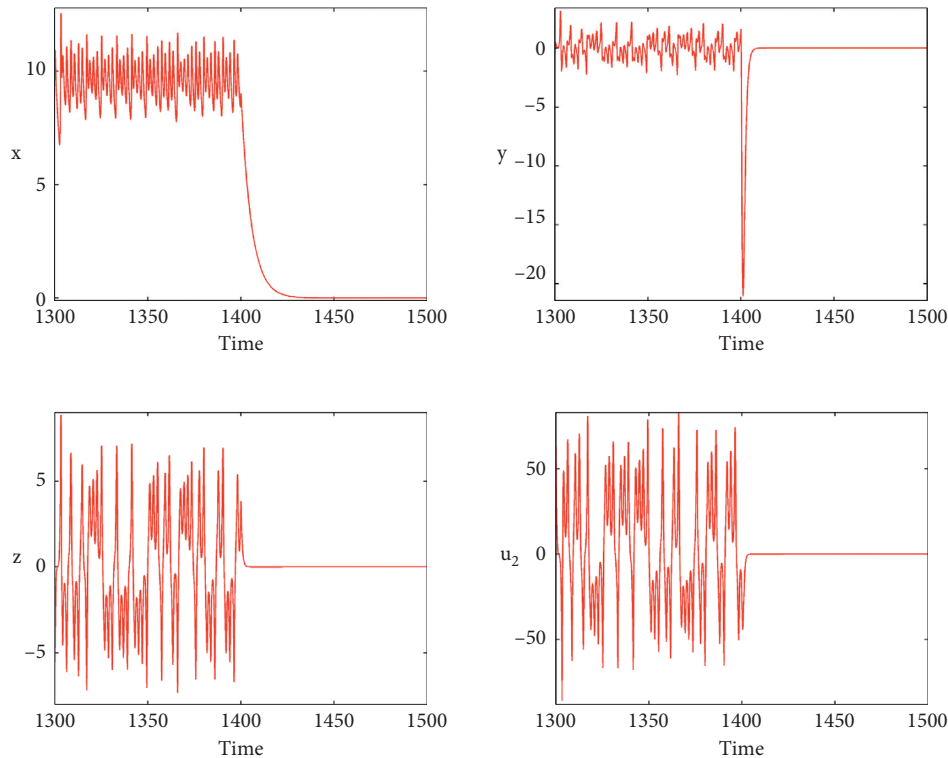
FIGURE 5: Time series of x, y, z, u_2 for $a = 3$, $b = 0.2$ and $c = 22$. The initial conditions are $(x(0), y(0), z(0)) = (0.1, 0.2, 0.2)$.

The results of Figure 6 show the efficiency of the controller u_3. From practical realization point of view, the single controllers 1 and 3 are preferred because of the inclusion of two states variables (i.e. y and z or x and z) in a single expression signifying a lesser requirement of sensing devices during their fabrication. Hence, this making the system to become cheap.

4. Circuit Implementation of SynRM without External Inputs and Chaos Suppression in SynRM without External Inputs

The electronic implementation of system (3a)–(3c) is depicted in Figure 7.

The electronic circuit of Figure 7 is made of three capacitors, thirteen resistors, six TL081 operational amplifiers, and three analog devices AD633 multipliers. Based on the circuit diagram of Figure 7, the phase portraits of dynamical behaviors found in SynRM without external inputs are illustrated in Figure 8 for specific values of capacitors and resistors.

The good qualitative agreement between the Pspice results of Figure 8 and the numerical simulations results of Figure 3 confirms the existence of the dynamical behavior found in SynRM without external inputs. The electronic implementations of the controlled systems (5a)–(5c), (9a)–(9c), and (13a)–(13c) are deduced from the electronic implementation of system (5a)–(5c) in Figure 7 (not shown). The time series of the state responses and the output of the single controller 1 generated from the circuit diagram of the controlled system (5a)–(5c) are shown in Figure 9.

The good qualitative agreement between the Pspice results of Figure 9 and the numerical simulations results of Figure 5 confirms the efficiency of proposed single controller 3. The time series of the state responses and the output of the single controller 2 generated from the circuit diagram of the controlled system (9a)–(9c) are shown in Figure 10.

The good qualitative agreement between the Pspice results of Figure 10 and the numerical simulations results of Figure 5 confirms the efficiency of proposed single controller 2. The time series of the state responses and the
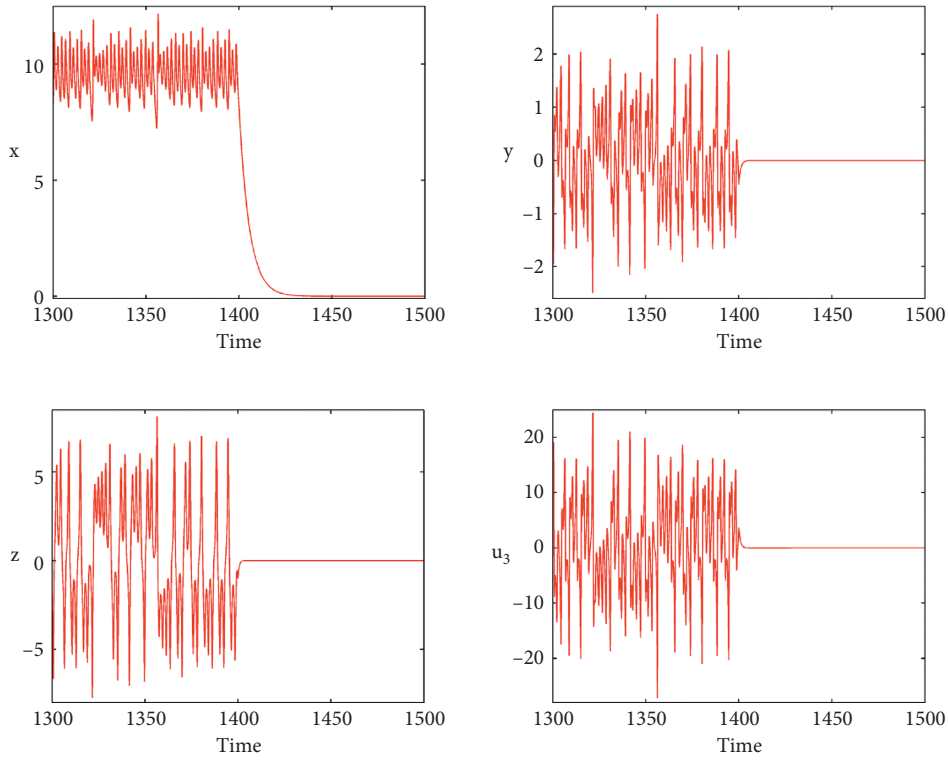
FIGURE 6: Time series of x, y, z, u_3 for $a = 3$, $b = 0.2$ and $c = 22$. The initial conditions are $(x(0), y(0), z(0)) = (0.1, 0.2, 0.2)$.
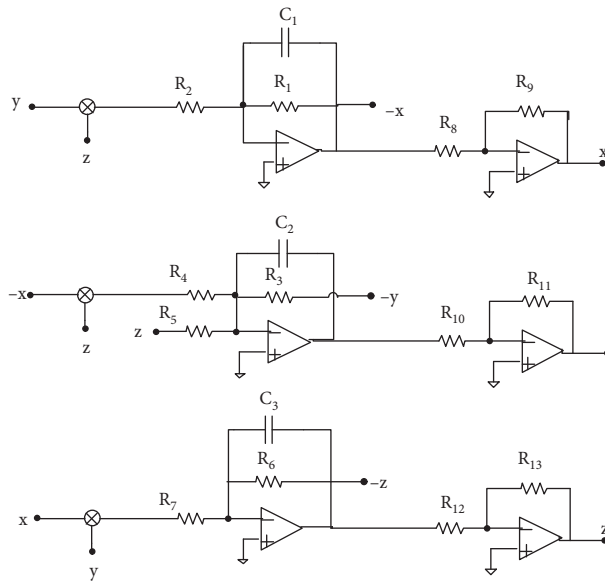
FIGURE 7: Circuit diagram of system (3a)–(3c) describing SynRM without external inputs.

output of the single controller 3 generated from the circuit diagram of the controlled system (13a)–(13c) are shown in Figure 11.

The good qualitative agreement between the Pspice results of Figure 11 and the numerical simulations results of Figure 6 confirms the efficiency of proposed single controller 3.
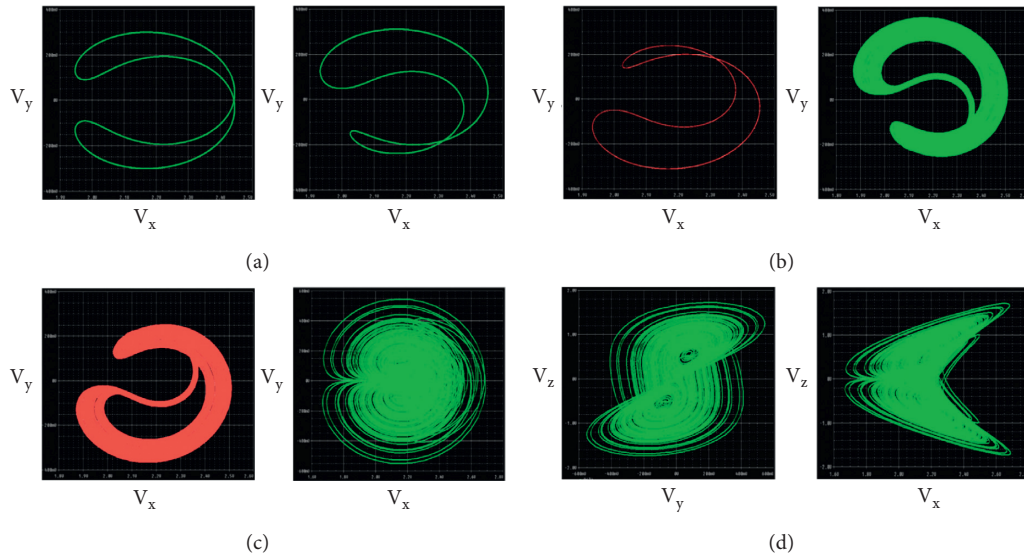
FIGURE 8: Phase planes of the dynamical behaviors of circuit in Figure 7 observed on the Pspice oscilloscope for specific values of R_6: (a) $R_6 = 6.67\,k\Omega$, (b) $R_6 = 5.56\,k\Omega$, (c)$R_6 = 5\,k\Omega$, and (d) $R_6 = 3.33\,k\Omega$. The others values are $C_1 = C_2 = C_3 = 10\,nF$, $R_3 = R_8 = R_9 = R_{10} = R_{11} = R_{12} = R_{13} = 10\,k\Omega$, $R_5 = 454.55\,k\Omega$, $R_1 = 50\,k\Omega$, $R_2 = R_4 = R_7 = 1\,k\Omega$.
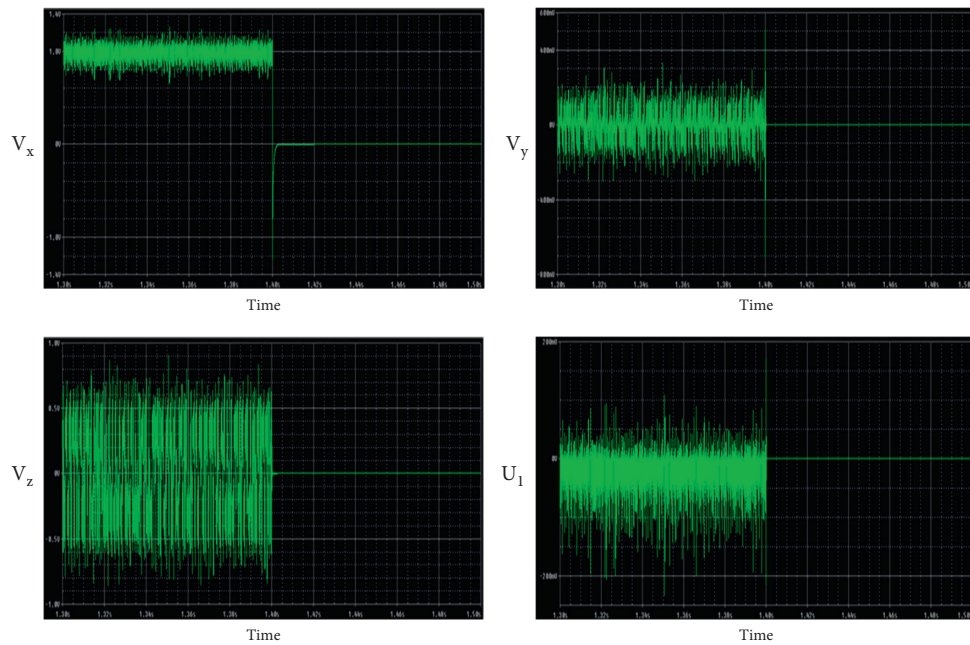
FIGURE 9: Time series of chaos suppression in SynRM without external inputs generated from the Pspice oscilloscope for the capacitors and resistors: $C_1 = C_2 = C_3 = 10\,nF$, $R_3 = R_8 = R_9 = R_{10} = R_{11} = R_{12} = R_{13} = 10\,k\Omega$, $R_5 = 454.55\,k\Omega$, $R_1 = 50\,k\Omega$, $R_2 = R_4 = R_7 = 1\,k\Omega$, $R_6 = 3.33\,k\Omega$.
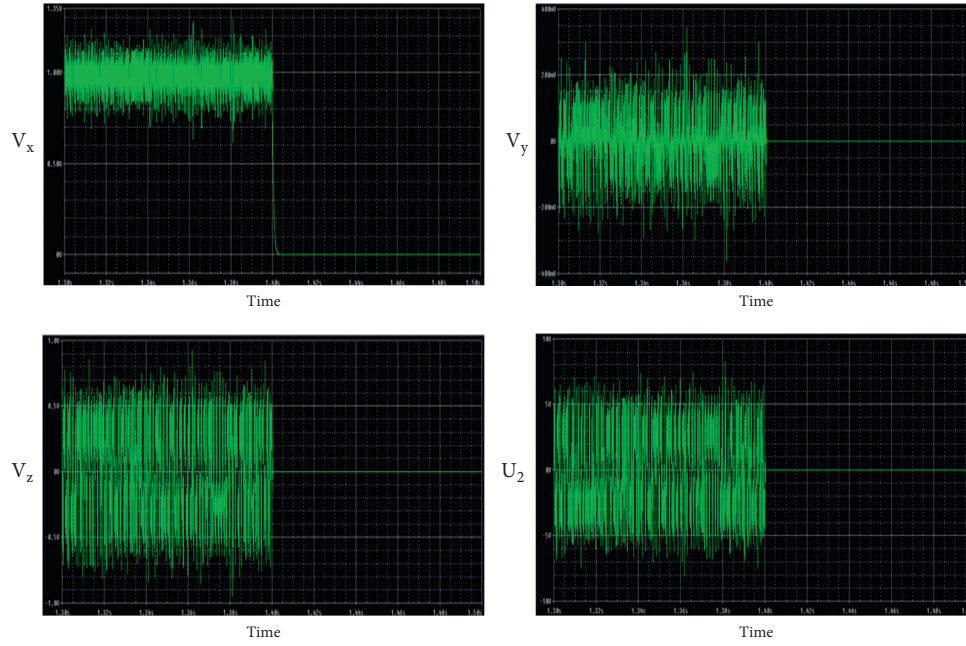
FIGURE 10: Time series of chaos suppression in SynRM without external inputs generated from the Pspice oscilloscope for the capacitors and resistors: $C_1 = C_2 = C_3 = 10\,nF$, $R_3 = R_8 = R_9 = R_{10} = R_{11} = R_{12} = R_{13} = 10\,k\Omega$, $R_5 = 454.55\,k\Omega$, $R_1 = 50\,k\Omega$, $R_2 = R_4 = R_7 = 1\,k\Omega$, $R_6 = 3.33\,k\Omega$.
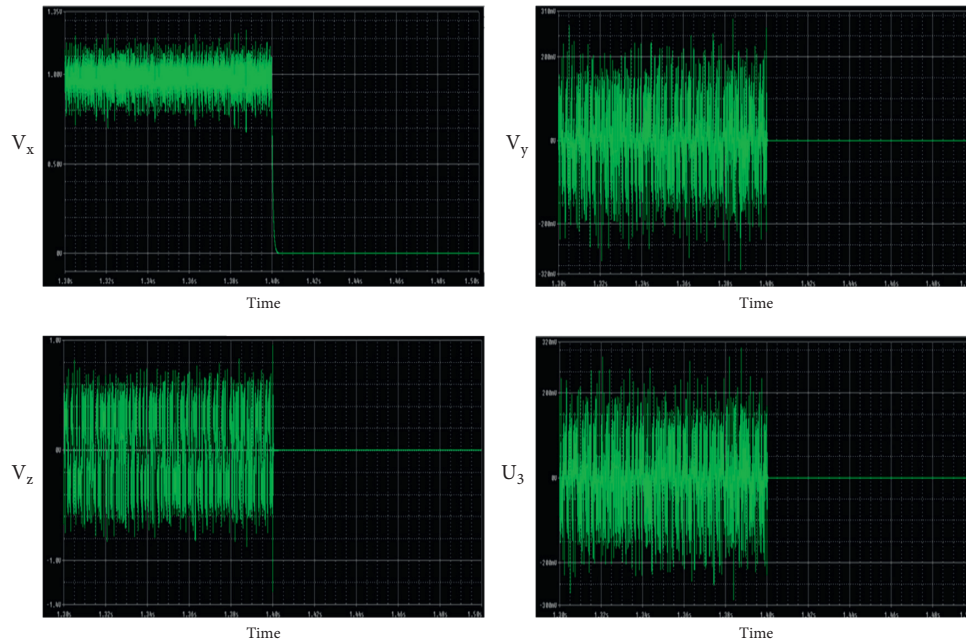
FIGURE 11: Time series of chaos suppression in SynRM without external inputs generated from the Pspice oscilloscope for the capacitors and resistors: $C_1 = C_2 = C_3 = 10\,nF$, $R_3 = R_8 = R_9 = R_{10} = R_{11} = R_{12} = R_{13} = 10\,k\Omega$, $R_5 = 454.55\,k\Omega$, $R_1 = 50\,k\Omega$, $R_2 = R_4 = R_7 = 1\,k\Omega$, $R_6 = 3.33\,k\Omega$.

5. Conclusion

This paper is dealt with the dynamical analysis, chaos suppression, and electronic implementation of synchronous reluctance motor without external inputs. The numerical analysis of synchronous reluctance motor without external inputs was revealed as monostable periodic attractors, bistable periodic attractors, monostable double-scroll chaotic attractors, and bistable one-scroll chaotic attractors. Thanks to the principle of Lyapunov's method for asymptotic global stability, three single controllers were designed to suppress chaotic behavior found in synchronous

reluctance motor without external inputs, and it was revealed that they were simple and easy to implement. The single controllers 1 and 3 could be a preferable choice because of the use of two states variables (i.e. y and z or x and z) in a single expression. Numerical simulations results were provided to demonstrate the efficiency of three proposed single controllers. To access the physical feasibility of three designed single controllers and the existence of the dynamical behaviors found in synchronous reluctance motor without external inputs, electronic circuits were implemented and validated on OrCAD-PSpice software. In the future works, it will be interesting to study the synchronous reluctance motor with external inputs such as the load torque and the stator voltage.

Data Availability

The data used to support the findings of this study are included within the article.

Conflicts of Interest

The authors declare that they have no conflicts of interest.

Acknowledgments

References

[1] A. E. Fitzgerald, C. Jr. Kingsley, and S. D. Umpans, *Electric Machinery*, McGraw-Hill, New York, NY, USA, 1991.

[2] J. Machowski, J. Bialek, and J. R. Bumby, *Power System Dynamics and Stability*, John Wiley & Sons, Hoboken, NJ, USA, 1997.

[3] A. Parra, A. Zubizarreta, J. Pérez, and M. Dendaluce, "Intelligent torque vectoring approach for electric vehicles with per-wheel motors," *Complexity*, vol. 2018, Article ID 7030184, 14 pages, 2018.

[4] F. Stîngă, M. Marian, and D. Selisteanu, "Robust estimation-based control strategies for induction motors," *Complexity*, vol. 2020, Article ID 9235701, 14 pages, 2020.

[5] Q. Ji and M. Ye, "Control of chaotic calcium oscillations in biological cells," *Complexity*, vol. 2021, Article ID 8861465, 14 pages, 2021.

[6] X. Hu and P. Zhou, "Coexisting three-scroll and four-scroll chaotic attractors in a fractional-order system by a three-scroll integer-order memristive chaotic system and chaos control," *Complexity*, vol. 2020, Article ID 5796529, 7 pages, 2020.

[7] I. Nagy, Z. Siitb, and L. Backhausz, "Periodic states of hysteresis current control of I.M," in *Proceedings of the 29th International Power Conversion and Intelligent Motion Conference (PCIM'SG)*, pp. 605–619, Nürnberg, Germany, May 1996.

[8] Z. Suto, I. Nagy, and Z. Jak, "Periodic responses of a nonlinear current conti-olled IM drive," in *Proceedings of the 7th European Conference on Power Electronics and Applications (EPE'S'I)*, vol. 3, Trondheim, Norway, September 1997.

[9] Z. Zhong Li, J. B. Jin Bae Park, Y. H. Young Hoon Joo, B. Bo Zhang, and G. Guanrong Chen, "Bifurcations and chaos in a permanent-magnet synchronous motor," *IEEE Transactions on Circuits and Systems I: Fundamental Theory and Applications*, vol. 49, no. 3, pp. 383–387, 2002.

[10] P. Pillay and R. Krishnan, "Modeling, analysis and simulation of a high performance vector controlled, permanent magnet synchronous motor drive," *Rec. Conf. IEEE-IAS Annul. Meeting*, pp. 253–262, 1987.

[11] N. Hemati, "Dynamic analysis of brushless motors based on compact representations of motion," in *Proceedings of the Conference Record of the IEEE Industry Applications Society Annual Meeting*, vol. 1, pp. 51–58, Toronto, ON, Canada, October 1993.

[12] N. Hemati, "Strange attractors in brushless DC motors," *IEEE Transactions on Circuits and Systems I: Fundamental Theory and Applications*, vol. 41, no. 1, pp. 40–45, 1994.

[13] Y. Gao and K. T. Chau, "Hopf bifurcation and chaos in synchronous reluctance motor drives," *IEEE Transactions on Energy Conversion*, vol. 19, no. 2, pp. 296–302, 2004.

[14] P. J. Lawrenson, "A brief status review of switched reluctance drives," *EPE Journal*, vol. 2, no. 3, pp. 133–144, 1992.

[15] C. C. Chan, Y. Zhan, Q. Jiang, and K. T. Chau, "A high performance switched reluctance motor drive for P-star EV project," in *Proceedings of the 13th International Electric Vehicle Symposium*, pp. 78–83, Osaka Japan, October 1996.

[16] N. Bianchi, S. Bolognani, D. Bon, and M. Dai Pre, "Torque harmonic compensation in a synchronous reluctance motor," *IEEE Transactions on Energy Conversion*, vol. 23, no. 2, pp. 466–473, 2008.

[17] M. Ferrari, N. Bianchi, A. Doria, and E. Fornasiero, "Design of synchronous reluctance motor for hybrid electric vehicles," *IEEE Transactions on Industry Applications*, vol. 51, no. 4, pp. 3030–3040, 2015.

[18] J. Kolehmainen, "Synchronous reluctance motor with form blocked rotor," *IEEE Transactions on Energy Conversion*, vol. 25, no. 2, pp. 450–456, 2010.

[19] S. T. Kingni, A. Cheukem, P. R. N. Tuwa, A. C. Chamgoué, V.-T. Pham, and S. Jafari, "Synchronous reluctance motor with load vibration perturbation: analysis, electronic implementation and adaptive backstepping sliding mode control," *Iranian Journal of Science and Technology, Transactions of Electrical Engineering*, vol. 45, no. 2, pp. 645–654, 2021.

[20] K. T. Chau and Z. Wang, *Chaos in Electric Drive Systems: Analysis, Control and Application*, John Wiley & Sons, Hoboken, NJ, USA, 2011.

[21] W. Du-Qu and L. Xiao-Shu, "Passive adaptive control of chaos in synchronous reluctance motor," *Chinese Physics B*, vol. 17, no. 1, pp. 92–97, 2008.

[22] M. Babaei, J. Nazarzadeh, and J. Faiz, "Nonlinear feedback control of chaos in synchronous reluctance motor drive systems," in *Proceedings of the IEEE conference Industrial Technology*, pp. 1–5, Chengdu, China, April 2008.

[23] F. Q. Tang, Y. N. Tong, and C. L. Li, "A controller for chaotic synchronous reluctance motor drive systems," in *Proceedings of the IEEE conference Computing, Control and Industrial Engineering*, pp. 316–319, Wuhan, China, September 2011.

[24] L. Xu, X. Xu, T. A. Lipo, and D. W. Novotny, "Vector control of a synchronous reluctance motor including saturation and Iron Loss," *IEEE Transactions on Industry Applications*, vol. 27, no. 5, pp. 977–985, 1991.

[25] M. K. Metwally and M. E. Ahmed, "Vector control of four switch three-phase inverter fed synchronous reluctance motor drive including saturation and iron losses effects based Maximum Torque Control," *Telkomnika*, vol. 11, pp. 6344–6351, 2013.

[26] E. M. Rashad, T. S. Radwan, and M. A. Rahman, "A maximum torque per ampere vector control strategy for synchronous reluctance motors considering saturation and iron losses, 39th IAS Annual Meeting," in *Proceedings of the IEEE Industry Applications Conference*, vol. 4, pp. 2411–2417, Seattle, WA, USA, October 2004.

[27] M. A. Fellani and D. E. Abaid, "Sliding-mode control of synchronous reluctance motor," *International Journal of Electronics, Circuits and Systems*, vol. 3, pp. 91–95, 2009.

[28] K. Rajagopal, F. Nazarimehr, A. Karthikeyan, A. Srinivasan, and S. Jafari, "Fractional order synchronous reluctance motor: analysis, chaos control and fpga implementation," *Asian Journal of Control*, vol. 20, pp. 1–15, 2018.

[29] X. Liao and P. Yu, *Absolute Stability of Nonlinear Control Systems*, Springer Science & Business Media, Berlin, Germany, 2008.

WILEY | Hindawi

Research Article

A Unified Power Quality Conditioner for Feeder Reconfiguration and Setting to Minimize the Power Loss and Improve Voltage Profile

Zhigao Huang [iD],[1] **Farid Shahbaazy,**[2] **and Afshin Davarpanah** [iD][3]

[1]*Wuhan Railway Vocational College Technology, Wuhan, Hubei 430205, China*
[2]*Department of Electrical Engineering, Islamic Azad University, Borujerd Branch, Borujerd, Iran*
[3]*Young Elite Researchers, Science and Research Branch, Islamic Azad University, Tehran, Iran*

Correspondence should be addressed to Zhigao Huang; zhigao-huang2021@163.com and Afshin Davarpanah; afshindpe@gmail.com

Using devices such as unified power quality conditioners (UPQCs) in distribution networks seems essential for higher electricity quality. Moreover, distribution network reconfiguration is a suitable model for improving network characteristics, including loss reduction and voltage increase for distribution networks, and is widely used in this era. Here, the study discusses the rechanging of distribution networks for UPQC via proposing an appropriate model for it. In addition to the optimum structure of distribution networks, the most appropriate branch where UPQC must be located and the most appropriate reactive power size with which series and shunt filters must be injected into the grid are determined. The simulations have been applied on two 69- and 84-standard-bus networks. The results of the simulations indicate much power loss reduction and much voltage increase in the presence of UPQC compensators.

1. Introduction

The important goal of companies for electric effectiveness is providing the sinusoidal voltage continuously and stable voltage to all customers. In previous studies, parameters of PQ including the harmonics power, voltage cell, frequency, power factor, and reactive power are examined by using the infusion generators. The problem of power eminence is yielded in separation of customer equipment by using some problems in current, deviation of frequency, and voltage. The subjects of PQ have engrossed high consideration from companies and clients because of utilization of various types of susceptible electronic devices. The differences of PQ regarding load switching are obtained through short circuits, voltage decrease, gleam and relief, and distortions of harmonics. The electrical misses have happened via burst in electrical cycles, sudden loads, firelight, and radiated frequency. The various types of disturbances of PQ are occurring in the outline of electrical power. The evaluation of

proficiency from PQ indicated that 50 percent of troubles of PQ are related to bonds of the ground, voltage neutral to the ground, and more ground-related problems. Distribution network reconfiguration is an effective way of reducing losses among the existing loss reduction methods in distribution networks. As distribution networks are designed in ring or mesh but are exploited in radial distribution, two customarily opened and normally closed switches exist. Reconfiguration represents selecting the open or closed state of these switches. However, the aim of reconfiguration may not be only to reduce losses. Previously, there have been several successful methods developed and employed. Improving voltage profile, balancing the load, and service restoration are some of the objectives mentioned in reconfiguration studies. In previous works, the heuristic model is proposed to obtain minimum loss configuration [1]. In [2], an innovative approach is provided for reducing losses and improving voltage profiles. In [3], a method is suggested to balance feeder load and reduce losses for

unbalanced distribution networks. In [4], models to provide network reconfiguration are proposed. Regardless of the aim of reconfiguration, reconfiguration studies can be categorized as far as the presence of different compensator devices is concerned.

1.1. In the Presence of a Capacitor.

Capacitors have various advantages in distribution networks, such as voltage regulation, power factor improvement, and losses reduction. Multiple studies have investigated reconfiguration and capacitors simultaneously. For instance, reconfiguration and capacitor control are investigated simultaneously using the simulated annealing method [5]. An algorithm is presented in a study [6] by considering different load levels based on MINLP for performing reconfiguration and capacitor allocation.

1.2. In the Presence of Distributed Generations (DGs).

DGs have many economic and operational advantages [7]. Various articles have investigated the distribution reconfiguration. For instance, distribution reconfiguration is used for DG via the genetic algorithm [8]. A study [9] has considered DG's active power generation cost in reconfiguration. Other objective functions that PSO optimize in this article include the operational power generation cost of distribution networks, the number of switches functions, and bus voltage deviation. A model is presented in a study [10] based on MINLP for distribution reconfiguration for DGs.

1.3. In the Presence of DSTATCOM.

Some advantages of DSTATCOM include voltage flicker reduction, harmonic reduction in-network, improving bus voltage, reducing losses, and continuous control of reactive power [11]. Distribution network reconfiguration and DSTATCOM placement are investigated simultaneously in a study [12]. The present study aims to reduce losses and improve voltage levels via DEA.

Today, the need for high power quality is felt more than ever. In general, it can be stated that low power quality causes additional costs for producers and consumers. For instance, an equipment malfunction, more network losses, consumer dissatisfaction, and life loss of equipment are examples of some extra charges imposed on producers and consumers due to low power quality. However, electricity distribution networks may not have high quality due to nonlinear loads, single-phase consumers, power electronics loads, etc. As a result, the use of devices that guarantee the power quality of distribution networks is essential. UPQC is one of the best devices which can improve power quality effectively [13]. UPQC has a series and a shunt filter that are connected back to back. The active series filter is responsible for damping feeding disturbance, and the active shunt filter damps the current quality generated by consumers [14].

In [15, 16], a model to assess the technical efficiency of PQ change strategy via FACTS devices is reported. In [17],

the control strategy is reported using UPQC. In [18], the flow pattern is recommended for feeder reconfiguration to obtain the best start in search models. In [19], a model is reported to optimize the NR problems in PDS to decrease VP in advance. In previous studies, NR was used to increase the VP and decrease power loss. In [20], a UPQC with two CAMCs in back-to-back connection is proposed. The hybrid modulation technique used in the CAMC made the implementation of the control objectives easier. Due to the applicability of power electronic devices in improving the FACTS performances, the expectancy of using various kinds of controllers for efficient shunt are increased. The devices of FACTS are answered to alter in-network positions. The implication of FACTS devices in transmission and analogous systems is implemented properly in distribution systems. The devices of distribution-FACTS are utilized to recover the problems of power in systems of distribution [1, 2] that happen at a measure of milliseconds. In the mentioned time, D-FACTS has injected the active power and reactive power in the system to recover sensitive loads [9]. The DSTATCOM as a converter of the voltage source is used to recover the problems of power quality [13–19]. The DVR as an important converter is utilized to recover the problems of power quality. In [7], ANFIS, which is related to a controller of hysteresis, is suggested to obtain the efficiency of power quality. The novel works were produced by the incorporation of fuzzy and neural networks. The suggested models of D-FACTS are used in systems of two bus distributions including the sensitive load and source. The D-FACTS effects on recovery of the problem of power quality are examined. But, the D-FACTS effects on the system of large distribution are not examined. Also, the D-FACTS impacts are investigated for a short duration but not examined for a long term.

Considering the importance of reconfiguration and the increasing importance of UPQC, this work investigates distribution reconfiguration for UPQC. In this paper, first, a model will be extracted for UPQC load flow. Then, based on this model and with the aid of a genetic algorithm, reconfiguration of distribution networks will be carried out in the presence of UPQC. Reducing losses and improving voltage profile are the objective functions based on the network form, by which the best UPQC location and the most appropriate injected power will be determined. To combine loss reduction and voltage improvement as one objective function, these objective functions should be normalized. In this study, Utopia Point and Nadir Point methods are used for normalizing objective functions.

2. The Problem's Objective Functions

As mentioned above, the present study aims to decrease the losses and increase voltage for networks. Objective functions considered for optimization purposes are total active losses, voltage deviation average, and the sum of the normalized values of these two objective functions. These objective functions can be formalized as follows [1–3]:

$$f_1 = \sum_{i=1}^{N_L} \frac{P_i^2 + Q_i^2}{V_i^2} = P_{\text{total,loss}}, \tag{1}$$

$$f_2 = \sum_{i=1}^{n} \frac{|1 - V_i|}{n}, \tag{2}$$

$$f_3 = \overline{f}_1 + \overline{f}_2, \tag{3}$$

where $P_{\text{total,loss}}$ is total power losses (W) and V_i is the voltage magnitude of bus i. Also, $\overline{f}_1$ and $\overline{f}_2$ are the normalized values of the first and second objective functions, respectively. n indicates the number of buses. N_L shows the number of lines. P (MW) and Q (Var) are active and reactive power, respectively. The constraints which should be considered in this optimization are as follows (constraints 1 and 2 must be regarded for common reconfiguration and constraints 3 and 4 for reconfiguration in the presence of UPQC):

(1) Bus voltage must not exceed the permitted limits:

$$V_{\text{min}} < V_i < V_{\text{max}}. \tag{4}$$

(2) The branch's current must not exceed the permitted limits:

$$|I_i| < I_{i,\text{max}}. \tag{5}$$

(3) The sum of UPQC injected series and shunt reactive power size is lower than reactive load power:

$$\sum_{I=1}^{N_{\text{UPQC}}} \left(Q_i^{\text{series}} + Q_i^{\text{shunt}} \le Q_{\text{Total,Load}} \right). \tag{6}$$

(4) The branch that the optimization algorithm proposes for opening must not be the same as UPQC's location.

In these equations, Q_i^{series} and Q_i^{shant} are injected reactive power by compensator i and N_{UPQC} is the total number of existing UPQCs in the network. V_{min} and V_{max} (V) are network voltage constraints, and I_i and I_{max} (A) are the branch current i and the maximum branch current i, respectively. V_{min} and V_{max} are lower and upper bounds of voltage, respectively. $Q_{\text{Total,Load}}$ is the total reactive power for the consumer. N_{UPQC} is the number of UPQC devices [20].

The sum of two different objective functions is considered one objective function for simultaneous optimization; it is necessary to normalize them because each function is in different units. In this study, Utopia Point and Nadir Point methods are used for normalizing objective functions [21]. If x_i^* is the best response for optimizing the single objective function i, then the normalized objective function i $\overline{f}_1$ will be defined as follows [21]:

$$\overline{f}_i = \frac{f_i - f_i^U}{f_i^N - f_i^U}, \tag{7}$$

where f_i^U is the Utopia Point and is defined as follows:

$$f^U = [f_1(x_1^*) f_2(x_2^*) \dots f_n(x_n^*)], \\ f_i^U = f_i(x_i^*). \tag{8}$$

Utopia Point f^U is obtained from the best data of Pareto solution, and a Utopia Point is computed as a result of optimization of n single criteria in time serving.

And, f_i^N is the Nadir Point that is defined as follows:

$$f_i^N = \max [f_i(x_1^*) f_i(x_2^*) \dots f_i(x_n^*)]. \tag{9}$$

Nadir Point f^N is obtained from the worst data of the Pareto solution, and finding a Nadir Point is difficult when the problems have three and more criteria. The given points via the user, Utopia Point $f^{U,}$ and Nadir Point f^N, define the piecewise function u.

3. UPQC Modeling

UPQC can inject active and reactive power and is used to increase sag and unbalance voltages [20, 22]. A very complicated PV model is presented in a study for modeling UPQC in a distribution network within which only the series part is controllable. In the present paper, a simpler and more appropriate model is presented for the placement of UPQC in the network by evolution algorithms. UPQC compensators can inject power. Figure 1 shows a general view of a UPQC installed between buses i and j, with its series and shunt parts specified.

The series for UPQCs operates entirely between each other for injecting power, and it has enough the power for reactive load of bus j for modeling shunt injected reactive power. The shunt injected reactive power is intended as a negative load for bus j as in Figure 2 [20]. The reactive load of bus j after modeling the shunt part of UPQC is changed, and in this equation, Q_{shunt} is the injected power for UPQC.

The series injected power to the line will be simulated after modeling the shunt part separately and as a reactive negative load. The single line diagram of Figure 2 is changed by voltage (Figure 3).

If the network's Norton equivalent circuit is achieved from the points of i and j, the Thevenin's circuit will be converted to Norton circuit as in Figure 4. In this situation, we can model the injected series power as loads of i and j buses:

$$I_s = \frac{V_s}{Z_s}. \tag{10}$$

The V_s, I_s, and Z_s are voltage, current, and impedance for buses, and these parameters are formulated as follows:

$$V_s = V_{sm} \angle \delta_{Vs}, \\ I_s = I_{sm} \angle \delta_{Is}, \tag{11}$$

where δ_{V_s} and δ_{Is} are the angle of voltage and current, respectively. V_{sm} and I_{sm} are the maximum values of voltage and current, respectively. Equal power is needed in the load flow. Therefore, the current source will be replaced with it by using equivalent power equations, and Figure 4 will be converted to Figure 5 subsequently.

The active power is obtained via [21]
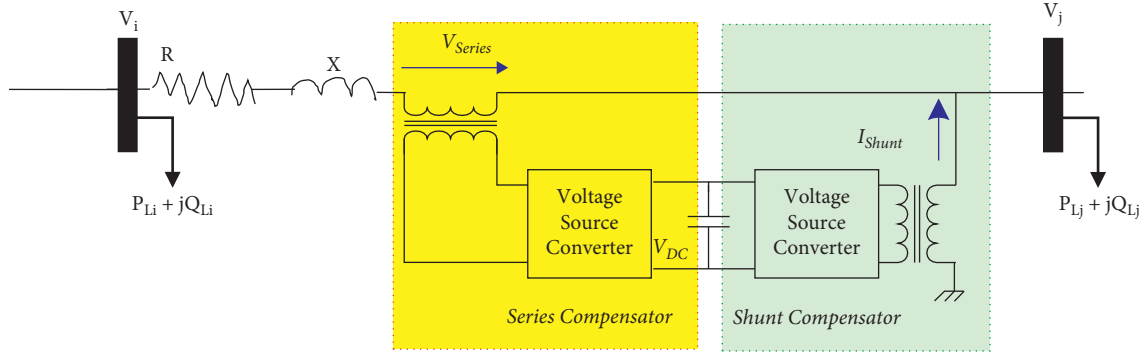
FIGURE 1: Single line diagram of the UPQC structure.
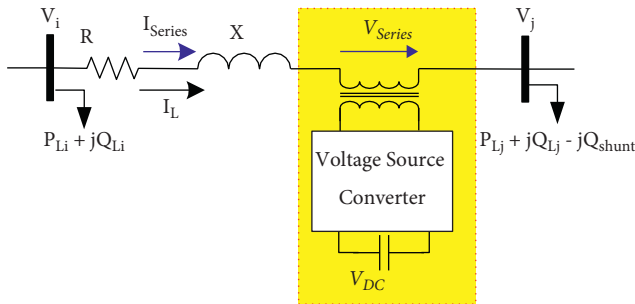
FIGURE 2: UPQC structure with modeling of the shunt part as the negative load for bus j.
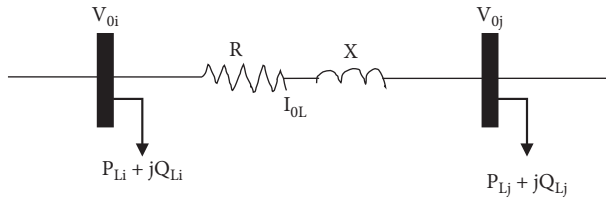
FIGURE 3: Thevenin's equivalent circuit for UPQC.
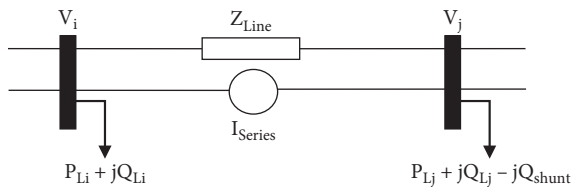
FIGURE 4: Norton equivalent circuit of the series part of UPQC.
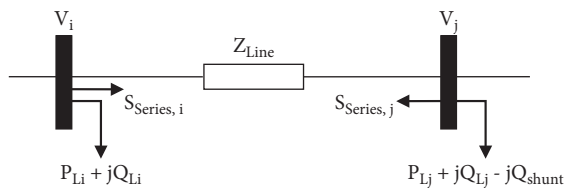
FIGURE 5: The load model for the series part of UPQC.

$$S_{\text{series},i} = V_i * \left(-I_s^*\right), \tag{12}$$

$$P_{\text{series},i} = \text{real}\left\{S_{\text{series},i}\right\}, \tag{13}$$

$$Q_{\text{series},i} = \text{Im}\left\{S_{\text{series},i}\right\}, \tag{14}$$

where $S_{\text{series},i}$ (VA), $P_{\text{series},i}$ (W), and $Q_{\text{series},i}$ (Var) are complex, active, and reactive power in series lines, respectively. The exact process will be conducted in bus j. These operations will be performed in each of the load flow iterations. Operational management cannot be used to inject and it is [21–23] as follows:

$$P_{\text{series},i} = \text{real}\left\{S_{\text{series},i}\right\} = 0. \tag{15}$$

The current angle of I_s will be calculated in the following way:

$$\delta_{Is} = \frac{\angle V_i + \pi}{2}. \tag{16}$$

Before calculating equations (12)–(14), first, the source current in each iteration is calculated with the aid of the following equation:

$$I_s = \frac{V_{sm}}{|Z_m|}\angle\frac{V_i + \pi}{2}. \tag{17}$$

Since I_s a constant amount, only its angle will be changed in each iteration to adjust to the injected reactive power. After completing the load flow iterations, the injected series voltage angle will be calculated using the following equation:

$$\delta_{Vs} = \angle\left(\frac{I_s}{Z_s}\right). \tag{18}$$

4. Performing Reconfiguration and UPQC Placement in a Distribution Network

The switch types are available in distribution networks, and each ring includes one typically opened switch. Performing rechanging by using intelligent algorithms can be simulated in

two ways: (a) all the switches should be considered open in the initial state and then by closing some of the switches, a network structure will be obtained that, in addition to being radial, must reduce the objective function to its minimize amount; (b) in the initial state of the problem, all switches should be considered closed and then by opening a specific number of switches, the radial limitation and minimization of the objective function will be met. The number of normally closed switches in distribution networks is much more than the number of customarily opened ones. Hence, if we perform the reconfiguration according to the second method, the problem will be less complicated.

The following states can be considered for performing reconfiguration concerning UPQC placement:

(1) First, reconfiguration and then UPQC placement
(2) First, UPQC placement and then reconfiguration
(3) Distribution network reconfiguration and UPQC placement simultaneously

The third method can have the characteristics of the other two ways at the same time. Here, the algorithm is used for optimization. In the first step of the genetic algorithm, the initial populations (chromosomes) are generated. For distribution network reconfiguration, concerning UPQC placement, each chromosome can be considered a structure as shown in Figure 6.

Step 1: the genes of this part represent the typically opened switch number. According to Graph's theory, the number of these genes or usually opened switches will be calculated by the following equation:

$$N = L - n + 1. \tag{19}$$

Here, N is the number of customarily opened switches, L is the branch number, and n is the network bus number.

Step 2: the genes in this part of the chromosome indicate the branches in which UPQC will be located.

Step 3: the genes in this part of the chromosome indicate the shunt injected reactive power of all UPQCs.

Step 4: the genes in this part of the chromosome indicate the series injected reactive power of all UPQCs.

For instance, for a 69-bus network with 73 branches with five typically opened switches and one UPQC, each chromosome has eight genes. Five of these genes are network switches that must be opened. The sixth gene indicates the branch in which UPQC will be located. The seventh gene indicates the shunt injected reactive power, and the eighth gene indicates the series injected reactive power of UPQC.

Once the initial population is generated randomly, the objective functions will be evaluated. After evaluating the objective function, genetic operators (usually three operators of selection, crossover, and mutation) will be applied in the initial population. The generated chromosomes will be reevaluated, and this process continues until the stopping conditions are met.

5. Simulation Results

In this paper, two 69- and 84-bus networks are considered for simulation. Data are compared by the following:

| Section 1 | Section 2 | Section 3 | Section 4 |
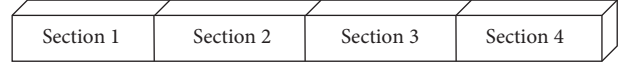
Figure 6: Chromosome structure for reconfiguration and UPQC setting optimization.

(1) The primary state of the network
(2) Network reconfiguration without the presence of UPQC
(3) Reconfiguration and UPQC to optimum the losses
(4) Reconfiguration and UPQC to improve the voltage level
(5) Reconfiguration and UPQC to decrease losses and to increase voltage levels simultaneously

5.1. 69-Bus Network. In this study, a system with 12.66 kV, 69-bus, 8-lateral radial distribution according to modern node counting with some corrections in demands of active power and reactive power is remarked as another test system. The whole load of the studied system is obtained as (4.0951 +j2.8630) MVA. The obtained results of the studied system are calculated from [22]. This distribution network has 69 buses and 73 branches. The total load over its feeders is 3.801 MW and 2.6944 MVAR. Data of this network are taken from [23]. The population size is assumed to be 50, and the iteration number is 200 for simulation. Based on equation (6), the amount of UPQC series and shunt injected power must not exceed 2.6944 MVAR (total reactive power of this network). Data of simultaneous network reconfiguration and UPQC placement are demonstrated in Table 1. The suitable effect of reconfiguration and UPQC placement can be observed clearly in this table. As can be observed, in optimizing the first objective function (f_1), the network losses have been reduced significantly and have decreased from 224.92 to 73.10 kW. Therefore, the objective function is improved by about 66% which is very considerable. In this state, switches 14, 58, 63, 69, and 70 are suggested to be open, and UPQC is located in line 60, and the shunt and series injected power are 1.1 and 0.91 MVAR, respectively. In optimizing the second objective function (f_2), a significant improvement is observed in the voltage level enhancement. As Table 1 shows, this function has decreased from 0.0265 PU to 0.0045 PU. The voltage means reached the ideal amount of 0.9955 PU that is rather suitable and noticeable. In this state, the opened switches are 10, 12, 18, 58, and 61, and the UPQC location is line 73, and its series and shunt injected power are 1.03 and 1.49 MVAR, respectively. For optimizing the fifth case or optimizing the third objective function, the amounts of f^U and f^N should be determined concerning the third and fourth cases:

$$f^N = [150.72 KW \, 0.0112 PU],$$
$$f^U = [73.1 KW \, 0.0044 PU]. \tag{20}$$

Thus, considering these obtained amounts and equations (3) and (7), the third objective function is as follows:

TABLE 1: The results of UPQC placement and reconfiguration simultaneously in 69-bus network.

			UPQC characteristics		Total losses (KW)	Voltage deviation	$V_{\min}$ (PU)	V_{ave} (PU)
	Tie switches	Line	Shunt power (MVAR)	Series power (MVAR)				
Case 1	69, 70, 71, 72, 73	-	-	-	224.92	0.0265	0.9091	0.9734
Case 2	12, 13, 58, 61, 69	-	-	-	99.88	0.0135	0.9427	0.9865
Case 3	14, 58, 63, 69, 70	60	1.1	0.91	73.10	0.0112	0.9654	0.9887
Case 4	10, 12, 18, 58, 61	73	1.49	1.031	150.72	0.0044	0.9688	0.9956
Case 5	14, 58, 64, 69, 70	61	1.78	0.384	84.85	0.0082	0.9719	0.9917

$$f_3 = \frac{f_1 - f_1^U}{f_1^N - f_1^U} + \frac{f_2 - f_2^U}{f_2^N - f_2^U} \tag{21}$$

$$= \frac{f_1 - 73.1}{77.62} + \frac{f_2 - 0.0044}{0.00068}.$$

This function is optimized as an objective function by a genetic algorithm; the first and second objective functions have the same importance from the optimizing algorithm perspective. According to Table 1, the optimizing algorithm suggested a response between the third and fourth cases in the fifth case, and a relative balance is established between these two functions. In this state, the loss is 84.85 kW and the average voltage of the network is 0.9917 PU. It should be noted that in (20), the f_1 (losses) must be in kW and the f_2 (voltage deviation) must be in the PU unit.

The voltage profile for all buses in different cases is presented in Figure 7. Following the figure, the voltage in the primary structure is not in an appropriate state. Still, after reconfiguration and UPQC placement for improving voltage levels (fourth case), it reaches the best state compared to other mentioned cases. Especially in the range of buses 1 to 50, the voltage levels are improved more than in other cases and it can be stated that the voltage is around one PU. But, in this state, the net loss is 150 kW. According to the figure, in the fifth case, where the voltage levels and network losses are optimized simultaneously, failures are more satisfying than in the fourth case. In bus 61, a considerable load is available which is the cause of voltage sag in this area. In the fifth case, voltage sag is compensated appropriately due to the placement of a compensator on this bus. When the effects of installation of D-FACTS devices in two states are investigated, it can be concluded that in the studied systems, the performances and effectiveness of D-FACTS devices are similar.

5.2. 84-Bus Network with 96 Branches.
The loads on this network are 28.35 MW and 20.70 MVAR, and lines 96–84 are open in the initial state. The operational losses and average voltage deviation in this network are 532.61 KW and 0.03078 PU, respectively. For more information, please refer to [23]. For this large network, two UPQCs are considered with 13 typically opened switches (tie switch) and considering two UPQCs, each chromosome has 19 genes. Due to the extent of each chromosome, more population and iteration numbers are considered compared to a 69-bus network. The population and iteration numbers are 50 and
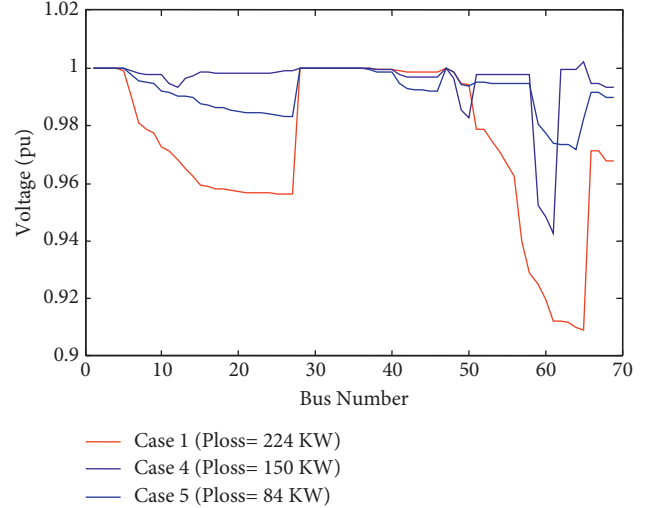
FIGURE 7: Voltage for cases of the 69-bus network.

— Case 1 (Ploss= 224 KW)
— Case 4 (Ploss= 150 KW)
— Case 5 (Ploss= 84 KW)

250, respectively. The UPQC characteristics and simulation results in different cases are shown in Tables 2 and 3. In addition to the proposed structure, the optimization of objective function $f1$ proposes the locations of two UPQCs at lines 79 and 7; this condition could reduce the network losses to 407.43 KW and increase over 20%. In $f2$ and the new proposed structure, lines 7 and 78 are designated for the placement of UPQCs. The voltage reached 0.0129 PU. The intermediate voltages reached 0.9888 PU, which is a satisfactory result. The line losses are too high and cannot be accepted (624.58 KW). As the previous network, for optimizing the third objective function, firstly, the f^U and f^N will be defined concerning the third and fourth cases in Table 3:

$$f^U = [407.43 KW \quad 0.0129 PU],$$
$$f^N = [624.58 KW \quad 0.0199 PU]. \tag{22}$$

Then, considering these obtained amounts and equations (3) and (7), we will receive

$$f_3 = \frac{f_1 - f_1^U}{f_1^N - f_1^U} + \frac{f_2 - f_2^U}{f_2^N - f_2^U} \tag{23}$$

$$= \frac{f_1 - 407.43}{217.15} + \frac{f_2 - 0.0129}{0.007}.$$

As the 69-bus network, in this case, the structure and location of UPQC are suggested precisely. These indicate the appropriate performance of normalization by Utopia Point

Table 2: UPQC characteristics for the 84-bus network.

	First UPQC characteristics			Second UPQC characteristics		
	Line	Shunt power (MVAR)	Series power (MVAR)	Line	Shunt power (MVAR)	Series power (MVAR)
Case 3	79	2.75	2.28	7	3.18	1.8
Case 4	7	5.63	1.355	78	8.14	5.506
Case 5	21	4.086	0.732	7	4.16	3.992

Table 3: Data of UPQC placement and reconfiguration for the 84-bus network.

	Tie switches	Total losses (KW)	Voltage deviation	$V_{\min}$ (PU)	V_{ave} (PU)
Case 1	84–96	532.61	0.03078	0.9285	0.9692
Case 2	7, 13, 34, 39, 42, 55, 62, 72, 83, 86, 89, 90, 92	470.26	0.0248	0.9532	0.9752
Case 3	7, 13, 34, 39, 42, 55, 64, 72, 86, 89, 90, 91,92	407.43	0.0199	0.9531	0.9801
Case 4	14, 20, 34, 39, 42, 54, 59, 71, 86, 88, 90, 92, 96	624.58	0.0129	0.948	0.9888
Case 5	6, 34, 39, 42, 54, 64, 72, 81, 86, 88, 89, 90, 92	459.32	0.0147	0.9531	0.9854
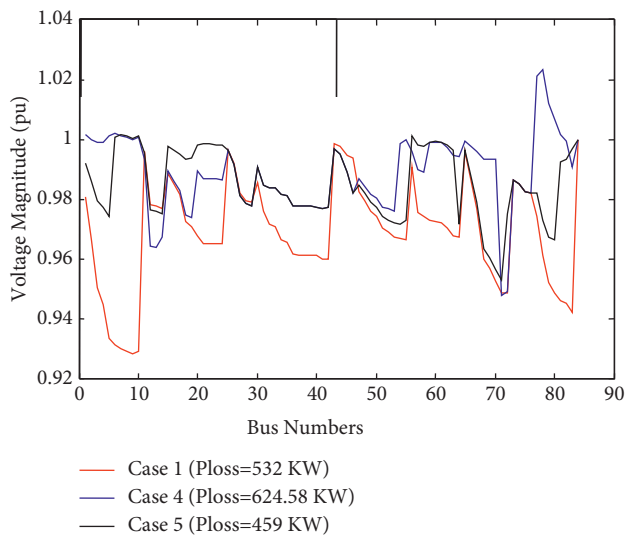
Figure 8: Voltage magnitude in different cases of the 84-bus network.

and Nadir Point methods. Although in this case, the voltage levels are less than those of the fourth case, the losses are not considered and the amount of network losses is acceptable (459.32 KW) compared to the initial state.

The voltage profile of all buses in different cases is presented in Figure 8. The voltage profile in the primary structure does not have an appropriate state. Still, after reconfiguration and placement, it is in the best state compared to the other mentioned cases.

To make a comparison with other methods, we have selected an 84-bus network in mode 1. The evolutionary algorithm optimization methods, linearized mathematical method, and simulated annealing algorithm have been considered. Accordingly, the obtained results from losses are 538.32 kW for the evolutionary algorithm, 541.43 kW for the mathematical linearization method, and 536.76 kW for the simulated refrigeration algorithm. From the obtained results, our method has received the best answer in comparison to other mentioned methods, that is, 1.2%, 1.7%, and 0.8%, respectively.

6. Conclusion

In this paper, the reconfiguration of the distribution network and the placement of UPQC were studied. A simple load flow model was proposed for the placement of UPQCs. In general, the location and size of UPQC and typically opened switch numbers were investigated for different purposes. Therefore, three objective functions were studied: losses, voltage deviation, and the combination of these two. It was found that the simultaneous combination of reconfiguration and UPQC placement reduces the active power losses to more than 50% of the primary structure and significantly improves the voltage characteristics. The sum of loss objective function and the voltage deviation objective function were considered as objective functions so that the optimization algorithm could optimize these two objective functions simultaneously. The normalization method was used to scale these objective functions, and the results obtained were quite desirable and logical. With careful consideration of the simulations, the improvement in voltage level and reduction in losses are obvious in the presence of UPQC.

Data Availability

No data were used to support this study.

Conflicts of Interest

The authors declare that there are no conflicts of interest.

References

[1] Y. Merzoug, B. Abdelkrim, and B. Larbi, "Distribution network reconfiguration for loss reduction using PSO method," *International Journal of Electrical and Computer Engineering*, vol. 10, no. 5, Article ID 5009, 2020.

[2] I. Benitez Cattani, E. Chaparro, and B. Baran, "Distribution system operation and expansion planning using network reconfiguration," *IEEE Latin America Transactions*, vol. 18, no. 05, pp. 845–852, 2020, þ.

[3] R. V. A. Monteiro, J. P. Bonaldo, R. F. da Silva, and A. S. Bretas, "Electric distribution network reconfiguration optimized for PV distributed generation and energy storage,"

Electric Power Systems Research, vol. 184, 2020 þ, Article ID 106319.

[4] S.-M. Park and Y.-G. Kim, "User profile system based on sentiment analysis for mobile edge computing," *Computers, Materials & Continua*, vol. 62, no. 2, pp. 569–590, 2020.

[5] D. Dan Jiang and R. Baldick, "Optimal electric distribution system switch reconfiguration and capacitor control," *IEEE Transactions on Power Systems*, vol. 11, no. 2, pp. 890–897, 1996.

[6] L. W. de Oliveira, S. Carneiro, E. J. de Oliveira et al., "Optimal reconfiguration and capacitor allocation in radial distribution systems for energy losses minimization," *International Journal of Electrical Power & Energy Systems*, vol. 32, no. 8, pp. 840–848, 2010.

[7] W. El-Khattam and M. M. A. Salama, "Distributed generation technologies, definitions and benefits," *Electric Power Systems Research*, vol. 71, no. 2, pp. 119–128, 2004.

[8] J. H. Choi and J. C. Kim, "Network reconfiguration at the power distribution system with dispersed generations for loss reduction," *Power engineering society winter meeting*, vol. 4, pp. 2363–2367, 2000.

[9] J. Olamaei, T. Niknam, and G. Gharehpetian, "Application of particle swarm optimization for distribution feeder reconfiguration considering distributed generators," *Applied Mathematics and Computation*, vol. 201, no. 1-2, pp. 575–586, 2008.

[10] J. F. Franco, M. J. Rider, M. Lavorato, and R. Romero, "A mixed-integer LP model for the reconfiguration of radial electric distribution systems considering distributed generation," *Electric Power Systems Research*, vol. 97, pp. 51–60, 2013.

[11] I. Wasiak, R. Mienski, R. Pawelek, and P. Gburczyk, "Application of DSTATCOM compensators for mitigation of power quality disturbances in low voltage grid with distributed generation," in *Proceedings of the 9th International conference on electrical power quality and utilizations*, Barcelona, Spain, October 2007.

[12] S. Jazebi, S. H. Hosseinian, and B. Vahidi, "DSTATCOM allocation in distribution networks considering reconfiguration using differential evolution algorithm," *Energy Conversion and Management*, vol. 52, no. 7, pp. 2777–2783, 2011.

[13] E. Ali, A. Nasiri, and B. Stoyan, *Uninterruptible Power Supplies And Active Filters*, CRC Press, Boca Raton, FL, USA, 2004.

[14] S. K. Khadem, M. Basu, and M. F. Conlon, *Integration of UPQC for Power Quality Improvement in Distributed Generation Network – A Review*, ISGT Europe 2011, Manchester UK, Dec 2011.

[15] T. Yuvaraj, K. Ravi, and K. R. Devabalaji, "DSTATCOM allocation in distribution networks considering load variations using bat algorithm," *Ain Shams Engineering Journal*, vol. 8, no. 3, pp. 391–403, 2017.

[16] T. Jin, Y. Chen, J. Guo, M. Wang, and M. A. Mohamed, "An effective compensation control strategy for power quality enhancement of unified power quality conditioner," *Energy Reports*, vol. 6, pp. 2167–2179, 2020, þ.

[17] Y. Qu, "A global optimum flow pattern for feeder reconfiguration to minimize power losses of unbalanced distribution systems," *International Journal of Electrical Power & Energy Systems*, vol. 131, 2021 þ, Article ID 107071.

[18] A. O. Salau, Y. W. Gebru, and D. Bitew, "Optimal network reconfiguration for power loss minimization and voltage profile enhancement in distribution systems," *Heliyon*, vol. 6, no. 6, Article ID e04233, 2020.

[19] I. Y. Kim and O. L. de Weck, "Adaptive weighted-sum method for bi-objective optimization: Pareto front generation," in *Proceedings of the The 45th Structural Dynamics, and Materials Conference*, pp. 19–22, Palm Springs, Boca raton, FL, USA, April 2004.

[20] M. Hosseini, H. A. Shayanfar, and M. Fotuhi-Firuzabad, "Modeling of unified power quality conditioner (UPQC) in distribution systems load flow," *Energy Conversion and Management*, vol. 50, no. 6, pp. 1578–1585, 2009.

[21] S. P. Kapse, S. Krishnapillai, and S. Krishnapillai, "An improved multi-objective particle swarm optimization based on utopia point guided search," *International Journal of Applied Metaheuristic Computing*, vol. 9, no. 4, pp. 71–96, 2018, þ.

[22] N. C. Sahoo and K. Prasad, "A fuzzy genetic approach for network reconfiguration to enhance voltage stability in radial distribution systems," *Energy Conversion and Management*, vol. 47, no. 18-19, pp. 3288–3306, 2006.

[23] J.-P. Chiou, C.-F. Chang, and C.-T. Su, "Variable scaling hybrid differential evolution for solving network reconfiguration of distribution systems," *IEEE Transactions on Power Systems*, vol. 20, no. 2, pp. 668–674, 2005.

WILEY | Hindawi

Research Article

On the Rejection of Random Perturbations and the Tracking of Random References in a Quadrotor

Jesus Alberto Meda-Campaña [iD],[1] **Jonathan Omega Escobedo-Alva** [iD],[2]
José de Jesús Rubio [iD],[3] **Carlos Aguilar-Ibañez** [iD],[4] **Jose Humberto Perez-Cruz** [iD],[3]
Guillermo Obregon-Pulido [iD],[5] **Ricardo Tapia-Herrera** [iD],[6] **Eduardo Orozco,**[3]
Daniel Andres Cordova,[3] **and Marco Antonio Islas** [iD][3]

[1]*Sección de Estudios de Posgrado e Investigación, ESIME Zacatenco, Instituto Politécnico Nacional,
Av. Instituto Politécnico Nacional, Col. Lindavista, México City 07738, Mexico*
[2]*ESIME Ticomán, Instituto Politécnico Nacional, Calz. Ticomán 600, San Joé Ticomán, Ciudad de México 07340, Mexico*
[3]*Sección de Estudios de Posgrado e Investigación, ESIME Azcapotzalco, Instituto Politécnico Nacional, Av. de las Granjas no. 682,
Col. Santa Catarina, Ciudad de México 02250, Mexico*
[4]*Centro de Investigación en Computación, Instituto Politécnico Nacional, Av. Juan de Dios Bátiz S/N, Col. San Pedro Zacatenco,
México City 07738, Mexico*
[5]*CUCEI, Universidad de Guadalajara, Guadalajara, Jalisco, Mexico*
[6]*CONACYT, Universidad Tecnológica de la Mixteca, Oaxaca, Mexico*

Correspondence should be addressed to José de Jesús Rubio; rubio.josedejesus@gmail.com

In this note, the problem of tracking random references and rejecting random perturbations in a quadrotor, both generated by an auxiliary system named exosystem, is solved by extending the deterministic tracking problem to the area of stochastic processes. Besides, it is considered that only a part of the state vector of the quadrotor is available through measurements. As a consequence, the state vector of the plant must be estimated in order to close the control loop. On this basis, a controller to track random references and to reject random perturbations is developed by combining a Kalman filter to estimate the references and perturbations of an exosystem and an observer to estimate the states of a quadrotor. Besides, to obtain a more practical controller, the analysis is carried out in discrete time. Numerical simulations are used in a quadrotor to confirm the validity and effectiveness of the proposed control.

1. Introduction

In the control field, the problem of imposing random references on some outputs of unmanned aerial vehicles is a very recurrent problem. This is because such scenarios appear in many disciplines of science and technology, and among them, aeronautics is one of those areas. Besides, the study of a quadrotor is gaining great interest because of their wide range of applications and low cost [1]. For instance, the chaotic approach [2–4], the chaotic attractors [5–7], the adaptive technique [8–10], the sliding mode strategy [11–13], the robust technique [14–16], the learning strategy [17–19], and the structure method [20, 21] are used for the tracking of quadrotors. As can be expected, the bibliography related to the control of quadrotors is vast and it goes on and on.

In other orders of ideas, the tracking theory is a well-posed frame of work providing the tools to ensure asymptotic stability while references are tracked and perturbations are rejected. Roughly speaking, the solution for the tracking problem is provided by a control vector achieving two goals: (1) the asymptotic stabilization of the equilibrium

of the quadrotor and (2) the tracking of random references and the rejecting of random perturbations, both produced by an auxiliary system named exosystem [22].

For the linear problem, the solution has been presented by [23]. There, the author showed that the existence of the desired control coincides with the existence of the solution of some simultaneous equations, which can be represented in a matrix form and they are named Francis equations. Afterward, the nonlinear tracking problem was analyzed and it was concluded that the linear result is a particular case of the nonlinear problem. However, some nonlinear partial differential equations need to be solved in order to obtain the nonlinear control. Unfortunately, in many cases, the solution of such nonlinear partial differential equations is very difficult to obtain [22]. Thus, the avoiding of such nonlinear partial differential equations has been also studied. For instance, Takagi-Sugeno fuzzy systems and neural networks have been successfully used to extrapolate the linear control to the nonlinear field, without involving nonlinear partial differential equations [24].

On the other hand, most of the references and perturbations in nature are not perfectly harmonic. For instance, the flight of butterflies, the behavior of the heart, brain, human march, among others, include a little bit of randomness, to say the least. To estimate these kinds of references and perturbations, the Kalman filter [25] has been and still is a very good alternative. In this sense, in [26], the Kalman filter is used for the quadrotors parameters identification, and in [27, 28], the Kalman filter is used for the quadrotors states estimation.

With all this in mind, the problem to be studied in current work can be stated as the problem of ensuring that the output of a quadrotor behaves as an external random perturbation while the stability property is maintained. Roughly speaking, the main contribution of this paper is the extension of the deterministic references tracking and deterministic perturbations rejection to the stochastic field, by assuming that the generator of references and perturbations is subject to random uncertainties.

Besides, in order to make the problem more realistic, it is assumed that only a part of the state is available. The novelty of the proposed approach is the combination of the Kalman filtering and the regulation theory to solve the references tracking and perturbations rejection; this problem cannot be solved by the Kalman filter or the regulation theory by themselves. In this sense, the desired controller must achieve two goals which are very similar to those considered in the tracking problem: (1) to stabilize the quadrotor around an operation point when the exosystem is affecting it and (2) to minimize the tracking error when the quadrotor is influenced by external perturbations. On the basis of the observer and Kalman filter, some random references will be imposed on the quadrotor, while some random perturbations are rejected as well.

The rest of the work is arranged in the following way: Brief reminders of the tracking and Kalman filter are given in Section 2. Besides, the numerical model of the quadrotor and the definition of the problem are also included there. Section 3 is devoted to obtaining the main results. The numerical

simulations of a quadrotor are analyzed in Section 4, while some conclusions are given in Section 5.

2. Problem Setup

In this section, the control problem is defined. But before that, the control, the Kalman filter, and the quadrotor are briefly introduced.

2.1. The Control for Deterministic Plants. Let the plant be

$$
\dot{x}(t) = Ax(t) + Bu(t) + Pw(t), z(t) \\
= C_z x(t),
\tag{1}
$$

where $x(t) \in \mathfrak{R}^n$ is the state of the plant, $u(t) \in \mathfrak{R}^p$ is the control input, $z(t) \in \mathfrak{R}^{m_z}$ is the output, and $w(t) \in \mathfrak{R}^\ell$ is the solution of the exosystem:

$$
\dot{w}(t) = A_{\text{exo}} w(t), z_{\text{ref}}(t) = C_{\text{exo}} w(t).
\tag{2}
$$

With $z_{\text{ref}}(t) \in \mathfrak{R}^{m_z}$ as the references to be tracked and $Pw(t)$ as the perturbations to be rejected, system (1) and (2) corresponds to the regulation problem in continuous time, where (1) is the plant to be regulated, while (2) is an auxiliary system used to model the references/perturbations signals.

Clearly, it is possible to construct a block diagonal matrix A_{exo}, such that each block on the diagonal describes the behavior of the references or perturbations to be generated by (2). So, C_{exo} and P can be viewed as output matrices for such an exosystem.

The tracking error is $e(t) = z(t) - z_{\text{ref}}(t)$, and the control $u(t)$ must achieve

$$
\lim_{t \to \infty} e(t) = 0.
\tag{3}
$$

In [22, 23], it has been shown that the control $u(t)$ which solves the control problem is

$$
u(t) = K(x(t) - \Pi w(t)) + \Gamma w(t),
\tag{4}
$$

where the steady-state $x_{ss}(t) = \Pi w(t)$ is invariant through $u_{ss}(t) = \Gamma w(t)$, where $\Pi \in \mathfrak{R}^{n \times \ell}$ and $\Gamma \in \mathfrak{R}^{p \times \ell}$ solve the Francis equations, defined as

$$
A\Pi + B\Gamma + P = \Pi A_{\text{exo}}, C_z \Pi - C_{\text{exo}} = 0.
\tag{5}
$$

Notice that equations (5) are a set of $(n \times \ell) + (m_z \times \ell)$ simultaneous equations with $(n \times \ell) + (p \times \ell)$ unknowns. These equations can be readily solved. These equations can be solved analytically or with the help of numerical tools, in general, when $p \geq m_z$. The following theorem summarizes the previous analysis.

Theorem 1. *Assuming that the exosystem is given by (2) and H1: There exists a matrix K which stabilizes the pair (A , B) and H2: There exists a solution for Francis equations (5) given by $\Pi \in \mathfrak{R}^{n \times \ell}$ and $\Gamma \in \mathfrak{R}^{p \times \ell}$, then, the tracking problem described by (1) and (2) can be solved by (4).*

Proof. Consider $e_{ss}(t) = x(t) - \Pi w(t)$ as the steady-state error. Now, its first-order derivative is

$$\dot{e}_{ss}(t) = \dot{x}(t) - \Pi\dot{w}(t), \Rightarrow \dot{e}_{ss}(t)$$
$$= Ax(t) + Bu(t) + Pw(t) - \Pi A_{exo}w(t). \quad (6)$$

At this point, it is easy to obtain

$$\dot{e}_{ss}(t) = (A + BK)e_{ss}(t) + A\Pi w(t) + B\Gamma w(t) + Pw(t) - \Pi A_{exo}w(t). \quad (7)$$

From (7), it is clear that $e_{ss}(t)$ is zeroed as $t \longrightarrow \infty$ if (1) $A + BK$ is Hurwitz (Assumption $H1$), and (2) $A\Pi + B\Gamma + P = \Pi A_{exo}$, which coincides with (5). Observe that (5) involves $n \times \ell$ equations with $n \times \ell + p \times \ell$ unknowns.

But, the tracking error is rewritten as

$$e(t) = C_z\left(e_{ss}(t) + \Pi w(t)\right) - C_{exo}w(t). \quad (8)$$

The missing equations are obtained. Notice that (8) coincides with (5), in steady-state, i.e., when $e_{ss}(t) = 0$. To conclude, notice that if $m_z = p$, then equation (5) may have a unique solution; if $p > m_z$, then an infinite of solutions may exist. And, if $p < m_z$, then (5) may not have solution, in general [23]. □

2.2. Kalman Filter (KF).

The Kalman filter is an iterative process based on the least square method, which is able to estimate the states of a plant in an optimal way [25].

Consider the following discrete-time plant:

$$x_{k+1} = Ax_k + Bu_k + M\xi_k, y_k$$
$$= Cx_k + N\eta_k, \quad (9)$$

where, as usual, the discrete time is represented by k, and $x_k \in \mathfrak{R}^n$, $u_k \in \mathfrak{R}^p$, and $y_k \in \mathfrak{R}^m$ are the state, input, and output vectors, respectively. The dynamic noise is $\xi_k \in \mathfrak{R}^q$ with normal distribution, zero mean, and variance $Q \in \mathfrak{R}^{q \times q}$, while the measurement noise is $\eta_k \in \mathfrak{R}^r$ with normal distribution, zero mean, and variance $R \in \mathfrak{R}^{r \times r}$. It is important to mention that matrices $A \in \mathfrak{R}^{n \times n}$, $B \in \mathfrak{R}^{n \times p}$, $C \in \mathfrak{R}^{m \times n}$, $M \in \mathfrak{R}^{n \times q}$, and $N \in \mathfrak{R}^{m \times r}$ are obtained by linearizing the discrete-time quadrotor plant around a suitable operation point. On this basis, the Kalman filter (KF) is defined by

$$\hat{x}_{k|k-1} = A\hat{x}_{k-1|k-1} + Bu_{k-1},$$
$$P_{k|k-1} = AP_{k-1|k-1}A^T + MQM^T,$$
$$G_k = P_{k|k-1}C^T\left(CP_{k|k-1}C^T + R\right)^{-1}, \quad (10)$$
$$\hat{x}_{k|k} = \hat{x}_{k|k-1} + G_k\left(y_k - C\hat{x}_{k|k-1}\right),$$
$$P_{k|k} = (I - G_kC)P_{k|k-1},$$

where $\hat{x}_{k-1|k-1}$ and $P_{k-1|k-1}$ are the estimations for the state x_{k-1} and error variance at iteration $k - 1$, respectively, while $\hat{x}_{k|k-1}$ and $P_{k|k-1}$ are the predictions for state x_k and variance at iteration k, respectively. And, $\hat{x}_{k|k}$ and $P_{k|k}$ are the updated

estimations, through the Kalman gain G_k, for state x_k and error variance at iteration k, respectively [25].

Evidently, the Kalman filter can be extended to the nonlinear domain by linearizing the quadrotor plant at every discrete instant and by applying the previous equations iteratively. Such a result is known as the extended Kalman filter (EKF).

2.3. The Mathematical Model of the Quadrotor.

The proposed controller will be tested on a quadrotor with sufficiently complex behavior; the quadrotor can be considered as an aerial robot. The free-body diagram of the quadrotor is given in Figure 1, while its mathematical model is [29]

$$\dot{x}(t) = f(x(t), u(t), w(t)), y(t)$$
$$= h(x(t)). \quad (11)$$

With $x(t) = [x_1(t) \dots x_{12}(t)]^T$, $u(t) = [u_1(t) \dots u_4(t)]^T$,

$$f(x, u) = \begin{bmatrix} x_2(t), \\[1ex] f_1(x(t), u(t)), \\[1ex] x_4(t), \\[1ex] f_2(x(t), u(t)), \\[1ex] x_6(t), \\[1ex] -g + (\cos(x_9(t))\cos(x_7(t))\dfrac{\beta_1}{m}, \\[1ex] x_8(t), \\[1ex] x_{10}(t)x_{12}(t)\dfrac{I_{yy} - I_{zz}}{I_{xx}} - \dfrac{J_{tp}}{I_{xx}}x_{10}(t)\omega + \dfrac{l\beta_2}{I_{xx}}, \\[1ex] x_{10}(t), \\[1ex] x_8(t)x_{12}(t)\dfrac{I_{zz} - I_{xx}}{I_{yy}} + \dfrac{J_{tp}}{I_{yy}}x_8(t)\omega + \dfrac{l\beta_3}{I_{yy}}, \\[1ex] x_{12}(t), \\[1ex] x_8(t)x_{10}(t)\dfrac{I_{xx} - I_{yy}}{I_{zz}} + \dfrac{\beta_4}{I_{zz}}. \end{bmatrix}. \quad (12)$$

With
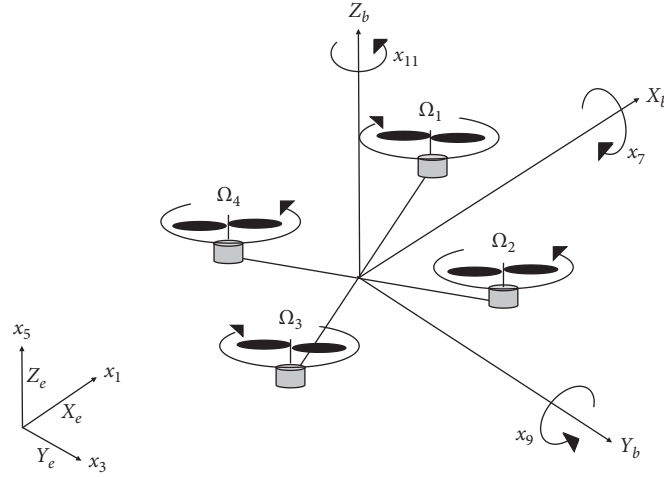
FIGURE 1: Quadrotor free-body diagram.

$$f_1(x(t), u(t)) = [\sin(x_{11}(t))\sin(x_7(t)) + \cos(x_{11}(t))\sin(x_9(t))\cos(x_7(t))]\frac{\beta_1}{m},$$

$$f_2(x(t), u(t)) = [-\cos(x_{11}(t))\sin(x_7(t)) + \sin(x_{11}(t))\sin(x_9(t))\cos(x_7(t))]\frac{\beta_1}{m},$$

$$\beta_1 = b[u_1(t)^2 + u_2(t)^2 + u_3(t)^2 + u_4(t)^2],$$

$$\beta_2 = b[u_4^2 + u_3^2 - u_1^2 - u_2^2],$$

$$\beta_3 = b[u_2(t)^2 + u_3(t)^2 - u_1(t)^2 - u_4(t)^2],$$

$$\beta_4 = d[u_1(t)^2 + u_3(t)^2 - u_2(t)^2 - u_4(t)^2],$$

$$\Omega = u_1(t) - u_2(t) + u_3(t) - u_4(t),$$

$$h(x(t)) = Cx(t),$$

$$(13)$$

where C is chosen,

$$h(x(t)) = [x_1(t) x_3(t) x_5(t) x_7(t) x_9(t) x_{11}(t)]^T. \qquad (14)$$

t is the continuous time. The frequencies of rotors 1, 2, 3, and 4, which are in fact the effective controls, are described by $u_1(t)$, $u_2(t)$, $u_3(t)$, and $u_4(t)$, respectively, and they are given in radians per second. The states $x_1(t)$, $x_3(t)$, and $x_5(t)$ are given in meters and they describe the linear movements along the Earth fixed axes X_e, Y_e, and Z_e, respectively. On the other hand, states $x_7(t)$, $x_9(t)$, and $x_{11}(t)$ are given in radians representing angular movements around the body-fixed axes X_b, Y_b, and Z_b, respectively. And, the even states can be easily identified as the velocities of abovementioned states.

The value of the parameters are as follows [29]: $b = 54.2 \times 10^{-6}$ N · s² is the thrust coefficient, $d = 1.1 \times 10^{-6}$ N · m · s² is the drag coefficient, $l = 0.24$ m is measured from the quadrotor's center to the rotors' middle point, $m = 1$ kg is the mass of the quadrotor, $g = 9.81$ m/s² is the gravity constant, $J_{tp} = 104 \times 10^{-6}$ N · m · s² is the rotors' momentum, and $Ixx = 8.1 \times 10^{-3}$ N · m · s², $Iyy = 8.1 \times 10^{-3}$ N · m · s², and $Izz = 14.2 \times 10^{-3}$ N · m · s² are the

momentum respect to X_e, Y_e, and Z_e, respectively. With these values, the quadrotor can be maintained in hovering when $u_{o1} = u_{o2} = u_{o3} = u_{o4} \approx 212.7183$rad/s, where $u_1 \ldots u_4$ are the static controls needed to keep the quadrotor in a static floating position.

The discrete-time approximation for equation (11) can be derived by means of the Euler discretization method [25]:

$$\dot{x}(t) \approx \frac{x(t+T) - x(t)}{T}, \qquad (15)$$

where T is the sampling time and it is sufficiently small such that the main features of the continuous-time system are preserved, while the controllability property is not affected. Thus,

$$x(t+T) \approx x(t) + T\dot{x}(t). \qquad (16)$$

Consequently, the discrete-time approximation for (11) is

$$\begin{aligned} x_{k+1} &= x_k + Tf(x_k, u_k, w_k), \\ y_k &= h(x_k, w_k), \end{aligned} \qquad (17)$$

with $f(\cdot,\cdot,\cdot)$ as in (12), with $T = (1/40)s$.

On the other hand, in order to produce the random references and random perturbations, the following stochastic exosystem is considered:

$$
\begin{aligned}
w_{k+1} &= A_{\text{exo}}w_k + qM_k\xi_k, \\
z_{\text{ref},k} &= C_{\text{exo}}w_k + rN_k\eta_k,
\end{aligned}
\tag{18}
$$

where for this case $A_{\text{exo}} \in \mathfrak{R}^{5\times5}$, $M_k = I_{5\times5}$, $C_{\text{exo}} \in \mathfrak{R}^{3\times5}$, and $N_k = I_{3\times3}$, while the dynamic and measurement noises are characterized by their standard deviations q and r, respectively, such that $Q = q^2M_k$ and $R = r^2N_k$. Equation (18) is the Euler discretization of the nonlinear model of the quadrotor, and equation (19) is the stochastic exosystem generating the references to be tracked and the perturbations to be rejected. In the following section, the dimensions of A_{exo} and C_{exo} are clarified.

2.4. The Problem of Tracking Random References in the Presence of Random Perturbations. In this work, it is supposed that only six from the twelve states of the quadrotor are available for measurement, namely, $x_1, x_3, x_5, x_7, x_9,$ and x_{11}; i.e., only the linear and angular displacements in the axes $X_e, Y_e, Z_e, X_b, Y_b,$ and Z_b are available. To overcome this problem, a full-state observer will be considered during the stabilization of the quadrotor.

Under such conditions, one random reference will be imposed on x_1, another on x_3, and the last one on x_5. Besides, a random perturbation will affect x_2.

Both the references and perturbations are generated by a set of equations similar to (9) and (19):

$$
\begin{aligned}
w_{k+1} &= A_{\text{exo}}w_k + M_k\xi_k, \\
z_{\text{ref},k} &= C_{\text{exo}}w_k + N_k\eta_k.
\end{aligned}
\tag{19}
$$

For the definition of structure of the exosystem, it is important to mention that the references and perturbations to be imposed on x_1, x_3 are pseudoperiodic with frequency of πrad/s, the reference to be imposed on x_5 is random with zero mean, and the perturbations affecting the state x_2 are also pseudo periodic of $(\pi/2)$(rad/s). Therefore, by considering the dimensions of system (11), one way of generating such references and perturbations is through (20) with matrices $A_{\text{exo}} = \{a_{\text{exo},ij}\} \in \mathfrak{R}^{5\times5}$, $C_{\text{exo}} = \{c_{\text{exo},ij}\} \in \mathfrak{R}^{3\times5}$, and $P = \{p_{ij}\} \in \mathfrak{R}^{12\times5}$, where $a_{\text{exo},11} = a_{\text{exo},22} = 0.997$, $a_{\text{exo},12} = -a_{\text{exo},21} = 0.078$, $a_{\text{exo},44} = a_{\text{exo},55} = 0.999$, and $a_{\text{exo},45} = -a_{\text{exo},54} = 0.039$, the other terms of A_{exo} have a value of 0, $c_{\text{exo},11} = c_{\text{exo},22} = c_{\text{exo},33} = 1$, the other terms of C_{exo} have a value of 0, $p_{25} = 1$, and the other terms of P have a value of 0. At this point, the perturbations can be defined as Pw_k.

Thus, as mentioned before, in order to track the random references and to reject the random perturbations, they will be estimated online by means of a Kalman filter. In the following section, the structure of the matrices involved in the estimation of the references and perturbations is thoroughly analyzed.

3. Main Result

To estimate the random references and random perturbations by means of the Kalman filter, it must be recalled that both matrices C_{exo} and P can be viewed as output matrices for the exosystem, and because of their dimension, they can be used to construct an overall output matrix for the exosystem, namely, $C_{\text{Tot}} = [C_{\text{exo}}^T P^T]^T$, with $C_{\text{Tot}} \in \mathfrak{R}^{15\times5}$.

With this in mind, and by considering the expressions for the exosystem, i.e., (20), the estimation problem for the references and perturbations can be solved by a Kalman iterative process like the one defined through equations (9) and (10), where $A = A_{\text{exo}}$, $B = 0$, and $C = C_{\text{Tot}}$, for all $k \geq 0$.

On the other hand, an observer capable of estimating the full state of a plant from the available outputs when it is subject to random perturbations must be designed. So, for system (21), a quasi-solution for the observability problem is given next.

Theorem 2. *Consider a plant in the form of*

$$
\begin{aligned}
x_{k+1} &= Ax_k + Bu_k + Pw_k, \\
z_k &= C_zx_k, \\
y_k &= Cx_k.
\end{aligned}
\tag{20}
$$

y_k is considered as the vector of available output and z_k as the set of output where the references are to be imposed. As before, $x_k \in \mathfrak{R}^n$, $u_k \in \mathfrak{R}^p$, $y_k \in \mathfrak{R}^m$, $z_k \in \mathfrak{R}^{m_z}$, and $w_k \in \mathfrak{R}^\ell$ as the solution of the exosystem

$$
\begin{aligned}
w_{k+1} &= A_{\text{exo}}w_k, \\
z_{\text{ref},k} &= C_{\text{exo}}w_k.
\end{aligned}
\tag{21}
$$

$z_{\text{ref},k} \in \mathfrak{R}^{m_z}$ are considered as the vector of references to be tracked. Then, the state x_k can be taken to a neighborhood around its equilibrium if the pair (A, B) is stabilizable, the pair (A, C) is detectable, and there exists an estimation for perturbation $p_k = Pw_k$. Moreover, the quasi-stabilizer is given by the dynamic system:

$$
\begin{aligned}
x_{o,k+1} &= Ax_{o,k} + Bu_k + \widehat{p}_k + L\big(y_k - y_{o,k}\big), y_{o,k} \\
&= Ax_{o,k}, u_k \\
&= Kx_{o,k},
\end{aligned}
\tag{22}
$$

where $x_{o,k}$ is the state of the observer.

Proof. Let the observer for (21) be (23) and $e_o = x_k - x_{o,k}$ with u_k as in (22) for both (21) and (23). Thus $e_{o,k+1}$ can be written as

$$
e_{o,k+1} = Ae_{o,k} + e_{p,k} + LCe_{o,k},
\tag{23}
$$

where $e_{p,k} = p_k - \widehat{p}_k$. Thus, by continuity, if the system (21) is detectable and if $e_{p,k}$ is sufficiently small, then gain L exists because $e_{p,k}$ could be disregarded. Besides, if (21) is stabilizable the gain K also exists and both state vectors x_k and $x_{o,k}$ tend to a neighborhood around the equilibrium by means of (22).

Notice that, previously, it has been supposed that p_k can be estimated by the Kalman filter.
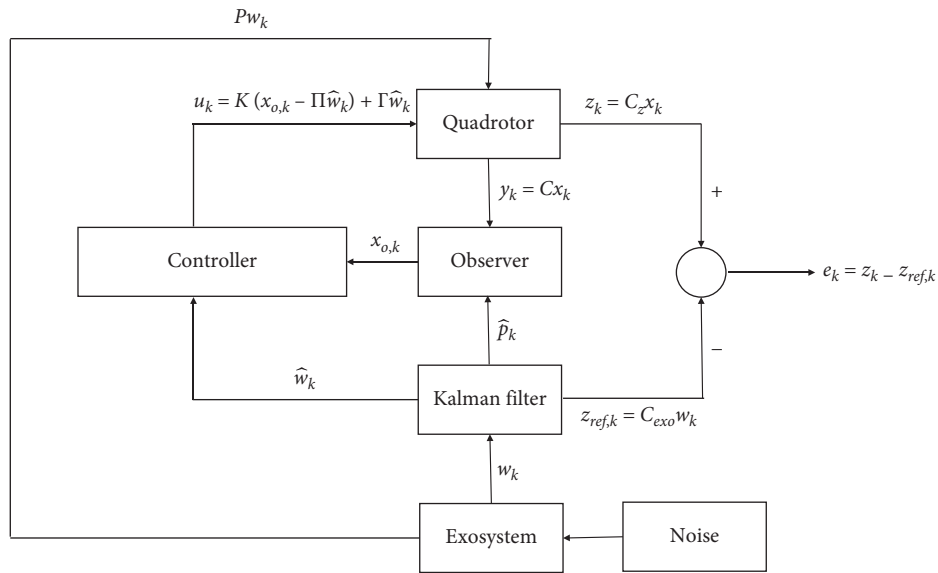
FIGURE 2: Control scheme.
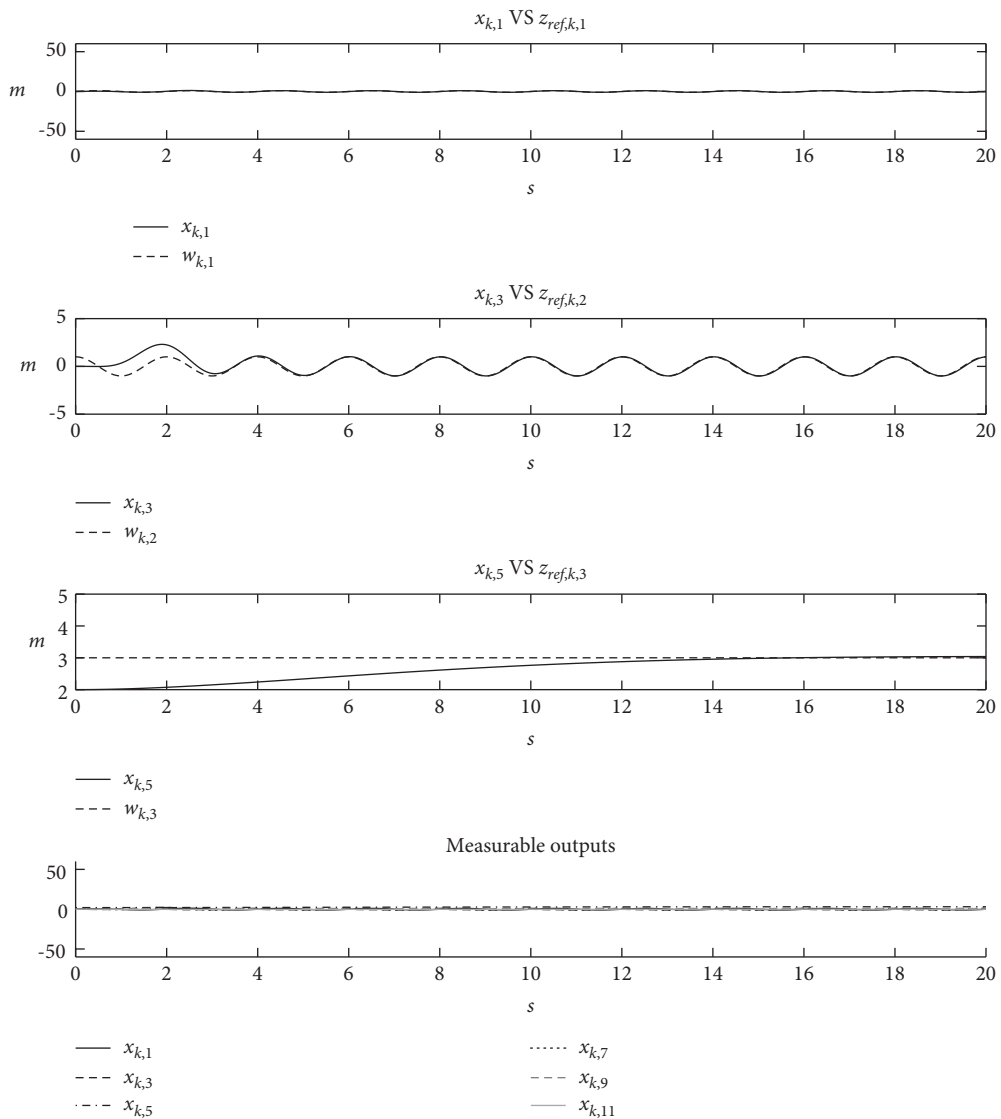
FIGURE 3: Tracking and available outputs when minimum randomness is considered.
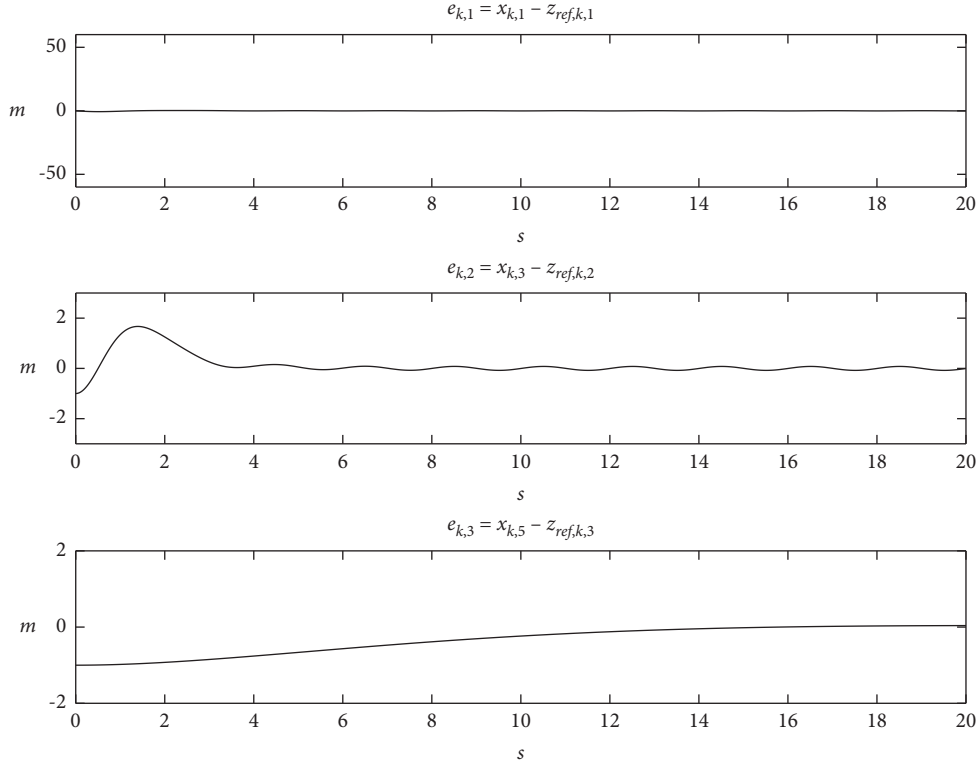
FIGURE 4: Tracking errors with minimum randomness.

Now, the regulation problem presented in Section 2.1 must be extended to the field of the discrete-time systems, but considering that the states and output of the exosystem are influenced by noise. To this end, consider the discrete-time plant (21) and the exosystem (20).

Thus, by mimicking the procedure in Section 2.1, the tracking error is given by $e_k = z_k - z_{ref,k}$, and the tracking problem for discrete time is solved by a control vector u_k such that

$$\lim_{k \longrightarrow \infty} e_k = 0. \tag{24}$$

As above, it will be considered that the tracking problem for discrete-time plants is solved by

$$u_k = K\left(x_{o,k} - \Pi \widehat{w}_k\right) + \Gamma \widehat{w}_k, \tag{25}$$

where $x_{o,k}$ is the observed state of the plant, $\widehat{w}_k$ is the Kalman estimation for w_k, the manifold of steady-state is $x_{ss,k} = \Pi \widehat{w}_k$, and the steady-state input is $u_{ss,k} = \Gamma \widehat{w}_k$, with $\Pi \in \mathfrak{R}^{n \times \ell}$ and $\Gamma \in \mathfrak{R}^{p \times \ell}$ as the solution of

$$A\Pi + B\Gamma + P = \Pi A_{exo}, C\Pi - C_{exo} = 0. \tag{26}$$

At this point, the following result naturally arises. □

Theorem 3. *Considering the tracking problem defined by (20) and (21), and assuming H1: There exists a matrix K which stabilizes (A, B), H2: There exists a matrix L, such that the pair (A, C) is detectable, and H3: There exists a solution for Francis equation (26) given by $\Pi \in \mathfrak{R}^{n \times \ell}$ and $\Gamma \in \mathfrak{R}^{p \times \ell}$, then,*

the tracking problem for the discrete-time system defined by (20) and (21) is solved by (25).

Proof. Let the steady-state error be $e_{ss,k} = x_{o,k} - \Pi \widehat{w}_k$. Thus,

$$e_{ss,k+1} = x_{o,k+1} - \Pi \widehat{w}_{k+1},$$
$$\Rightarrow e_{ss,k+1} = Ax_{o,k} + Bu_k + Pw_k - \Pi A_{exo}\widehat{w}_k. \tag{27}$$

By the definition of $e_{ss,k}$ and by substituting (26) in (27), one gets

$$e_{ss,k+1} = (A + BK)e_{ss,k} + A\Pi \widehat{w}_k + B\Gamma \widehat{w}_k + P\widehat{w}_k - \Pi A_{exo}\widehat{w}_k. \tag{28}$$

From (28), it is obvious that $e_{ss,k}$ dissipates when (1) matrices $A + BK$ and $A - LC$ have their eigenvalues inside the unit circle [30] (Assumptions $H1$ and $H2$), and (2) $A\Pi + B\Gamma + P = \Pi A_{exo}$, which coincides with (26). As in Theorem 1, by considering the tracking error $e_k = z_k - z_{ref,k}$ in steady-state, the missing equations are obtained from

$$e_k = C_z\left(e_{ss,k} + \Pi \widehat{w}_k\right) - C_{exo}\widehat{w}_k. \tag{29}$$

In steady-state it coincides with (26). As above, this analysis entirely relies on the fact that the Kalman estimation $\widehat{w}_k$ is sufficiently close to w_k. The rest of the proof follows the same path as in Theorem 1. □

Remark 1. Theorems 1 and 2 correspond to results in continuous time and discrete time, where no uncertainties were considered. However, Theorem 3 states the conditions
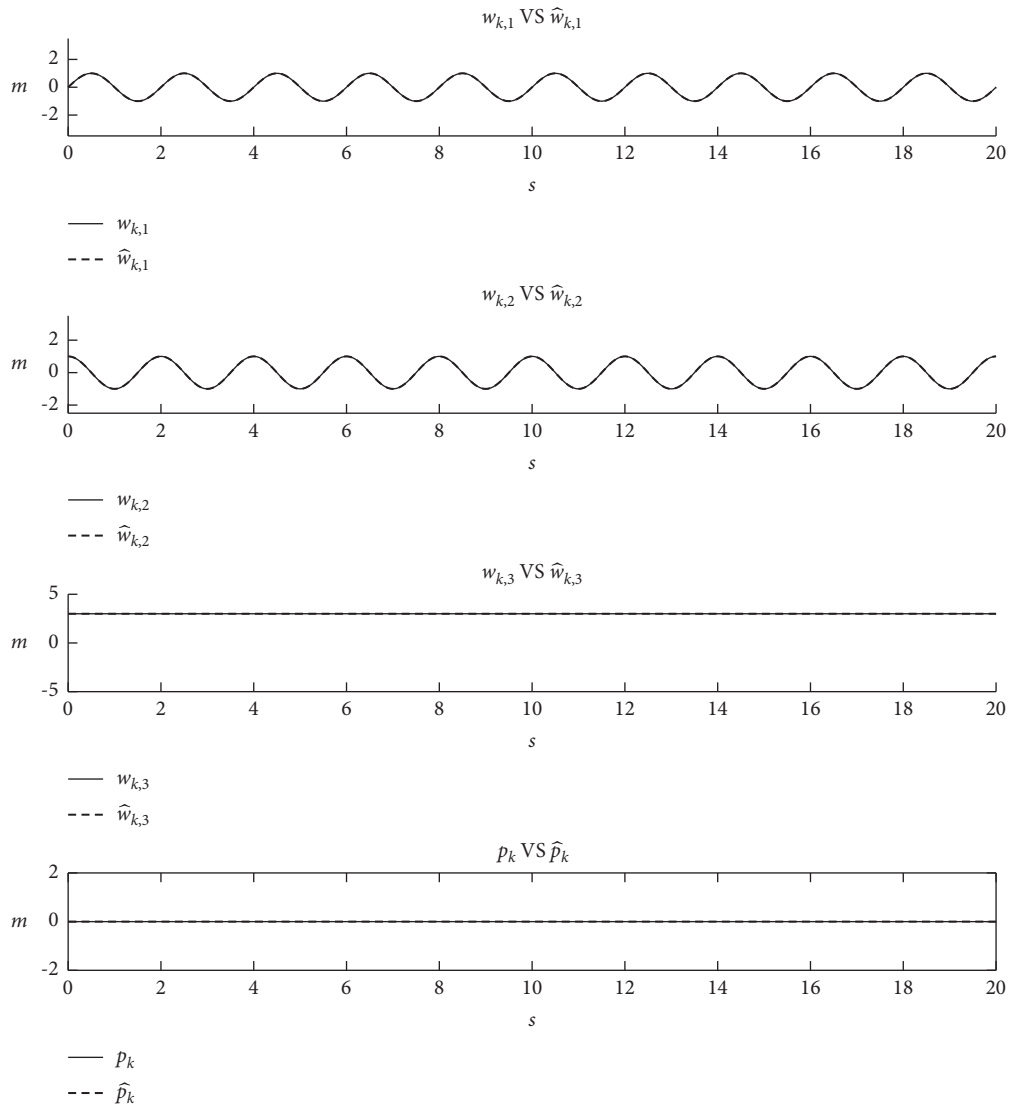
FIGURE 5: Estimation of references and perturbation with minimum randomness.
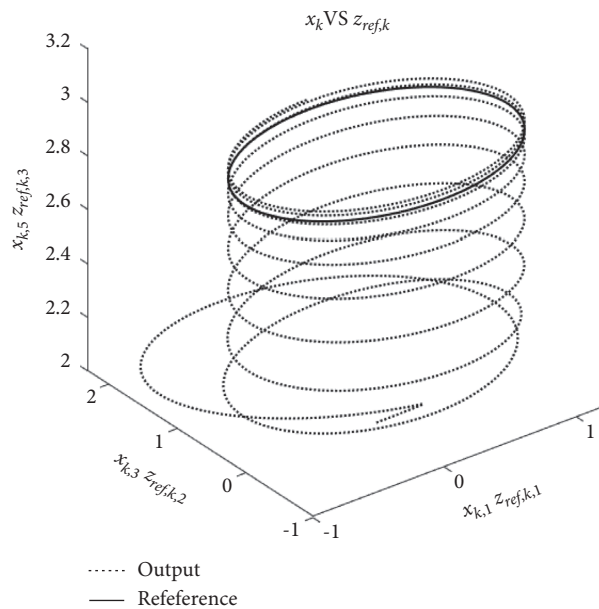
FIGURE 6: Behavior of the quadrotor when minimum randomness references are tracking.
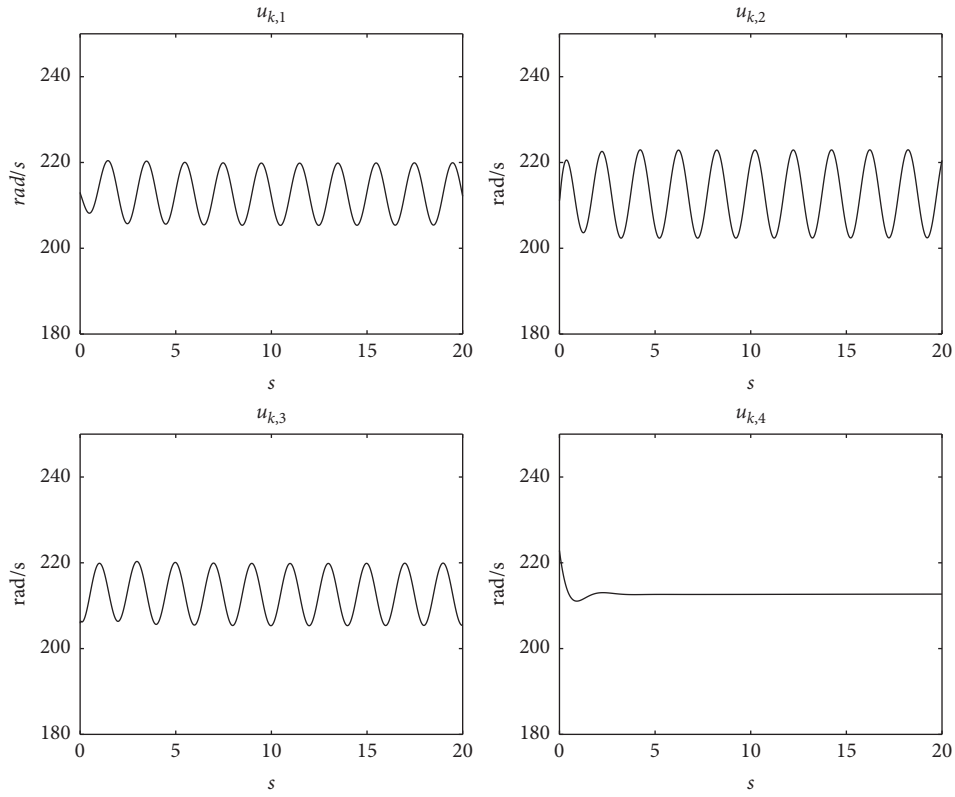
Figure 7: Rotors frequencies for minimum randomness tracking.
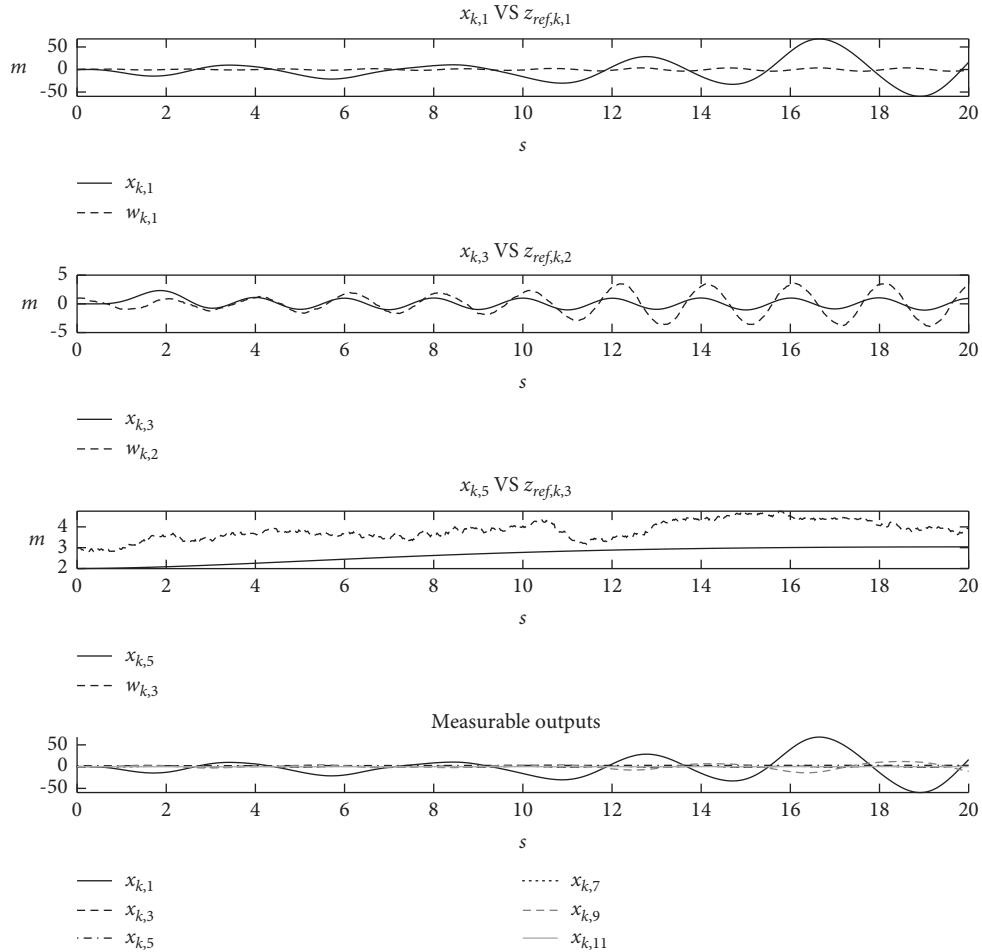
Figure 8: Tracking random references considering the structure method.
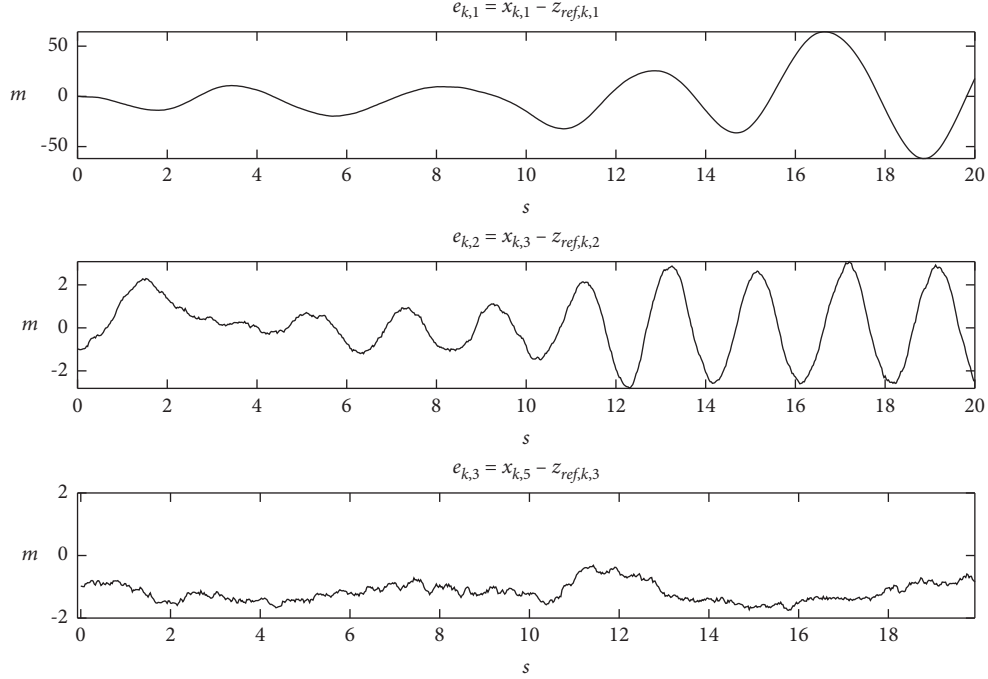
FIGURE 9: Tracking errors for random references considering the structure method.

under which that regulation problem can be solved, even if the exosystem is subject to uncertainties.

Remark 2. The proposed approach entirely relies on the estimation of the Kalman filter. For that reason, the proposed exosystem complies with the requirements established by the Kalman theory, and A_{exo} must be known. Future works may be oriented to estimate the elements of A_{exo} when such matrix is unknown, but that problem exceeds the scope of the present work.

The control scheme is graphically described in the block diagram of Figure 2.

4. Numerical Simulations

Please refer to Appendix where a detailed description of the matrices considered to construct the control is given.

The numerical simulations are carried out considering a linearization of (17) around the origin, because the ground effect is not considered in the mathematical model. Consequently, the observer (23) is construct from the matrices $A = \{a_{ij}\} \in \mathfrak{R}^{12 \times 12}$, $B = \{b_{ij}\} \in \mathfrak{R}^{12 \times 4}$, $C = \{c_{ij}\} \in \mathfrak{R}^{6 \times 12}$, and $L = \{l_{ij}\} \in \mathfrak{R}^{12 \times 6}$, and L has been computed by considering the set of desired eigenvalues:

$$\lambda = \left\{ \begin{array}{cccccc} 0.435 & 0.44 & 0.445 & 0.45 & 0.455 & 0.46 \\ 0.465 & 0.47 & 0.475 & 0.48 & 0.485 & 0.49 \end{array} \right\}. \quad (30)$$

The control (26) is formed from the matrix $K = \{k_{ij}\} \in \mathfrak{R}^{12 \times 4}$. K has been computed by the dlqr algorithm with $Q = 10^3 I_{12}$, and $R = 10^{-3} I_4$ with I_j as the identity matrix of dimension j, and the solution for (27) is given by $\Pi = \{\pi_{ij}\} \in \mathfrak{R}^{12 \times 5}$ and $\Gamma = \{\gamma_{ij}\} \in \mathfrak{R}^{4 \times 5}$, A_{exo}, C_{exo}, and P are given in Section 2.4.

Remark 3. The design of the controller has been performed on the linear model of the quadrotor, although the results presented correspond to the response of the nonlinear system under the action of the designed controller.

With all of the basis stated in previous sections, the results are given next.

Example 1. Minimum randomness with the proposed method.

At first, the simulations are carried out with very small randomness in order to validate the approach in the quasi-deterministic case. As mentioned before $M_k = I_{5 \times 5}$, $N_k = I_{3 \times 3}$, while the dynamic and measurement noises are characterized by their standard deviations q and r, respectively, such that $Q = q^2 M_k$ and $R = r^2 N_k$. The results are given in Figures 2 to 6.

So, for this example, the standard deviation values are $q = 1 \times 10^{-6}$ and $r = 1 \times 10^{-6}$. The initial conditions for the nonlinear model of the quadrotor (18) are $x_0 = [0, 1, 0, 0, 2, 0, 0, 0, 0, 0, 0, 0]^T$, while the initial state for the observer is $x_{o,0} = [0, 1 + \varepsilon_1, 0, 0, 2 + \varepsilon_2, 0, 0, 0, 0, 0, 0, 0]^T$, where ε_1 and ε_2 are random numbers with zero mean and standard deviation q. On the other hand, the references and perturbations are generated by the exosystem (19) with initial conditions $w_0 = [0, 1, 3, 0, 0]^T$, while the initial state for the Kalman filter is $\hat{w}_0 = w_0 + [\eta_1, \eta_2, \eta_3, \eta_4, \eta_5]^T$, where $\eta_1 \ldots \eta_5$ are random numbers with zero mean and standard deviation r. Under these conditions, the obtained results are depicted from Figures 3 to 7.

In Figure 3 are shown the tracking outputs against the corresponding reference. It can be observed how the proposed controller achieves the desired goals. Besides, in the same figure, the available outputs are depicted also. Figure 4 might be more helpful to determine the efficacy of the controller by
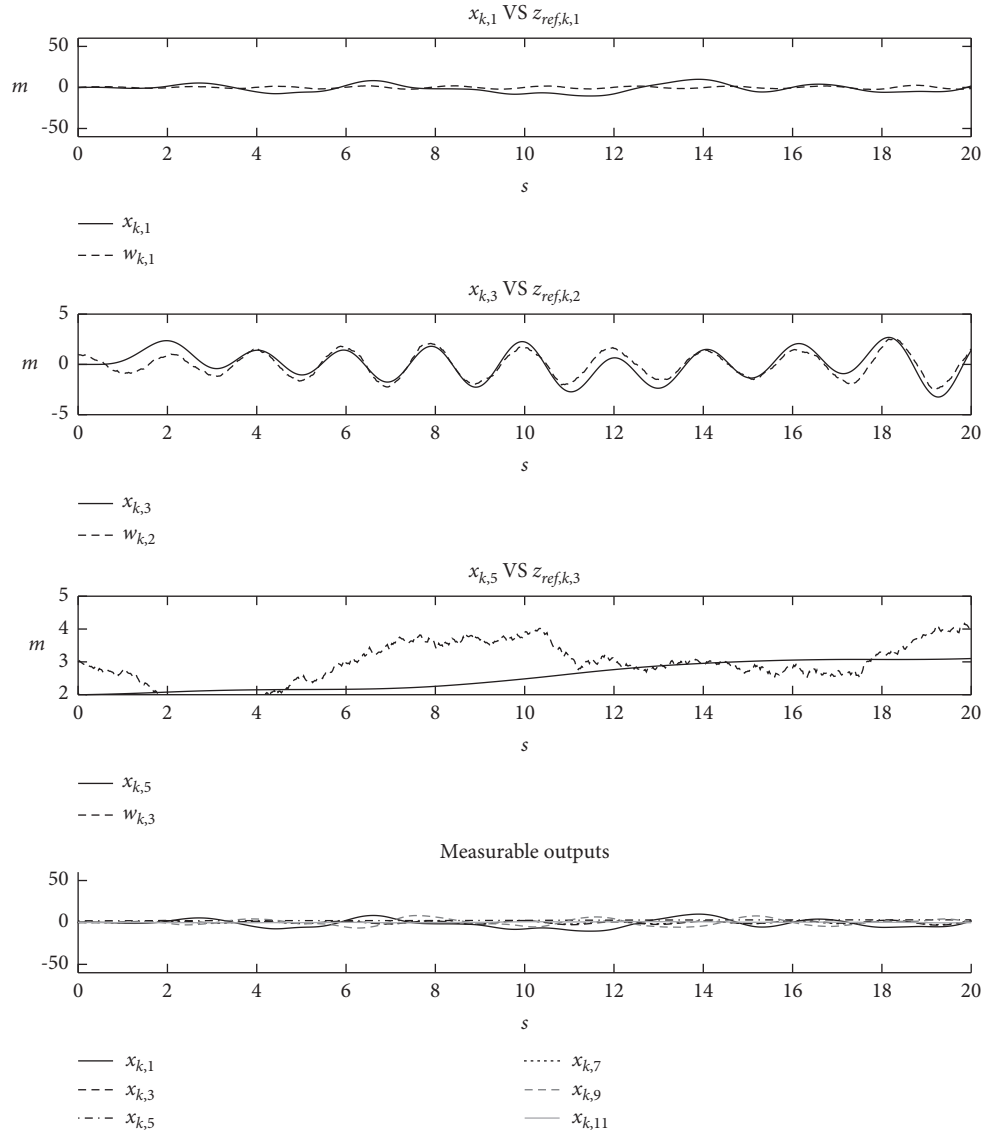
FIGURE 10: Tracking random references and available outputs.

showing the tracking errors under the mentioned conditions. Please, note that the oscillations presented in such a figure are due to the fact that a controller is applied to a quadrotor. In other words, persistent oscillations can be reduced or even eliminated by means of a nonlinear controller; however, such analysis exceeds the scope of the present work.

The estimation of the references and the perturbations can be viewed in Figure 5. From there, it can be concluded that the estimates provided by the Kalman filter are acceptable, at least in this case.

Thus, the 3D behavior of the quadrotor is shown in Figure 6 and the rotors' frequencies appear in Figure 7. It is worth mentioning that the frequencies of the rotors remain positive, all of them. This is an important feature of the quadrotor that must be kept all the time because the rotors of such system rotate in one and only one direction.

Notice also that the frequencies of the rotors are not the same. This is due to the fact that the quadrotor is describing circles during its operation.

Example 2. Stochastic problem with the structure method.

Now, a more interesting case is simulated with bigger values for q and r; i.e., the randomness of the problem is now notably increased. In this case $q = 0.05$ and $r = 0.5$. The rest of the parameters remain as those considered in Example 1. The results are given in Figures 8 to 9.

The simulation considers the same situation presented in the previous example, but the structure method of [20, 21] is used in which the Kalman estimating is omitted and it is assumed that the structure method is sufficient to describe both the references and the perturbation even when they are, in fact, random. The results are given in Figures 8 and 9. Notice now
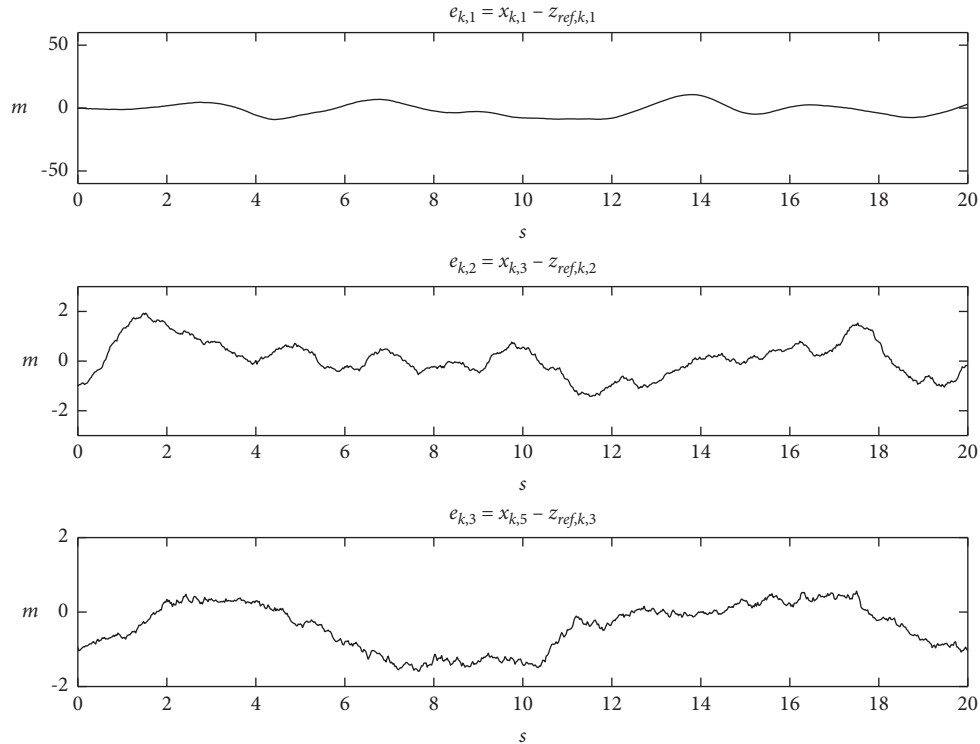
FIGURE 11: Tracking errors for random references and random perturbation.

that the references are much more complex due to the random nature of the exosystem provoked by the values of q and r.

In this case, the boundedness of the tracking errors can not be ensured, which totally justifies the use of the proposed method of the next example.

Example 3. Stochastic problem with the proposed method.

This numerical experiment considers the same situation presented in Example 2; i.e., $q = 0.05$ and $r = 0.5$. However, in this case the Kalman estimation is considered. The rest of the parameters remain as those considered in Example 1. The results are given in Figures 10 to 14.

In Figure 10 are depicted the tracking outputs against their respective references. The tracking errors are shown in Figure 11. Observe how, in this case, the errors are smaller than those obtained in Example 2.

The performance of the Kalman filter can be assessed through the results given in Figure 12. From there, one can conclude that the estimations of the references and the perturbation are acceptable again despite the randomness introduced in the exosystem, corroborating in this way, that the main issue of the tracking problem, in this case, is the nature of the linear control.

Finally, the 3D behavior of the quadrotor is shown in Figure 13 and the rotors' frequencies appear in Figure 14. Observe that the random reference is changing so abruptly that the quadrotor is unable to track it exactly because of its own physical restrictions. However, the quadrotor is kept in a neighborhood around the reference, meaning that the tracking errors are bounded. Again, the frequencies are all positives, which implies that the controller is imposing normal behavior in the rotors. Obviously, the strange behavior of the quadrotor is due to complex response of the rotors.

Comparison of Examples 1–3:

Finally, the mean squared error (MSE) between the tracking states of the quadrotor and the corresponding states of the exosystem for Examples 1–3 is depicted in Table 1.

Clearly, the inclusion of the Kalman filter for estimating the states of the stochastic exosystem drastically reduces the MSEs. Therefore, its use cannot be neglected when the reference or perturbation is not fully known.

Remark 4. Example 3 should be compared with Example 2 because the same big noises with standard deviation values of $q = 0.05$ and $r = 0.5$ are used in Examples 2 and 3; the difference of this comparison is that the Kalman estimating is omitted in Example 2, while the Kalman estimating is used in Example 3. Example 1 should not be compared with Examples 2 and 3 because small noises with standard deviation values of $q = 1 \times 10^{-6}$ and $r = 1 \times 10^{-6}$ are used in Example 1, and the Kalman estimating is omitted in Example 1.
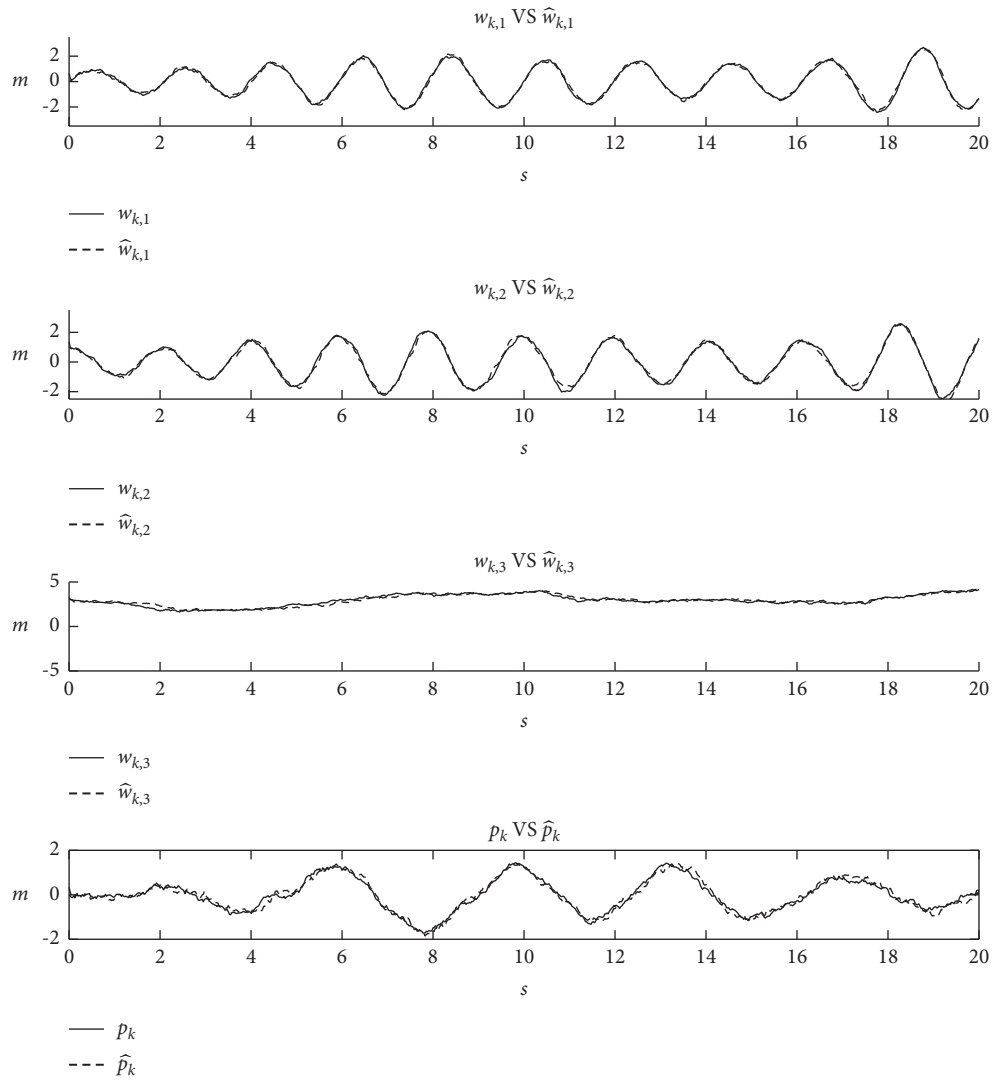
Figure 12: Estimation of random references and random perturbation.
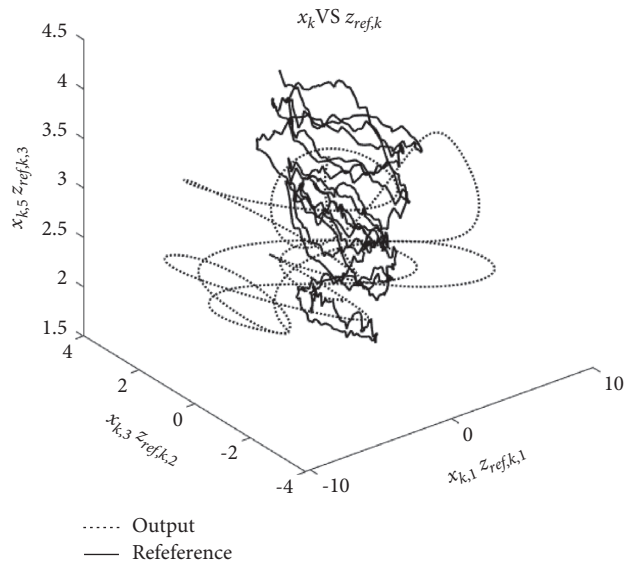
Figure 13: Behavior of the quadrotor when random references are tracking.
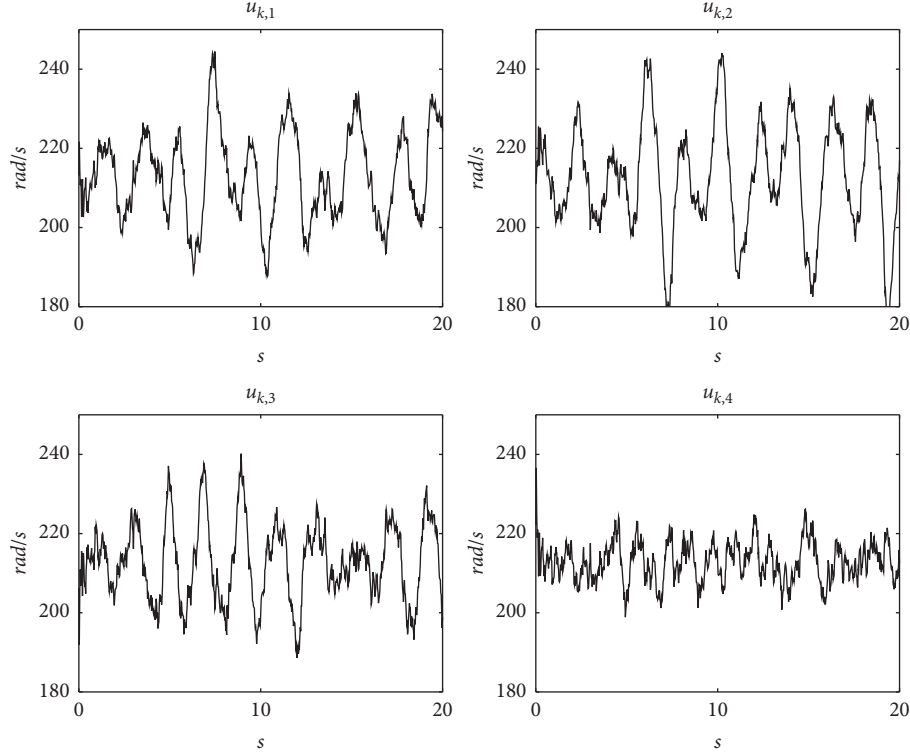
FIGURE 14: Rotors frequencies for random tracking.

TABLE 1: MSEs for Examples 1–3.

	$x_{k,1}$ vs $z_{\mathrm{ref},k,1}$	$x_{k,3}$ vs $z_{\mathrm{ref},k,2}$	$x_{k,5}$ vs $z_{\mathrm{ref},k,3}$
1	0.01832414	0.1837935	0.2471288
2	1835.705	0.7743019	1.995679
3	26.1942	0.5449	0.5347

5. Conclusion

On the basis of the observer and Kalman filter, an approach to track random references while random perturbations are rejected has been proposed. The control scheme analyzed in this work can be viewed as an extension of the deterministic tracking problem to the area of stochastic processes. It has been shown that the estimation of the references and perturbation makes a great difference because, in general, the controller is constructed on the basis that the same matrices need to solve the deterministic case. The validity of the approach has been illustrated by several numerical simulations considering the mathematical model of a quadrotor. In the future work, for the case where the quadrotor includes random dynamics, then the observer will be substituted for an unscented Kalman filter, an extended Kalman filter, or another estimator as the James-Stein filter.

Appendix

The terms of the matrix $A = \left\{a_{ij}\right\} \in \mathfrak{R}^{12 \times 12}$ are $a_{11} = a_{22} = a_{33} = a_{44} = a_{55} = a_{66} = 1$, $a_{77} = a_{88} = a_{99} = a_{10,10} = a_{11,11} = a_{12,12} = 1$, $a_{12} = a_{34} = a_{56} = a_{78} = a_{9,10} = a_{11,12} = \alpha_1$, $a_{29} = \alpha_2$, $a_{47} = -\alpha_2$, $\alpha_1 = 0.025$, $\alpha_2 = 0.24525$, and the other terms of A have a value of 0.

The terms of the matrix $B = \left\{b_{ij}\right\} \in \mathfrak{R}^{12 \times 4}$ are $b_{61} = b_{62} = b_{63} = b_{64} = \beta_1$, $b_{81} = b_{82} = b_{83} = b_{84} = \beta_2$, $b_{10,1} = b_{10,2} = b_{10,3} = b_{10,4} = \beta_2$, $b_{12,1} = b_{12,2} = b_{12,3} = b_{12,4} = \beta_3$, $\beta_1 = 0.00057$, $\beta_2 = 0.01708$, $\beta_3 = 0.00082$, and the other terms of B have a value of 0.

The terms of the matrix $C = \left\{c_{ij}\right\} \in \mathfrak{R}^{6 \times 12}$ are $c_{11} = c_{23} = c_{35} = c_{47} = c_{59} = c_{6,11} = 1$, the rest of the terms of C are equal to zero.

The terms of the matrix $L = \left\{l_{ij}\right\} \in \mathfrak{R}^{12 \times 6}$ are $l_{11} = 1.045$, $l_{12} = -0.004849$, $l_{13} = -0.00187$, $l_{14} = 0.004604$, $l_{15} = -3.917 \times 10^{-5}$, $l_{16} = 0.0001877$, $l_{21} = 10.91$, $l_{22} = -0.1019$, $l_{23} = -0.03905$, $l_{24} = 0.09537$, $l_{25} = 0.2462$, $l_{26} = 0.003895$, $l_{31} = -0.004303$, $l_{32} = 1.047$, $l_{33} = -0.001568$, $l_{34} = 0.006485$, $l_{35} = -0.01585$, $l_{36} = 0.000152$, $l_{41} = -0.09043$, $l_{42} = 10.97$, $l_{43} = -0.03272$, $l_{44} = -0.1107$, $l_{45} = -0.3324$, $l_{46} = 0.003145$, $l_{51} = -0.0002392$, $l_{52} = -0.0002246$, $l_{53} = 1.101$, $l_{54} = 0.0001867$, $l_{55} = -0.0001424$, $l_{56} = 0.02143$, $l_{61} = -0.005185$, $l_{62} = -0.004869$, $l_{63} = 12.12$, $l_{64} = 0.004052$, $l_{65} = -0.003096$, $l_{66} = 0.4646$, $l_{71} = 0.003847$, $l_{72} = 0.004632$, $l_{73} = 0.001292$, $l_{74} = 1.044$, $l_{75} = 0.007422$, $l_{76} = -0.0001401$, $l_{81} = 0.07979$, $l_{82} = 0.09622$, $l_{83} = 0.02687$, $l_{84} = 10.89$, $l_{85} = 0.1542$, $l_{86} = -0.002901$, $l_{91} = -6.892 \times 10^{-5}$, $l_{92} = -0.001195$, $l_{93} = -8.156 \times 10^{-5}$, $l_{94} = 0.0007677$, $l_{95} = 1.104$, $l_{96} = 9.086 \times 10^{-6}$, $l_{10,1} = -0.001524$, $l_{10,2} = -0.0264$, $l_{10,3} = -0.001802$, $l_{10,4} = 0.01696$, $l_{10,5} = 12.19$, $l_{10,6} = 0.0002007$, $l_{11,1} = 4.419 \times 10^{-5}$, $l_{11,2} = 4.014 \times 10^{-5}$, $l_{11,3} = 0.001739$, $l_{11,4} = -4.137 \times 10^{-5}$, $l_{11,5} = 3.991 \times 10^{-5}$, $l_{11,6} = 1.109$, $l_{12,1} = 0.0009928$, $l_{12,2} = 0.0009018$, $l_{12,3} = 0.0389$, $l_{12,4} = -0.0009294$, $l_{12,5} = 0.0008965$, $l_{12,6} = 12.29$.

The terms of the matrix $K = \left\{k_{ij}\right\} \in \mathfrak{R}^{12 \times 4}$ are $k_{11} = k_{14} = k_{33} = k_{34} = -0.4646$,

$k_{12} = k_{13} = k_{31} = k_{32} = 0.4646$, $\quad k_{21} = k_{24} = k_{43} = k_{44} = -0.8851$, $\quad k_{22} = k_{23} = k_{41} = k_{42} = 0.8851$, $\quad k_{71} = k_{72} = k_{91} = k_{94} = -5.884$, $\quad k_{73} = k_{74} = k_{92} = k_{93} = 5.884$, $\quad k_{81} = k_{82} = k_{10,1} = k_{10,4} = -2.143$, $\quad k_{83} = k_{84} = k_{10,2} = k_{10,3} = 2.143$, $k_{51} = k_{52} = k_{53} = k_{54} = 0.4981$, $k_{61} = k_{62} = k_{63} = k_{64} = 3.33$, $k_{11,1} = k_{11,3} = 0.4977$, $k_{11,2} = k_{11,4} = -0.4977$, $k_{12,1} = k_{12,3} = 2.799$, $k_{12,2} = k_{12,4} = -2.799$.

The terms of the matrix $\Pi = \{\pi_{ij}\} \in \mathfrak{R}^{12 \times 5}$ are $\pi_{11} = \pi_{33} = \pi_{55} = 1$, $\quad \pi_{21} = \pi_{42} = -0.1233$, $\quad \pi_{71} = \pi_{92} = -0.0789$, $\pi_{81} = \pi_{10,2} = -3.136$, $\pi_{22} = 3.138$, $\pi_{41} = -3.138$, $\pi_{72} = 1.002$, $\pi_{91} = -1.002$, $\pi_{82} = -0.3712$, $\pi_{10,1} = 0.3712$, $\pi_{95} = -4.077$, $\pi_{10,4} = 6.403$, $\pi_{10,5} = 0.1257$, $\pi_{11,1} = 0.04455$, $\pi_{11,2} = 0.05216$, $\pi_{11,5} = 0.1967$, $\pi_{12,1} = -0.1692$, $\pi_{12,2} = 0.1334$, $\pi_{14,4} = -0.3089$, $\pi_{12,5} = -0.006065$, and the other terms of Π have a value of 0.

The terms of the matrix $\Gamma = \{\gamma_{ij}\} \in \mathfrak{R}^{4 \times 5}$ are $\gamma_{11} = \gamma_{32} = -7.17$, $\gamma_{12} = -1.136$, $\gamma_{31} = 1.136$, $\gamma_{14} = 0.289$, $\gamma_{24} = -0.289$, $\gamma_{15} = -7.356$, $\gamma_{25} = 7.356$, $\gamma_{21} = 6.034$, $\gamma_{22} = 8.306$, and the other terms of Γ have a value of 0.

Data Availability

The simulation data used to support this research are available from the third author upon request to the e-mail: rubio.josedejesus@gmail.com.

Conflicts of Interest

The authors declare that there are no conflicts of interest regarding the publication of this paper.

Acknowledgments

References

[1] V. T. Pham, S. Vaidyanathan, and T. Kapitaniak, "Complexity, dynamics, control, and applications of nonlinear systems with multistability," *Complexity*, vol. 2020, Article ID 8510930, 7 pages, 2020.

[2] G. D. Leutcho, T. F. Fozin, A. N. Negou et al., "A novel megastable Hamiltonian system with infinite hyperbolic and nonhyperbolic equilibria," *Complexity*, vol. 2020, Article ID 9260823, 12 pages, 2020.

[3] A. Sambas, S. Vaidyanathan, T. Bonny et al., "Mathematical model and FPGA realization of a multi-stable chaotic dynamical system with a closed butterfly-like curve of equilibrium points," *Applied Sciences*, vol. 11, no. 788, pp. 1–16, 2021.

[4] X. Wang, A. Akgul, U. Cavusoglu, V. T. Pham, D. V. Hoang, and X. Q. Nguyen, "A chaotic system with infinite equilibria and its S-box constructing application," *Applied Sciences*, vol. 8, no. 2132, pp. 1–12, 2018.

[5] A. T. Azar, F. E. Serrano, Q. Zhu et al., "Robust stabilization and synchronization of a novel chaotic system with input saturation constraints," *Entropy*, vol. 23, no. 1110, pp. 1–27, 2021.

[6] J. M. Muñoz-Pacheco, D. K. Guevara-Flores, O. G. Felix-Beltran, E. Tlelo-Cuautle, J. E. Barradas-Guevara, and C. K. Volos, "Experimental verification of optimized multi-scroll chaotic oscillators based on irregular saturated functions," *Complexity*, vol. 2018, Article ID 3151840, 17 pages, 2018.

[7] X. Wang, V.-T. Pham, S. Jafari, C. Volos, J. M. Munoz-Pacheco, and E. Tlelo-Cuautle, "A new chaotic system with stable equilibrium: from theoretical model to circuit implementation," *IEEE Access*, vol. 5, pp. 8851–8858, 2017.

[8] A. R. Ajel, A. J. Humaidi, I. K. Ibraheem, and A. T. Azar, "Robust model reference adaptive control for tail-sitter VTOL aircraft," *Actuators*, vol. 10, no. 162, pp. 1–19, 2021.

[9] H. Jahanshahi, N. N. Sari, V. T. Pham, F. E. Alsaadi, and T. Hayat, "Optimal adaptive higher order controllers subject to sliding modes for a carrier system," *International Journal of Advanced Robotic Systems*, vol. 15, pp. 1–11, 2018.

[10] H. Jahanshahi, M. Shahriari-Kahkeshi, R. Alcaraz, X. Wang, V. P. Singh, and V. T. Pham, "Entropy analysis and neural network-based adaptive control of a non-equilibrium four-dimensional chaotic system with hidden attractors," *Entropy*, vol. 21, no. 156, pp. 1–15, 2019.

[11] S. Mobayen, A. Fekih, S. Vaidyanathan, and A. Sambas, "Chameleon chaotic systems with quadratic nonlinearities: an adaptive finite-time sliding mode control approach and circuit simulation," *IEEE Access*, vol. 9, Article ID 64558, 2021.

[12] S. Wang, A. Yousefpour, A. Yusuf et al., "Synchronization of a non-equilibrium four-dimensional chaotic system using a disturbance-observer-based adaptive terminal sliding mode control method," *Entropy*, vol. 22, no. 271, pp. 1–15, 2020.

[13] G. Zhu, S. Wang, L. Sun, W. Ge, and X. Zhang, "Output feedback adaptive dynamic surface sliding-mode control for quadrotor UAVs with tracking error constraints," *Complexity*, vol. 2020, Article ID 8537198, 23 pages, 2020.

[14] P. Bagheri, A. Ramirez-Serrano, and J. K. Pieper, "Adaptive nonlinear robust control of a novel unconventional unmaned aerial vehicle," *Control and Intelligent Systems*, vol. 43, no. 1, 2015.

[15] Q. Guo, C. J. Macna, and J. K. Pieper, "Robust control of a rigid articulated hopper," *International Journal of Robotics and Automation*, vol. 27, no. 1, 2012.

[16] Y. Zhang, N. Xu, G. Zhu, L. Sun, S. Cao, and X. Zhang, "Adaptive robust dynamic surface integral sliding mode control for quadrotor UAVs under parametric uncertainties and external disturbances," *Complexity*, vol. 2020, Article ID 8879364, 20 pages, 2020.

[17] G. A. R. Ibraheem, A. T. Azar, I. K. Ibraheem, and A. J. Humaidi, "A novel design of a neural network-based fractional PID controller for mobile robots using hybridized fruit fly and particle swarm optimization," *Complexity*, vol. 2020, Article ID 3067024, 18 pages, 2020.

[18] M. M. Ferdaus, M. Pratama, S. G. Anavatti, M. A. Garratt, and E. Lughofer, "PAC: a novel self-adaptive neuro-fuzzy controller for micro aerial vehicles," *Information Sciences*, vol. 512, pp. 481–505, 2020.

[19] A. T. Azar, A. Koubaa, N. A. Mohamed et al., "Drone deep reinforcement learning: a review," *Electronics*, vol. 10, no. 999, pp. 1–30, 2021.

[20] J. De Jesus Rubio, G. Ochoa, D. Mujica-Vargas et al., "Structure regulator for the perturbations attenuation in a quadrotor," *IEEE Access*, vol. 7, Article ID 138244, 2019.

[21] J. d. J. Rubio, "Structure control for the disturbance rejection in two electromechanical processes," *Journal of the Franklin Institute*, vol. 353, no. 14, pp. 3610–3631, 2016.

[22] A. Isidori, *Nonlinear Control Systems*, Springer, Berlin, Germany, 1995.

[23] B. A. Francis, "The linear multivariable regulator problem," *SIAM Journal on Control and Optimization*, vol. 15, pp. 486–505, 1997.

[24] J. A. Meda-Campana, J. C. Gomez-Mancilla, and B. Castillo-Toledo, "Exact output regulation for nonlinear systems described by Takagi-Sugeno fuzzy models," *IEEE Transactions on Fuzzy Systems*, vol. 20, no. 2, pp. 235–247, 2012.

[25] C. K. Chui and G. Chen, *Kalman Filtering with Real-Time Applications*, Springer-Verlag, Berlin Heidelberg, 1987.

[26] E. Lughofer, "Improving the robustness of recursive consequent parameters learning in evolving neuro-fuzzy systems," *Information Sciences*, vol. 545, pp. 555–574, 2021.

[27] T. Gao, S. Yin, H. Gao, X. Yang, J. Qiu, and O. Kaynak, "A locally weighted project regression approach-aided nonlinear constrained tracking control," *IEEE Transactions on Neural Networks and Learning Systems*, vol. 29, no. 12, pp. 5870–5879, 2018.

[28] Z. Li, J. Teng, J. Qiu, and H. Gao, "Filtering design for multirate sampled-data systems," *IEEE Transactions on Systems, Man, and Cybernetics: Systems*, vol. 50, no. 11, pp. 4224–4232, 2020.

[29] J. A. Meda-Campana, "On the estimation and control of nonlinear systems with parametric uncertainties and noisy outputs," *IEEE Access*, vol. 6, pp. 31968–31973, 2018.

[30] T. Kailath, *Linear Systems*, Prentice-Hall, Englewood Cliffs, NJ, USA, 1980.

WILEY | Hindawi

Research Article

New Stabilization Properties of Pendulum Models Applying a Large Parameter

A. I. Ismail [ID]**[1,2] and Hamza A. Ghulman[1]**

[1]*Mechanical Engineering Department, College of Engineering and Islamic Architecture, Umm Al-Qura University,*
 P.O. Box 5555, Makkah, Saudi Arabia
[2]*Mathematics Department, Faculty of Science, Tanta University, P.O. Box 31527, Tanta, Egypt*

Correspondence should be addressed to A. I. Ismail; aiismail@uqu.edu.sa

In the present paper, we introduce new models of pendulum motions for two cases: the first model consists of a pendulum with mass M moving at the end of a string with a suspended point moving on an ellipse and the second one consists of a pendulum with mass M moving at the end of a spring with a suspended point on an ellipse. In both models, we use the Lagrangian functions for deriving the equations of motions. The derived equations are reduced to a quasilinear system of the second order. We use a new mathematical technique named a large parameter method for solving both models' systems. The analytical solutions are obtained in terms of the generalized coordinates. We use the numerical techniques represented by the fourth-order Runge–Kutta method to solve the autonomous system for both cases. The stabilities of the obtained solutions are studied using the phase diagram procedure. The obtained numerical solutions and analytical ones are compared to examine the accuracy of the mathematical and numerical techniques. The large parameter technique gives us the advantage to obtain the solutions at infinity in opposite with the famous Poincare's (small parameters) method which was used by many outstanding scientists in the last two centuries.

1. Introduction

The pendulum motions are considered as one of the important problems in theoretical mechanics. These problems are studied by many authors in [1–5]. The authors used the small parameter technique for solving their problems. In [6], the author studied the properties of the relative periodic motions of a coherent object suspended by a flexible wire at a regular rotating vertical plane. He used Lagrange's equations to obtain the motion equations while neglecting nonlinear boundaries. He found periodic solutions to equations using the small parameter method. In [7], the movement of a variable-length pendulum was studied and perturbation analysis [8] was used to determine the properties of the movement. In [9], the authors studied a simple pendulum revolving around an axis that has a double linear torque and is subject to periodic movements. The researchers showed that this natural system becomes an effective way to

determine the change in the median resonance (parametric). In [10], the author concluded solutions for a simple pendulum in the presence of excitation in the polar direction.

Nobody thought about using another technique especially the large parameter method although this technique allows us to give the problem new conditions that cannot be assumed previously. Also, this technique gives us the chance to study the problems in a new domain of the problem (at infinity). The applied work has many applications in the rotary planet motions around the Sun and the rotary motions of bodies around the Earth. Also, there are many applications in satellite motions, antennas, and navigations. In the first problem, the angular velocity ω is the one for the point Q instead of point A in the previous works (see Figure 1). Also, the angle ωt is the angle between the line OQ and the fixed vertical downward x-axis in the plane xy instead of the angle between the line OA and the x-axis. However, in the second problem, we take a rigid body M
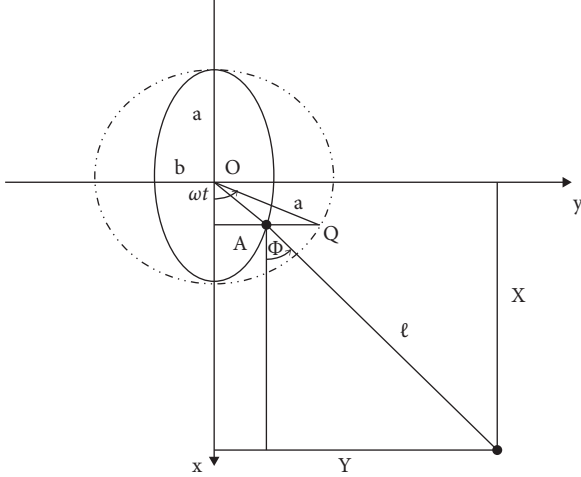
FIGURE 1: The pendulum motion on an ellipse.

instead of a particle in the first one and spring instead of a string in the first. So, the second problem takes a complicated study and procedure for obtaining the solutions in terms of three generalized coordinates instead of one in the first problem. We take into consideration the mentioned descriptions above for studying the following two models and constructing the equations of motions using the Lagrangian function. We achieve the solutions by the large parameter method instead of the small one. This method is considered as a new procedure [11] which gives new considerations for these problems.

2. The First Pendulum Model

In this section, we study a pendulum of mass M and string length ℓ with suspended point A moving on an ellipse (see Figure 1). For this case, we take a point Q on the auxiliary circle of radius a to correspond the point A on the ellipse. Let O be the common center of both the ellipse and the circle such that the line AQ is perpendicular on the major axis of the ellipse. When point A moves on the ellipse, the point Q moves on the circle with angular velocity ω in the plane xy. Let A begin the motion at the initial moment $t = 0$ in an anticlockwise direction. After a time t, the coordinates of the point A becomes (x_A, y_A) such that

$$\omega t = \cos^{-1}\left(\frac{x_A}{a}\right) = \sin^{-1}\left(\frac{y_A}{b}\right), \tag{1}$$

where $2a$ and $2b$ are the major and the minor axes of the ellipse, respectively. The coordinates (X, Y) of m are obtained as

$$\omega t = \cos^{-1}\left[\frac{(X - \ell\cos\Phi)}{a}\right] = \sin^{-1}\left[\frac{(Y - \ell\sin\Phi)}{b}\right], \tag{2}$$

where Φ is the angle between the string and the vertical axis. Assume the following parameters [12],

$$\mu = \frac{b}{\ell} >> 1, \tag{3}$$

$$a = b\nu,$$

where μ is a large parameter, that is, $\ell << b$.

Also, we assume the variables

$$\ell\omega_n^2 = g,$$

$$\omega\Omega = \omega_n,$$

$$\Phi = \mu^{-1}\varphi, \tag{4}$$

$$\frac{\tau}{\omega} = t,$$

where g is the gravity of acceleration, ω_n is the normal angular velocity, and φ is the generalized coordinate for the problem.

2.1. Equation of Motion.
Using Lagrange's equation, we get the equation of motion of the pendulum in the form as follows:

$$\frac{d}{d\tau}\left[\frac{\partial(T - V)}{\partial\varphi'}\right] - \left[\frac{\partial(T - V)}{\partial\varphi}\right] = 0, \tag{5}$$

where T is the kinetic energy and V is the potential one. Substituting (2), (3), and (4) into (5), we get

$$\varphi'' + \Omega^2\varphi = \sin\tau - \mu^{-1}\nu\varphi\cos\tau - 0.5\mu^{-2}\varphi^2\sin\tau + 0.17\mu^{-3}\nu\varphi^3\cos\tau. \tag{6}$$

The solution of this equation means that we obtain φ in terms of the large parameter and the time.

2.2. Approximate Periodic Solution.
Now, we will find the approximated periodic solutions for the nonresonance case [12]; that is Ω is irrational value. However, here we use the large parameter technique instead of the small one which was used previously. The solutions of (6) are obtained in the form of power series expansions of powers of $1/\mu$ as follows:

$$\varphi(\tau, \mu) = \varphi_0(\tau) + \mu^{-1}\varphi_1(\tau) + \mu^{-2}\varphi_2(\tau) + \mu^{-3}\varphi_3(\tau) + \ldots. \tag{7}$$

Substituting from (7) into (6) and equating coefficients of like powers of $(1/\mu)$ of both sides, we get a system of differential equations containing $\varphi_i, i = 1, 2, 3, \ldots$, which is solved to obtain the following:

$$\left(\Omega^2 - 1\right)\varphi\left(\tau, \mu\right) = \sin\tau - \mu^{-1}\frac{\nu}{\left(\Omega^2 - 4\right)}\sin\tau\cos\tau$$

$$+ \mu^{-2}\left[\frac{2\nu^2\left(\Omega^2 - 1\right) - 3\left(\Omega^2 - 4\right)}{8\left(\Omega^2 - 1\right)^2\left(\Omega^2 - 4\right)}\sin\tau + \frac{2\nu^2\left(\Omega^2 - 1\right) + \left(\Omega^2 - 4\right)}{8\left(\Omega^2 - 1\right)\left(\Omega^2 - 4\right)\left(\Omega^2 - 9\right)}\sin 3\tau\right]$$

$$+ \nu\sin 2\tau\mu^{-3}\left[\begin{array}{c}\dfrac{\left(5\Omega^4 - 62\Omega^2 + 123\right) - 3\nu^2\left(\Omega^2 - 1\right)\left(\Omega^2 - 5\right)}{12\left(\Omega^2 - 1\right)^2\left(\Omega^2 - 4\right)^2\left(\Omega^2 - 9\right)} \\ \\ -\dfrac{\left(5\Omega^4 - 44\Omega^2 + 51\right) + 3\nu^2\left(\Omega^2 - 1\right)^2}{12\left(\Omega^2 - 1\right)^2\left(\Omega^2 - 4\right)\left(\Omega^2 - 9\right)\left(\Omega^2 - 16\right)}\cos 2\tau\end{array}\right] + \cdots.$$

$$(8)$$

3. The Second Pendulum Model

In this section, we consider a rigid body pendulum of mass M suspended with a massless spring with a length $\rho(t)$ which is suspended at a point O_1 on the ellipse [3]. According to [3], the point Q moves on the auxiliary circle with constant angular velocity ω and corresponds to point O_1 on the ellipse. Consider that the circle has radius b and the angle between the line OQ and the horizontal axis depends on t only. Consider the motion in the plane xy. From [3], the point O_1 moves from $t = 0, \theta = 0$, and $\varphi = 0$ in the counterclockwise direction.

3.1. Determining of Lagrangian Function.
After a while t, the point O_1 will create an angle (ωt) with the horizontal axis, that is:

$$\omega t = \cos^{-1}\left(\frac{x_{O_1}}{a}\right) = \sin^{-1}\left(\frac{y_{O_1}}{b}\right), \tag{9}$$

where $2a$ and $2b$ are the minor and major diagonal of the ellipse, respectively.

Consider that the coordinates of the center of mass of the body are given by

$$X_c = a\cos\omega t + \rho\sin\theta + h\sin\varphi, \tag{10}$$

$$Y_c = b\sin\omega t + \rho\cos\theta + h\cos\varphi. \tag{11}$$

We calculate the velocity of the center c by differentiating (9) and (10). Consider the following parameters and variables [3]:

$$\mu = \frac{h}{d} \gg 1,$$

$$\rho(t) = d + \beta(t),$$

$$\omega_n^2 = \frac{K}{M\omega^2}, \tag{12}$$

$$J\sigma^2 = Mh\left(\frac{g}{\omega^2} + \gamma\right),$$

$$\gamma\omega^2 = \frac{K(d - l)}{M - g},$$

$$\theta = \mu^{-1}\Theta, \quad (\theta\varphi), \tag{13}$$

where d is the spring length at relative equilibrium, J denotes the principal moment of inertia for the axis $c\zeta$, l is the free length of the spring, μ is a large parameter, K is the force constant of the spring, and β, Θ, and Φ are the generalized coordinates. Use (9), (10), (11), and (13) to find the kinetic energy and potential one and then construct the Lagrangian = kinetic energy–potential one in terms of the generalized coordinates as follows:

$$
\frac{2L}{\omega^2} = M \begin{bmatrix} \beta'^2 + (d+\beta)^2 \mu^{-2}\Theta'^2 + h^2\mu^{-2}\Phi'^2 + a^2\sin^2\tau + b^2\cos^2\tau \\[2mm] +2h\beta'\mu^{-2}\Phi'\left(\begin{array}{c} \Theta - \dfrac{1}{6}\mu^{-2}\Theta^3 - \dfrac{1}{2}\mu^{-2}\Theta\Phi^2 + \dfrac{1}{12}\mu^{-4}\Theta^3\Phi^2 - \Phi + \dfrac{1}{2}\mu^{-2}\Theta^2\Phi \\[3mm] + \dfrac{1}{6}\mu^{-2}\Phi^3 - \dfrac{1}{12}\mu^{-4}\Theta^2\Phi^3 \end{array} \right) \\[6mm] +2(d+\beta)h\mu^{-2}\Theta'\Phi'\left(\begin{array}{c} 1 - \dfrac{1}{2}\mu^{-2}\Theta^2 - \dfrac{1}{2}\mu^{-2}\Phi^2 \\[3mm] + \dfrac{1}{4}\mu^{-4}\Theta^2\Phi^2 + \mu^{-2}\Theta\Phi - \dfrac{1}{6}\mu^{-4}\Theta^3\Phi - \dfrac{1}{6}\mu^{-4}\Theta\Phi^3 + \dfrac{1}{36}\mu^{-6}\Theta^3\Phi^3 \end{array} \right) \\[6mm] -2\beta'\mu^{-1}\left(a\Theta\sin\tau - \dfrac{1}{6}\mu^{-2}a\Theta^3\sin\tau - \mu b\cos\tau + \dfrac{1}{2}\mu^{-1}b\Theta^2\cos\tau \right) \\[4mm] -2(d+\beta)\mu^{-1}\Theta'\left(a\sin\tau - \dfrac{1}{2}\mu^{-2}a\Theta^2\sin\tau + \mu^{-1}b\Theta\cos\tau - \dfrac{1}{6}\mu^{-3}b\Theta^3\cos\tau \right) \\[4mm] -2h\mu^{-1}\Phi'\left(a\sin\tau - \dfrac{1}{2}\mu^{-2}a\Phi^2\sin\tau + \mu b\Phi\cos\tau - \dfrac{1}{6}\mu^{-3}b\Phi^3\cos\tau \right) \end{bmatrix}
$$
$$
+ J\mu^{-2}\Phi'^2 + Mg/\omega^2\left[(d+\beta)\left(2 - \mu^{-2}\Theta^2\right) + h\left(2 - \mu^{-2}\Phi^2\right) \right] - \frac{K(d+\beta-\ell)^2}{\omega^2}. \tag{14}
$$

3.2. Equations of Motion.

Making use of Lagrange's equations (14), (11), and (13), we get the equations of motion as follows:

$$
\beta'' + \omega_n{}^2\beta = b\sin\tau - \gamma + \mu^{-1}\left[a\Theta\cos\tau + h\Theta'^2 \right]
$$
$$
+ \mu^{-2}\left[h\left(\Phi''\Phi - \Phi''\Theta + \Phi'^2\right) + \beta\Theta'^2 + 0.5\Theta^2\left(\frac{g}{\omega^2} - b\sin\tau\right) \right], \tag{15}
$$

$$
h\Theta'' = a\cos\tau - \mu^{-1}\left[2\beta'\Theta' + \Theta\left(b\sin\tau + \frac{g}{\omega^2}\right) + h\Phi'' \right] - 0.5a\mu^{-2}\Theta^2\cos\tau, \tag{16}
$$

$$
\mu^{-1}\left[\left(h + \frac{J}{Mh}\right)\Phi'' + \frac{g}{\omega^2}\Phi \right] = a\cos\tau - h\Theta'' + \mu^{-1}\left[-2\beta'\Theta' - \beta\Theta'' + \beta''\Phi - b\Phi\sin\tau \right]
$$
$$
+ \mu^{-2}\left[-\frac{1}{2}a\Phi^2\cos\tau + \frac{1}{2}h\Theta''\left(\Theta^2 + \Phi^2\right) - h\left(\Theta''\Theta\Phi - \Theta\Theta'^2 + \Theta'^2\Phi\right) \right]
$$
$$
+ \mu^{-3}\left[(\Theta - \Phi)^2\left(\beta'\Theta' + \frac{1}{2}\beta\Theta''\right) + \beta\Theta'^2(\Theta - \Phi) + \frac{1}{6}\beta''(\Theta - \Phi)^3 + \frac{1}{6}b\Phi^3\sin\tau \right]. \tag{17}
$$

Substituting (15) and (16) into (17), we get

$$\left(\Phi'' + \sigma^2\Phi\right)J = Mh\left[\begin{array}{l}\Theta\left(g/\omega^2 + b\,\sin\tau\right) - \omega_n^{\,2}\beta\Phi + \mu^{-1}\left[\begin{array}{l}\Phi\left(a\Theta\,\cos\tau + h\Theta'^{\,2}\right)\\[6pt]+0.5a\,\cos\tau\left(\Theta^2 - \Phi^2\right) + 0.5h\Theta''\left(\Theta - \Phi\right)^2 + h\Theta'^{\,2}\left(\Theta - \Phi\right)\end{array}\right]\\[24pt]+\mu^{-2}\left[\begin{array}{l}h\Phi\Phi''\left(\Phi - \Theta\right) + \Phi\left(h\Phi'^{\,2} + b\Theta\Theta'\,\cos\tau\right) - 0.5b\Phi\,\sin\tau\left(\Theta^2 + 0.33\Phi^2\right)\\[6pt]+\dfrac{g}{\omega^2}\Theta^2\Phi + \beta'\Theta'\left(\Theta - \Phi\right)^2 + 0.5\beta\Theta''\left(\Theta - \Phi\right)^2 + \beta\Theta\Theta'^{\,2} + 0.17\beta''\left(\Theta - \Phi\right)^3\end{array}\right]\end{array}\right]. \tag{18}$$

Equations (15),(16), and (18) are a quasilinear system of the second order which describes the pendulum equations for this model. We aim to solve this system by a new procedure named the large parameter method [11] to get the approximated periodic solutions.

3.3. *Approximate Periodic Solutions.* In this section, we search the approximated periodic solutions for the case of nonresonance using the large parameter technique. Assuming the solutions for (15–18), the following is obtained:

$$\beta(\tau,\mu) = \beta_0 + \mu^{-1}\beta_1 + \mu^{-2}\beta_2 + \ldots, \tag{19}$$

$$\Theta(\tau,\mu) = \Theta_0 + \mu^{-1}\Theta_1 + \mu^{-2}\Theta_2 + \ldots, \tag{20}$$

$$\Phi(\tau,\mu) = \Phi_0 + \mu^{-1}\Phi_1 + \mu^{-2}\Phi_2 + \ldots. \tag{21}$$

Substituting (18), (19), and (20) into (15), (16), and (18) and equating coefficients of same powers of μ in both sides,

we get a system of nine equations which give the following solutions [3]:

$$\beta(\tau,\mu) = \frac{b}{\omega_n^2 - 1}\sin\tau - \frac{\gamma}{\omega_n^2} - \mu^{-1}\frac{a^2}{h\left(\omega_n^2 - 4\right)}\cos 2\,\tau + \ldots,$$

$$\Theta(\tau,\mu) = -\frac{a}{h}\cos\tau + \mu^{-1}\left(a\,\sin 2\,\tau - \Gamma\,\cos\tau\right) + \ldots, \tag{22}$$

$$\Phi(\tau,\mu) = -\left(\frac{Ma}{J}\right)\left[\frac{g}{\omega^2\left(\sigma^2 - 1\right)}\cos\tau - \frac{b}{2\left(\omega_n^2 - 1\right)\left(\sigma^2 - 4\right)}\sin 2\,\tau\right] + \ldots.$$

The force of the spring will be

$$F = k\left[d - \left(l + \frac{\gamma}{\omega_n^2}\right) + \frac{b}{\omega_n^2 - 1}\sin\tau - \mu\frac{a^2}{h\left(\omega_n^2 - 4\right)}\cos 2\,\tau + \ldots\right]. \tag{23}$$

4. Numerical Considerations

In this section, we treat the previously mentioned models by nine programs for obtaining both the analytical and the numerical solutions for different cases of the motions. We use the fourth-order Runge–Kutta method for obtaining the numerical solutions for systems of motions of the different problems. So, we obtain five tables of results and 33 figures for a description of the motions at different values of the

pendulum parameters. These tables and figures describe the behavior of the motion and the influence of the different parameters on the solutions.

4.1. *The Numerical Considerations of the First Model.* In this section, we discuss the analytical and numerical solutions for the first model mentioned above. We compare these solutions, and we will discuss the maximum value of the angle Φ. We divide the problem into the following cases.

4.1.1. *The First Case* ($\nu = 0\ and\ \mu = 5000$). Since $\nu = a/b = 0$, then $a = 0$, that is, the pendulum moves horizontally on a straight line of length $2b$ [13]. From Table 1, we note that the amplitude of the vibrations and the angular velocity decrease when Ω increases. Also, we note from the table that for every

TABLE 1: φ_{max} of the first case $(\nu = 0, \mu = 5000)$.

Ω	analytical φ_{max}	numerical φ_{max}
2.1	0.2933488	0.2930785
2.3	0.2331735	0.2331879
2.5	0.1905422	0.1905665
2.7	0.1590564	0.1590581
2.8	0.146291	0.1463126
3.1	0.1160335	0.1161796
3.3	0.1010852	0.1011365
3.5	0.08887673	0.08893137
3.7	0.07879558	0.07887411
4.1	0.06324854	0.06334555
4.3	0.0571738	0.05724992
4.5	0.05194685	0.05202674
4.7	0.04741498	0.0474991
5.2	0.03840205	0.03847147
5.4	0.03551105	0.03557474

value of Ω there is a great value for Φ (the angle between the pendulum rib and the vertical axis). This case is represented (see Figure 2).

At the initial moment $(\tau = 0)$, the pendulum is suspended at point O and its rib is represented by the vector $\underline{OB}$, i.e., $(\Phi = 0)$. The angle Φ increases counterclockwise until it reaches the maximum value when the suspension point is at $A(\tau = \pi/2)$. At $\tau = \pi$ the suspension, the point returns to the initial position O. Then, the angle Φ increases in a clockwise direction until it reaches its maximum value at the point $A'(\tau = 3\pi/2)$. The suspension point will then be directed towards the point O until it reaches the initial position $(\tau = 2\pi)$. In this case, the graphical representations of analytical and numerical solutions appear (see Figures 3 and 4).

4.1.2. The Second Case $(\nu = 1 \ and \ \mu = 5000)$.
In this case, $\nu = a/b = 1$ and then $a = b$; this means that the point of suspension of the pendulum moves on a circle of radius a. It is obvious from Table 2 that when the value of Ω increases, the angular velocity decreases and the amplitude of the vibrations decreases. The movement of the suspension point on the circumference of a circle can be illustrated (see Figure 5). At the initial moment $(\tau = 0)$, the point of suspension of the pendulum is at S and its rib is represented by the vector $\underline{SB}$, i.e., $(\Phi = 0)$. Then, the pendulum's suspension point moves counterclockwise towards point A. The angle Φ increases counterclockwise until it reaches the maximum value when the suspension point is at $A(\tau = \pi/2)$. When the suspension point reaches the point $S'(\tau = \pi)$, the angle Φ becomes zero and the pendulum rib becomes vertical again. Then, the angle Φ increases until it reaches its maximum value at the point $A'(\tau = 3\pi/2)$. After that, the suspended point will be directed towards point S until it reaches the primary position $(\tau = 2\pi)$ and completes the period. As for this case, the graphical representations for both analytical and numerical solutions appear (see Figures 6 and 7).
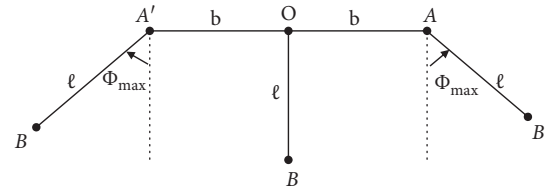
FIGURE 2: Description of the pendulum motion for case (i) in Section 4.1.
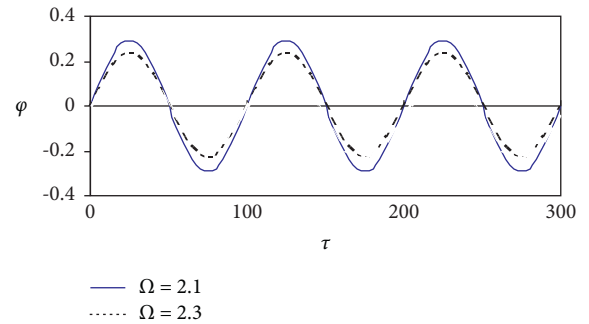
FIGURE 3: The analytical solutions for case (i) in Section 4.1.
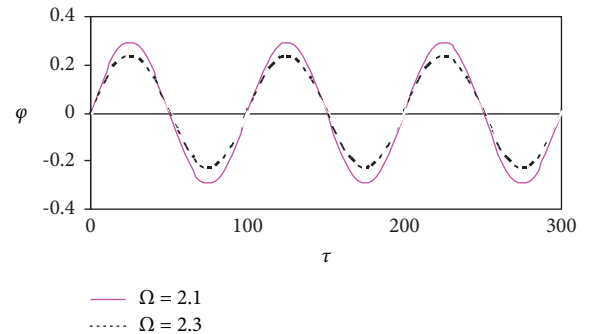
FIGURE 4: The numerical solutions for case (i) in Section 4.1.

TABLE 2: φ_{max} of the second case $(\nu = 1, \mu = 5000)$.

Ω	$\varphi_{max}^{analytical}$	$\varphi_{max}^{numerical}$
2.1	0.3213152	0.3233396
2.3	0.2336605	0.2339807
2.5	0.19085	0.1909746
2.7	0.159339	0.1591531
2.8	0.1466192	0.1466426
3.1	0.1156941	0.1158647
3.3	0.1010075	0.1010626
3.5	0.08884358	0.0889034
3.7	0.07877824	0.07885911
4.1	0.06324223	0.06336687
4.3	0.05716965	0.0572462
4.5	0.05194401	0.05202422
4.7	0.04741298	0.0474967
5.2	0.03840113	0.03846995
5.4	0.03551035	0.03557364

FIGURE 7: The numerical solutions for case (ii) in Section 4.1.

TABLE 3: φ_{max} of the third case $(\nu = 1.5, \mu = 5000)$.

Ω	$\varphi_{max}^{analytical}$	$\varphi_{max}^{numerical}$
2.1	0.3433021	0.3466265
2.3	0.2382122	0.2389854
2.5	0.1912348	0.1914796
2.7	0.1596922	0.1597867
2.8	0.1470294	0.1470511
3.1	0.1152698	0.1154751
3.3	0.1009105	0.1009705
3.5	0.08880214	0.08886883
3.7	0.07875657	0.07884256
4.1	0.06323432	0.06333476
4.3	0.05716445	0.0572428
4.5	0.05194046	0.05202207
4.7	0.04741048	0.04749489
5.2	0.03839997	0.03846891
5.4	0.03550947	0.03557289

FIGURE 5: Description of the pendulum motion for case (ii) in Section 4.1.
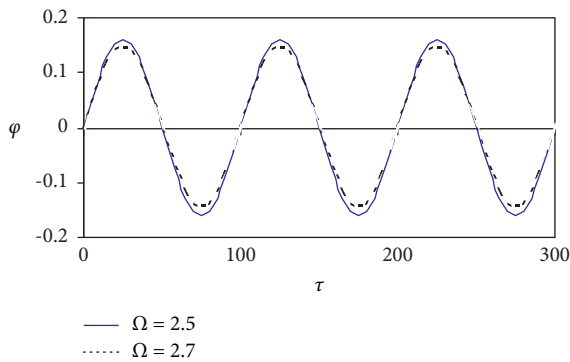
FIGURE 6: The analytical solutions for case (ii) in Section 4.1.
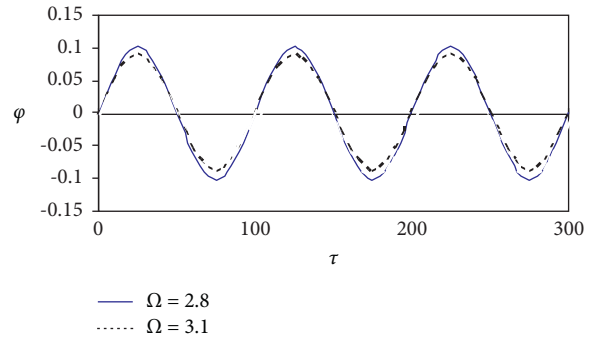
FIGURE 8: The analytical solutions for case (iii) in Section 4.1.

4.1.3. The Third Case $(\nu = 1.5 \, and \, \mu = 5000)$. It is clear from Table 3 that the amplitude of the vibrations decreases when the value of Ω increases and thus the angular velocity decreases. The graphical representations of the analytical and numerical solutions are shown (see Figures 8 and 9).

4.1.4. The Fourth Case $(\Omega = 1.5 \, and \, \mu = 1250)$. Table 4 shows the analytical and numerical solutions of different values of ν belonging to the period [0, 1]. From Table 4, we conclude that the higher the value μ makes the smaller the amplitude of the vibrations. The graphical representations for this case are obtained (see Figures 10 and 11).

4.1.5. The Fifth Case $(\Omega = 2.5 \, and \, \mu = 1250)$. Table 5 gives the analytical and numerical solutions for different values of ν belonging to the period [0, 1]. We conclude that the higher
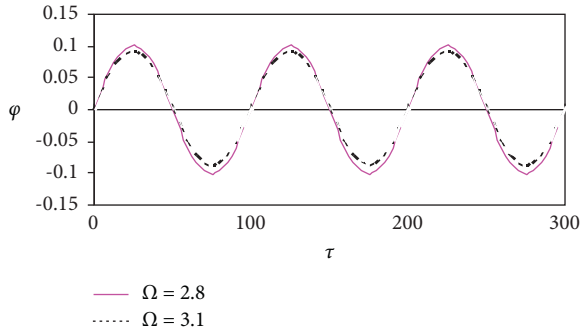
FIGURE 9: The numerical solutions for case (iii) in Section 4.1.

TABLE 5: $\varphi_{\max}$ of the fifth case $(\Omega = 2.5, \mu = 1250)$.

ν	analytical $\varphi_{\max}$	numerical $\varphi_{\max}$
0	0.1904803	0.190602
0.1	0.1904805	0.1906011
0.2	0.1904811	0.1906013
0.3	0.1904821	0.1906015
0.4	0.1904834	0.1906024
0.5	0.1904851	0.1906038
0.6	0.1904873	0.1906058
0.7	0.1904897	0.1906083
0.8	0.1904926	0.1906113
0.9	0.1904959	0.1906149
1	0.1904996	0.1906189

TABLE 4: $\varphi_{\max}$ of the fourth case $(\Omega = 1.5, \mu = 1250)$.

ν	analytical $\varphi_{\max}$	numerical $\varphi_{\max}$
0	0.8000296	0.8000393
0.1	0.8000292	0.800032
0.2	0.800028	0.8000173
0.3	0.8000258	0.7998232
0.4	0.8000228	0.7998127
0.5	0.8000191	0.799799
0.6	0.8000144	0.799782
0.7	0.8000089	0.7997616
0.8	0.8000026	0.7997379
0.9	0.7999954	0.7997114
1	0.7999873	0.7996807
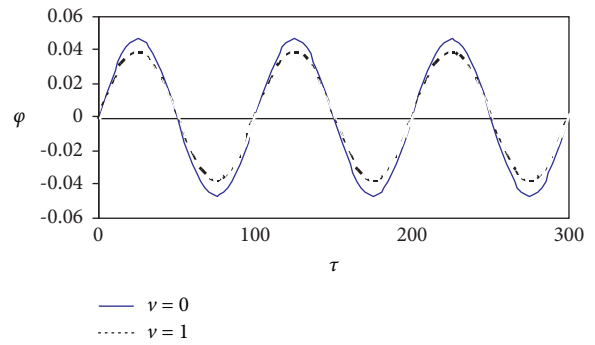
FIGURE 12: The analytical solutions for case (v) in Section 4.1.

the value ν, the slower the amplitude of the vibrations will increase. From Table 5, we find that the difference between numerical and analytical results is very small and can be neglected. Moreover, the graphic representations of this case are shown (see Figures 12 and 13).

4.2. The Numerical Considerations of the Second Model.
This section will be devoted to verifying the accuracy of the analytical solutions resulting in the second model mentioned above by using computer programs. These solutions will be represented graphically in several cases as follows.

4.2.1. The First Case $(b = 0 \text{ and } \mu = 2500)$.
Since $b = 0$, this means that the movement of the pendulum is horizontal along its longitude $2a$. This is evident from the graphical representations of the analytical solutions shown through the graphs (see Figures 14–16). In this case, we note the stability of the solutions that we obtained as evidence (see Figures 17–19).

4.2.2. The Second Case $(a = b \text{ and } \mu = 2500)$.
In this case, the point of suspension of the pendulum moves over a circle of radius a. We obtain the graphic representations of the analytical solutions in a suitable manner of the case (i) (see Figures 20–22). We note the stability of solutions in this case, as evidenced (see Figures 23–25).

FIGURE 10: The analytical solutions for case (iv) in Section 4.1.

FIGURE 11: The numerical solutions for case (iv) in Section 4.1.
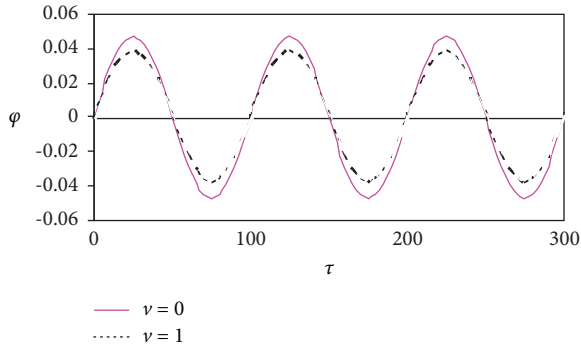
Figure 13: The numerical solutions for case (v) in Section 4.1.

Figure 14: The analytical solution β for case (i) in Section 4.1.

Figure 15: The analytical solution Θ for case (i) in Section 4.2.

Figure 16: The analytical solution Φ for case (i) in Section 4.2.
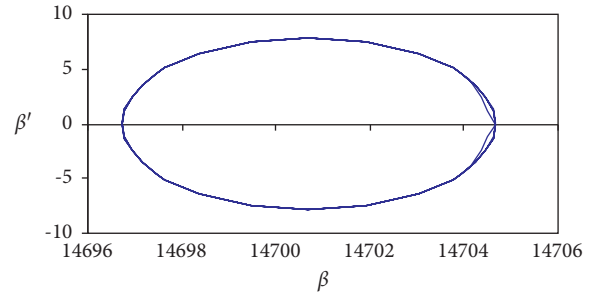
Figure 17: The stability phrase β' and β for case (i) in Section 4.2.
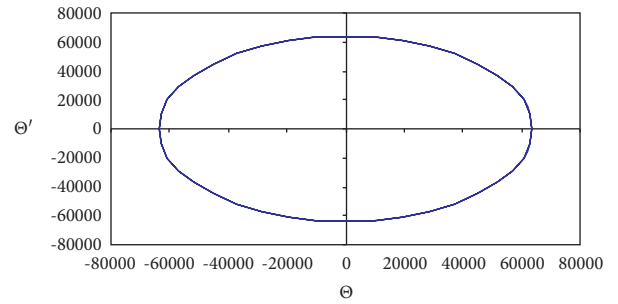
Figure 18: The stability phrase Θ' and Θ for case (i) in Section 4.2.
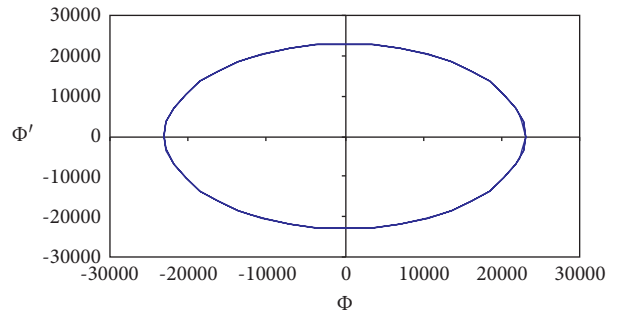
Figure 19: The stability phrase Φ' and Φ for case (i) in Section 4.2.
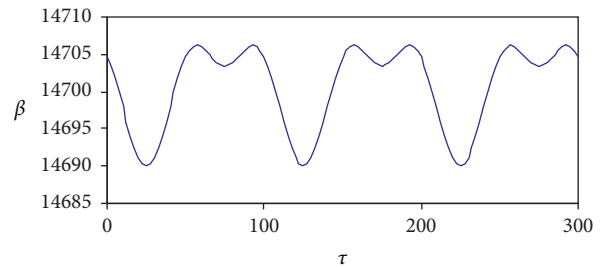
Figure 20: The analytical solution β for case (ii) in Section 4.2.
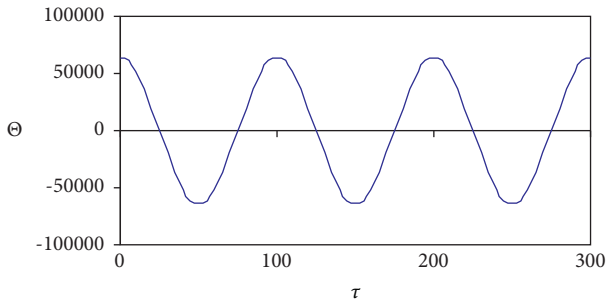
Figure 21: The analytical solution Θ for case (ii) in Section 4.2.

Figure 22: The analytical solution Φ for case (ii) in Section 4.2.

Figure 23: The stability phrase β' and β for case (ii) in Section 4.2.

Figure 24: The stability phrase Θ' and Θ for case (ii) in Section 4.2.

Figure 25: The stability phrase Φ' and Φ for case (ii) in Section 4.2.
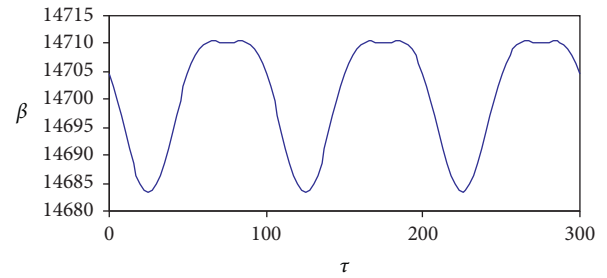
Figure 26: The analytical solution β for case (iii) in Section 4.2.
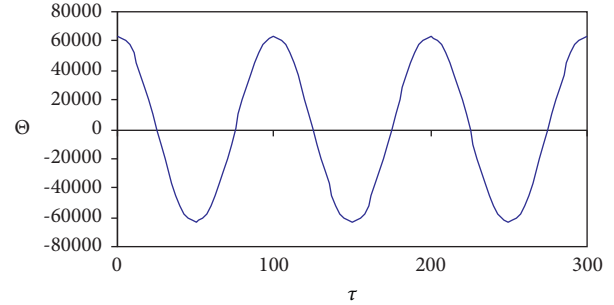
Figure 27: The analytical solution Θ for case (iii) in Section 4.2.
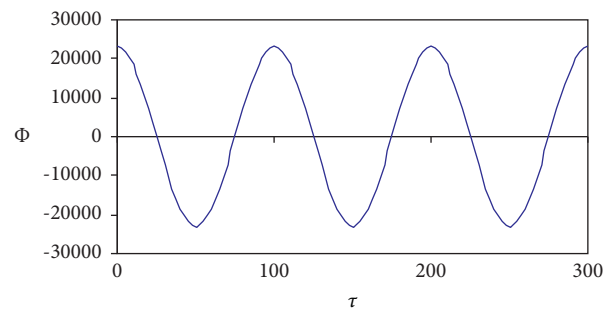
Figure 28: The analytical solution Φ for case (iii) in Section 4.2.
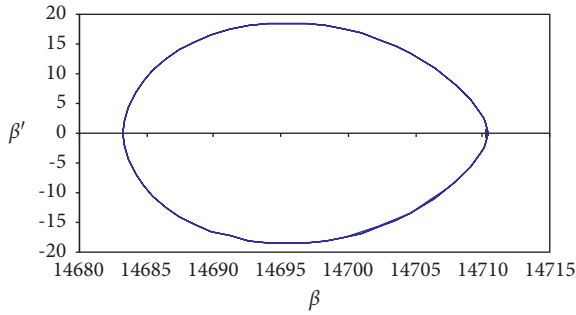
FIGURE 29: The stability phrase β' and β for case (iii) in Section 4.2.

FIGURE 30: The stability phrase Θ' and Θ for case (iii) in Section 4.2.
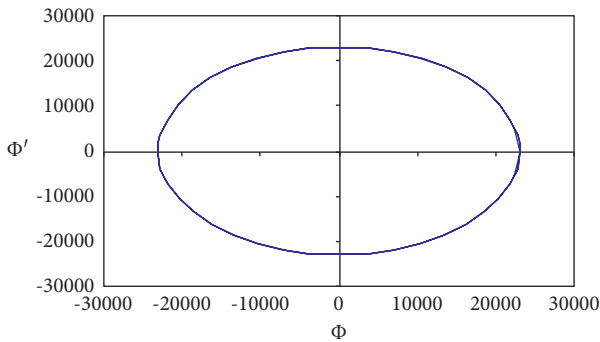
FIGURE 31: The stability phrase Φ' and Φ for case (iii) in Section 4.2.
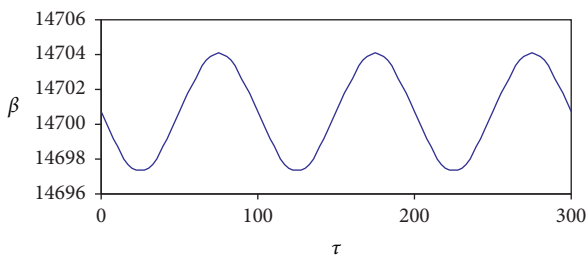
FIGURE 32: The analytical solution β for case (iv) in Section 4.2.

4.2.3. The Third Case ($b = 2a \, and \, \mu = 2500$). In this case, the pendulum's suspension point moves on the ellipse of its largest and minimum axial as a and b, respectively. Concerning this case, the graphic representations of the analytical solutions appear suitably for case (i) (see

FIGURE 33: The stability phrase β' and β for case (iv) in Section 4.2.

Figures 26–28). We note the stability of solutions in this case, as evidenced (see Figures 29–31).

4.2.4. The Fourth Case ($a = 0$). The pendulum, in this case, moves vertically along a vertical line along its length, and the graphic representations of the analytical solutions are represented (see Figure 32). In this case, we note the stability of the solutions as shown (see Figure 33). In this case, we deduce that $\Theta(\tau) = \Phi(\tau) = 0$.

5. Conclusions

Two new models have been introduced for the movement of the pendulum in the presence of new primary conditions that are not previously defined. Poincare's method fails to solve these problems in the presence of the new condition so we must search for a new technique that matches these changes. A large parameter was defined to achieve a large parameter method for solving this problem under the new assumptions. The equations for the motility of the models are deduced and solved using the large parameter method for obtaining the solutions analytically. The fourth-order Ronge–Kutta numerical method is presented for solving the system of equations numerically through computer programs. Also, numerical and analytical solutions were compared by 5 tables and 33 graphs. It turned out that the analytical solutions conform to the numerical solutions, which proves the validity of the serious methods used in the solutions. The solutions stabilities are given by the phase diagrams procedure. This paper is a generalization of many previous works. The two models are classified into nine cases depending on the parameters of the motion. From this, we conclude that the cases studied were implemented in research [6, 7, 10, 13]. There are generalized cases of the pendulum movement because of introducing the coherent body instead of the particle as well as the movement on an ellipse instead of moving on a circle and taking a flexible wire instead of a string. The previous solutions are obtained as special cases of solutions in this paper. We also conclude the following points:

(1) The approximate periodic solutions are obtained using the large parameter method because Poincare's technique is failed in this case

(2) The amount of angular velocity in the case of nonresonant vibrations must take no integer values to avoid the singularity in the solution

(3) The approximate periodic solutions were obtained in terms of periodic functions.

Data Availability

Conflicts of Interest

The authors declare that there are no conflicts of interest.

Authors' Contributions

AI carried out the design of the article and the immunoassays, participated in the sequence alignment, analyzed and interpreted the methods, performed the results, concluded the study, was a major contributor in writing the manuscript, and conceived and coordinated the study. HA carried out the numerical analysis, participated in writing and revising the sequence alignment, drafted the manuscript, participated in the design of the study, and performed the numerical analysis. All authors read and approved the final manuscript.

Acknowledgments

References

[1] F. A. El-Barki, A. I. Ismail, M. O. Shaker, and T. S. Amer, "On the motion of the pendulum on an Ellipse," *Zeitschrift für Angewandte Mathematik und Mechanik*, vol. 79, no. 1, pp. 65–72, 1999.

[2] S. J. Liao, "A second-order approximate analytical solution of a simple pendulum by the process analysis method," *Journal of Applied Mechanics*, vol. 59, no. 4, pp. 970–975, 1992.

[3] A. I. Ismail, "Relative periodic motion of a rigid body pendulum on an ellipse," *Journal of Aerospace Engineering*, vol. 22, no. 1, 2009.

[4] W. S. Amer, M. A. Bek, and M. K. Abohamer, "On the motion of a pendulum attached with tuned absorber near resonances," *Results in Physics*, vol. 11, pp. 291–301, 2018.

[5] T. S. Amer, B. Ma, and I. S. Hamada, "On the motion of harmonically excited spring pendulum in the elliptic path near resonances," *Advances in Mathematical Physics*, 2016.

[6] N. V. Stoianov, "On the relative periodic motions of a pendulum," *Journal of Applied Mathematics and Mechanics*, vol. 28, no. 1, pp. 160–163, 1964.

[7] A. Werner and C. J. Eliezer, "The lengthening pendulum," *Journal of the Australian Mathematical Society*, vol. 9, no. 3-4, pp. 331–336, 1969.

[8] A. H. Nayfeh, "A perturbation method for treating nonlinear oscillation problems," *Journal of Mathematics and Physics*, vol. 44, no. 1-4, pp. 368–374, 1965.

[9] W. K. Tso and K. G. Asmis, "Parametric excitation of a pendulum with bilinear hysteresis," *Journal of Applied Mechanics*, vol. 37, no. 4, pp. 1061–1068, 1970.

[10] B. A. Schmidt, "The radially flexible pendulum subjected to a high-frequency excitation," *Journal of Applied Mechanics*, vol. 50, no. 2, pp. 443–448, 1983.

[11] A. I. Ismail, "Solving a problem of rotary motion for a heavy solid using the large parameter method," *Advances in Astronomy*, vol. 2020, Article ID 2764867, 7 pages, 2020.

[12] T. Van Baak, "A new and wonderful pendulum period equation (PDF)," *Horological Science Newsletter*, vol. 2013, no. 5, pp. 22–30, 2013.

[13] K. Ochs, "A comprehensive analytical solution of the nonlinear pendulum," *European Journal of Physics*, vol. 32, no. 2, pp. 479–490, 2011.

WILEY | Hindawi

Research Article

A New Chaotic System with Only Nonhyperbolic Equilibrium Points: Dynamics and Its Engineering Application

Maryam Zolfaghari-Nejad [ID],[1] **Mostafa Charmi** [ID],[1] **and Hossein Hassanpoor** [ID][2,3]

[1]*Department of Electrical Engineering, Faculty of Engineering, University of Zanjan, Zanjan, Iran*
[2]*Department of Cognitive Sciences, Dade Pardazi Shenakht Mehvare Atynegar (DSA) Institute, Tehran, Iran*
[3]*Department of Medical Engineering, Energy Institute of Higher Education, Saveh, Iran*

Correspondence should be addressed to Mostafa Charmi; charmi.mostafa@znu.ac.ir

In this work, we introduce a new non-Shilnikov chaotic system with an infinite number of nonhyperbolic equilibrium points. The proposed system does not have any linear term, and it is worth noting that the new system has one equilibrium point with triple zero eigenvalues at the origin. Also, the novel system has an infinite number of equilibrium points with double zero eigenvalues that are located on the z-axis. Numerical analysis of the system reveals many strong dynamics. The new system exhibits multistability and antimonotonicity. Multistability implies the coexistence of many periodic, limit cycle, and chaotic attractors under different initial values. Also, bifurcation analysis of the system shows interesting phenomena such as periodic window, period-doubling route to chaos, and inverse period-doubling bifurcations. Moreover, the complexity of the system is analyzed by computing spectral entropy. The spectral entropy distribution under different initial values is very scattered and shows that the new system has numerous multiple attractors. Finally, chaos-based encoding/decoding algorithms for secure data transmission are developed by designing a state chain diagram, which indicates the applicability of the new chaotic system.

1. Introduction

In recent decades, particular attention has been paid to the chaos that arises in nonlinear dynamic systems. This is due to various potential applications of chaotic systems in science and engineering fields. With special attention accorded to chaotic dynamics, many researchers strive to develop new chaotic systems with interesting properties and complex behaviors SPROTT [1]. Recently, some chaotic systems are reported with different characteristics of equilibrium points Sprott [2], with no equilibria Zhang et al. [3], only stable equilibrium point Deng et al. [4], with different shapes of equilibria Pham et al. [5], and with a line equilibrium Jafari and Sprott [6].

The equilibrium point of the system is defined as the simplest possible solution of its differential equation $\dot{x}(t) = f((x)) = 0$. The equilibrium points could be hyperbolic or nonhyperbolic. If all eigenvalues of the corresponding Jacobian matrix have nonzero real parts, the equilibrium of the system is hyperbolic. In these systems, the existence of

chaos is proved by using the Shilnikov theorem Lawande and Maiti [11]. According to the Shilnikov theorem, a system must have at least one equilibrium point of saddle-focus type with three eigenvalues γ, $\delta \pm i\omega$ that should satisfy $\gamma\delta < 1$, $|\gamma| > |\delta| > 0$, and $\omega \neq 0$. Suppose that there are homoclinic/heteroclinic orbits; then, chaos can be shown to exist (Kingni et al. [12]; Leonov [13]). In contrast, if at least one of the real parts of the corresponding eigenvalues is zero, the equilibrium is nonhyperbolic Izhikevich [14]. So far, a few chaotic systems with nonhyperbolic equilibrium points, namely, non-Shilnikov chaotic systems, are formulated and studied (Li and Xiong [10]; Cai et al. [8]; Singh and Roy [15]). For example, a new Lorenz-like chaotic system with two nonhyperbolic equilibrium points of the type double zero eigenvalues is introduced in Kamdem Kuate et al. [7]. Also, a grid multiwing chaotic system with nonhyperbolic equilibria is investigated in Zhang et al. [3]. In Chen et al. [9], a 3D chaotic system with only one equilibrium point at the origin is proposed that has three zero eigenvalues. The reported non-Shilnikov chaotic

systems with various nature of equilibrium points and several types of nonlinearities are given in Table 1. To the best of our knowledge, there has been little research on nonhyperbolic equilibria with triple or double zero eigenvalues in dynamical systems.

In the investigation of chaos theory, it is important to design new chaotic systems with some interesting phenomena such as period-subtracting phenomenon by Zolfaghari-Nejad et al. [16], multistability Dong et al. [17], antimonotonicity Liu and Iu [18]; the phenomena of asymmetric bistability by Li et al. [19]; hidden chaotic attractor by Jahanshahi et al. [20]; and some features related to their equilibria. A system is called multistable if there are different coexisting attractors in the constant parameters and various initial conditions by Jafari and Kapitaniak [21]. It is generally believed that the system with coexisting attractors has better flexibility and plasticity in performance (Lai et al. [22]). In Li and Sprott [23], Pisarchik and Grebogi [24], and Li et al. [25], the authors gave a comprehensive analysis of the coexisting attractors in Lorenz systems. In Lai et al. [22], the authors consider creating a new autonomous chaotic system with many coexisting attractors. The system in Lai et al. [22] generates multiple coexisting attractors by increasing the number of equilibrium points, but no application is mentioned for them. It is well recognized from different works that multiple coexisting attractors depend on the number of equilibrium points. As a result, some periodic functions like sine can be used to design chaotic systems with multiple coexisting attractors such as Lai et al. [26] and Li et al. [25].

The phenomenon of antimonotonicity is observed in various nonlinear systems such as Kengne et al. [27], Kingni et al. [28], and Signing et al. [29]. In this phenomenon, periodic orbits can be yielded from period-doubling bifurcation and then annihilated via reverse period-doubling as a control parameter is slowly altered.

In general, chaotic systems have a linear term in addition to a nonlinear one Kengne et al. [30]. Chaotic systems without linear terms have rarely been investigated in the literature Zhang et al. [31], Xu and Wang [32], Pham et al. [33], and Vaidyanathan [34]. A simple chaotic system without linear terms is proposed in Pham et al. [35]. Furthermore, a chaotic system with only quadratic and constant terms is introduced in Mobayen et al. [36].

A chaotic system is used in many engineering applications in Guanrong [37]. The most valuable application is secure communication. During the past few years, many chaotic substitution boxes (S-box) have been proposed such as Çavuşoğlu et al. [38], Wang et al. [39], García-Guerrero et al. [40], and Ullah et al. [41]. S-box is the most basic unit in encryption algorithms (Mobayen et al. [42]). On the other hand, some applications have used chaotic systems to achieve secure data transmission as in Gan et al. [43], Tirandaz and Karami-Mollaee [44], Dhall et al. [45], and Nesa et al. [46] and image encryption as in Shaukat et al. [47]. Data confidentiality is obligatory during transmission, especially in the military, medical, and financial applications (Noura et al. [48]). In this work, we propose chaos-based encoding/decoding algorithms for a secure data transmission scheme using the novel chaotic system.

In this paper, a new three-dimensional chaotic system with only nonhyperbolic equilibrium points is introduced. The main characteristics of the system can be summarized as follows: (i) the novel system has triple zero eigenvalues at the origin; (ii) the system has many equilibria with double zero eigenvalues; (iii) the chaotic system does not have any linear term; (iv) the new system has no reflection symmetry property about any axis; (v) the phenomenon of infinite coexistence of multiple periodic, limit cycle, and chaotic attractors is observed; (vi) this system can exhibit antimonotonicity phenomena such as chaotic bubbles and period-2 bubbles; (v) it has very scattered spectral entropy (SE) distribution under different initial values. Furthermore, we address chaos-based encoding and decoding algorithms for a secure data transmission scheme by designing a state chain (SC) diagram, which indicates the applicability of the new chaotic system.

The rest of this paper is organized as follows. In Section 2, we describe the chaotic mathematical model and analyze the equilibrium points. In Section 3, we will show the nonlinear characteristics of the system in terms of bifurcation diagrams, Lyapunov exponents (LEs) spectrum, phase portrait, and spectral entropy (SE) distributions. In Section 4, we describe the details of the engineering application of the proposed system comprising chaos-based encoding/decoding algorithms for a secure data transmission scheme. The performance of this scheme is analyzed in Section 5. Finally, the conclusion of the current research work is summarized in Section 6.

2. Description and Analysis of the Proposed System

2.1. The System Model. The structure of the proposed system is as follows:

$$\dot{x} = -p_1 x^3 + p_2 y^3 + p_3 xz^2,$$
$$\dot{y} = p_4 \sin(xy - z) - p_5 x^3, \qquad (1)$$
$$\dot{z} = p_6 \sin(xyz) + p_7 \sin(x),$$

where (x, y, z) are state variables and p_i $(i = 1, 2, \ldots, 7)$ are (real) positive parameters of the system. System (1) is a third-order autonomous with seven nonlinearity terms. Notice that the nonlinearity terms are either sine or cubic. It is clearly seen the chaotic system does not have any linear or constant term. System (1) has no reflection symmetry property about any axis, which indicates the system could not have bistability or symmetric attractors.

When the parameters are set to $(p_1, p_2, p_3, p_4, p_5, p_6, p_7) = (3.964, 7, 7, 5, 4.5, 2.9, 1)$ and the initial value is set as $(x_0, y_0, z_0) = (-1, -1, -1)$, the proposed system generates a chaotic attractor. In this case, the three Lyapunov exponents are calculated as $LE_1 = 0.2603$, $LE_2 = 0.002$, and $LE_3 = -5.491$ (by using ode45 numerical solver and the simulation time $T = 1000$ s). At this initial value, the fractional Kaplan-York dimension is $D_{KY} = 2 + ((LE_1 + LE_2))/(|LE_3|) = 2.0478$, which confirms the chaotic behavior $(D_{KY} > 2)$. Figure 1 shows the corresponding phase portraits of this strange attractor in x-y, x-z, and y-z planes, from left to right, respectively.

TABLE 1: Type of nonlinearities in non-Shilnikov chaotic systems with various nature of their equilibria.

Reference of papers	Type of nonlinearities	Nature/number of equilibrium points
Kamdem Kuate et al. [7]	Absolute value and signum	Double zero eigenvalues/2
Cai et al. [8]	Quadratic and absolute value	One pair of pure-imaginary eigenvalues/Infinite
Chen et al. [9]	Quadratic	Triple zero eigenvalues/1
Li and Xiong [10]	Quadratic and exponential	One pair of pure-imaginary eigenvalues/2
This work	Sine and cubic	Double and triple zero eigenvalues/Infinite

(a)

(b)

(c)
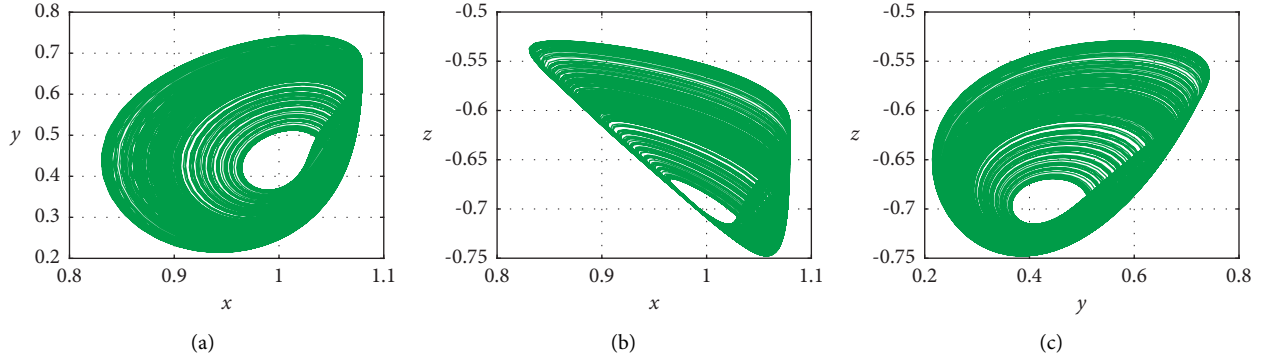
FIGURE 1: Phase portraits of the system with $(p_1, p_2, p_3, p_4, p_5, p_6, p_7) = (3.964, 7, 7, 5, 4.5, 2.9, 1)$ and initial value $(-1, -1, -1)$ projected on (a) x-y plane, (b) x-z plane, and (c) y-z plane.

2.2. Analysis of Equilibrium Points. Suppose that $P(x_*, y_*, z_*)$ is the equilibrium point of the system (1); then,

$$-p_1 (x_*)^3 + p_2 (y_*)^3 + p_3 x_* (z_*)^2 = 0,$$
$$p_4 \sin(x_* y_* - z_*) - p_5 (x_*)^3 = 0, \qquad (2)$$
$$p_6 \sin(x_* y_* z_*) + p_7 \sin(x_*) = 0.$$

We have a system with nonlinear equations and three unknowns. Nonlinear equations cannot be solved analytically in general. We used Newton's method for solving this system, which involves using the Jacobian matrix. Newton's method is one of the most popular numerical methods and is referred to in Courtney [49]. By solving equation (2), we have $x_* = y_* = 0$ and $z_* = k\pi$ ($k = 0, \pm 1, \pm 2, \pm 3, \pm 4, \ldots$). It is clear that one equilibrium point is located at the origin, and the others are located on the z-axis. The Jacobian matrix is obtained by the linearizing system (1) at $P(x_*, y_*, z_*)$ as

$$J = \begin{bmatrix} p_3 z_*^2 & 0 & 0 \\ 0 & 0 & -p_4 \cos(z_*) \\ p_7 & 0 & 0 \end{bmatrix}. \qquad (3)$$

The characteristic equation of J is

$$\lambda^3 - p_3 (z_*)^2 \lambda^2 = 0, \qquad (4)$$

Equation (4) has triple zero eigenvalues in its equilibrium point at the origin. This equilibrium point is nonhyperbolic and characterized by a 3D center manifold. Also, the corresponding eigenspace gives rise to a slow manifold. In Jiang et al. [50], Gamero et al. [51], and Freire et al. [52], some methods have been suggested to derive the normal forms on the center manifold, which can be used to study the dynamics near triple zero eigenvalues. The stability of this

equilibrium point cannot be determined under the Shilnikov criteria. So, the stability of this case is investigated numerically by tracking the final state of the system with initial values around the equilibrium point (Faghani et al. [53]). The result of this investigation shows that the origin is unstable.

The characteristic equation (4) indicates that the Jacobian matrix (3) has double zero eigenvalues ($\lambda_{1,2} = 0$) and one nonzero eigenvalue $\lambda_3 = p_3 k^2 \pi^2$ for the other equilibrium points. λ_3 is always positive since p_3 is a positive real parameter. So, these equilibria ($P(0, 0, k\pi), k \in \mathbb{Z}$ and $k \neq 0$) are nonhyperbolic and characterized by a 2D center manifold and 1D stable manifold. The numerical investigations show that all equilibrium points are unstable. An equilibrium point is stable when trajectories starting in its proximity remain close or converge toward it.

3. Numerical Analysis of the New System

In this section, we will show the dynamical behaviors of system (1). The use of well-known tools such as bifurcation diagram, Lyapunov Exponents (LEs) spectrum, phase portrait, and SE complexity helps us to demonstrate the chaotic behavior of the proposed system. The largest LE is an important tool for detecting chaos. SE algorithm is a powerful measure of the chaotic characteristics of the system Liu et al. [54]. Here, all the simulations are made by using numerical tools based on an ode45 solver with a time step fixed at $\Delta t = 0.001$ s.

3.1. Bifurcation Behavior. In this subsection, the bifurcation diagrams and the corresponding LE spectrums with respect to the control parameters such as p_1, p_5, p_6, and p_7 have

been investigated in detail. At first, to reveal the dynamic behaviors of system (1), we consider the parameter $p_1 \in [3.92, 4.1]$. For the parameters $(p_2, p_3, p_4, p_5, p_6, p_7) = (7, 7, 5, 4.5, 2.9, 1)$ and initial value $(-1, -1, -1)$, the bifurcation diagram and the corresponding LE spectrum with respect to p_1 are shown in Figure 2. When the system parameter p_1 is increased from 3.92 to 4.1, Figure 2(a) shows that the system changes from chaotic state to periodic state, alternatively. There exists a periodic window in $p_1 = 3.929$, and we observe a periodic motion with order-5 when $p_1 = 3.93$. Also, chaotic bubbles are presented in Figure 2(a) (for $p_1 \in [4.03, 4.1]$) that exhibit a complex behavior of the nonlinear system. In addition, the spectrum of LEs in Figure 2(b) well matches the bifurcation diagram. As it is known, when $LE_1 > 0$, $LE_2 = 0$, and $LE_3 < 0$, the proposed system is in a chaotic state.

When p_5 varies from 4.2 to 5.3, the bifurcation diagram and corresponding Ls spectrum with initial values $(-1, -1, -1)$ are plotted in Figures 3(a) and 3(c), respectively. Figure 3(a) shows that the system is alternately changing from a nonchaotic state to a chaotic state. For some values of p_5, the system has a small positive maximum LE, and the system is in a weak chaotic state. As shown in Figure 3(c), there are large fluctuations in the curve, which indicates the change has a great impact on the dynamical behavior of system (1).

Also, the bifurcation diagram and LEs spectrum versus the parameter $p_6 \in [3.94, 4.05]$ are presented in Figures 3(b) and 3(d). The bifurcation diagram in Figure 3(b) shows that the local maxima of the coordinate z directly illustrate an important phenomenon. This phenomenon is period-adding bifurcation, and we observe two sequences that overlap with each other. In this phenomenon, the oscillation period successively increases in different sequences by system parameter alteration.

Let the system parameters be $(p_1, p_2, p_3, p_4, p_5, p_6) = (4.4, 7, 7, 5, 4.5, 2.9)$ and initial value $(-1, -1, -1)$. The bifurcation diagram versus $p_7 \in [0.25, 1.3]$ is plotted in Figure 4(a). As it can be seen from this diagram, there are disconnected chaotic and periodic areas. For more details and revealing more interesting phenomena, the red frames of the bifurcation diagram of Figure 4(a) are magnified in Figure 5 and Figures 4(b) and 4(c), respectively. In the next subsection, we address the period-2 bubbles that are observed on the left side of the graph in Figure 4. Chaotic motions, periodic windows, and period-doubling bifurcation are also seen in Figure 4(b). The intermittent transition from period-1 motion to chaotic motion occurred in $p_7 = 0.9881$ (In Figure 4(c)). Also, the period-3 window occurs near $p_7 = 1.02$ after reverse period-doubling. Moreover, the route to chaos via period-doubling bifurcation is strongly visible in Figure 4(c).

3.2. Antimonotonicity.

The phenomenon of antimonotonicity has been found in many dynamical systems including 3D autonomous systems without linear terms in Kengne et al. [30]. In this phenomenon, periodic orbits can be created and then destroyed via reverse period-doubling

bifurcation as a control parameter is varied (Zolfaghari-Nejad et al. [16]). In order to demonstrate this phenomenon in system (1), we have illustrated some bifurcation diagrams as the parameter p_7 is varied in the range $0.52 < p_7 < 0.75$ for some discrete values of the control parameter p_6. Sample results are shown in Figure 5. In Figure 5(a), four period-2 bubbles are observed in $p_6 = 2.9$ (the left red frame in Figure 4(a)). Also, we have stable period-4 bubbles at $p_6 = 2.97$ (Figure 5(b)). Similarly, more bubbles are created for $p_6 = 3.01$ (Figure 5(c)), and an infinite tree finally occurs at $p_6 = 3.15$ (full Feigenbaum remerging tree in Figure 5(d)).

3.3. Multistability.

In order to uncover the coexisting characteristic, we select the system parameters as $(p_1, p_2, p_3, p_4, p_5, p_6, p_7) = (4, 7, 7, 5, 4.785, 4, 1)$, and let the initial value be $(-1, -1, z_0)$. Figure 6 presents the phase portraits of eight coexisting attractors of system (1). However, they are samples of an infinite number of attractors which form along the z-axis in phase space and could be detected with other initial values.

The coexistence of multiple periodic, limit cycle, and chaotic attractors with different topologies is one of the most attractive properties considered in this work. The corresponding bifurcation diagram versus z_0 as a control parameter is provided in Figure 6(a), which can be observed as multistability in system (1). When $z_0 = -1$, we can observe a strange attractor in Figure 6(c). For the initial value $z_0 = -1.1$, the existence of the order-3 period is proven in Figure 6(d). In Figures 6(e) and 6(f), order-1 period, limit cycle, and chaotic attractors coexist together for selected initial values, and they are asymmetric.

3.4. Spectral Entropy Analysis.

Spectral entropy has been used to determine the unpredictability of time-series Kengne et al. [30]. Spectral entropy is defined as

$$SE(N) = -\sum_{k=1}^{N} P_k \ln P_k, \tag{5}$$

where P_k is given by

$$P_k = \frac{|\lambda_k|^2}{\sum_i |\lambda_i|^2}. \tag{6}$$

Here, $|\lambda_k|^2$ is the Fourier power spectrum of a time-series at frequency λ_k Legendre and Legendre [55].

For the purpose of revealing the effect of the two parameters p_1 and p_6 on the chaotic behavior of system (1), we plot the spectrum of SE complexity as Figure 7(a). Fixing $(p_2, p_3, p_4, p_5, p_7) = (7, 7, 5, 5.005, 1)$, the initial value $(-1, -1, -1)$, and varying p_1 and p_6 from 3 to 5, SE distribution of the system is obtained as Figure 7(a). The darker areas are separated by a curved line. Also, a curved line is observed in lighter areas where around it the more chaotic state and nonchaotic state are repeated alternatively. We use the SE complexity algorithm in parameter selection for the novel system in real applications.

(a)

(b)
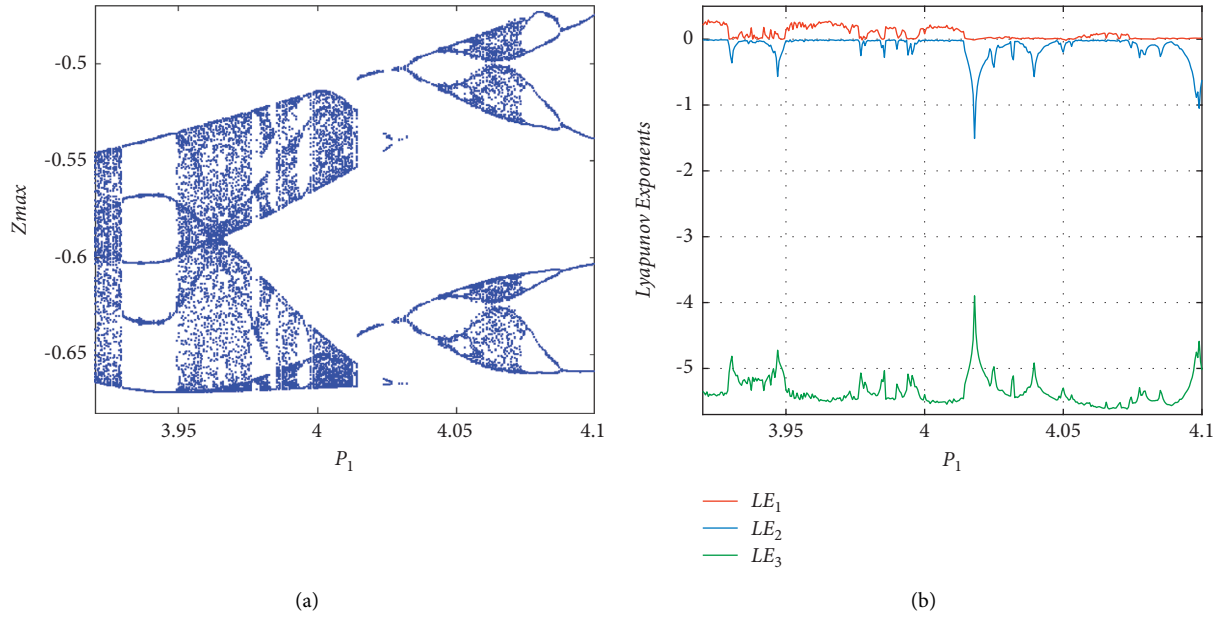
FIGURE 2: Bifurcation diagram and LEs spectrum of system (1) with the initial value $(-1, -1, -1)$ and $(p_1, p_2, p_3, p_4, p_5, p_6, p_7) = (p_1 \in [3.92, 4.1], 7, 7, 5, 4.5, 2.9, 1)$. (a) Bifurcation diagram; (b) LEs spectrum.

(a)

(b)
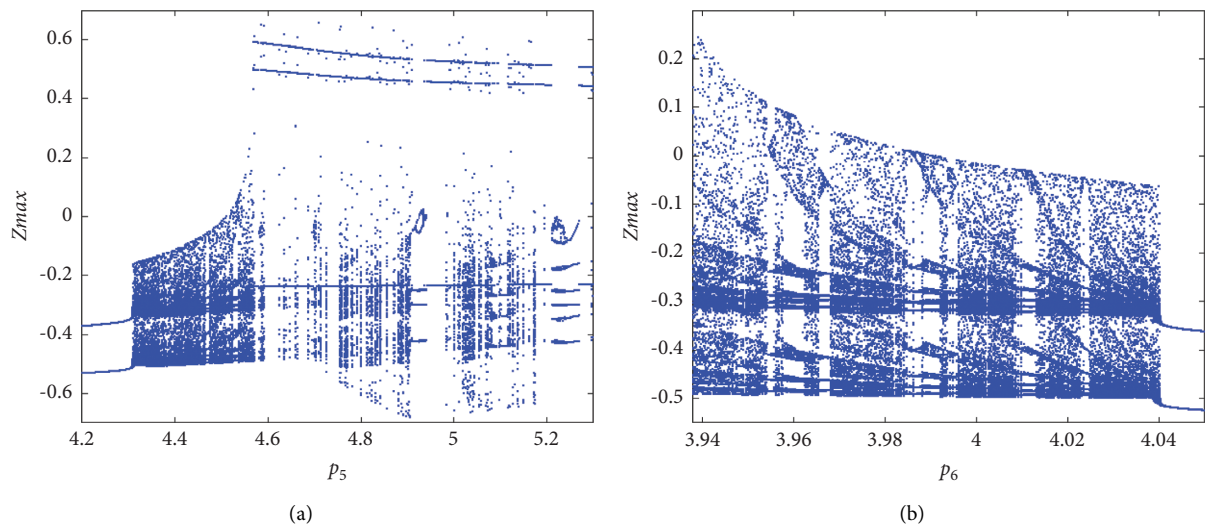
FIGURE 3: Continued.

(c)

(d)
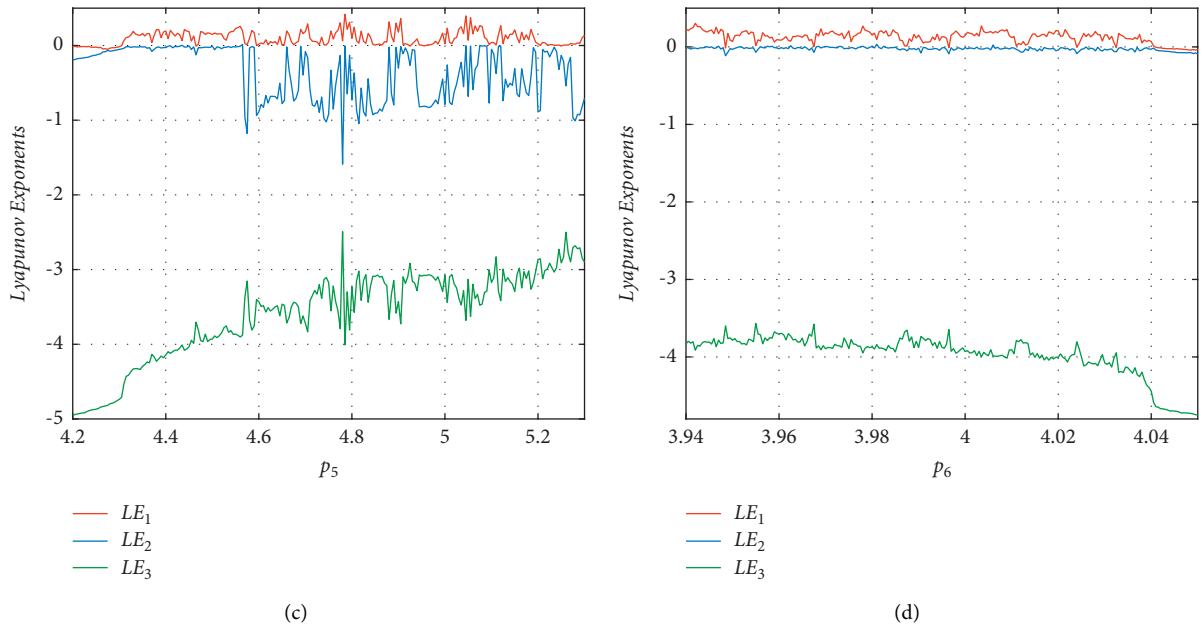
FIGURE 3: Bifurcation diagrams and LEs spectrum of system (1) with the initial value $(-1, -1, -1)$ and $(p_1, p_2, p_3, p_4, p_5, p_6, p_7) = (4, 7, 7, 5, 1)$. (a) Bifurcation diagram with respect to p_5 ($p5 \in [4.2, 5.3]$, $p_6 = 2.9$). (b)Bifurcation diagram with respect to p_6 ($p_5 = 4.5$, $p_6 \in [2.94, 4.05]$). (c) The corresponding LE spectrum with (a). (d) The corresponding LE spectrum with (b).

(a)

(b)

(c)
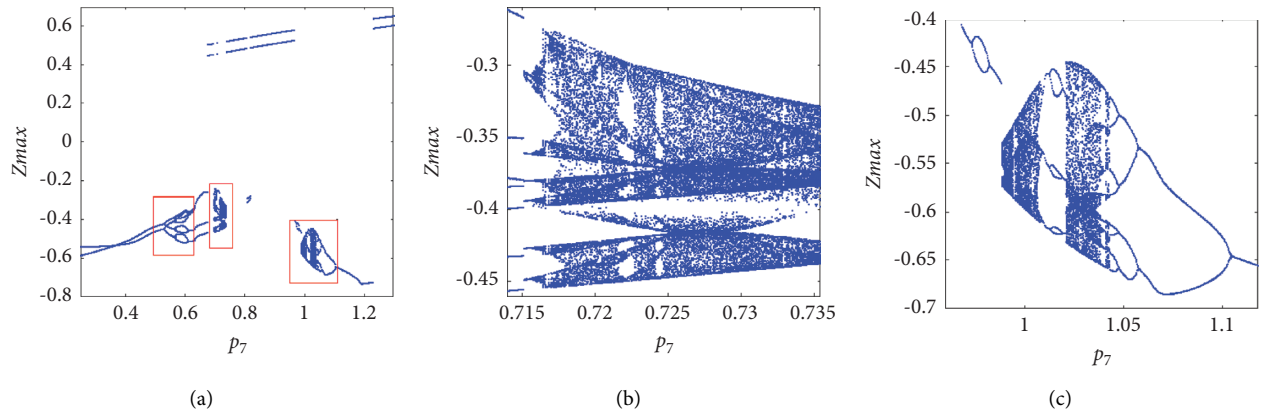
FIGURE 4: (a) Bifurcation diagram of the system with $(p_1, p_2, p_3, p_4, p_5, p_6, p_7) = (4.4, 7, 7, 5, 4.5, 2.9, p_7 \in [0.25, 1.3])$ and initial value $(-1, -1, -1)$. A magnified version of the bifurcation diagram versus (b)$p_7 \in [0.714, 0.735]$ and (c) $p_7 \in [0.968, 1.118]$.

(a)

(b)

(c)

(d)
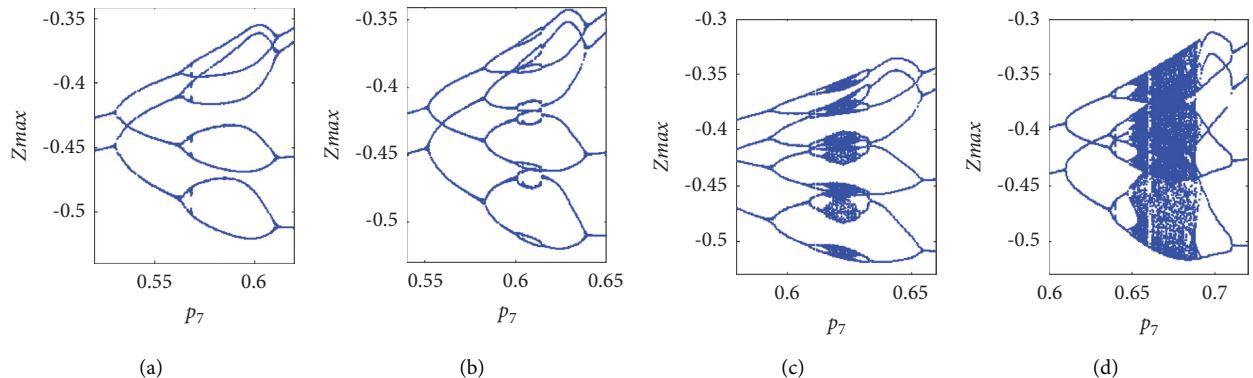
FIGURE 5: Bifurcation diagram for remerging Feigenbaum tree (bubbling): (a) period-2 bubble for $p_6 = 2.9$; (b) period-4 bubble for $p_6 = 2.97$; (c) and (d) full Feigenbaum remerging tree at $p_6 = 3.01$ and $p_6 = 3.15$; the initial value is $(-1, -1, -1)$.
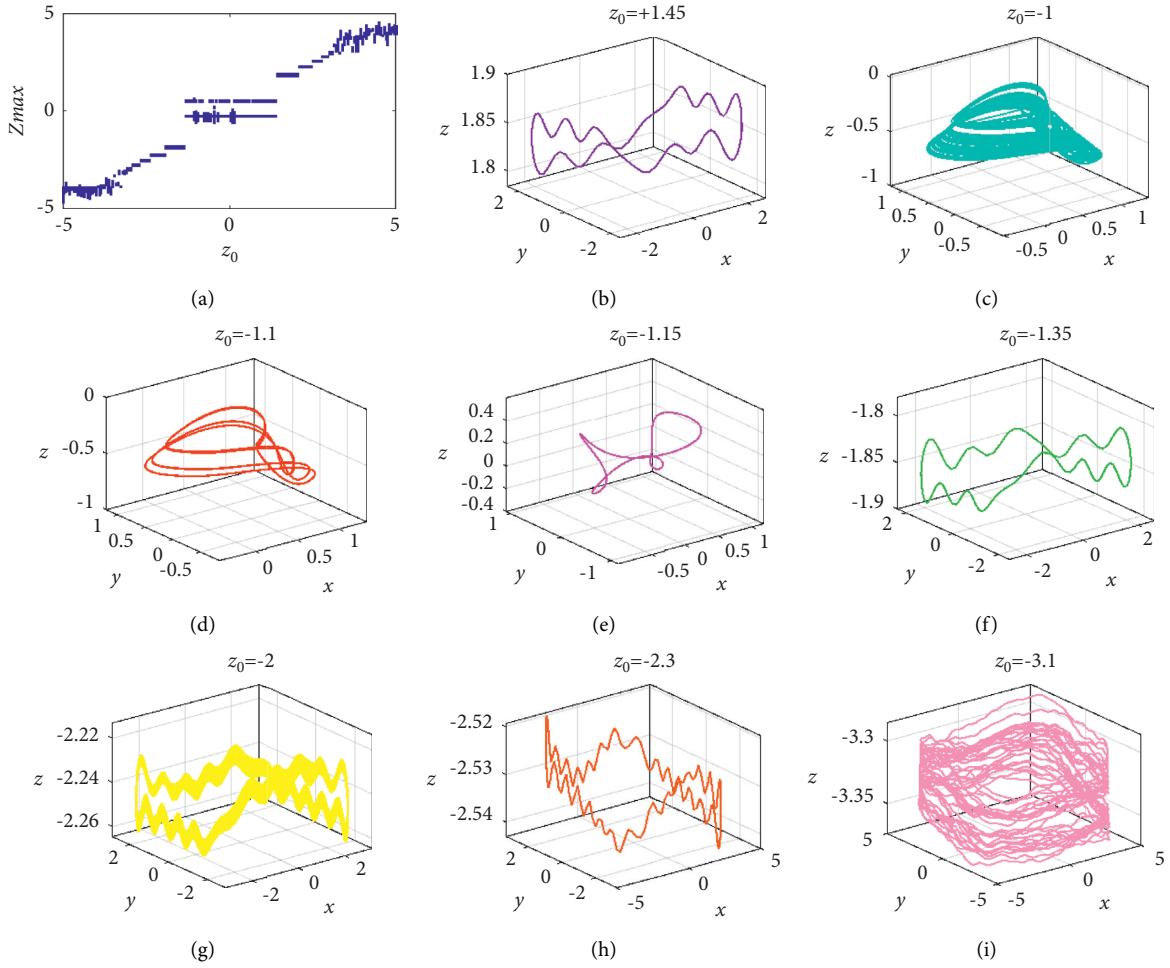
Figure 6: Sample phase portraits of system (1) under $(p_1, p_2, p_3, p_4, p_5, p_6, p_7) = (4, 7, 7, 5, 4.785, 4, 1)$, $x_0 = -1$, $y_0 = -1$ showing the occurrence of multiple attractors. (a) Bifurcation diagram of the system versus z_0, (b) period-1 cycle, (c) spiral chaotic attractor, (d) period-3 cycle, (e, f) period-1 cycle with different topologies, (g) limit cycle, (h) period-1 cycle, and (i) limit cycle.
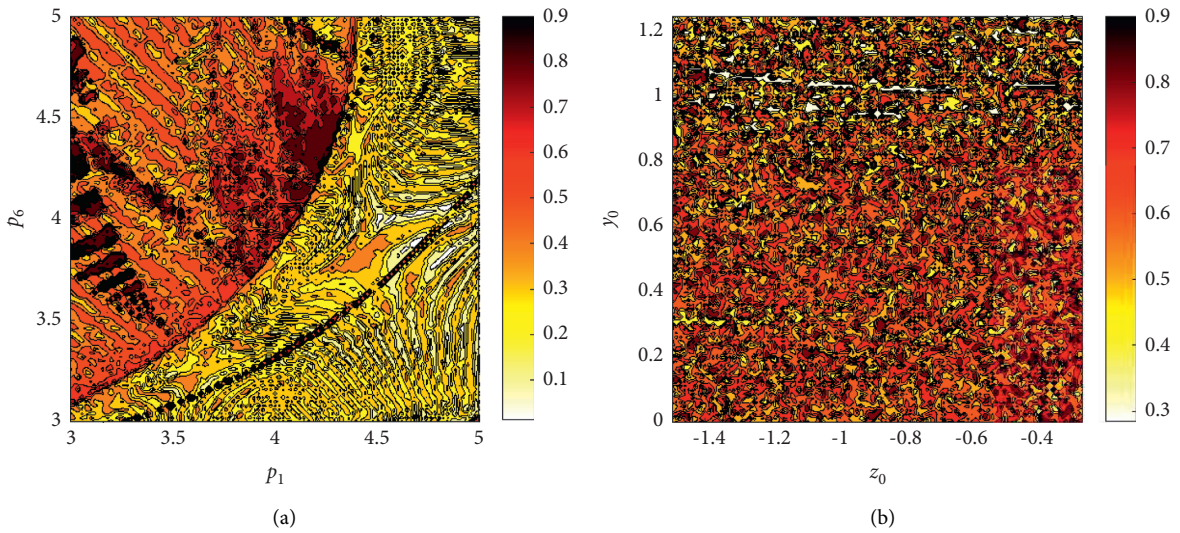
Figure 7: Spectral entropy distribution of the system in the (a) $p_6 - p_1$ plane and (b) $y_0 - z_0$ plane.

We can see the SE distribution of system (1) in $y_0 - z_0$ plane in Figure 7(b). Here, the system parameters remain unchanged and $p_1 = 4$, $p_6 = 4$, and $x_0 = -1$. The SE complexity is computed when $z_0 \in [-1.5, -0.25]$ and $y_0 \in [0, 1.25]$. Figure 7(b) reflects the SE distribution under different initial values of y_0 and z_0. The color distribution in $y_0 - z_0$ plane is very scattered which demonstrates that the novel system is very sensitive to the initial values. Other than small areas with lighter colors at the top of the plane, in the entire area, numerous small black spots are diffused. Moreover, this figure illustrates that different initial values have a great impact on the complexity of system (1). Also, we observe that the system has multiple coexisting attractors.

4. A Secure Data Transmission Scheme Using the Proposed Chaotic System

In this section, we give a complete description of the proposed secure data transmission scheme. Chaotic systems are used as one of the potential alternative encoding techniques in secure data transmissions. Chaos-based encoding/decoding algorithms offer high flexibility in secure data transmission schemes due to numerous numbers of chaotic systems and many possible secret keys. However, chaotic systems are often applied in designing pseudorandom number generators (PRNGs) with a high degree of randomness as the most basic unit in secure transmission schemes. In this work, the proposed chaotic system has been used to design a new encoding/decoding algorithm with an evolutionary approach.

Deterministic secure data transmission schemes have predictable behavior because there is always only one output for each constant data. So, these schemes can never amount to the level of high security. In contrast, a probabilistic scheme produces different outputs at different times even when the algorithm is applied with the same key to the same input data. As a result, probabilistic secure transmission schemes possess resistance against chosen-plaintext and ciphertext-only attacks (Dhall et al. [45]). In this section, we propose a new inherently probabilistic scheme that provides high security and has unpredictable behavior.

4.1. Problem Formulation. Figure 8 summarizes the secure data transmission setup. Suppose Alice wants to send an l-bit message $m = (m_i)_{i=1}^l \in \{0, 1\}^l$ through the public channel to Bob. She first encodes the message by a chaos-based encoding algorithm and produces a set of codewords. While encoding a message, she utilizes the preagreed secret key which may drive the encoding step when producing codewords. Codewords $c = \{c_0, \ldots, c_s\}$ are sent through the channel and inspected by Eve. Suppose Eve wants to understand the confidential message between Alice and Bob; however, she does not have the secret key. If codewords are delivered to Bob, he extracted the message by inverting the encoding operation via a chaos-based decoding algorithm.

In this work, chaos-based encoding/decoding algorithms are realized by applying a designed SC diagram using different steady states. There are several possible final steady states for a set of parameters in chaotic systems with multiple coexisting attractors. The final state depends on the initial values of the system and is determined by an evolutionary rule that the system goes from the current state to which state. In these systems, the SE distribution of the system under different initial values is very dispersive (see Figure 7(b)). Our main idea for encoding a message is also the use of SE complexity distribution.

The SC diagram determines the relationship between the steady states of the system and message bits. Figure 9 shows a simple designed SC diagram. In this structure, three final states A, B, and C are considered. Each edge is labeled with $q_i \in \{0, 1\}$, where it shows one bit of message m. For each bit of the message, the sender generates the corresponding codeword, so that the chaotic system evolves into a final steady state in the receiver. Also, it should be noted that when assigning q_i, to (from) each state, at least one "0" and one "1" should be entered (be exited). The assignment process of q_i to edges is pseudorandom and can be considered as a part of the secret key. We have different paths through the SC diagram that lead all paths toward a specified message. This is due to the existence of several possible final steady states and many different initial values for the evolution of the system. The number of paths varies depending on the length of the message, the number of considered states, and the number of initial values for the realization of each state.

The final steady states A, B, and C can be obtained under different initial values. For instance, Figure 10 indicates three different states obtained by $y_0 \in [-1.5, -0.25]$ and $z_0 \in [0, 1.25]$, which reflects the SE distribution of system (1). The system parameters and x_0 are fixed as shown in Section 3.4. Figure 10(a) shows the dispersion of $SE \le 0.55$ with black dots (state A). The state B is defined as $0.55 < SE < 0.7$ (Figure 10(b)), and state C is obtained by $SE \ge 0.7$ as shown in Figure 10(c). As is shown in these figures, there are many initial values for the realization of each state. Also, the distribution of these initial values in each state is random and unpredictable.

4.2. Algorithm Description. The proposed algorithms for the encoding and decoding procedure are described in Figure 11 using pseudocode and based on the SC diagram of Figure 9. For the decoding procedure, we need to know how to label the edges in the SC diagram (q_i). Therefore, we are able to reconstruct the paths of the SC diagram in the receiver. As mentioned, the process of assigning the labels is considered as a part of the secret key shared between the sender and the receiver.

In this construction, the length of codewords can be $n \in \{4, 8, 16, \ldots\}$ according to the SC diagram. The codewords refer to the initial value that creates a determined state. The set of codewords $c = \{c_0, \ldots, c_s\}$ generated for each message can be represented as a path through the SC diagram. So, different sets of codewords can be sent each time for a fixed message. In this section, we first describe the encoding/decoding algorithms in their general form, and later, in Section 4.2.1, we give two simple examples for better understanding.
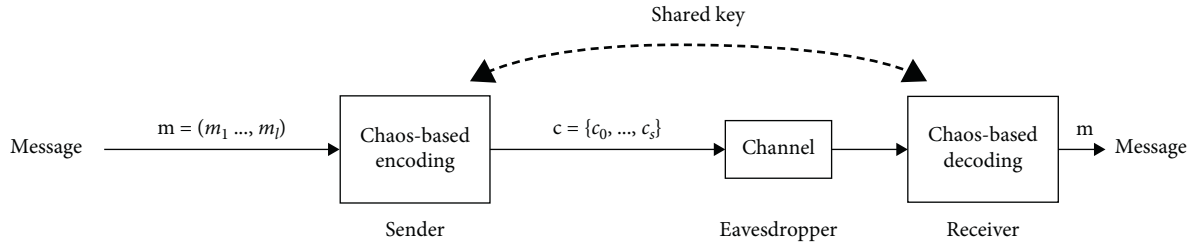
FIGURE 8: Model of secure data transmission scheme.
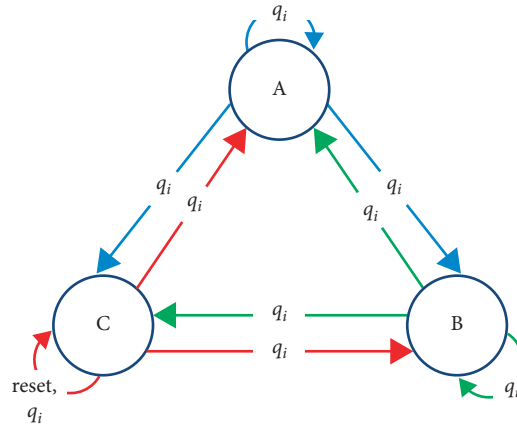
FIGURE 9: The state chain diagram with $q_i \in \{0, 1\}$.

(a)

(b)

(c)
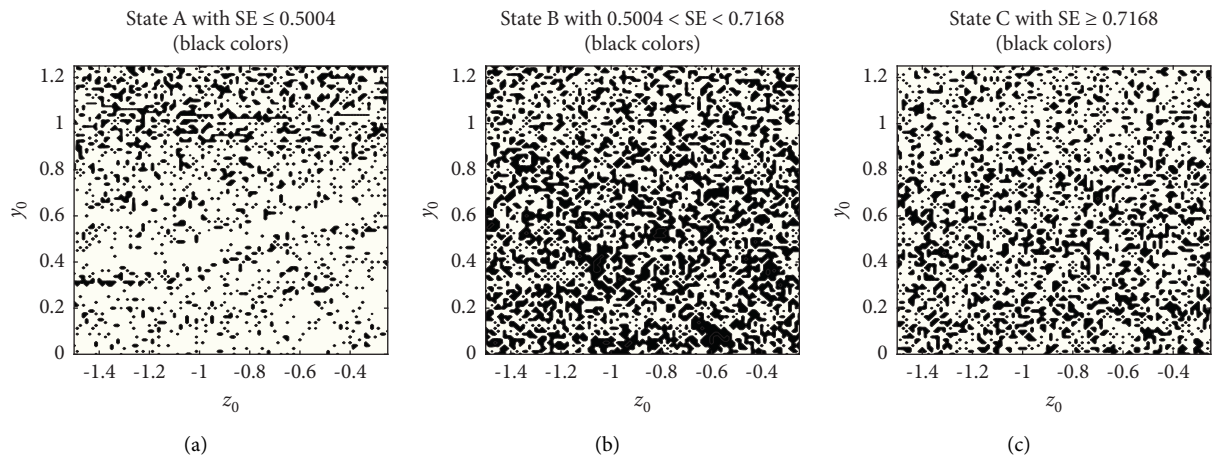
FIGURE 10: Dispersion of spectral entropy in the $y_0 - z_0$ plane, (a) SE ≤ 0.55, (b) $0.55 < $ SE < 0.7, and (c) SE ≥ 0.7.

In Algorithm 1 of Figure 11 (Encoding procedure), the SE complexity of the chaotic system (1) under different initial values is first computed, and then one codeword will be assigned to each initial value. Also, the states *A*, *B*, and *C* are set based on computed spectral entropy. In general, the message *m* is divided into equal blocks $b = \{b_1, \ldots, b_s\}$. In fact, the encoding process is done in block form. Based on the SC diagram in Figure 9, there are three steady states. So, the length of each block is equal to one, and each block represents one bit of the message ($l = s$).

In the following, one state is randomly selected named as the current state. Depending on the current state, one codeword is randomly selected (c_0). As we explain this procedure, the reader is advised to inspect Algorithm 1 of Figure 11. According to the SC diagram, the current state, and the first block of m (b_1), the next state is determined. The edge between the current state and the next state is labeled with $q_i = b_j$. Then, another codeword is randomly selected according to the next state (c_j). In the following, the next state replaces the current state, and the process is repeated.

Algorithm 1: Encoding procedure	Algorithm 2: Decoding procedure
Input: $\mathbf{m} = (m_1 \ldots, m_l)$ Output: $\mathbf{c} = \{c_0 \ldots, c_s\}$ 1. $\{SE_{11}, \ldots, SE_{nm}\}$ ←compute the spectral entropy of chaotic system (1) under different initial values 2. determine codewords and set the states **A**, **B** and **C** based on spectral entropy 3. divide **m** into equal blocks $\mathbf{b} = \{b_1, \ldots, b_s\}$ 4. select *current_state* $\in \{\mathbf{A}, \mathbf{B}, \mathbf{C}\}$ randomly 5. c_0 ←select on codeword randomly from current_state 6. j ← 1 7. while j ≤ num of blocks (*s*) do 8. switch *current_state* 9. case **A**: 10. switch b_j 11. select *next_state* according to q_i between (*current_state*, **A**) 12. end 13. case **B**: 14. switch b_j 15. select *next_state* according to q_i between (*current_state*, **B**) 16. case **C**: 17. switch b_j 18. select *next_state* according to q_i between (*current_state*, **C**) 19. if (*next_state*==**C**) then 20. reset 21. c_j ←select one codeword randomly from *next_state* 22. *current_state*←*next_state* 23. $j ← j + 1$ 24. end while	Input: $\mathbf{c} = \{c_0 \ldots, c_s\}$ Output: $\mathbf{m} = (m_1 \ldots, m_l)$ 1. (x_{00}, y_{00}, z_{00}) ←determine initial value based on codeword c_0 2. SE_0 ←compute the spectral entropy of chaotic system (1) with (x_{00}, y_{00}, z_{00}) 3. select *current_state* $\in \{\mathbf{A}, \mathbf{B}, \mathbf{C}\}$ based on SE_0 4. j ← 1 5. while j ≤ num of blocks (*s*) do 6. (x_{0j}, y_{0j}, z_{0j}) ←determine initial value based on codeword c_j 7. SE_j ←compute the spectral entropy of chaotic system (1) with (x_{0j}, y_{0j}, z_{0j}) 8. choose next_state $\in \{\mathbf{A}, \mathbf{B}, \mathbf{C}\}$ based on SE_j 9. $b_j ← q_i$ between (*current_state, next_state*) 10. if (*current_state* and *next_state*=**C**) then 11. reset 12. *current_state* ←*next_state* 13. $j ← j + 1$ 14. end while 15. **m** ←concatenate blocks of $\mathbf{b} = \{b_1, \ldots, b_s\}$

FIGURE 11: Pseudocode of the encoding and decoding procedures.

This algorithm continues until all message blocks are mapped to the corresponding codewords.

In the encoding procedure, whenever the state C is repeated twice times in succession, the algorithm resets. Therefore, depending on the current block of m, the system parameters are changed. Then, the SE complexity of system (1) under initial values is recomputed. This process causes a more complicated algorithm. As a result, the proposed algorithm becomes more resistant to eavesdropping attacks. Finally, a generated set of codewords $c = \{c_0, \ldots, c_s\}$ is sent to the receiver.

The decoding procedure (Algorithm 2 of Figure 11) starts with the first transmitted codeword (c_0), and the initial value (x_{00}, y_{00}, z_{00}) is determined based on it. Then, the SE complexity of system (1) is calculated by knowing the initial value and system parameters extracted from the secret key. SE_0 determines the current state. In the same way, the next codeword specifies the next state. In the SC diagram, the edge that connects the current state with the next state is labeled q_i and assigns the first block of the message m (b_1). The next state replaces the current state, and the second codeword (c_1) determines the initial value (x_{01}, y_{01}, z_{01}). By calculating the SE complexity of the system, the next state is specified, and the second block of m (b_2) is obtained. The decoding procedure continues until all blocks of m are specified. Finally, the blocks $b = \{b_1, \ldots, b_s\}$ concatenates, and the confidential message is restored.

4.2.1. Two Examples of the Proposed Algorithm. In this subsection, the algorithm for secure data transmission is explained with two small examples. Let the labels assignment of the edges in the SC diagram of Figure 9 be as in Figure 12(a). We assume $l/s = 1$ and thus q_i represent one bit of message m. In the first example, suppose that the

message is $m_1 = (0, 1, 1, 0)$. As shown in Figure 12(b), the encoding algorithm starts with a random selection of one of the states (A, B, C). Suppose state B is selected. Depending on state B, one codeword is randomly selected (c_{10}). This codeword refers to the initial value which causes system (1) to evolve to the state B. Two edges are exited from this state that is labeled "0" (m_{11}). The first edge connects state B to state C, and the second edge connects B to itself. We select one of the states C or B, randomly. Suppose that state B is selected again as the next state. So, the second codeword randomly picks up from state B (c_{11}). Depending on the second bit of m_1, one edge is exited from this state that is labeled "1". Then, the next state is A, and c_{12} is determined. The state A has two exited edges labeled "1" that equals to m_{13}. These edges connect state A to the states B and C. With random selection between B and C, c_{13} is also determined. If the state C is selected, the final state will be A, because just one exited edge from C is labeled "0" (according to the last bit of m_1). So, c_{14} is randomly selected from state A. The codewords $c = \{c_{10}, c_{11}, c_{12}, c_{13}, c_{14}\}$ are sent through the public channel and are delivered in the receiver.

In the receiver, m_1 is restored using the secret key by running Algorithm 2 of Figure 11. In the first step, (x_{00}, y_{00}, z_{00}) is determined based on the codeword c_{10}, and then SE_0 is calculated for this initial value. Also, based on SE_0, the current state is determined. The second initial value (x_{01}, y_{01}, z_{01}) is determined by the codeword c_{11}, and the corresponding SE of system (1) is computed. Indeed, SE_1 specifies the next state. The edge between the current state and the next state labeled q_i corresponds to the first bit of the message m_1. So, the next state replaces the current state, and the third initial value resulting from c_{12} determines the next state. This procedure continues until the last bit of m_1 has been extracted.
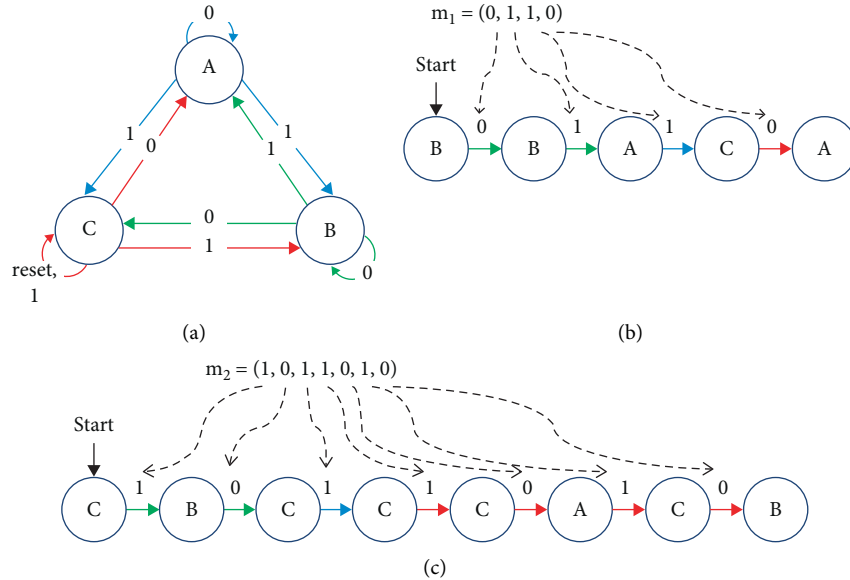
FIGURE 12: (a) The state chain diagram with assignments. (b) Selected path through the SC diagram of (a) for $m_1 = (0, 1, 1, 0)$. (c) Selected path through the SC diagram of (a) for $m_2 = (1, 0, 1, 1, 0, 1, 0)$.

In the second example, suppose the message is $m_2 = (1, 0, 1, 1, 0, 1, 0)$. Figure 12(c) represents the selected path through the SC diagram of Figure 12(a) for this example. Suppose state C is randomly selected first as the current state. Depending on state C, one codeword is randomly selected. Two edges that connect state C with itself and state B are labeled "1" (according to m_{21}). Suppose state B is selected as the next state. So, the next codeword is randomly determined based on state B. In this step, state B replaces the current state, and the second bit m_2 (m_{22}) determines the next state. Then, the next state is B or C. Suppose the state C is selected, and the third codeword is randomly chosen from state C. Similarly, m_{23} determines the next state. Suppose the next state is state C, again. Therefore, state C is repeated twice times in succession, and the encoding algorithm resets. Depending on the current bit of m_2, we change the system parameters based on the preshared agreement between the sender and the receiver. So, we recompute SE complexity of system (1) under initial values. Then, the codeword c_3 is randomly chosen from new state C. This algorithm continues to encode the other message bits. At the receiver, depending on the received codewords, the initial values are extracted, and the system evolves to the desired states based on the SC diagram. As a result, we can extract the message m_2 correctly on the receiver side.

4.2.2. Extended State Chain Diagram. The SC diagram in Figure 9 is an example of a simple model, in which each state represents the final steady state of the chaotic system (1) based on the SE complexity. In this model, the length of each block of m is one, and each edge is labeled with q_i equal to one bit of the message. As a result, the number of transmitted codewords is equal to the number of message bits. When the message length is short, the number of generated

codewords is low enough. However, by increasing the message length, the number of codewords is increased. We can design an extended SC diagram with more states to improve the efficiency of the proposed secure transmission scheme. For example, the extended SC diagram in Figure 13 has nine states. These states can be obtained by dividing the SE distribution of Figure 7(b) into nine parts. Each edge is labeled with $r_i \in \{000, 001, 010, 011, 100, 101, 110, 111\}$ which represents different modes for each block of m. Therefore, one codeword is generated for one block of the message with a length of three bits. As a result, the number of generated codewords is decreased than before.

5. Performance Analysis and Experimental Results

In this section, experimental observations are given to demonstrate the performance and validity of the proposed scheme. In Section 4, we described the details of the proposed chaos-based encoding/decoding algorithms for a secure data transmission scheme. As mentioned, the transferred data through the public channel is a set of codewords in the form of $c \in \{0, 1\}^n$. Each codeword refers to the initial value which causes system (1) to evolve to the desired state. At the receiver, with the dynamic evolution of the chaotic system, the original data is restored based on the SC diagram. The proposed scheme is independent of data type, and we can send any type of confidential digital data such as image, text, and numeric data. Also, this scheme is capable of sending data in different paths through the SC diagram. As a result, the proposed scheme is inherently probabilistic and provides high security. For the evaluation of the proposed scheme, we used the extended SC diagram in Figure 13.
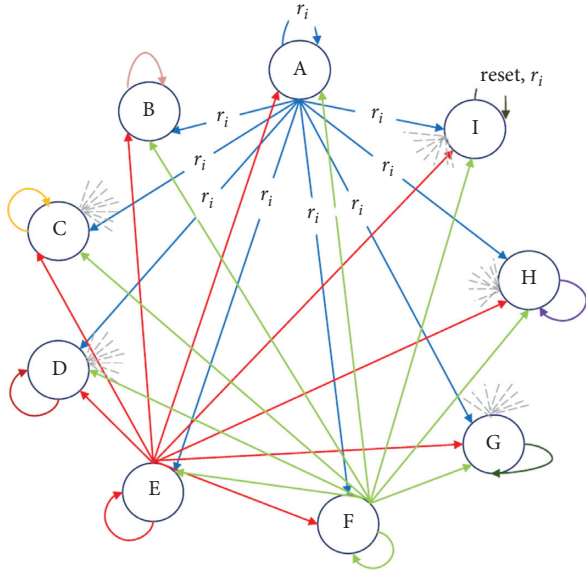
FIGURE 13: Extended state chain diagram ($r_i \in \{000, 001, \ldots, 111\}$).

5.1. Security Analysis.

At first, common security analyses are evaluated including keyspace and sensitivity to mismatched keys. Then, statistical analyses are examined.

(1) *Keyspace.* For the evolution of the dynamical system, we need to know the parameters of the system. Also, how to label the edges with q_i (or r_i) in the SC diagram is required. The proposed scheme uses 17 parameters as keys, and these keys are coded with 17×16 bits. Then. the total keyspace is equal to 2^{272}. The keyspace of this framework is greater than 2^{100} and is considered secure (Alvarez and Li [56]). So, the proposed scheme is infallible against brute force attacks. (2) *Sensitivity to Mismatched Secret Key.* We tested the sensitivity of the proposed scheme to the mismatched secret key. The dynamical system is very sensitive to small changes in the value of the parameters. Thus, even one wrong bit in the secret key results in a completely different message at the receiver. Figure 14 shows the original image and the extracted image at the receiver with one wrong bit in the secret key. In this case, one bit of the secret key is randomly selected and is flipped. (3) *Dissimilarity Matrix for a Constant Message.* The proposed chaos-based encoding algorithm is capable of sending data in different paths. Since there are many initial values for each state, the proposed algorithm corresponding to the SC diagram has different paths for data transmission. We consider the message in general form $m = (m_i)_{i=1}^{l} \in \{0,1\}^l$, and a constant secret key is used. Figure 15 illustrates the dissimilarity matrix for a constant message with the length of 25, 100, 1000, and 10 000 bytes. For each constant message, the proposed encoding algorithm is run 100 times. Each time different codewords are generated. Cosine similarity in Kornaropoulos and Efstathopoulos [57] is used to estimate the similarity between two vectors of codewords. As you see, for all cases, the Cosine similarity is less than 0.5. (4) *Histogram Analysis.* Figures 16(a) and 16(b) show the histogram distribution graphs of a random plaintext with 3000 bytes and transmitted data, respectively. As can be seen from

Figure 16(b), the transmitted data has a balanced histogram distribution and includes all codeword values (0 to 255). Therefore, the proposed method is robust against frequency attack.

5.2. Information Entropy.

Information entropy exhibits the discrete probability of random events and can be used to measure system confusion. The ideal value for information entropy should be 8 (Tong et al. [58]). The system information entropy is calculated according to (7), where $P(c_i)$ is the probability of each codeword in the output:

$$H(c) = \sum_c P(c_i) \log_2 \frac{1}{P(c_i)}. \tag{7}$$

The information entropy for a given sample message with the lengths of 5000 bytes is 7.997 2. So, the proposed chaos-based encoding algorithm has high performance, because the value of information entropy is close to 8. Also, the information entropy is more close to eight, if the length of data increases. For example, if the message length increases to 100 000 bytes, the information entropy is obtained equal to 7.999 1. Furthermore, for a given message with all zero bits, information entropy equals 7.793 4 (message length = 5000 bytes). If all bits of the given message are one, entropy is 7.892 3. The information entropy of codewords in these cases is close to 8. As a result, the proposed scheme generates a set of codewords with more confusion and can resist information entropy attacks well.

The results obtained from observations prove the strength of the scheme against data eavesdropping attacks. Also, the system parameters change adaptively to the message content during running the algorithm, which increases the data security by reducing the time available for statistical attacks on the transmitted codewords. On the other hand, there are about 6000 different sets of codewords to send only one byte of constant data corresponding to the extended SC diagram in Figure 13 (using the same key). Also, there are many different sets of codewords for data with more than six bytes length. As a result, the proposed scheme for secure data transmission is inherently probabilistic and provides high security.

5.3. Comparison.

In this section, the proposed scheme is compared with the existing secure data transmission methods in recent years. The comparison is made from four main perspectives: application of chaos in secure data transmission, probabilistic scheme, data type, and keyspace of scheme, as illustrated in Table 2. Chaos-based PRNG is the most common application of chaotic systems in secure data transmission. In Nesa et al. [46], a PRNG is proposed that is based on a logarithmic chaotic map and has been utilized in encrypting sensor data. The authors in Nesa et al. [46] proposed a new deterministic encryption algorithm that generates the same ciphertext for the same plaintext with the same key. As a result, it does not provide a high level of security. In Dhall et al. [45], a random bit insertion phase is employed, which contributes to the probabilistic nature of

(a)

(b)
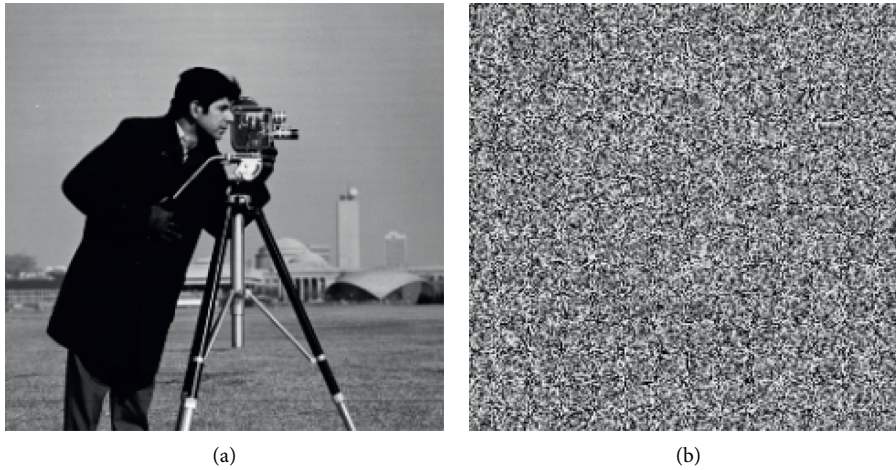
FIGURE 14: (a) Original image and (b) extracted image in the receiver with one wrong bit in the secret key.

(a)

(b)

(c)

(d)
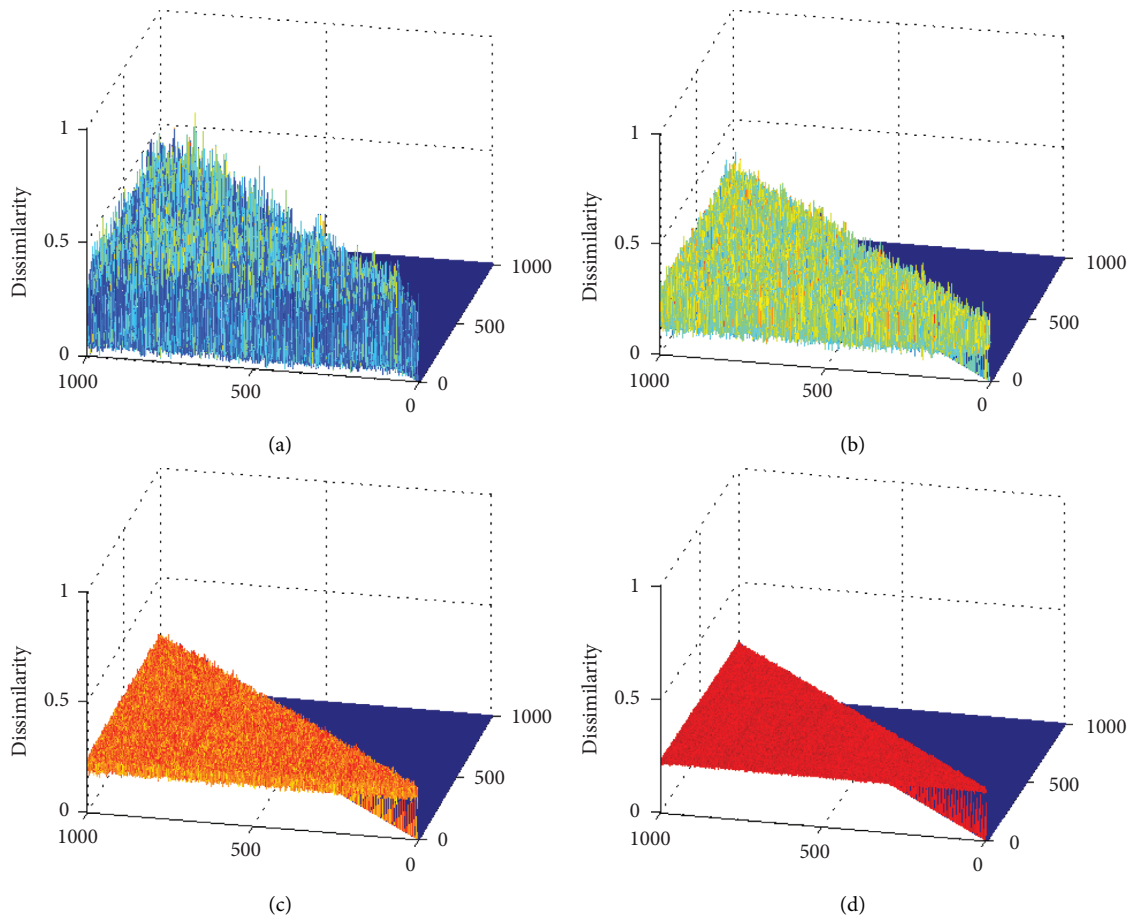
FIGURE 15: Dissimilarity matrix for a constant message: (a) message length = 25 bytes; (b) message length = 100 bytes; (c) message length = 1000; (d) message length = 10,000.

the encryption scheme. The proposed scheme in Dhall et al. [45] uses chaos for generating keystream which is utilized to perform permutation and substitution operations. This probabilistic scheme is suitable for encrypting images. In Srich and San-Um [59], a data encryption scheme is

proposed using the chaotic map in order to generate the chaotic matrix. The proposed scheme in Srich and San-Um [59] can also be applied to any data type such as image, text, and excel files. However, it has a deterministic approach and is vulnerable to a chosen-plaintext attack. In this work, we

(a)

(b)
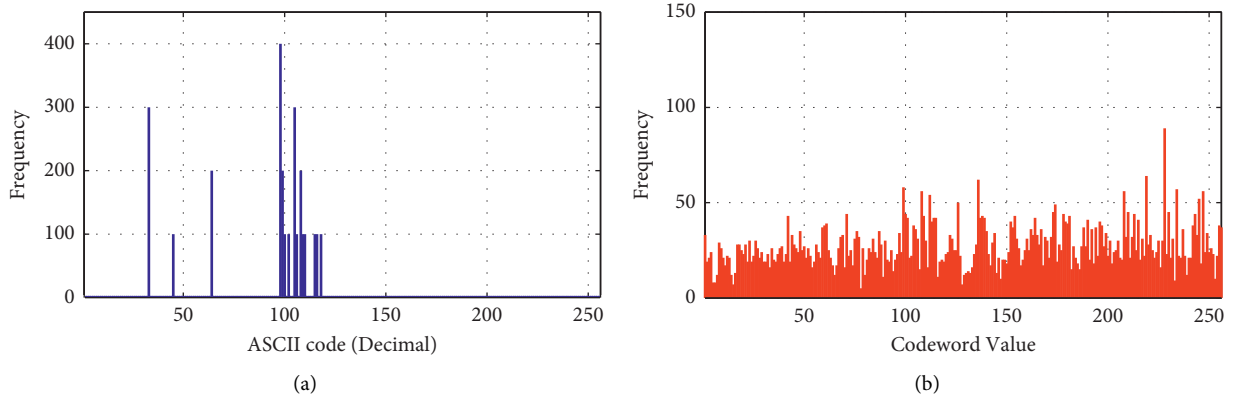
FIGURE 16: Histogram distribution graph of (a) the plaintext and (b) transmitted data.

TABLE 2: Comparison between the proposed secure data transmission scheme and the other works.

Scheme	Application of chaos	Probabilistic	Data type	Keyspace
Nesa et al. [46]	Chaos-based PRNG	No	Numeric sensor data	2^{148}
Dhall et al. [45]	Chaos-based permutation and substitution	Probabilistic with random bits insertion	Image	2^{256}
Srich and San-Um [59]	Chaotic matrix construction	No	Image/Text/Excel files	$2^{(w+3)}10^{36}$ (w: a parameter)
Proposed scheme	Chaos-based encoding/decoding algorithms	Inherently probabilistic	Any type of digital data	2^{272}

proposed a new approach for secure data transmission using chaotic systems with multiple coexisting attractors. The proposed chaos-based encoding/decoding algorithms make an evolutionary approach to transmitting confidential data. These algorithms are realized by applying an SC diagram using different steady states. Also, the proposed scheme is inherently probabilistic. The data transmission scheme is flexible since it could be applied to a different type of digital data. The keyspace is large enough to make the attack infeasible in all schemes.

6. Conclusions

In this paper, a new non-Shilnikov chaotic system with an infinite number of nonhyperbolic equilibrium points is introduced and analyzed. The novel system has one equilibrium point with triple zero eigenvalues at the origin and many equilibrium points with double zero eigenvalues. Such chaotic systems are very rare in the literature. Also, all equilibrium points are unstable and are located on the z-axis. By numerical analysis of the new chaotic system in terms of the phase portrait, bifurcation diagram, Lyapunov exponents, and spectral entropy distribution, a wide variety of dynamics are revealed. The phenomenon of anti-monotonicity such as chaotic bubbles and period-2 bubbles is observed in bifurcation diagrams. Also, it is shown that the novel system can exhibit the phenomenon of the infinitely coexistence of multiple periodic, limit cycle, and chaotic attractors. So, the novel chaotic system is multistable. Moreover, the complexity of the system is analyzed by SE.

The SE distribution under different initial values of y_0 and z_0 is very scattered, which indicates the coexistence of multiple attractors. Finally, we developed chaos-based encoding/decoding algorithms for a secure data transmission scheme using the proposed chaotic system. For this purpose, an SC diagram with different steady states is designed. These states are determined by computing the SE complexity of the novel system under different initial values. The proposed secure data transmission scheme is inherently probabilistic and provides high security against different attacks.

As a future task, system (1) will be more investigated by using various functions instead of $\sin(xy - z)$. In a nutshell, the proposed system will be extended and enriched by some proper nonlinearities. More work on constructing many coexisting attractors with non-Shilnikov chaotic systems will be addressed in future research. From an engineering application point of view, we continue to forward the research about secure data transmission schemes via constructing chaotic systems with infinitely equilibrium points. Also, an interesting future direction could be designing the new SC diagrams to improve the efficiency of the secure data transmission scheme.

Data Availability

In fact, there is not any specific data used in the research work. The authors have solved differential equations in MATLAB. Furthermore, a chaos-based encoding/decoding scheme was applied to the Cameraman image which is well known and could be found everywhere. Overall, there is no data to share with the research community.

Conflicts of Interest

The authors declare that they have no conflicts of interest.

References

[1] J. Sprott, "Do we need more chaos examples?" *Chaos Theory and Applications*, vol. 2, pp. 49–51, 2020.

[2] J. C. Sprott, "Strange attractors with various equilibrium types," *The European Physical Journal-Special Topics*, vol. 224, no. 8, pp. 1409–1419, 2015.

[3] S. Zhang, Y. Zeng, Z. Li, M. Wang, X. Zhang, and D. Chang, "A novel simple no-equilibrium chaotic system with complex hidden dynamics," *International Journal of Dynamics and Control*, vol. 6, no. 4, pp. 1465–1476, 2018.

[4] Q. Deng, C. Wang, and L. Yang, "Four-wing hidden attractors with one stable equilibrium point," *International Journal of Bifurcation and Chaos*, vol. 30, no. 6, Article ID 2050086, 2020.

[5] V. T. Pham, S. Jafari, X. Wang, and J. Ma, "A chaotic system with different shapes of equilibria," *International Journal of Bifurcation and Chaos*, vol. 26, Article ID 1650069, 2016.

[6] S. Jafari and J. C. Sprott, "Simple chaotic flows with a line equilibrium," *Chaos, Solitons and Fractals*, vol. 57, pp. 79–84, 2013.

[7] P. D. K. Kamdem, Q. Lai, and H. Fotsin, "Dynamics, synchronization and electronic implementations of a new lorenz-like chaotic system with nonhyperbolic equilibria," *International Journal of Bifurcation and Chaos*, vol. 29, no. 14, Article ID 1950197, 2019.

[8] X. Cai, L. Liu, Y. Wang, and C. Liu, "A 3D chaotic system with piece-wise lines shape non-hyperbolic equilibria and its predefined-time control," *Chaos, Solitons and Fractals*, vol. 146, Article ID 110904, 2021.

[9] L. Chen, F. Nazarimehr, S. Jafari, E. T. Cuautle, and I. Hussain, "Investigation of early warning indexes in a three-dimensional chaotic system with zero eigenvalues," *Entropy*, vol. 22, no. 3, 2020.

[10] C.-L. Li and J.-B. Xiong, "A simple chaotic system with non-hyperbolic equilibria," *Optik*, vol. 128, pp. 42–49, 2017.

[11] Q. V. Lawande and N. Maiti, "Role of nonlinear dynamics and chaos in applied sciences," Technical Report, Bhabha Atomic Research Centre, Mumbai, Maharashtra, 2000.

[12] S. T. Kingni, L. Keuninckx, P. Woafo, G. Van der Sande, and J. Danckaert, "Dissipative chaos, Shilnikov chaos and bursting oscillations in a three-dimensional autonomous system: theory and electronic implementation," *Nonlinear Dynamics*, vol. 73, no. 1-2, pp. 1111–1123, 2013.

[13] G. A. Leonov, "Shilnikov chaos in Lorenz-like systems," *International Journal of Bifurcation and Chaos*, vol. 23, Article ID 1350058, 2013.

[14] E. Izhikevich, "Equilibrium," *Scholarpedia*, vol. 2, no. 10, 2007.

[15] J. P. Singh and B. K. Roy, "Five new 4-d autonomous conservative chaotic systems with various type of non-hyperbolic and lines of equilibria," *Chaos, Solitons and Fractals*, vol. 114, pp. 81–91, 2018.

[16] M. Zolfaghari-Nejad, H. Hassanpoor, and M. Charmi, "Numerical analysis of a novel 3d chaotic system with period-subtracting structures," *International Journal of Bifurcation and Chaos*, vol. 31, no. 11, Article ID 2150169, 2021.

[17] E. Dong, M. Yuan, S. Du, and Z. Chen, "A new class of Hamiltonian conservative chaotic systems with multistability and design of pseudo-random number generator," *Applied Mathematical Modelling*, vol. 73, pp. 40–71, 2019.

[18] Y. Liu and H. H.-C. Iu, "Antimonotonicity, chaos and multidirectional scroll attractor in autonomous odes chaotic system," *IEEE Access*, vol. 8, Article ID 77178, 2020.

[19] Y. Li, Y. Zeng, and J. Zeng, "A unique jerk system with abundant dynamics: symmetric or asymmetric bistability, tristability, and coexisting bubbles," *Brazilian Journal of Physics*, vol. 50, no. 2, pp. 153–163, 2020.

[20] H. Jahanshahi, A. Yousefpour, J. M. P. Munoz, I. Moroz, Z. Wei, and O. Castillo, "A new multi-stable fractional-order four-dimensional system with self-excited and hidden chaotic attractors: dynamic analysis and adaptive synchronization using a novel fuzzy adaptive sliding mode control method," *Applied Soft Computing*, vol. 87, Article ID 105943, 2020.

[21] S. Jafari and T. Kapitaniak, "Special chaotic systems," *The European Physical Journal Special Topics*, vol. 229, no. 6-7, pp. 877–886, 2020.

[22] Q. Lai, C. Chen, X. W. Zhao, J. Kengne, and C. Volos, "Constructing chaotic system with multiple coexisting attractors," *IEEE Access*, vol. 7, Article ID 24056, 2019.

[23] C. Li and J. C. Sprott, "Multistability in the Lorenz system: a broken butterfly," *International Journal of Bifurcation and Chaos*, vol. 24, no. 10, Article ID 1450131, 2014.

[24] A. N. Pisarchik and C. Grebogi, "Editorial," *International Journal of Bifurcation and Chaos*, vol. 18, pp. 1605-1606, 2008.

[25] C. Li, W. J. C. Thio, J. C. Sprott, H. H. C. Iu, and Y. Xu, "Constructing infinitely many attractors in a programmable chaotic circuit," *IEEE Access*, vol. 6, Article ID 29012, 2018.

[26] Q. Lai, P. D. K. Kuate, F. Liu, and H. H. C. Iu, "An extremely simple chaotic system with infinitely many coexisting attractors," *IEEE Transactions on Circuits and Systems II: Express Briefs*, vol. 67, pp. 1129–1133, 2019.

[27] J. Kengne, A. N. Negou, and D. Tchiotsop, "Antimonotonicity, chaos and multiple attractors in a novel autonomous memristor-based jerk circuit," *Nonlinear Dynamics*, vol. 88, no. 4, pp. 2589–2608, 2017.

[28] S. T. Kingni, C. Tchodimou, D. F. Platou, P. Djorwe, and S. G. E. Nana, "Antimonotonicity, coexisting attractors and bursting oscillations in optomechanical system: analysis and electronic implementation," *The European Physical Journal-Special Topics*, vol. 229, no. 6-7, pp. 1117–1132, 2020.

[29] V. R. F. Signing, J. Kengne, and J. R. M. Pone, "Antimonotonicity, chaos, quasi-periodicity and coexistence of hidden attractors in a new simple 4-d chaotic system with hyperbolic cosine nonlinearity," *Chaos, Solitons and Fractals*, vol. 118, pp. 187–198, 2019.

[30] J. Kengne, S. Jafari, Z. T. Njitacke, M. Yousefi Azar Khanian, and A. Cheukem, "Dynamic analysis and electronic circuit implementation of a novel 3d autonomous system without linear terms," *Communications in Nonlinear Science and Numerical Simulation*, vol. 52, pp. 62–76, 2017.

[31] S. Zhang, Y. Zeng, and Z. Li, "Chaos in a novel fractional order system without a linear term," *International Journal of Non-Linear Mechanics*, vol. 106, pp. 1–12, 2018.

[32] Y. Xu and Y. Wang, "A new chaotic system without linear term and its impulsive synchronization," *Optik*, vol. 125, no. 11, pp. 2526–2530, 2014.

[33] V. T. Pham, S. Jafari, C. Volos, and L. Fortuna, "Simulation and experimental implementation of a line-equilibrium system without linear term," *Chaos, Solitons and Fractals*, vol. 120, pp. 213–221, 2019.

[34] S. Vaidyanathan, "A novel four-dimensional conservative chaotic system without linear term, its analysis and adaptive control via integral sliding mode control," *International*

Journal of Modelling, Identification and Control, vol. 30, no. 2, pp. 132–142, 2018.

[35] V. T. Pham, S. Vaidyanathan, A. T. Azar, and V. H. Duy, "A new chaotic system without linear term, its backstepping control, and circuit design," *Backstepping Control of Nonlinear Dynamical Systems*, Elsevier, Amsterdam, Netherlands, pp. 33–52, 2021.

[36] S. Mobayen, S. T. Kingni, V.-T. Pham, F. Nazarimehr, and S. Jafari, "Analysis, synchronisation and circuit design of a new highly nonlinear chaotic system," *International Journal of Systems Science*, vol. 49, no. 3, pp. 617–630, 2018a.

[37] C. Guanrong, "Chaos theory and applications: a new trend," *Chaos Theory and Applications*, vol. 3, pp. 1-2, 2021.

[38] Ü. Çavuşoğlu, S. Kaçar, I. Pehlivan, and A. Zengin, "Secure image encryption algorithm design using a novel chaos based s-box," *Chaos, Solitons and Fractals*, vol. 95, pp. 92–101, 2017.

[39] X. Wang, U. Çavuşoğlu, S. Kacar et al., "S-box based image encryption application using a chaotic system without equilibrium," *Applied Sciences*, vol. 9, no. 4, p. 781, 2019.

[40] E. E. G. García, E. G. Inzunza, O. R. B. López, J. R. V. Cárdenas, and E. T. Cuautle, "Randomness improvement of chaotic maps for image encryption in a wireless communication scheme using pic-microcontroller via zigbee channels," *Chaos, Solitons and Fractals*, vol. 133, Article ID 109646, 2020.

[41] A. Ullah, A. Javeed, and T. Shah, "A scheme based on algebraic and chaotic structures for the construction of substitution box," *Multimedia Tools and Applications*, vol. 78, no. 22, Article ID 32484, 2019.

[42] S. Mobayen, C. K. Volos, S. Kaçar, U. Çavuşoğlu, and B. Vaseghi, "A chaotic system with infinite number of equilibria located on an exponential curve and its chaos-based engineering application," *International Journal of Bifurcation and Chaos*, vol. 28, Article ID 1850112, 2018.

[43] H. Gan, S. Xiao, and Y. Zhao, "A novel secure data transmission scheme using chaotic compressed sensing," *IEEE Access*, vol. 6, pp. 4587–4598, 2017.

[44] H. Tirandaz and A. K. Mollaee, "On active synchronization of fractional-order Bloch chaotic system and its practical application in secure image transmission," *International Journal of Intelligent Computing and Cybernetics*, vol. 11, no. 1, 2018.

[45] S. Dhall, S. K. Pal, and K. Sharma, "A chaos-based probabilistic block cipher for image encryption," *Journal of King Saud University-Computer and Information Sciences*, vol. 34, no. 1, pp. 1533–1543, 2018.

[46] N. Nesa, T. Ghosh, and I. Banerjee, "Design of a chaos-based encryption scheme for sensor data using a novel logarithmic chaotic map," *Journal of Information Security and Applications*, vol. 47, pp. 320–328, 2019.

[47] S. Shaukat, A. Arshid, A. Eleyan et al., "Chaos theory and its application: an essential framework for image encryption," *Chaos Theory and Applications*, vol. 2, pp. 17–22, 2020.

[48] H. Noura, C. Guyeux, A. Chehab, M. Mansour, and R. Couturier, "Efficient chaotic encryption scheme with OFB mode," *International Journal of Bifurcation and Chaos*, vol. 29, Article ID 1950059, 2019.

[49] R. Courtney, *Numerical Methods for Solving Systems of Nonlinear Equations*, Lakehead University, Thunder Bay, Ontario, Canada, 2012.

[50] J. Jiang, Y. Song, and P. Yu, "Delay-induced triple-zero bifurcation in a delayed leslie-type predator-prey model with additive allee effect," *International Journal of Bifurcation and Chaos*, vol. 26, Article ID 1650117, 2016.

[51] E. Gamero, E. Freire, A. J. Rodríguez-Luis, E. Ponce, and A. Algaba, "Hypernormal form calculation for triple-zero degeneracies," *Bulletin of the Belgian Mathematical Society Simon Stevin*, vol. 6, pp. 357–368, 1999.

[52] E. Freire, E. Gamero, A. J. Rodríguez-Luis, and A. Algaba, "A note on the triple-zero linear degeneracy: normal forms, dynamical and bifurcation behaviors of an unfolding," *International Journal of Bifurcation and Chaos*, vol. 12, no. 12, pp. 2799–2820, 2002.

[53] Z. Faghani, F. Nazarimehr, S. Jafari, and J. C. Sprott, "A new category of three-dimensional chaotic flows with identical eigenvalues," *International Journal of Bifurcation and Chaos*, vol. 30, Article ID 2050026, 2020.

[54] L. Liu, C. Du, L. Liang, and X. Zhang, "A high spectral entropy (se) memristive hidden chaotic system with multi-type quasi-periodic and its circuit," *Entropy*, vol. 21, no. 10, 2019.

[55] P. Legendre and L. Legendre, *Numerical Ecology*, Elsevier, Amsterdam, Netherlands, 2012.

[56] G. Alvarez and S. Li, "Some basic cryptographic requirements for chaos-based cryptosystems," *International Journal of Bifurcation and Chaos*, vol. 16, pp. 2129–2151, 2006.

[57] E. M. Kornaropoulos and P. Efstathopoulos, "Breaking and fixing secure similarity approximations: dealing with adversarially perturbed inputs," *Work*, vol. 40, p. 63, 2017.

[58] X. J. Tong, Z. Wang, Y. Liu, M. Zhang, and L. Xu, "A novel compound chaotic block cipher for wireless sensor networks," *Communications in Nonlinear Science and Numerical Simulation*, vol. 22, no. 1–3, pp. 120–133, 2015.

[59] W. Srich and W. San-Um, "Data encryption scheme based on rules of cellular automata and chaotic map function for information security," *IJ Network Security*, vol. 18, pp. 1130–1142, 2016.

Research Article

Some Real-Life Applications of a Newly Designed Algorithm for Nonlinear Equations and Its Dynamics via Computer Tools

Amir Naseem ⓘ,[1] **M. A. Rehman** ⓘ,[1] **and Jihad Younis** ⓘ[2]

[1]*Department of Mathematics, University of Management and Technology, Lahore 54770, Pakistan*
[2]*Department of Mathematics, Aden University, Khormaksar P.O.Box, Aden 6014, Yemen*

Correspondence should be addressed to Amir Naseem; amir.kasuri89@gmail.com and Jihad Younis; jihadalsaqqaf@gmail.com

In this article, we design a novel fourth-order and derivative free root-finding algorithm. We construct this algorithm by applying the finite difference scheme on the well-known Ostrowski's method. The convergence analysis shows that the newly designed algorithm possesses fourth-order convergence. To demonstrate the applicability of the designed algorithm, we consider five real-life engineering problems in the form of nonlinear scalar functions and then solve them via computer tools. The numerical results show that the new algorithm outperforms the other fourth-order comparable algorithms in the literature in terms of performance, applicability, and efficiency. Finally, we present the dynamics of the designed algorithm via computer tools by examining certain complex polynomials that depict the convergence and other graphical features of the designed algorithm.

1. Introduction

The role of computers in the fields of applied Mathematics cannot be denied in the modern age. Using different computer programs such as Mathematica, Matlab, and Maple, a plethora of different types of complex problems can be solved easily. In recent years, mathematicians employed the excessive use of computers in different branches of Mathematics especially in the determination of approximated roots of the transcendental and nonlinear algebraic equations which have played an important role in different branches of computational and applied mathematics. In many engineering disciplines, a lot of problems exist which can be easily converted into nonlinear forms by employing different mathematical techniques. Analytical methods cannot find the solution needed for these problems, and therefore, we need iterative algorithms for solving out these problems. To execute an iterative algorithm, we always need a starting point (initial guess) which is refined after every iteration, and we find the approximated root up to the required accuracy after some finite iterations. The convergence rate and convergence order of an iterative algorithm are relied upon the selection of that starting point. Some of the most popular and ancient iterative algorithms are given in [1–8] and the references

are cited therein. In the 15th century, Newton [1, 2] introduced a quadratic-order root-finding algorithm which has been used successfully for many years. Over the time, many experts worked on iterative algorithms and brought several modified versions of Newton's algorithm with higher-order convergence which involve predictor and corrector steps and are often referred to as multistep iterative algorithms. For more information, one can see [9–20] and the references are cited therein. In general, the convergence order of a multistep algorithm is higher because of predictor and corrector steps, but it results in a higher computational cost which is the downside of these algorithms. It is really difficult to handle the cost of computing and the convergence rate of an algorithm because these two terms are inversely proportional to each other.

Over the past few years, mathematicians have focused on the aforementioned issues and have tried to design some new iterative algorithms with higher convergence and low cost of computing by employing several mathematical methods. In [21], the authors introduced a new two-step Halley's method with sixth order convergence and then replaced its second derivative for reducing computing cost and proposed a new fifth order second derivative free algorithm. In [22], Hafiz and Al-Goria established a novel family of optimal eighth order

iterative algorithms and then studied their dynamics. In [23], the authors introduced seventh and ninth orders novel iterative algorithms with the help of the predictor-corrector technique and Simpson quadrature formulae. By employing the Newton interpolation technique along with weight functions, Salimi et al. [24] introduced a new family of eighth order optimal root-finding algorithms. In [25], the authors constructed some novel optimal iterative algorithms with higher convergence and demonstrated the applicability of the suggested methods by solving some engineering problems. Recently, Chu et al. [26] proposed a novel family iteration scheme and discussed the dynamics of the presented methods with the help of computer tools.

In the present research article, we introduce a new fourth-order and derivative free algorithm for solving engineering problems in the form of scalar nonlinear functions. The construction of this algorithm is based upon the finite difference scheme on Ostrowski's method. We also certify that the designed algorithm has fourth-order convergence. The designed algorithm is then applied to some real-world engineering problems for certifying its better performance and applicability among the other fourth-order algorithms in the literature. The dynamical comparison of the designed algorithm with the other comparable ones has been also presented via the computer program Mathematica 12.0.

2. Main Results

Consider the nonlinear problem of the following form:

$$\psi(u) = 0, \tag{1}$$

where ψ is a real-valued function with an open interval domain.

Suppose that α is a root of (1) with u_0 as an initial guess near to the exact root α, then the implication of Taylor's series around u_0 for (1) gives us

$$\psi(u_0) - (u - u_0)\psi'(u_0) + \frac{(u - u_0)^2 \psi''(u_0)}{2!} + \cdots = 0. \tag{2}$$

If $\psi'(u_0)$ is nonzero, then the above expression implies

$$u_{i+1} = u_i - \frac{\psi(u_i)}{\psi'(u_i)}, \tag{3}$$

which is Newton's root-finding algorithm [1, 2] for scalar nonlinear functions.

By taking it as a predictor, Ostrowski designed the following two-step iterative algorithm:

$$v_i = u_i - \frac{\psi(u_i)}{\psi'(u_i)},$$

$$u_{i+1} = v_i - \frac{\psi(v_i)\psi(u_i)}{\psi'(u_i)[\psi(u_i) - 2\psi(v_i)]}, \tag{4}$$

which is well-known Ostrowski's root-finding algorithm [11] for scalar nonlinear functions.

By including Newton's algorithm, the above two-step method may be converted to three-step in the following form:

$$v_i = u_i - \frac{\psi(u_i)}{\psi'(u_i)},$$

$$w_i = v_i - \frac{\psi(v_i)}{\psi'(v_i)}, \tag{5}$$

$$u_{i+1} = w_i - \frac{\psi(w_i)\psi(v_i)}{\psi'(v_i)[\psi(v_i) - 2\psi(w_i)]},$$

which is a three-step iteration scheme for calculating zeros of nonlinear scalar equations. The main drawback of the above algorithm is its high computational cost per iteration as it requires six evaluations for its execution. To lower its computational cost make it more effective, we approximate its first derivatives and make it derivative free, so that it can be easily applied on those nonlinear scalar functions whose first derivative becomes infinite or does not exist. To approximate $\psi'(u)$ in the predictor step, we employ the forward difference approximation as

$$\psi'(u_i) = \frac{\psi(u_i + \psi(u_i))}{\psi(u_i)} = g(u_i). \tag{6}$$

To approximate $\psi'(v)$, we utilize the finite difference scheme as

$$\psi'(v_i) = \frac{\psi(v_i) - \psi(u_i)}{v_i - u_i} = h(u_i, v_i). \tag{7}$$

Using (6) and (7) in (5), we can write Algorithm 1.

Algorithm 1. For a given u_0, compute the approximate solution u_{i+1} by the following iterative schemes

$$v_i = u_i - \psi(u_i)/g(u_i), i = 0, 1, 2, \ldots,$$
$$w_i = v_i - \psi(v_i)/h(u_i, v_i),$$
$$u_{i+1} = w_i - \psi(w_i)\psi(v_i)/h(u_i, v_i)[\psi(v_i) - 2\psi(w_i)]$$

Algorithm 1 is a new iteration scheme for calculating the approximated roots of scalar nonlinear equations and needs only four evaluations per iteration. The main characteristic of the suggested algorithm is that it is derivative free and easily applicable to all those scalar functions whose derivatives become undefined within the domain. In this sense, the proposed algorithm's computing cost is minimal which results in a higher efficiency index.

3. Convergence Analysis

In the present section, we shall discuss the convergence criterion of the newly designed algorithm, i.e., Algorithm 1.

Theorem 1. *Suppose that α is the root of the equation $\psi(u) = 0$. If $\psi(u)$ is sufficiently smooth in the neighborhood of α, then the order of convergence of Algorithm 1 is at least four.*

TABLE 1: Comparison among different fourth-order algorithms.

Methods	IT	u_{i+1}	$|\psi(u_{i+1})|$	$\sigma = |u_{i+1} - u_i|$	η
OM	04	0.3426482058114499	$9.186801e^{-17}$	$2.728697e^{-05}$	4
TM	05	0.3426482058114499	$4.236557e^{-23}$	$1.848727e^{-14}$	4
ZM	05	0.3426482058114499	$7.675869e^{-25}$	$1.516654e^{-07}$	4
Algorithm 1	04	0.3426482058114499	$5.362719e^{-18}$	$1.131404e^{-06}$	4

Proof. To analyze the convergence criterion of the iteration scheme (1), we assume that α is a root of equation $\psi(u) = 0$ and e_i be the error at i^{th} iteration; then, $e_i = u_i - \alpha$, and by using Taylor's series expansion, we have

$$\psi(u_i) = \psi'(\alpha)e_i + \frac{1}{2!}\psi''(\alpha)e_i^2 + \frac{1}{3!}\psi'''(\alpha)e_i^3 + \frac{1}{4!}\psi^{(iv)}(\alpha)e_i^4 + O(e_i^5),$$

$$\psi(u_i) = \psi'(\alpha)\left[e_i + d_2 e_i^2 + d_3 e_i^3 + d_4 e_i^4 + O(e_i^5)\right], \tag{8}$$

where

$$d_i = \frac{1}{i!}\frac{\psi^{(i)}(\alpha)}{\psi'(\alpha)},$$

$$g(u_i) = \psi'(\alpha)\left[1 + 3d_2 e_i + (7d_3 + d_2^2)e_i^2 + (6d_2 d_3 + 15d_2^4)e_i^3 + (18d_2 d_4 + 31d_5 + d_3 d_2^2 + 5d_3^2)e_i^4 + O(e_i^5)\right]. \tag{9}$$

With the help of equations (8) and (9), we get

$$v_i = \alpha + 2d_2 e_i^2 + (6d_3 - 5d_2^2)e_i^3 + (14d_4 - 26d_3 d_2 + 13d_2^3)e_i^4 + O(e_i^5), \tag{10}$$

$$\psi(v_i) = \psi'(\alpha)\left[2d_2 e_i^2 + (6d_3 - 5d_2^2)e_i^3 + (14d_4 - 26d_3 d_2 + 13d_2^3)e_i^4 + O(e_i^5)\right], \tag{11}$$

$$h(u_i, v_i) = \psi'(\alpha)\left[1 + d_2 e_i + (d_3 + d_2^2)e_i^2 + (8d_2 d_3 - 5d_2^3 + d_4)e_i^3 + (13d_2^4 - 27d_3 d_2^2 + 16d_4 d_2 + +d_5 + 6d_3^2)e_i^4 + O(e_i^5)\right], \tag{12}$$

$$w_i = \alpha + 2d_2 e_i^3 + (8d_2 d_3 - 7d_2^3)e_i^4 + O(e_i^5), \tag{13}$$

$$\psi(w_i) = \psi'(\alpha)\left[2d_2 e_i^3 + (8d_2 d_3 - 7d_2^3)e_i^4 + O(e_i^5)\right]. \tag{14}$$

Using equations (8)–(14) in Algorithm 1 gives us the following equality:

$$u_{i+1} = \alpha - 2d_2^3 e_i^4 + O(e^5), \tag{15}$$

which implies that

$$e_{i+1} = -2d_2^3 e_i^4 + O(e^5). \tag{16}$$

The above equation shows that the designed algorithm is of fourth-order convergence. □

4. Real-Life Applications

In this section, we take five real-world problems in the form of scalar nonlinear functions to exhibit the applicability, validity, and efficiency of the newly designed fourth-order algorithm. We compare it with other well-known fourth-order algorithms, namely, Ostrowski's method (OM) [11], Traub's method (TM) [12], and Zhanlav method (ZM) [27].

Example 1. Fluid permeability problem:

The hydraulic permeability is actually the measurement of the flow resistance. It relates the pressure gradient to fluid

velocity and may be expressed as

$$\kappa = \frac{r_e u^3}{20(1-u)^2},$$ (17)

$$r_e u^3 - 20k(1-u)^2 = 0,$$

where κ denotes the specific hydraulic permeability, r_e stands for the radius, and $0 \le u \le 1$ is the porosity. For further details see [28] and the reference cited therein. By taking the values of $r_e = 100$ and $\kappa = 0.4655$ in (14), we obtain the above problem in the following nonlinear function:

$$\psi_1(u) = 100u^3 - 9.31(1-u)^2.$$ (18)

To solve ψ_1, the initial guess has been chosen as $u_0 = 2.0$ for starting the iteration process, and the results are given in Table 1.

Example 2. Blood rheology model.

Blood rheology is a branch of science that works to study the physical and flow properties of blood [29]. Blood is actually a non-Newtonian fluid and treated as Caisson fluid. The model of Caisson fluid shows that the flow of simple fluids in a tube is such a way that the center core of the fluids will move as a plug with little deformation and velocity gradient occurs near the wall.

To study the plug flow of Caisson fluids flow, we consider the following function in the form of nonlinear equation as

$$H = 1 - \frac{16}{7}\sqrt{u} + \frac{4}{3}u - \frac{1}{21}u^4,$$ (19)

where flow rate reduction is computed by H. Using $H = 0.40$ in (19), we have

$$\psi_2(u) = \frac{1}{441}u^8 - \frac{8}{63}u^5 - 0.05714285714u^4 + \frac{16}{9}u^2 - 3.624489796u + 0.3.$$ (20)

To solve ψ_2, the initial guess has been chosen as $u_0 = 0.9$ for starting the iteration process, and the results are given in Table 2.

Example 3. Van Der Wall's equation.

The well-known equation for examining the behaviour of real and ideal gas was introduced by Van Der Wall's [30], with the following expression:

$$\left(P + \frac{C_1 n^2}{V^2}\right)(V - nC_2) = iRT.$$ (21)

Equation (21) may be easily transformed into the following nonlinear function by taking the particular values of the parameters:

$$\psi_3(u) = 0.986u^3 - 5.181u^2 + 9.067u - 5.289,$$ (22)

where u is the gas volume that may be easily determined by solving ψ_2. Because the polynomial's degree is three, it must have three roots. There is only one positive real root 1.9298462428 among these which is physically possible since the gas volume can never be negative. To solve ψ_3, the initial guess has been chosen as $u_0 = 1.0$ for starting the iteration process, and the results are given in Table 3.

Example 4. Plank's radiation law.

The energy density within the black isothermal body is calculated using Planck's radiation law [31] given as follows:

$$\varphi(\gamma) = \frac{8\pi Pc}{\gamma^5 \left(e^{Pc/\gamma Tk} - 1\right)}.$$ (23)

Suppose we want to calculate wavelength γ_1 for the peak value of the energy density $\varphi(\gamma_1)$. To transform (23) in nonlinear form, we assume $u = Pc/\gamma Tk$ and obtain the following nonlinear expression:

$$\psi_4(u) = -1 + \frac{u}{5} + e^{-u}.$$ (24)

One of the estimated roots of ψ_4 is -0.0000000000000000 which represents the maximum amount of the wavelength of the radiation. To solve ψ_4, the initial point has been chosen as $u_0 = -2.0$ for starting the iteration process, and the results are given in Table 4.

Example 5. The problem of beam designing.

In Physics and Engineering sciences, the beam designing problem [32] regarding the embedment u of a sheet pile wall in the form of scalar nonlinear function is expressed as

$$\psi_5(u) = \frac{u^3 + 2.87u^2 - 4.62u - 10.28}{4.62}.$$ (25)

To solve ψ_5, the initial guess has been chosen as $u_0 = 3.0$ for starting the iteration process, and the results are given in Table 5.

Here, we choose the accuracy $\varepsilon = 10^{-15}$ in the following stopping criterion of the computer program:

$$|u_{i+1} - u_i| < \varepsilon.$$ (26)

We used the computer application Maple 13 to solve all numerical problems.

Tables 1–5 exhibit the numerical comparison of the designed fourth-order algorithm with Ostrowski's method (OM), Traub's method (TM), and Zhanlav's method (ZM). In the columns of the above tables, IT stands for the number of iterations, $|\psi(u)|$ indicates the positive value of the function $\psi(u)$, u_{i+1} indicates the estimated root, σ indicates the absolute difference of the consecutive estimations u_{i+1},

TABLE 2: Comparison among different fourth-order algorithms.

Methods	IT	u_{i+1}	$|\psi(u_{i+1})|$	$\sigma = |u_{i+1} - u_i|$	η
OM	03	0.0864335580522918	$2.960661e^{-18}$	$4.952936e^{-05}$	4
TM	03	0.0864335580522916	$3.697508e^{-16}$	$1.642942e^{-04}$	4
ZM	12	0.0864335580522918	$1.957052e^{-25}$	$5.571776e^{-07}$	4
Algorithm 1	03	0.0864335580522917	$1.940272e^{-17}$	$3.210544e^{-06}$	4

TABLE 3: Comparison among different fourth-order algorithms.

Methods	IT	u_{i+1}	$|\psi(u_{i+1})|$	$\sigma = |u_{i+1} - u_i|$	η
OM	09	1.9298462428478622	$1.626245e^{-22}$	$1.858593e^{-06}$	4
TM	10	1.9298462428478622	$4.578052e^{-27}$	$1.235520e^{-07}$	4
ZM	44	1.9298462428478622	$1.365062e^{-19}$	$6.456152e^{-06}$	4
Algorithm 1	06	1.9298462428478622	$1.335843e^{-29}$	$3.841021e^{-10}$	4

TABLE 4: Comparison among different fourth-order algorithms.

Methods	IT	u_{i+1}	$|\psi(u_{i+1})|$	$\sigma = |u_{i+1} - u_i|$	η
OM	04	−0.0000000000000000	$1.030994e^{-51}$	$3.261218e^{-13}$	4
TM	04	−0.0000000000000000	$1.706136e^{-36}$	$1.719178e^{-09}$	4
ZM	04	−0.0000000000000000	$1.383001e^{-20}$	$1.153483e^{-05}$	4
Algorithm 1	04	−0.0000000000000000	$2.759067e^{-45}$	$6.858899e^{-14}$	4

TABLE 5: Comparison of different fourth-order algorithms.

Methods	IT	u_{i+1}	$|\psi(u_{i+1})|$	$\sigma = |u_{i+1} - u_i|$	η
OM	03	2.0021187789538273	$1.247083e^{-31}$	$2.494230e^{-08}$	4
TM	03	2.0021187789538273	$1.271632e^{-29}$	$7.400791e^{-08}$	4
ZM	03	2.0021187789538273	$1.334997e^{-21}$	$5.297174e^{-06}$	4
Algorithm 1	03	2.0021187789538273	$1.760330e^{-28}$	$1.073092e^{-09}$	4

and u_i and η represent the approximated computational order of convergence given as

$$\eta \approx \frac{\ln\left(|u_{i+1} - \alpha|/|u_i - \alpha|\right)}{\ln\left(|u_i - \alpha|/|u_{i-1} - \alpha|\right)}, \tag{27}$$

which was introduced by Weerakoon and Fernando [33].

5. Dynamical Analysis via Computer Technology

In this section, we give a detailed graphical comparison of the newly designed fourth-order algorithm with the other fourth-order algorithms via computer technology by considering some complex polynomials in the form of polynomiographs. A polynomiograph is a graphical object generated in a process known as polynomiography, introduced by Dr. Bahman Kalantri in 2005 [34]. It is defined as "the algorithmic visualization of polynomial equations by employing different iterative techniques" [35].

To draw dynamics by employing computer technology using various iterative algorithms, an initial rectangle $\mathscr{R}$ which includes the root of the investigated complex polynomial has been chosen. Then, for every point w_0 in $\mathscr{R}$, we perform the process of iteration. The image's quality is usually correlated with the discretization of $\mathscr{R}$, i.e., if the rectangle $\mathscr{R}$ has been discretized into a 2000×2000 grid, then the quality of the produced image will be better.

Typically, the colors of produced polynomiographs are fully associated with the number of iterations required to find the approximated roots with a given precision and a selected iterative algorithm. The main algorithm for the production of a polynomiograph is given in Algorithm 1.

A stopping criterion is always required for an iterative algorithm that includes the repetition of steps, since it informs us about the convergence or divergence of the investigated iterative algorithm. Such a criterion is commonly referred to as a convergence test with the following mathematical expression:

$$|w_{i+1} - w_i| < \varepsilon, \tag{28}$$

Input: $q \in \mathbb{C}$—polynomial, $\mathbb{A} \subset \mathbb{C}$—area, K—maximum No. of iterations, I—iterative algorithm, ε—accuracy, colormap $[0 \ldots C-1]$—colormap with C colors
Output: polynomiograph for the complex polynomial q in the area $\mathbb{A}$
for $w_0 \in \mathbb{A}$, **do**
    $i = 0$
    while $i \leq K$ do
        $w_{i+1} = I(w_i)$
            if $|w_{i+1} - w_i| < \epsilon$, then
                break
        $i = i + 1$
    color $\mathbf{w}_0$ via colormap

ALGORITHM 1: Polynomiograph's generation.

where w_{i+1} and w_i denote the successive iterations, and $\varepsilon > 0$ stands for the accuracy in the stopping criterion. The convergence test $(w_{i+1}, w_i, \varepsilon)$ is considered TRUE if the iterative algorithm under consideration is converged and FALSE if it is diverged. The abovementioned stopping criterion (28) is also used in this study. The variety of polynomiographs' colors is correlated with the performed iterations to find out the root with given precision ε. Using various iterative algorithms, a variety of aesthetically pleasant polynomiographs can be produced by altering the parameter K, where K specifies the upper limit of the number of iterations. For further information regarding polynomiography along with its applications in different fields, one can see [36–44] and the references cited therein.

For drawing polynomiographs through different iterative algorithms, we consider the following four complex polynomials:

$$
\begin{aligned}
q_1(w) &= w^3 - 1, \\
q_2(w) &= \left(w^3 - 1\right)^2, \\
q_3(w) &= w^4 - 1, \\
q_4(w) &= \left(w^4 - 1\right)^2.
\end{aligned}
\tag{29}
$$

The colormap used for the coloring of iterations in the generation of polynomiographs is shown in Figure 1:

Example 6. Polynomiographs for the polynomial q_1 through different fourth-order algorithms.

In the first example, we consider a cubic-degree polynomial $q_1(w) = w^3 - 1$, having three distinct roots $1, -1/2 + \sqrt{3}/2i$, and $-1/2 - \sqrt{3}/2i$. We used a computer program to run all the methods to get the simple roots of the under consideration polynomial q_1, and the results are shown in Figure 2.

Example 7. Polynomiographs for the polynomial q_2 through different fourth-order algorithms.

In the second example, we take a sextic-degree polynomial $q_2(w) = (w^3 - 1)^2$, which has three unique roots $1, -1/2 + \sqrt{3}/2i$, and $-1/2 - \sqrt{3}/2i$ with multiplicity two. We perform the process of iteration for all iterative algorithms for drawing polynomiographs, and the results are shown in Figure 3.

Example 8. Polynomiographs for the polynomial q_3 through different fourth-order algorithms.

In the third example, we consider a quartic-degree polynomial $q_3(w) = w^4 - 1$, which has four unique roots $1, -1, i,$ and $-i$. We created the graphical objects by executing all iterative algorithms, and the results are shown in Figure 4.

Example 9. Polynomiographs for the polynomial q_4 through different fourth-order algorithms.

In the fourth example we take an eighth-degree complex polynomial $q_4(w) = (w^4 - 1)^2$ with four unique roots $1, -1, i,$ and $-i$ of multiplicity two. We used a computer program to run all methods for drawing polynomiographs, and the results in the form of visually attractive pictures are shown in Figure 5.

In above examples, we compared the developed algorithm to various fourth-order iterative algorithms using a computer program by taking into account different degrees complex polynomials. Two key features may be identified from the produced graphics. The first is the iteration scheme's speed of convergence, and the second feature is the iteration scheme's dynamics. Low dynamics are seen in places with little color variation, and high dynamics are found in areas with a lot of color variety. The black coloring in the graphics denotes areas where the solution cannot be reached in the specified number of iterations. The darker zone in the above-presented pictures indicates that the iterative algorithm under consideration requires fewer iterations for finding the solution of the given problem. The same-colored regions in the graphical objects represent the same number of iterations necessary to find the required solution with the given accuracy. Note that the polynomiographs created using our proposed iterative algorithm have considerably brighter and darker regions and no black areas as compared to other similar order algorithms in the literature. Furthermore, the polynomiographs of the proposed iterative algorithm show larger convergence areas than the other comparable techniques which demonstrate the better efficiency of the suggested algorithm.

We drew all graphical objects with the computer program Mathematica 12.0 by using the values of parameters as $\varepsilon = 0.001$ and $K = 20$, where ε and K indicate the accuracy and the upper bound of the number of iterations, respectively.

Figure 1: The colormap used for generating polynomiographs.

(a)	(b)	(c)	(d)
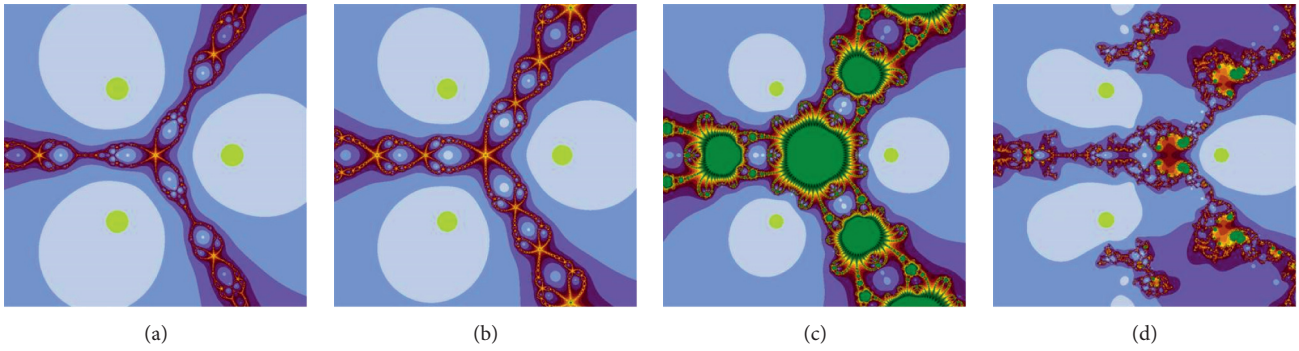
Figure 2: Polynomiographs related to the complex polynomial q_1. (a) Ostrowski's method. (b) Traub's method. (c) Zhanlav's method. (d) Algorithm 1.

(a)	(b)	(c)	(d)
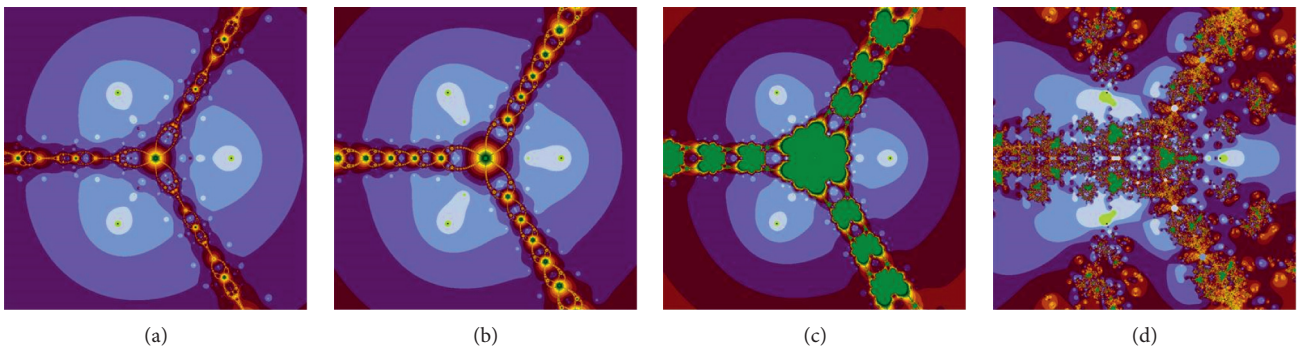
Figure 3: Polynomiographs related to the complex polynomial q_2. (a) Ostrowski's method. (b) Traub's method. (c) Zhanlav's method. (d) Algorithm 1.

(a)	(b)	(c)	(d)
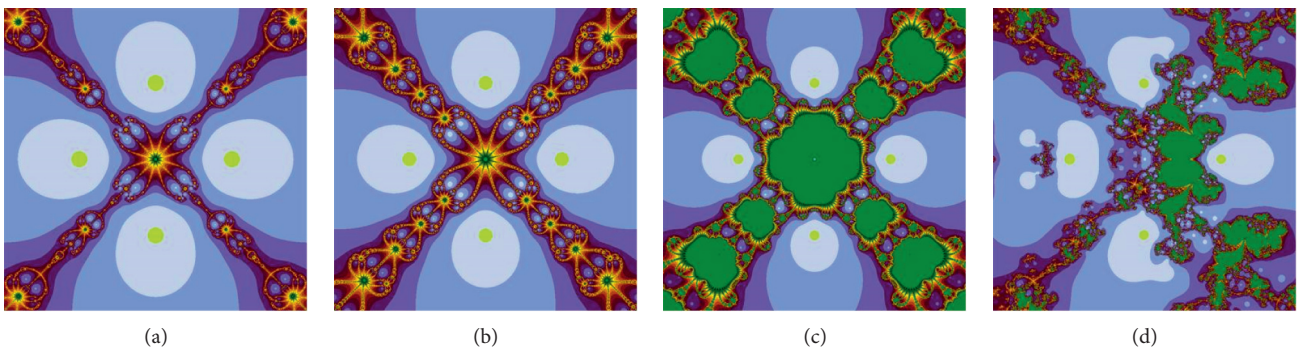
Figure 4: Polynomiographs related to the complex polynomial q_3. (a) Ostrowski's method. (b) Traub's method. (c) Zhanlav's method. (d) Algorithm 1.

(a)   (b)   (c)   (d)
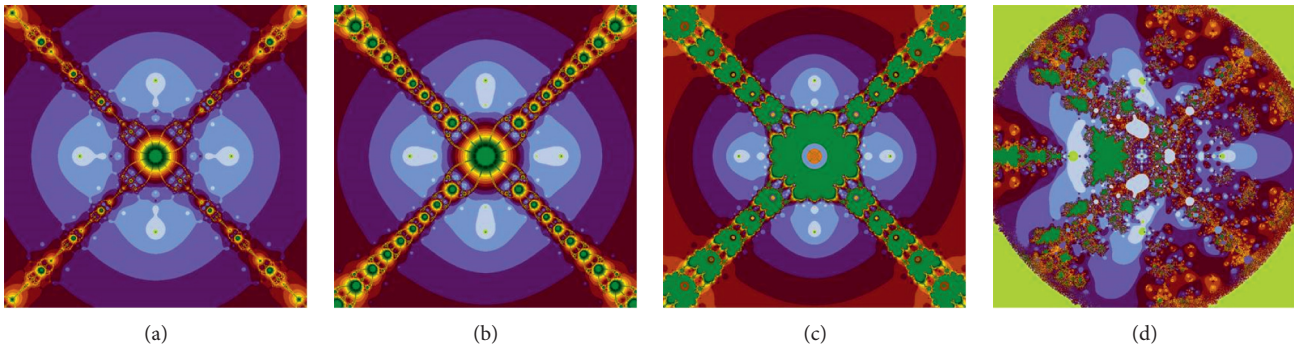
Figure 5: Polynomiographs related to the complex polynomial q_4. (a) Ostrowski's method. (b) Traub's method. (c) Zhanlav's method. (d) Algorithm 1.

6. Conclusion

By employing the finite difference scheme on Ostrowski's method, we designed a new derivative free algorithm for calculating the approximate zeros of nonlinear scalar equations that possesses the fourth-order convergence. To analyze the applicability of the designed algorithm, we took some real-life engineering problems and solved them via computer tools. The numerical results given in Tables 1–5 proved the better performance and applicability of the designed algorithm against the other fourth-order algorithms. We have also presented the dynamics of the designed algorithm and gave a detailed comparison with the other comparable fourth-order algorithms in the literature via computer tools that revealed the convergence and other graphical characteristics of the designed algorithm. A new family of derivative free root-finding algorithms can be constructed by applying the finite difference scheme to the existing methods in the literature.

Data Availability

The data used to support this study are included within the article.

Conflicts of Interest

The authors declare that they have no conflicts of interest.

Authors' Contributions

All authors contributed equally to this study.

References

[1] D. E. Kincaid and E. W. Cheney, *Numerical Analysis*, Brooks/Cole Publishing Company, Pacific Grove, CA, USA, 1990.

[2] C. Chun, "Construction of Newton-like iteration methods for solving nonlinear equations," *Numerische Mathematik*, vol. 104, no. 3, pp. 297–315, 2006.

[3] J. M. Hernández and M. A. Hernandez, "A family of Chebyshev-Halley type methods in Banach spaces," *Bulletin of the Australian Mathematical Society*, vol. 55, no. 1, pp. 113–130, 1997.

[4] R. L. Burden and J. D. Faires, *Numerical Analysis*, Brooks/Cole Publishing Company, Pacific Grove, CA, USA, 6th edition, 1997.

[5] J. Stoer and R. Bulirsch, *Introduction to Numerical Analysis*, Springer-Verlag, New York, NY, USA, 3rd edition, 2002.

[6] J.-H. He, "Homotopy perturbation technique," *Computer Methods in Applied Mechanics and Engineering*, vol. 178, no. 3-4, pp. 257–262, 1999.

[7] I. K. Argyros, "A note on the Halley method in Banach spaces," *Applied Mathematics and Computation*, vol. 58, pp. 215–224, 1993.

[8] S. Householder, *The Numerical Treatment of a Single Nonlinear Equation*, McGraw-Hill, New York, NY, USA, 1970.

[9] A. Kumar, P. Maroju, R. Behl, D. K. Gupta, and S. S. Motsa, "A family of higher order iterations free from second derivative for nonlinear equations in R," *Journal of Computational and Applied Mathematics*, vol. 330, pp. 215–224, 2018.

[10] A. Golbabai and M. Javidi, "A third-order Newton type method for nonlinear equations based on modified homotopy perturbation method," *Applied Mathematics and Computation*, vol. 191, no. 1, pp. 199–205, 2007.

[11] A. M. Ostrowski, *Solution of Equations and Systems of Equations*, Academic Press, Cambridge, MA, USA, 2nd edition, 1966.

[12] J. F. Traub, *Iterative Methods for the Solution of Equations*, Chelsea Publishing company, New York, NY, USA, 1982.

[13] J. Kuo, "The improvements of modified Newton's method," *Applied Mathematics and Computation*, vol. 189, no. 1, pp. 602–609, 2007.

[14] A. Naseem, M. A. Rehman, and T. Abdeljawad, "Numerical algorithms for finding zeros of nonlinear equations and their dynamical aspects," *Journal of Mathematics*, vol. 2020, Article ID 2816843, 11 pages, 2020.

[15] A. Naseem, M. A. Rehman, and T. Abdeljawad, "Some new iterative algorithms for solving one-dimensional non-linear equations and their graphical representation," *IEEE Access*, vol. 9, pp. 8615–8624, 2021.

[16] R. Behl and E. Martinez, "A new high-order and efficient family of iterative techniques for nonlinear models," *Hindawi Complexity*, vol. 2020, Article ID 1706841, 11 pages, 2020.

[17] F. Ahmad, E. Tohidi, M. Z. Ullah, and J. A. Carrasco, "Higher order multi-step Jarratt-like method for solving systems of nonlinear equations: application to PDEs and ODEs," *Computers & Mathematics with Applications*, vol. 70, no. 4, pp. 624–636, 2015.

[18] M. A. Rehman, A. Naseem, and T. Abdeljawad, "Some novel sixth-order iteration schemes for computing zeros of

nonlinear scalar equations and their applications in engineering," *Journal of Function Spaces*, vol. 2021, p. 11, Article ID 5566379, 2021.

[19] F. Ahmad, E. Tohidi, and J. A. Carrasco, "A parameterized multi-step Newton method for solving systems of nonlinear equations," *Numerical Algorithms*, vol. 71, no. 3, pp. 631–653, 2016.

[20] A. Naseem, M. A. Rehman, T. Abdeljawad, and Y.-M. Chu, "Some engineering applications of newly constructed algorithms for one-dimensional non-linear equations and their fractal behavior," *Journal of King Saud University Science*, vol. 33, no. 5, Article ID 101457, 2021.

[21] M. A. Noor, W. A. Khan, and A. Hussain, "A new modified Halley method without second derivatives for nonlinear equation," *Applied Mathematics and Computation*, vol. 189, no. 2, pp. 1268–1273, 2007.

[22] M. S. Rhee, Y. I. Kim, and B. Neta, "An optimal eighth-order class of three-step weighted Newton's methods and their dynamics behind the purely imaginary extraneous fixed points," *International Journal of Computer Mathematics*, vol. 95, no. 11, pp. 2174–2211, 2017.

[23] M. A. Hafiz and S. M. H. Al-Goria, "New ninth and seventh order methods for solving nonlinear equations," *European Scientific Journal*, vol. 8, no. 27, pp. 83–95, 2012.

[24] M. Salimi, N. M. A. Nik Long, S. Sharifi, and B. A. Pansera, "A multi-point iterative method for solving nonlinear equations with optimal order of convergence," *Japan Journal of Industrial and Applied Mathematics*, vol. 35, no. 2, pp. 497–509, 2018.

[25] O. S. Solaiman and I. Hashim, "Efficacy of optimal methods for nonlinear equations with chemical engineering applications," *Mathematical Problems in Engineering*, vol. 2019, Article ID 1728965, 11 pages, 2019.

[26] Y. Chu, N. Rafiq, M. Shams, S. Akram, N. A. Mir, and H. Kalsoom, "Computer methodologies for the comparison of some efficient derivative free simultaneous iterative methods for finding roots of non-linear equations," *Computers, Materials & Continua*, vol. 66, no. 1, pp. 275–290, 2021.

[27] T. Zhanlav, O. Chuluunbaatar, and G. Ankhbayar, "On Newton-type methods with fourth and fifth-order convergence," *Discrete and Continuous Models and Applied Computational Science*, vol. 2, pp. 30–35, 2010.

[28] W. M. Saltzman, *Drug Delivery: Engineering Principal for Drug Therapy*, Oxford University Press, New York, NY, USA, 2001.

[29] R. L. Fournier, *Basic Transport Phenomena in Biomedical Engineering*, pp. 1–611, Taylor & Francis, New York, NY, USA, 2007.

[30] V. D. Waals and J. Diderik, "Over de continuiteit van den gas-envloeistoftoestand (on the continuity of the gas and liquid state)," Ph.D. thesis, Leiden University, Leiden, The Netherlands, 1873.

[31] M. Planck, "The theory of heat radiation," in *Translated by Masius, M*, P. Blakiston's Son & Co., Philadelphia, PA, USA, 2nd ed. edition, 1914.

[32] M. Shams, N. Ahmad Mir, N. Rafiq, A. O. Almatroud, and S. Akram, "On dynamics of iterative techniques for nonlinear equation with applications in engineering," *Mathematical Problems in Engineering*, vol. 2020, Article ID 5853296, 17 pages, 2020.

[33] S. Weerakoon and T. G. I. Fernando, "A variant of Newton's method with accelerated third-order convergence," *Applied Mathematics Letters*, vol. 13, no. 8, pp. 87–93, 2000.

[34] B. Kalantari, "Polynomiography: from the fundamental theorem of algebra to art," *Leonardo*, vol. 38, no. 3, pp. 233–238, 2005.

[35] B. Kalantari, "Method of creating graphical works based on polynomials," U.S. Patent 6 894 705, 2005.

[36] B. Kalantari and E. H. Lee, "Newton-Ellipsoid polynomiography," *Journal of Mathematics and the Arts*, vol. 13, no. 4, pp. 336–352, 2019.

[37] A. Naseem, M. A. Rehman, and T. Abdeljawad, "Computational methods for non-linear equations with some real-world applications and their graphical analysis," *Intelligent Automation & Soft Computing*, vol. 30, no. 3, pp. 805–819, 2021.

[38] K. Gdawiec, "Fractal patterns from the dynamics of combined polynomial root finding methods," *Nonlinear Dynamics*, vol. 90, no. 4, pp. 2457–2479, 2017.

[39] A. Naseem, M. A. Rehman, and T. Abdeljawad, "Higher-order root-finding algorithms and their basins of attraction," *Journal of Mathematics*, vol. 2020, Article ID 5070363, 11 pages, 2020.

[40] K. Gdawiec, W. Kotarski, and A. Lisowska, "Visual analysis of the Newton's method with FractionalOrder derivatives," *Symmetry*, vol. 11, no. 9, 2019.

[41] A. Naseem, M. A. Rehman, T. Abdeljawad, and Y.-M. Chu, "Novel iteration schemes for computing zeros of non-linear equations with engineering applications and their dynamics," *IEEE Access*, vol. 9, pp. 92246–92262, 2021.

[42] A. Naseem, M. A. Rehman, and T. Abdeljawad, "Numerical methods with engineering applications and their visual analysis via polynomiography," *IEEE Access*, vol. 9, pp. 99287–99298, 2021.

[43] J. R. Sharma and H. Arora, "A new family of optimal eighth order methods with dynamics for nonlinear equations," *Applied Mathematics and Computation*, vol. 273, pp. 924–933, 2016.

[44] B. Neta, M. Scott, and C. Chun, "Basins of attraction for several methods to find simple roots of nonlinear equations," *Applied Mathematics and Computation*, vol. 218, no. 21, pp. 10548–10556, 2012.

WILEY | Hindawi

Research Article

Dissipative Filter Design for Nonlinear Time-Varying-Delay Singular Systems against Deception Attacks

Guobao Liu [ORCID],[1] **Shibin Shen** [ORCID],[1] **and Xianglei Jia** [ORCID][2]

[1]*School of Electrical and Automation, Nanjing Normal University, Nanjing 210046, China*
[2]*School of Automation, Hangzhou Dianzi University, Hangzhou 310018, China*

Correspondence should be addressed to Shibin Shen; shen112233@139.com

This paper applies a T-S fuzzy model to depict a class of nonlinear time-varying-delay singular systems and investigates the dissipative filtering problem for these systems under deception attacks. The measurement output is assumed to encounter random deception attacks during signal transmission, and a Bernoulli distribution is used to describe this random phenomena. In this case, the filtering error system modeled by a stochastic singular T-S fuzzy system is established and stochastic admissibility for this kind of system is defined firstly. Then, by combining some integral inequalities and using the Lyapunov–Krasovskii functional approach, sufficient delay-dependent conditions are presented based on linear matrix inequality techniques, where the system of filtering error can be stochastically admissible and strictly $(\mathbb{Q}, \mathbb{S}, \mathbb{R})$-dissipative against randomly occurring deception attacks. Moreover, parameters of the desired filter can be obtained via the solutions of the established conditions. The validity of our work is illustrated through a mostly used example of the nonlinear system.

1. Introduction

In order to study various actual systems, such as large-scale systems, circuit systems, and biological systems, scholars have widely used the singular system model to describe these systems. In contrast with ordinary state space systems, singular systems can describe the performance characteristics of physical systems better [1]. On the other hand, time delay is a major factor that leads to system instability and performance degradation. Because of the coupling of the delay term and the functional equation, the study of singular time-delay systems is much more difficult than that of the standard time-delay systems [2]. Not only stability but also regularity and absence of impulse (or causality) are involved in the admissible analysis problem for singular time-delay systems. Up to now, various results for studying singular time-delay systems have been published. Reachable set estimation for continuous-time singular delay systems [3–5], sliding mode control for discrete-time singular delay systems [6–8], and H_∞ control for singular time-delay systems with Markovian jump parameters [9–11] are just a few examples of so many research works.

In the past decade, control researchers discovered that in practical or industrial applications, nonlinearities in system dynamics behavior can be fairly accurately described as a set of locally linear models mixed together with fuzzy membership functions. Thus, any complex nonlinear systems can be fuzzified and effectively approximated as a set of linear models by using the T-S fuzzy model approach [12]. In this case, a similar way to linear systems can be extended to analyze and synthesize nonlinear systems and lots of fruitful studies on the fields of stability theories, adaptive tracking control, H_∞ filter design, etc., have been achieved for T-S fuzzy systems [13–18]. Recently, using the T-S fuzzy model to approximate singular nonlinear systems has also been published in many literature studies. To mention a few, the problems of admissibility analysis and controller design for singular T-S fuzzy systems with mismatched membership functions were investigated in [19,20]; the problems of adaptive sliding mode controller design for T-S fuzzy singular systems were considered in [21,22]; and asynchronous filtering problems for T-S fuzzy singular

systems with Markovian jump parameters were investigated in [23,24].

On another active research frontier, cyber-attacks have become more and more important factors to threaten network security in the network control system since they could lead to the leakage of a large amount of confidential information. So far, denial-of-service attacks and deception attacks are two main kinds of cyber-attacks widely studied by scholars [25–29]. Especially, deception attacks are more secluded and harder to detect which import mendacious data in the process of signal transmission and lead to performance damage of the target system. Therefore, it is very important to design a security filter for the system with deception attacks. For example, the topics include distributed recursive filtering for discrete time-delayed stochastic systems subject to both uniform quantization and deception attacks, recursive filtering for stochastic nonlinear time-varying complex networks with deception attacks, and event-triggered filter design for T-S fuzzy systems with deception attacks had been investigated in [30–32], respectively. As far as we know, control and filtering problems for T-S fuzzy singular systems with time-varying delays against deception attacks have not been fully investigated, not mention to dissipative filter design. Dissipativity, in simple terms, generally indicates that the increase in a system's internal energy storage does not exceed the external energy supply of the system. The dissipativity has been analysed for large amounts of nonlinear systems and widely used in control theory and practice [33–35]. All the aforementioned facts motivate our research.

The main contribution of this paper is centered on dealing with the problem of dissipative filtering for T-S fuzzy singular systems with time-varying delays subject to deception attacks, where the measurement output is assumed to encounter random deception attacks based on a Bernoulli distribution during signal transmission. In this case, the filtering error system modeled by a stochastic singular T-S fuzzy system is established and the stochastic admissibility for this kind of system is defined. By using the Lyapunov–Krasovskii functional (LKF) approach and based on linear matrix inequality (LMI) techniques, sufficient delay-dependent conditions are established to guarantee the stochastic admissibility and strictly $(\mathbb{Q}, \mathbb{S}, \mathbb{R})$-dissipativity of the filtering error with randomly occurring deception attacks. Furthermore, based on these feasible conditions, parameters of the desired filter can be obtained. At last, we give an example of the nonlinear system to show the effectiveness of our result.

Notations. In this work, the dimensions of all the matrices are generally considered to be compatible. $\mathbf{R}^n$ denotes the Euclidean space with n dimension; $\mathbf{R}^{n \times m}$ represents the real matrices with $n \times m$ dimension; I represents an identity matrix, and 0 denotes a zero matrix with appropriate dimension; $\| \cdot \|$ denotes the Euclidean norm of a vector and its induced norm of a matrix; $A + A^T$ is described by $\mathrm{sym}(A)$; $\mathscr{L}_2[0, \infty)$ is the space of integral vector over $[0, \infty)$; for any real function $x, y \in \mathscr{L}_2[0, \infty)$ and real matrix M, we define $\langle x, My \rangle_d = \int_0^d x^T(t) M y(t) dt$; the mathematical expectation operator is denoted as $\mathbb{E}\{\cdot\}$.

2. Problem Formulation

For the description of an interval time-varying-delay nonlinear singular system, a delayed T-S fuzzy model is adopted in terms of r plant rules as follows.

Rule 1. If $\theta_1(t)$ is μ_{i1}, and ..., and $\theta_p(t)$ is μ_{ip}, then

$$\begin{cases} E\dot{x}(t) = A_i x(t) + A_{di} x(t - d(t)) + B_i \omega(t), \\ y(t) = C_i x(t) + C_{di} x(t - d(t)) + D_i \omega(t), \\ z(t) = L_i x(t), \\ x(t) = \phi(t), \quad \forall t \in [-d_2, 0], \end{cases} \quad (1)$$

where $x(t) \in \mathbf{R}^n$, $y(t) \in \mathbf{R}^m$, and $\omega(t) \in \mathbf{R}^l$ stand for the state vector, the measurement output, and the disturbance input, respectively; $z(t) \in \mathbf{R}^q$ is the signal to be estimated; $\phi(t)$ is the initial condition; the premise variable vector is described by $\theta(t) = [\theta_1(t), \theta_2(t), \ldots, \theta_p(t)]$, and the fuzzy sets are $\mu_{ij}(i = 1, \ldots, r, j = 1, \ldots, p)$; the time-varying delay $d(t)$ satisfies the conditions of $0 \le d_1 \le d(t) \le d_2$, $\dot{d}(t) \le \varpi$, and d_1, d_2, and $0 \le \varpi < 1$ are constant scalars; $E \in \mathbf{R}^{n \times n}$ may be a singular matrix with $\mathrm{rank}(E) = g \le n$; and A_i, A_{di}, B_i, C_i, C_{di}, D_i, and L_i are known real constant matrices with appropriate dimensions.

Then, we can generate the model of the T-S fuzzy singular systems when time-varying delay is considered:

$$\begin{cases} E\dot{x}(t) = \sum_{i=1}^r h_i(\theta(t))[A_i x(t) + A_{di} x(t - d(t)) + B_i \omega(t)], \\ y(t) = \sum_{i=1}^r h_i(\theta(t))[C_i x(t) + C_{di} x(t - d(t)) + D_i \omega(t)], \\ z(t) = \sum_{i=1}^r h_i(\theta(t)) L_i x(t), \end{cases} \quad (2)$$

where

$$h_i(\theta(t)) = \frac{\prod_{j=1}^p \mu_{ij}(\theta_j(t))}{\sum_{i=1}^r \prod_{j=1}^p \mu_{ij}(\theta_j(t))} \quad (3)$$

and $\mu_{ij}(\theta_j(t))$ stand for the grade of membership for $\theta_j(t)$ in μ_{ij}. It is easy to verify that

$$h_i(\theta(t)) \ge 0, \quad \sum_{i=1}^r h_i(\theta(t)) = 1. \quad (4)$$

In this paper, for calculating the signal $z(t)$, a fuzzy filter is derived as

$$\begin{cases} E\dot{x}_f(t) = \sum_{i=1}^r h_i(\theta(t))[A_{fi} x_f(t) + B_{fi} y_a(t)], \\ z_f(t) = \sum_{i=1}^r h_i(\theta(t)) C_{fi} x_f(t), \end{cases} \quad (5)$$

where $x_f(t) \in \mathbf{R}^n$ and $z_f(t) \in \mathbf{R}^q$ represent the filter state and the filter output, respectively. $y_a(t)$ is the sensor

measurement under randomly occurring deception attacks which can be given as

$$y_a(t) = y(t) + \alpha(t)(-y(t) + \sigma(t)). \tag{6}$$

$\sigma(t)$ defines the deception signal imported into the output which is assumed to satisfy $\|\sigma(t)\| \le \|Wy(t)\|$, and W is considered to be an appropriate dimension matrix; $\alpha(t)$ is a Bernoulli-distributed variable and we have the following assumptions on $\alpha(t)$:

$$
\begin{aligned}
\text{Prob}\{\alpha(t) = 1\} &= \mathbb{E}\{\alpha(t)\} = \alpha, \\
\text{Prob}\{\alpha(t) = 0\} &= 1 - \alpha.
\end{aligned}
\tag{7}
$$

Remark 1. The model of deception attacks considered in this paper is established in (6). A Bernoulli distribution is applied

to describe the random property of deception attacks. It is easy to say that $\alpha(t) = 1$ or $\alpha(t) = 0$ means sensor measurement is under deception attacks or not, respectively. Furthermore, the deception attacks are supposed to be norm bounded in (6), since there usually exists an upper bound for the attack signals to avoid detection.

We define the initial condition of system (5) as $x_f(0) = x_{f0}$, and for any $t \in [-d_2, 0]$, assume that $x_f(t) = x_{f0}$. A_{fi}, B_{fi}, and C_{fi} are filter gains to be determined.

Then, define $e_f(t) = z(t) - z_f(t)$ and $\eta(t) = \left[x^T(t) \ x_f^T(t) \right]^T$. By combining systems (2) and (5), we can obtain the following filtering error system:

$$
\begin{cases}
\hat{E}\dot{\eta}(t) = \displaystyle\sum_{i=1}^{r}\sum_{j=1}^{r} h_i(\theta(t))h_j(\theta(t))\left[\left(\hat{A}_{ij} - \hat{\alpha}(t)\hat{B}_{f1ij} \right)\eta(t) + \left(\hat{A}_{di\,j} - \hat{\alpha}(t)\hat{B}_{f2ij} \right)\eta(t - d(t)) \right. \\
\left. + \left(\hat{B}_{ij} - \hat{\alpha}(t)\hat{B}_{f3ij} \right)\omega(t) + \alpha\hat{B}_{f4j}\sigma(t) + \hat{\alpha}(t)\hat{B}_{f4j}\sigma(t) \right], \\
e_f(t) = \displaystyle\sum_{i=1}^{r}\sum_{j=1}^{r} h_i(\theta(t))h_j(\theta(t))\hat{L}_{ij}\eta(t), \\
\eta(t) = \hat{\phi}(t) = \left[\phi^T(t) \ x_{f0}^T \right]^T, \quad \forall t \in [-d_2, 0],
\end{cases}
\tag{8}
$$

where

$$
\begin{aligned}
\hat{E} &= \begin{bmatrix} E & 0 \\ 0 & E \end{bmatrix}, \\
\hat{A}_{ij} &= \begin{bmatrix} A_i & 0 \\ (1 - \alpha)B_{fj}C_i & A_{fj} \end{bmatrix}, \\
\hat{A}_{di\,j} &= \begin{bmatrix} A_{di} & 0 \\ (1 - \alpha)B_{fj}C_{di} & 0 \end{bmatrix}, \\
\hat{B}_{ij} &= \begin{bmatrix} B_i \\ (1 - \alpha)B_{fj}D_i \end{bmatrix}, \\
\hat{B}_{f1ij} &= \begin{bmatrix} 0 & 0 \\ B_{fj}C_i & 0 \end{bmatrix}, \\
\hat{B}_{f2ij} &= \begin{bmatrix} 0 & 0 \\ B_{fj}C_{di} & 0 \end{bmatrix}, \\
\hat{B}_{f3ij} &= \begin{bmatrix} 0 \\ B_{fj}D_i \end{bmatrix}, \\
\hat{B}_{f4j} &= \begin{bmatrix} 0 \\ B_{fj} \end{bmatrix}, \\
\hat{L}_{ij} &= \begin{bmatrix} L_i & -C_{fj} \end{bmatrix}, \\
\hat{\alpha}(t) &= \alpha(t) - \alpha.
\end{aligned}
\tag{9}
$$

Denoting

$$
\begin{aligned}
\hat{A}(t) &= \sum_{i=1}^{r}\sum_{j=1}^{r} h_i(\theta(t))h_j(\theta(t))\left(\hat{A}_{ij} - \hat{\alpha}(t)\hat{B}_{f1ij} \right), \\
\hat{A}_d(t) &= \sum_{i=1}^{r}\sum_{j=1}^{r} h_i(\theta(t))h_j(\theta(t))\left(\hat{A}_{di\,j} - \hat{\alpha}(t)\hat{B}_{f2ij} \right), \\
\hat{B}(t) &= \sum_{i=1}^{r}\sum_{j=1}^{r} h_i(\theta(t))h_j(\theta(t))\left(\hat{B}_{ij} - \hat{\alpha}(t)\hat{B}_{f3ij} \right), \\
\hat{B}_1(t) &= \sum_{j=1}^{r} h_j(\theta(t))\left(\alpha\hat{B}_{f4j} + \hat{\alpha}(t)\hat{B}_{f4j} \right), \\
\hat{L}(t) &= \sum_{i=1}^{r}\sum_{j=1}^{r} h_i(\theta(t))h_j(\theta(t))\hat{L}_{ij},
\end{aligned}
\tag{10}
$$

system (8) can be given as

$$
\begin{cases}
\hat{E}\dot{\eta}(t) = \hat{A}(t)\eta(t) + \hat{A}_d(t)\eta(t - d(t)) + \hat{B}(t)\omega(t) + \hat{B}_1(t)\sigma(t), \\
e_f(t) = \hat{L}(t)\eta(t).
\end{cases}
\tag{11}
$$

Remark 2. Due to a stochastic variable of Bernoulli distribution, filtering error system (11) is established as a stochastic T-S fuzzy singular system. In this condition, the definition of admissibility in [19] does not work for the stochastic T-S fuzzy singular system in (11) anymore. Motivated by the stochastic admissibility defined in [36] of

the discrete time case, we can generalize the definition of admissibility in [19] naturally and have the following definition of stochastic admissibility for system (11).

Definition 1 (see [36]).

(1) System (11) is said to be stochastically regular if $\det(\mathbb{E}\{sE - \hat{A}(t)\})$ is not identically zero

(2) System (11) is said to be stochastically impulse-free if $\deg(\det(\mathbb{E}\{sE - \hat{A}(t)\})) = \mathrm{rank}(E)$

(3) System (11) with $\omega(t) = 0$ is said to be stochastically stable if there exists a scalar $\mathcal{M} > 0$ such that

$$\lim_{t \to \infty} \mathbb{E}\left\{\int_0^t \eta^T(s, \overset{\wedge}{\phi}(t))\eta(s, \overset{\wedge}{\phi}(t)) ds\right\} \leq \mathcal{M}, \qquad (12)$$

where $\eta(s, \overset{\wedge}{\phi}(t))$ represents the system solution

(4) System (11) with $\omega(t) = 0$ is said to be stochastically admissible if it is stochastically regular, impulse-free, and stable

Definition 2 (see [33]). Give real symmetric matrices $\mathbb{Q}$ and $\mathbb{R}$ and matrix $\mathbb{S}$. For a scalar $\gamma > 0$, if the equation

$$\begin{aligned} \mathbb{E}\{\langle e_f, \mathbb{Q}e_f\rangle_{t_*}\} &+ 2\mathbb{E}\{\langle e_f, \mathbb{S}\omega\rangle_{t_*}\} \\ &+ \mathbb{E}\{\langle \omega, \mathbb{R}\omega\rangle_{t_*}\} \geq \gamma\mathbb{E}\{\langle \omega, \omega\rangle_{t_*}\} \end{aligned} \qquad (13)$$

holds under zero initial state with $t_* > 0$, system (11) is said to be strictly $(\mathbb{Q}, \mathbb{S}, \mathbb{R})$-$\gamma$-dissipative. Furthermore, we suppose $\mathbb{Q} \leq 0$ and $-\mathbb{Q} = \mathbb{Q}_-^T \mathbb{Q}_-$ for some $\mathbb{Q}_-$.

Before discussing the main results, we present a few lemmas that we need to use.

Lemma 1 (see [37]). *For a matrix $Z > 0$, the following inequality holds:*

$$-(k_2 - k_1)\int_{k_1}^{k_2} \dot{x}^T(s)Z\dot{x}(s)\mathrm{d}s \leq -\Pi^T \mathrm{diag}(Z, 3Z, 5Z)\Pi, \qquad (14)$$

where $\Pi = \begin{bmatrix} x(k_2) - x(k_1) \\ x(k_2) + x(k_1) - 2/k_2 - k_1 \int_{k_1}^{k_2} x(s)ds \\ x(k_2) - x(k_1) - 6/k_2 - k_1 \int_{k_1}^{k_2} \varsigma_{k_1,k_2}(s)x(s)ds \end{bmatrix}$

and $\varsigma_{k_1,k_2}(s) = 2(s - k_1/k_2 - k_1) - 1$.

Lemma 2 (see [38]). *Given a real scalar $\beta \in (0, 1)$, matrices $Z_1 > 0$ and $Z_2 > 0$, and any matrices $\mathcal{W}_1$ and $\mathcal{W}_2$, the inequality*

$$\begin{bmatrix} \dfrac{1}{\beta}Z_1 & 0 \\ \\ 0 & \dfrac{1}{1-\beta}Z_2 \end{bmatrix} \geq \begin{bmatrix} Z_1 + (1-\beta)\mathcal{T}_1 & (1-\beta)\mathcal{W}_1 + \beta\mathcal{W}_2 \\ \\ \mathring{a} & Z_2 + \beta\mathcal{T}_2 \end{bmatrix} \qquad (15)$$

holds,   where $\mathcal{T}_1 = Z_1 - \mathcal{W}_2 Z_2^{-1}\mathcal{W}_2^T$ and $\mathcal{T}_2 = Z_2 - \mathcal{W}_1^T Z_1^{-1}\mathcal{W}_1$.

Lemma 3 (see [13]). *If*

$$\Xi_{ii} < 0, \quad i = 1, 2, \dots, r,$$

$$\frac{2}{r-1}\Xi_{ii} + \Xi_{ij} + \Xi_{ji} < 0, \quad i \neq j, \, i, j = 1, 2, \dots, r, \qquad (16)$$

then $\sum_{i=1}^r \sum_{j=1}^r h_i(\theta(t))h_j(\theta(t))\Xi_{ij} < 0$, *where* $h_i(\theta(t))$, $i = 1, 2, \dots, r$, *satisfy (3) and (4)*.

3. Main Results

In this section, we will design a dissipative filter for system (1) with randomly occurring deception attacks. First, we give some notations in order to simplify the presentation:

$$\varsigma_1(s) = 2\frac{s + d_1}{d_1} - 1,$$

$$\varsigma_2(s) = 2\frac{s + d(t)}{d(t) - d_1} - 1,$$

$$\varsigma_3(s) = 2\frac{s + d_2}{d_2 - d(t)} - 1,$$

$$\varsigma_4(s) = 2\frac{s + d_2}{d_2 - d_1} - 1,$$

$$\zeta(t) = \left[\begin{array}{cccc} \eta^T(t)\hat{E}^T & \displaystyle\int_{t-d_1}^{t} \eta^T(s)\hat{E}^T \, ds & \displaystyle\int_{t-d_1}^{t} \varsigma_1(s)\eta^T(s)\hat{E}^T \, ds & \displaystyle\int_{t-d_2}^{t-d_1} \eta^T(s)\hat{E}^T \, ds \end{array}\right.$$
$$\left. (d_2-d_1)\displaystyle\int_{t-d_2}^{t-d_1} \varsigma_4(s)\eta^T(s)\hat{E}^T \, ds \right]^T,$$

$$\xi_1(t) = \left[\begin{array}{ccccc} \eta^T(t) & \dot{\eta}^T(t)\hat{E}^T & \eta^T(t-d_1) & \eta^T(t-d(t)) & \eta^T(t-d_2) \end{array}\right]^T,$$

$$\xi_2(t) = \frac{1}{d_1}\left[\begin{array}{cc} \displaystyle\int_{t-d_1}^{t} \eta^T(s)\hat{E}^T \, ds & \displaystyle\int_{t-d_1}^{t} \varsigma_1(s)\eta^T(s)\hat{E}^T \, ds \end{array}\right]^T,$$

$$\xi_3(t) = \frac{1}{d(t)-d_1}\left[\begin{array}{cc} \displaystyle\int_{t-d(t)}^{t-d_1} \eta^T(s)\hat{E}^T \, ds & \displaystyle\int_{t-d(t)}^{t-d_1} \varsigma_2(s)\eta^T(s)\hat{E}^T \, ds \end{array}\right]^T,$$

$$\xi_4(t) = \frac{1}{d_2-d(t)}\left[\begin{array}{cc} \displaystyle\int_{t-d_2}^{t-d(t)} \eta^T(s)\hat{E}^T \, ds & \displaystyle\int_{t-d_2}^{t-d(t)} \varsigma_3(s)\eta^T(s)\hat{E}^T \, ds \end{array}\right]^T,$$

$$\xi_5(t) = (d(t)-d_1)\xi_3(t),$$
$$\xi_6(t) = (d_2-d(t))\xi_4(t),$$
$$\xi(t) = \left[\begin{array}{cccccccc} \xi_1^T(t) & \xi_2^T(t) & \xi_3^T(t) & \xi_4^T(t) & \xi_5^T(t) & \xi_6^T(t) & \sigma^T(t) & \omega^T(t) \end{array}\right]^T,$$

$$\Pi_1 = \left[\begin{array}{c} \Psi_3 \\ \Psi_4 \end{array}\right]^T \left[\begin{array}{cc} 2\tilde{R}_2 & \mathscr{W}_1 \\ \mathring{a} & \tilde{R}_2 \end{array}\right]\left[\begin{array}{c} \Psi_3 \\ \Psi_4 \end{array}\right],$$

$$\Pi_2 = \Psi_3^T \mathscr{W}_2 \tilde{R}_2^{-1} \mathscr{W}_2^T \Psi_3,$$

$$\Pi_3 = \left[\begin{array}{c} \Psi_3 \\ \Psi_4 \end{array}\right]^T \left[\begin{array}{cc} \tilde{R}_2 & \mathscr{W}_2 \\ \mathring{a} & 2\tilde{R}_2 \end{array}\right]\left[\begin{array}{c} \Psi_3 \\ \Psi_4 \end{array}\right],$$

$$\Pi_4 = \Psi_4^T \mathscr{W}_1^T \tilde{R}_2^{-1} \mathscr{W}_1 \Psi_4,$$

$$\Psi_1(d(t)) = \left[\begin{array}{cccccc} \mathscr{I}_1^T\hat{E}^T & d_1\mathscr{I}_6^T & d_1\mathscr{I}_7^T & \mathscr{I}_{12}^T + \mathscr{I}_{14}^T & (d_2-d(t))(\mathscr{I}_{12}^T + \mathscr{I}_{15}^T) & (d(t)-d_1)(\mathscr{I}_{13}^T - \mathscr{I}_{14}^T) \end{array}\right]^T,$$

$$\Psi_2 = \left[\begin{array}{ccccc} \mathscr{I}_2^T & (\mathscr{I}_1^T - \mathscr{I}_3^T)\hat{E}^T & (\mathscr{I}_1^T + \mathscr{I}_3^T)\hat{E}^T - 2\mathscr{I}_6^T & (\mathscr{I}_3^T - \mathscr{I}_5^T)\hat{E}^T \end{array}\right.$$
$$\left. (d_2-d_1)(\mathscr{I}_3^T + \mathscr{I}_5^T)\hat{E}^T - 2(\mathscr{I}_{12}^T + \mathscr{I}_{14}^T) \right]^T,$$

$$\Psi_3 = \left[\begin{array}{ccc} (\mathscr{I}_3^T - \mathscr{I}_4^T)\hat{E}^T & (\mathscr{I}_3^T + \mathscr{I}_4^T)\hat{E}^T - 2\mathscr{I}_8^T & (\mathscr{I}_3^T - \mathscr{I}_4^T)\hat{E}^T - 6\mathscr{I}_9^T \end{array}\right]^T,$$

$$\Psi_4 = \left[\begin{array}{ccc} (\mathscr{I}_4^T - \mathscr{I}_5^T)\hat{E}^T & (\mathscr{I}_4^T + \mathscr{I}_5^T)\hat{E}^T - 2\mathscr{I}_{10}^T & (\mathscr{I}_4^T - \mathscr{I}_5^T)\hat{E}^T - 6\mathscr{I}_{11}^T \end{array}\right]^T,$$

$$f_1(d(t)) = (d(t)-d_1)\left[\begin{array}{c} \mathscr{I}_8 \\ \mathscr{I}_9 \end{array}\right] - \left[\begin{array}{c} \mathscr{I}_{12} \\ \mathscr{I}_{13} \end{array}\right],$$

$$f_2(d(t)) = (d_2-d(t))\left[\begin{array}{c} \mathscr{I}_{10} \\ \mathscr{I}_{11} \end{array}\right] - \left[\begin{array}{c} \mathscr{I}_{14} \\ \mathscr{I}_{15} \end{array}\right],$$

$$\mathscr{I}_i = \left[\begin{array}{cccc} 0_{2n\times(i-1)2n} & I_{2n} & 0_{2n\times(15-i)2n} & 0_{2n\times(m+l)} \end{array}\right], \quad i=1,\ldots,15,$$

$$\mathscr{I}_{16} = \left[\begin{array}{ccc} 0_{m\times30n} & I_m & 0_{m\times l} \end{array}\right],$$

$$\mathscr{I}_{17} = \left[\begin{array}{cc} 0_{l\times(30n+m)} & I_l \end{array}\right],$$

$$\mathscr{I}_{18} = \left[\begin{array}{cc} I_n & 0_{n\times(29n+m+l)} \end{array}\right],$$

$$\mathscr{I}_{19} = \left[\begin{array}{ccc} 0_{n\times6n} & I_n & 0_{n\times(23n+m+l)} \end{array}\right],$$

$$\tilde{R}_2 = \mathrm{diag}\{R_2, 3R_2, 5R_2\}. \tag{17}$$

Theorem 1. *For given scalars* α, $\gamma > 0$, $0 \le d_1 < d_2$, *and* $0 \le \omega < 1$, *matrices* W *and* $\mathbb{S}$, *symmetric matrices* $\mathbb{Q}$ *and* $\mathbb{R}$ *with* $\mathbb{Q} \le 0$, *and full column rank matrix* Γ *with* $\hat{E}^T \Gamma = 0$, *system (11) is said to be stochastically admissible and strictly* $(\mathbb{Q}, \mathbb{S}, \mathbb{R})$-$\gamma$-*dissipative, if there exist matrices* $P =$
$$\begin{bmatrix} P_{11} & P_{12} & P_{13} & P_{14} & P_{15} \\ * & P_{22} & P_{23} & P_{24} & P_{25} \\ * & * & P_{33} & P_{34} & P_{35} \\ * & * & * & P_{44} & P_{45} \\ * & * & * & * & P_{55} \end{bmatrix} > 0, \; Q_1 > 0, \; Q_2 > 0, \; Q_3 > 0, \; R_1 > 0,$$

$R_2 > 0$, Υ, $\mathscr{U}_1$, $\mathscr{U}_2$, $\mathscr{W}_1$, $\mathscr{W}_2$, $\mathscr{T}_1$, *and* $\mathscr{T}_2$ *such that the following matrix inequalities hold:*

$$\Omega(d_1) - \Pi_1 + \Pi_2 < 0, \tag{18}$$

$$\Omega(d_2) - \Pi_3 + \Pi_4 < 0, \tag{19}$$

where

$$
\begin{aligned}
\Omega(d(t)) = {} & \operatorname{sym}\left(\Psi_1^T(d(t)) P \Psi_2 + \mathscr{I}_1^T \Upsilon \Gamma^T \mathscr{I}_2 + \mathscr{U}_1 f_1(d(t)) + \mathscr{U}_2 f_2(d(t)) + \left(\mathscr{I}_1^T \mathscr{T}_1 + \mathscr{I}_2^T \mathscr{T}_2\right)\Phi - \left(\hat{L}(t)\mathscr{I}_1\right)^T \mathbb{S}\mathscr{I}_{17}\right) \\
& + \alpha\left(C(t)\mathscr{I}_{18} + C_d(t)\mathscr{I}_{19} + D(t)\mathscr{I}_{17}\right)^T W^T W \left(C(t)\mathscr{I}_{18} + C_d(t)\mathscr{I}_{19} + D(t)\mathscr{I}_{17}\right) - \alpha \mathscr{I}_{16}^T \mathscr{I}_{16} \\
& - \left(\hat{L}(t)\mathscr{I}_1\right)^T \mathbb{Q}\left(\hat{L}(t)\mathscr{I}_1\right) - \mathscr{I}_{17}^T (\mathbb{R} - \gamma I)\mathscr{I}_{17} + \mathscr{I}_1^T(Q_1 + Q_2 + Q_3)\mathscr{I}_1 - \mathscr{I}_3^T Q_1 \mathscr{I}_3 \\
& - (1 - \omega)\mathscr{I}_4^T Q_2 \mathscr{I}_4 - \mathscr{I}_5^T Q_3 \mathscr{I}_5 + \mathscr{I}_2^T\left(d_1^2 R_1 + (d_2 - d_1)^2 R_2\right)\mathscr{I}_2 - \left(\mathscr{I}_1 - \mathscr{I}_3\right)^T \hat{E}^T R_1 \hat{E}\left(\mathscr{I}_1 - \mathscr{I}_3\right) \\
& - 3\left(\hat{E}\mathscr{I}_1 + \hat{E}\mathscr{I}_3 - 2\mathscr{I}_6\right)^T R_1 \left(\hat{E}\mathscr{I}_1 + \hat{E}\mathscr{I}_3 - 2\mathscr{I}_6\right) - 5\left(\hat{E}\mathscr{I}_1 - \hat{E}\mathscr{I}_3 - 6\mathscr{I}_7\right)^T R_1 \left(\hat{E}\mathscr{I}_1 - \hat{E}\mathscr{I}_3 - 6\mathscr{I}_7\right), \\
\Phi = {} & \left[\tilde{A}(t) \quad -I_{2n} \quad 0_{2n} \quad \tilde{A}_d(t) \quad 0_{2n \times 22n} \quad \tilde{B}_1(t) \quad \tilde{B}(t)\right], \\
\tilde{A}(t) = {} & \sum_{i=1}^r \sum_{j=1}^r h_i(\theta(t)) h_j(\theta(t)) \hat{A}_{ij}, \\
\tilde{A}_d(t) = {} & \sum_{i=1}^r \sum_{j=1}^r h_i(\theta(t)) h_j(\theta(t)) \hat{A}_{di\,j}, \\
\tilde{B}_1(t) = {} & \sum_{j=1}^r h_j(\theta(t))\left(\alpha \hat{B}_{f4j}\right), \\
\tilde{B}(t) = {} & \sum_{i=1}^r \sum_{j=1}^r h_i(\theta(t)) h_j(\theta(t)) \hat{B}_{ij}, \\
C(t) = {} & \sum_{i=1}^r h_i(\theta(t)) C_i, \\
C_d(t) = {} & \sum_{i=1}^r h_i(\theta(t)) C_{di}, \; D(t) = \sum_{i=1}^r h_i(\theta(t)) D_i.
\end{aligned}
$$
$$\tag{20}$$

Proof. First, we will show the stochastic admissibility for system (11) with $\omega(t) = 0$. It can be obtained from (18) and (19) that

$$
\begin{bmatrix}
\mathfrak{M}_{11} - \hat{L}(t)^T \mathbb{Q} \hat{L}(t) + Q_1 + Q_2 + Q_3 & \mathfrak{M}_{12} & \sharp_1 \\
\ast & \mathfrak{M}_{22} + d_1^2 R_1 + (d_2 - d_1)^2 R_2 & \sharp_2 \\
\ast & \ast & \sharp_3
\end{bmatrix} < 0, \tag{21}
$$

where

$$\mathfrak{M}_{11} = \mathrm{sym}\left(\mathscr{T}_1 \widetilde{A}(t) + \hat{E}^T P_{12} \hat{E} + \hat{E}^T P_{13} \hat{E} \right)$$
$$- \hat{E}^T R_1 \hat{E} - 3\hat{E}^T R_1 \hat{E} - 5\hat{E}^T R_1 \hat{E}, \tag{22}$$

$$\mathfrak{M}_{12} = \hat{E}^T P_{11} + \Upsilon\Gamma^T - \mathscr{T}_1 + \widetilde{A}(t)^T \mathscr{T}_2^T, \quad \mathfrak{M}_{22} = -\left(\mathscr{T}_2 + \mathscr{T}_2^T \right).$$

$\sharp_1$, $\sharp_2$, and $\sharp_3$ represent matrices which have compatible dimensions and will not be used in the following discussion. Since $Q_1 > 0$, $Q_2 > 0$, $Q_3 > 0$, $R_1 > 0$, $R_2 > 0$, and $-\mathbb{Q} \geq 0$, we have

$$\begin{bmatrix} \mathfrak{M}_{11} & \mathfrak{M}_{12} \\ \mathring{a} & \mathfrak{M}_{22} \end{bmatrix} < 0. \tag{23}$$

Premultiplying and postmultiplying (23) by $[I \ \widetilde{A}(t)^T]$ and $[I \ \widetilde{A}(t)^T]^T$, we can obtain

$$\mathrm{sym}\left(\left(\hat{E}^T P_{11} + \Upsilon\Gamma^T \right) \widetilde{A}(t) + \hat{E}^T P_{12} \hat{E} + \hat{E}^T P_{13} \hat{E} \right)$$
$$- \hat{E}^T R_1 \hat{E} - 3\hat{E}^T R_1 \hat{E} - 5\hat{E}^T R_1 \hat{E} < 0. \tag{24}$$

According to Theorem 10.1 of [1] and from (24), we have that the pair $(\hat{E}, \widetilde{A}(t))$ is regular and impulse-free. It should be noted that

$$\det\left(\mathbb{E}\left\{ s\hat{E} - \hat{A}(t) \right\} \right) = \det\left(\left\{ s\hat{E} - \widetilde{A}(t) \right\} \right),$$

$$\deg\left(\det\left(\mathbb{E}\left\{ s\hat{E} - \hat{A}(t) \right\} \right) \right) = \deg\left(\det\left(\left\{ s\hat{E} - \widetilde{A}(t) \right\} \right) \right). \tag{25}$$

By Definition 1, we can conclude system (11) is stochastically regular and impulse-free. Choose the LKF as follows:

$$V(\eta_t) = \zeta^T(t) P\zeta(t) + \int_{t-d_1}^t \eta^T(s) Q_1 \eta(s)\mathrm{d}s + \int_{t-d(t)}^t \eta^T(s) Q_2 \eta(s)\mathrm{d}s + \int_{t-d_2}^t \eta^T(s) Q_3 \eta(s)\mathrm{d}s$$
$$+ d_1 \int_{-d_1}^0 \int_{t+\theta}^t \dot{\eta}^T(s) \hat{E}^T R_1 \hat{E}\dot{\eta}(s)\mathrm{d}s\mathrm{d}\theta + (d_2 - d_1) \int_{-d_2}^{-d_1} \int_{t+\theta}^t \dot{\eta}^T(s) \hat{E}^T R_2 \hat{E}\dot{\eta}(s)\mathrm{d}s\mathrm{d}\theta. \tag{26}$$

Set

$$\hat{\xi}(t) = \left[\xi_1^T(t) \ \xi_2^T(t) \ \xi_3^T(t) \ \xi_4^T(t) \ \xi_5^T(t) \ \xi_6^T(t) \right]^T,$$

$$\hat{\mathscr{I}}_i = \left[0_{2n\times(i-1)2n} \ I_{2n} \ 0_{2n\times(15-i)2n} \right], \quad i = 1, \ldots, 15,$$

$$\hat{\mathscr{I}}_{16} = \left[0_{m\times30n} \ I_m \right],$$

$$\hat{\mathscr{I}}_{18} = \left[I_n \ 0_{n\times(29n+m)} \right],$$

$$\hat{\mathscr{I}}_{19} = \left[0_{n\times6n} \ I_n \ 0_{n\times(23n+m)} \right],$$

$$\hat{\Psi}_1(d(t)) = \left[\hat{\mathscr{I}}_1^T \hat{E}^T \ d_1 \hat{\mathscr{I}}_6^T \ d_1 \hat{\mathscr{I}}_7^T \ \hat{\mathscr{I}}_{12}^T + \hat{\mathscr{I}}_{14}^T \ (d_2 - d(t))\left(\hat{\mathscr{I}}_{12}^T + \hat{\mathscr{I}}_{15}^T \right) + (d(t) - d_1)\left(\hat{\mathscr{I}}_{13}^T - \hat{\mathscr{I}}_{14}^T \right) \right]^T,$$

$$\hat{\Psi}_2 = \left[\hat{\mathscr{I}}_2^T \ \left(\hat{\mathscr{I}}_1^T - \hat{\mathscr{I}}_3^T \right)\hat{E}^T \ \left(\hat{\mathscr{I}}_1^T + \hat{\mathscr{I}}_3^T \right)\hat{E}^T - 2\hat{\mathscr{I}}_6^T \ \left(\hat{\mathscr{I}}_3^T - \hat{\mathscr{I}}_5^T \right)\hat{E}^T \right.$$
$$\left. (d_2 - d_1)\left(\hat{\mathscr{I}}_3^T + \hat{\mathscr{I}}_5^T \right)\hat{E}^T - 2\left(\hat{\mathscr{I}}_{12}^T + \hat{\mathscr{I}}_{14}^T \right) \right]^T,$$

$$\hat{\Psi}_3 = \left[\left(\hat{\mathscr{I}}_3^T - \hat{\mathscr{I}}_4^T \right)\hat{E}^T \ \left(\hat{\mathscr{I}}_3^T + \hat{\mathscr{I}}_4^T \right)\hat{E}^T - 2\hat{\mathscr{I}}_8^T \ \left(\hat{\mathscr{I}}_3^T - \hat{\mathscr{I}}_4^T \right)\hat{E}^T - 6\hat{\mathscr{I}}_9^T \right]^T,$$

$$\hat{\Psi}_4 = \left[\left(\hat{\mathscr{I}}_4^T - \hat{\mathscr{I}}_5^T \right)\hat{E}^T \ \left(\hat{\mathscr{I}}_4^T + \hat{\mathscr{I}}_5^T \right)\hat{E}^T - 2\hat{\mathscr{I}}_{10}^T \ \left(\hat{\mathscr{I}}_4^T - \hat{\mathscr{I}}_5^T \right)\hat{E}^T - 6\hat{\mathscr{I}}_{11}^T \right]^T,$$

$$\hat{f}_1(d(t)) = (d(t) - d_1)\begin{bmatrix} \hat{\mathscr{I}}_8 \\ \hat{\mathscr{I}}_9 \end{bmatrix} - \begin{bmatrix} \hat{\mathscr{I}}_{12} \\ \hat{\mathscr{I}}_{13} \end{bmatrix},$$

$$\hat{f}_2(d(t)) = (d_2 - d(t))\begin{bmatrix} \hat{\mathscr{I}}_{10} \\ \hat{\mathscr{I}}_{11} \end{bmatrix} - \begin{bmatrix} \hat{\mathscr{I}}_{14} \\ \hat{\mathscr{I}}_{15} \end{bmatrix}$$

$$\overset{\wedge}{\Phi} = \left[\; \widetilde{A}(t) \;\; -I_{2n} \;\; 0_{2n} \;\; \widetilde{A}_d(t) \;\; 0_{2n \times 22n} \;\; \widetilde{B}_1(t) \;\right],$$

$$\overset{\wedge}{\Pi}_1 = \begin{bmatrix} \overset{\wedge}{\Psi}_3 \\ \overset{\wedge}{\Psi}_4 \end{bmatrix}^T \begin{bmatrix} 2\widetilde{R}_2 & \mathscr{W}_1 \\ \text{å} & \widetilde{R}_2 \end{bmatrix} \begin{bmatrix} \overset{\wedge}{\Psi}_3 \\ \overset{\wedge}{\Psi}_4 \end{bmatrix},$$

$$\overset{\wedge}{\Pi}_2 = \overset{\wedge}{\Psi}_3^T \mathscr{W}_2 \widetilde{R}_2^{-1} \mathscr{W}_2^T \overset{\wedge}{\Psi}_3,$$

$$\overset{\wedge}{\Pi}_3 = \begin{bmatrix} \overset{\wedge}{\Psi}_3 \\ \overset{\wedge}{\Psi}_4 \end{bmatrix}^T \begin{bmatrix} \widetilde{R}_2 & \mathscr{W}_2 \\ \text{å} & 2\widetilde{R}_2 \end{bmatrix} \begin{bmatrix} \overset{\wedge}{\Psi}_3 \\ \overset{\wedge}{\Psi}_4 \end{bmatrix},$$

$$\overset{\wedge}{\Pi}_4 = \overset{\wedge}{\Psi}_4^T \mathscr{W}_1^T \widetilde{R}_2^{-1} \mathscr{W}_1 \overset{\wedge}{\Psi}_4.$$

$$(27)$$

Define the infinitesimal $\mathscr{L}$ as $\mathscr{L}V(\eta_t) = \lim_{\Delta \to 0^+} 1/\Delta \{\mathbb{E}\{V(\eta_{t+\Delta}|\eta_t)\} - V(\eta_t)\}$. Along the trajectory of (11) with $\omega(t) = 0$, we have

$$\mathbb{E}\{\mathscr{L}V(\eta_t)\} \leq \overset{\wedge}{\xi}^T(t)\left(\mathrm{sym}\left(\overset{\wedge}{\Psi}_1^T(d(t))P\overset{\wedge}{\Psi}_2 \right) + \overset{\wedge}{\mathscr{I}}_1^T (Q_1 + Q_2 + Q_3)\overset{\wedge}{\mathscr{I}}_1 - \overset{\wedge}{\mathscr{I}}_3^T Q_1 \overset{\wedge}{\mathscr{I}}_3 \right.$$
$$\left. -(1 - \eth)\overset{\wedge}{\mathscr{I}}_4^T Q_2 \overset{\wedge}{\mathscr{I}}_4 - \overset{\wedge}{\mathscr{I}}_5^T Q_3 \overset{\wedge}{\mathscr{I}}_5 + \overset{\wedge}{\mathscr{I}}_2^T \left(d_1^2 R_1 + (d_2 - d_1)^2 R_2 \right)\overset{\wedge}{\mathscr{I}}_2 \right)\overset{\wedge}{\xi}(t)$$
$$- d_1 \int_{t-d_1}^t \dot{\eta}^T(s)\hat{E}^T R_1 \hat{E}\dot{\eta}(s)\mathrm{d}s - (d_2 - d_1) \int_{t-d_2}^{t-d_1} \dot{\eta}^T(s)\hat{E}^T R_2 \hat{E}\dot{\eta}(s)\mathrm{d}s.$$

$$(28)$$

Using Lemma 1, it can be generated that

$$-d_1 \int_{t-d_1}^t \dot{\eta}^T(s)\hat{E}^T R_1 \hat{E}\dot{\eta}(s)\mathrm{d}s \leq -\overset{\wedge}{\xi}^T(t)\left(\left(\overset{\wedge}{\mathscr{I}}_1 - \overset{\wedge}{\mathscr{I}}_3 \right)^T \hat{E}^T R_1 \hat{E}\left(\overset{\wedge}{\mathscr{I}}_1 - \overset{\wedge}{\mathscr{I}}_3 \right) \right.$$
$$+ 3\left(\hat{E}\overset{\wedge}{\mathscr{I}}_1 + \hat{E}\overset{\wedge}{\mathscr{I}}_3 - 2\overset{\wedge}{\mathscr{I}}_6 \right)^T R_1 \left(\hat{E}\overset{\wedge}{\mathscr{I}}_1 + \hat{E}\overset{\wedge}{\mathscr{I}}_3 - 2\overset{\wedge}{\mathscr{I}}_6 \right)$$
$$\left. + 5\left(\hat{E}\overset{\wedge}{\mathscr{I}}_1 - \hat{E}\overset{\wedge}{\mathscr{I}}_3 - 6\overset{\wedge}{\mathscr{I}}_7 \right)^T R_1 \left(\hat{E}\overset{\wedge}{\mathscr{I}}_1 - \hat{E}\overset{\wedge}{\mathscr{I}}_3 - 6\overset{\wedge}{\mathscr{I}}_7 \right) \right)\overset{\wedge}{\xi}(t),$$

$$(29)$$

$$-(d_2 - d_1) \int_{t-d_2}^{t-d_1} \dot{\eta}^T(s)\hat{E}^T R_2 \hat{E}\dot{\eta}(s)\mathrm{d}s$$
$$= -(d_2 - d_1)\left\{ \int_{t-d(t)}^{t-d_1} \dot{\eta}^T(s)\hat{E}^T R_2 \hat{E}\dot{\eta}(s)\mathrm{d}s + \int_{t-d_2}^{t-d(t)} \dot{\eta}^T(s)\hat{E}^T R_2 \hat{E}\dot{\eta}(s)\mathrm{d}s \right\}$$
$$\leq -\overset{\wedge}{\xi}^T(t)\left(\frac{d_2 - d_1}{d(t) - d_1}\overset{\wedge}{\Psi}_3^T \widetilde{R}_2 \overset{\wedge}{\Psi}_3 + \frac{d_2 - d_1}{d_2 - d(t)}\overset{\wedge}{\Psi}_4^T \widetilde{R}_2 \overset{\wedge}{\Psi}_4 \right)\overset{\wedge}{\xi}(t).$$

$$(30)$$

Then, by Lemma 2, we can obtain

$$-(d_2 - d_1) \int_{t-d_2}^{t-d_1} \dot{\eta}^T(s)\hat{E}^T R_2 \hat{E}\dot{\eta}(s)\mathrm{d}s \leq -\frac{d_2 - d(t)}{d_2 - d_1}\overset{\wedge}{\xi}^T(t)\left(\overset{\wedge}{\Pi}_1 - \overset{\wedge}{\Pi}_2 \right)\overset{\wedge}{\xi}(t)$$
$$-\frac{d(t) - d_1}{d_2 - d_1}\overset{\wedge}{\xi}^T(t)\left(\overset{\wedge}{\Pi}_3 - \overset{\wedge}{\Pi}_4 \right)\overset{\wedge}{\xi}(t).$$

$$(31)$$

Note that $\hat{\xi}_5(t) = (d(t) - d_1)\hat{\xi}_3(t)$ and $\hat{\xi}_6(t) = (d_2 - d(t))\hat{\xi}_4(t)$. Thus, it is easy to see that for matrices $\mathcal{U}_1$ and $\mathcal{U}_2$,

$$2\hat{\xi}^T(t)\left(\mathcal{U}_1\hat{f}_1(d(t)) + \mathcal{U}_2\hat{f}_2(d(t))\right)\hat{\xi}(t) = 0. \qquad (32)$$

$$2\mathbb{E}\left\{\left[\eta^T(t)\mathcal{T}_1 + (\hat{E}\dot{\eta}(t))^T\mathcal{T}_2\right]\left[-\hat{E}\dot{\eta}(t) + \hat{A}(t)\eta(t) + \hat{A}_d(t)\eta(t-d(t)) + \hat{B}_1(t)\sigma(t)\right]\right\} = 0. \qquad (33)$$

It is easy to obtain from (33) that

$$2\hat{\xi}^T(t)\left(\hat{\mathcal{F}}_1^T\mathcal{T}_1 + \hat{\mathcal{F}}_2^T\mathcal{T}_2\right)\hat{\Phi}\hat{\xi}(t) = 0. \qquad (34)$$

Noticing $\hat{E}^T\Gamma = 0$, we can obtain that for matrix Υ with appropriate dimension,

Given matrices $\mathcal{T}_1$ and $\mathcal{T}_2$ from (11), we have

$$2\hat{\xi}^T(t)\hat{\mathcal{F}}_1^T\Upsilon\Gamma^T\hat{\mathcal{F}}_2\hat{\xi}(t) = 0. \qquad (35)$$

Considering the definition of deception attacks, it is easy to obtain

$$y^T(t)W^TWy(t) - \sigma^T(t)\sigma(t) \geq 0, \qquad (36)$$

which means

$$\hat{\xi}^T(t)\left(\alpha\left(C(t)\hat{\mathcal{F}}_{18} + C_d(t)\hat{\mathcal{F}}_{19}\right)^T W^TW\left(C(t)\hat{\mathcal{F}}_{18} + C_d(t)\hat{\mathcal{F}}_{19}\right) - \alpha\hat{\mathcal{F}}_{16}^T\hat{\mathcal{F}}_{16}\right)\hat{\xi}(t) \geq 0. \qquad (37)$$

From (28)–(37), it can be verified that

$$\mathbb{E}\{\mathscr{L}V(\eta_t)\} \leq \hat{\xi}^T(t)\left(\hat{\Omega}(d(t)) - \frac{d_2 - d(t)}{d_2 - d_1}\left(\hat{\Pi}_1 - \hat{\Pi}_2\right) - \frac{d(t) - d_1}{d_2 - d_1}\left(\hat{\Pi}_3 - \hat{\Pi}_4\right)\right)\hat{\xi}(t), \qquad (38)$$

where

$$\begin{aligned}
\hat{\Omega}(d(t)) = \operatorname{sym}&\left(\hat{\Psi}_1^T(d(t))P\hat{\Psi}_2 + \hat{\mathcal{F}}_1^T\Upsilon\Gamma^T\hat{\mathcal{F}}_2 + \mathcal{U}_1\hat{f}_1(d(t)) + \mathcal{U}_2\hat{f}_2(d(t)) + \left(\hat{\mathcal{F}}_1^T\mathcal{T}_1 + \hat{\mathcal{F}}_2^T\mathcal{T}_2\right)\hat{\Phi}\right) - \hat{\mathcal{F}}_3^TQ_1\hat{\mathcal{F}}_3 \\
&+ \alpha\left(C(t)\hat{\mathcal{F}}_{18} + C_d(t)\hat{\mathcal{F}}_{19}\right)^T W^TW\left(C(t)\hat{\mathcal{F}}_{18} + C_d(t)\hat{\mathcal{F}}_{19}\right) - \alpha\hat{\mathcal{F}}_{16}^T\hat{\mathcal{F}}_{16} + \hat{\mathcal{F}}_1^T(Q_1 + Q_2 + Q_3)\hat{\mathcal{F}}_1 \\
&- (1-\omega)\hat{\mathcal{F}}_4^TQ_2\hat{\mathcal{F}}_4 - \hat{\mathcal{F}}_5^TQ_3\hat{\mathcal{F}}_5 + \hat{\mathcal{F}}_2^T\left(d_1^2R_1 + (d_2 - d_1)^2R_2\right)\hat{\mathcal{F}}_2 - \left(\hat{\mathcal{F}}_1 - \hat{\mathcal{F}}_3\right)^T\hat{E}^TR_1\hat{E}\left(\hat{\mathcal{F}}_1 - \hat{\mathcal{F}}_3\right) \\
&- 3\left(\hat{E}\hat{\mathcal{F}}_1 + \hat{E}\hat{\mathcal{F}}_3 - 2\hat{\mathcal{F}}_6\right)^TR_1\left(\hat{E}\hat{\mathcal{F}}_1 + \hat{E}\hat{\mathcal{F}}_3 - 2\hat{\mathcal{F}}_6\right) - 5\left(\hat{E}\hat{\mathcal{F}}_1 - \hat{E}\hat{\mathcal{F}}_3 - 6\hat{\mathcal{F}}_7\right)^TR_1\left(\hat{E}\hat{\mathcal{F}}_1 - \hat{E}\hat{\mathcal{F}}_3 - 6\hat{\mathcal{F}}_7\right).
\end{aligned} \qquad (39)$$

We can obtain from (18) and (19) that $\mathbb{E}\{\mathscr{L}V(\eta_t)\} < 0$. Hence, we can find a scalar $\beta > 0$ so that $\mathbb{E}\{\mathscr{L}V(\eta_t)\} \leq -\beta\|\eta(t)\|^2$. Using Dynkin's formula, it can be derived that

$$\mathbb{E}\{V(\eta_t)\} - \mathbb{E}\{V(\eta_0)\} \leq -\beta\mathbb{E}\left\{\int_0^t \|\eta(s)\|^2 ds\right\}, \qquad (40)$$

which implies

$$\mathbb{E}\left\{\int_0^t \|\eta(s)\|^2 ds\right\} \leq \beta^{-1}\mathbb{E}\{V(\eta_0)\}. \qquad (41)$$

From Definition 1, it can be concluded that system (11) in the condition of $\omega(t) = 0$ is considered to be stochastically stable.

To verify the dissipativity for system (11), by (18), (19), and (25), it can be derived that

$$\mathscr{L}V(\eta_t) - e_f^T(t)\mathbb{Q}e_f(t) - 2e_f^T(t)\mathbb{S}\omega(t) - \omega^T(t)(\mathbb{R} - \gamma I)\omega(t)$$

$$= \xi^T(t)\left(\Omega(d(t)) - \frac{d_2 - d(t)}{d_2 - d_1}(\Pi_1 - \Pi_2) - \frac{d(t) - d_1}{d_2 - d_1}(\Pi_3 - \Pi_4)\right)\xi(t) < 0. \tag{42}$$

Thus, for any $t_* \geq 0$, it is easy to see that

$$\mathbb{E}\left\{V(\eta_{t_*}) - V(\eta_0) - \int_0^{t_*} e_f^T(t)\mathbb{Q}e_f(t)\mathrm{d}t - \int_0^{t_*} 2e_f^T(t)\mathbb{S}\omega(t)\mathrm{d}t \right.$$

$$\left. - \int_0^{t_*} \omega^T(t)(\mathbb{R} - \gamma I)\omega(t)\mathrm{d}t\right\} < 0. \tag{43}$$

Considering $\mathbb{E}\{V(\eta_{t_*})\} \geq 0$ and $V(\eta_0) = 0$ under zero initial condition, by (43), we can obtain that (13) holds, which shows that system (11) is strictly $(\mathbb{Q}, \mathbb{S}, \mathbb{R}) - \gamma$–dissipative. □

Theorem 2. *For given scalars α, $\gamma > 0$, $0 \leq d_1 < d_2$, and $0 \leq \omega < 1$, matrices W and $\mathbb{S}$, symmetric matrices $\mathbb{Q}$ and $\mathbb{R}$ with $\mathbb{Q} \leq 0$ and $-\mathbb{Q} = \mathbb{Q}_-^T\mathbb{Q}_-$, and full column rank matrix Γ*

with $\hat{E}^T \Gamma = 0$, if there are matrices $P = \begin{bmatrix} P_{11} & P_{12} & P_{13} & P_{14} & P_{15} \\ * & P_{22} & P_{23} & P_{24} & P_{25} \\ * & * & P_{33} & P_{34} & P_{35} \\ * & * & * & P_{44} & P_{45} \\ * & * & * & * & P_{55} \end{bmatrix} > 0, Q_1 > 0, Q_2 > 0, Q_3 > 0, R_1 > 0,$ and $R_2 > 0$, an invertible matrix Y, matrices Υ, $\mathscr{U}_1$, $\mathscr{U}_2$, $\mathscr{W}_1$, $\mathscr{W}_2$, Y_1, Y_2, Y_3, Y_4, $\overline{A}_{fj}$, $\overline{B}_{fj}$, and $\overline{C}_{fj}$, $j = 1, 2, \ldots, r$, such that the following linear matrix inequalities hold:

$$\Xi_{ii}(d_k) < 0, \ i = 1, 2, \ldots, r, \ k = 1, 2, \tag{44}$$

$$\Xi_{ij}(d_k) + \Xi_{ji}(d_k) < 0, \ i < j, \ i = 1, 2, \ldots, r, \ k = 1, 2, \tag{45}$$

where

$$\Xi_{ij}(d_1) = \begin{bmatrix} \Omega_{ij}(d_1) - \Pi_1 & \Psi_3^T\mathscr{W}_2 & (\overline{L}_{ij}e_1)^T\mathbb{Q}_- \\ \mathring{a} & -\widetilde{R}_2 & 0 \\ \mathring{a} & \mathring{a} & -I \end{bmatrix},$$

$$\Xi_{ij}(d_2) = \begin{bmatrix} \Omega_{ij}(d_2) - \Pi_3 & \Psi_4^T\mathscr{W}_1^T & (\overline{L}_{ij}e_1)^T\mathbb{Q}_- \\ \mathring{a} & -\widetilde{R}_2 & 0 \\ \mathring{a} & \mathring{a} & -I \end{bmatrix},$$

$$\Omega_{ij}(d(t)) = \mathrm{sym}\left(\Psi_1^T(d(t))P\Psi_2 + \mathscr{I}_1^T\Upsilon\Gamma^T\mathscr{I}_2 + \mathscr{U}_1 f_1(d(t)) + \mathscr{U}_2 f_2(d(t)) + \mathscr{I}_1^T\overline{\Theta}_{ij} + \mathscr{I}_2^T\breve{\Theta}_{ij} - (\overline{L}_{ij}\mathscr{I}_1)^T\mathbb{S}\mathscr{I}_{17}\right)$$

$$- \mathscr{I}_{17}^T(\mathbb{R} - \gamma I)\mathscr{I}_{17} + \alpha(C_i\mathscr{I}_{18} + C_{di}\mathscr{I}_{19} + D_i\mathscr{I}_{17})^T W^T W(C_i\mathscr{I}_{18} + C_{di}\mathscr{I}_{19} + D_i\mathscr{I}_{17}) - \alpha\mathscr{I}_{16}^T\mathscr{I}_{16}$$

$$+ \mathscr{I}_1^T(Q_1 + Q_2 + Q_3)\mathscr{I}_1 - \mathscr{I}_3^TQ_1\mathscr{I}_3 - (1 - \omega)\mathscr{I}_4^TQ_2\mathscr{I}_4 - \mathscr{I}_5^TQ_3\mathscr{I}_5 + \mathscr{I}_2^T(d_1^2 R_1 + (d_2 - d_1)^2 R_2)\mathscr{I}_2$$

$$- (\mathscr{I}_1 - \mathscr{I}_3)^T\hat{E}^T R_1\hat{E}(\mathscr{I}_1 - \mathscr{I}_3) - 3(\hat{E}\mathscr{I}_1 + \hat{E}\mathscr{I}_3 - 2\mathscr{I}_6)^T R_1(\hat{E}\mathscr{I}_1 + \hat{E}\mathscr{I}_3 - 2\mathscr{I}_6)$$

$$- 5(\hat{E}\mathscr{I}_1 - \hat{E}\mathscr{I}_3 - 6\mathscr{I}_7)^T R_1(\hat{E}\mathscr{I}_1 - \hat{E}\mathscr{I}_3 - 6\mathscr{I}_7),$$

$$\overline{\Theta}_{ij} = \begin{bmatrix} \overline{A}_{ij} & -\mathscr{I}_1 & 0_{2n} & \overline{A}_{di\,j} & 0_{2n\times 22n} & \overline{B}_{1j} & \overline{B}_{ij} \end{bmatrix},$$

$$\breve{\Theta}_{ij} = \begin{bmatrix} \breve{A}_{ij} & -\mathscr{I}_2 & 0_{2n} & \breve{A}_{di\,j} & 0_{2n\times 22n} & \breve{B}_{1j} & \breve{B}_{ij} \end{bmatrix},$$

$$\overline{A}_{ij} = \begin{bmatrix} Y_1 A_i + (1 - \alpha)\overline{B}_{fj}C_i & \overline{A}_{fj} \\ Y_2 A_i + (1 - \alpha)\overline{B}_{fj}C_i & \overline{A}_{fj} \end{bmatrix},$$

$$\breve{A}_{ij} = \begin{bmatrix} Y_3 A_i + (1 - \alpha)\overline{B}_{fj}C_i & \overline{A}_{fj} \\ Y_4 A_i + (1 - \alpha)\overline{B}_{fj}C_i & \overline{A}_{fj} \end{bmatrix},$$

$$\overline{A}_{di\,j} = \begin{bmatrix} Y_1 A_{di} + (1-\alpha)\overline{B}_{fj}C_{di} & 0 \\ Y_2 A_{di} + (1-\alpha)\overline{B}_{fj}C_{di} & 0 \end{bmatrix},$$

$$\breve{A}_{di\,j} = \begin{bmatrix} Y_3 A_{di} + (1-\alpha)\overline{B}_{fj}C_{di} & 0 \\ Y_4 A_{di} + (1-\alpha)\overline{B}_{fj}C_{di} & 0 \end{bmatrix},$$

$$\overline{B}_{1j} = \breve{B}_{1j}$$

$$\overline{B}_{ij} = \begin{bmatrix} Y_1 B_i + (1-\alpha)\overline{B}_{fj}D_i \\ Y_2 B_i + (1-\alpha)\overline{B}_{fj}D_i \end{bmatrix},$$

$$\breve{B}_{ij} = \begin{bmatrix} Y_3 B_i + (1-\alpha)\overline{B}_{fj}D_i \\ Y_4 B_i + (1-\alpha)\overline{B}_{fj}D_i \end{bmatrix},$$

$$\overline{L}_{ij} = \begin{bmatrix} L_i & -\overline{C}_{fj} \end{bmatrix},$$

$$\mathcal{T}_1 = \begin{bmatrix} Y_1 & Y \\ Y_2 & Y \end{bmatrix},$$

$$\mathcal{T}_2 = \begin{bmatrix} Y_3 & Y \\ Y_4 & Y \end{bmatrix}.$$

$$(46)$$

Then, fuzzy filter (5) can guarantee system (11) to be stochastically admissible and strictly $(\mathbb{Q}, \mathbb{S}, \mathbb{R})$-$\gamma$-*dissipative. Furthermore, from LMIs (44) and (45), the parameters of fuzzy filter (5) can be obtained by*

$$A_{fj} = Y^{-1}\overline{A}_{fj},$$
$$B_{fj} = Y^{-1}\overline{B}_{fj}, \qquad (47)$$
$$C_{fj} = \overline{C}_{fj}.$$

Proof. Using Lemma 3 and from (44) and (45), it can be verified that

$$\sum_{i=1}^{r}\sum_{j=1}^{r} h_i(\theta(t)) h_j(\theta(t)) \left(\Omega_{ij}(d_1) - \left(\overline{L}_{ij}\mathcal{I}_1\right)^T \mathbb{Q}\left(\overline{L}_{ij}\mathcal{I}_1\right) - \Pi_1 + \Pi_2 \right) < 0, \qquad (48)$$

$$\sum_{i=1}^{r}\sum_{j=1}^{r} h_i(\theta(t)) h_j(\theta(t)) \left(\Omega_{ij}(d_2) - \left(\overline{L}_{ij}\mathcal{I}_1\right)^T \mathbb{Q}\left(\overline{L}_{ij}\mathcal{I}_1\right) - \Pi_3 + \Pi_4 \right) < 0. \qquad (49)$$

By substituting the filter parameters in (44) into (45) and (46), from Theorem 1, we can proof that Theorem 2 holds. □

Remark 3. From Theorem 1 and Theorem 2, we can find that fuzzy filter (5) is designed successfully for a class of time-varying-delay T-S fuzzy singular systems subject to randomly occurring deception attacks based on the LKF approach and LMI techniques. According to Definitions 1 and 2, the filtering error system is guaranteed to be stochastically

admissible and satisfy strictly $(\mathbb{Q}, \mathbb{S}, \mathbb{R})$-$\gamma$-dissipativity by conditions (44) and (45). Furthermore, Lemmas 1 and 2 are applied in (29)–(31) to lessen the estimation gaps of (47), which have been shown to reduce the conservatism in dealing with time delays in [37,38], respectively.

4. Numerical Example

Consider a time-delay nonlinear system which is borrowed from [39]:

$$(1 + a\cos\varphi(t))\ddot{\varphi}(t) = -b\dot{\varphi}^3(t) + c\varphi(t) + c_d\varphi(t-d(t)) + f\omega(t), \qquad (50)$$

where $\dot{\varphi}(t)$ is supposed to satisfy $|\dot{\varphi}(t)| < \psi$. Choose $\psi = 2$, $a = -0.01$, $b = 0.5$, $c = -0.5$, $c_d = -0.05$, $f = -0.2$, and $d(t) = 0.3 + 0.2 \sin 0.5\, t$. Set $x_1(t) = \varphi(t)$, $x_2(t) = \dot{\varphi}(t)$, and $x_3(t) = \ddot{\varphi}(t)$. Introduce a new variable $x(t) = [x_1^T(t)\ x_2^T(t)\ x_3^T(t)]^T$, and the nonlinear system in (31) can be exactly modeled as

$$
\begin{cases}
E\dot{x}(t) = \sum_{i=1}^{3} h_i \left[A_i x(t) + A_{di} x(t - d(t)) + B_i \omega(t) \right], \\
y(t) = \sum_{i=3}^{r} h_i \left[C_i x(t) + C_{di} x(t - d(t)) + D_i \omega(t) \right], \\
z(t) = \sum_{i=3}^{r} h_i \left[L_i x(t) \right].
\end{cases}
\tag{51}
$$

The parameters are given as

$$
h_1 = \frac{x_2^2(t)}{\psi^2 + 2},
$$

$$
h_2 = \frac{1 + \cos x_1(t)}{\psi^2 + 2},
$$

$$
h_3 = \frac{\psi^2 - x_2^2(t) + 1 - \cos x_1(t)}{\psi^2 + 2},
$$

$$
E = \begin{bmatrix} 1 & 0 & 0 \\ 0 & 1 & 0 \\ 0 & 0 & 0 \end{bmatrix},
$$

$$
A_1 = \begin{bmatrix} 0 & 1 & 0 \\ 0 & 0 & 1 \\ c & -b(\psi^2 + 2) & a - 1 \end{bmatrix},
$$

$$
A_2 = \begin{bmatrix} 0 & 1 & 0 \\ 0 & 0 & 1 \\ c & 0 & -a - 1 - a\psi^2 \end{bmatrix},
$$

$$
A_3 = \begin{bmatrix} 0 & 1 & 0 \\ 0 & 0 & 1 \\ c & 0 & a - 1 \end{bmatrix},
$$

$$
A_{d1} = A_{d2} = A_{d3} = \begin{bmatrix} 0 & 0 & 0 \\ 0 & 0 & 0 \\ c_d & 0 & 0 \end{bmatrix},
$$

$$
B_1 = B_2 = B_3 = \begin{bmatrix} 0 \\ 0 \\ f \end{bmatrix},
$$

$$
C_1 = [\, 0 \ \ 1 \ \ 0 \,],
$$

$$
C_2 = [\, 0.6 \ \ 0 \ \ -0.4 \,],
$$

$$
C_3 = [\, -0.2 \ \ 0.1 \ \ 0.55 \,],
$$

$$
C_{d1} = [\, -0.25 \ \ 0.3 \ \ 0 \,],
$$

$$
C_{d2} = [\, 0.12 \ \ -0.6 \ \ 0 \,],
$$

$$
C_{d3} = [\, 0 \ \ 0.8 \ \ 0 \,],
$$

$$
L_1 = [\, 0.1 \ \ -0.5 \ \ 1 \,],
$$

$$
L_2 = [\, 1 \ \ 0.5 \ \ -0.5 \,],
$$

$$
L_3 = [\, -1 \ \ 0 \ \ 2 \,],
$$

$$
D_1 = -0.36,
$$

$$
D_2 = 2.5,
$$

$$
D_3 = 1,
$$

$$
W = 0.09,
$$

$$
\alpha = 0.2,
$$

$$
\mathbb{Q} = -0.01,
$$

$$
\mathbb{S} = -1.1, \mathbb{R}
$$

$$
\tag{52}
$$

For $\gamma = 0.5$, we can obtain from conditions (44)–(47) in Theorem 2 that the desired filter parameters are

$$
A_{f1} = \begin{bmatrix} -0.2502 & 0.5137 & -0.0001 \\ 0.5429 & -1.8529 & 1.0002 \\ -0.2868 & 0.4149 & -0.9900 \end{bmatrix},
$$

$$
A_{f2} = \begin{bmatrix} -0.2839 & -0.1028 & 0.0290 \\ 0.3353 & -0.2848 & 0.9769 \\ -0.3028 & -0.0022 & -1.0297 \end{bmatrix},
$$

$$
A_{f3} = \begin{bmatrix} -0.3269 & -0.1942 & 0.3735 \\ 0.3252 & -0.3790 & 0.9439 \\ -0.2717 & 0.1739 & -1.0781 \end{bmatrix},
$$

$$
B_{f1} = \begin{bmatrix} 0.1762 \\ -1.6414 \\ 0.3855 \end{bmatrix},
\tag{53}
$$

$$
B_{f2} = \begin{bmatrix} -0.0724 \\ 0.0577 \\ 0.0994 \end{bmatrix},
$$

$$
B_{f3} = \begin{bmatrix} 0.6792 \\ -0.1021 \\ -0.1602 \end{bmatrix},
$$

$$
C_{f1} = [\, -0.2313 \ \ 0.8816 \ \ -1.0000 \,],
$$

$$
C_{f2} = [\, -2.3880 \ \ 2.7310 \ \ 0.5015 \,],
$$

$$
C_{f3} = [\, 0.2935 \ \ 1.2410 \ \ -2.0008 \,].
$$
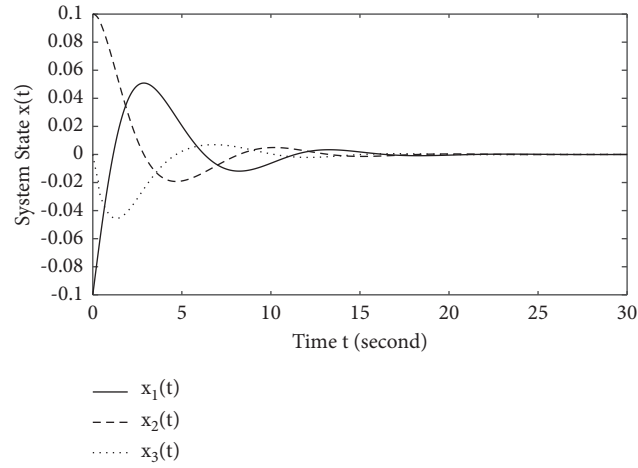
FIGURE 1: System state $x(t)$.
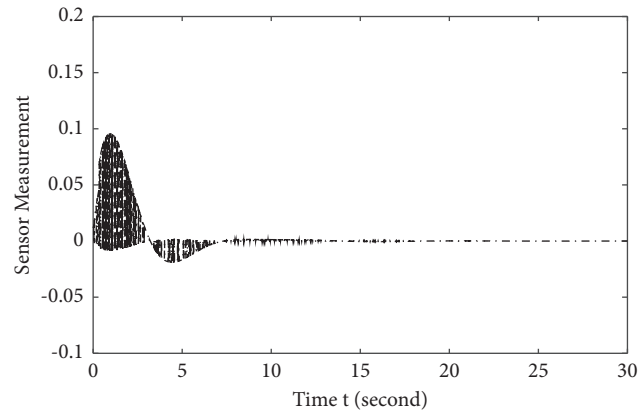
FIGURE 2: Sensor measurement $y_a(t)$ under randomly occurring deception attack.
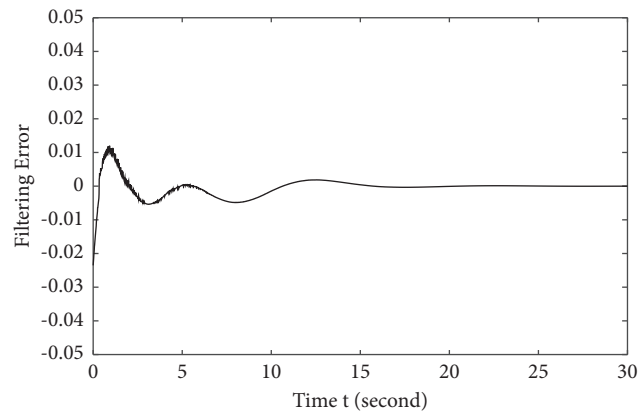
FIGURE 3: Filtering error $e_f(t)$.

Next, we will provide the simulation results to demonstrate the effectiveness of our filter design method against randomly occurring deception attacks. Let the initial condition be $[-0.1\,0.1\,0]^T$ and the disturbance be $\omega(t) = 0.1e^{-0.5t}\sin t$. Figure 1 shows the system state response $x(t)$. The deception attack function is given as $\sigma(t) = -\tanh(0.09y(t))$. The sensor measurement $y_a(t)$ under randomly occurring deception attack is given in Figure 2. Figure 3 is the filtering error $e_f(t)$. From Figures 1–3, we can find that our results are effective.

5. Conclusions

In this work, a method for dealing with the problem of dissipative filtering associated with T-S fuzzy singular systems with time-varying delays subject to deception attacks has been developed. Since the measurement output is supposed to encounter random deception attacks based on a Bernoulli distribution during signal transmission, the filtering error system is modeled by a stochastic singular T-S fuzzy system and the definition of stochastic admissibility for this kind of system has been presented. By using the LKF approach and LMI techniques, sufficient delay-dependent results have been generated, where the filtering error system can be stochastically admissible and strictly $(\mathbb{Q}, \mathbb{S}, \mathbb{R})$-dissipative against randomly occurring deception attacks. Besides, the desired filter parameters can be obtained by these solvable conditions. Finally, a frequently used example of the nonlinear system has been given to show the effectiveness of our work.

Data Availability

The data used to support the findings of this study are available from the corresponding author upon request.

Conflicts of Interest

The authors declare that there are no conflicts of interest.

Acknowledgments

References

[1] S. Xu and J. Lam, *Robust control and filtering of singular systems*, Springer, Berlin, Germany, 2006.

[2] S. Shengyuan Xu, P. Van Dooren, R. Stefan, and J. Lam, "Robust stability and stabilization for singular systems with state delay and parameter uncertainty," *IEEE Transactions on Automatic Control*, vol. 47, no. 7, pp. 1122–1128, 2002.

[3] Z. Feng and J. Lam, "On reachable set estimation of singular systems," *Automatica*, vol. 52, pp. 146–153, 2015.

[4] Y. Li, Y. He, W.-J. Lin, and M. Wu, "Reachable set estimation for singular systems via state decomposition method," *Journal of the Franklin Institute*, vol. 357, no. 11, pp. 7327–7342, 2020.

[5] J. Zhao, "A new result on reachable set estimation for time-varying delay singular systems," *International Journal of Robust and Nonlinear Control*, vol. 31, no. 3, pp. 806–816, 2021.

[6] J. Hu, Z. Wang, H. Gao, and L. K. Stergioulas, "Robust H_∞ sliding mode control for discrete time-delay systems with stochastic nonlinearities sliding mode control for discrete time-delay systems with stochastic nonlinearities," *Journal of the Franklin Institute*, vol. 349, no. 4, pp. 1459–1479, 2012.

[7] Y. Han, Y. Kao, and C. Gao, "Robust sliding mode control for uncertain discrete singular systems with time-varying delays

and external disturbances," *Automatica*, vol. 75, pp. 210–216, 2017.

[8] X. Fan, Q. Zhang, and J. Ren, "Event-triggered sliding mode control for discrete-time singular system," *IET Control Theory & Applications*, vol. 12, no. 17, pp. 2390–2398, 2018.

[9] S. Xu, J. Lam, and X. Mao, "Delay-dependent H_∞ control and filtering for uncertain markovian jump systems with time-varying delays," *IEEE Transactions on Circuits and Systems I: Regular Papers*, vol. 54, no. 9, pp. 2070–2077, 2007.

[10] J. Wang, H. Wang, A. Xue, and R. Lu, "Delay-dependent H_∞ control for singular Markovian jump systems with time delay control for singular Markovian jump systems with time delay," *Nonlinear Analysis: Hybrid Systems*, vol. 8, pp. 1–12, 2013.

[11] Y. Tian and Z. Wang, "Bounded real lemma and H_∞ control for singular Markovian jump systems with mode-dependent derivative-term coefficient control for singular Markovian jump systems with mode-dependent derivative-term coefficient," *Journal of the Franklin Institute*, vol. 358, no. 1, pp. 723–736, 2021.

[12] T. Takagi and M. Sugeno, "Fuzzy identification of systems and its applications to modeling and control," *IEEE Transactions on Systems, Man, and Cybernetics*, vol. SMC-15, no. 1, pp. 116–132, 1985.

[13] X. Chang and G. Yang, "Non-fragile H_∞ filtering of continuous-time fuzzy systems," *IEEE Transactions on Signal Processing*, vol. 59, pp. 1528–1538, 2010.

[14] X. Chang and G. Yang, "Non-fragile H_∞ filter design for T-S fuzzy systems in standard form," *IEEE Transactions on Industrial Electronics*, vol. 61, pp. 3448–3458, 2013.

[15] Z. Liu, F. Wang, Y. Zhang, X. Chen, and C. Chen, "Adaptive tracking control for a class of nonlinear systems with a fuzzy dead-zone input," *IEEE Transactions on Fuzzy Systems*, vol. 23, pp. 193–204, 2014.

[16] Y. Liu, B.-Z. Guo, and J. H. Park, "Non-fragileH_∞filtering for delayed Takagi-Sugeno fuzzy systems with randomly occurring gain variations filtering for delayed Takagi-Sugeno fuzzy systems with randomly occurring gain variations," *Fuzzy Sets and Systems*, vol. 316, pp. 99–116, 2017.

[17] P. Cheng, S. He, V. Stojanovic, X. Luan, and F. Liu, "Fuzzy fault detection for Markov jump systems with partly accessible hidden information: An event-triggered approach," *IEEE Transactions on Cybernetics*, pp. 1–10, 2021.

[18] X. Zhang, H. Wang, V. Stojanovic et al., "Asynchronous Fault Detection for Interval Type-2 Fuzzy Nonhomogeneous Higher-level Markov Jump Systems with Uncertain Transition Probabilities," *IEEE Transactions on Fuzzy Systems*, p. 1, 2021.

[19] Z. Feng and P. Shi, "Admissibilization of singular interval-valued fuzzy systems," *IEEE Transactions on Fuzzy Systems*, vol. 25, pp. 1765–1776, 2016.

[20] Z. Feng, H. Zhang, H. Du, and Z. Jiang, "Admissibilisation of singular interval type-2 Takagi-Sugeno fuzzy systems with time delay," *IET Control Theory & Applications*, vol. 14, no. 8, pp. 1022–1032, 2020.

[21] M. Kchaou, H. Gassara, and A. El-Hajjaji, "Adaptive sliding mode control for fuzzy singular systems with time delay and input nonlinearity," *International Journal of Adaptive Control and Signal Processing*, vol. 32, no. 3, pp. 464–479, 2018.

[22] X. Sun and Q. Zhang, "Observer-based adaptive sliding mode control for T-S fuzzy singular systems," *IEEE Trans. Syst. Man Cybern. Syst.*vol. 50, pp. 4438–4446, 2018.

[23] Y. Wang, G. Zhuang, and F. Chen, "Event-based asynchronous dissipative filtering for T-S fuzzy singular Markovian

jump systems with redundant channels," *Nonlinear Analysis: Hybrid Systems*, vol. 34, pp. 264–283, 2019.

[24] G. Zhuang, S.-F. Su, J. Xia, and W. Sun, "HMM-based asynchronous H_{∞} filtering for fuzzy singular markovian switching systems with retarded time-varying delays filtering for fuzzy singular markovian switching systems with retarded time-varying delays," *IEEE Transactions on Cybernetics*, vol. 51, no. 3, pp. 1189–1203, 2021.

[25] J. Liu, M. Yang, X. Xie, C. Peng, and H. Yan, "Finite-time H_{∞} filtering for state-dependent uncertain systems with event-triggered mechanism and multiple attacks," *IEEE Transactions on Circuits and Systems*, vol. 67, pp. 1021–1034, 2019.

[26] L. Su and D. Ye, "Static output feedback control for discrete-time hidden Markov jump systems against deception attacks," *International Journal of Robust and Nonlinear Control*, vol. 29, no. 18, pp. 6616–6637, 2019.

[27] N. Rong and Z. Wang, "State-dependent asynchronous intermittent control for IT2 T-S fuzzy interconnected systems under deception attacks," *Nonlinear Dynamics*, vol. 100, no. 4, pp. 3433–3448, 2020.

[28] J. Song, L.-Y. Huang, H. R. Karimi, Y. Niu, and J. Zhou, "ADP-based security decentralized sliding mode control for partially unknown large-scale systems under injection attacks," *IEEE Transactions on Circuits and Systems I: Regular Papers*, vol. 67, no. 12, pp. 5290–5301, 2020.

[29] H. Zhao, Y. Niu, and T. Jia, "Security control of cyber-physical switched systems under round-robin protocol: input-to-state stability in probability," *Information Sciences*, vol. 508, pp. 121–134, 2020.

[30] D. Ding, Z. Wang, D. W. C. Ho, and G. Wei, "Distributed recursive filtering for stochastic systems under uniform quantizations and deception attacks through sensor networks," *Automatica*, vol. 78, pp. 231–240, 2017.

[31] B. Shen, Z. Wang, D. Wang, and Q. Li, "State-saturated recursive filter design for stochastic time-varying nonlinear complex networks under deception attacks," *IEEE Transactions on Neural Networks and Learning Systems*, vol. 31, pp. 3788–3800, 2019.

[32] Z. Gu, X. Zhou, T. Zhang, F. Yang, and M. Shen, "Event-triggered filter design for nonlinear cyber-physical systems subject to deception attacks," *ISA Transactions*, vol. 104, pp. 130–137, 2020.

[33] Z. Wu, J. Lam, H. Su, and J. Chu, "Stability and dissipativity analysis of static neural networks with time delay," *IEEE Transactions on Neural Networks and Learning Systems*, vol. 23, pp. 199–210, 2011.

[34] L. Zhou, "Dissipativity of a class of cellular neural networks with proportional delays," *Nonlinear Dynamics*, vol. 73, no. 3, pp. 1895–1903, 2013.

[35] X. Zhang, S. He, V. Stojanovic, X. Luan, and F. Liu, "Finite-time asynchronous dissipative filtering of conic-type nonlinear Markov jump systems," *Science China Information Sciences*, vol. 64, no. 5, pp. 1–12, 2021.

[36] X. Yao, L. Wu, and W. X. Zheng, "Fault Detection Filter Design for Markovian Jump Singular Systems With Intermittent Measurements," *IEEE Transactions on Signal Processing*, vol. 59, no. 7, pp. 3099–3109, 2011.

[37] K. Liu, A. Seuret, and Y. Xia, "Stability analysis of systems with time-varying delays via the second-order Bessel-Legendre inequality," *Automatica*, vol. 76, pp. 138–142, 2017.

[38] C.-K. Zhang, Y. He, L. Jiang, M. Wu, and Q.-G. Wang, "An extended reciprocally convex matrix inequality for stability analysis of systems with time-varying delay," *Automatica*, vol. 85, pp. 481–485, 2017.

[39] C. Chong Lin, Q. Qing-Guo Wang, and T. H. Tong Heng Lee, "Stability and stabilization of a class of fuzzy time-delay descriptor systems," *IEEE Transactions on Fuzzy Systems*, vol. 14, no. 4, pp. 542–551, 2006.

WILEY | Hindawi

Research Article

Blow-Up of Solutions for a Coupled Nonlinear Viscoelastic Equation with Degenerate Damping Terms: Without Kirchhoff Term

Salah Mahmoud Boulaaras [1,2] **Abdelbaki Choucha,**[3] **Mohamed Abdalla** [4,5] **Karthikeyan Rajagopal** [6] **and Sahar Ahmed Idris**[7,8]

[1]*Department of Mathematics, College of Sciences and Arts, ArRas, Qassim University, Buraydah, Saudi Arabia*
[2]*Laboratory of Fundamental and Applied Mathematics of Oran (LMFAO), University of Oran 1, Oran 31000, Algeria*
[3]*Department of Mathematics, Faculty of Exact Sciences, University of El Oued, El Oued, Algeria*
[4]*Department of Mathematics, Faculty of Science, King Khalid University, Abha 61471, Saudi Arabia*
[5]*Mathematics Department, Faculty of Science, South Valley University, Qena 83523, Egypt*
[6]*Center for Nonlinear Systems, Chennai Institute of Technology, Chennai, Tamil Nadu 600069, India*
[7]*College of Industrial Engineering, King Khalid University, Abha 62529, Saudi Arabia*
[8]*Department of Mathematics, College of Sciences, Juba University, Juba, Sudan*

Correspondence should be addressed to Salah Mahmoud Boulaaras; s.boularas@qu.edu.sa

In this work, we consider a quasilinear system of viscoelastic equations with degenerate damping and source terms without the Kirchhoff term. Under suitable hypothesis, we study the blow-up of solutions.

1. Introduction

In this paper, we consider the following problem:

$$
\begin{cases}
|u_t|^\eta u_{tt} - \Delta u + \int_0^t h_1(t-s)\Delta u(s)ds + \left(|u|^k + |v|^l\right)|u_t|^{j-1}u_t \\
\quad = f_1(u,v), \ (x,t) \in \Omega \times (0,T), \\
|v_t|^\eta v_{tt} - \Delta v + \int_0^t h_2(t-s)\Delta v(s)ds + \left(|v|^\theta + |u|^\varrho\right)|v_t|^{s-1}v_t \\
\quad = f_2(u,v), \ (x,t) \in \Omega \times (0,T), \\
u(x,t) = v(x,t) = 0, \quad (x,t) \in \partial\Omega \times (0,T), \\
u(x,0) = u_0(x), u_t(x,0) = u_1(x), \quad x \in \Omega, \\
v(x,0) = v_0(x), v_t(x,0) = v_1(x), \quad x \in \Omega,
\end{cases}
\tag{1}
$$

where $k, l, \theta, \varrho \geq 0$; $j, s \geq 1$ for $N = 1, 2$, and $0 \leq j, s \leq (N + 2/N - 2)$ for $N \geq 3$; and $\eta \geq 0$ for $N = 1, 2$, and $0 < \eta \leq (2/N - 2)$ for $N \geq 3$; and $h_i(.): R^+ \longrightarrow R^+$ $(i = 1, 2)$ are positive relaxation functions which will be specified later. $(|(.)|^a + |(.)|^b)|(.)_t|^{\tau-1}(.)_t$ is the degenerate damping term, and

$$
\begin{cases}
f_1(u,v) = a_1|u+v|^{2(p+1)}(u+v) + b_1|u|^p.u.|v|^{p+2}, \\
f_2(u,v) = a_1|u+v|^{2(p+1)}(u+v) + b_1|v|^p.v.|u|^{p+2}.
\end{cases}
\tag{2}
$$

The motivation of our problem firstly is by the initial boundary value problem for the quasilinear equation of the form

$$
|u_t|^\eta u_{tt} - \Delta u + \int_0^t h(t-s)\Delta u(s)ds + g(u,u_t) = f(u).
\tag{3}
$$

This type of problem is frequently found in some mathematical models in applied sciences, especially in the theory of viscoelasticity. Problem (3) has been studied by various authors, and several results concerning asymptotic behavior and blow-up have been studied (case $\eta \geq 0$). For example, in the case $(g(u, u_t) = 0)$, problem (3) has been investigated in [1] and the author proved the blow-up result. In the case $(g(u, u_t) = 0)$ of boundary value problem and in the presence of the dispersion term $(-\Delta u_{tt})$, Liu [2] studied a general decay of solutions. And, in [3], the authors applied the potential well method to indicate the global existence and uniform decay of solutions $(g(u; u_t)) = 0$ instead of Δu_t). Furthermore, the authors obtained a blow-up result. In the case $(g(u, u_t) = |u_t|^m u_t)$, in [4], Wu studied a general decay of solution. Later, the same author in [5] considered the same problem but $(g(u, u_t) = u_t)$ and discussed the decay rate of solution. Recently, in [6], the authors proved the existence of global solution and a general stability result.

There are several works in case $(\eta = 0)$, where the authors have studied the blow-up of solutions of problem (3) (for example, see [3, 7–12]).

For a coupled system, He [13] considered the following problem:

$$
\begin{cases}
|u_t|^\eta u_{tt} - \Delta u + \int_0^t h_1(t-s)\Delta u(s)ds - \Delta u_{tt} + g_1(u, u_t) \\
\quad = f_1(u, v), \\
|v_t|^\eta v_{tt} - \Delta v + \int_0^t h_2(t-s)\Delta v(s)ds - \Delta v_{tt} + g_2(v, v_t) \\
\quad = f_2(u, v),
\end{cases}
$$

$$(4)$$

where $\eta > 0$; $j, s \geq 2$; and $g_1(u, u_t) = |u_t|^{j-2}u_t$ and $g_2(v, v_t) = |v_t|^{s-2}v_t$. The author proved general and optimal decay of solutions. Then, in [14], the author investigated the same problem without damping term and established a general decay of solutions. Furthermore, the author obtained a blow-up of solutions. In addition, in problem (1) with $\eta = 0$, in [15], Wu proved a general decay of solutions. Later, in [16], Piskin and Ekinci established a general decay and blow-up of solutions with nonpositive initial energy for problem (1) case (Kirchhoff type). In recent years, some other authors investigate the hyperbolic type system with degenerate damping terms (see [17–20]). Very recently, in the presence of the dispersion term $(-\Delta u_{tt})$, our problem (1) has been studied in [21]. Under some restrictions on the initial datum and standard conditions on relaxation functions, the authors have established the global existence and proved the general decay of solutions.

Based on all of the abovementioned discussion, we believe that the combination of these terms of damping (memory term, degenerate damping, and source terms) constitutes a new problem worthy of study and research, different from the above that we will try to shed light on, especially the blow-up of solutions.

Our paper is divided into several sections: In Section 2, we lay down the hypotheses, concepts, and lemmas we need.

In Section 3, we prove our main result. Finally, we give some concluding remarks in the last section.

2. Preliminaries

We prove the blow-up result under the following suitable assumptions:

(A1) $h_i: \mathbb{R}_+ \longrightarrow \mathbb{R}_+$ are differentiable and decreasing functions such that

$$h_i(t) \geq 0, 1 - \int_0^\infty h_i(s)ds = l_i > 0, \quad i = 1, 2. \quad (5)$$

(A2) There exist a constants $\xi_1, \xi_2 > 0$ such that

$$h_i'(t) \leq -\xi_i h_i(t), \quad t \geq 0, i = 1, 2. \quad (6)$$

Lemma 1. *There exists a function $F(u, v)$ such that*

$$F(u, v) = \frac{1}{2(p+2)}[uf_1(u, v) + vf_2(u, v)],$$

$$(7)$$

$$\frac{1}{2(p+2)}\left[a_1|u+v|^{2(p+2)} + 2b_1|uv|^{p+2}\right] \geq 0,$$

where

$$\frac{\partial F}{\partial u} = f_1(u, v),$$

$$(8)$$

$$\frac{\partial F}{\partial v} = f_2(u, v).$$

We take $a_1 = b_1 = 1$ for convenience.

Lemma 2 (see [18]). *There exist two positive constants c_0 and c_1 such that*

$$\frac{c_0}{2(p+2)}\left(|u|^{2(p+2)} + |v|^{2(p+2)}\right) \leq F(u, v)$$

$$(9)$$

$$\leq \frac{c_1}{2(p+2)}\left(|u|^{2(p+2)} + |v|^{2(p+2)}\right).$$

Now, we state the local existence theorem that can be established by combining arguments of [13, 16].

Theorem 1. *Assume (5) and (6) hold. Let*

$$
\begin{cases}
-1 < p < \dfrac{4-n}{n-2}, & n \geq 3, \\
p \geq -1, & n = 1, 2.
\end{cases}
$$

$$(10)$$

Then, for any initial datum,

$$(u_0, u_1, v_0, v_1) \in \mathcal{H}. \quad (11)$$

Problem (1) has a unique solution, for some $T > 0$:

$$u, v \in C\left([0, T]; H^2(\Omega) \cap H_0^1(\Omega)\right),$$

$$u_t \in C\left([0, T]; H_0^1(\Omega)\right) \cap L^{j+1}(\Omega), \qquad (12)$$

$$v_t \in C\left([0, T]; H_0^1(\Omega)\right) \cap L^{s+1}(\Omega),$$

where

$$\mathscr{H} = H_0^1(\Omega) \times L^2(\Omega) \times H_0^1(\Omega) \times L^2(\Omega). \qquad (13)$$

Now, we define the energy functional.

Lemma 3. *Assume (5), (6), and (10) hold; let (u, v) be a solution of (1); then, $E(t)$ is nonincreasing, that is,*

$$E(t) = \frac{1}{\eta + 2}\left[\|u_t\|_{\eta+2}^{\eta+2} + \|v_t\|_{\eta+2}^{\eta+2}\right],$$

$$+ \frac{1}{2}\left[\left(1 - \int_0^t h_1(s)ds\right)\|\nabla u\|_2^2\right.$$

$$+ \left(1 - \int_0^t h_2(s)ds\right)\|\nabla u\|_2^2\right],$$

$$+ \frac{1}{2}\left[(h_1 o \nabla u)(t) + (h_2 o \nabla u)(t)\right] - \int_\Omega F(u, v)\mathrm{d}x,$$

$$(14)$$

which satisfies

$$E'(t) \le \frac{1}{2}\left[(h_1' o \nabla u)(t) + (h_2' o \nabla u)\right](t)$$

$$- \frac{1}{2}\left[h_1(t)\|\nabla u\|_2^2 + h_2(t)\|\nabla u\|_2^2\right],$$

$$- \int_\Omega \left(|u|^k + |v|^l\right)|u_t|^{j+1}dx - \int_\Omega \left(|v|^\theta + |u|^\varrho\right)|v_t|^{s+1}dx,$$

$$\le 0.$$

$$(15)$$

Proof. By multiplying the first and second equations in (1) by u_t, v_t and integrating over Ω, we get

$$\frac{d}{dt}\left\{\frac{1}{\eta+2}\|u_t\|_{\eta+2}^{\eta+2} + \frac{1}{\eta+2}\|v_t\|_{\eta+2}^{\eta+2} + \frac{1}{2}\left(-1\int_0^t h_1(s)ds\right)\|\nabla u\|_2^2 + \frac{1}{2}\left(-1\int_0^t h_2(s)ds\right)\|\nabla u\|_2^2 + \frac{1}{2}(h_1 o \nabla u)(t)\right.$$

$$\left. + \frac{1}{2}(h_2 o \nabla u)(t) - \int_\Omega F(u, v)dx\right\}, \qquad (16)$$

$$= -\int_\Omega \left(|u|^k + |v|^l\right)|u_t|^{j+1}dx - \int_\Omega \left(|v|^\theta + |u|^\varrho\right)|v_t|^{s+1}dx + \frac{1}{2}(h_1' o \nabla u) - \frac{1}{2}h_1(t)\|\nabla u\|_2^2 + \frac{1}{2}(h_2' o \nabla u) - \frac{1}{2}h_2(t)\|\nabla u\|_2^2.$$

We obtain (14) and (15).   □

3. Blow-Up

In this section, we prove the blow-up result of solution of problem (1).

First, we define the functional as

$$\mathbb{H}(t) = -E(t) = -\frac{1}{\eta+2}\left[\|u_t\|_{\eta+2}^{\eta+2} + \|v_t\|_{\eta+2}^{\eta+2}\right] - \frac{1}{2}\left(1 - \int_0^t h_1(s)ds\right)\|\nabla u\|_2^2 + \frac{1}{2}\left(1 - \int_0^t h_2(s)ds\right)\|\nabla v\|_2^2$$

$$- \frac{1}{2}\left[(h_1 o \nabla u)(t) + (h_2 o \nabla u)(t)\right]$$

$$+ \frac{1}{2(p+2)}\left[\|u + v\|_{2(p+2)}^{2(p+2)} + \|uv\|_{2(p+2)}^{2(p+2)}\right]. \qquad (17)$$

Theorem 4. *Assume that (5), (6), and (10) hold, and suppose that $E(0) < 0$ and*

$$2(p+2) > \max\{k+j+1; l+j+1; \theta+s+1; \varrho+s+1\}. \tag{18}$$

Then, the solution of problem (1) blows up in finite time.

Proof. From (14), we have

$$E(t) \leq E(0) \leq 0. \tag{19}$$

Therefore,

$$\mathbb{H}'(t) = -E'(t) \geq \int_{\Omega} \left(|u|^k + |v|^l\right)|u_t|^{j+1} dx$$
$$+ \int_{\Omega} \left(|v|^\theta + |u|^\varrho\right)|v_t|^{s+1} dx. \tag{20}$$

Hence,

$$\mathbb{H}'(t) \geq \int_{\Omega} \left(|u|^k + |v|^l\right)|u_t|^{j+1} dx \geq 0,$$
$$\mathbb{H}'(t) \geq \int_{\Omega} \left(|v|^\theta + |u|^\varrho\right)|v_t|^{s+1} dx \geq 0. \tag{21}$$

By (9) and (17), we have

$$0 \leq \mathbb{H}(0) \leq \mathbb{H}(t) \leq \frac{1}{2(p+2)} \left[\|u+v\|_{2(p+2)}^{2(p+2)} + 2\|uv\|_{2(p+2)}^{2(p+2)}\right],$$
$$\leq \frac{c_1}{2(p+2)} \left[\|u_t\|_{\eta+2}^{\eta+2} + \|v_t\|_{\eta+2}^{\eta+2}\right]. \tag{22}$$

We set

$$\mathcal{K}(t) = \mathbb{H}^{1-\alpha} + \frac{\varepsilon}{\eta+1} \int_{\Omega} \left[u|u_t|^\eta u_t + v|v_t|^\eta v_t\right] dx, \tag{23}$$

where $\varepsilon > 0$ is to be assigned later and

$$0 < \alpha < \min\left\{\left(1 - \frac{1}{2(p+2)} - \frac{1}{\eta+2}\right), \frac{2p+3-(k+j)}{2j(p+2)}, \frac{2p+3-(l+j)}{2j(p+2)}, \frac{2p+3-(\theta+s)}{2s(p+2)}, \frac{2p+3-(\varrho+s)}{2s(p+2)}\right\} < 1. \tag{24}$$

By multiplying the first and second equations in (1) by u, v and with a derivative of (23), we get

$$\mathcal{K}'(t) = (1-\alpha)\mathbb{H}^{-\alpha}\mathbb{H}'(t) + \frac{\varepsilon}{\eta+1}\left(\|u_t\|_{\eta+2}^{\eta+2} + \|v_t\|_{\eta+2}^{\eta+2}\right) + \underbrace{\varepsilon \int_{\Omega} \nabla u \int_0^t g(t-s)\nabla u(s) ds\, dx}_{J_1} + \underbrace{\varepsilon \int_{\Omega} \nabla v \int_0^t h(t-s)\nabla u(s) ds\, dx}_{J_2}$$

$$\underbrace{- \varepsilon \int_{\Omega}\left(|u|^k + |v|^l\right)|u_t|^{j-1} u_t. u\, dx}_{J_3} \underbrace{- \varepsilon \int_{\Omega}\left(|v|^\theta + |u|^\varrho\right)|v_t|^{s-1} v_t. v\, dx}_{J_4} - \varepsilon\left(\|\nabla u\|_2^2 + \|\nabla v\|_2^2\right) + \underbrace{\varepsilon\left[\|u+v\|_{2(p+2)}^{2(p+2)} + 2\|uv\|_{2(p+2)}^{2(p+2)}\right]}_{J_5}, \tag{25}$$

where we have

$$J_1 = \varepsilon \int_0^t h_1(t-s) ds \int_{\Omega} \nabla u. (\nabla u(s) - \nabla u(t)) dx\, ds$$
$$+ \varepsilon \int_0^t h_1(s) ds\, \|\nabla u\|_2^2, \tag{26}$$
$$\geq \frac{\varepsilon}{2} \int_0^t h_1(s) ds\, \|\nabla u\|_2^2 - \frac{\varepsilon}{2} (h_1 o \nabla u),$$

$$J_2 = \varepsilon \int_0^t h_2(t-s) ds \int_{\Omega} \nabla u. (\nabla u(s) - \nabla u(t)) dx\, ds$$
$$+ \varepsilon \int_0^t h_2(s) ds\, \|\nabla u\|_2^2, \tag{27}$$
$$\geq \frac{\varepsilon}{2} \int_0^t h_2(s) ds\, \|\nabla u\|_2^2 - \frac{\varepsilon}{2} (h_2 o \nabla u).$$

From (25), we find that

$$\mathcal{K}'(t) \geq (1-\alpha)\mathbb{H}^{-\alpha}\mathbb{H}'(t) + \frac{\varepsilon}{\eta+1}\left(\|u_t\|_{\eta+2}^{\eta+2} + \|v_t\|_{\eta+2}^{\eta+2}\right)$$

$$- \varepsilon\left[\left(1 - \frac{1}{2}\int_0^t h_1(s) ds\right)\|\nabla u\|_2^2\right.$$

$$\left. + \left(1 - \frac{1}{2}\int_0^t h_2(s) ds\right)\|\nabla v\|_2^2\right]$$

$$- \frac{\varepsilon}{2}(h_1 o \nabla u) - \frac{\varepsilon}{2}(h_2 o \nabla u) - J_3 - J_4 + J_5. \tag{28}$$

At this point, we use Young's inequality; for $\delta > 0$,

$$XY \leq \frac{\delta^\alpha X^\alpha}{\alpha} + \frac{\delta^{-\beta} X^\beta}{\beta}, \alpha, \beta > 0, \frac{1}{\alpha} + \frac{1}{\beta} = 1, \tag{29}$$

We get that for $\delta_1, \delta_2 > 0,$

$$\left|u|u_t|^{j-1}u_t\right| \le \frac{\delta_1^{j+1}}{j+1}|u_t|^{j+1} + \frac{j}{j+1}\delta_1^{-(j+1/j)}|u_t|^{j+1},$$

$$\left|v|v_t|^{s-1}v_t\right| \le \frac{\delta_2^{s+1}}{s+1}|v_t|^{s+1} + \frac{s}{s+1}\delta_2^{-(s+1/s)}|v_t|^{s+1}. \tag{30}$$

Hence, we have

$$J_3 \le \varepsilon \frac{\delta_1^{j+1}}{j+1}\int_\Omega \left(|u|^k + |v|^l\right)|u_t|^{j+1}dx$$

$$+ \varepsilon \frac{j\delta_1^{-(j+1/j)}}{j+1}\int_\Omega \left(|u|^k + |v|^l\right)|u_t|^{j+1}dx\,dx,$$

$$J_4 \le \varepsilon \frac{\delta_2^{s+1}}{s+1}\int_\Omega \left(|v|^\theta + |u|^\varrho\right)|v_t|^{s+1}dx$$

$$+ \varepsilon \frac{s\delta_2^{-(s+1/s)}}{s+1}\int_\Omega \left(|v|^\theta + |u|^\varrho\right)|v_t|^{s+1}dx\,. \tag{31}$$

Therefore, using (21) and by setting δ_1, δ_2 so that

$$\frac{j\delta_1^{-(j+1/j)}}{j+1} = \frac{\kappa\mathbb{H}^{-\alpha}(t)}{2},$$

$$\frac{s\delta_2^{-(s+1/s)}}{s+1} = \frac{\kappa\mathbb{H}^{-\alpha}(t)}{2}, \tag{32}$$

and substituting in (28), we get

$$\mathcal{K}'(t) \ge [(1-\alpha) - \varepsilon\kappa]\mathbb{H}^{-\alpha}\mathbb{H}'(t) + \frac{\varepsilon}{\eta+1}\left(\|u_t\|_{\eta+2}^{\eta+2} + \|v_t\|_{\eta+2}^{\eta+2}\right) - \varepsilon\left[\left(1 - \frac{1}{2}\int_0^t h_1(s)ds\right)\|\nabla u\|_2^2 + \left(1 - \frac{1}{2}\int_0^t h_2(s)ds\right)\|\nabla v\|_2^2\right]$$

$$- \frac{\varepsilon}{2}(h_1 o \nabla u) - \frac{\varepsilon}{2}(h_2 o \nabla u) - \varepsilon C_1(\kappa)\mathbb{H}^{\alpha j}(t)\int_\Omega \left(|u|^k + |v|^l\right)|u_t|^{j+1}dx - \varepsilon C_2(\kappa)\mathbb{H}^{\alpha j}(t)\int_\Omega \left(|v|^\theta + |u|^\varrho\right)|v_t|^{s+1} + J_5, \tag{33}$$

where

$$C_1(\kappa):\; = \left(\frac{2j}{\kappa(j+1)}\right)^{j+1}\frac{1}{j+1},$$

$$C_2(\kappa):\; = \left(\frac{2s}{\kappa(s+1)}\right)^{s+1}\frac{1}{s+1}. \tag{34}$$

We have

$$\int_\Omega \left(|u|^k + |v|^l\right)|u_t|^{j+1}dx = \|u\|_{k+j+1}^{k+j+1} + \int_\Omega |v|^l|u|^{j+1}dx\,,$$

$$\int_\Omega \left(|v|^\theta + |u|^\varrho\right)|v_t|^{s+1}dx = \|v\|_{\theta+s+1}^{\theta+s+1} + \int_\Omega |u|^\varrho|v|^{s+1}dx\,. \tag{35}$$

By Young's inequality, we find that for $\delta_3, \delta_4 > 0$,

$$\int_\Omega |v|^l|u|^{j+1}dx \le \frac{l}{l+j+1}\delta_3^{(l+j+1/l)}\|v\|_{l+j+1}^{l+j+1}$$

$$+ \frac{j+1}{l+j+1}\delta_3^{-(l+j+1/l)}\|u\|_{l+j+1}^{l+j+1},$$

$$\int_\Omega |u|^\varrho|v|^{s+1}dx \le \frac{\varrho}{\varrho+s+1}\delta_4^{(\varrho+s+1/\varrho)}\|u\|_{\varrho+s+1}^{\varrho+s+1}$$

$$+ \frac{s+1}{\varrho+s+1}\delta_4^{-((\varrho+s+1/\varrho))}\|v\|_{\varrho+s+1}^{\varrho+s+1}. \tag{36}$$

Hence,

$$\mathbb{H}^{\alpha j}(t)\int_\Omega \left(|u|^k + |v|^l\right)|u_t|^{j+1}dx \le \mathbb{H}^{\alpha j}(t)\|u\|_{k+j+1}^{k+j+1} + \frac{l\mathbb{H}^{\alpha j}(t)}{l+j+1}\delta_3^{(l+j+1/l)}\|v\|_{l+j+1}^{l+j+1} + \frac{(j+1)\mathbb{H}^{\alpha j}(t)}{l+j+1}\delta_3^{-((l+j+1/l))}\|u\|_{l+j+1}^{l+j+1},$$

$$\mathbb{H}^{\alpha j}(t)\int_\Omega \left(|v|^\theta + |u|^\varrho\right)|v_t|^{s+1}dx \le \mathbb{H}^{\alpha s}(t)\|v\|_{\theta+s+1}^{\theta+s+1} + \frac{\varrho\mathbb{H}^{\alpha s}(t)}{\varrho+s+1}\delta_4^{(\varrho+s+1/\varrho)}\|u\|_{\varrho+s+1}^{\varrho+s+1} + \frac{(s+1)\mathbb{H}^{\alpha s}(t)}{\varrho+s+1}\delta_4^{-((\varrho+s+1/\varrho))}\|v\|_{\varrho+s+1}^{\varrho+s+1}. \tag{37}$$

Since (10) holds, we obtain the following by using (22) and (24):

$$
\begin{aligned}
&\mathbb{H}^{\alpha j}(t)\|u\|_{k+j+1}^{k+j+1} \le c_1\left(\|u\|_{2(p+2)}^{2\alpha j(p+2)+k+j+1} + \|v\|_{2(p+2)}^{2\alpha j(p+2)}\|u\|_{k+j+1}^{k+j+1}\right),\\
&\mathbb{H}^{\alpha j}(t)\|v\|_{k+j+1}^{k+j+1} \le c_2\left(\|v\|_{2(p+2)}^{2\alpha j(p+2)+k+j+1} + \|u\|_{2(p+2)}^{2\alpha j(p+2)}\|v\|_{k+j+1}^{k+j+1}\right),\\
&\mathbb{H}^{\alpha s}(t)\|v\|_{\theta+s+1}^{\theta+s+1} \le c_3\left(\|v\|_{2(p+2)}^{2\alpha s(p+2)+\theta+s+1} + \|u\|_{2(p+2)}^{2\alpha s(p+2)}\|v\|_{\theta+s+1}^{\theta+s+1}\right),\\
&\mathbb{H}^{\alpha s}(t)\|u\|_{\theta+s+1}^{\theta+s+1} \le c_4\left(\|u\|_{2(p+2)}^{2\alpha s(p+2)+\theta+s+1} + \|v\|_{2(p+2)}^{2\alpha s(p+2)}\|u\|_{\theta+s+1}^{\theta+s+1}\right),
\end{aligned}
\tag{38}
$$

for some positive constants $c_i, i = 1, ..4$. By using (24) and the algebraic inequality

$$
B^\varsigma \le (B+1) \le \left(1+\frac{1}{b}\right)(B+b), \forall B>0, 0<\varsigma<1, b>0,
\tag{39}
$$

we have, $\forall t>0$,

$$
\begin{aligned}
&\|u\|_{2(p+2)}^{2\alpha j(p+2)+k+j+1} \le d\left(\|u\|_{2(p+2)}^{2(p+2)} + \mathbb{H}(0)\right) \le d\left(\|u\|_{2(p+2)}^{2(p+2)} + \mathbb{H}(t)\right),\\
&\|v\|_{2(p+2)}^{2\alpha j(p+2)+k+j+1} \le d\left(\|v\|_{2(p+2)}^{2(p+2)} + \mathbb{H}(0)\right) \le d\left(\|v\|_{2(p+2)}^{2(p+2)} + \mathbb{H}(t)\right),\\
&\|v\|_{2(p+2)}^{2\alpha s(p+2)+\theta+s+1} \le d\left(\|v\|_{2(p+2)}^{2(p+2)} + \mathbb{H}(0)\right) \le d\left(\|v\|_{2(p+2)}^{2(p+2)} + \mathbb{H}(t)\right),\\
&\|u\|_{2(p+2)}^{2\alpha s(p+2)+\theta+s+1} \le d\left(\|u\|_{2(p+2)}^{2(p+2)} + \mathbb{H}(0)\right) \le d\left(\|u\|_{2(p+2)}^{2(p+2)} + \mathbb{H}(t)\right),
\end{aligned}
\tag{40}
$$

where $d = 1 + (1/\mathbb{H}(0))$. Also, since

$$
(X+Y)^\gamma \le C(X^\gamma + Y^\gamma), X, Y > 0, \gamma > 0,
\tag{41}
$$

we conclude that

$$
\begin{aligned}
&\|v\|_{2(p+2)}^{2\alpha j(p+2)}\|u\|_{k+j+1}^{k+j+1} \le c_5\left(\|v\|_{2(p+2)}^{2(p+2)} + \|u\|_{2(p+2)}^{2(p+2)}\right),\\
&\|u\|_{2(p+2)}^{2\alpha j(p+2)}\|v\|_{k+j+1}^{k+j+1} \le c_6\left(\|u\|_{2(p+2)}^{2(p+2)} + \|v\|_{2(p+2)}^{2(p+2)}\right),\\
&\|u\|_{2(p+2)}^{2\alpha s(p+2)}\|v\|_{\theta+s+1}^{\theta+s+1} \le c_7\left(\|v\|_{2(p+2)}^{2(p+2)} + \|u\|_{2(p+2)}^{2(p+2)}\right),\\
&\|v\|_{2(p+2)}^{2\alpha s(p+2)}\|u\|_{\theta+s+1}^{\theta+s+1} \le c_8\left(\|v\|_{2(p+2)}^{2(p+2)} + \|u\|_{2(p+2)}^{2(p+2)}\right).
\end{aligned}
\tag{42}
$$

Substituting (40) and (42) in (38), we get

$$
\begin{aligned}
&\mathbb{H}^{\alpha j}(t)\|u\|_{k+j+1}^{k+j+1} \le c_9\left(\|v\|_{2(p+2)}^{2(p+2)}\right) + \left(\|u\|_{2(p+2)}^{2(p+2)} + \mathbb{H}(t)\right),\\
&\mathbb{H}^{\alpha j}(t)\|v\|_{k+j+1}^{k+j+1} \le c_{10}\left(\|v\|_{2(p+2)}^{2(p+2)}\right) + \left(\|u\|_{2(p+2)}^{2(p+2)} + \mathbb{H}(t)\right),\\
&\mathbb{H}^{\alpha j}(t)\|v\|_{k+j+1}^{k+j+1} \le c_{11}\left(\|v\|_{2(p+2)}^{2(p+2)}\right) + \left(\|u\|_{2(p+2)}^{2(p+2)} + \mathbb{H}(t)\right),\\
&\mathbb{H}^{\alpha j}(t)\|u\|_{k+j+1}^{k+j+1} \le c_{12}\left(\|v\|_{2(p+2)}^{2(p+2)}\right) + \left(\|u\|_{2(p+2)}^{2(p+2)} + \mathbb{H}(t)\right).
\end{aligned}
\tag{43}
$$

Hence, by fixing $\delta_3, \delta_4 > 0$, we get

$$
\begin{aligned}
&\mathbb{H}^{\alpha j}(t)\int_\Omega \left(|u|^k + |v|^l\right)|u_t|^{j+1}dx \le M_1\left(1 + \frac{l\delta_3^{(l+j+1/l)}}{l+j+1} + \frac{(j+1)\delta_3^{-(l+j+1/l)}}{l+j+1}\right)\left(\|v\|_{2(p+2)}^{2(p+2)} + \|u\|_{2(p+2)}^{2(p+2)} + \mathbb{H}(t)\right),\\
&\mathbb{H}^{\alpha s}(t)\int_\Omega \left(|v|^\theta + |u|^\varrho\right)|v_t|^{s+1}dx \le M_2\left(1 + \frac{\varrho\delta_4^{(\varrho+s+1/\varrho)}}{\varrho+s+1} + \frac{(s+1)\delta_4^{-(\varrho+s+1/\varrho)}}{\varrho+s+1}\right)\left(\|v\|_{2(p+2)}^{2(p+2)} + \|u\|_{2(p+2)}^{2(p+2)} + \mathbb{H}(t)\right),
\end{aligned}
\tag{44}
$$

for some constants $M_1, M_2 > 0$.

Now, for $0 < a < 1$, from (17),

$$
\begin{aligned}
J_5 &= \varepsilon\left[\|u+v\|_{2(p+2)}^{2(p+2)} + 2\|uv\|_{p+2}^{p+2}\right] = \varepsilon a\left[\|u+v\|_{2(p+2)}^{2(p+2)} + 2\|uv\|_{p+2}^{p+2}\right] + \frac{2\varepsilon(p+2)(1-a)}{\eta+2}\left(\|u_t\|_{\eta+2}^{\eta+2} + \|v_t\|_{\eta+2}^{\eta+2}\right)\\
&\quad + \varepsilon(p+2)(1-a)\left(1 - \int_0^t g(s)ds\right)\|\nabla u\|_2^2 + \varepsilon(p+2)(1-a)\left(1 - \int_0^t h(s)ds\right)\|\nabla v\|_2^2\\
&\quad - \varepsilon(p+2)(1-a)\left((h_1 o\nabla u) + (h_2 o\nabla u)\right) + \varepsilon 2(p+2)(1-a)\mathbb{H}(t).
\end{aligned}
\tag{45}
$$

Substituting in (33) and by using (9), we get

$$\mathcal{K}'(t) \geq \{(1-a) - \varepsilon\kappa\}\mathbb{H}^{-\alpha}\mathbb{H}'(t) + \varepsilon\left\{\frac{2\varepsilon(p+2)(1-a)}{\eta+2} + \frac{1}{\eta+1}\right\}\left(\|u_t\|_{\eta+2}^{\eta+2} + \|v_t\|_{\eta+2}^{\eta+2}\right),$$

$$+ \varepsilon\left\{(p+2)(1-a)\left(1 - \int_0^t h_1(s)ds\right) - \left(1 - \frac{1}{2}\int_0^t h_1(s)ds\right)\right\}\|\nabla u\|_2^2$$

$$+ \varepsilon\left\{(p+2)(1-a)\left(1 - \int_0^t h_2(s)ds\right) - \left(1 - \frac{1}{2}\int_0^t h_2(s)ds\right)\right\}\|\nabla v\|_2^2 \tag{46}$$

$$+ \varepsilon\left\{(p+2)(1-a) - \frac{1}{2}\right\}(h_1 o\nabla u + h_2 o\nabla v) + \varepsilon\{c_0 a - (M_3 C_1(\kappa) + M_4 C_2(\kappa))\}\left(\|u\|_{2(p+2)}^{2(p+2)} + \|v\|_{2(p+2)}^{2(p+2)}\right)$$

$$+ \varepsilon\{2(p+2)(1-a) - (M_3 C_1(\kappa) + M_4 C_2(\kappa))\}\mathbb{H}(t),$$

where

$$M_3 := M_1\left(1 + \frac{l\delta_3^{(l+j+1/l)}}{l+j+1} + \frac{(j+1)\delta_3^{-(l+j+1/l)}}{l+j+1}\right) > 0,$$

$$M_4 := M_2\left(1 + \frac{\varrho\delta_4^{(\varrho+s+1/\varrho)}}{\varrho+s+1} + \frac{(s+1)\delta_4^{-(\varrho+s+1/\varrho)}}{\varrho+s+1}\right) > 0. \tag{47}$$

In this stage, we take $a > 0$ small enough so that

$$\lambda_1 = (p+2)(1-a) - 1 > 0, \tag{48}$$

and we assume that

$$\max\left\{\int_0^\infty h_1(s)ds, \int_0^\infty h_2(s)ds\right\} < \frac{(p+2)(1-a) - 1}{((p+2)(1-a) - (1/2))}$$

$$= \frac{2\lambda_1}{2\lambda_1 + 1} \tag{49}$$

gives

$$\lambda_2 = \left\{((p+2)(1-a) - 1) - \int_0^t h_1(s)ds\left((p+2)(1-a) - \frac{1}{2}\right)\right\} > 0,$$

$$\lambda_3 = \left\{((p+2)(1-a) - 1) - \int_0^t h_2(s)ds\left((p+2)(1-a)) - \frac{1}{2}\right)\right\} > 0. \tag{50}$$

Then, we choose κ so large such that

$$\lambda_4 = ac_0 - (M_3 C_1(\kappa) + M_4 C_2(\kappa)) > 0,$$
$$\lambda_5 = 2(p+2)(1-a) - (M_3 C_1(\kappa) + M_4 C_2(\kappa)) > 0. \tag{51}$$

Finally, we fix κ and a and we appoint ε small enough so that

$$\lambda_6 = (1-\alpha) - \varepsilon\kappa > 0. \tag{52}$$

Thus, for some $\beta > 0$, estimate (46) becomes

$$\mathcal{K}'(t) \geq \beta\left\{\mathbb{H}(t) + \|u_t\|_{\eta+2}^{\eta+2} + \|v_t\|_{\eta+2}^{\eta+2} + \|\nabla u\|_2^2 + \|\nabla v\|_2^2 + (h_1 o\nabla u) + (h_2 o\nabla v) + \|u\|_{2(p+2)}^{2(p+2)} + \|u\|_{2(p+2)}^{2(p+2)}\right\}. \tag{53}$$

By (9), for some $\beta_1 > 0$, we obtain

$$\mathcal{K}'(t) \geq \beta_1\left\{\mathbb{H}(t) + \|u_t\|_{\eta+2}^{\eta+2} + \|v_t\|_{\eta+2}^{\eta+2} + \|\nabla u\|_2^2 + \|\nabla v\|_2^2 + (h_1 o\nabla u) + (h_2 o\nabla v) + \|u+v\|_{2(p+2)}^{2(p+2)} + 2\|uv\|_{(p+2)}^{(p+2)}\right\} \tag{54}$$

and

$$\mathcal{K}(t) \geq \mathcal{K}(0) > 0, t > 0. \tag{55}$$

Next, using Hölder's and Young's inequalities, we have

$$\left|\int_\Omega\left(u|u_t|^\eta u_t + v|v_t|^\eta v_t\right)dx\right|^{(1/1-\alpha)}$$

$$\leq C\left[\|u\|_{2(p+2)}^{(\theta/1-\alpha)} + \|u_t\|_{\eta+2}^{(\mu/1-\alpha)} + \|v\|_{2(p+2)}^{(\theta/1-\alpha)} + \|v_t\|_{\eta+2}^{(\mu/1-\alpha)}\right], \tag{56}$$

where $(1/\mu) + (1/\theta) = 1$.

We take $\mu = (\eta + 2)(1 - \alpha)$, to get

$$\frac{\theta}{1-\alpha} = \frac{\eta+2}{(1-\alpha)(\eta+2)-1} \le 2(p+2). \quad (57)$$

Subsequently, by using (24), (22), and (39), we obtain

$$\|u\|_{2(p+2)}^{(\eta+2/(1-\alpha)(\eta+2)-1)} \le d\left(\|u\|_{2(p+2)}^{2(p+2)} + \mathbb{H}(t)\right),$$

$$\|v\|_{2(p+2)}^{(\eta+2/(1-\alpha)(\eta+2)-1)} \le d\left(\|v\|_{2(p+2)}^{2(p+2)} + \mathbb{H}(t)\right), \forall t \ge 0. \quad (58)$$

Therefore,

$$\left|\int_\Omega \left(u|u_t|^\eta u_t + v|v_t|^\eta v_t\right)dx\right|^{(1/1-\alpha)}$$

$$\le c_{13}\left[\|u\|_{2(p+2)}^{2(p+2)} + \|v\|_{2(p+2)}^{2(p+2)} + \|u_t\|_{\eta+2}^{\eta+2} + \|v_t\|_{\eta+2}^{\eta+2} + H(t)\right]. \quad (59)$$

Hence, by substituting (59) into (23), we get

$$\begin{aligned}
\mathscr{K}^{(1/1-\alpha)}(t) &= \left(\mathbb{H}^{1-\alpha} + \frac{\varepsilon}{\eta+1}\int_\Omega \left(u|u_t|^\eta u_t + v|v_t|^\eta v_t\right)dx\right)^{(1/1-\alpha)}, \\
&\le c\left(\mathbb{H}(t) + \left|\int_\Omega \left(u|u_t|^\eta u_t + v|v_t|^\eta v_t\right)dx\right|^{(1/1-\alpha)}\right), \\
&\le c\left(\mathbb{H}(t) + \|u_t\|_{\eta+2}^{\eta+2} + \|v_t\|_{\eta+2}^{\eta+2} + \|u\|_{2(p+2)}^{2(p+2)} + \|v\|_{2(p+2)}^{2(p+2)}\right), \\
&\le c\left(\mathbb{H}(t) + \|u_t\|_{\eta+2}^{\eta+2} + \|v_t\|_{\eta+2}^{\eta+2} + \|\nabla u\|_2^2 + \|\nabla v\|_2^2 + (h_1 o \nabla u) + (h_2 o \nabla v) + \|u\|_{2(p+2)}^{2(p+2)} + \|v\|_{2(p+2)}^{2(p+2)}\right).
\end{aligned} \quad (60)$$

From (53) and (60), we get

$$\mathscr{K}'(t) \ge \lambda \mathscr{K}^{(1/1-\alpha)}(t), \quad (61)$$

where $\lambda > 0$, and this depends only on β and c.

By integration of (61), we obtain

$$\mathscr{K}^{(\alpha/1-\alpha)}(t) \ge \frac{1}{\mathscr{K}^{(-\alpha/1-\alpha)}(0) - \lambda(\alpha/1-\alpha)t}. \quad (62)$$

Hence, $\mathscr{K}(t)$ blows up in time

$$T \le T^* = \frac{1-\alpha}{\lambda \alpha \mathscr{K}^{(\alpha/1-\alpha)}(0)}. \quad (63)$$

Then, the proof is completed. □

4. Conclusion

The objective of this work is the study of the blow-up of solutions for a quasilinear viscoelastic system with degenerate damping. This type of problem is frequently found in some mathematical models in applied sciences, especially in the theory of viscoelasticity. What interests us in this current work is the combination of these terms of damping (memory term, degenerate damping, and source terms), which dictates the emergence of these terms in the system.

In the next work, we will try using the same method with the same problem in addition to other damping terms (dispersion term, Balakrishnan–Taylor damping, and delay term).

Data Availability

No data were used.

Conflicts of Interest

The authors declare that they have no conflicts of interest.

Acknowledgments

References

[1] H. Song, "Global nonexistence of positive initial energy solutions for a viscoelastic wave equation," *Nonlinear Analysis*, vol. 125, pp. 260–269, 2015.

[2] W. Liu, "General decay and blow-up of solution for a quasilinear viscoelastic problem with nonlinear source," *Nonlinear Analysis: Theory, Methods & Applications*, vol. 73, no. 6, pp. 1890–1904, 2010.

[3] G. Liang, Y. Zhaoqin, and L. Guonguang, "Blow up and global existence for a nonlinear viscoelastic wave equation with strong damping and nonlinear damping and source terms," *Applied Mathematics*, vol. 6, pp. 806–816, 2015.

[4] S. T. Wu, "General decay of solutions for a viscoelastic equation with nonlinear damping and source terms," *Acta Mathematica Scientia*, vol. 318, pp. 1436–1448, 2011.

[5] S. T. Wu, "General decay of energy for a viscoelastic equation with damping and source terms," *Taiwanese Journal of Mathematics*, vol. 16, no. 1, pp. 113–128, 2012.

[6] H. Yang, S. Fang, F. Liang, and M. Li, "A general stability result for second order stochastic quasilinear evolution equations with memory," *Boundary Value Problems*, vol. 62, pp. 1–16, 2020.

[7] A. M. Alghamdi, S. Gala, M. A. Ragusa, and Z. Zhang, "A regularity criterion for the 3D density-dependent MHD equations," *Bulletin of the Brazilian Mathematical Society, New Series*, vol. 52, no. 2, pp. 241–251, 2020.

[8] A. Mohammad Alghamdi, S. Gala, S. Gala, C. Qian, and M. Alessandra Ragusa, "The anisotropic integrability logarithmic regularity criterion for the 3D MHD equations," *Electronic research archive*, vol. 28, no. 1, pp. 183–193, 2020.

[9] A. Choucha, D. Ouchenane, and S. Boulaaras, "Blow-up of a nonlinear viscoelastic wave equation with distributed delay combined with strong damping and source terms," *Journal of Nonlinear Functional Analysis*, vol. 31, 2020.

[10] H. Song and D. Xue, "Blow up in a nonlinear viscoelastic wave equation with strong damping," *Nonlinear Analysis: Theory, Methods & Applications*, vol. 109, pp. 245–251, 2014.

[11] H. Song and C. Zhong, "Blow-up of solutions of a nonlinear viscoelastic wave equation," *Nonlinear Analysis: Real World Applications*, vol. 11, no. 5, pp. 3877–3883, 2010.

[12] A. Zarai, A. Draifia, and S. Boulaaras, "Blow-up of solutions for a system of nonlocal singular viscoelastic equations," *Applicable Analysis*, vol. 97, no. 13, pp. 2231–2245, 2018.

[13] L. He, "On decay and blow-up of solutions for a system of equations," *Applicable Analysis*, vol. 100, no. 11, pp. 2449–2477, 2019.

[14] L. He, "On decay of solutions for a system of coupled viscoelastic equations," *Acta Applicandae Mathematica*, vol. 167, no. 1, pp. 171–198, 2020.

[15] S.-T. Wu, "General decay of solutions for a nonlinear system of viscoelastic wave equations with degenerate damping and source terms," *Journal of Mathematical Analysis and Applications*, vol. 406, no. 1, pp. 34–48, 2013.

[16] E. Pişkin and F. Ekinci, "General decay and blow up of solutions for coupled viscoelastic equation of Kirchhoff type with degenerate damping terms," *Mathematical Methods in the Applied Sciences*, vol. 42, no. 16, pp. 5468–5488, 2019.

[17] M. M. Cavalcanti, V. N. Domingos Cavalcanti, and J. Ferreira, "Existence and uniform decay for a non-linear viscoelastic equation with strong damping," *Mathematical Methods in the Applied Sciences*, vol. 24, no. 14, pp. 1043–1053, 2001.

[18] D. Ouchenane, K. Zennir, and M. Bayoud, "Global nonexistence of solutions for a system of nonlinear viscoelastic wave equation with degenerate damping and source terms," *Ukrainian Mathematical Journal*, vol. 65, no. 7, 2013.

[19] E. Pişkin and F. Ekinci, "Blow up of solutions for a coupled Kirchhoff-type equations with degenerate damping terms, applications and applied Mathematics," *International Journal*, vol. 14, no. 2, pp. 942–956, 2019.

[20] N. Mezouar and S. Boulaaras, "Global existence and decay of solutions of a singular nonlocal viscoelastic system with damping terms," *Topological Methods in Nonlinear Analysis*, vol. 1, 2020.

[21] F. Ekinci, E. Piskin, S. M. Boulaaras, and I. Mekawy, "Global existence and general decay of solutions for a quasilinear system with degenerate damping terms," *Journal of function Spaces*, vol. 2021, Article ID 4316238, 2021.

WILEY | Hindawi

Research Article

Delayed Feedback Control of Hidden Chaos in the Unified Chaotic System between the Sprott C System and Yang System

Huijian Zhu and Lijie Li [ID]

*Guangxi Colleges and Universities Key Laboratory of Complex System Optimization and Big Data Processing,
Yulin Normal University, Yulin 537000, Guangxi, China*

Correspondence should be addressed to Lijie Li; lijieguangxi@126.com

In this paper, the influence of delayed feedback on the unified chaotic system from the Sprott C system and Yang system is studied. The Hopf bifurcation and dynamic behavior of the system are fully studied by using the central manifold theorem and bifurcation theory. The explicit formula, bifurcation direction, and stability of the periodic solution of bifurcation are given correspondingly. The Hopf bifurcation diagram and chaotic phenomenon are also analyzed by numerical simulation to prove the correctness of the theory. It shows that this delay control can only be applied to the hidden chaos with two stable equilibria.

1. Introduction

Since Lorentz inadvertently discovered chaos in a three-dimensional autonomous system [1] in 1963, more and more scholars began to study the chaos of various systems. Sprott [2–4] found nineteen simple chaotic systems, which may have no equilibra, one equilibrium, or two equilibra. Some classical three-dimensional autonomous chaotic systems, such as Lorentz system [1] and Chen system [5], have a saddle point and two unstable saddle foci. Other three-dimensional chaotic systems [6] have two unstable saddle foci. A chaotic system with one saddle and two stable node foci was discovered by Yang and Chen [7]. Some current studies on these systems including theoretical proof and numerical simulation can be found in the literature [8–19].

In 2000, Yang, Wei, and Chen [20] introduced a new three-dimensional chaotic system that is very similar to Lorentz system and Chen system, but it has only two stable node foci. The related types of chaotic systems have been analyzed and numerically studied in detail [21–24]. It has become very important to study the local and global properties of systems with chaotic phenomena. As it is known, hidden attractors are known as the kind of attractors whose domain of attraction is outside the equilibrium points; meanwhile, the domain of attraction in self-excited attractors is related to the unstable equilibrium points [25–27]. Finding hidden attractors in complex variable chaotic systems is even more difficult than finding their real variable counterparts. In recent years, an increasing number of scholars have paid attention to the control and utilization of chaos [28–31] for stabilizing the system with chaotic behaviors. It is also worth noting that theories and methods of controlling hidden chaos in continuous dynamical systems have been developed. This paper mainly studies the following unified chaotic system from [2, 20, 24]:

$$
\begin{cases}
\dot{x} = a(y - x) \\
\dot{y} = -cy - xz + k(y(t - \tau) - y), \\
\dot{z} = -b + k_1 xy + k_2 y^2,
\end{cases}
\tag{1}
$$

where $a, b,$ and c are the positive real parameters, $k, k_1,$ and k_2 are the control parameters, and τ is the delay parameter. For parameter values $(a, b, c, k, k_1, k_2) = (1, 1, 0, 0, 0, 1)$, system (1) becomes the Sprott C system. For parameter values $(k, k_1, k_2) = (0, 1, 0)$, system (1) is a general expression for the Yang system. Moreover, for parameter values $(a, b, c, k, k_1, k_2) = (10, 100, 9.8, 0, 0.08, 0.01)$, system (1) without delay has two

stable equilibria, whose three characteristic values are $\lambda_1 = -19.3894$ and $\lambda_{2,3} = -0.2053 \pm 10.1542i$. Figures 1(a) and 1(b), respectively, show time series and the projection of chaotic attractors on the $y - z$ plane. Therefore, system (1) has a hidden attractor coexisting with two stable node foci for initial values $(0.98, -1.82, 0.49)$. Therefore, we want to consider the stability of system (1) with direct delay feedback from theoretical analysis and numerical study. At the same time, when all equilibria are stable, we want to show the results that system (1) will turn to chaotic attractor from Hopf bifurcation [32].

The organization of this paper is as follows: In Section 2, the bifurcation conditions of Hopf bifurcation in delayed system (1) are discussed. In Section 3, based on the central manifold theorem and bifurcation theory, the direction and stability of Hopf bifurcation are analyzed in detail. In Section 4, numerical simulations illustrate our theoretical results. Finally, the conclusion is given in Section 5.

2. Existence of Hopf Bifurcation in System (1)

If $k_1 + k_2 > 0$, system (1) possesses two equilibria $E_{1,2}$ $(\pm\sqrt{b}/\sqrt{k_1 + k_2}, \pm\sqrt{b}/\sqrt{k_1 + k_2}, -c)$. Because of the symmetry of E_1 and E_2, it is sufficient to analyze the properties of only one of them. So, the rest of the discussion is going to be about E_1. By the following linear transformation to shift E_1 to the origin,

$$x_1 = x - \frac{\sqrt{b}}{\sqrt{k_1 + k_2}},$$

$$y_1 = y - \frac{\sqrt{b}}{\sqrt{k_1 + k_2}}, \tag{2}$$

$$z_1 = x + c,$$

the controlled system (1) is

$$\begin{cases} \dot{x}_1 = a(y_1 - x_1), \\ \dot{y}_1 = c(x_1 - y_1) - \frac{\sqrt{b}}{\sqrt{k_1 + k_2}}z_1 - x_1 z_1 + k[y_1(t - \tau) - y_1], \\ \dot{z}_1 = \frac{\sqrt{b}\,k_1}{\sqrt{k_1 + k_2}}x_1 + \frac{\sqrt{b}\,(k_1 + 2k_2)}{\sqrt{k_1 + k_2}}y_1 + k_1 x_1 y_1 + k_2 y_1^2. \end{cases} \tag{3}$$

The characteristic equation corresponding to the linear matrix of equation (3) is

$$\lambda^3 + (a + c + k)\lambda^2 + \left(\frac{k_1 + 2k_2}{k_1 + k_2}b + ak\right)\lambda + 2ab \tag{4}$$

$$-\left(\lambda^2 + a\lambda\right)ke^{-\lambda\tau} = 0.$$

When $\tau = 0$, equation (4) becomes

$$\lambda^3 + (a + c)\lambda^2 + \frac{k_1 + 2k_2}{k_1 + k_2}b\lambda + 2ab = 0. \tag{5}$$

According to the Routh–Hurwitz criterion, in equation (5), under the following conditions, there are three roots in the negative real part:

$$k_2 > \max\left\{-k_1, -\frac{1}{2}(c - a)k_1\right\}. \tag{6}$$

The classification conditions of reference equilibrium point, E_1, and E_2 are local stable nodes or focal points.

For the sake of analysis, let us reduce equation (4) to

$$\lambda^3 + a_2\lambda^2 + a_1\lambda + a_0 + \left(b_2\lambda^2 + b_1\lambda\right)e^{-\lambda\tau} = 0, \tag{7}$$

where $a_2 = a + c + k, a_1 = (k_1 + 2k_2)/\ (k_1 + k_2)b + ak, a_0 = 2ab, b_2 = -k$, and $b_1 = -ak$.

Since Hopf bifurcations must have a pair of pure imaginary roots at the system equilibrium point, we might as well establish system (1) having a pair of pure imaginary roots, that is, $i\rho$, so we can substitute the roots into equation (4):

$$-\rho^3 i - a_2\rho^2 + a_1\rho i + a_0 + \left(-b_2\rho^2 + b_1\rho i\right) \\ \cdot\left[\cos(\rho\tau) - i\sin(\rho\tau)\right] = 0, \tag{8}$$

where we separate the real part from the imaginary part:

$$\begin{cases} \rho^3 - a_1\rho = b_2\rho^2\sin(\rho\tau) + b_1\rho\cos(\rho\tau), \\ a_2\rho^2 - a_0 = b_1\rho\sin(\rho\tau) - b_2\rho^2\cos(\rho\tau), \end{cases} \tag{9}$$

which leads to

$$\rho^6 + \left(a_2^2 - b_2^2 - 2a_1\right)\rho^4 + \left(a_1^2 - 2a_0 a_2 - b_1^2\right)\rho^2 + a_0^2 = 0. \tag{10}$$

Let $s = \rho^2$ and let us denote $p = a_2^2 - b_2^2 - 2a_1, q = a_1^2 - 2a_0 a_2 - b_1^2$, and $r = a_0^2$; then, equation (10) becomes

$$s^3 + ps^2 + qs + r = 0. \tag{11}$$

Let

$$h(s) = s^3 + ps^2 + qs + r. \tag{12}$$

From equation (11), we have

$$h'(s) = 3s^2 + 2ps + q. \tag{13}$$

Denote $\Delta = p^2 - 3q$. When $\Delta > 0$ and $r > 0$, we can solve for two real roots of equation $h'(s) = 0$ as follows:

$$s_1^* = \frac{-p + \sqrt{\Delta}}{3},$$

$$s_2^* = \frac{-p - \sqrt{\Delta}}{3}. \tag{14}$$

Noticing that $r = a_0^2 > 0$ and $\lim_{s \longrightarrow +\infty} h(s) = +\infty$, we can get results similar to [9].

Lemma 1. *The following results hold:*

(1) Equation (11) does not have positive real roots if $\Delta = p^2 - 3q \leq 0$

(a)

(b)
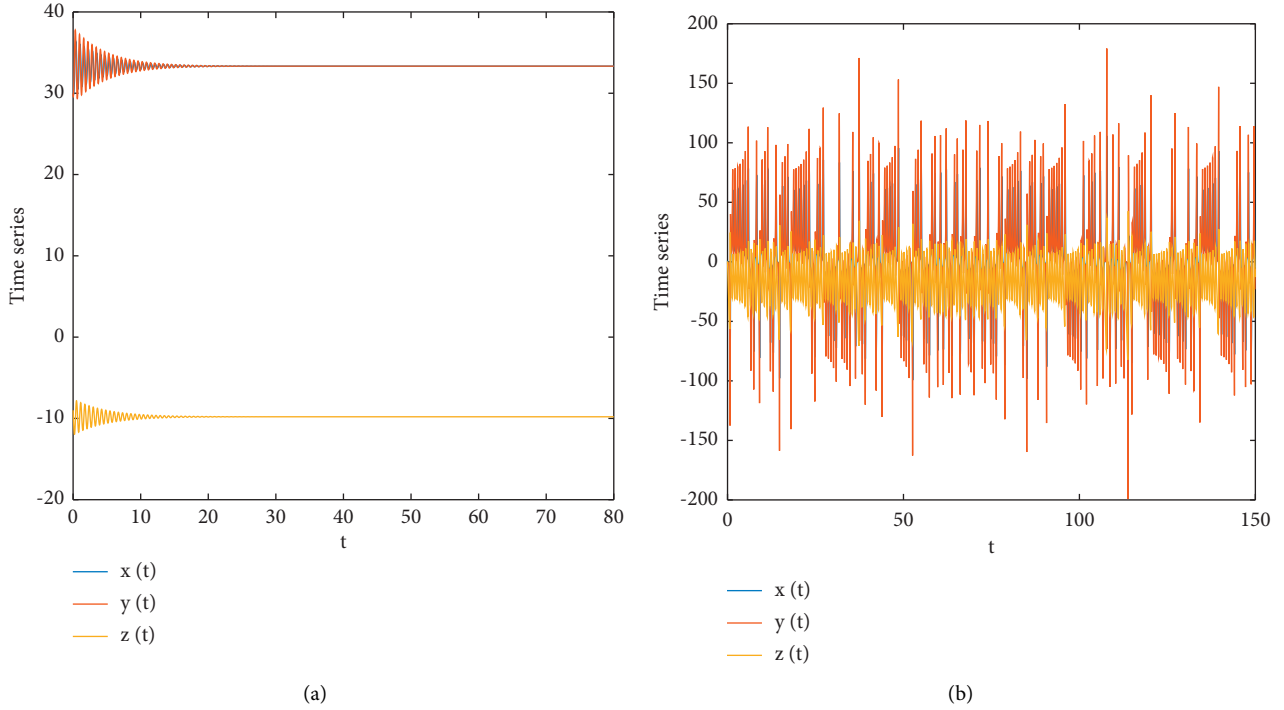
Figure 1: For parameter values $(a, b, c, k, k_1, k_2) = (10, 100, 9.8, 0, 0.08, 0.01)$, system (1) without delay has two stable equilibria: (a) system (1) without delay tends to stable equilibrium when IC = $(30, 30, -9)$; (b) system (1) without delay has a chaotic attractor when IC = $(0.98, -1.82, 0.01)$.

(2) Otherwise, if and only if $s_1^* = (-p + \sqrt{\Delta})/3 > 0$ and $h(s_1^*) \leq 0$, equation (11) has positive roots

From the second point of Lemma 1, we can make an assumption to obtain the two positive roots of equation (11), and when $s_1 < s_2$, then $h'(s_1) < 0$ and $h'(s_2) > 0$:

$$\Delta = p^2 - 3q > 0,$$

$$s_1^* = \frac{-p + \sqrt{\Delta}}{3} > 0, \tag{15}$$

$$h(s_1^*) < 0.$$

Substituting $\rho_k = \sqrt{k} (k = 1, 2)$ into equation (9), we have

$$\tau_k^j = \begin{cases} \dfrac{1}{\rho_k} [\arccos(P) + 2j\pi], & Q \geq 0, \\[2mm] \dfrac{1}{\rho_k} [2\pi - \arccos(P) + 2j\pi], & Q < 0, \end{cases} \tag{16}$$

where

$$P = \frac{b_1 \rho_k^2 - a_1 b_1 + a_0 b_2 - a_2 b_2 \rho_k^2}{b_2^2 \rho_k^2 + b_1^2},$$

$$Q = \frac{b_2 \rho_k^4 - a_1 b_2 \rho_k^2 + a_2 b_1 \rho_k^2 - a_0 b_1}{\rho_k (b_2^2 \rho_k^2 + b_1^2)}, \tag{17}$$

and $j = 0, 1, \ldots$. The following lemma comes naturally.

Lemma 2. *If Lemma 2 holds, when $\tau = \tau_k^j (k = 1, 2; j = 0, 1, 2, \ldots)$, the root of a system (7) consists of a number of pure imaginary roots and nonzero real parts.*

By substituting $\lambda(\tau)$ into equation (7) and taking the derivative of τ, we can obtain

$$\left[\frac{d(\text{Re}\lambda)}{d\tau}\right]_{\tau = \tau_k^j}^{-1} = \text{Re}\left[\frac{3\lambda^2 + 2a_2\lambda + a_1}{\lambda(b_2\lambda^2 + b_1\lambda)e^{-\lambda\tau}}\right]_{\tau = \tau_k^j}$$

$$+ \text{Re}\left[\frac{2b_2\lambda + b_1}{\lambda(b_2\lambda^2 + b_1\lambda)}\right]_{\tau = \tau_k^j}$$

$$= \text{Re}\left[\frac{3\lambda^2 + 2a_2\lambda + a_1}{-\rho_k^2(b_1 + ib_2\rho_k)}\left(\cos(\rho_k\tau_k^j) + i\sin(\rho_k\tau_k^j)\right)\right]$$

$$+ \text{Re}\left[\frac{2b_2\lambda + b_1}{-\rho_k^2(b_1 + ib_2\rho_k)}\right]$$

$$= \frac{s_k}{\Lambda}\left[3\rho_k^4 + 2(a_2^2 - b_2^2 - 2a_1)\rho_k^2 + a_1^2 - 2a_0a_2 - b_1^2\right]$$

$$= \frac{s_k}{\Lambda}h'(s_k), \tag{18}$$

where $\Lambda = \rho_k^4(b_1^2 + b_2^2\rho_k^2)$. Since $s_k > 0$, we conclude that $[d(\text{Re}\lambda)/d\tau]_{\tau = \tau_k^j}^{-1}$ and $h'(s_k)$ have the same sign. Note that $h'(s_1) < 0$ and $h'(s_2) > 0$.

Thus, the following crucial lemma can be obtained.

Lemma 3. *If (15) holds, then the transversality condition of Hopf bifurcation holds:* $[d(\mathrm{Re}\lambda)/d\tau]^{-1}_{\tau=\tau_1^j} < 0,\ [d(\mathrm{Re}\lambda)/d\tau]^{-1}_{\tau=\tau_2^j} > 0$, *where* $j = 0, 1, \ldots.$

The results discussed above and the basic conditions for Hopf bifurcation (transversality and nondegradation) are also applicable to differential equations with time delay, and the important theorem in this section holds [33].

Theorem 1. *Suppose that (6) and (15) are satisfied, then system (1) undergoes a Hopf bifurcation at the equilibria $E_{1,2}$ when $\tau = \tau_k^j (k = 1, 2; j = 0, 1, 2, \ldots)$. Moreover, if $\tau_1^0 > \tau_2^0$, then there exists $m \in N$ such that $\tau_2^0 < \tau_1^0 < \tau_2^1 < \tau_1^1 < \cdots < \tau_2^m < \tau_1^m < \tau_2^{m+1} < \tau_2^{m+2} < \tau_1^{m+1}$ and equilibria $E_{1,2}$ of system (1) are asymptotically stable for $\tau \in [0, \tau_2^0) \bigcup (\tau_1^0, \tau_2^1) \bigcup \cdots \bigcup (\tau_1^{m-1}, \tau_2^m) \bigcup (\tau_1^m, \tau_2^{m+1})$ and unstable for $\tau \in [\tau_2^0, \tau_1^0) \bigcup (\tau_2^1, \tau_1^1) \bigcup \cdots \bigcup (\tau_2^m, \tau_1^m) \bigcup (\tau_2^{m+1}, +\infty)$. Furthermore, system (1) undergoes a Hopf bifurcation at the equilibria $E_{1,2}$ when $\tau = \tau_k^j (k = 1, 2; j = 0, 1, \ldots).$*

Remark. Theorem 3 shows that when the delay passes a certain critical value, the chaotic attractor generated by system (1) with only two stable node foci can be transformed into stable and unstable periodic orbits or another chaotic attractor. Thus, the chaos generated by system (1) is controllable.

3. Direction and Stability of Hopf Bifurcation

The Hopf bifurcation theory of the smooth autonomous system has been very advanced [33–35]. In this section, we use bifurcation theory to study Hopf bifurcation of system (1), determine the bifurcation direction and stability, and obtain the corresponding parameter conditions through detailed calculation. Due to the symmetry of the equilibrium point, we only study the Hopf bifurcation of E_1 at $\tau = \tau_k$.

Let $m_1 = x - x_0, m_2 = y - y_0, m_3 = z - z_0, \overline{m_i}(t) = m_i(\tau t)$, and $\tau = \omega + \tau_k$; for convenience, we are dropping the bars. Nonlinear system (1) can be transformed into an FDE in $C \in C([-1, 0], R^3)$ as

$$\dot{m}(t) = L_\omega(m_t) + g(\omega, m_t), \tag{19}$$

where $m(t) = (m_1(t), m_2(t), m_3(t))^T \in R^3$ and $L_\omega: C \longrightarrow R^3$ and $g: R \times C \longrightarrow R$ are given, respectively, by

$$L_\omega(\phi) = (\omega + \tau_k) \begin{pmatrix} -a & a & 0 \\ c & -k-c & -\dfrac{\sqrt{b}}{\sqrt{k_1+k_2}} \\ \dfrac{\sqrt{b}\,k_1}{\sqrt{k_1+k_2}} & \dfrac{\sqrt{b}\,(k_1+2k_2)}{\sqrt{k_1+k_2}} & 0 \end{pmatrix} \begin{pmatrix} \phi_1(0) \\ \phi_2(0) \\ \phi_3(0) \end{pmatrix} + (\omega + \tau_k) \begin{pmatrix} 0 & 0 & 0 \\ 0 & k & 0 \\ 0 & 0 & 0 \end{pmatrix} \begin{pmatrix} \phi_1(-1) \\ \phi_2(-1) \\ \phi_3(-1) \end{pmatrix},$$

$$g(\omega, m_t) = (\omega + \tau_k) \begin{pmatrix} 0 \\ -\phi_1(0)\phi_3(0) \\ k_1\phi_1(0)\phi_2(0) + k_2\phi_2^2(0) \end{pmatrix}. \tag{20}$$

Based on the Reese representation theorem in functional analysis,

$$L_\omega(\phi) = \int_{-1}^{0} d\mu(\varepsilon, \omega)\phi(\varepsilon), \quad \text{for } \phi \in C. \tag{21}$$

where $\mu(\varepsilon, \omega)$ is a bounded variation function in $\varepsilon \in [-1, 0]$ and can be selected as

$$\mu(\varepsilon, \omega) = (\omega + \tau_k) \begin{pmatrix} -a & a & 0 \\ c & -k-c & -\dfrac{\sqrt{b}}{\sqrt{k_1+k_2}} \\ \dfrac{\sqrt{b}\,k_1}{\sqrt{k_1+k_2}} & \dfrac{\sqrt{b}\,(k_1+2k_2)}{\sqrt{k_1+k_2}} & 0 \end{pmatrix} \delta(\varepsilon) - (\omega + \tau_k) \begin{pmatrix} 0 & 0 & 0 \\ 0 & k & 0 \\ 0 & 0 & 0 \end{pmatrix} \delta(\varepsilon + 1), \tag{22}$$

where $\delta(\cdot)$ is a Dirac function.

Let us define $A(\omega)\phi$ and $R(\omega)\phi$ on $\phi \in C([-1,0], R^3)$, and let $m_t(\varepsilon) = m(t+\varepsilon), \varepsilon \in [-1,0]$. Rewrite the system as equation (31):

$$A(\omega)\phi = \begin{cases} \dfrac{d\phi(\varepsilon)}{d\varepsilon}, & \varepsilon \in [-1,0), \\[2mm] \displaystyle\int_{-1}^{0} d\mu(\varepsilon,s)\phi(s), & \varepsilon = 0, \end{cases} \quad (23)$$

and

$$R(\omega)\phi = \begin{cases} 0, & \varepsilon \in [-1,0), \\ g(\omega,\phi), & \varepsilon = 0, \end{cases} \quad (24)$$

$$\dot{m}(t) = A(\omega)m_t + R(\omega)m_t.$$

For $\psi \in C^1([0,1], (R^3)^*)$, we can define $A^*\psi(\theta)$; when $\theta = 0$, $A^*\psi(\theta) = \int_{-1}^{0} d\mu^T(t,0)\psi(-t)$; Otherwise, when $\theta \in (0,1]$, $A^*\psi(\theta) = -d\psi(\theta)/d\theta$ and we get a bilinear inner product

$$\langle \psi, \phi \rangle = \overline{\psi}(0)\phi(0) - \int_{-1}^{0}\int_{\xi=0}^{\varepsilon} \overline{\psi}(\xi-\varepsilon)d\mu(\varepsilon)\phi(\xi)d\xi, \quad (25)$$

where $\mu(\varepsilon) = \mu(\varepsilon,0)$.

According to the properties of matrix eigenvalues, we can get that the eigenvalues of A^* are the same as those of $A(0)$. Therefore, the eigenvalue of $A(0)$ is $\pm i\rho_k\tau_k$. We need to calculate the $i\rho_k\tau_k$ and $-i\rho_k\tau_k$ corresponding to the eigenvectors of $A(0)$ and A^*. Let $A(0)q(\varepsilon) = i\rho_k\tau_k q(\varepsilon)$, i.e., $q(\varepsilon) = e^{i\varepsilon\rho_k\tau_k}(1,\alpha,\beta)^T$, be the eigenvectors of $A(0)$; then, we have

$$\begin{pmatrix} i\rho_k + a & -a & 0 \\[2mm] -c & i\rho_k + k + c - ke^{-i\rho_k\tau_k} & \dfrac{\sqrt{b}}{\sqrt{k_1+k_2}} \\[3mm] -\dfrac{\sqrt{b}\,k_1}{\sqrt{k_1+k_2}} & -\dfrac{\sqrt{b}\,(k_1+2k_2)}{\sqrt{k_1+k_2}} & i\rho_k \end{pmatrix} q(0) = \begin{pmatrix} 0 \\ 0 \\ 0 \end{pmatrix}. \quad (26)$$

Through calculation, there are

$$q(0) = (1,\alpha,\beta)^T$$

$$= \left(1, \frac{a+i\rho_k}{a}, \frac{\sqrt{b}\,(-2ia(k_1+k_2)+(k_1+2k_2)w_k)}{a\sqrt{k_1+k_2}\,w_k}\right)^T. \quad (27)$$

Similarly, we can assume that $q^*(\theta) = e^{i\theta\rho_k\tau_k}D(1,\alpha^*,\beta^*)$ is the eigenvector of A^* corresponding to $-i\rho_k\tau_k$, that is, $A^*q^*(\theta) = -i\rho_k\tau_k q^*(\theta)$, and we have

$$q^*(\theta) = D(1,\alpha^*,\beta^*)e^{i\theta\rho_k\tau_k}$$

$$= D\left(1, \frac{(k_1+k_2)(a-i\rho_k)\rho_k}{-ibk_1 + c(k_1+k_2)\rho_k}, \frac{\sqrt{b(k_1+k_2)}\,(a-i\rho_k)}{bk_1 + ic(k_1+k_2)\rho_k}\right)e^{i\theta\rho_k\tau_k}. \quad (28)$$

By (25), we can replace ψ and ϕ with $q(0)$ and $q^*(\theta)$. At this time, $<q^*(\theta), q(\varepsilon)> = 1$, so we can calculate D, shown as follows:

$$\langle q^*(\theta), q(\varepsilon)\rangle = \overline{D}\left\{1 + \alpha\overline{\alpha^*} + \beta\overline{\beta^*} + k\tau_k\alpha\overline{\alpha^*}e^{-i\rho_k\tau_k}\right\} = 1. \quad (29)$$

Therefore, we can obtain

$$D = \frac{1}{\left\{1 + \alpha\overline{\alpha^*} + \beta\overline{\beta^*} + k\tau_k\alpha\overline{\alpha^*}e^{-i\rho_k\tau_k}\right\}}. \quad (30)$$

The central manifold C_0 must be calculated at $\omega = 0$. We can make m_t the solution of (29) when $\omega = 0$. Define

$$z(t) = \langle q^*, m_t\rangle, G(t,\varepsilon) = m_t(\varepsilon) - 2\mathrm{Re}\{z(t)q(\varepsilon)\}. \quad (31)$$

Then,

$$G(t,\varepsilon) = G(z(t),\overline{z}(t),\varepsilon) = G_{20}(\varepsilon)\frac{z^2}{2} + G_{11}(\varepsilon)z\overline{z}$$
$$+ G_{02}(\varepsilon)\frac{\overline{z}^2}{2} + G_{30}(\varepsilon)\frac{z^3}{6} + \cdots, \quad (32)$$

where z and $\overline{z}$ are the local coordinates for the center manifold C_0 in the directions of q^* and $\overline{q}^*$. Note that since m_t is real, then G is also real, so we only deal with real solutions. For solution $m_t \in C_0$, since $\omega = 0$, we have

$$\dot{z}(t) = i\rho_k\tau_k z + \langle q^*(\varepsilon), f(0, G(z(t), t\overline{z}n(t)), \varepsilon + t2nReq\{z(t)q(\varepsilon)\})\rangle$$
$$= i\rho_k\tau_k z + q^*(0)f(0, G(z(t),\overline{z}(t),0) + 2\mathrm{Re}\{z(t)q(0)\}). \quad (33)$$

Let $g(0, G(z(t),\overline{z}(t),0) + 2\mathrm{Re}\{z(t)q(0)\}) = g_0(z,\overline{z})$; then,

$$\dot{z}(t) = i\rho_k\tau_k z + q^*(0)g_0(z,\overline{z}). \quad (34)$$

Now, we consider

$$\dot{z}(t) = i\rho_k\tau_k z + f(z,\overline{z}), \quad (35)$$

where

$$f(z,\overline{z}) = f_{20}\frac{z^2}{2} + f_{11}z\overline{z} + f_{02}\frac{\overline{z}^2}{2} + f_{21}\frac{z^2\overline{z}}{2} + \cdots. \quad (36)$$

Since $q(\varepsilon) = (1, \alpha, \beta)^T e^{i\varepsilon\rho_k\tau_k}$ and $m_t(\varepsilon) = (m_{1t}(\varepsilon), m_{2t}(\varepsilon), m_{3t}(\varepsilon)) = G(t, \varepsilon) + z(t)q(\varepsilon) + \overline{z}(t)\overline{q}(\varepsilon)$, we have

$$m_{1t}(0) = z + \overline{z} + G_{20}^{(1)}\frac{z^2}{2} + G_{11}^{(1)}z\overline{z} + G_{02}^{(1)}\frac{\overline{z}^2}{2} + \cdots,$$

$$m_{2t}(0) = \alpha z + \overline{\alpha z} + G_{20}^{(2)}\frac{z^2}{2} + G_{11}^{(2)}z\overline{z} + G_{02}^{(2)}\frac{\overline{z}^2}{2} + \cdots, \quad (37)$$

$$m_{3t}(0) = \beta z + \overline{\beta z} + G_{20}^{(3)}\frac{z^2}{2} + G_{11}^{(3)}z\overline{z} + G_{02}^{(3)}\frac{\overline{z}^2}{2} + \cdots.$$

$$f(z, \overline{z}) = q^*(0)g_0(z, \overline{z})$$

$$= \overline{D}\tau_k(1, \alpha^*, \beta^*)\begin{pmatrix} 0 \\ -m_{1t}(0)m_{3t}(0) \\ k_1 m_{1t}(0)m_{2t}(0) + k_2 m_{2t}^2(0) \end{pmatrix}$$

$$= \overline{D}\tau_k\Bigg[-\alpha^*\left(z + \overline{z} + G_{20}^{(1)}\frac{z^2}{2} + G_{11}^{(1)}z\overline{z} + G_{02}^{(1)}\frac{\overline{z}^2}{2} + \cdots\right)\left(\beta z + \overline{\beta z} + G_{20}^{(3)}\frac{z^2}{2} + G_{11}^{(3)}z\overline{z} + G_{02}^{(3)}\frac{\overline{z}^2}{2} + \cdots\right) \quad (38)$$

$$+ k_1\beta^*\left(z + \overline{z} + G_{20}^{(1)}\frac{z^2}{2} + G_{11}^{(1)}z\overline{z} + G_{02}^{(1)}\frac{\overline{z}^2}{2} + \cdots\right)\left(\alpha z + \overline{\alpha z} + G_{20}^{(2)}\frac{z^2}{2} + G_{11}^{(2)}z\overline{z} + G_{02}^{(2)}\frac{\overline{z}^2}{2} + \cdots\right)$$

$$+ k_2\beta^*\left(\alpha z + \overline{\alpha z} + G_{20}^{(2)}\frac{z^2}{2} + G_{11}^{(2)}z\overline{z} + G_{02}^{(2)}\frac{\overline{z}^2}{2} + \cdots\right)^2\Bigg].$$

Comparing the coefficients with (36), we have

$$f_{20} = 2\overline{D}\tau_k\left(k_1\alpha\overline{\beta^*} - \beta\overline{\alpha^*} + k_2\alpha^2\beta^*\right),$$

$$f_{11} = \overline{D}\tau_k\left(2k_1\beta^*\mathrm{Re}\{\alpha\} - 2\overline{\alpha^*}\mathrm{Re}\{\beta\} + 2k_2\beta^*\alpha\overline{\alpha}\right),$$

$$f_{02} = 2\overline{D}\tau_k\left(k_1\overline{\beta^*}\alpha - \overline{\alpha^*}\beta + k_2\overline{\alpha}^2\right),$$

$$f_{21} = -\overline{D}\tau_k\alpha^*\left[2G_{11}^{(3)}(0) + G_{20}^{(3)}(0) + 2\beta G_{11}^{(1)}(0) + \overline{\beta}G_{20}^{(1)}(0)\right]$$
$$+ k_1\overline{D}\tau_k\beta^*\left[2G_{11}^{(2)}(0) + G_{20}^{(2)}(0) + 2\alpha G_{11}^{(1)}(0) + \overline{\alpha}G_{20}^{(1)}(0)\right]$$
$$+ 2k_2\overline{D}\tau_k\beta^*\left[\overline{\alpha}G_{20}^{(2)}(0) + 2\alpha G_{11}^{(2)}(0)\right].$$

$$(39)$$

Then, we need to compute $G_{20}(\varepsilon)$ and $G_{11}(\varepsilon)$. From (24) and (31), we have

$$\dot{G} = \dot{m}_t - \dot{z}q - \dot{\overline{z}}\,\overline{q} = \begin{cases} A(0)G - 2\mathrm{Re}\{\overline{q^*}(0)g_0q(\varepsilon)\}, \varepsilon \in [-1, 0) \\ A(0)G - 2\mathrm{Re}\{\overline{q^*}(0)g_0q(\varepsilon)\} + g_0, \varepsilon = 0. \end{cases}$$

$$(40)$$

Let

From (36), we have

$$M(z, \overline{z}, \varepsilon) = \begin{cases} 2\mathrm{Re}\{\overline{q^*}(0)g_0q(\varepsilon)\}, & \varepsilon \in [-1, 0) \\ 2\mathrm{Re}\{\overline{q^*}(0)g_0q(\varepsilon)\} + g_0, & \varepsilon = 0. \end{cases} \quad (41)$$

We can rewrite (40) as

$$\dot{G} = A(0)G + M(z, \overline{z}, \varepsilon), \quad (42)$$

where

$$M(z, \overline{z}, \varepsilon) = M_{20}(\varepsilon)\frac{z^2}{2} + M_{11}(\varepsilon)z\overline{z} + M_{02}(\varepsilon)\frac{\overline{z}^2}{2} + \cdots.$$

$$(43)$$

According to the definition of (40) and (43) and G, using the series expansion and comparison of coefficients, we have

$$(A(0) - 2i\rho_k\tau_k)G_{20}(\varepsilon) = -M_{20}(\varepsilon), A(0)G_{11}(\varepsilon) = -M_{11}(\varepsilon), \ldots.$$

$$(44)$$

From (40), we know that for $\varepsilon \in [-1, 0)$,

$$M(z, \overline{z}, \varepsilon) = -\overline{q^*}(0)g_0q(\varepsilon) - q^*(0)\overline{g_0}\overline{q}(\varepsilon)$$
$$= -f(z, \overline{z})q(\varepsilon) - \overline{f}(z, \overline{z})\overline{q}(\varepsilon). \quad (45)$$

Comparing the coefficients of equation (45) with those of equation (43), we have

$$M_{20}(\varepsilon) = -f_{20}q(\varepsilon) - \overline{f}_{02}\overline{q}(\varepsilon),$$
$$M_{11}(\varepsilon) = -f_{11}q(\varepsilon) - \overline{f}_{11}\overline{q}(\varepsilon). \tag{46}$$

Therefore, the following equation can be obtained:

$$\dot{G}_{20} = 2i\rho_k\tau_k G_{20}(\varepsilon) + f_{20}q(\varepsilon) + \overline{f}_{02}\overline{q}(\varepsilon). \tag{47}$$

From $q(\varepsilon) = (1, \alpha, \beta)^T e^{i\varepsilon\omega_k\tau_k}$, we can calculate the solution of the previous equation:

$$G_{20}(\varepsilon) = \frac{if_{20}}{\rho_k\tau_k}q(0)e^{i\varepsilon\rho_k\tau_k} + \frac{i\overline{f}_{02}}{3\rho_k\tau_k}\overline{q}(0)e^{-i\varepsilon\rho_k\tau_k} + W_1 e^{2i\varepsilon\rho_k\tau_k} \tag{48}$$

and, similarly,

$$G_{11}(\varepsilon) = \frac{if_{11}}{\rho_k\tau_k}q(0)e^{i\varepsilon\rho_k\tau_k} + \frac{i\overline{f}_{11}}{\rho_k\tau_k}\overline{q}(0)e^{-i\varepsilon\rho_k\tau_k} + W_2, \tag{49}$$

where $W_1 = (W_1^{(1)}, W_1^{(2)}, W_1^{(3)})^T \in R^3$ and $W_2 = (W_2^{(1)}, W_2^{(2)}, W_2^{(3)})^T \in R^3$ are the constant vectors corresponding to the initial conditions.

We find the values of W_1 and W_2 now. For (44), we have

$$\dot{G}_{20}(\varepsilon) = \int_{-1}^0 d\mu(\varepsilon)G_{20}(\varepsilon) = 2i\varepsilon\rho_k\tau_k G_{20}(0) - M_{20}(0) \tag{50}$$

and

$$\dot{G}_{11}(\varepsilon) = \int_{-1}^0 d\mu(\varepsilon)G_{11}(\varepsilon) = -M_{11}(0), \tag{51}$$

where $\mu(\varepsilon) = \mu(\varepsilon, 0)$. From equation (40), we have

$$M_{20}(0) = -f_{20}q(0) - \overline{f}_{02}\overline{q}(0) + 2\tau_k(0, -\beta, k_1\alpha + k_2\alpha^2)^T \tag{52}$$

and

$$M_{11}(0) = -f_{11}q(0) - \overline{f}_{11}\overline{q}(0) + 2\tau_k(0, -\mathrm{Re}\{\beta\}, k_1\mathrm{Re}\{\alpha\} + k_2\alpha\overline{\alpha})^T. \tag{53}$$

The eigenvector corresponding to eigenvalue $i\rho_k\tau_k$ by $A(0)$ is $q(0)$. We obtain

$$\left(i\rho_k\tau_k - \int_{-1}^0 e^{i\varepsilon\rho_k\tau_k}d\mu(f)\right)q(0)$$
$$= 0, \left(-i\rho_k\tau_k - \int_{-1}^0 e^{-i\varepsilon\rho_k\tau_k}d\mu(f)\right)\overline{q}(0) = 0. \tag{54}$$

Substituting equations (48) and (52) into equation (50), we obtain

$$\left(2i\rho_k\tau_k I - \int_{-1}^0 e^{2i\varepsilon\rho_k\tau_k}d\mu(f)\right)E_1 = 2\tau_k(0, -\beta, k_1\alpha + k_2\alpha^2)^T. \tag{55}$$

That is,

$$\begin{pmatrix} 2i\rho_k + a & -a & 0 \\[2mm] -c & 2i\rho_k + k + c - ke^{-i\rho_k\tau_k} & \dfrac{\sqrt{b}}{\sqrt{k_1 + k_2}} \\[3mm] -\dfrac{\sqrt{b}\,k_1}{\sqrt{k_1 + k_2}} & -\dfrac{\sqrt{b}\,(k_1 + 2k_2)}{\sqrt{k_1 + k_2}} & 2i\rho_k \end{pmatrix} E_1$$
$$= 2\begin{pmatrix} 0 \\ -\beta \\ k_1\alpha + k_2\alpha^2 \end{pmatrix}. \tag{56}$$

It follows that

$$W_1^{(1)} = \frac{\Delta_{11}}{\Delta_1},$$
$$W_1^{(2)} = \frac{\Delta_{12}}{\Delta_1}, \tag{57}$$
$$W_1^{(3)} = \frac{\Delta_{13}}{\Delta_1},$$

where

$$\Delta_{11} = 2 \begin{vmatrix} 0 & -a & 0 \\ -\beta & 2i\rho_k + k + c - ke^{-i\rho_k\tau_k} & \dfrac{\sqrt{b}}{\sqrt{k_1 + k_2}} \\ k_1\alpha + k_2\alpha^2 & -\dfrac{\sqrt{b}\,(k_1 + 2k_2)}{\sqrt{k_1 + k_2}} & 2i\rho_k \end{vmatrix},$$

$$\Delta_{12} = 2 \begin{vmatrix} 2i\rho_k + a & 0 & 0 \\ -c & -\beta & \dfrac{\sqrt{b}}{\sqrt{k_1 + k_2}} \\ -\dfrac{\sqrt{b}\,k_1}{\sqrt{k_1 + k_2}} & k_1\alpha + k_2\alpha^2 & 2i\rho_k \end{vmatrix},$$

$$\Delta_{13} = 2 \begin{vmatrix} 2i\rho_k + a & -a & 0 \\ -c & 2i\rho_k + k + c - ke^{-i\rho_k\tau_k} & -\beta \\ -\dfrac{\sqrt{b}\,k_1}{\sqrt{k_1 + k_2}} & -\dfrac{\sqrt{b}\,(k_1 + 2k_2)}{\sqrt{k_1 + k_2}} & k_1\alpha + k_2\alpha^2 \end{vmatrix},$$

$$\Delta_1 = \begin{vmatrix} 2i\rho_k + a & -a & 0 \\ -c & 2i\rho_k + k + c - ke^{-i\rho_k\tau_k} & \dfrac{\sqrt{b}}{\sqrt{k_1 + k_2}} \\ -\dfrac{\sqrt{b}\,k_1}{\sqrt{k_1 + k_2}} & -\dfrac{\sqrt{b}\,(k_1 + 2k_2)}{\sqrt{k_1 + k_2}} & 2i\rho_k \end{vmatrix}. \tag{58}$$

Similarly, substituting equations (49) and (53) into equation (51), we have

$$\begin{pmatrix} a & -a & 0 \\ -c & c & \dfrac{\sqrt{b}}{\sqrt{k_1 + k_2}} \\ -\dfrac{\sqrt{b}\,k_1}{\sqrt{k_1 + k_2}} & -\dfrac{\sqrt{b}\,(k_1 + 2k_2)}{\sqrt{k_1 + k_2}} & 0 \end{pmatrix} E_2$$

$$= 2 \begin{pmatrix} 0 \\ -\mathrm{Re}\{\beta\} \\ k_1\mathrm{Re}\{\alpha\} + k_2\alpha\overline{\alpha} \end{pmatrix}. \tag{59}$$

It follows that

$$W_2^{(1)} = \frac{\Delta_{21}}{\Delta_2},$$

$$W_2^{(2)} = \frac{\Delta_{22}}{\Delta_2}, \tag{60}$$

$$W_2^{(3)} = \frac{\Delta_{23}}{\Delta_2},$$

where

$$\Delta_{21} = 2 \begin{vmatrix} 0 & -a & 0 \\ -\mathrm{Re}\{\beta\} & c & \dfrac{\sqrt{b}}{\sqrt{k_1 + k_2}} \\ k_1\mathrm{Re}\{\alpha\} + k_2\alpha\overline{\alpha} & -\dfrac{\sqrt{b}\,(k_1 + 2k_2)}{\sqrt{k_1 + k_2}} & 0 \end{vmatrix},$$

$$\Delta_{22} = 2 \begin{vmatrix} a & 0 & 0 \\ -c & -\mathrm{Re}\{\beta\} & \dfrac{\sqrt{b}}{\sqrt{k_1 + k_2}} \\ -\dfrac{\sqrt{b}\,k_1}{\sqrt{k_1 + k_2}} & k_1\mathrm{Re}\{\alpha\} + k_2\alpha\overline{\alpha} & 0 \end{vmatrix},$$

$$\Delta_{23} = 2 \begin{vmatrix} a & -a & 0 \\ -c & c & -\mathrm{Re}\{\beta\} \\ -\dfrac{\sqrt{b}\,k_1}{\sqrt{k_1 + k_2}} & -\dfrac{\sqrt{b}\,(k_1 + 2k_2)}{\sqrt{k_1 + k_2}} & k_1\mathrm{Re}\{\alpha\} + k_2\alpha\overline{\alpha} \end{vmatrix},$$

$$\Delta_2 = \begin{vmatrix} a & -a & 0 \\ -c & c & \dfrac{\sqrt{b}}{\sqrt{k_1 + k_2}} \\ -\dfrac{\sqrt{b}\,k_1}{\sqrt{k_1 + k_2}} & -\dfrac{\sqrt{b}\,(k_1 + 2k_2)}{\sqrt{k_1 + k_2}} & 0 \end{vmatrix}. \tag{61}$$

We can determine $G_{20}(0)$ and $G_{11}(0)$, and therefore, all f_{ij} can be determined by (39).

In summary, the properties of Hopf bifurcation are determined by the following parameters: ω_2 determines the direction of Hopf bifurcation, β_2 determines the stability of bifurcation periodic solutions, and T_2 determines the period of bifurcation periodic solutions, and the specific values are shown as follows. The main theories and methods are from [34, 35]:

FIGURE 2: For system (1) with parameter values $(a, b, c, k, k_1, k_2) = (10, 100, 9.8, -0.5, 0.08, 0.01)$ and initial values $(30, 30, -9)$ when $\tau = 0.16$, the equilibrium E_1 is asymptotically stable.
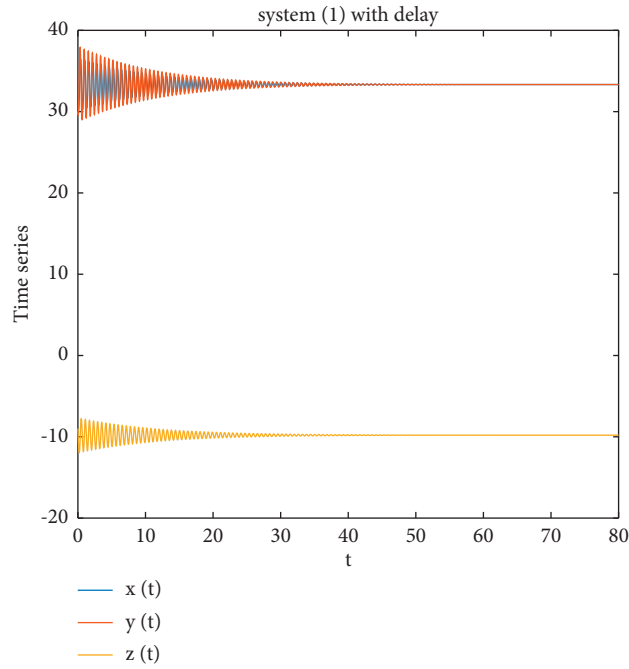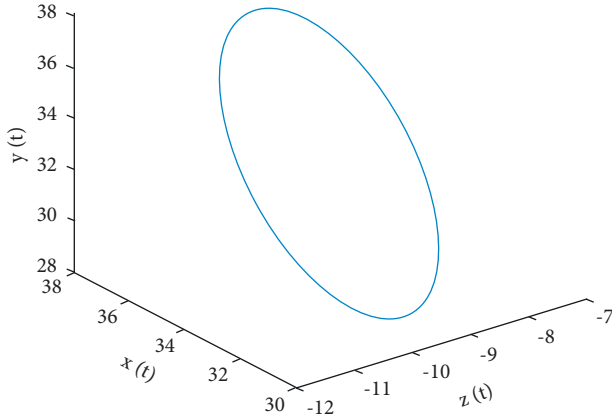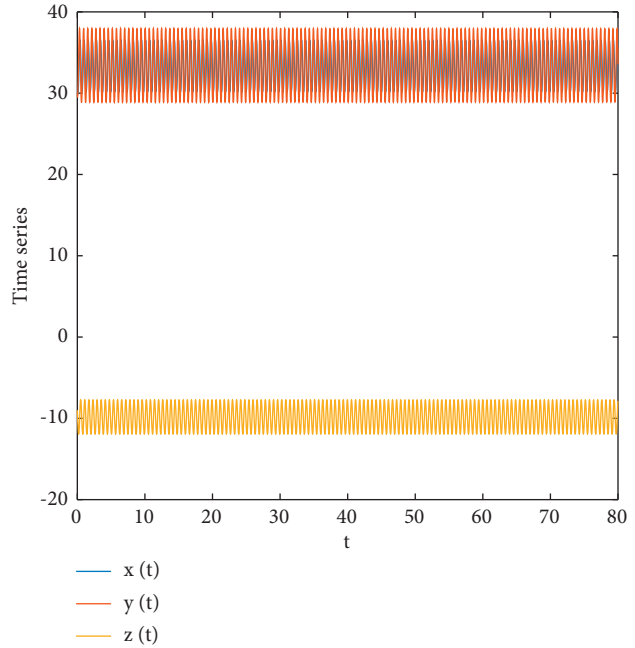

(a)

(b)

FIGURE 3: A bifurcation diagram for system (1) with parameter values $(a, b, c, k, k_1, k_2) = (10, 100, 9.8, -0.5, 0.08, 0.01)$ and initial values $(30, 30, -9)$ when $\tau = 0.2095 < \tau_2^0$ is close to τ_2^0: (a) phase portrait; (b) time series of $z(t)$.
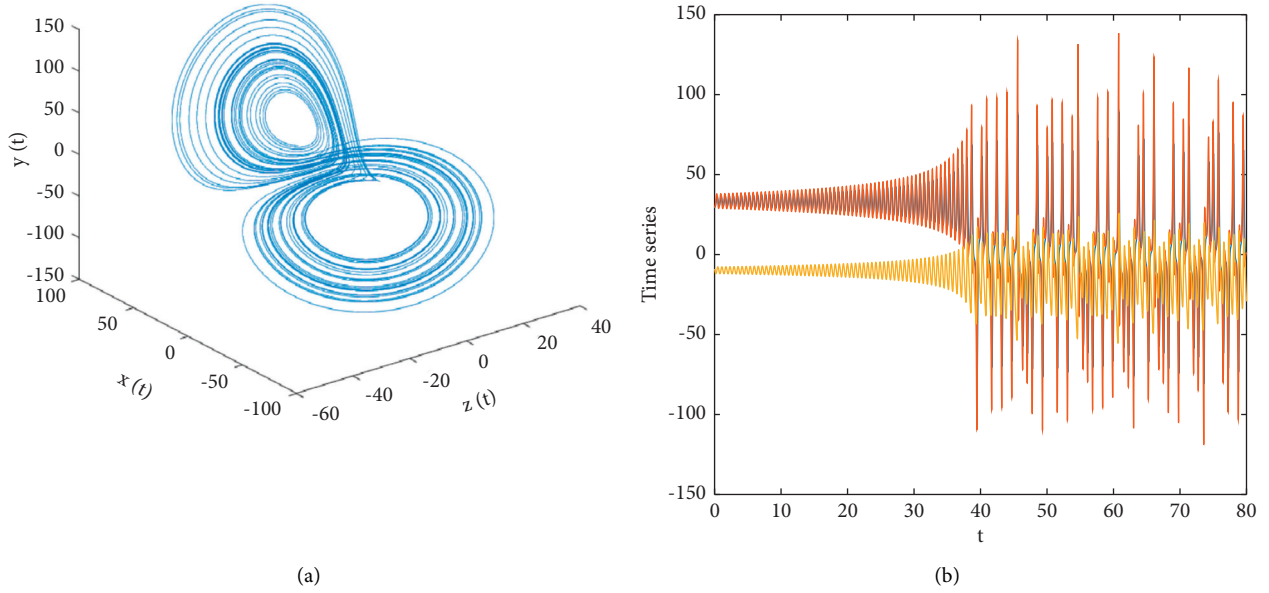
(a)

(b)

Figure 4: When τ is closer to τ_2^0, $\tau = 0.23 > \tau_2^0$ is taken and system (1) is chaotic at the initial values $(30, 30, -9)$: (a) the chaotic attractor of system (1); (b) the time series of $z(t)$.

$$C_1(0) = \frac{i}{2\rho_k \tau_k}\left(f_{20}f_{11} - 2|f_{11}|^2 - \frac{1}{3}|f_{02}|^2\right) + \frac{f_{21}}{2},$$

$$\omega_2 = -\frac{\mathrm{Re}\{C_1(0)\}}{\mathrm{Re}\{d\lambda(\tau_k)/d\tau\}},$$

$$T_2 = -\frac{\mathrm{Im}C_1(0) + \omega_2\mathrm{Im}\{d\lambda(\tau_k)/d\tau\}}{\rho_k \tau_k},$$

$$\beta_2 = 2\mathrm{Re}\{C_1(0)\}.$$

(62)

Therefore, the following main results are obtained in this section.

Theorem 2. *In equation (62), when $\tau > \tau_k$ or $\tau < \tau_k$, system (1) has Hopf bifurcations with the following properties: if $\omega_2 > 0 \, (\omega_2 < 0)$, the Hopf bifurcation is supercritical (subcritical); if $\beta_2 < 0 \, (\beta_2 > 0)$, the orbit is stable (unstable); if $T_2 > 0 \, (T_2 < 0)$, then the period increases (decreases).*

4. Numerical Results

In the previous two sections, we have proved the parameter conditions for Hopf bifurcation in system (1) and analyzed the bifurcation direction and bifurcation stability. In this section, we select appropriate parameters and use the MATLAB toolkit for numerical simulation to verify our theoretical analysis. When the parameter values are $a = 10, c = 9.8$, and $b = 100$, the two equilibria are $E_1(100/3, 100/3, -9.8)$ and $E_2(-100/3, -100/3, -9.8)$.

$$\begin{cases} \dot{x} = 10(y - x), \\ \dot{y} = -9.8y - xz + k[y(t - \tau) - y], \\ \dot{z} = -100 + xy. \end{cases}$$

(63)

Through the previous analysis and numerical simulation from the finite difference method (FDM), as shown in Figure 1, the equilibrium points $E_{1,2}$ of system (63) are asymptotically stable when $\tau = 0$ and a chaotic attractor appears. If we choose the parameter $k = -0.5$, we can get that equation (10) has two positive roots $\rho_1 = 10.0521$ and $\rho_2 = 10.3648$. Therefore, there are, respectively,

$$\begin{aligned} \tau_1^j &= 0.467983 + 0.625063j, \\ \tau_2^j &= 0.211299 + 0.606205j, \end{aligned}$$

(64)

where $j = 0, 1, 2, \ldots$. From formula (62), it follows that $\tau_2^0 = 0.211299$, $C_1(0) = 0.000588642 + 0.000658409i$, $\omega_2 = -0.000362443$, $T_2 = -0.000204142$, and $\beta_2 = 0.00117728$. Therefore, as shown by computer simulation, when $0 < \tau < \tau_2^0$, the equilibria $E_{1,2}$ are stable (see Figure 2). E_1 loses its stability and Hopf bifurcation occurs as τ crosses the critical value τ_2^0. According to the properties of Hopf bifurcation, Hopf bifurcation is subcritical and the bifurcation direction is $\tau < \tau_2^0$, when $\omega_2 < 0$ and $\beta_2 > 0$. At this time, an unstable bifurcation periodic solution appears, as shown in Figures 3(a) and 3(b).

Otherwise, as shown in Figures 4(a) and 4(b), numerical simulation shows that when τ reaches the region $\tau > \tau_2^0$, Hopf bifurcation periodic solution disappears and chaos occurs.

5. Conclusion

In previous studies, few scholars have analyzed the time-delay feedback chaotic system with two stable node foci coexisting. In this paper, a unified chaotic system control model is established by using the delay feedback control law. The corresponding parameter range is obtained according to the conditions of Hopf bifurcation. Central manifold theory and normal form method are the most classical methods to

study the properties of Hopf bifurcation. This paper also uses this method to study the direction of Hopf bifurcation and the stability of bifurcation periodic solution of system (1). Theoretical results and numerical simulation show that chaos can be controlled using a delay system (1). Numerical simulation shows that the periodic solution is transformed into a chaotic attractor with further increase in delay. It is worth noting that the results obtained in this paper are of great significance for controlling chaos in systems with only two stable node foci. The dynamic behavior of the new system is still rich and complex, and its topology needs to be thoroughly studied and developed. In future studies, we will provide more credible theoretical analysis and data results.

Data Availability

The data that support the findings of this study are included within the article.

Conflicts of Interest

The authors declare that there are no conflicts of interest regarding the publication of this paper.

Acknowledgments

References

[1] E. N. Lorenz, "Deterministic nonperiodic flow," *Journal of the Atmospheric Sciences*, vol. 20, no. 2, pp. 130–141, 1963.

[2] J. C. Sprott, "Some simple chaotic flows," *Physical Review. E, Statistical Physics, Plasmas, Fluids, and Related Interdisciplinary Topics*, vol. 50, pp. R647–R650, 1994.

[3] J. C. Sprott, "A new class of chaotic circuit," *Physics Letters A*, vol. 266, no. 1, pp. 19–23, 2000.

[4] J. C. Sprott, "Simplest dissipative chaotic flow," *Physics Letters A*, vol. 228, no. 4-5, pp. 271–274, 1997.

[5] G. R. Chen G and T. Ueta, "Yet another chaotic attractor," *International Journal of Bifurcation and Chaos*, vol. 09, no. 7, pp. 1465-1466, 1999.

[6] G. van der Schrier and L. R. M. Maas, "The diffusionless Lorenz equations; Shil'nikov bifurcations and reduction to an explicit map," *Physica D: Nonlinear Phenomena*, vol. 141, no. 1-2, pp. 19–36, 2000.

[7] Q. Yang and G. Chen, "A chaotic system with one saddle and two stable node-foci," *International Journal of Bifurcation and Chaos*, vol. 18, no. 5, pp. 1393–1414, 2008.

[8] C. Sparrow, *The Lorenz Equations: Bifurcation, Chaos, and Strange Attractor*, Springer-Verlag, New York, NY, USA, 1982.

[9] T. Zhou, Y. Tang, and G. Chen, "Complex dynamical behaviors of the chaotic chen's system," *International Journal of Bifurcation and Chaos*, vol. 13, no. 9, pp. 2561–2574, 2003.

[10] Q. Yang, G. Chen, and T. Zhou, "A unified Lorenz-type system and its canonical form," *International Journal of Bifurcation and Chaos*, vol. 16, no. 10, pp. 2855–2871, 2006.

[11] H. Kokubu and R. Roussarie, "Existence of a singularly degenerate heteroclinic cycle in the lorenz system and its dynamical consequences: Part I," *Journal of Dynamics and Differential Equations*, vol. 16, no. 2, pp. 513–557, 2004.

[12] M. Messias, "Dynamics at infinity and the existence of singularly degenerate heteroclinic cycles in the Lorenz system," *Journal of Physics A: Mathematical and Theoretical*, vol. 42, no. 11, Article ID 115101, 2009.

[13] L. F. Mello and S. F. Coelho, "Degenerate Hopf bifurcations in the Lü system," *Physics Letters A*, vol. 373, no. 12-13, pp. 1116–1120, 2009.

[14] J. Li and J. Zhang, "New treatment on bifurcations of periodic solutions and homoclinic orbits at high r in the lorenz equations," *SIAM Journal on Applied Mathematics*, vol. 53, no. 4, pp. 1059–1071, 1993.

[15] D. Huang, "Periodic orbits and homoclinic orbits of the diffusionless Lorenz equations," *Physics Letters A*, vol. 309, no. 3-4, pp. 248–253, 2003.

[16] Z. Wei and Q. Yang, "Controlling the diffusionless Lorenz equations with periodic parametric perturbation," *Computers and Mathematics with Applications*, vol. 58, no. 10, pp. 1979–1987, 2009.

[17] I. Pehlivan and Y. Uyaroglu, "A new chaotic attractor from general lorenz system family and its electronic experimental implementation," *Turkish Journal of Electrical Engineering and Computer Sciences*, vol. 18, pp. 171–184, 2010.

[18] Z. Wang, "Existence of attractor and control of a 3D differential system," *Nonlinear Dynamics*, vol. 60, no. 3, pp. 369–373, 2009.

[19] Z. Wei, B. Zhu, J. Yang, M. Perc, and M. Slavinec, "Bifurcation analysis of two disc dynamos with viscous friction and multiple time delays," *Applied Mathematics and Computation*, vol. 347, pp. 265–281, 2019.

[20] Q. Yang, Z. Wei, and G. Chen, "An unusual 3D autonomous quadratic chaotic system with two stable node-foci," *International Journal of Bifurcation and Chaos*, vol. 20, no. 04, pp. 1061–1083, 2010.

[21] Z. Wei and Q. Yang, "Dynamical analysis of a new autonomous 3-D chaotic system only with stable equilibria," *Nonlinear Analysis: Real World Applications*, vol. 12, no. 1, pp. 106–118, 2011.

[22] Z. Wei and Q. Yang, "Anti-control of Hopf bifurcation in the new chaotic system with two stable node-foci," *Applied Mathematics and Computation*, vol. 217, no. 1, pp. 422–429, 2010.

[23] Z. C. Wei, W. Zhang, I. Moroz, and N. V. Kuznetsov, "Codimension one and two bifurcations in Cattaneo Christov heat-flux model," *Discrete and Continuous Dynamical Systems—Series B*, vol. 26, no. 10, pp. 5305–5319, 2021.

[24] Z. Wang, F. Parastesh, K. Rajagopal, I. I. Hamarash, and I. Hussain, "Delay-induced synchronization in two coupled chaotic memristive Hopfield neural networks," *Chaos, Solitons & Fractals*, vol. 134, Article ID 109702, 2020.

[25] G. A. Leonov, N. V. Kuznetsov, and T. N. Mokaev, "Hidden attractor and homoclinic orbit in Lorenz-like system describing convective fluid motion in rotating cavity," *Communications in Nonlinear Science and Numerical Simulation*, vol. 28, no. 1-3, pp. 166–174, 2015.

[26] M.-F. Danca and M. Lampart, "Hidden and self-excited attractors in a heterogeneous Cournot oligopoly model," *Chaos, Solitons & Fractals*, vol. 142, Article ID 110371, 2021.

[27] N. Wang, G. Zhang, N. V. Kuznetsov, and H. Bao, "Hidden attractors and multistability in a modified Chua's circuit," *Communications in Nonlinear Science and Numerical Simulation*, vol. 92, Article ID 105494, 2021.

[28] K. Pyragas and A. Tamaševičius, "Experimental control of chaos by delayed self-controlling feedback," *Physics Letters A*, vol. 180, no. 1-2, pp. 99–102, 1993.

[29] Z. Wei, A. Yousefpour, H. Jahanshahi, U. Erkin Kocamaz, and I. Moroz, "Hopf bifurcation and synchronization of a five-dimensional self-exciting homopolar disc dynamo using a new fuzzy disturbance-observer-based terminal sliding mode control," *Journal of the Franklin Institute*, vol. 358, no. 1, pp. 814–833, 2021.

[30] Z. Wang, X. Xi, L. Kong, and Z. Wei, "Infinity dynamics and DDF control for a chaotic system with one stable equilibrium," *The European Physical Journal—Special Topics*, vol. 229, no. 6, pp. 1319–1333, 2020.

[31] Z. Wang, W. Sun, Z. Wei, and S. Zhang, "Dynamics and delayed feedback control for a 3D jerk system with hidden attractor," *Nonlinear Dynamics*, vol. 82, no. 1, pp. 577–588, 2015.

[32] C. Xu, Z. Liu, M. Liao, P. Li, Q. Xiao, and S. Yuan, "Fractional-order bidirectional associate memory (BAM) neural networks with multiple delays: the case of Hopf bifurcation," *Mathematics and Computers in Simulation*, vol. 182, pp. 471–494, 2021.

[33] J. Hale, *Theory of Functional Differential Equations*, Springer, New York, NY, USA, 1977.

[34] B. Hassard, N. Kazarinoff, and Y. Wan, *Theory and Application of Hopf Bifurcation*, Cambridge University Press, Cambridge, UK, 1981.

[35] Y. Song and J. Wei, "Bifurcation analysis for Chen's system with delayed feedback and its application to control of chaos☆," *Chaos, Solitons and Fractals*, vol. 22, no. 1, pp. 75–91, 2004.

WILEY | Hindawi

Research Article

New Properties on Degenerate Bell Polynomials

Taekyun Kim [iD],[1] **Dae San Kim** [iD],[2] **Hyunseok Lee** [iD],[3] **Seongho Park** [iD],[1]
and Jongkyum Kwon [iD][1]

[1]*Department of Mathematics, Kwangwoon University, Seoul 139-701, Republic of Korea*
[2]*Department of Mathematics, Sogang University, Seoul 121-742, Republic of Korea*
[3]*Department of Mathematics Education, Gyeongsang National University, Jinju 52828, Republic of Korea*

Correspondence should be addressed to Jongkyum Kwon; mathkjk26@gnu.ac.kr

The aim of this paper is to study the degenerate Bell numbers and polynomials which are degenerate versions of the Bell numbers and polynomials. We derive some new identities and properties of those numbers and polynomials that are associated with the degenerate Stirling numbers of both kinds.

1. Introduction

The Bell number Bel_n counts the number of partitions of a set with n elements into disjoint nonempty subsets. The Bell polynomials $\text{Bel}_n(x)$, also called Touchard or exponential polynomials, are natural extensions of Bell numbers. The partial and complete Bell polynomials, which are multivariate generalizations of the Bell polynomials, have diverse applications not only in mathematics but also in physics and engineering as well (see [1]).

For instance, the following formula, due to Faà di Bruno formula:

$$\frac{d^n}{dt^n} f \circ g(t) = \sum_{k=0}^{n} f^{(k)}(g(t)) B_{n,k}$$
$$\left(g'(t), g''(t), \ldots, g^{(n-k+1)}(t) \right), \tag{1}$$

gives an explicit formula for higher derivatives of composite functions. Here, the partial Bell polynomials $B_{n,k}(x_1, x_2, \ldots, x_{n-k+1})$ are defined by

$$B_{n,k}(x_1, x_2, \ldots, x_{n-k+1})$$
$$= \sum \frac{n!}{\prod_{l=1}^{n-k+1} i_l! \prod_{l=1}^{n-k+1} \left(\frac{x_l}{l!} \right)^{i_l}}, \quad (n \geq k \geq 0), \tag{2}$$

where the sum runs over all nonnegative integers $i_1, i_2, \ldots, i_{n-k+1}$, satisfying $i_1 + i_2 + \cdots + i_{n-k+1} = k$ and $i_1 + 2i_2 + \cdots (n-k+1)i_{n-k+1} = n$ (see [1], p. 133). Then, the complete Bell polynomials are given by $B_n(x|x_1, \ldots, x_n) = \sum_{k=1}^{n} B_{n,k}(x_1, x_2, \ldots, x_{n-k+1})x^k$, $(n \geq 1)$, and $B_n(x|1, 1, \ldots, 1) = \sum_{k=1}^{n} B_{n,k}(1, 1, \ldots, 1)x^k = \text{Bel}(x)$, $(n \geq 1)$.

As a degenerate version of those Bell polynomials and numbers, the degenerate Bell polynomials $\text{Bel}_{n,\lambda}(x)$ and numbers $\text{Bel}_{n,\lambda}$ (see (17)) are introduced and studied under the different names of the partially degenerate Bell polynomials and numbers in [2]. Some interesting identities for them were obtained in connection with Stirling numbers of the first and second kinds [2]. We hope that we will be able to find many interesting applications of these polynomials and numbers in near future.

In [3], Carlitz initiated the exploration of degenerate Bernoulli and Euler polynomials, which are degenerate versions of the ordinary Bernoulli and Euler polynomials. Along the same line as Carlitz's pioneering work, intensive studies have been done for degenerate versions of quite a few special polynomials and numbers (see [2–10] and the references therein). It is worthwhile to mention that these studies of degenerate versions have been done not only for some special numbers and polynomials but also for transcendental functions like gamma functions (see [8]). The studies have been carried out by various means like combinatorial methods, generating functions, differential equations, umbral calculus techniques, p-adic analysis, and probability theory.

The aim of this paper is to further investigate the degenerate Bell polynomials and numbers by means of generating functions. In more detail, we derive several properties and identities of those numbers and polynomials which include recurrence relations for degenerate Bell polynomials (see Theorems 1, 3, 4, and 8), and expressions for them that can be derived from repeated applications of certain operators to the exponential functions (see Theorem 2, Proposition 1), the derivatives of them (Corollary 1), the antiderivatives of them (see Theorem 6), and some identities involving them (see Theorems 5, 9). For the rest of this section, we recall some necessary facts that are needed throughout this paper.

For any $\lambda \in \mathbb{R}$, the degenerate exponential functions are defined by

$$e_\lambda^x(t) = \sum_{k=0}^\infty \frac{(x)_{k,\lambda}}{k!} t^k, \qquad (3)$$

(see [9]), where

$$(x)_{0,\lambda} = 1, (x)_{n,\lambda} = x(x - \lambda) \cdots (x - (n-1)\lambda), \ (n \geq 1). \qquad (4)$$

When $x = 1$, we see use the notation $e_\lambda(t) = e_\lambda^1(t)$.

In [3], Carlitz introduced the degenerate Bernoulli numbers given by

$$\frac{t}{e_\lambda(t) - 1} = \sum_{n=0}^\infty \beta_{n,\lambda} \frac{t^n}{n!}. \qquad (5)$$

Note that $\lim_{\lambda \to 0} \beta_{n,\lambda} = B_n$, where B_n are the ordinary Bernoulli numbers given by

$$\frac{t}{e^t - 1} = \sum_{n=0}^\infty B_n \frac{t^n}{n!}, \qquad (6)$$

(see [1–14]).

From (5), we deduce that

$$\beta_{0,\lambda} = 1, \ \sum_{l=0}^{n-1} \binom{n}{l} (1)_{n-l,\lambda} \beta_{l,\lambda} = 0, \quad (n \geq 2), \qquad (7)$$

from which we compute the first few values of $\beta_{n,\lambda}$ as follows:

$$\beta_{0,\lambda} = 1, \ \beta_{1,\lambda} = \frac{1}{2}\lambda - \frac{1}{2}, \ \beta_{2,\lambda} = -\frac{1}{6}\lambda^2 + \frac{1}{6},$$

$$\beta_{3,\lambda} = \frac{1}{4}\lambda^3 - \frac{1}{4}\lambda, \ \beta_{4,\lambda} = -\frac{19}{30}\lambda^4 + \frac{2}{3}\lambda^2 - \frac{1}{30},$$

$$\beta_{5,\lambda} = \frac{9}{4}\lambda^5 - \frac{5}{2}\lambda^3 + \frac{1}{4}\lambda, \ \beta_{6,\lambda} = -\frac{863}{84}\lambda^6 + 12\lambda^4 - \frac{7}{4}\lambda^2 + \frac{1}{42},$$

$$\beta_{7,\lambda} = \frac{1375}{24}\lambda^7 - 70\lambda^5 + \frac{105}{8}\lambda^3 - \frac{5}{12}\lambda,$$

$$\beta_{8,\lambda} = -\frac{33953}{90}\lambda^8 + 480\lambda^6 - \frac{1624}{15}\lambda^4 + \frac{50}{9}\lambda^2 - \frac{1}{30}. \qquad (8)$$

It is well known that the Stirling numbers of the first kind are defined by

$$(x)_n = \sum_{k=0}^n S_1(n,k) x^k, \frac{1}{k!} (\log(1+t))^k = \sum_{n=k}^\infty S_1(n,k) \frac{t^n}{n!}, \qquad (9)$$

(see [14]), where $(x)_0 = 1$, $(x)_n = x(x-1) \cdots (x-n+1)$, $(n \geq 1)$.

As the inversion formula of (9), the Stirling numbers of the second kind are given by

$$x^n = \sum_{k=0}^n S_2(n,k)(x)_k, \frac{1}{k!}(e^t - 1)^k = \sum_{n=k}^\infty S_2(n,k) \frac{t^n}{n!}, \qquad (10)$$

(see [14]).

The degenerate Stirling numbers of the first kind are defined by

$$(x)_n = \sum_{k=0}^n S_{1,\lambda}(n,k)(x)_{k,\lambda}, \frac{1}{k!}(\log_\lambda(1+t))^k = \sum_{n=k}^\infty S_{1,\lambda}(n,k) \frac{t^n}{n!}, \qquad (11)$$

(see [5]), and the degenerate Stirling numbers of the second kind are given by

$$(x)_{n,\lambda} = \sum_{k=0}^n S_{2,\lambda}(n,k)(x)_k, \frac{1}{k!}(e_\lambda(t) - 1)^k = \sum_{n=k}^\infty S_{2,\lambda}(n,k) \frac{t^n}{n!}, \qquad (12)$$

(see [5, 7]).

Here, $\log_\lambda(1+t)$ is the degenerate logarithm given by (18).

We also recall the degenerate absolute Stirling numbers of the first kind that are defined by

$$\langle x \rangle_n = \sum_{k=0}^n \begin{bmatrix} n \\ k \end{bmatrix}_\lambda \langle x \rangle_{k,\lambda}, \qquad (13)$$

(see [10]), where

$$\langle x \rangle_0 = 1, \quad \langle x \rangle_n = x(x+1)\cdots(x+n-1), \quad (n \geq 1),$$
$$\langle x \rangle_{0,\lambda} = 1, \quad \langle x \rangle_{n,\lambda} = x(x+\lambda)(x+2\lambda)\cdots(x+(n-1)\lambda),$$
$$(n \geq 1). \tag{14}$$

It is well known that the Bell polynomials are defined by

$$e^{x(e^t-1)} = \sum_{n=0}^{\infty} \mathrm{Bel}_n(x)\frac{t^n}{n!}, \tag{15}$$

(see [12, 13]).

When $x = 1$, $\mathrm{Bel}_n = \mathrm{Bel}_n(1)$ are called the Bell numbers. From (12), we note that

$$\mathrm{Bel}_n(x) = \sum_{k=0}^{n} S_2(n,k)x^k, \tag{16}$$

(see [12, 13]).

In [2], the degenerate Bell polynomials are defined by

$$e^{x(e_\lambda(t)-1)} = \sum_{n=0}^{\infty} \mathrm{Bel}_{n,\lambda}(x)\frac{t^n}{n!}. \tag{17}$$

Note that $\lim_{\lambda \to 0}\mathrm{Bel}_{n,\lambda}(x) = \mathrm{Bel}_n(x)$. For $x = 1$, $\mathrm{Bel}_{n,\lambda} = \mathrm{Bel}_{n,\lambda}(1)$ are called the degenerate Bell numbers.

The compositional inverse of $e_\lambda(t)$ is given by $\log_\lambda(t)$, namely, $e_\lambda(\log_\lambda(t)) = t = \log_\lambda(e_\lambda(t))$, where

$$\log_\lambda(1+t) = \frac{1}{\lambda}\left((1+t)^\lambda - 1\right) = \sum_{n=1}^{\infty} \lambda^{n-1}(1)_{n,\frac{1}{\lambda}}\frac{t^n}{n!}, \tag{18}$$

(see [5]).

Note that $\lim_{\lambda \to 0}\log_\lambda(1+t) = \log(1+t)$.

From (17), we note that

$$\mathrm{Bel}_{n,\lambda}(x) = e^{-x}\sum_{k=0}^{\infty} \frac{(k)_{n,\lambda}}{k!}x^k = \sum_{k=0}^{n} S_{2,\lambda}(n,k)x^k, \tag{19}$$

(see [2]).

From (12), we can deduce the recurrence relation given by

$$S_{2,\lambda}(n+1,k) = S_{2,\lambda}(n,k-1) + (k-n\lambda)S_{2,\lambda}(n,k), \quad (n \geq k \geq 1), \tag{20}$$

and the values

$$S_{2,\lambda}(n,0) = 0, \quad (n \geq 1), \; S_{2,\lambda}(n,n) = 1, \quad (n \geq 0), \tag{21}$$

Now, we compute from (19), (3), and (21) the first few degenerate Bell polynomials as follows:

$$\mathrm{Bel}_{0,\lambda}(x) = 1, \; \mathrm{Bel}_{1,\lambda}(x) = x, \; \mathrm{Bel}_{2,\lambda}(x) = (-x)\lambda + \left(x^2 + x\right),$$
$$\mathrm{Bel}_{3,\lambda}(x) = (2x)\lambda^2 + \left(-3x^2 - 3x\right)\lambda + \left(x^3 + 3x^2 + x\right),$$
$$\mathrm{Bel}_{4,\lambda}(x) = (-6x)\lambda^3 + \left(11x^2 + 12x\right)\lambda^2 + \left(-6x^3 - 18x^2 - 7x\right)\lambda + \left(x^4 + 6x^3 + 7x^2 + x\right),$$
$$\mathrm{Bel}_{5,\lambda}(x) = (24x)\lambda^4 + \left(-50x^2 - 60x\right)\lambda^3 + \left(35x^3 + 110x^2 + 50x\right)\lambda^2 + \left(-10x^4 - 60x^3 - 75x^2 - 15x\right)\lambda$$
$$+ \left(x^5 + 10x^4 + 25x^3 + 15x^2 + x\right),$$
$$\mathrm{Bel}_{6,\lambda}(x) = (-120x)\lambda^5 + \left(274x^2 + 274x\right)\lambda^4 + \left(-225x^3 - 675x^2 - 225x\right)\lambda^3$$
$$+ \left(85x^4 + 510x^3 + 595x^2 + 85x\right)\lambda^2 + \left(-15x^5 - 150x^4 - 375x^3 - 225x^2 - 15x\right)\lambda$$
$$+ \left(x^6 + 15x^5 + 65x^4 + 90x^3 + 31x^2 + x\right),$$
$$\mathrm{Bel}_{7,\lambda}(x) = (720x)\lambda^6 + \left(-1764x^2 - 1764x\right)\lambda^5 + \left(1624x^3 + 4872x^2 + 1624x\right)\lambda^4$$
$$+ \left(-735x^4 - 4410x^3 - 5145x^2 - 735x\right)\lambda^3 + \left(175x^5 + 1750x^4 + 4375x^3 + 2625x^2 + 175x\right)\lambda^2$$
$$+ \left(-21x^6 - 315x^5 - 1365x^4 - 1890x^3 - 651x^2 - 21x\right)\lambda + \left(x^7 + 21x^6 + 140x^5 + 350x^4 + 301x^3 + 63x^2 + x\right),$$
$$\mathrm{Bel}_{8,\lambda}(x) = (-5040x)\lambda^7 + \left(13068x^2 + 13068x\right)\lambda^6 + \left(-13132x^3 - 39396x^2 - 13132x\right)\lambda^5$$
$$+ \left(6769x^4 + 40614x^3 + 47383x^2 + 6769x\right)\lambda^4 + \left(-1960x^5 - 19600x^4 - 49000x^3 - 29400x^2 - 1960x\right)\lambda^3$$
$$+ \left(332x^6 + 4830x^5 + 20930x^4 + 28980x^3 + 9982x^2 + 322x\right)\lambda^2$$
$$+ \left(-28x^7 - 588x^6 - 3920x^5 - 9800x^4 - 8428x^3 - 1764x^2 - 28x\right)\lambda$$
$$+ \left(x^8 + 28x^7 + 266x^6 + 1050x^5 + 1701x^4 + 966x^3 + 127x^2 + x\right). \tag{22}$$
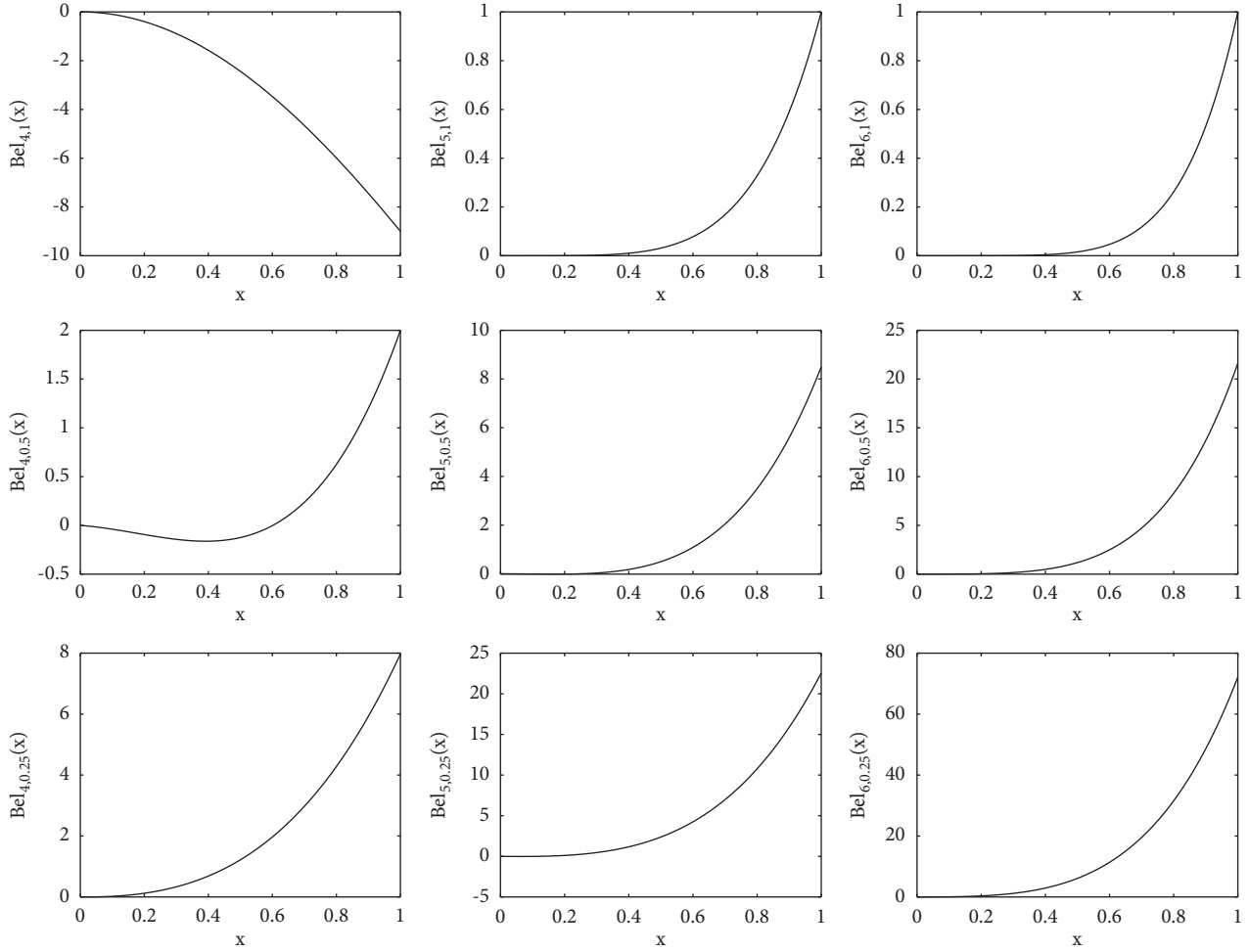
Figure 1: The shapes of Bell polynomials $\mathrm{Bel}_{k,\lambda}(x)$.

In Figure 1, we plot the shapes of Bell polynomial $\mathrm{Bel}_{k,\lambda}(x)$. The upper-left graph looks different from the others. However, of course they all go to infinity as x tends to infinity.

2. Some New Properties on Degenerate Bell Polynomials

Let a be a nonzero constant. First, we observe that

$$
\begin{aligned}
\frac{d^n}{dt^n}e^{a(e_\lambda(t))} &= \frac{d^n}{dt^n}\sum_{k=0}^{\infty}\frac{a^k}{k!}e_\lambda^k(t) = \sum_{k=0}^{\infty}\frac{a^k}{k!}(k)_{n,\lambda}e_\lambda^{k-n\lambda}(t) \\
&= \sum_{k=0}^{\infty}\frac{(k)_{n,\lambda}}{k!}a^k e_\lambda^k(t)\frac{1}{(1+\lambda t)^n} \\
&= \left(\sum_{k=0}^{\infty}\frac{(k)_{n,\lambda}}{k!}(ae_\lambda(t))^k e^{-ae_\lambda(t)}\right)e^{ae_\lambda(t)}\frac{1}{(1+\lambda t)^n} \\
&= \frac{1}{(1+\lambda t)^n}\mathrm{Bel}_{n,\lambda}(ae_\lambda(t))e^{ae_\lambda(t)}.
\end{aligned}
\tag{23}
$$

Therefore, by (23), we obtain the following lemma.

Lemma 1. *For $n \geq 0$, the nth derivative of $e^{a(e_\lambda(t))}$ is given by*

$$
\frac{d^n}{dt^n}e^{a(e_\lambda(t))} = \frac{1}{(1+\lambda t)^n}\mathrm{Bel}_{n,\lambda}(ae_\lambda(t))e^{ae_\lambda(t)}.
\tag{24}
$$

Let $x = e_\lambda(t)$ in (23). Then, we have

$$
\frac{d}{dt} = \frac{dx}{dt}\frac{d}{dx} = \frac{1}{1+\lambda t}e_\lambda(t)\frac{d}{dx} = x^{1-\lambda}\frac{d}{dx}.
\tag{25}
$$

By Lemma 1 and (25), we get

$$
\left(x^{1-\lambda}\frac{d}{dx}\right)^n e^{ax} = x^{-n\lambda}\mathrm{Bel}_{n,\lambda}(ax)e^{ax}, \quad (n \geq 0).
\tag{26}
$$

Let

$$
S_{n,\lambda} = \sum_{k=0}^{\infty}\frac{(k)_{n,\lambda}}{k!}, \quad n = 0, 1, 2, \ldots.
\tag{27}
$$

Then, we note from (19) that we have

$$
e\mathrm{Bel}_{n,\lambda} = S_{n,\lambda}.
\tag{28}
$$

The generating function of $S_{n,\lambda}$ is given by

$$e^{e_\lambda(t)} = \sum_{n=0}^{\infty} S_{n,\lambda} \frac{t^n}{n!}. \tag{29}$$

Indeed, this can be seen from the following:

$$\sum_{n=0}^{\infty} S_{n,\lambda} \frac{t^n}{n!} = e \sum_{n=0}^{\infty} \mathrm{Bel}_{n,\lambda}(1) \frac{t^n}{n!} = e e^{e_\lambda(t)-1} = e^{e_\lambda(t)}. \tag{30}$$

Taking the derivative with respect to t on both sides of (30), we have

$$\sum_{n=0}^{\infty} S_{n+1,\lambda} \frac{t^n}{n!} = \frac{d}{dt} e^{e_\lambda(t)} = e_\lambda^{1-\lambda}(t) e^{e_\lambda(t)}$$

$$= \sum_{l=0}^{\infty} (1-\lambda)_{l,\lambda} \frac{t^l}{l!} \sum_{m=0}^{\infty} S_{m,\lambda} \frac{t^m}{m!}$$

$$= \sum_{n=0}^{\infty} \left(\sum_{m=0}^{n} \binom{n}{m} S_{m,\lambda} (1-\lambda)_{n-m,\lambda} \right) \frac{t^n}{n!} \tag{31}$$

$$= \sum_{n=0}^{\infty} \left(\sum_{m=0}^{n} \binom{n}{m} S_{m,\lambda} (1)_{n-m+1,\lambda} \right) \frac{t^n}{n!}.$$

Thus, by comparing the coefficients on both sides of (31) and from (28), we obtain the following theorem.

Theorem 1. *For $n \geq 0$, the following recurrence relation holds:*

$$\mathrm{Bel}_{n+1,\lambda} = \sum_{m=0}^{n} \binom{n}{m} \mathrm{Bel}_{m,\lambda} (1)_{n-m+1,\lambda}. \tag{32}$$

Assume that the following identity holds:

$$\left(x^{1-\lambda} \frac{d}{dx} \right)^n e^x = \sum_{k=0}^{\infty} \frac{(k)_{n,\lambda}}{k!} x^{k-n\lambda}. \tag{33}$$

Then, we have

$$\left(x^{1-\lambda} \frac{d}{dx} \right)^{n+1} e^x = x^{1-\lambda} \frac{d}{dx} \sum_{k=0}^{\infty} \frac{(k)_{n,\lambda}}{k!} x^{k-n\lambda}$$

$$= x^{1-\lambda} \sum_{k=0}^{\infty} \frac{(k)_{n,\lambda}}{k!} (k - n\lambda) x^{k-n\lambda-1} \tag{34}$$

$$= \sum_{k=0}^{\infty} \frac{(k)_{n+1,\lambda}}{k!} x^{k-(n+1)\lambda}.$$

This together with (26) gives the next result.

Theorem 2. *For $n \geq 0$, the following relations hold true:*

$$\left(x^{1-\lambda} \frac{d}{dx} \right)^n e^x = \sum_{k=0}^{\infty} \frac{(k)_{n,\lambda}}{k!} x^{k-n\lambda} = x^{-n\lambda} \mathrm{Bel}_{n,\lambda}(x) e^x. \tag{35}$$

From the first equality in (35) and (27), we see that we have

$$S_{n,\lambda} = \left(x^{1-\lambda} \frac{d}{dx} \right)^n e^x |_{x=1}. \tag{36}$$

Clearly, $S_{0,\lambda} = S_{1,\lambda} = e$. We can check that

$$\left(x^{1-\lambda} \frac{d}{dx} \right)^2 e^x = (1-\lambda) x^{1-2\lambda} e^x + x^{2-2\lambda} e^x,$$

$$\left(x^{1-\lambda} \frac{d}{dx} \right)^3 e^x = x^{1-3\lambda} e^x \left((1-\lambda)_{2,\lambda} + (1-\lambda)x \right) \tag{37}$$

$$+ x^{2-3\lambda} e^x (2 - 2\lambda + x).$$

From (36) and (37), we have $S_{2,\lambda} = (2-\lambda)e$, $S_{3,\lambda} = (2\lambda^2 - 6\lambda + 5)e$.

By taking $x(d/dx)$ in the second equality of (35), on the one hand, we have

$$x \frac{d}{dx} \left(x^{-n\lambda} \mathrm{Bel}_{n,\lambda}(x) e^x \right) = \sum_{k=0}^{\infty} \frac{(k)_{n+1,\lambda}}{k!} x^{k-n\lambda}. \tag{38}$$

On the other hand, we also have

$$x \frac{d}{dx} \left(x^{-n\lambda} \mathrm{Bel}_{n,\lambda}(x) e^x \right) = x x^{-n\lambda} \left(\mathrm{Bel}'_{n,\lambda}(x) + \mathrm{Bel}_{n,\lambda}(x) \right) e^x$$

$$- n\lambda x^{-n\lambda} \mathrm{Bel}_{n,\lambda}(x) e^x, \tag{39}$$

where $\mathrm{Bel}'_{n,\lambda}(x) = (d/dx) \mathrm{Bel}_{n,\lambda}(x)$.

From (38) and (39) and Theorem 2, we note that

$$\sum_{k=0}^{\infty} \frac{(k)_{n+1,\lambda}}{k!} x^k = \left(\sum_{k=0}^{\infty} \frac{(k)_{n+1,\lambda}}{k!} x^k e^{-x} \right) e^x = \mathrm{Bel}_{n+1,\lambda}(x) e^x$$

$$= x \left(\mathrm{Bel}'_{n,\lambda}(x) + \mathrm{Bel}_{n,\lambda}(x) \right) e^x - n\lambda \mathrm{Bel}_{n,\lambda}(x) e^x. \tag{40}$$

Therefore, by (40) and Theorem 2, we obtain the following theorem.

Theorem 3. *For $n \geq 0$, the following identity holds:*

$$\mathrm{Bel}_{n+1,\lambda}(x) = x \left(\mathrm{Bel}'_{n,\lambda}(x) + \mathrm{Bel}_{n,\lambda}(x) \right) - n\lambda \mathrm{Bel}_{n,\lambda}(x), \tag{41}$$

where $\mathrm{Bel}'_{n,\lambda}(x) = (d/dx) \mathrm{Bel}_{n,\lambda}(x)$.

From (17), we note that

$$\sum_{n=0}^{\infty} \frac{d}{dx} \mathrm{Bel}_{n,\lambda}(x) \frac{t^n}{n!} = \frac{\partial}{\partial x} e^{x(e_\lambda(t)-1)} = (e_\lambda(t)-1) e^{x(e_\lambda(t)-1)}$$

$$= \left(\sum_{l=0}^{\infty} (1)_{l,\lambda} \frac{t^l}{l!} - 1 \right) \sum_{m=0}^{\infty} \mathrm{Bel}_{m,\lambda}(x) \frac{t^m}{m!}$$

$$= \sum_{n=0}^{\infty} \left(\sum_{m=0}^{n} \binom{n}{m} \mathrm{Bel}_{m,\lambda}(x) (1)_{n-m,\lambda} - \mathrm{Bel}_{n,\lambda}(x) \right) \frac{t^n}{n!}$$

$$= \sum_{n=0}^{\infty} \left(\sum_{m=0}^{n-1} \binom{n}{m} \mathrm{Bel}_{m,\lambda}(x) (1)_{n-m,\lambda} \right) \frac{t^n}{n!}.$$

(42)

Thus, by comparing the coefficients on both sides of (42), we get

$$\frac{d}{dx} \mathrm{Bel}_{n,\lambda}(x) = \mathrm{Bel}'_{n,\lambda}(x) = \sum_{m=0}^{n-1} \binom{n}{m} \mathrm{Bel}_{m,\lambda}(x) (1)_{n-m,\lambda},$$

$$(n \geq 1).$$

(43)

Taking the derivative with respect to t on both sides of (17), we have

$$\frac{d}{dt} e^{x(e_\lambda(t)-1)} = \sum_{n=0}^{\infty} \mathrm{Bel}_{n+1,\lambda}(x) \frac{t^n}{n!}.$$

(44)

On the other hand,

$$\frac{d}{dt} e^{x(e_\lambda(t)-1)} = x e_\lambda^{1-\lambda}(t) e^{x(e_\lambda(t)-1)}$$

$$= x \sum_{l=0}^{\infty} (1-\lambda)_{l,\lambda} \frac{t^l}{l!} \sum_{m=0}^{\infty} \mathrm{Bel}_{m,\lambda}(x) \frac{t^m}{m!}$$

$$= x \sum_{n=0}^{\infty} \left(\sum_{m=0}^{n} \binom{n}{m} \mathrm{Bel}_{n,\lambda}(x) (1-\lambda)_{n-m,\lambda} \right) \frac{t^n}{n!}$$

$$= \sum_{n=0}^{\infty} \left(x \sum_{m=0}^{n} \binom{n}{m} \mathrm{Bel}_{m,\lambda}(x) (1)_{n-m+1,\lambda} \right) \frac{t^n}{n!}.$$

(45)

Therefore, by (44) and (45), we obtain the following theorem.

Theorem 4. *. For $n \geq 0$, the following recurrence relation is valid:*

$$\mathrm{Bel}_{n+1,\lambda}(x) = x \sum_{m=0}^{n} \binom{n}{m} \mathrm{Bel}_{m,\lambda}(x) (1)_{n-m+1,\lambda}.$$

(46)

Remark 1. Theorems 3 and 4 and (43) give us the following:

$$\mathrm{Bel}_{n+1,\lambda}(x) = x \sum_{m=0}^{n} \binom{n}{m} \mathrm{Bel}_{m,\lambda}(x) (1)_{n-m,\lambda} - n\lambda \mathrm{Bel}_{n,\lambda}(x)$$

$$= x \sum_{m=0}^{n} \binom{n}{m} \mathrm{Bel}_{m,\lambda}(x) (1)_{n-m,\lambda} (1 - (n-m)\lambda).$$

(47)

This implies that the following identity must hold true:

$$n \mathrm{Bel}_{n,\lambda}(x) = x \sum_{m=0}^{n} \binom{n}{m} (n-m) \mathrm{Bel}_{m,\lambda}(x) (1)_{n-m,\lambda}, \quad (48)$$

the validity of which follows from Theorem 4.

From Theorem 3, we note that

$$x \mathrm{Bel}'_{n,\lambda}(x) = x \frac{d}{dx} \mathrm{Bel}_{n,\lambda}(x) = \mathrm{Bel}_{n+1,\lambda}(x) - x \mathrm{Bel}_{n,\lambda}(x)$$

$$+ n\lambda \mathrm{Bel}_{n,\lambda}(x)$$

$$= \mathrm{Bel}_{n+1,\lambda}(x) - (x - n\lambda) \mathrm{Bel}_{n,\lambda}(x)$$

$$= x \sum_{m=0}^{n-1} \binom{n}{m} \mathrm{Bel}_{m,\lambda}(x) (1)_{n+1-m,\lambda} + n\lambda \mathrm{Bel}_{n,\lambda}(x).$$

(49)

Therefore, by (49), we obtain the following corollary.

Corollary 1. *For $n \geq 1$, we have the following identity:*

$$x \frac{d}{dx} \mathrm{Bel}_{n,\lambda}(x) = x \sum_{m=0}^{n-1} \binom{n}{m} \mathrm{Bel}_{m,\lambda}(x) (1)_{n+1-m,\lambda} + n\lambda \mathrm{Bel}_{n,\lambda}(x).$$

(50)

We observe that

$$x^{1-\lambda}\frac{d}{dx}\left(x^{-n\lambda}\mathrm{Bel}_{n,\lambda}(x)e^x\right) = x^{1-\lambda}\frac{d}{dx}\left(x^{-n\lambda}\sum_{k=0}^{\infty}\frac{(k)_{n,\lambda}}{k!}x^k\right)$$

$$= \sum_{k=0}^{\infty}\frac{(k)_{n+1,\lambda}}{k!}x^{k-(n+1)\lambda}$$

$$= x^{-(n+1)\lambda}\left(\sum_{k=0}^{\infty}\frac{(k)_{n+1,\lambda}}{k!}x^k e^{-x}\right)e^x$$

$$= x^{-(n+1)\lambda}\mathrm{Bel}_{n+1,\lambda}(x)e^x, \quad (n\geq 0). \tag{51}$$

Thus, by (51), we get

$$x^{1-\lambda}\frac{d}{dx}\left(x^{-n\lambda}\mathrm{Bel}_{n,\lambda}(x)e^x\right) = x^{-(n+1)\lambda}\mathrm{Bel}_{n+1,\lambda}(x)e^x, \quad (n\geq 0). \tag{52}$$

From (17), we have

$$\sum_{n=0}^{\infty}\mathrm{Bel}_{n,\lambda}(x+y)\frac{t^n}{n!} = e^{(x+y)(e_\lambda(t)-1)} = e^{x(e_\lambda(t)-1)}\cdot e^{y(e_\lambda(t)-1)}$$

$$= \sum_{l=0}^{\infty}\mathrm{Bel}_{l,\lambda}(x)\frac{t^l}{l!}\sum_{m=0}^{\infty}\mathrm{Bel}_{m,\lambda}(x)\frac{t^m}{m!}$$

$$= \sum_{n=0}^{\infty}\left(\sum_{l=0}^{n}\binom{n}{l}\mathrm{Bel}_{l,\lambda}(x)\mathrm{Bel}_{n-l,\lambda}(y)\right)\frac{t^n}{n!}. \tag{53}$$

Therefore, by comparing the coefficients on both sides of (53), we obtain the following theorem.

Theorem 5. *For $n\geq 0$, the following binomial identity holds:*

$$\mathrm{Bel}_{n,\lambda}(x+y) = \sum_{l=0}^{n}\binom{n}{l}\mathrm{Bel}_{l,\lambda}(x)\mathrm{Bel}_{n-l,\lambda}(y). \tag{54}$$

From (17), we note that

$$\sum_{n=0}^{\infty}\int_0^x \mathrm{Bel}_{n,\lambda}(x)dx\frac{t^n}{n!} = \int_0^x e^{x(e_\lambda(t)-1)}dx. \tag{55}$$

On the other hand, we also have

$$\int_0^x e^{x(e_\lambda(t)-1)}dx = \frac{1}{e_\lambda(t)-1}\left[e^{x(e_\lambda(t)-1)}\right]_0^x$$

$$= \frac{1}{e_\lambda(t)-1}\left(e^{x(e_\lambda(t)-1)}-1\right) = \frac{1}{e_\lambda(t)-1}\sum_{k=1}^{\infty}\mathrm{Bel}_{k,\lambda}(x)\frac{t^k}{k!}$$

$$= \frac{t}{e_\lambda(t)-1}\sum_{k=0}^{\infty}\frac{\mathrm{Bel}_{k+1,\lambda}(x)}{k+1}\frac{t^k}{k!} = \sum_{l=0}^{\infty}\beta_{l,\lambda}\frac{t^l}{l!}\sum_{k=0}^{\infty}\frac{\mathrm{Bel}_{k+1,\lambda}(x)}{k+1}\frac{t^k}{k!}$$

$$= \sum_{n=0}^{\infty}\left(\sum_{k=0}^{n}\binom{n}{k}\frac{\mathrm{Bel}_{k+1,\lambda}(x)}{k+1}\beta_{n-k,\lambda}\right)\frac{t^n}{n!} \tag{56}$$

$$= \sum_{n=0}^{\infty}\left(\frac{1}{n+1}\sum_{k=0}^{n}\binom{n+1}{k+1}\mathrm{Bel}_{k+1,\lambda}(x)\beta_{n-k,\lambda}\right)\frac{t^n}{n!}$$

$$= \sum_{n=0}^{\infty}\left(\frac{1}{n+1}\sum_{k=1}^{n+1}\binom{n+1}{k}\mathrm{Bel}_{k,\lambda}(x)\beta_{n+1-k,\lambda}\right)\frac{t^n}{n!}.$$

Therefore, by (55) and (56), we obtain the following theorem.

Theorem 6. *For $n \geq 0$, the antiderivative of $\mathrm{Bel}_{n,\lambda}(x)$ is given by*

$$\int_0^x \mathrm{Bel}_{n,\lambda}(x)\mathrm{d}x = \frac{1}{n+1}\sum_{k=1}^{n+1}\binom{n+1}{k}\beta_{n+1-k,\lambda}\mathrm{Bel}_{k,\lambda}(x), \tag{57}$$

where $\beta_{n,\lambda}$ are Carlitz's degenerate Bernoulli numbers given by $(t/(e_\lambda(t)-1)) = \sum_{n=0}^{\infty}\beta_{n,\lambda}(t^n/n!)$.

For $k \geq 0$, by (12), we get

$$\sum_{n=k}^{\infty}S_{2,\lambda}(n,k)\frac{t^n}{n!} = \frac{1}{k!}(e_\lambda(t)-1)^k = \frac{1}{k!}\sum_{j=0}^{k}(-1)^{k-j}e_\lambda^j(t)\binom{k}{j}$$

$$= \sum_{n=0}^{\infty}\left(\frac{1}{k!}\sum_{j=0}^{k}\binom{k}{j}(-1)^{k-j}(j)_{n,\lambda}\right)\frac{t^n}{n!}. \tag{58}$$

By comparing the coefficients on both sides of (58), we have

$$\frac{1}{k!}\sum_{j=0}^{k}\binom{k}{j}(-1)^{k-j}(j)_{n,\lambda} = \begin{cases} S_{2,\lambda}(n,k), & \text{if } n \geq k, \\ 0, & \text{if } \$0 \leq n \leq k-1\$. \end{cases} \tag{59}$$

Let $D = (d/dx)$, and let $y = x^p$. As $x^{1-\lambda}D = py^{1-(\lambda/p)}(d/dy)$, we have

$$\left(x^{1-\lambda}D\right)^n e^{ax^p} = \left(py^{1-(\lambda/p)}\frac{d}{dy}\right)^n e^{ay} = p^n\left(y^{1-(\lambda/p)}\frac{d}{dy}\right)^n e^{ay}$$

$$= p^n y^{-(n\lambda/p)}\mathrm{Bel}_{n,(\lambda/p)}(ay)e^{ay} = p^n x^{-n\lambda}\mathrm{Bel}_{n,(\lambda/p)}(ax^p)e^{ax^p}. \tag{60}$$

Thus, we have

$$\left(x^{1-\lambda}D\right)^n e^{ax^p} = p^n x^{-n\lambda}\mathrm{Bel}_{n,(\lambda/p)}(ax^p)e^{ax^p}, \quad (n \geq 0). \tag{61}$$

Therefore, by (61), we obtain the following proposition.

Proposition 1. *For $n \geq 0$, we have the following operational formula:*

$$x^{n\lambda}\left(x^{1-\lambda}D\right)^n e^{ax^p} = p^n\mathrm{Bel}_{n,(\lambda/p)}(ax^p)e^{ax^p}, \tag{62}$$

where $D = (d/dx)$.

From (12), we note that

$$\sum_{k=0}^{n+1}S_{2,\lambda}(n+1,k)(x)_k = (x)_{n+1,\lambda} = (x-n\lambda)(x)_{n,\lambda}$$

$$= (x-n\lambda)\sum_{k=0}^{n}S_{2,\lambda}(n,k)(x)_k = \sum_{k=0}^{n}S_{2,\lambda}(n,k)(x-k+k-n\lambda)(x)_k$$

$$= \sum_{k=0}^{n}S_{2,\lambda}(n,k)(x)_{k+1} + \sum_{k=0}^{n}S_{2,\lambda}(n,k)(k-n\lambda)(x)_k \tag{63}$$

$$= \sum_{k=1}^{n+1}S_{2,\lambda}(n,k-1)(x)_k + \sum_{k=0}^{n}S_{2,\lambda}(n,k)(k-n\lambda)(x)_k$$

$$= \sum_{k=0}^{n+1}\left(S_{2,\lambda}(n,k-1) + S_{2,\lambda}(n,k)(k-n\lambda)\right)(x)_k.$$

By (63), we get

$$S_{2,\lambda}(n+1,k) = S_{2,\lambda}(n,k-1) + (k-n\lambda)S_{2,\lambda}(n,k), \quad (64)$$

where $0 \le k \le n+1$.

We prove the next theorem by induction on n.

Theorem 7. *Assume that f is an infinitely differentiable function. Then, for $n \ge 0$, the following operational formula holds:*

$$\left(x^{1-\lambda}D\right)^n f = \sum_{k=0}^n S_{2,\lambda}(n,k) x^{k-n\lambda} D^k f, \quad (65)$$

where $D = (d/dx)$.

Proof. The statement is obviously true for $n = 0$. Assume that it is true for n, $(n \ge 0)$.

$$
\begin{aligned}
\left(x^{1-\lambda}D\right)^{n+1} f(x) &= \left(x^{1-\lambda}D\right) \sum_{k=0}^n S_{2,\lambda}(n,k) x^{k-n\lambda} D^k f(x) \\
&= x^{1-\lambda} \sum_{k=0}^n S_{2,\lambda}(n,k)\left\{(k-n\lambda)x^{k-1-n\lambda} D^k f(x) + x^{k-n\lambda} D^{k+1} f(x)\right\} \\
&= \sum_{k=0}^n S_{2,\lambda}(n,k)\left\{(k-n\lambda)x^{k-(n+1)\lambda} D^k f(x) + x^{k+1-(n+1)\lambda} D^{k+1} f(x)\right\} \\
&= \sum_{k=0}^{n+1} S_{2,\lambda}(n,k)(k-n\lambda)x^{k-(n+1)\lambda} D^k f(x) + \sum_{k=0}^{n+1} S_{2,\lambda}(n,k-1) x^{k-(n+1)\lambda} D^k f(x) \\
&= \sum_{k=0}^{n+1} \left\{S_{2,\lambda}(n,k)(k-n\lambda) + S_{2,\lambda}(n,k-1)\right\} x^{k-(n+1)\lambda} D^k f(x) \\
&= \sum_{k=0}^{n+1} S_{2,\lambda}(n+1,k) x^{k-(n+1)\lambda} D^k f(x).
\end{aligned}
\quad (66)
$$

Let $f(x) = e^x$. Then, we have

$$
\begin{aligned}
x^{n\lambda}\left(x^{1-\lambda}D\right)^n e^x &= \left(\sum_{k=0}^n S_{2,\lambda}(n,k)x^k\right)e^x \\
&= \mathrm{Bel}_{n,\lambda}(x)e^x.
\end{aligned}
\quad (67)
$$

Observe that, for any α, we have

$$\left(x^{1-\lambda}D\right)^n x^\alpha = (\alpha)_{n,\lambda} x^{\alpha-n\lambda}. \quad (68)$$

By the Leibniz rule, we get

$$\left(x^{1-\lambda}D\right)^n (fg) = \sum_{l=0}^n \binom{n}{l}\left[\left(x^{1-\lambda}D\right)^{n-l} f\right]\left[\left(x^{1-\lambda}D\right)^l g\right]. \quad (69)$$

From Theorem 2, we note that

$$
\begin{aligned}
x^{-(n+m)\lambda} e^x \mathrm{Bel}_{n+m,\lambda}(x) &= \left(x^{1-\lambda}D\right)^{n+m} e^x = \left(x^{1-\lambda}D\right)^n \left(x^{1-\lambda}D\right)^m e^x \\
&= \left(x^{1-\lambda}D\right)^n \left(x^{-m\lambda} \mathrm{Bel}_{m,\lambda}(x)e^x\right).
\end{aligned}
\quad (70)
$$

By (69) and (70), we get

$$
\begin{aligned}
x^{-(n+m)\lambda} e^x \mathrm{Bel}_{n+m,\lambda}(x) &= \left(x^{1-\lambda}D\right)^n \left(x^{-m\lambda} \mathrm{Bel}_{m,\lambda} e^x\right) \\
&= \sum_{k=0}^n \binom{n}{k}\left[\left(x^{1-\lambda}D\right)^{n-k}\left(x^{-m\lambda} \mathrm{Bel}_{m,\lambda}(x)\right)\right]\left[\left(x^{1-\lambda}D\right)^k e^x\right] \\
&= \sum_{k=0}^n \binom{n}{k} x^{-k\lambda} \mathrm{Bel}_{k,\lambda}(x)e^x\left[\left(x^{1-\lambda}D\right)^{n-k}\left(x^{-m\lambda} \mathrm{Bel}_{m,\lambda}(x)\right)\right].
\end{aligned}
\quad (71)
$$

On the other hand,

$$
\begin{aligned}
\left(x^{1-\lambda}D\right)^{n-k}\left(x^{-m\lambda} \mathrm{Bel}_{m,\lambda}(x)\right) &= \sum_{j=0}^m S_{2,\lambda}(m,j)\left[\left(x^{1-\lambda}D\right)^{n-k} x^{j-m\lambda}\right] \\
&= \sum_{j=0}^m S_{2,\lambda}(m,j)(j-m\lambda)_{n-k,\lambda} x^{j-m\lambda-(n-k)\lambda} = \sum_{j=0}^m S_{2,\lambda}(m,j)(j-m\lambda)_{n-k,\lambda} x^{j-(m+n)\lambda+k\lambda} \\
&= \sum_{j=0}^m S_{2,\lambda}(m,j) \frac{(j)_{m+n-k,\lambda}}{(j)_{m,\lambda}} x^{j-(m+n)\lambda+k\lambda}.
\end{aligned}
\quad (72)
$$

By (71) and (72), we get

$$x^{-(n+m)\lambda}e^x \mathrm{Bel}_{n+m,\lambda}(x)$$

$$= \sum_{k=0}^{n}\binom{n}{k}x^{-k\lambda}\mathrm{Bel}_{k,\lambda}(x)e^x\sum_{j=0}^{m}S_{2,\lambda}(m,j)\frac{(j)_{m+n-k,\lambda}}{(j)_{m,\lambda}}x^{j-(m+n)\lambda+k\lambda}$$

$$= x^{-(m+n)\lambda}e^x\sum_{k=0}^{n}\sum_{j=0}^{m}\binom{n}{k}S_{2,\lambda}(m,j)\mathrm{Bel}_{k,\lambda}(x)\frac{(j)_{m+n-k,\lambda}}{(j)_{m,\lambda}}x^{j}.$$

$$(73)$$

Therefore, by comparing the coefficients on both sides of (73), we obtain the following theorem. □

Theorem 8. *For $m, n \geq 0$, we have the following expression:*

$$\mathrm{Bel}_{n+m,\lambda}(x) = \sum_{k=0}^{n}\sum_{j=0}^{m}\binom{n}{k}S_{2,\lambda}(m,j)\mathrm{Bel}_{k,\lambda}(x)\frac{(j)_{m+n-k,\lambda}}{(j)_{m,\lambda}}x^{j}.$$

$$(74)$$

Taking $x = 1$ in (74), we have

$$\mathrm{Bel}_{n+m,\lambda} = \sum_{k=0}^{n}\sum_{j=0}^{m}\binom{n}{k}S_{2,j}(m,j)\mathrm{Bel}_{k,\lambda}\frac{(j)_{n+m-k,\lambda}}{(j)_{m,\lambda}}.$$

$$(75)$$

From (19) and (68), we note that

$$\left(x^{1-\lambda}D\right)^n\mathrm{Bel}_{m,\lambda}(x) = \left(x^{1-\lambda}D\right)^n\sum_{k=0}^{m}S_{2,\lambda}(m,k)x^k$$

$$= \sum_{k=0}^{m}S_{2,\lambda}(m,k)(k)_{n,\lambda}x^{k-n\lambda}.$$

$$(76)$$

On the other hand, by Leibniz rule (69) and Theorem 2, we get

$$\left(x^{1-\lambda}D\right)^n\mathrm{Bel}_{m,\lambda}(x) = \left(x^{1-\lambda}D\right)^n\left[\left(e^{-x}x^{m\lambda}\right)\left(\mathrm{Bel}_{m,\lambda}(x)e^x x^{-m\lambda}\right)\right]$$

$$= \sum_{k=0}^{n}\binom{n}{k}\left[\left(x^{1-\lambda}D\right)^{n-k}\left(x^{m\lambda}e^{-x}\right)\right]\left[\left(x^{1-\lambda}D\right)^{k}\left(\mathrm{Bel}_{m,\lambda}(x)e^x x^{-m\lambda}\right)\right]$$

$$= \sum_{k=0}^{n}\binom{n}{k}\left[\left(x^{1-\lambda}D\right)^{n-k}\left(x^{m\lambda}e^{-x}\right)\right]\left[\left(x^{1-\lambda}D\right)^{m+k}e^x\right]$$

$$= \sum_{k=0}^{n}\binom{n}{k}\left[\left(x^{1-\lambda}D\right)^{n-k}\left(x^{m\lambda}e^{-x}\right)\right]x^{-(m+k)\lambda}\mathrm{Bel}_{m+k,\lambda}(x)e^x.$$

$$(77)$$

By (68) and (69) and Theorem 2, we easily get

$$\left(x^{1-\lambda}D\right)^{n-k}\left(x^{m\lambda}e^{-x}\right) = \sum_{j=0}^{n-k}\binom{n-k}{j}\left[\left(x^{1-\lambda}D\right)^{j}x^{m\lambda}\right]\left[\left(x^{1-\lambda}D\right)^{n-k-j}e^{-x}\right]$$

$$= \sum_{j=0}^{n-k}\binom{n-k}{j}(m\lambda)_{j,\lambda}x^{m\lambda-j\lambda}e^{-x}\mathrm{Bel}_{n+k-j,\lambda}(-x)x^{-(n-k-j)\lambda}$$

$$= \sum_{j=0}^{n-k}\binom{n-k}{j}(m\lambda)_{j,\lambda}x^{m\lambda-n\lambda+k\lambda}\mathrm{Bel}_{n-k-j,\lambda}(-x)e^{-x}.$$

$$(78)$$

From (77) and (78), we have

$$
\begin{aligned}
\left(x^{1-\lambda} D\right)^n &\mathrm{Bel}_{m,\lambda}(x) \\
&= \sum_{k=0}^{n} \binom{n}{k} x^{-m\lambda - k\lambda} \mathrm{Bel}_{m+k,\lambda}(x) e^x \sum_{j=0}^{n-k} \binom{n-k}{j} (m\lambda)_{j,\lambda} x^{m\lambda - n\lambda + k\lambda} \mathrm{Bel}_{n-k-j,\lambda}(-x) e^{-x} \\
&= \sum_{k=0}^{n} \sum_{j=0}^{n-k} \binom{n}{k} \binom{n-k}{j} \mathrm{Bel}_{m+k,\lambda}(x) \mathrm{Bel}_{n-k-j,\lambda}(-x)(m\lambda)_{j,\lambda} x^{-n\lambda}.
\end{aligned}
\tag{79}
$$

Therefore, by (76) and (79), we obtain the following theorem.

Theorem 9. *For $m, n \geq 0$, the following identity holds true.*

$$
\begin{aligned}
\sum_{k=0}^{m} &S_{2,\lambda}(m,k)(k)_{n,\lambda} x^k \\
&= \sum_{k=0}^{n} \sum_{j=0}^{n-k} \binom{n}{k}\binom{n-k}{j} \mathrm{Bel}_{m+k,\lambda}(x)\mathrm{Bel}_{n-k-j,\lambda}(-x)(m\lambda)_{j,\lambda}.
\end{aligned}
\tag{80}
$$

By (11) and (13), we easily get

$$
(-1)^{n-k} S_{1,\lambda}(n,k) = \begin{bmatrix} n \\ k \end{bmatrix}_{\lambda}, \quad (0 \leq k \leq n).
\tag{81}
$$

Indeed,

$$
\begin{aligned}
\sum_{n=0}^{\infty} \langle x \rangle_n \frac{t^n}{n!} &= \left(\frac{1}{1-t}\right)^x = e_\lambda^{-x}\left(\log_\lambda(1-t)\right) \\
&= \sum_{k=0}^{\infty} (-x)_{k,\lambda} \frac{1}{k!}\left(\log_\lambda(1-t)\right)^k \\
&= \sum_{k=0}^{\infty} (-1)^k \langle x \rangle_{k,\lambda} \sum_{n=k}^{\infty} S_{1,\lambda}(n,k)\frac{(-t)^n}{n!} \\
&= \sum_{n=0}^{\infty} \left(\sum_{k=0}^{n} (-1)^{n-k} S_{1,\lambda}(n,k)\langle x \rangle_{k,\lambda}\right) \frac{t^n}{n!}.
\end{aligned}
\tag{82}
$$

Therefore, by (82), we get

$$
\langle x \rangle_n = \sum_{k=0}^{n} (-1)^{n-k} S_{1,\lambda}(n,k)\langle x \rangle_{k,\lambda}.
\tag{83}
$$

Replacing t by $\log_\lambda(1+t)$ in (17), we get

$$
\begin{aligned}
e^{xt} &= \sum_{k=0}^{\infty} \mathrm{Bel}_{k,\lambda}(x)\frac{1}{k!}\left(\log_\lambda(1+t)\right)^k \\
&= \sum_{k=0}^{\infty} \mathrm{Bel}_{k,\lambda}(x) \sum_{n=k}^{\infty} S_{1,\lambda}(n,k)\frac{t^n}{n!} \\
&= \sum_{n=0}^{\infty} \left(\sum_{k=0}^{n} \mathrm{Bel}_{k,\lambda}(x) S_{1,\lambda}(n,k)\right)\frac{t^n}{n!}.
\end{aligned}
\tag{84}
$$

Thus, from (81) and (84), we get

$$
x^n = \sum_{k=0}^{n} \mathrm{Bel}_{k,\lambda}(x)(-1)^{n-k} \begin{bmatrix} n \\ k \end{bmatrix}_{\lambda}.
\tag{85}
$$

From (13), we note that

$$
\begin{aligned}
\sum_{k=0}^{n+1} &\begin{bmatrix} n+1 \\ k \end{bmatrix}_{\lambda} \langle x \rangle_{k,\lambda} = \langle x \rangle_{n+1} = (x+n)\langle x \rangle_n \\
&= (x+n) \sum_{k=0}^{n} \begin{bmatrix} n \\ k \end{bmatrix}_{\lambda} \langle x \rangle_{k,\lambda} \\
&= \sum_{k=0}^{n} \begin{bmatrix} n \\ k \end{bmatrix}_{\lambda} (x+k\lambda + n - k\lambda)\langle x \rangle_{k,\lambda} \\
&= \sum_{k=0}^{n} \begin{bmatrix} n \\ k \end{bmatrix}_{\lambda} \langle x \rangle_{k+1,\lambda} + \sum_{k=0}^{n} (n-k\lambda)\begin{bmatrix} n \\ k \end{bmatrix}_{\lambda} \langle x \rangle_{k,\lambda} \\
&= \sum_{k=0}^{n+1} \begin{bmatrix} n \\ k-1 \end{bmatrix}_{\lambda} \langle x \rangle_{k,\lambda} + \sum_{k=0}^{n+1} (n-k\lambda)\begin{bmatrix} n \\ k \end{bmatrix}_{\lambda} \langle x \rangle_{k,\lambda} \\
&= \sum_{k=0}^{n+1} \left(\begin{bmatrix} n \\ k-1 \end{bmatrix}_{\lambda} + (n-k\lambda)\begin{bmatrix} n \\ k \end{bmatrix}_{\lambda}\right)\langle x \rangle_{k,\lambda}.
\end{aligned}
\tag{86}
$$

Thus, by comparing the coefficients on both sides of (86), we get

$$
\begin{bmatrix} n+1 \\ k \end{bmatrix}_{\lambda} = \begin{bmatrix} n \\ k-1 \end{bmatrix}_{\lambda} + (n-k\lambda)\begin{bmatrix} n \\ k \end{bmatrix}_{\lambda}, \quad (0 \leq k \leq n+1).
\tag{87}
$$

3. Conclusion

Here, we studied by means of generating functions the degenerate Bell polynomials which are degenerate versions of the Bell polynomials. In more detail, we derived recurrence relations for degenerate Bell polynomials (see Theorems 1, 3, 4, and 8), and expressions for them that can be derived from repeated applications of certain operators to the exponential functions (see Theorem 2 and Proposition 1), the derivatives of them (Corollary 1), the antiderivatives of them (see Theorem 6), and some identities involving them (see Theorems 5 and 9).

As one of our future projects, we would like to continue to study degenerate versions of certain special polynomials and numbers and their applications to physics, science, and

engineering as well as to mathematics. An earlier version of this paper has been presented as preprint in [15].

Data Availability

No data were used to support this study.

Disclosure

Conflicts of Interest

The authors declare that they have no conflicts of interest.

Acknowledgments

References

[1] L. Comtet, *Advanced Combinatorics: The Art of Finite and Infinite Expansions*, Springer, Dordrecht, Netherlands, 1974.

[2] T. Kim, D. S. Kim, and D. V. Dolgy, "On partially degenerate Bell numbers and polynomials," *Proceedings of the Jangjeon Mathematical Society*, vol. 20, no. 3, pp. 337–345, 2017.

[3] L. Carlitz, "Degenerate stirling, Bernoulli and eulerian numbers," *Utilitas Mathematica*, vol. 15, pp. 51–88, 1979.

[4] M. Acikgoz and U. Duran, "Unified degenerate central Bell polynomials," *Journal of Mathematical Analysis*, vol. 11, no. 2, pp. 18–33, 2020.

[5] D. S. Kim and T. Kim, "A note on a new type of degenerate Bernoulli numbers," *Russian Journal of Mathematical Physics*, vol. 27, no. 2, pp. 227–235, 2020.

[6] H. K. Kim, "Fully degenerate Bell polynomials associated with degenerate Poisson random variables," *Open Mathematics*, vol. 19, no. 1, pp. 284–296, 2021.

[7] T. Kim, "A note on degenerate stirling polynomials of the second kind," *Proceedings of the Jangjeon Mathematical Society*, vol. 20, no. 3, pp. 319–331, 2017.

[8] T. Kim and D. S. Kim, "Note on the degenerate gamma function," *Russian Journal of Mathematical Physics*, vol. 27, no. 3, pp. 352–358, 2020.

[9] T. Kim and D. S. Kim, "Degenerate zero-truncated Poisson random variables," *Russian Journal of Mathematical Physics*, vol. 28, no. 1, pp. 66–72, 2021.

[10] T. Kim, D. S. Kim, H. Lee, and J.-W. Park, "A note on degenerate r-stirling numbers," *Journal of Inequalities and Applications*, vol. 225, p. 12, 2020.

[11] S. Araci, M. Acikgoz, and E. Sen, "Some new formulae for Genocchi numbers and polynomials involving Bernoulli and Euler polynomials," *International Journal of Mathematics and Mathematical Sciences*, vol. 2014, Article ID 760613, 7 pages, 2014.

[12] E. T. Bell, "Exponential numbers," *The American Mathematical Monthly*, vol. 41, no. 7, pp. 411–419, 1934.

[13] K. N. Boyadzhiev, "Exponential polynomials, stirling numbers, and evaluation of some gamma integrals," *Abstract and Applied Analysis*, vol. 2009, Article ID 168672, 18 pages, 2009.

[14] S. Roman, "The umbral calculus," *Pure and Applied Mathematics*, Academic Press, Inc. [Harcourt Brace Jovanovich, Publishers], New York, NY, USA, 1984.

[15] T. Kim, D. S. Kim, H. Lee, and S. Park, "Some new properties on degenerate bell polynomials," Preprint.